

1 NOAA Technical Memorandum NMFS-AFSC-

2
3
4
5
6 Advancing Model-Based Essential Fish Habitat
7 Descriptions for North Pacific Species
8 in the Aleutian Islands
9

10
11
12
13 by
14 J. Harris, E. A. Laman, J. L. Pirtle, M. C. Siple, C. N. Rooper, T. P. Hurst,
15 and C. L. Conrath
16

17
18
19 Resource Assessment and Conservation Engineering
20 Groundfish Assessment Program
21 Alaska Fisheries Science Center
22 National Marine Fisheries Service
23 National Oceanic and Atmospheric Administration
24 7600 Sand Point Way NE
25 (206) 526-4832
26

27 Jeremy.Harris@NOAA.gov
28

29
30
31
32 Ned.Laman@NOAA.gov, Jodi.Pirtle@NOAA.gov, Margaret.Siple@NOAA.gov,
33 Chris.Rooper@dfo-mpc.gc.ca, Thomas.Hurst@NOAA.gov,
34 Christina.Conrath@NOAA.gov
35

36
37
38 **Submitted to RPTS 21 December 2021**
39 November 2021

40
41

ABSTRACT

42
43 Advancing model-based descriptions of essential fish habitat (EFH) for federally managed fishes and
44 invertebrates is a key component of the 5-year Review process mandated for EFH information in Fishery
45 Management Plans. The analyses presented here demonstrate refinements and advances built on the
46 habitat based species distribution modeling (SDM) approach established in the previous EFH 5-year
47 Review. All of the ensemble SDMs constructed for Aleutian Island species in this present work predict
48 EFH Level 2 information (habitat related abundance), meeting a key objective of the EFH Research Plan
49 for Alaska. We also met another objective of the Research Plan by introducing maps of EFH Level 3
50 information (habitat related vital rates) for settled early juvenile walleye pollock in the Aleutian Islands
51 for the first time. In the present work, we describe 53 EFH maps in the Aleutian Islands accounting for 25
52 North Pacific groundfish species with up to 3 life stages per species as well as for 2 crab species and
53 octopus. The SDM ensemble approach achieved good predictive performance over a variety of species,
54 and was particularly effective for flatfish species. SDM predictions were less accurate for species with
55 few occurrences in the trawl survey (e.g. invertebrate) or highly variable trawl catches (e.g. Atka
56 mackerel). In general, geographic position, bottom depth and bottom currents were the most influential
57 covariate predictors in the SDMs. The maps and descriptions presented here represent the “best available
58 science” to form a basis for assessing anthropogenic impacts to habitats in Alaska and are extensible to
59 other fishery management and ecosystem information needs. Recommended future research includes
60 developing methods for combining disparate data sources to expand spatial and seasonal coverage of
61 Alaska species distribution and abundance as well as increasing the scope of EFH research to address
62 rapidly changing environmental conditions in the region.

64
65
66
67
68
69
70
71
72
73
74
75
76
77
78
79
80
81
82
83
84
85
86
87
88
89
90
91
92
93
94
95
96
97

TABLE OF CONTENTS

ABSTRACT.....	3
INTRODUCTION	8
MATERIALS AND METHODS	10
Study Area	10
Dependent Variables: Fish and Invertebrate Data	11
Large-mesh Bottom-trawl Survey.....	11
Independent Covariates: Habitat Data	13
Bottom Depth and Temperature.....	14
Water Movement	15
Geographic Position.....	17
Seafloor Terrain	18
Seafloor Rockiness.....	19
Biogenic Structure	20
Statistical Modeling	21
Maximum Entropy Models (MaxEnt).....	22
Generalized Additive Models (GAM)	23
Cross-Validation and Skill Testing	25
Ensemble Models and Uncertainty	26
Species Distribution Model Performance Metrics	28
Essential Fish Habitat (EFH) Maps	30
Species Complexes	31
EFH Level 3 Habitat Related Vital Rates	32
RESULTS	44
Flatfishes	44
Arrowtooth flounder (<i>Atheresthes stomias</i>)	44
Flathead sole (<i>Hippoglossoides elassodon</i>)	59
Greenland turbot (<i>Reinhardtius hippoglossoides</i>)	74
Kamchatka flounder (<i>Atheresthes evermani</i>).....	81
Northern rock sole (<i>Lepidopsetta polyxystra</i>).....	92
Other Flatfish Stock Complex.....	107
Dover sole (<i>Microstomus pacificus</i>) –	111
Rex sole (<i>Glyptocephalus zachirus</i>)	129
Southern rock sole (<i>Lepidopsetta bilineata</i>)	140

98	Roundfishes.....	151
99	Atka mackerel (<i>Pleurogrammus monopterygius</i>)	151
100	Pacific cod (<i>Gadus macrocephalus</i>)	162
101	Sablefish (<i>Anoplopoma fimbria</i>).....	173
102	Walleye pollock (<i>Gadus chalcogrammus</i>).....	184
103	Rockfishes.....	203
104	Northern rockfish (<i>Sebastes polyspinis</i>)	203
105	Pacific ocean perch (<i>Sebastes alutus</i>)	214
106	Shortraker rockfish (<i>Sebastes borealis</i>)	229
107	Complex: Rougheye/Blackspotted rockfish (<i>Sebastes aleutianus/Sebastes melanostictus</i>).....	240
108	Stock Complex: Other Rockfishes.....	251
109	Dusky rockfish (<i>Sebastes variabilis</i>)	254
110	Harlequin rockfish (<i>Sebastes variegatus</i>)	265
111	Shortspine thornyhead (<i>Sebastolobus alascanus</i>).....	272
112	Skates - Stock Complex	283
113	Alaska skate (<i>Bathyraja parmifera</i>).....	287
114	Aleutian skate (<i>Bathyraja aleutica</i>)	298
115	Mud skate (<i>Bathyraja taranetzi</i>).....	309
116	Whiteblotched skate (<i>Bathyraja maculata</i>)	320
117	Invertebrates.....	331
118	Golden king crab (<i>Lithodes aequispinus</i>)	331
119	Red king crab (<i>Paralithodes camtschaticus</i>)	338
120	Octopus (<i>Enteroctopus dofleini</i>)	345
121	Future Recommendations	352
122	PRIORITIZE AND IMPROVE EFH FOR SELECT SPECIES	352
123	Leverage existing species distribution data	353
124	Leverage environmental data	356
125	Leverage life history information and process studies.....	357
126	Combine disparate datasets.....	359
127	Consider diverse constituent models.....	360
128	INCREASE SCOPE AND APPLICABILITY OF EFH RESEARCH	360
129	Describe prey species habitat.....	361
130	Expand to EFH Levels 3 and 4 where appropriate	362
131	Continue to advance and apply dynamic SDM methods	362

132	IMPROVE PROCESS AND COMMUNICATION	367
133	Communicate confidence in EFH designations	368
134	Develop thresholds for EFH mapping and test them	368
135	Add more opportunities for communication.....	369
136	Streamline workflows and reproducibility.....	369
137	CONCLUSIONS	370
138	ACKNOWLEDGEMENTS	372
139	REFERENCES	373

INTRODUCTION

140

141 The purpose of this project is to advance levels of essential fish habitat (EFH) information for federally
142 managed groundfish and crab species in the Aleutian Islands (AI) using species distribution models
143 (SDMs). We are guided by the Alaska EFH Research Plan (Sigler et al. 2017) Research Priority #1 near
144 term objectives and by the Magnuson-Stevens Act (MSA) EFH requirements.

145 Alaska EFH Research Plan, Research Priority #1 – Characterize habitat utilization and productivity by
146 using the best available science to accomplish –

147 Objective #1 – Develop EFH Level 1 information (distribution) for life stages and areas where
148 missing, and

149 Objective #2 – Raise EFH level from 1 or 2 (habitat-related densities or abundance) to Level 3
150 (habitat-related growth, reproduction, or survival rates).

151 The Final Environmental Impact Statement for EFH Identification and Conservation in Alaska¹ defines
152 EFH as the area inhabited by 95% of a species' population (NMFS 2005). Our habitat-based modeling
153 approach characterizes EFH for life stages of species within North Pacific Fishery Management Council
154 (NPFMC) Fishery Management Plans (FMPs) as the area circumscribing the top 95% of the SDM-
155 predicted abundance. To meet the research priority and objectives described above, we applied SDMs to
156 predict the distribution and abundance of species' life stages by incorporating new and updated data
157 sources to develop SDM EFH Level 1 and 2 maps, and we used habitat-related vital rates to map EFH
158 Level 3 information as an adjunct to the SDM EFH Level 1 and 2 maps.

159 The MSA defines EFH as those waters and substrate necessary to fish for spawning, breeding,
160 feeding, or growth to maturity ([50 CFR 600.10](#)). EFH regulations require that the National Marine
161 Fisheries Service (NMFS) and Fishery Management Councils (Councils) describe and identify EFH for

¹ <https://repository.library.noaa.gov/view/noaa/17391>

162 managed species and minimize to the extent practicable the adverse effects of anthropogenic activities
163 (e.g., fishing, mineral and oil extraction, coastal development). As part of this requirement, EFH text
164 descriptions and maps (EFH component 1, descriptions and identification) are necessary for each life
165 stage of species in an FMP ([50 CFR 600.815\(a\)\(1\)](#)) with an overarching consideration that the science
166 related to this effort meets the standards of best available science (NMFS National Standard 2 – Scientific
167 Information [50 CFR 600.315](#)). There are two separate and complementary FMPs for managing
168 groundfishes² and crabs³ in the Bering Sea and Aleutian Islands (BSAI) management area.

169 Councils and NMFS must also periodically review the EFH components of FMPs and revise or
170 amend these components with new information at least every 5 years ([50 CFR 600.815\(a\)\(10\)](#)). In the
171 2017 EFH 5-year Review, habitat-based SDMs incorporating Level 1 and 2 EFH information were
172 developed for many FMP species and their life stages in the AI (Turner et al. 2017). That project, along
173 with related projects in the Bering Sea (Laman et al. 2017, 2018) and Gulf of Alaska
174 (Rooney et al. 2018), replaced qualitative EFH Level 1 maps that were based on adult distributions
175 (Fisheries Leadership and Sustainability Forum 2016; Simpson et al. 2017) with SDM-based estimates for
176 individual life stages, substantially refining Alaska groundfish and crab EFH designation and, in many
177 cases, producing EFH Level 2 information for the first time. The EFH descriptions and maps produced for
178 the 2017 EFH 5-year Review were approved by the US Secretary of Commerce as part of the EFH
179 Omnibus Amendment package ([83 FR 31340](#), July 5, 2018) to revise the FMPs⁴.

180 In this EFH 5-year Review, we assessed the forecasting accuracy of the 2017 SDM approach for
181 describing EFH⁵ (e.g., Laman et al. 2017, 2018), refined our modeling approach, and updated our data
182 sources. EFH in this present work is now represented as life stage-specific and spatially-explicit
183 population percentiles predicted from an ensemble of best-performing constituent SDMs for 25 species

² <http://www.fisheries.noaa.gov/alaska/sustainable-fisheries/alaska-groundfish-fisheries-management>

³ <http://www.fisheries.noaa.gov/alaska/sustainable-fisheries/bering-sea-and-aleutian-islands-bsai-crab-fisheries>

⁴ <https://alaskafisheries.noaa.gov/portal/apps/webappviewer>

⁵ Pirtle et al. 2020 and our June 2020 SSC presentation links available at <https://www.npfmc.org/efh-distribution/>

184 across up to three life stages per species of Aleutian Islands (AI) groundfishes, two crabs, and one
185 octopus species. To achieve this, we expanded the SDM approach from the 2017 5-year EFH Review to
186 include up to five constituent models (three SDMs were assessed in 2017) in an ensemble and refined our
187 methodology by using the lowest cross-validated root mean square error (RMSE) to identify the best
188 fitting models. We enhanced existing data sets with recent survey results (von Szalay and Raring 2020 -
189 summer bottom trawl surveys 1991–2019), updated independent predictor variables (e.g., survey-
190 dependent bottom temperature observations), and added new covariates for bathymetric position index
191 (BPI) and rockiness. We separately modeled settled early juvenile life stages to extend consideration of
192 EFH to critical ontogenetic habitat transitions and revised SDMs for species where maturity schedules or
193 life stage definitions were recently updated (e.g., yellowfin sole and flathead sole; Tenbrink and
194 Wilderbuer 2015).

195 **MATERIALS AND METHODS**

196 **Study Area**

197 The Aleutian Islands are a chain of volcanic islands stretching from southwest Alaska across the North
198 Pacific, separating the western Gulf of Alaska (GOA) from the Bering Sea (Figure 1). The continental
199 shelf and upper continental slope represent a diverse mosaic of benthic habitats from Unimak Pass
200 (165°W) in the eastern Aleutian Islands to Stalemate Bank in the western Aleutians (170.5°E). The
201 Alaska Coastal Stream flows westward on the Pacific side of the Aleutians, while on the Bering Sea side,
202 the Aleutian North Slope Current flows eastward (Stabeno et al. 1999, Stabeno et al. 2002,
203 Ladd et al. 2005). There is extensive transport to the north through passes in the island chain from the
204 Pacific side to the Bering Sea. In the Aleutians, there is a very narrow continental shelf that ranges in
205 width from 20 km to greater than 200 km. The continental slope is steep and features multiple passes
206 incising the continental shelf. The seafloor of the Aleutian Islands is diverse, with extensive rocky
207 substrate resulting from volcanic activity dominating the continental shelf (Zimmermann et al. 2013).

Dependent Variables: Fish and Invertebrate Data

Large-mesh Bottom-trawl Survey

Alaska Fisheries Science Center (AFSC) Resource Assessment and Conservation Engineering-Groundfish Assessment Program (RACE-GAP) summer bottom trawl surveys document the distribution and abundance of federally managed fish and invertebrate species (Table 1) in the Aleutian Islands (AI) archipelago from Unimak Pass to Stalemate Bank (Figure 1). For these EFH analyses, our data set combined the AI and the Gulf of Alaska (GOA) surveys west of the faunal barrier represented by Unimak Pass (Stabeno et al. 2002). The two surveys have been conducted at regular intervals since 1991 and are collectively referred to in this document as the AI survey. Triennial surveys were conducted between 1991 and 2000 in the AI and biennial surveys were conducted from 2002 to 2018 (von Szalay and Raring 2020). The western portion of the GOA survey characterizes the eastern portion of the Aleutian chain south of the archipelago and was conducted triennially from 1993 to 1999 and then biennially from 2001 to 2019 (von Szalay and Raring 2018). Both of these fishery-independent AFSC RACE-GAP surveys used a stratified random sampling design. For our analysis data set, trawlable AI survey stations located on a contiguous survey grid between Unimak Pass and Samalga Pass north of the archipelago and from Samalga Pass to Stalemate Bank north and south of the archipelago were included. Strata in the AI were based on four depth intervals (10–100 m, 101–200 m, 201–300 m, and 301–500 m) and established survey districts. The AI survey area is contained within the North Pacific Fishery Management Council’s (NPFMC) Bering Sea-Aleutian Islands (BSAI) management zone. For the western portion of the GOA survey appended to the AI survey area for these analyses (Unimak to Samalga Pass south of the archipelago), the survey randomly trawled stations from a continuous survey grid constrained in some years by the 700 m isobath (2011, 2013, 2017, 2019) and in other years by the 1,000 m isobath (1993, 1996, 1999, 2001, 2003, 2005, 2007, 2009, 2015). Strata in the GOA were based on up to six depth intervals (10–100 m, 101–200 m, 201–300 m, 301–500 m, 501–700 m, and 701–1,000 m) and established survey districts. Assignment of sampling effort within strata for both surveys was determined using a

233 Neyman optimum allocation sampling strategy (Cochran 1977) which considers relative abundance and
234 variance of commercially important groundfish species from previous surveys of the area as well as the
235 previous year's ex-vessel price for select species. During the time period of these data collections,
236 changes in taxonomic classifications have resulted in different effective time series for different species
237 and these are reflected in the analyses presented here (see Table 1). For example, dusky and dark
238 rockfishes were considered a single species prior to the 1996 survey so that only data since that survey
239 were used to separately model these two species. All fishes and invertebrates captured by the trawl net
240 were either identified to species or into higher level taxonomic groups and weighed. Non-colonial taxa
241 were also counted or estimates of total count were made. For species where length-based definitions of
242 life stages were available, length ranges for settled early juveniles, subadults, and adults were used to
243 partition the catch based on proportionality estimated from the random length subsample taken from each
244 catch. These length-based definitions of ontogenetic life stages came from the extant scientific literature,
245 web resources (e.g., the Ichthyoplankton Information System, AFSC RACE:
246 <https://access.afsc.noaa.gov/ichthyo/speciesdict.php>), or length data collected in beach seines, purse
247 seines, and small-mesh bottom-trawls and recorded in the updated Nearshore Fish Atlas (as described in
248 Grüss et al. 2021a).

249 The fishing gear used on the RACE-GAP AI and GOA bottom trawl surveys consists of a Poly
250 Nor'Eastern high-opening bottom trawl with a 27.2 m headrope, a 36.3 m footrope, and 24.2 m roller gear
251 constructed with 36 cm rubber bobbins separated by 10 cm rubber disks (Stauffer 2004). Under fishing
252 conditions, the average net width is 16.0 m and average height is 6.7 m based on acoustic net mensuration
253 equipment mounted on the wing-tips and headrope of the trawl. Each trawl was certified as conforming to
254 measurements and dimension standards prior to its use in the survey as stipulated in the National
255 Trawling Standards (Stauffer 2004).

256
257
258
259
260
261
262
263
264
265
266
267
268
269
270
271
272
273
274
275
276
277

Independent Covariates: Habitat Data

The independent covariates used to parameterize SDMs (Table 2) were chosen on the basis of their potential to influence the distribution and abundance of North Pacific groundfish and crab life stages in the regions where we sample. Some of these independent covariates (or predictor variables) were dynamic or static habitat attributes typically collected on the bottom trawl survey (Figure 2). Others were derived and modeled variables describing the marine environment in the study area (e.g., NEP5 ROMS; Danielson et al. 2011). They were combined into a suite of independent covariates used to parameterize the SDMs. We used variance inflation factors (VIF; Table 3) calculated using the methods in Zuur et al. (2009) to eliminate strongly collinear terms ($VIF \geq 5.0$; Sigler et al. 2015). Independent habitat covariates from the time series (1991–2018) were interpolated on regular spatial grids ranging from 0.1–1 km² using natural neighbor interpolation (Sibson 1981), inverse distance weighting (Watson and Philip 1985), ordinary kriging (Venables and Ripley 2002) with an exponential semi-variogram, or empirical Bayesian kriging with a semi-variogram estimated using restricted maximum likelihood (REML; Diggle and Ribeiro 2002). Interpolation by inverse distance weighting and ordinary kriging were calculated on the R computing platform⁶ (R Core Development Team 2020) and Bayesian kriging was generated in ESRI ArcGIS mapping software⁷. Rasters for our analyses in the AI were gridded at a resolution of 1 km². All rasters were projected in the Alaska Albers Equal Area Conic (EAC) projection (standard parallels = 55° and 65°N and center longitude = 154°W). To represent local conditions in the SDMs and to incorporate inter-annual variability in our EFH maps and descriptions, we used a mixture of observed and derived predictors extracted from these rasters at the bottom trawl stations by averaging the raster values along the towpath of each haul. These variables were used to train and identify the best-fitting SDMs. Rasterized multi-year averages of habitat covariates in each raster cell were used to

⁶ R version 3.6.3 “Holding the Windsock”

⁷ ESRI 2018, version 10.7

278 represent average conditions in the study area over time and were input into the best-fitting SDMs when
279 predicting species distributions and abundances.

280 To represent local conditions in the SDMs and to incorporate inter-annual variability in our EFH
281 maps and descriptions, we utilized a mixture of observed, modeled, and derived predictors. For the
282 RACE-GAP survey data, covariate raster values were extracted as averaged values along the towpaths at
283 the bottom trawl stations. For species data sources supporting the settled early juvenile stage models only,
284 covariate raster values were extracted at point locations representing the geographic location of each
285 sampling site. In both cases, these extracted predictors were used to train and identify the best fitting
286 SDMs. When predicting species distribution and abundance, the complete raster of each retained
287 covariate was used as input into the final models for a species and life stage. In the case of observed,
288 dynamic predictor variables such as bottom temperature from the RACE-GAP survey, the observed
289 values were kriged and rasterized over the study duration (1991–2019) to represent average conditions in
290 the study area over time.

291 **Bottom Depth and Temperature**

292 Bottom depth and temperature were routinely collected during each trawl haul, but different
293 instruments were used to measure these values over the survey years (Buckley et al. 2009). From 1982 to
294 1992, depth and temperature were recorded using expendable bathythermographs (XBTs). In 1993, the
295 XBTs were replaced by the Brancker XL200 digital bathythermographic data logger (Richard Brancker
296 Research, Ltd., Kanata, Ontario, Canada) mounted on the headrope of the trawl net. With the advent of
297 continuous recording devices, the survey began reporting on-bottom depth and temperature averaged over
298 the tow duration. Starting in 2004, the Brancker data logger was replaced by the SeaBird SBE-39
299 microbathythermograph (Sea-Bird Electronics, Inc., Bellevue, WA). In 1993–1995, mean gear depth
300 measured at the headrope was equated with bottom depth. Since 1996, mean gear depth has been added to
301 mean net height measured during the on-bottom period of the trawl to estimate mean bottom depth.

302 We used two kinds of bathymetry data when formulating the SDMs used to model groundfish and
303 crab distributions and abundances in the AI. When identifying the best fitting constituent SDMs for the
304 subadult and adult life stages, the bottom depth measured at each trawl station was used as a covariate
305 predictor variable to train and test those SDMs. When predicting groundfish distribution and abundance
306 for all life stages modeled, we used a bathymetry raster built from two sources that included data from the
307 Aleutian Islands and the western GOA (Zimmermann et al. 2013, 2019). The primary sources for the
308 bathymetry raster were depth soundings from digitized NOAA National Ocean Service (NOS) smooth
309 sheets from early hydrographic (Hawley 1931) and other surveys (hydrographic and non-hydrographic)
310 that used manual soundings (e.g., lead lines), single-beam, or multi-beam acoustic echosounders. Details
311 on the preparation and processing of the bathymetry datasets were documented in Zimmermann and
312 Benson (2013). Point data from these compiled bathymetry datasets were gridded to the recommended
313 resolution of 100 m², and also to create a raster surface using natural neighbor interpolation (Sibson 1981)
314 in ArcMap. To achieve the 1 km² resolution used in our analyses, we averaged the 100 m² point data over
315 1 km² grid cells.

316 Similar to how we used depth data, we used temperatures measured at each trawl station in the AI
317 (1991–2018) to train and identify the best-fitting SDMs and used a raster surface of those temperatures to
318 predict groundfish and crab distributions and abundances from the for the subadult and adult life
319 stagesbest-fitting models. The bottom temperature raster was created by interpolating the observed
320 temperatures at each trawl station over the study area and time series using empirical Bayesian kriging in
321 ArcGIS (Diggle and Ribeiro 2002) with a semi-variogram estimated using restricted maximum likelihood
322 (REML). The raster was interpolated over a 1 km² grid of the AI study area.

323 **Water Movement**

324 Three attributes of water movement were used as habitat covariates in modeling and prediction:
325 maximum tidal speed, bottom current speed and direction, and variability in bottom current. We estimated

326 maximum tidal speed at each survey station over a lunar year (369 consecutive days between January 1,
327 2009 and January 4, 2010) using a tidal inversion program parameterized for the AI on a 1 km² grid
328 (Egbert and Erofeeva 2002). This tidal prediction model was used to produce a series of tidal currents for
329 spring and neap cycles at every bottom trawl survey station. The maximum of the lunar annual series of
330 predicted tidal current was then extracted at each bottom trawl survey haul location. A 1 km² raster
331 surface of maximum tidal current speed was kriged over the AI using an exponential semi-variogram and
332 values were extracted and averaged along individual trawl haul towpaths to use as input to the best fitting
333 SDMs when predicting distribution and abundance.

334 The second water movement variable was the predicted bottom water layer current speed and
335 direction from NEP5 ROMS model runs from 1969 to 2005 (Danielson et al. 2011). These long-term
336 current projections are available as points on a 10 km² grid. The ROMS model was based on a three-
337 dimensional grid with 60 depth tiers for each grid cell. For example, a point at 60 m water depth would
338 have 60 depth bins at 1 m intervals, while a point at 120 m depth would have 60 depth bins at 2 m depth
339 intervals, etc.). The bottom current speed and direction for the deepest depth bin at each point (closest to
340 the seafloor) was used in our analyses. These regularly spaced projections were interpolated to a 100 m²
341 raster grid covering the AI using inverse distance weighting and then averaged over a 1 km² and across
342 survey years (1991–2018) for our analyses. To characterize current at each bottom trawl station, ROMS
343 current velocity components were extracted along each trawl towpath and the mean northing and easting
344 values were computed for each trawl haul. The interpolated bottom current raster served as covariate
345 input to the best fitting SDMs when making spatial predictions.

346 Bottom current variability across summer months (May to September) was included as a third
347 bottom current-related predictor in the SDMs. It was computed separately as the pooled standard
348 deviation (*Pooled SD_i*) of the northing and easting components of bottom current at each NEP5 ROMS
349 prediction locus through time such that:

350

$$Pooled\ SD_j = \sqrt{\frac{\sum_{i=1}^k [(n_i - 1) * s_{ij}^2]}{\sum_{i=1}^k [n_i - 1]}}$$

351 where j is the location of a prediction on the ROMS grid, n_i is the number of months in year i , s_{ij}^2 is the
352 variance at location j in year i , and k is the total number of survey years (12 in the AI). Bottom current
353 variability can be considered a proxy for current stability near the bottom.

354 **Geographic Position**

355 Spatial modeling, such as the SDMs presented here, often include a location variable to represent
356 geographic position and account for spatial autocorrelation (Ciannelli et al. 2008, Politou et al. 2008,
357 Boldt et al. 2012). To reduce the effects of spatial autocorrelation on the results, we chose to combine
358 latitude and longitude into a smoothed bivariate geographic position term included as an independent
359 predictor in SDM formulations. Rooper et al. (2020) demonstrated that this approach can reduce spatial
360 autocorrelation in the modeled results. Geographic position was collected during each haul using a variety
361 of positioning systems through time (e.g., manual charting, long range navigation (LORAN-C), digital
362 global positioning system [dGPS]). Since 2006, start and end positions for the vessel during the on-
363 bottom portion of the trawl haul were collected from a dGPS receiver mounted on the vessel. We
364 corrected vessel position to represent the position of the bottom trawl by triangulating how far the trawl
365 net was behind the vessel (based on the seafloor depth and the length of wire out) and subtracting this
366 distance from the vessel position. We assumed that the bottom trawl was directly behind the vessel during
367 the tow and that all bottom trawl hauls were conducted in a straight line from the beginning to the end
368 point. The mid-point of the net's trawl path between the start and end positions was used as the location
369 variable in the SDMs. The EAC projected longitude and latitude data for each haul (and all other
370 geographical data for this study) were transformed into eastings and northings for modeling.

371 **Seafloor Terrain**

372 Several seafloor terrain metrics were derived from the bathymetry surface and describe attributes
373 of seafloor morphology. The attributes included in the present study were slope, aspect, curvature, and
374 bathymetric position index (BPI). Seafloor terrain metrics were derived at the original scale of the
375 compiled bathymetry surface (100 m²) using neighborhood-based analytical methods in ArcGIS 10.7
376 (ESRI) with the Benthic Terrain Modeler (Wright et al. 2012, Walbridge et al. 2018). All seafloor terrain
377 metrics were derived using a 3 x 3 neighborhood of grid cells, with the exception of BPI. Computation
378 algorithms are provided by Walbridge et al. (2018).

379 Seafloor slope is the rate of change in bathymetry over a defined area. Slope is the first derivative
380 of the bathymetry surface and was reported in degrees of incline (Horn 1981, Dolan and Lucieer 2014).
381 Terrain slope may be a determinant of colonization since flatter areas support different substrata and
382 communities than those found on steeper slopes (Pirtle et al. 2019).

383 Aspect measures the direction of the maximum gradient of slope and was expressed as angular
384 compass direction, which is a circular variable (Horn 1981). Aspect was decomposed into sine (west-east
385 or “eastness”) and cosine (south-north or “northness”) components to be used in the SDMs as continuous
386 surfaces ranging from -1.0 to 1.0, where negative values indicate westness or southness and positive
387 values indicate eastness or northness (e.g., Walbridge et al. 2018). Aspect eastness and northness were
388 derived from the aspect surface. Terrain aspect is considered an indirect indicator of current velocity over
389 and around seafloor terrain features (Mienis et al. 2007, Dolan et al. 2008).

390 Terrain curvature is the second derivative of the bathymetry surface and the first derivative of the
391 slope (Zevenbergen and Thorne 1987, Schmidt et al. 2003). Curvature defines convex, concave, and
392 linear slopes and can be used to identify seafloor features such as mounds and depressions that may be
393 ecologically meaningful (Wilson et al. 2007). Curvature is also an indicator of how currents interact with
394 the seafloor, either accelerating or decelerating parallel to the direction of slope and converging or

395 diverging perpendicular to the direction of slope. We derived standard curvature as a single terrain
396 surface, incorporating curvature in directions parallel and perpendicular to the slope (Zevenbergen and
397 Thorne 1987, Schmidt et al. 2003). With this surface, positive values are convex slopes where currents
398 may decelerate or diverge, negative values are concave slopes where currents may accelerate or converge,
399 and values near zero are linear slopes where the rate and direction of flow is not expected to change.

400 Bathymetric position index (BPI) describes the elevation of one location relative to the mean of
401 neighboring locations in an annulus-shaped neighborhood around a central cell or cells
402 (Guisan et al. 1999, Weiss 2001). BPI emphasizes features shallower or deeper than the surrounding
403 landscape area, such as ridges and valleys and places with abrupt changes in slope such as the continental
404 shelf break and the base of the continental slope. Broad-scale measures of BPI (> 1 km) have been useful
405 in distinguishing between areas of trawlable and untrawlable seafloor encountered by the RACE-GAP
406 bottom-trawl survey (Pirtle et al. 2015). BPI has been used as an SDM covariate describing groundfish
407 habitat in the GOA (Pirtle et al. 2019) and in other habitat analyses (Wilson et al. 2007,
408 Howell et al. 2011). We derived BPI from AI bathymetry using a 65-cell radius neighborhood with an
409 inner radius of 3-cells. This is equivalent to a horizontal scale of 6.5 km, representing relatively broad-
410 scale terrain features in our study area. In the resulting surface, positive values are shallower than the
411 surrounding area (e.g., ridges and crests) and negative values are deeper (e.g., channels and valleys). In
412 the visualization of this covariate, we artificially stretched the scale to highlight the heterogeneity that
413 exists in the study area.

414 **Seafloor Rockiness**

415 A seafloor rockiness surface was developed for the AI based on a compilation of rock features
416 and sediment attributes to represent a continuous gradient from areas with high occurrence of rocky
417 substrate to areas with low occurrence of rocky substrate, using methods similar to Pirtle et al. (2019).
418 The following datasets were included for the AI region: 1) sediment and substrate features from digitized

419 smooth sheets (Zimmermann et al. 2013); 2) EBSSSED-2 regional selection of samples collected from
420 grabs and cores (Richwine et al. 2018); 3) modeled untrawable and trawable seafloor based on a
421 generalized linear model of multibeam acoustic backscatter and terrain available as a 6 m² raster dataset
422 (Pirtle et al. 2015) that was regridded to 1 km² and exported as point locations, where model predictions
423 of untrawable and trawable locations are proxies for high and low occurrence of rocky substrate; and 4)
424 RACE GAP bottom-trawl survey historic haul locations, including hauls that incurred gear damage from
425 seafloor contact to represent locations where untrawable rocky features were likely encountered and
426 hauls with good performance to represent locations where untrawable rocky seafloor was likely not
427 encountered, using the corrected start positions of the on-bottom portion of tows. Compiled point location
428 data from the four datasets was gridded using natural neighbor interpolation to produce a raster surface of
429 1 km² resolution (ArcGIS 10.7, ESRI).

430 For all of these seafloor terrain and substrate variables, values were extracted from their raster
431 surfaces along the towpath at each trawl station and were used when training the models and identifying
432 the best-fit SDM. The complete terrain raster was used to predict species distributions and abundances
433 when a terrain covariate was retained in the best-fitting model.

434 **Biogenic Structure**

435 Previous studies have indicated that structure forming invertebrates (SFI) such as sponges, corals,
436 and Pennatulaceans (sea pens and sea whips) can form important structural habitat for temperate marine
437 fishes (Heifetz et al. 2005, Malecha et al. 2005, Marliave and Challenger 2009, Rooper et al. 2010,
438 Stone et al. 2011, Laman et al. 2015). The occurrence of SFIs can also be indicative of substratum type
439 (Du Preez and Tunnicliffe 2011) because these sponges and corals attach to rocks and hard substrata,
440 whereas sea pens and sea whips anchor into soft substrata. Therefore, we included the presence and
441 absence of SFIs as binomial factors in the suite of habitat covariates. Rasters of these SFIs were used to

442 predict distributions and abundances from best-fit SDMs (Rooper et al. 2014, 2016, 2017a;
443 Sigler et al. 2015).

444 **Statistical Modeling**

445 Our modeling strategy for this 5-year EFH Review has been to fit multiple environmental- and
446 habitat-based SDMs to fish and crab abundances, skill test among SDMs using the root-mean-square-
447 error to indicate model performance (RMSE; Hastie et al. 2009), and incorporate the best performing
448 models into an ensemble in R (R Core Team 2020). Ensemble models essentially average predictions
449 across constituent models, making them more robust to overfitting and less sensitive to differences in
450 predictive performance among constituents. Rooper et al. (2017b) found that ensembles performed better
451 than the generalized linear or generalized additive models alone when predicting distributions of
452 structure-forming invertebrates. Overall, the ensemble modeling approach provides a universal SDM
453 application across multiple FMPs and can be easily expanded to consider additional constituent models in
454 the future.

455 Previous EFH descriptions in Alaska (e.g., Turner et al. 2017), were based on habitat-related
456 SDMs modeling species abundances from 4th-root transformed catch-per-unit-effort (CPUE; kg·ha⁻¹)
457 using the area swept method (Wakabayashi et al. 1985) and assuming a Gaussian distribution. Modeling
458 4th-root transformed CPUE has several shortcomings with respect to our study objectives, including: (1)
459 residuals were not informative due to the zero-inflation and overdispersion that cannot be properly
460 addressed by a Gaussian distribution; (2) the *a priori* and *ad hoc* nature of deciding to use a 4th-root
461 transformation relative to other equally defensible transformations; (3) the inability to interpret the scale
462 of the output, which is in units of 4th-root CPUE and hence must be back-transformed to calculate a total
463 predicted CPUE in any subarea; and (4) the scale-dependence of results, where the 4th-root transformation
464 implies that density would change if the area swept in the survey changed (i.e., if sampling had occurred
465 at a different scale). To improve on the challenges associated with using the 4th-root transformed CPUE,

466 we directly modeled numerical abundance with an area-swept offset to generate EFH descriptions that
467 were less derived than those using a transformed CPUE approach; this more precisely represents fishing
468 effort.

469 For this cycle, we modeled numerical abundance using five different SDMs (Table 4): a
470 maximum entropy model (MaxEnt), a presence-absence gam (paGAM), a hurdle GAM (hGAM), and two
471 forms of standard gam using the Poisson distribution (GAM_P) and the negative binomial distribution
472 (GAM_{nb}). The MaxEnt and paGAM use presence or presence-absence data to estimate probabilities of
473 occurrence (Phillips et al. 2006, Wood 2017). Using these models in conjunction with the complementary
474 log-log (cloglog) link function allowed us to approximate abundance from the estimated probabilities
475 (Scharf et al. 2019). Transforming these native model outputs (probability) into approximate numerical
476 abundance yields predictions in the same units as the response variables from the other 3 SDMs which
477 facilitated skill testing and model comparison while meeting the requirements to qualify predictions as
478 EFH Level 2, habitat-related density or abundance. Because some models, (notably MaxEnt) produce
479 results on different scales, a scaling factor was calculated for each model by dividing the mean of the
480 observed abundance by the mean of the model predictions. This ensured that predictions from all models
481 were directly comparable and could be used to construct a weighted ensemble (Figure 3).

482 **Maximum Entropy Models (MaxEnt)**

483 Maximum entropy modeling was developed to model probability of suitable habitat or species
484 occurrence with presence-only data (Phillips et al. 2006) in cases of rare species and when presence-only
485 or presence-absence data were available from multiple surveys with varied sampling designs
486 (Guisan et al. 2007, Elith et al. 2011). This newer version of the MaxEnt model, implemented with the
487 *maxnet* package in R (Phillips et al. 2017, R Core Team 2020), reformulates the model as an
488 inhomogeneous Poisson process (Fithian et al. 2015), which constructs the predicted probabilities as a
489 proportion of the product of underlying relative abundance and sampling probabilities. Because of this, it

490 was possible to estimate the species abundance by treating the cloglog link output of the MaxEnt model
491 as if it were the linear predictor in a Poisson model. The relative abundance estimate was then calculated
492 by adding an additional parameter, the entropy, to the cloglog linear predictor and exponentiating the
493 sum.

494 The MaxEnt model utilized the same suite of covariates as the GAMs, but omitted geographic
495 position (lat/lon) from the suite of predictor variables because MaxEnt does not separately distinguish
496 spatial variation in sampling probability from spatial variation in resource density (Elith et al. 2011). The
497 MaxEnt algorithm automatically constructed and selected terms based on several feature classes
498 determining relationships between the species response data and covariates. The default feature set was
499 used in this study, which includes linear, quadratic, and product interaction terms. By default, hinge
500 features were included in models with more than 80 presence records and threshold features were not
501 used. As part of the fitting process, a variety of these different features were tested in different
502 combinations. MaxEnt uses a regularization multiplier to determine the penalty applied to larger models
503 and to help regulate overall model complexity. Here, we evaluated regularization multiplier values
504 between 0.5 and 3.0 in intervals of 0.5 with the best value determined by the lowest RMSE after 10-fold
505 cross-validation as described below (see subsection *Cross-Validation and Skill Testing*).

506 **Generalized Additive Models (GAM)**

507 We used three classes of GAMs in this study: the paGAM (Wood 2017), the hGAM (Cragg 1971,
508 Barry and Welsh 2002, Potts and Elith 2006), and the standard GAM with a Poisson distribution (GAM_P;
509 Hastie and Tibshirani 1990); and a negative-binomial GAM (GAM_{nb}; Zuur et al. 2009). All GAMs were
510 fit using the *mgcv* package (Wood 2011) in R. The paGAM uses the binomial distribution and the cloglog
511 link function, which allowed numerical abundance to be approximated from model predicted encounter
512 probabilities (Fithian et al. 2015). The hGAM models presence-absence and abundance in two stages and
513 accounts for zero-inflation commonly seen in field collected data (McCullagh and Nelder 1989). In the
514 first stage of the hGAM, the probability of occurrence was predicted from presence-absence data using a

515 paGAM and binomial distribution. In the second stage of the hGAM, a standard GAM was constructed
516 for the positive catches using a “zero-adjusted” (Zuur et al. 2009) Poisson distribution. Finally, an
517 abundance estimate was obtained by multiplying the predicted probability of presence from step one with
518 the abundance estimate from step two (Barry and Welsh 2002). The GAM_P estimates abundance directly
519 using the Poisson distribution and a log link. The GAM_{nb} was structurally similar to the GAM_P but used a
520 negative binomial distribution with a log link, allowing the GAM_{nb} to account for overdispersion in the
521 data (McCullagh and Nelder 1989).

522 For all GAMs, we used iterative backward stepwise term elimination to remove covariate terms
523 based on minimizing the model-dependent generalized cross-validation (GCV) or unbiased risk estimator
524 (UBRE) scores thereby identifying the best fitting model formulations (Weinberg and Kotwicky 2008,
525 Zuur et al. 2009). Since the Poisson and negative-binomial GAMs were structurally very similar models,
526 we used RMSE-based skill testing to identify and keep the best performing model (lowest RMSE) of this
527 pair in the ensemble.

528 All GAMs in this study used a variety of two dimensional smoothing terms, one dimensional
529 smoothing terms, and categorical variables to fit the data. To avoid overfitting in the GAMs, the basis
530 degrees of freedom used in the smoothing function for each habitat covariate were constrained following
531 the methods of Weinberg and Kotwicky (2008). However, attempting to extrapolate model predictions
532 into areas with few data points requires additional consideration. In particular, the default smoother when
533 fitting GAMs, a “thin-plate spline,” sometimes produces exaggerated predictions in areas of sparse data
534 (Wood 2003). To counter this behavior in one dimensional smooth terms, we used a smoothing penalty
535 based on the first derivative (as opposed to the default second derivative), which tended to push the effect
536 curve towards zero where data were unavailable. For two dimensional smooth terms, the same method
537 was applied, but “Duchon” splines were used instead of thin-plate or cubic splines (Duchon 1977) which
538 did a better job of penalizing the smooth function in areas with sparse data. Finally, if a GAM based on
539 thin-plate splines failed, a second version using cubic splines in the one dimensional smooth terms was

540 attempted. If both versions failed to converge or produced unreasonable results, that particular GAM was
541 excluded from the final ensemble.

542 **Cross-Validation and Skill Testing**

543 Species distribution models were subjected to k -fold cross-validation to estimate RMSE and to
544 assess accuracy and uncertainty. We computed the error at each cross-validation fold (k) by fitting an
545 SDM to a randomly selected “in-bag” partition containing 90% of the observed abundance at trawl
546 stations (i), predicting abundance at the remaining “out-of-bag” partition containing the other 10% of
547 trawl stations, and comparing the predicted (y) and observed (x) values for the testing subset. The k -fold
548 cross-validation was repeated 10 times until every point in the data set had been tested and the RMSE
549 from the accumulated out-of-bag sample was calculated as:

$$550 \quad RMSE = \sqrt{\frac{\sum_{k=1}^{10} \sum_{i=1}^{n_k} (y_{ki} - x_{ki})^2}{\sum_{k=1}^{10} n_k}}$$

551 where y_{ki} is the predicted numerical abundance in cross-validation fold k , x_{ki} is the observed numerical
552 abundance at trawl station i in cross-validation fold k , and n_k is the number of stations sampled in the k th
553 fold. This process provides a test of prediction skill at unsampled locations within the cross-validation,
554 and provides a measure of performance that can be used to compare models. The RMSE provides a metric
555 of the ability of a model to accurately predict the abundance at a series of locations. The model with the
556 lowest RMSE value was considered the best performer (Hastie et al. 2009). The cross-validation also
557 allows for a consistent method of calculating the variance in model predictions by computing it at each
558 location across folds.

559 Skill testing was used to eliminate constituent SDMs from the ensemble by identifying and
560 dropping low-performing models with high RMSEs. Constituent SDMs retained in the ensemble were
561 weighted by the inverse squared RMSE following the formula,

562

$$w_i = \frac{RMSE_i^{-2}}{\sum_{i=1}^m RMSE_i^{-2}}$$

563
564

where w_i is the weight for model i , $RMSE_i$ is the cross-validated RMSE for model i , and m is the number of constituent models. The inclusion of poor performing models may degrade ensemble performance so if any constituent SDM received less than a 10% relative weight, it was eliminated from the ensemble and the weights of the remaining SDMs in the ensemble were recalculated.

567
568
569
570
571
572
573
574
575
576

The ensemble extrapolated abundance predictions into areas along the edges of the survey grid that were rarely sampled as well as across regions in the Bering Sea like the EBS Slope and NBS which have been sampled at much lower frequency than the EBS shelf. Under these conditions, SDMs that fit the majority of the data quite well can still produce unacceptable predictions around the edges and in these unfrequented regions. The unacceptable predictions usually take the form of unrealistically high abundance. To address this challenge, a criterion was implemented so that any SDM generating abundance predictions > 10 times the highest observed survey abundance was excluded from the ensemble. The resulting cumulative ensemble-predicted numerical abundance, based on the combined effects of all retained constituent SDMs, was translated into a map of the complete EFH area for each species.

577 **Ensemble Models and Uncertainty**

578
579
580
581
582
583
584

Ensemble modeling is a robust method to predict species distributions and abundances (Araujo and New 2007). Potential advantages include better estimates of uncertainty, reduced bias, and results that are less sensitive to minor changes in the underlying data (e.g., accumulating data through annual surveys; Stewart and Hicks 2018). In the present study, we combined the best-fit constituent SDMs into single species life stage-specific ensemble predictions of habitat-related abundance to inform descriptions of EFH. In practice, this means we first identified the best performing MaxEnt, paGAM, hGAM, and GAM SDMs. In the MaxEnt models, this entailed testing a range of regularization multipliers, while in the

585 GAMs this involved backwards stepwise term elimination. For the standard GAM, the Poisson and
 586 negative binomial error distributions were modeled separately and skill testing using the RMSE was
 587 employed to select the distribution that best characterized the data. The set of best SDMs from each
 588 category was then weighted by the inverse of its cross-validated RMSE and constituent SDM weights
 589 were normalized to sum to one. Predictions from the ensemble were made by multiplying each constituent
 590 prediction by its weight and summing the weighted predictions across SDMs. The result of this exercise
 591 was a final ensemble for each species' subadult and adult life stage that predicts habitat-related
 592 abundance.

593 The variance of the ensemble prediction can be obtained based on a weighted combination of the
 594 variance in the predictions of each constituent model. For each constituent, 10 abundance prediction
 595 rasters were made using the 10 models fit during cross-validation. The variance across these 10 folds at
 596 each location was then calculated to provide a variance estimate for that constituent model. After
 597 repeating this process for all constituent models in the ensemble, we adapted the following equation from
 598 Burnham and Anderson (2002), substituting our RMSE derived weights for their AIC weights:

$$599 \quad SD_j(ensemble) = \sum_{i=1}^m w_i \times \sqrt{var_{ij} + (y_j^* - y_{ij})^2}$$

600 where SD_j is the standard deviation of the ensemble at location j , w_i is the weight for model i , m is the
 601 number of constituent models, var_{ij} is the variance for model i at location j , y_j^* is the ensemble abundance
 602 prediction at location j , and y_{ij} is the abundance prediction for model i at location j . Then we computed the
 603 coefficient of variation (CV) from the $SD(ensemble)$ as:

$$604 \quad CV_j = \frac{SD_j}{y_j^* + c}$$

605 Where CV_j is the coefficient of variation at location j , SD_j is the ensemble standard deviation at location j ,
 606 and y_j^* is the ensemble prediction at location j . Because the term y_j^* in the denominator can sometimes be

607 zero, a small constant c , which was set at 1% of the max predicted abundance for that species and life
608 stage, must be added to all abundance estimates when calculating the CV.

609 **Species Distribution Model Performance Metrics**

610 In addition to the RMSE described above for skill testing among SDMs and constituent model
611 weighting in the ensemble, we computed three commonly used metrics of SDM performance for
612 constituent models and the ensembles. The three fit metrics we reported were the Spearman's rank
613 correlation coefficient (ρ), the area under the receiver-operator-characteristics curve (AUC; Hosmer and
614 Lemeshow 2005), and the deviance explained based on the Poisson distribution (PDE). Each fit metric
615 measures a different aspect of model performance, as well as having distinct strengths and weaknesses. A
616 model that scores poorly on one metric may still be useful once the others are considered, and all models
617 should be assessed with reference to the underlying biology of the species being studied.

618 The ρ score compares predicted densities with observations for each sample, computing their rank
619 correlation, and measuring how well a model accurately distinguished between high and low density areas
620 (Best and Roberts 1975, Zar 1984). We employ the ρ instead of the more familiar Pearson correlation
621 because the ρ is more appropriate to count data that do not follow a normal distribution (Legendre and
622 Legendre 2012). Additionally, the EFH maps produced in this project are based on ranked percentiles of
623 abundance, and ρ may provide some insight to the accuracy of the EFH maps. While there is no objective
624 standard for what constitutes a "good enough" correlation, for this project, we will adopt the framework
625 that less than 0.2 represents "poor" predictive performance, between 0.2 and 0.4 is "fair", between 0.4 and
626 0.6 is "good," and greater than 0.6 is "excellent." Our framework is based on our knowledge of the
627 ecology of the species being modeled and the available data. Because ρ is the rank correlation, a high
628 value is easiest to obtain when there is a large difference between the lowest and highest abundances,
629 such that small prediction errors do not affect the rankings. Conversely, a low value can result if the
630 observed densities occupy a narrow range and a small prediction error will change the rankings.

631 The AUC is a measure of the ability of a model to discriminate between binary outcomes, such as
632 presence and absence. The value of the curve at any point represents the ratio of true positives to false
633 positives at that point, and the total area under the curve is a representation of the overall performance
634 across the entire range of values. The AUC has a minimum value of 0.5 (i.e. random 50/50 chance) and a
635 maximum of 1, and values under 0.7 are generally considered poor, values between 0.7 and 0.9 are
636 average to good, and values greater than 0.9 suggest excellent discrimination ability (Hosmer and
637 Lemeshow 2005). The AUC provides a measure of discrimination ability that is standardized across the
638 range of probability predictions, which makes it useful as a summary of discrimination ability. In this
639 case, discriminating where the RACE-GAP bottom trawl survey catches individuals and where it does
640 not. However, it can sometimes be misleading in situations where an overwhelming majority of
641 observations are either present or absent and only a small portion of the probability space has been
642 adequately sampled.

643 The PDE provides a generalization of “variance explained” for the constituent SDMs as well as
644 the ensemble. We assume the Poisson distribution when computing the deviance explained for these
645 models because count data are not normally distributed and traditional estimates of the variance explained
646 tend to be misleading. Additionally, with the Poisson distribution, as other distributions the size of errors
647 is expected to change with the mean of the predictions. Therefore, it is common to compute the deviance
648 explained by a model. This value is a measure of the percent reduction in the residual deviance of a model
649 compared to a naïve null model, which contains only an intercept and no predictor terms (Pardoe 2012).
650 Because we employ a variety of models that utilize different distributions (binomial, Poisson, negative
651 binomial), and different underlying data types (presence-absence, count), we estimate the deviance
652 explained in comparison to a fixed null Poisson model. Therefore, the PDE represents the percent
653 deviance explained in relation to a null Poisson model, which allows for a fairer comparison of the
654 different models. In this case, we adopt a similar metric to the correlation, where less than 0.2 indicates
655 “poor” performance, between 0.2 and 0.4 “fair” performance, between 0.4 and 0.6 “good” performance,

656 and greater than 0.6 is “excellent” performance. A high PDE can result when model predictions are
657 accurate, or when the observed data are highly variable and the model represents a significant
658 improvement over a simple null model. Similarly, a low value can sometimes occur even when
659 predictions are accurate if there is no improvement over the null model, indicating that a simpler method
660 would probably be acceptable. Deviance is calculated as,

$$661 \quad D = 2 \sum_{i=1}^n \left[x_i \ln \left(\frac{x_i}{\exp(y_i)} \right) - (x_i - \exp(y_i)) \right]$$

$$662 \quad D_0 = 2 \sum_{i=1}^n \left[x_i \ln \left(\frac{x_i}{\exp(\bar{x})} \right) - (x_i - \exp(\bar{x})) \right]$$

$$663 \quad PDE = \frac{D}{D_0}$$

664 where D represents the deviance of a given model, D_0 is the deviance of the null model, x_i represents the
665 observed abundance for data point i , \bar{x} represents the mean of observed abundance, and y_i represents the
666 predicted abundance for data point i (Pardoe 2012).

667 **Essential Fish Habitat (EFH) Maps**

668 Maps⁸ of species’ habitat-related abundance predicted from the ensembles were used to describe
669 and map EFH for this EFH 5-year Review. These maps were produced as population percentiles based on
670 all areas where the given species and life stage was present, which was defined as having an encounter
671 probability greater than or equal to 5%. To calculate the probability of encounter, we began by assuming
672 that the ensemble predicted abundance approximately follows a Poisson distribution. Under this
673 assumption, the probability of encounter was equal to one minus the likelihood of zero abundance, given
674 the ensemble estimated abundance at that location. Locations with a probability of encounter below 0.05

⁸ Sean-Rohan-NOAA (2021) akghmaps [Source Code]. <https://github.com/sean-rohan-NOAA/akghmaps>

675 were eliminated, and the remaining locations were ordered by increasing abundance. Four percentiles
676 were identified from the percentiles computed above for each species' life stage and were then mapped to
677 the areas containing the upper 95%, 75%, 50%, and 25% of locations based on the predicted numerical
678 abundance. The 95% level corresponds to the definition of EFH area in Alaska⁹ (NMFS 2005,
679 Sigler et al. 2012). Each percentile describing subareas of the EFH area defines a more focused partition
680 of the total EFH area. The area containing the upper 75% of ensemble abundance predictions will be
681 referred to as the principal EFH area. For the fishing effects analysis in EFH Component 2 of the 2017
682 EFH 5-year Review (Simpson et al. 2017), the top 50% of SDM abundance predictions were termed the
683 “core EFH area” and we have applied this terminology to our results. We also produced a shape for the
684 top 25% of ensemble abundance predictions which we refer to as EFH hot spots. Mapping habitat
685 percentiles for EFH subareas like these helps demonstrate the heterogeneity of fish and crab distributions
686 over available habitat within the larger area identified as EFH and aligns our results with those of other
687 EFH-related projects.

688 **Species Complexes**

689 Some groundfishes in Alaska are managed as members of a stock complexes (e.g., the Other
690 Flatfish Stock Complex in the Bering Sea – Aleutian Islands). While EFH must be designated for each
691 managed species, EFH may be designated for assemblages of species with justification or scientific
692 rationale provided ([50 CFR 600.815\(a\)\(1\)\(iv\)\(E\)](#)). In the present study, and for the first time in an EFH
693 5-year Review, we presented EFH descriptions of multi-species stock complexes using aggregated single
694 species SDMs to produce descriptions of EFH which served as proxies for individual species in the stock
695 complex where an SDM EFH map was not possible due to data limitations (i.e., < less than 50 catches
696 over the study period). To achieve this, we first generated multi-species abundance maps by summing the
697 ensemble predicted abundances at each raster cell for each species in the complex that supported an

⁹ URL: <http://www.npfmc.org/habitat-protections/essential-fish-habitat-efh/> [accessed 15 November 2016]

698 ensemble. Then, using the same method described above for single species maps, we constructed an EFH
699 map for the stock complex. In complexes where there was a mixture of available life history information
700 (e.g., some species with known length-based life stage definitions and some without), life stages were
701 combined for the species mapped together from the complex. See the introductory section of each species
702 complex chapter (see section *Results*) for details about the species and life stages that were included.

703 **EFH Level 3 Habitat Related Vital Rates**

704 We advanced EFH information to Level 3 (habitat related vital rates) in the AI by integrating a
705 temperature-dependent growth rate developed from field and laboratory studies (Laurel et al. 2016,
706 Copeman et al. 2017) with habitat-linked SDM predictions of walleye pollock numerical abundance (EFH
707 Level 2) to achieve a key Alaska EFH Research Plan objective for this 5-year Review (Sigler et al. 2017).
708 Laurel et al. (2016) described the temperature-dependent growth rate of early juvenile walleye pollock as:

$$709 \quad GR = 0.2023 + 0.0092 * T + 0.0335 * T^2 - 0.0019 * T^3.$$

710 where *GR* is the growth rate expressed as the percent change in body weight per day (% body weight per
711 day) and *T* is temperature in degrees Celsius. Copeman et al (2017) describe the lipid accumulation rate
712 (*LAR*) for early juvenile walleye pollock as:

$$713 \quad LAR = 11.6 * \exp \left[-0.5 \left(\frac{T - 14.37}{6.39} \right)^2 \right]$$

714 where *LAR* is the lipid accumulation rate (% lipids per % body weight per day) and *T* is the temperature
715 (°C).

716 We constructed these surfaces by first mapping the spatially explicit vital rates across the survey
717 study area, using the bottom temperature covariate raster derived from the trawl-mounted temperature
718 measurements as the temperature value in the vital rate equations. Next, we computed the product of the
719 vital rate map and the SDM-predicted abundance map by multiplying the two rasters together. The

720 product map was then transformed onto a relative scale ranging from zero to one where zero indicates
721 areas of low abundance and low habitat-related temperature-dependent growth potential and one indicates
722 areas of high abundance and high habitat-related growth potential. This process was carried out twice,
723 producing separate EFH Level 3 maps for growth rate and lipid accumulation rate in early juvenile
724 walleye pollock.

725 Table 1. North Pacific groundfish and crab species from AFSC RACE-GAP summer bottom trawl surveys modeled to re-describe essential fish
 726 habitat in the Aleutian Islands: the years modeled were determined by taxonomic validity; life stage length ranges are fork lengths (F.L.) in mm
 727 with sources indicated (“--“ indicates no length known from literature); “All” years modeled = 1991-2019, “1996“-“ indicates 1996 to 2019.

Common Names	Years Modeled	Life Stage Length Ranges			Source
		early juvenile	subadult	adult	
<u>flatfishes</u>					
yellowfin sole	All	30–140	141–296	> 296	NFA ¹ , Doyle et al. 2019, Yeung and Cooper 2020, Tenbrink and Wilderbuer 2015
northern rock sole	1996-	20–140	141–309	> 309	NFA, Doyle et al. 2019, Yeung and Cooper 2020, Stark 2012a
arrowtooth flounder	1992-	35–160	161–480	> 480	NFA, Debenham et al. 2019, Doyle et al. 2018, 2019, Stark 2012b
Dover sole	All	30–140	141–439	> 439	Doyle et al. 2019, Abookire and Macewicz 2003
flathead sole	All	20–140	141–342	> 342	NFA, Doyle et al. 2019, Tenbrink and Wilderbuer 2015
Greenland turbot	All	--	49–580	> 580	IIS, Cooper et al. 2007, Helser et al. 2019 (NPRB #1605)
Kamchatka flounder	1992-	--	49–550	> 550	IIS, Stark 2012b
rex sole	All	70–140	141–352	> 352	Doyle et al. 2019, Abookire 2006
southern rock sole	1996-	--	17–347	> 347	Doyle et al. 2019, Stark 2012a
<u>roundfishes</u>					
walleye pollock	All	40–140	141–381	> 381	Doyle et al. 2019, Pirtle et al. 2019, Stahl and Kruse 2008
Pacific cod	All	40–150	151–580	> 580	Pirtle et al. 2019, Stark 2007
sablefish	All	150–399	400–585	> 585	Sasaki 1985, Hanselman pers. comm.
Atka mackerel	All	--	49–340	> 340	Cooper et al. 2010
<u>rockfishes</u>					
Pacific ocean perch	All	25–200	201–250	> 250	IIS, Moser 1996, Pirtle et al. 2019, Rooper 2008
northern rockfish	All	--	25–277	> 277	IIS, Moser 1996, Tenbrink and Spencer 2013
rougheye rockfish	2006-	--	25–450	> 450	IIS, Moser 1996, Conrath 2017

Common Names	Years Modeled		Life Stage Length Ranges		Source
blackspotted rockfish	2006-	--	25–453	> 453	IIS, Moser 1996, Conrath 2017
dusky rockfish	1996-	--	25-365	> 365	Chilton 2010
harlequin rockfish	All	--	25-188	> 188	Tenbrink and Helser 2021
shortraker rockfish	All	--	25–499	> 499	IIS, Moser 1996, Conrath 2017
shortspine thornyhead	All	--	20–215	> 215	IIS, Rooper 2008
<u>sharks and skates</u>					
Alaska skate	1999-	--	<= 930	> 930	Matta and Gunderson 2007
Aleutian skate	1999-	--	<= 1320	> 1320	Ebert et al. 2007
mud skate	1999-	--	<= 595	> 595	Ebert 2005
whiteblotched skate	1999-	--	<=964	>964	Ebert 2005
<u>invertebrates</u>					
golden king crab	All	--	--	--	
red king crab	All	--	--	--	
giant octopus	All	--	--	--	

728

729 ¹NFA = Updated Nearshore Fish Atlas, NMFS Auke Bay Laboratories, Juneau, AK (as described in Grüss et al. 2021a)

730 ²IIS = Ichthyoplankton Information System, Alaska Fisheries Science Center, Resource Assessment and Conservation Engineering:

731 <https://access.afsc.noaa.gov/ichthyo/speciesdict.php>

732 Table 2. Covariates used in habitat-based species distribution models (SDM) to fit (identify best-fitting formulation) and then predict distributions
 733 and abundances from the of the best -fitting models of North Pacific groundfish and crab species in Alaska and describe essential fish habitat
 734 (EFH).

Variable	Unit	Description of Prediction Raster	Interpolation method	Data Source and Usage
Bottom temperature	°C	Mean bottom temperatures measured on bottom trawls during AFSC RACE-GAP summer trawl surveys (1982–2019)	Empirical Bayesian kriging	Temperature data collected at bottom trawl hauls
Bottom current Northing and Easting	m·sec ⁻¹	Seafloor ocean current components predicted from the NEP5 ROMS (Danielson et al. 2011) averaged for the bottom layer across summer years (1991–2018)	Inverse distance weighting	Training: mean towpath value Prediction: raster of bottom current
Bottom current Northing and Easting variability	m·sec ⁻¹	Pooled standard deviation of seafloor ocean current components predicted from the NEP5 ROMS (Danielson et al. 2011) averaged for the bottom layer across summer years (1991–2018)	Inverse distance weighting	Training: mean towpath value Prediction: raster of bottom current pooled standard deviation
Maximum tidal current	cm·sec ⁻¹	Predicted tidal current maximum at each bottom trawl location over a lunar year cycle (Egbert and Erofeeva 2002)	Ordinary kriging	Training: mean towpath value Prediction: kriged surface of tidal maxima
Position	Latitude, Longitude	Midpoint of bottom trawl hauls corrected for position of the trawl net relative to the vessel in Alaska Albers Equal Area conic projection	--	Training: position collected during bottom trawl hauls. Prediction: raster of positions
Bottom Depth	meters (m)	Bathymetry of the seafloor based on acoustic seafloor mapping data and digitized, position corrected NOS charts	Natural neighbor	Training: mean bottom depth of trawl Prediction: raster of bathymetry soundings data ^a
Slope	degrees	Maximum gradient in depth between adjacent cells, derived from bathymetry	--	Training: mean towpath value Prediction: raster of slopes derived from bathymetry

Variable	Unit	Description of Prediction Raster	Interpolation method	Data Source and Usage
		(Horn 1981) applied with Benthic Terrain Modeler in ArcGIS (Walbridge et al. 2018)		
Bathymetric Position Index	--	Relative difference of elevation between neighboring locations, illustrates bathymetric highs and lows across the landscape, derived from bathymetry (Guisan et al. 1999) applied in ArcGIS (Walbridge et al. 2018)	--	Training: mean towpath value Prediction: raster of bathymetric position index derived from bathymetry
Aspect Eastness and Northness	--	Describes concavity/convexity as well as sloping nature, derived from bathymetry (Horn 1981) applied in ArcGIS (Walbridge et al. 2018)	--	Training: mean towpath value Prediction: raster of aspect derived from bathymetry
Curvature	--	Combined plan and profile curvature to return “standard” curvature; derived from bathymetry (Schmidt et al. 2003) applied in ArcGIS (Walbridge et al. 2018)	--	Training: mean towpath value Prediction: raster of curvature derived from bathymetry
Rockiness	--	Continuous surface of compiled datasets representing locations of rocky and not rocky substrate (updated from Pirtle et al. 2019)	Natural neighbor	Training: mean towpath value Prediction: raster of seafloor rockiness.
Coral presence or absence	probability	Coral presence-absence in bottom trawl catches / model-predicted coral presence-absence (Sigler et al. 2015; Rooper et al. 2014)	--	Training: presence-absence of corals in trawl catches Prediction: Raster of model-predicted binary presence-absence of coral (Rooper et al. 2014)
Sponge presence or absence	probability	Sponge presence-absence in bottom trawl catches / model-predicted sponge presence-absence (Sigler et al. 2015; Rooper et al. 2014)	--	Training: presence-absence of sponge in trawl catches Prediction: Raster of model-predicted binary presence-absence of sponge (Rooper et al. 2014)

Variable	Unit	Description of Prediction Raster	Interpolation method	Data Source and Usage
Pennatulacean presence-absence	probability	Pennatulacean presence-absence in bottom trawl catches / model-predicted penn. presence-absence (Sigler et al. 2015; Rooper et al. 2014)	--	Training: presence-absence of Pennatulaceans in trawl catches Prediction: Raster of model-predicted binary presence-absence of Pennatulaceans (Rooper et al. 2014)

735 a – Zimmermann et al. 2013; Zimmermann et al. 2019.

736 Table 3. Variance inflation factors (VIF) of covariates used as predictors in species distribution models
 737 (SDM) for federally managed groundfishes and invertebrates in the Aleutian Islands; SD = pooled
 738 standard deviation.

Covariate	VIF
*Longitude	3.32
*Latitude	3.05
Bottom depth	1.88
Slope	1.50
Aspect Eastness	1.07
Aspect Northness	1.28
Curvature	1.69
Bottom temperature	1.45
*Bottom Current Eastings	1.57
*Bottom Current Northings	1.64
*SD bottom current Eastings	2.24
*SD bottom current Northings	2.32
Tidal maximum current	1.32
Rockiness	1.18
Bathymetric position index	2.13
Sponge presence-absence	1.03
Coral presence-absence	1.03
Pennatulacean presence-absence	1.02

739
 740 *represent components of covariates that form bivariate smoothed interaction terms in the generalized
 741 additive models (Longitude and Latitude = “position”, Eastings and Northings = “bottom current”, SD
 742 Eastings and SD Northings = “bottom current SD”).

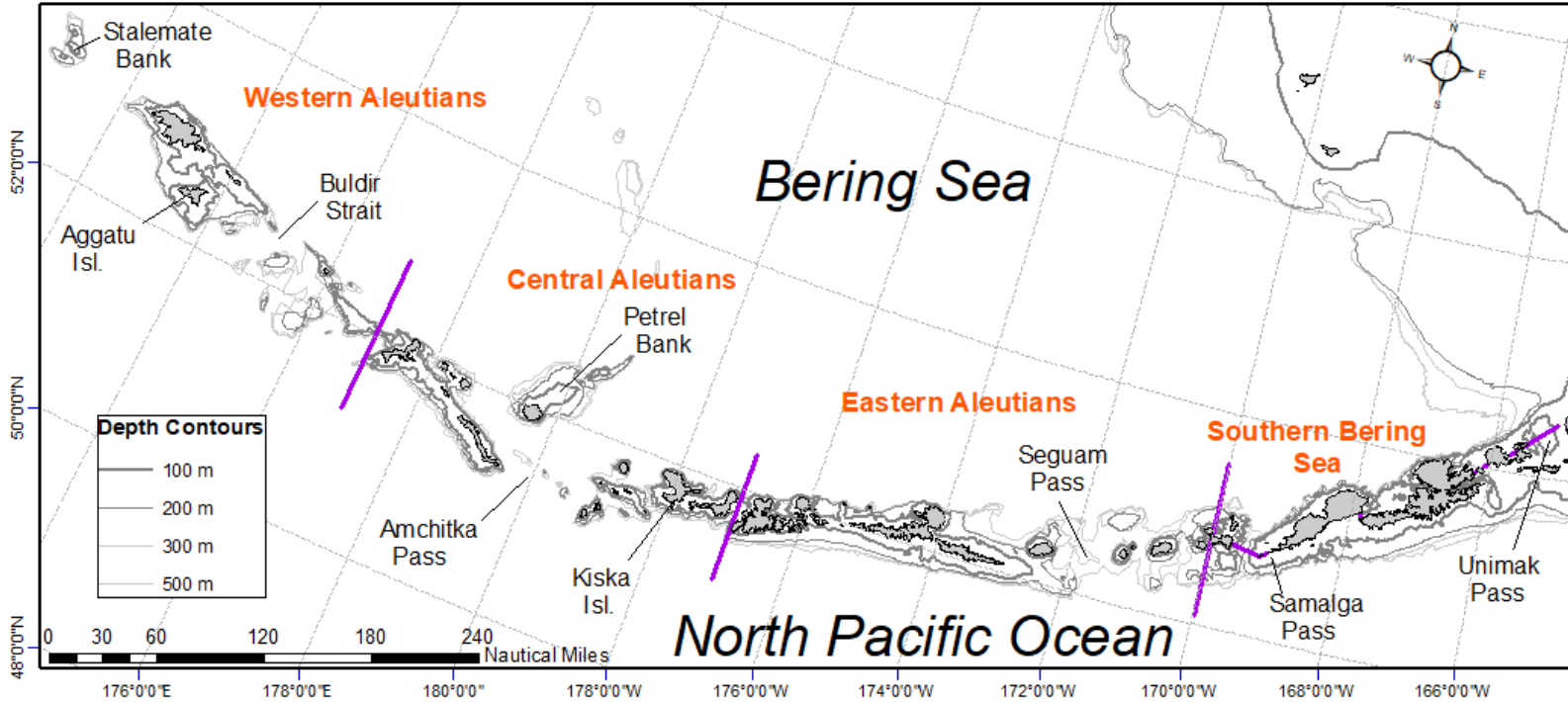
743 Table 4. Species distribution models (SDMs) trained and skill tested for inclusion in an ensemble; the
 744 Maximum Entropy model (MaxEnt) uses the *maxnet*^a package and the generalized additive models
 745 (GAMs) use the *mgcv*^b package.

Species Distribution Model (SDM)	Family	Link	Documentation
Maximum Entropy (MaxEnt)	*	cloglog approx.	Phillips et al. (2017)
Generalized Additive Models (GAM)			
presence-absence GAM (paGAM)	binomial	cloglog	Wood (2011)
hurdle GAM (hGAM)	zero-adjusted Poisson	cloglog and log	Zuur et al. (2009); Wood (2011)
standard GAM (GAM _p)	Poisson	log	Wood (2011)
negative-binomial GAM (GAM _{nb})	negative-binomial	log	Wood (2011)

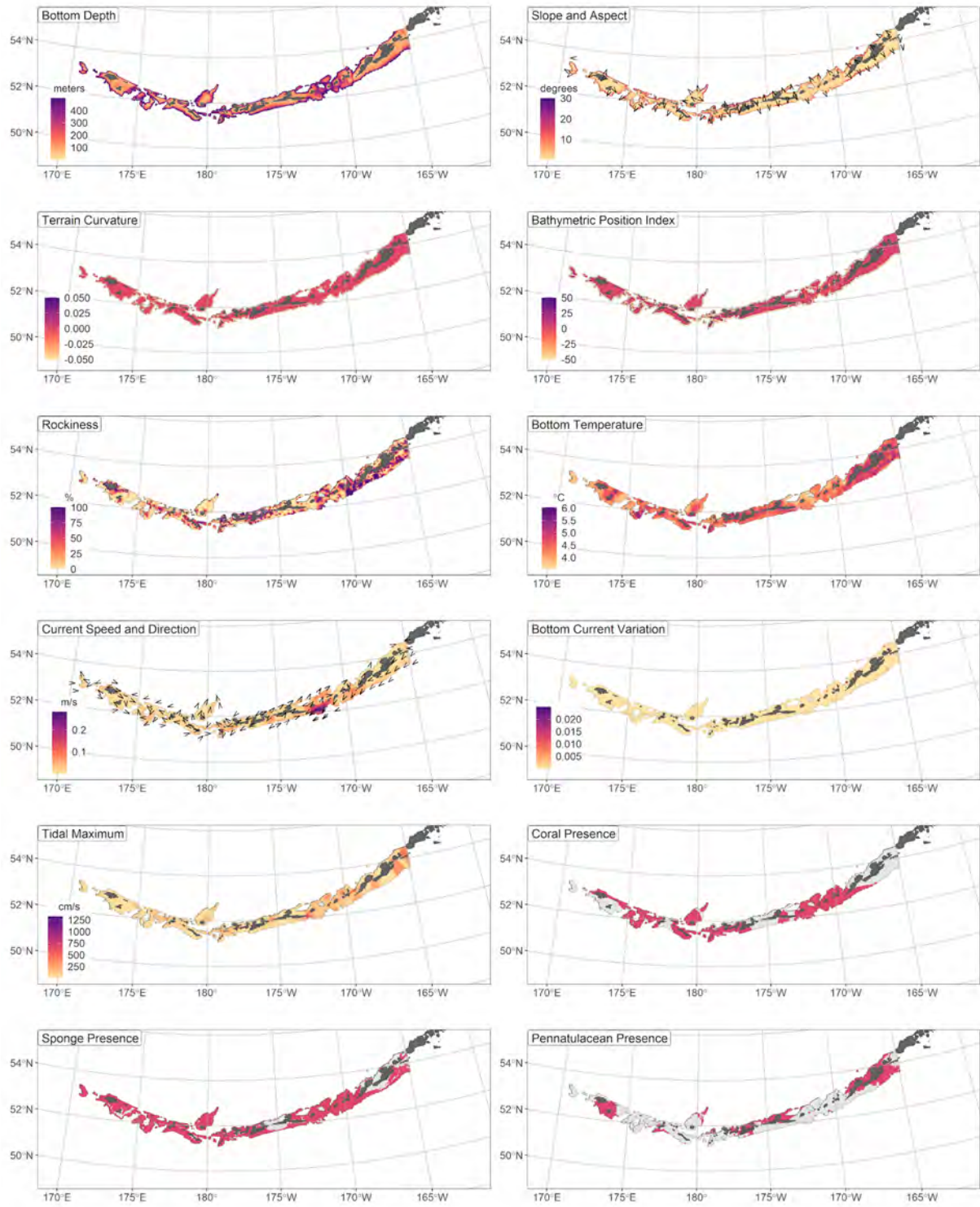
746
 747 * - the distribution applied to the MaxEnt model is a heavily modified Poisson distribution representing
 748 an inhomogeneous Poisson process

749 *a* - R v3.6.1; Fitting 'MaxEnt' species distribution models with 'glmnet'; *maxnet*: R package version
 750 0.1.2.

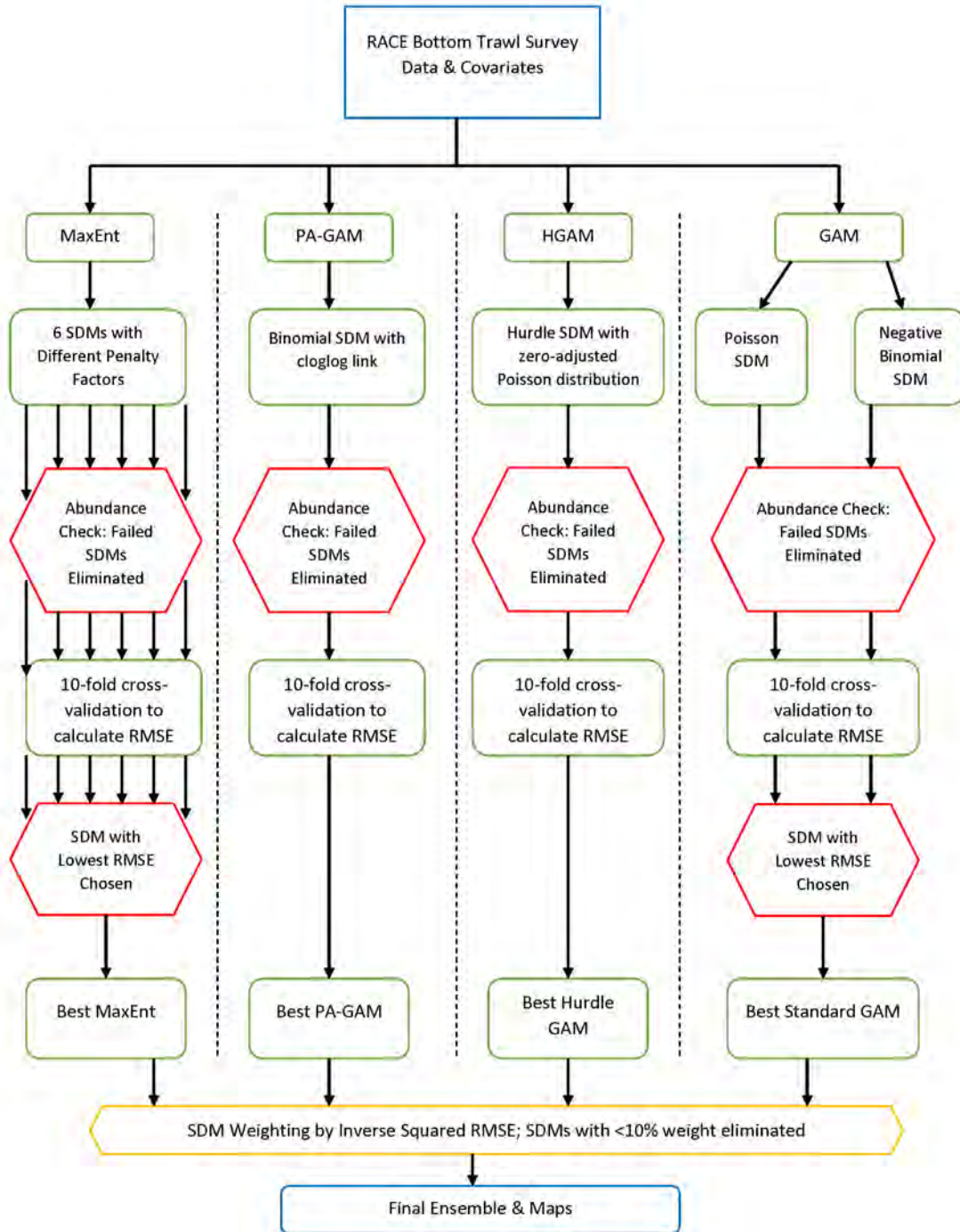
751 *b* - R v3.6.1; Fast stable restricted maximum likelihood and marginal likelihood estimation of
 752 semiparametric generalized linear models; *mgcv*: R package version 1.8-29



753
 754 Figure 1. Aleutian Islands (AI) from Unimak Pass to Stalemate Bank where data for this modeling study were collected on Alaska Fisheries
 755 Science Center (AFSC), Resource Assessment and Conservation Engineering-Groundfish Assessment Program (RACE-GAP) summer bottom
 756 trawl surveys (1991-2019).



757
 758 Figure 2. Predictor variables used to represent environmental and habitat covariates in the Aleutian
 759 Islands; scale of structure-forming invertebrates (SFI: corals, sponges, and pennatulacean) is light
 760 shading = absent and darker shading = present.



761
 762 Figure 3. Pathways to formulation and assessment of five species distribution models
 763 (MaxEnt = maximum entropy, paGAM = presence-absence generalized additive model, hGAM = hurdle
 764 GAM, GAM = standard Poisson GAM, GAM_{nb} = standard negative-binomial GAM) for inclusion in or
 765 elimination from a final ensemble predicting habitat-related distribution and abundance used to describe
 766 and map essential fish habitat (EFH) in Alaska: RMSE = root mean square error.

767
768
769
770
771
772
773
774
775
776
777
778
779
780
781
782
783
784
785
786
787
788

RESULTS

Flatfishes

Arrowtooth flounder (*Atheresthes stomias*)

Arrowtooth flounder (ATF; *Atheresthes stomias*) is a large bodied flatfish distributed from the Kuril Islands to California (Shotwell et al. 2020a). The species is morphologically similar to the less common Kamchatka flounder (*A. evermani*), and the two were not routinely distinguished in assessment surveys until 1992 (Shotwell et al. 2020a). The settled early juvenile life stage was defined as all fish between 35 mm (maximum size range of transformed pelagic early juveniles; Doyle et al. 2019) and 160 mm when ATF undergo an ontogenetic shift in habitat (Doyle et al. 2018). Female ATF have a length at 50% maturity (L_{50}) of 480 mm F. L. (Stark 2012b), and although the length at maturity is consistent across regions, the age of maturity can vary considerably (Shotwell et al. 2020a). Given its large size, this species is highly predatory and is thought to be an important part of the marine food web; in particular it is a major predator of juvenile walleye pollock (*Gadus chalcogrammus*) (Yang and Livingston, 1986). This species was managed as a stock complex with Kamchatka flounder until 2011, when the start of a directed fishery prompted the development of separate management plans (Shotwell et al. 2020a). ATF are often captured during long-line surveys and these may represent a useful data source in the future.

Settled early juvenile arrowtooth flounder distribution and predicted abundance from RACE-GAP summer bottom trawl surveys in the Aleutian Islands –

Settled early juvenile ATF were relatively uncommon in the RACE-GAP summer survey of the AI compared to older life stages (Figure 4). However, this may be an artifact of the sampling design, and smaller mesh sampling would likely catch this life stage in greater numbers¹⁰. Available trawl data indicate that settled early juvenile ATF were most concentrated towards the eastern AI near Unimak Pass,

¹⁰ A recommendation to add additional survey data types if possible to future SDM ensemble EFH mapping efforts for this species will be included as a future recommendation for research directions from the 2022 EFH 5-year Review.

789 but occurred in several pockets across the survey area. The final ensemble contained four SDMs with
790 approximately equal weights, and showed a fair to good performance in terms of model fit (Table 5).
791 Specifically, the ensemble did a fair job of distinguishing high and low abundance areas ($\rho = 0.357$), but
792 performed better in terms of deviance explained (PDE = 0.531). This pattern, in conjunction with the fact
793 that best performing constituents were the hGAM and the GAM_{nb}, indicates that the ensemble is useful
794 for predicting the patches where this life stage occurs in high numbers. Additionally, the ensemble does
795 an excellent job of predicting presence or absence in a given haul (AUC = 0.906). Geographic position,
796 bottom depth, tidal current maximum, and bottom currents were the most important covariates and
797 accounted for 77.2% of the deviance explained by the model (Table 6). In general, predicted abundance
798 was high in locations that were further east, with shallow depths (<150 m), and with weak tides
799 (Figure 5). Predicted abundance was highest in shallow, sheltered inshore areas, particularly those near
800 Unalaska Island (Figure 5), though secondary pockets of high abundance were also predicted near Atka
801 Island and Agattu Island. The predicted CV of abundance was higher in further west areas of the AI,
802 though the pattern was not strong (Figure 2). Encounter probabilities for settled early juvenile ATF were
803 high near the areas described above, and close to zero in most places beyond the 100m depth contour
804 (Figure 6).

805 **Subadult arrowtooth flounder distribution and predicted abundance from RACE-GAP summer**
806 **bottom trawl surveys in the Aleutian Islands –**

807 Subadult ATF were ubiquitous within RACE-GAP summer survey area (Figure 7). They were
808 present in the highest abundance in the eastern AI. The final ensemble contains three SDMs, with the
809 paGAM weighted slightly less than the others, and it demonstrated good predictive performance
810 (Table 5). Specifically, the ensemble was excellent at identifying hauls that would have a relatively high
811 or low density of this life stage ($\rho = 0.632$), but the lower deviance explained metric suggests that it was
812 less effective at predicting the exact density values (PDE = 0.381). The ensemble also performed well at
813 predicting presence and absence (AUC = 0.794). Geographic position and bottom depth were the most

814 important covariates and accounted for 66.2% of the total deviance explained, though bottom currents and
815 tidal maximum were also relatively important (Table 6). Like early juveniles, subadult ATF were
816 associated with areas with weak tidal forces and weak bottom currents. Based on the covariates,
817 abundance should be highest in the eastern and central AI, and at depths between 100 m and 300 m
818 (Figure 8). Overall abundance of this life stage was relatively high throughout the AI, but was highest in
819 the eastern part of the region, near Unalaska Island (Figure 8). The predicted CV of abundance tended to
820 be high in areas away from the areas of high abundance, reflecting the greater variability of these more
821 marginal areas (Figure 8). Subadult ATF are very common in the AI, and the encounter probability was
822 near 100% across the survey area (Figure 9).

823 **Adult arrowtooth flounder distribution and predicted abundance from RACE-GAP summer**
824 **bottom trawl surveys in the Aleutian Islands –**

825 Adult ATF catches were universally common throughout the RACE-GAP summer survey area in
826 the AI (Figure 10). High abundances were observed across the entire AI area, but were somewhat more
827 frequent in the eastern parts of the AI. The final ensemble contained three SDMs with the paGAM
828 weighted slightly less than the hGAM or GAM_p, and the predictions generated by the ensemble had a
829 good fit to the data (Table 5). Similar to subadults, the ensemble demonstrated good performance at
830 identifying hauls that caught relatively high or low numbers of adult ATF ($\rho = 0.504$), but was less able to
831 predict the density in those catches (PDE = 0.288). The ensemble displayed a fair ability to predict
832 presence in survey catches (AUC = 0.765), though this is likely a conservative estimate, as there are
833 almost no locations in the AI where ATF are never caught. Similar to earlier life stages, bottom depth,
834 geographic position, current, and current variability were the most important covariates, and they
835 accounted for a combined 80.7% of the deviance explained by the ensemble (Table 6). Adult ATF are
836 predicted to be abundant in moderately deep waters, in the eastern AI, and at locations with weak bottom
837 currents (Figure 11). Adult ATF appear in somewhat lower numbers than subadults, but are still one of
838 the most common flatfish species throughout the AI. The highest abundance areas were in the eastern AI,

839 near Unalaska Island and the Islands of Four Mountains, and predicted abundance was higher between
840 100 m and 300 m (Figure 11). The predicted CV of abundance tended to be higher in western areas, as
841 well as in shallow areas (Figure 11). Like subadults, adult ATF had a nearly 100% encounter probability
842 in most of the survey area, with lower encounter probabilities in shallow water close to shore (Figure 12).

843 **Essential fish habitat of settled early juvenile, subadult, and adult arrowtooth flounder in the**
844 **Aleutian Islands –**

845 Habitat related abundance predictions based on RACE-GAP summer bottom trawl data (1992–
846 2019) were translated into EFH area and additional subareas (Figure 13). The EFH area for settled early
847 juvenile ATF is smaller than that of the other life stages. Settled early juveniles had substantial EFH hot
848 spots in the eastern AI around Unalaska Island, more centrally around Atka Island, and a third, smaller
849 area in the far west near Agattu Island. These cases are supported by the maps of trawl catches (Figure 4),
850 and hot spots in these sheltered inshore areas are consistent with positive density responses to shallow
851 water with low currents (Figure 5). The subadult and adult life stages had very similar EFH maps, with
852 large hot spots around Unalaska and Atka Islands, but almost the entire survey area was included in the
853 95% EFH area. These life stages both had an EFH area of 77,700 km² (Table 5), which was the maximum
854 EFH area attainable using our current methods and reflected the ubiquity of this species in the AI.

855 Table 5. Constituent species distribution models (SDMs) used to construct Essential Fish Habitat (EFH)
 856 for a) settled early juvenile, b) subadult, and c) adult arrowtooth flounder: MaxEnt = Maximum entropy;
 857 paGAM = presence-absence generalized additive model; hGAM = hurdle GAM; GAM_P = standard
 858 Poisson GAM; and GAM_{nb} = standard negative-binomial GAM. Ensemble performance (ρ = Spearman's
 859 rank correlation coefficient), root-mean-square-error (RMSE), the area under the receiver operating
 860 characteristic (AUC), and the Poisson deviance explained (PDE) were generated from k-fold cross-
 861 validation. The "--" in a field indicates that this SDM was not included in the final ensemble.

862 **a) settled early juvenile arrowtooth flounder**

Models	RMSE	Relative Weight	ρ	AUC	PDE	EFH area (km²)
MaxEnt	1.70	0.245	0.342	0.890	0.416	40,900
paGAM	1.67	0.253	0.358	0.908	0.480	39,100
hGAM	1.69	0.249	0.354	0.908	0.572	32,200
GAM _P	1.68	0	--	--	--	--
GAM _{nb}	1.68	0.252	0.359	0.906	0.516	32,100
ensemble	1.60	1	0.357	0.906	0.531	37,400

863 **b) subadult arrowtooth flounder**

Models	RMSE	Relative Weight	ρ	AUC	PDE	EFH area (km²)
MaxEnt	259.0	0	--	--	--	--
paGAM	92.7	0.303	0.640	0.826	0.267	77,700
hGAM	86.1	0.351	0.618	0.826	0.398	77,700
GAM _P	86.7	0.346	0.599	0.767	0.388	77,700
GAM _{nb}	103.0	0	--	--	--	--
ensemble	85.5	1	0.632	0.794	0.381	77,700

864 **c) adult arrowtooth flounder**

Models	RMSE	Relative Weight	ρ	AUC	PDE	EFH area (km²)
MaxEnt	187.0	0	--	--	--	--
paGAM	45.2	0.319	0.544	0.803	0.131	77,700
hGAM	43.7	0.341	0.466	0.802	0.304	77,700
GAM _P	43.8	0.340	0.444	0.725	0.289	77,700
GAM _{nb}	48.9	0	--	--	--	--
ensemble	42.7	1	0.504	0.765	0.288	77,700

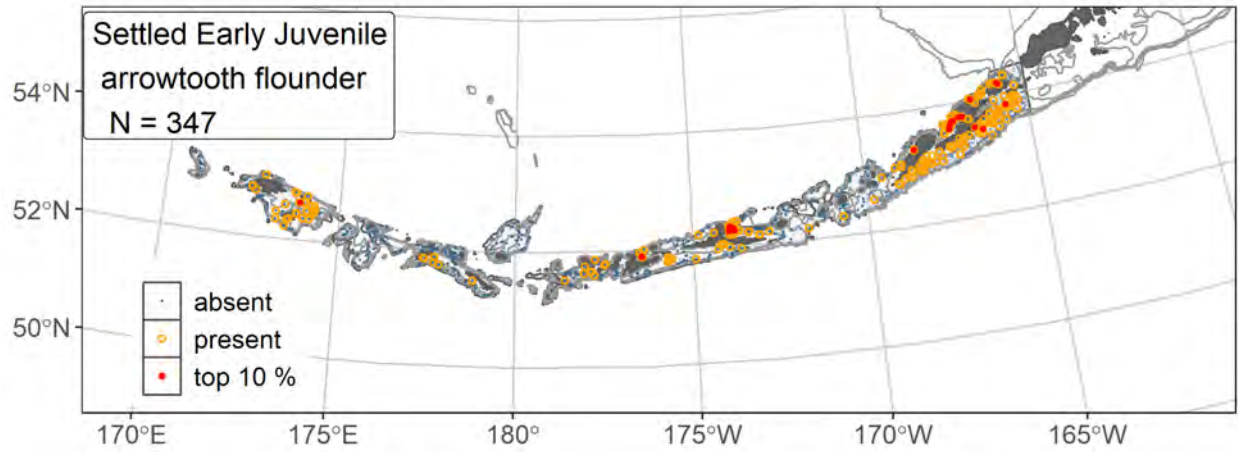
865

866 Table 6. Covariates retained in the a) settled early juvenile, b) subadult, and c) adult arrowtooth flounder
 867 species distribution model (SDM) final ensembles, the percent contribution to the ensemble deviance
 868 explained by each, and the cumulative percent deviance: SD = standard deviation, and BPI = bathymetric
 869 position index.

arrowtooth flounder	Covariate	% Contribution	Cumulative % Contribution
a) settled early juvenile	position	24.6	24.6
	tidal maximum	20.6	45.3
	bottom depth	18.6	63.9
	current	13.3	77.2
	BPI	7.3	84.6
	aspect east	3.2	87.7
	aspect north	2.7	90.4
	bottom temperature	2.1	92.5
	slope	2.0	94.5
	curvature	1.6	96.1
	current SD	1.3	97.5
	rockiness	1.1	98.5
	coral presence	0.9	99.5
	sponge presence	0.4	99.9
	pennatulacean presence	0.1	100
b) subadult	position	40.2	40.2
	bottom depth	26.0	66.2
	tidal maximum	9.4	75.6
	current	7.8	83.4
	current SD	3.5	86.9
	slope	2.6	89.6
	BPI	2.3	91.9
	coral presence	1.8	93.7
	aspect north	1.7	95.4
	bottom temperature	1.1	96.5
	sponge presence	0.9	97.4
	aspect east	0.8	98.2
	rockiness	0.8	98.9
	curvature	0.6	99.5
	pennatulacean presence	0.5	100
c) adult	bottom depth	36.3	36.3
	position	27.6	63.9
	current	9.3	73.1
	current SD	7.6	80.7
	aspect north	3.5	84.2
	tidal maximum	3.2	87.4

arrowtooth flounder	Covariate	% Contribution	Cumulative % Contribution
	bottom temperature	3.0	90.4
	aspect east	2.4	92.9
	rockiness	1.5	94.4
	slope	1.2	95.6
	BPI	1.2	96.8
	sponge presence	1.2	98.0
	coral presence	1.1	99.1
	curvature	0.5	99.5
	pennatulacean presence	0.5	100

870



871

872

Figure 4. Distribution of settled early juvenile arrowtooth flounder catches (N = 347) in 1992–2019

873

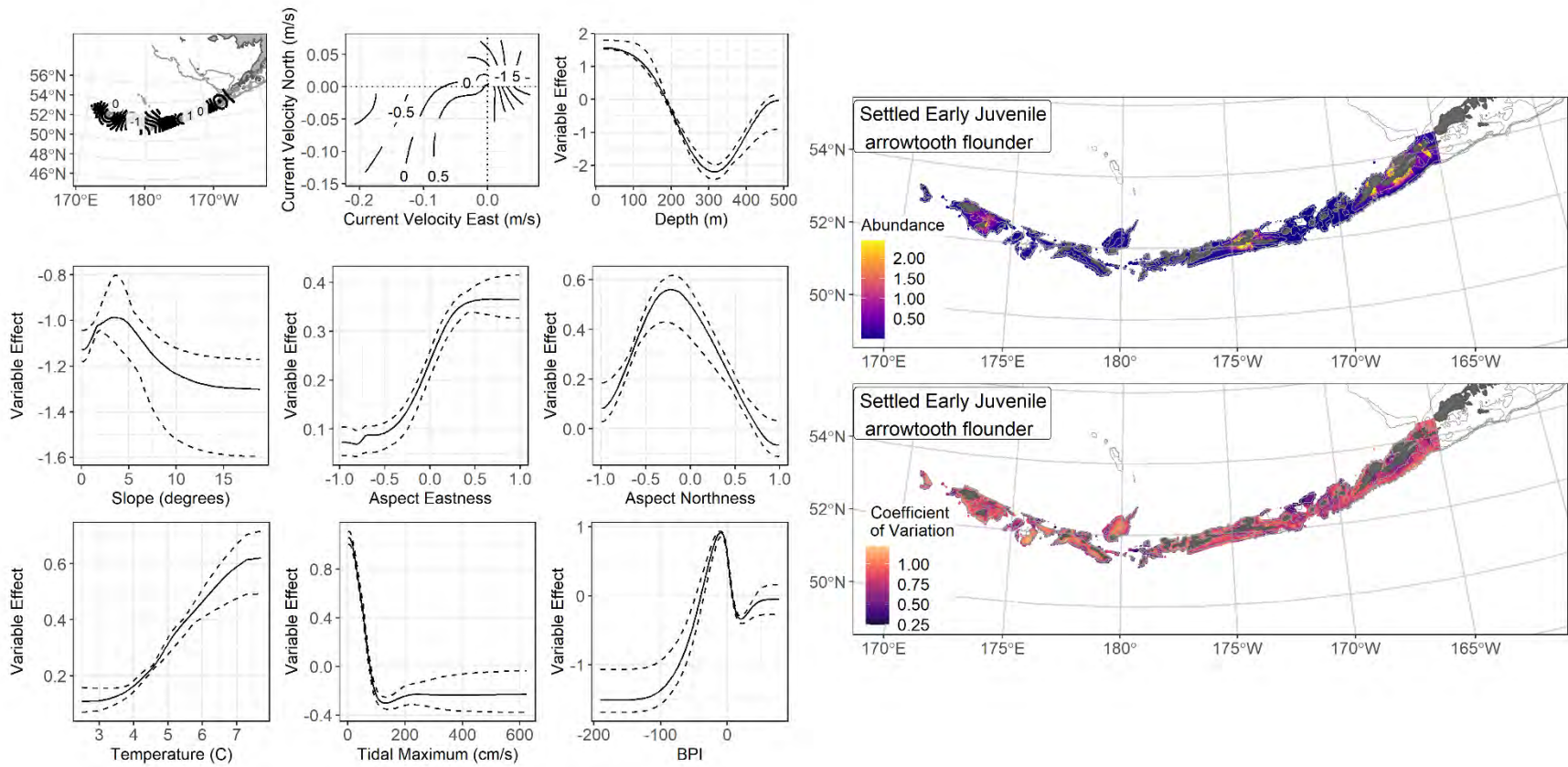
AFSC RACE-GAP summer bottom trawl surveys of the Aleutian Islands with the 100 m, 300 m, and

874

500 m isobaths indicated; filled red circles indicate locations in top 10% of overall abundance, open

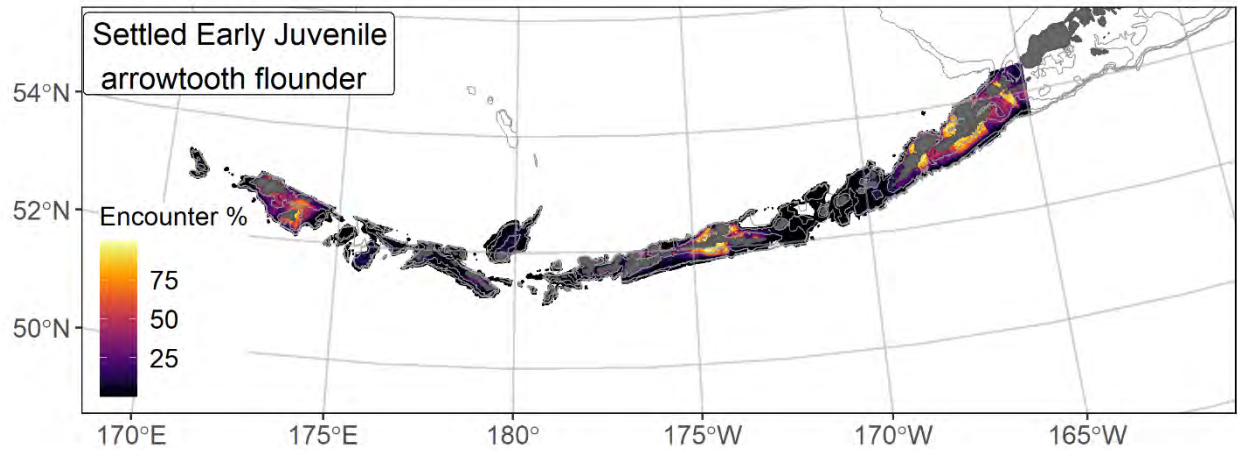
875

orange circles indicate presence in remaining catches, and small blue dots indicate absence.



876

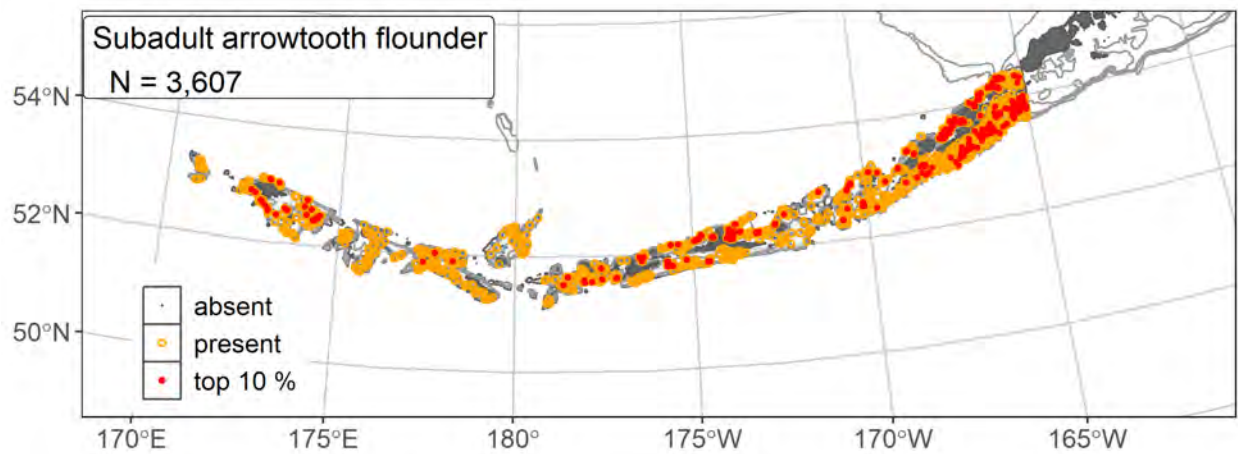
877 Figure 5. The top nine covariate effects (left panel) on ensemble-predicted settled early juvenile arrowtooth flounder numerical abundance across
 878 the Aleutian Islands (upper right panel) alongside the coefficient of variation of the ensemble predictions (lower right panel).



879

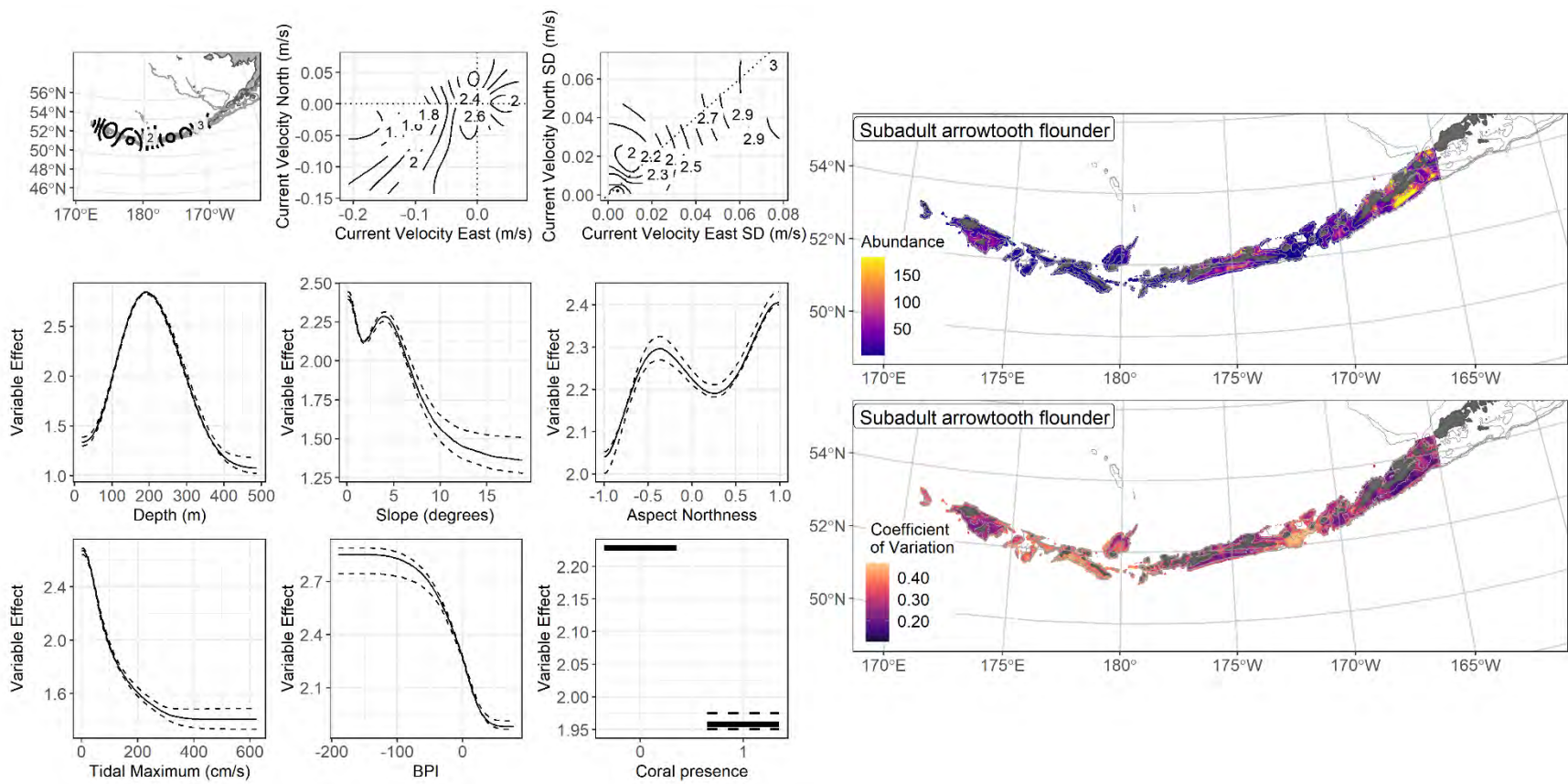
880 Figure 6. Encounter probability of settled early juvenile arrowtooth flounder from AFSC RACE-GAP
 881 summer bottom trawl surveys (1992–2019) of the Aleutian Islands with the 100 m, 300 m, and 500 m
 882 isobaths indicated.

883



884

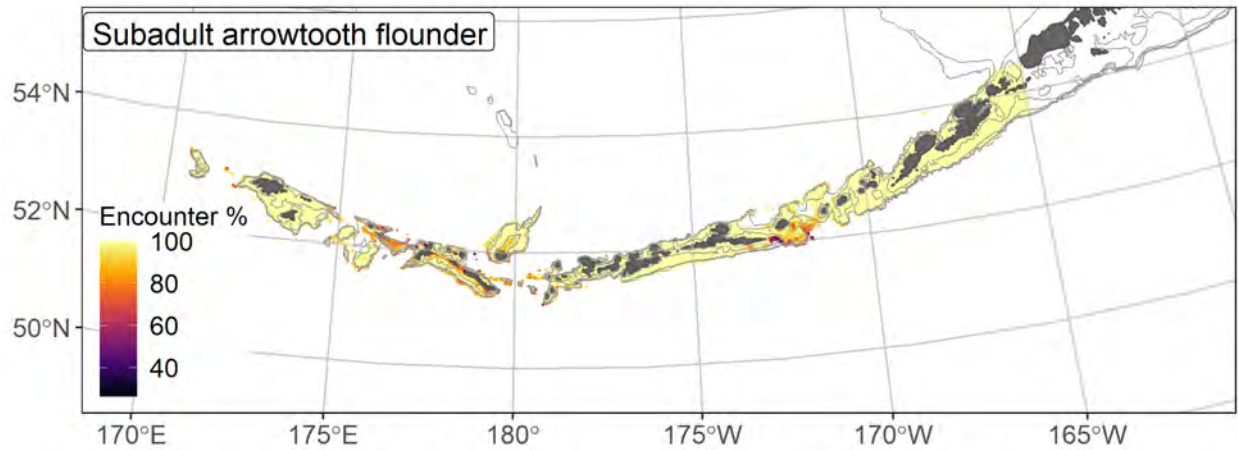
885 Figure 7. Distribution of subadult arrowtooth flounder catches (N = 3,607) in 1992–2019 AFSC RACE-
 886 GAP summer bottom trawl surveys of the Aleutian Islands with the 100 m, 300 m, and 500 m isobaths
 887 indicated; filled red circles indicate locations in top 10% of overall abundance, open orange circles
 888 indicate presence in remaining catches, and small blue dots indicate absence.



889

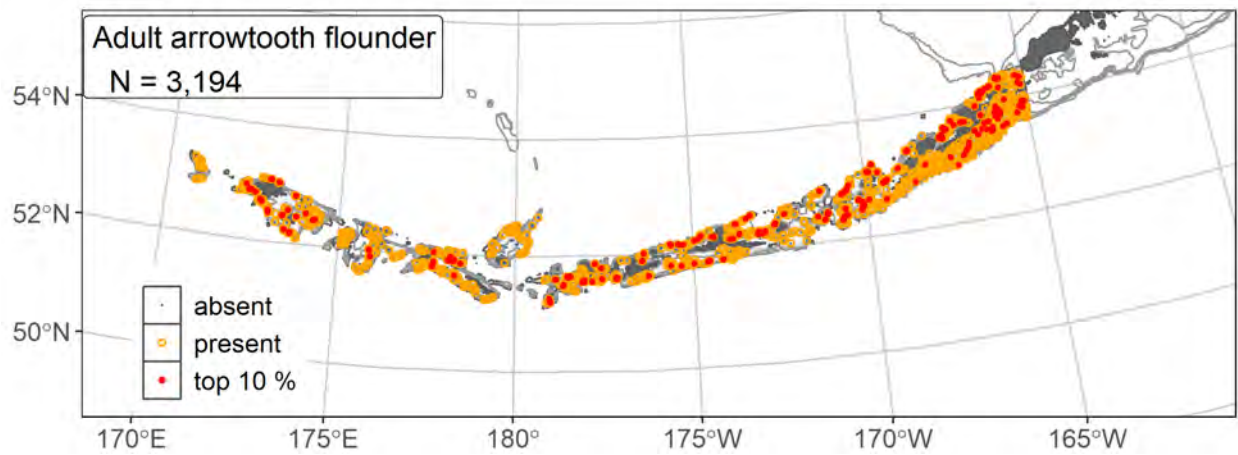
890 Figure 8. The top nine covariate effects (left panel) on ensemble-predicted subadult arrowtooth flounder numerical abundance across the Aleutian

891 Islands (upper right panel) alongside the coefficient of variation of the ensemble predictions (lower right panel).

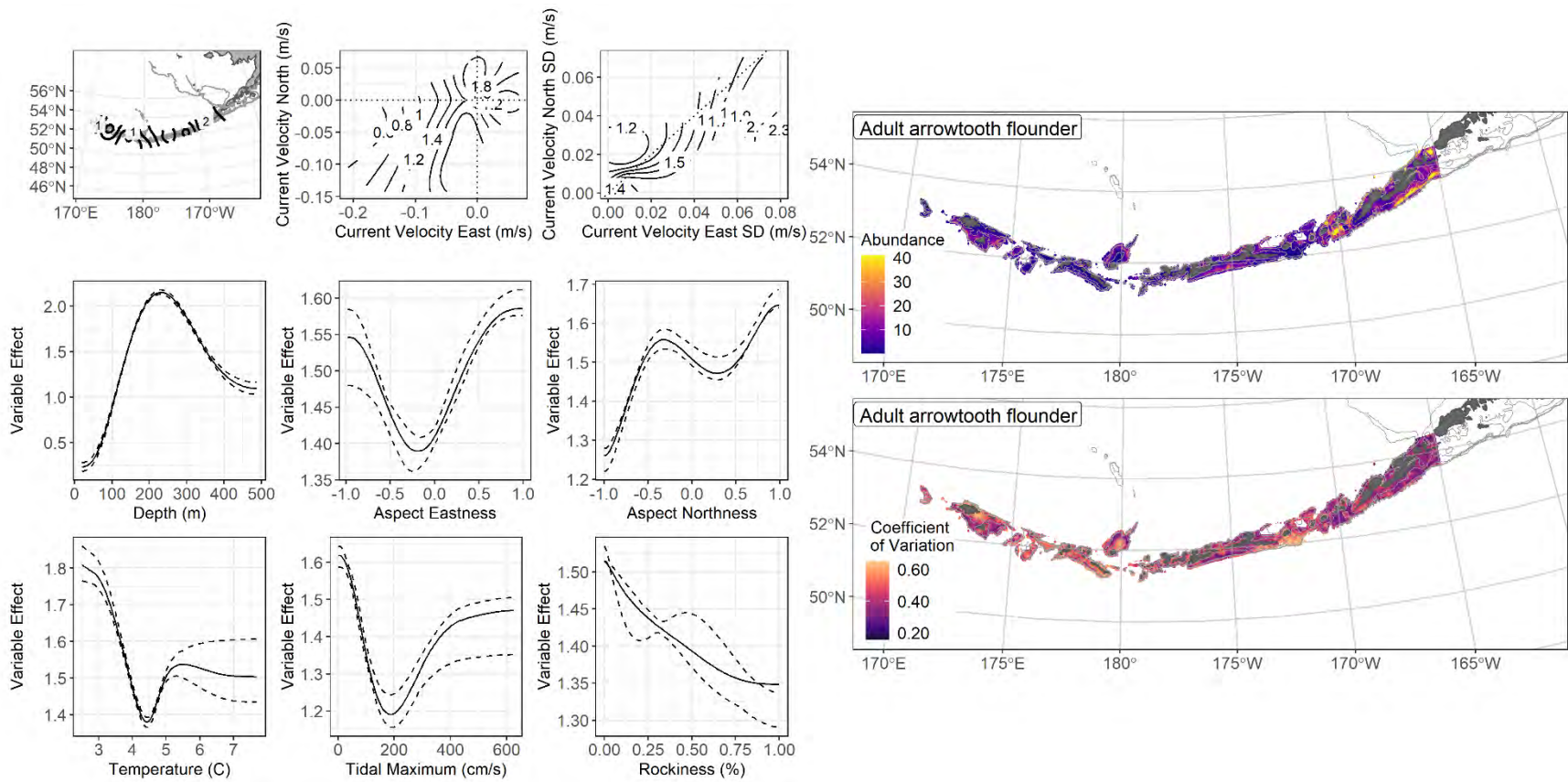


892
893 Figure 9. Encounter probability of subadult arrowtooth flounder from AFSC RACE-GAP summer bottom
894 trawl surveys (1992–2019) of the Aleutian Islands with the 100 m, 300 m, and 500 m isobaths indicated.

895



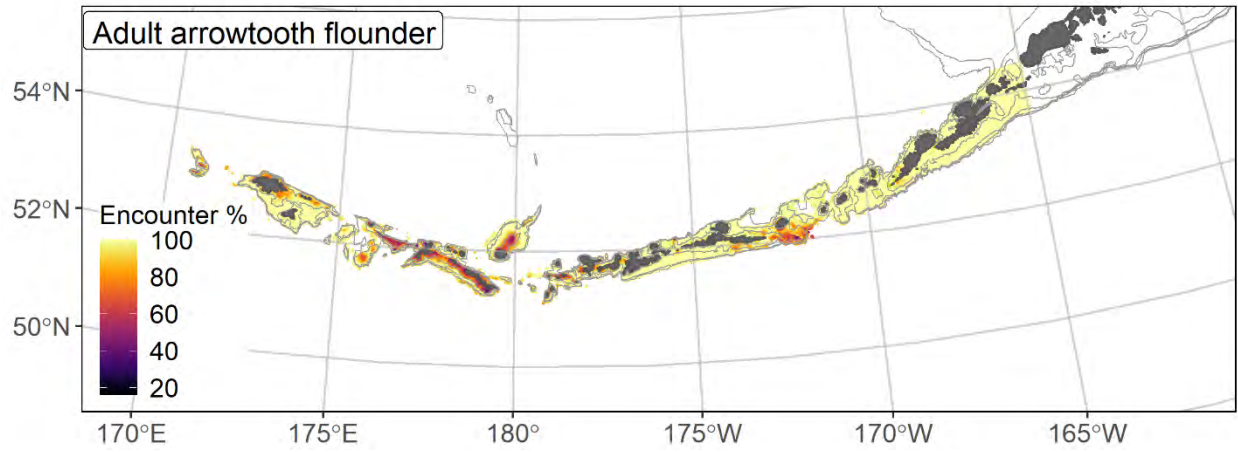
896
897 Figure 10. Distribution of adult arrowtooth flounder catches (N = 3,194) in 1992–2019 AFSC RACE-
898 GAP summer bottom trawl surveys of the Aleutian Islands with the 100 m, 300 m, and 500 m isobaths
899 indicated; filled red circles indicate locations in top 10% of overall abundance, open orange circles
900 indicate presence in remaining catches, and small blue dots indicate absence.



901

902 Figure 11. The top nine covariate effects (left panel) on ensemble-predicted adult arrowtooth flounder numerical abundance across the Aleutian

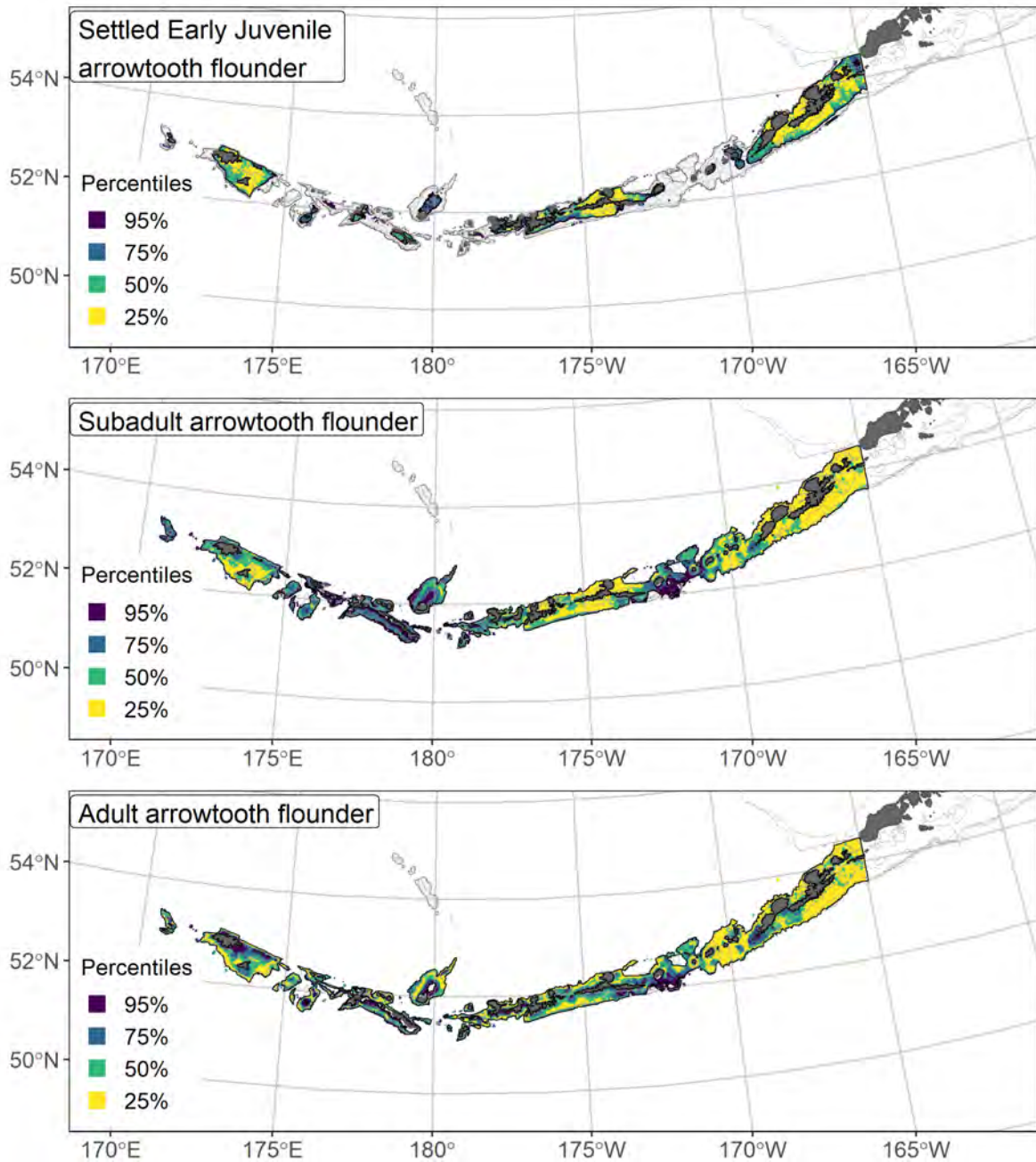
903 Islands (upper right panel) alongside the coefficient of variation of the ensemble predictions (lower right panel)



904

905 Figure 12. Encounter probability of adult arrowtooth flounder from AFSC RACE-GAP summer bottom

906 trawl surveys (1992–2019) of the Aleutian Islands with the 100 m, 300 m, and 500 m isobaths indicated.



907

908 Figure 13. Essential fish habitat (EFH) area defined as the top 95% of numerical abundance predictions
 909 from a habitat-based ensemble model fitted to settled early juvenile (top), subadult (middle), and adult
 910 (bottom) arrowtooth flounder distribution and abundance in AFSC RACE-GAP summer bottom trawl
 911 surveys (1992–2019) with 100 m, 300 m, and 500 m isobaths indicated; internal to the EFH map are the
 912 subareas of the top 25% (EFH hot spots), top 50% (core EFH area), and top 75% (principal EFH area) of
 913 habitat related, ensemble-predicted numerical abundance.

914 **Flathead sole (*Hippoglossoides elassodon*)**

915 Flathead sole (*Hippoglossoides elassodon*) is distributed across the north Pacific, from northern
916 California across the Aleutian islands and Bering Sea at least as far as the Kuril archipelago (Hart 1973).
917 Spawning occurs between March and June on the continental shelf, usually in bays or other shallow
918 habitats close to inshore nursery areas (Porter, 2005). Larvae undergo transformation at 20 mm T.L.
919 (Doyle et al. 2019) and remain in near shore habitats as settled early juveniles until they reach 140 mm
920 T.L. (NFA). Most flathead sole reach maturity at 342 mm T.L. (L₅₀; Tenbrink and Wilderbuer 2015) and
921 adults may grow up to 520 mm and live more than 30 years. In the BSAI region, flathead sole is managed
922 as the dominant component (>94%) of a mixed stock that also includes Bering flounder (*Hippoglossoides*
923 *robustus*; Monnahan and Haehn, 2020), though Bering flounder are not typically caught in the AI.

924 **Settled early juvenile flathead sole distribution and predicted abundance from RACE-GAP**
925 **summer bottom trawl surveys in the Aleutian Islands –**

926 Settled early juvenile flathead sole were not common in the RACE-GAP summer survey of the
927 Aleutian Islands compared to older life stages (Figure 14), likely because of their small size relative to the
928 selectivity of the trawl gear used¹¹. Catches occurred near shore and in shallow water around Unalaska,
929 Atka, or Agattu Islands. The final ensemble contained three SDMs, with the MaxEnt model assigned less
930 weight than the others, and the ensemble fit was good overall, though the fit metrics suggest a
931 complicated picture (Table 7). The ensemble performed excellently in terms of AUC and deviance
932 explained (AUC = 0.939; PDE = 0.810), but it scored only fair in its ability to estimate high or low
933 abundance areas ($\rho = 0.279$). Because the Spearman's correlation is based on ranking, when many
934 observed values are zero this metric can sometimes produce low values. By comparison, the excellent
935 score for AUC indicates that the ensemble is quite good at estimating presence vs. absence, and the high

¹¹ A recommendation to add additional survey data types if possible to future SDM ensemble EFH mapping efforts for this species will be included as a future recommendation for research directions from the 2022 EFH 5-year Review.

936 PDE suggests that it captures a majority of the variation in abundance. Finally, the map of predicted
937 abundance (Figure 15) agreed with the map of observed catches (Figure 14), so this model is likely to
938 provide accurate information. Geographic position, bottom depth, BPI, and tidal maximum were the most
939 important covariates and explained 66.1% of the total deviance (Table 8). In general, the ensemble
940 predicts high abundance in the far east and far west of the AI, in areas of moderate to shallow depth, weak
941 tidal currents, and a low BPI (which indicates terrain that includes troughs or valleys; Figure 15).
942 Predicted abundance matched the map of catches and was high in areas around Unalaska, Atka, and
943 Agattu Islands (Figure 15). The predicted CV of abundance was moderate throughout most areas and very
944 high in areas with high predicted abundance, reflecting uncertainty around the ensemble predictions in
945 high abundance areas (Figure 15). Encounter probabilities followed the same pattern with a few isolated
946 areas of high probability (Figure 16).

947 **Subadult flathead sole distribution and predicted abundance from RACE-GAP summer bottom**
948 **trawl surveys in the Aleutian Islands –**

949 In contrast to early juveniles, subadult flathead sole catches were widespread and very common
950 in the RACE-GAP summer survey area (Figure 17), following the same pattern as early juveniles with
951 high abundance catches around Unalaska, Atka, and Agattu Islands. The final ensemble contains four
952 SDMs, with the hGAM and GAM_P given more weight than the others, and it demonstrated excellent
953 predictive performance with regards to model fit (Table 7). All three fit metrics had high values
954 ($\rho = 0.599$; AUC = 0.893; PDE = 0.756), suggesting that the ensemble predictions are accurate.
955 Geographic position, bottom depth, tidal maximum, current speed, and current variability were the most
956 important covariates and accounted for 71.6% of the deviance explained by the ensemble (Table 8). In
957 general, the ensemble model predicted high abundance in patches around the major islands, as well as in
958 areas with depths between 100-200 m, weak tidal currents, and currents that run in north or south
959 directions (Figure 18). However, predicted abundance was very high overall, and even predicted low-
960 abundance areas had averages well above zero. Predicted abundance was much higher overall for the

961 subadult life stage, but was located in the same areas as settled early juveniles around Unalaska, Atka, and
962 Agattu Islands (Figure 18). The predicted CV of abundance tended to be high around places with
963 increased abundance (Figure 18). These places have low average predicted abundance with occasional
964 large catches. Predicted encounter probabilities for subadult flathead sole were high in areas shallower
965 than 300 m, with the exception of major passes between the islands (Figure 19).

966 **Adult flathead sole distribution and predicted abundance from RACE-GAP summer bottom trawl**
967 **surveys in the Aleutian Islands –**

968 Adult flathead sole catches were common in the RACE-GAP summer survey area in the AI
969 (Figure 20). The distribution of adult catches follows the same general pattern as subadults and settled
970 early juveniles, with high abundance catches centered around Unalaska, Atka, and Agattu Islands. The
971 ensemble contained four equally weighted SDMs and ensemble predictions had a good overall fit to the
972 data (Table 7). All three fit metrics indicated a good fit ($\rho = 0.564$; AUC = 0.863; PDE = 0.467),
973 suggesting that the ensemble provides good accuracy. Similar to earlier life stages, bottom depth,
974 geographic position, tidal maximum, and current were the most important covariates, and they accounted
975 for 67.9% of the deviance explained by the ensemble (Table 8). Adult flathead sole are predicted to be
976 abundant in 100-250 m deep waters, and areas with a low tidal maximum and southerly currents
977 (Figure 21). The estimated abundance of adults is lower overall than that of subadults, but otherwise
978 shows the same distribution pattern with high abundance predicted near Unalaska, Atka, and Agattu
979 Islands (Figure 21). The predicted CV of abundance was higher overall for adults than the other life
980 stages (Figure 21). Encounter probabilities were predicted to be high around the larger islands in the AI,
981 and to be low in deeper areas and in the passes, similar to earlier life stages (Figure 22).

982 **Essential fish habitat of settled early juvenile, subadult, and adult flathead sole in the Aleutian**
983 **Islands –**

984 The habitat related abundance predictions based on RACE-GAP summer bottom trawl data
985 (1991–2019) were translated into EFH area and subareas (Figure 23). The EFH areas for all three life
986 stages show the same overall pattern, with hot spots around Unalaska, Atka, and Agattu Islands. Although
987 the settled early juvenile model did not perform well in terms of Spearman’s ρ , high scores for AUC and
988 PDE suggest it is still reliable for describing long-term average bottom trawl catches. Additionally, the
989 correspondence between the early juvenile maps and the maps made by the better performing subadult
990 and adult models suggests that the early juvenile ensemble still provides useful predictions. The settled
991 early juvenile EFH area is much smaller than the EFH area for other life stages and is restricted to those
992 few spots. By contrast, subadult and adult EFH descriptions extended much further and covered most
993 areas with depths <300 m. Areas around the major passes in the islands, such as Seguam and Amchitka
994 Passes, were not EFH. Subadult and adult EFH maps were nearly identical, and overall, this species does
995 not seem to change habitats as it grows and reaches maturity.

996 Table 7. Constituent species distribution models (SDMs) used to construct Essential Fish Habitat (EFH)
 997 for a) settled early juvenile, b) subadult, and c) adult flathead sole: MaxEnt = Maximum entropy;
 998 paGAM = presence-absence generalized additive model; hGAM = hurdle GAM; GAM_P = standard
 999 Poisson GAM; and GAM_{nb} = standard negative-binomial GAM. Ensemble performance (ρ = Spearman's
 1000 rank correlation coefficient), root-mean-square-error (RMSE), the area under the receiver operating
 1001 characteristic (AUC), and the Poisson deviance explained (PDE) were generated from k-fold cross-
 1002 validation. The "--" in a field indicates that this SDM was not included in the final ensemble.

1003 **a) settled early juvenile flathead sole**

Models	RMSE	Relative Weight	ρ	AUC	PDE	EFH area (km ²)
MaxEnt	9.27	0.225	0.258	0.906	0.705	37,400
paGAM	6.88	0.409	0.290	0.941	0.701	29,700
hGAM	--	0	--	--	--	--
GAM _P	7.27	0.366	0.310	0.918	0.841	12,600
GAM _{nb}	11.1	0	--	--	--	--
ensemble	5.46	1	0.279	0.939	0.810	31,200

1004 **b) subadult flathead sole**

Models	RMSE	Relative Weight	ρ	AUC	PDE	EFH area (km ²)
MaxEnt	97.8	0.200	0.572	0.878	0.436	70,400
paGAM	94.9	0.211	0.608	0.902	0.462	72,000
hGAM	78.9	0.307	0.561	0.902	0.770	49,600
GAM _P	82.3	0.282	0.533	0.845	0.768	45,400
GAM _{nb}	111.0	0	--	--	--	--
ensemble	68.8	1	0.599	0.893	0.768	69,000

1005 **c) adult flathead sole**

Models	RMSE	Relative Weight	ρ	AUC	PDE	EFH area (km ²)
MaxEnt	14.7	0.245	0.522	0.839	0.248	68,700
paGAM	14.5	0.253	0.570	0.870	0.358	68,800
hGAM	14.6	0.248	0.530	0.869	0.481	58,500
GAM _P	14.4	0.254	0.524	0.834	0.480	59,600
GAM _{nb}	15.1	0	--	--	--	--
ensemble	13.8	1	0.564	0.863	0.467	68,300

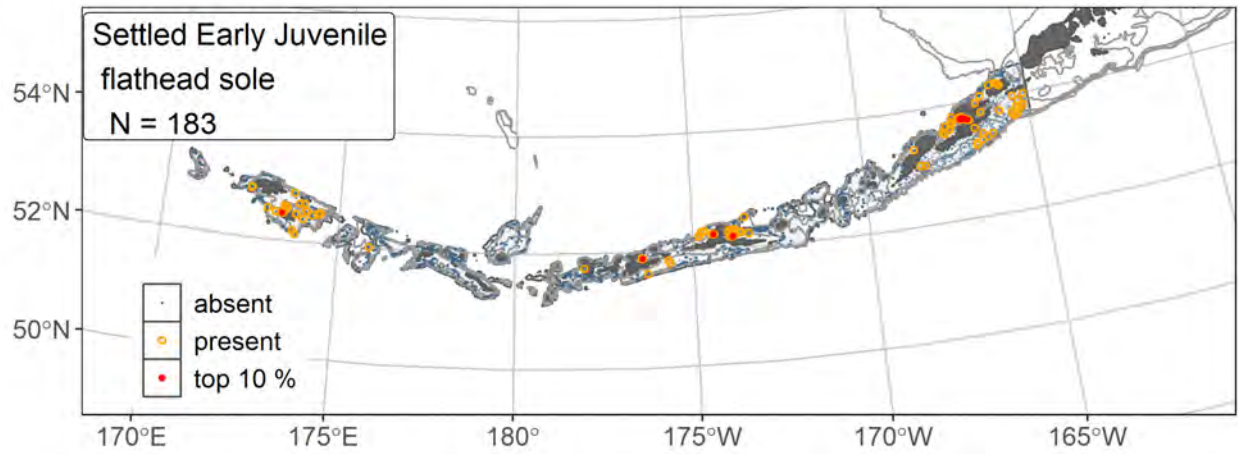
1006

1007 Table 8. Covariates retained in the a) settled early juvenile, b) subadult, and c) adult flathead sole species
 1008 distribution model (SDM) final ensembles, the percent contribution to the ensemble deviance explained
 1009 by each, and the cumulative percent deviance: SD = standard deviation, and BPI = bathymetric position
 1010 index.

flathead sole	Covariate	% Contribution	Cumulative % Contribution
a) settled early juvenile	position	24.0	24.0
	bottom depth	17.8	41.9
	BPI	12.4	54.3
	tidal maximum	11.8	66.1
	current	7.3	73.4
	pennatulacean presence	5.4	78.9
	slope	4.4	83.3
	current SD	4.1	87.4
	aspect east	3.3	90.7
	aspect north	2.3	93.0
	rockiness	1.9	94.9
	bottom temperature	1.8	96.7
	curvature	1.5	98.2
	coral presence	1.4	99.6
	sponge presence	0.4	100
b) subadult	position	23.0	23.0
	bottom depth	16.1	39.1
	tidal maximum	14.1	53.2
	current SD	9.3	62.5
	current	9.1	71.6
	aspect north	4.8	76.4
	rockiness	4.5	80.9
	slope	4.2	85.1
	BPI	4.1	89.2
	pennatulacean presence	3.0	92.2
	aspect east	2.4	94.6
	bottom temperature	1.7	96.3
	curvature	1.5	97.8
	sponge presence	1.1	98.9
	coral presence	1.1	100
c) adult	position	30.3	30.3
	bottom depth	14.7	45.0
	tidal maximum	14.3	59.3
	current	8.6	67.9
	current SD	5.9	73.8
	slope	3.6	77.4

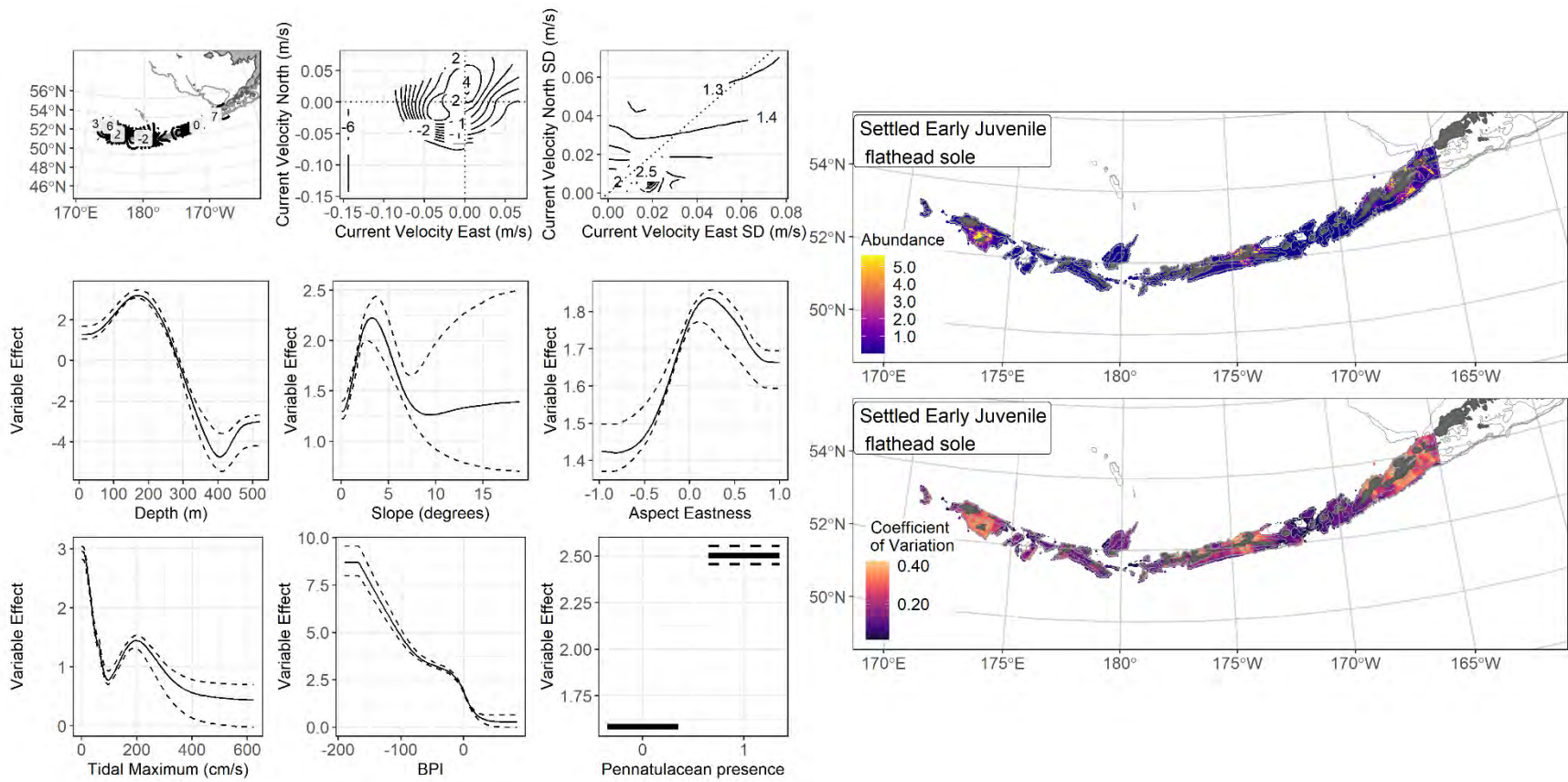
flathead sole	Covariate	% Contribution	Cumulative % Contribution
	aspect east	3.6	81.0
	BPI	3.4	84.4
	aspect north	3.2	87.6
	pennatulacean presence	2.8	90.4
	coral presence	2.5	92.9
	bottom temperature	2.4	95.3
	curvature	2.0	97.3
	rockiness	1.8	99.1
	sponge presence	0.9	100

1011



1012

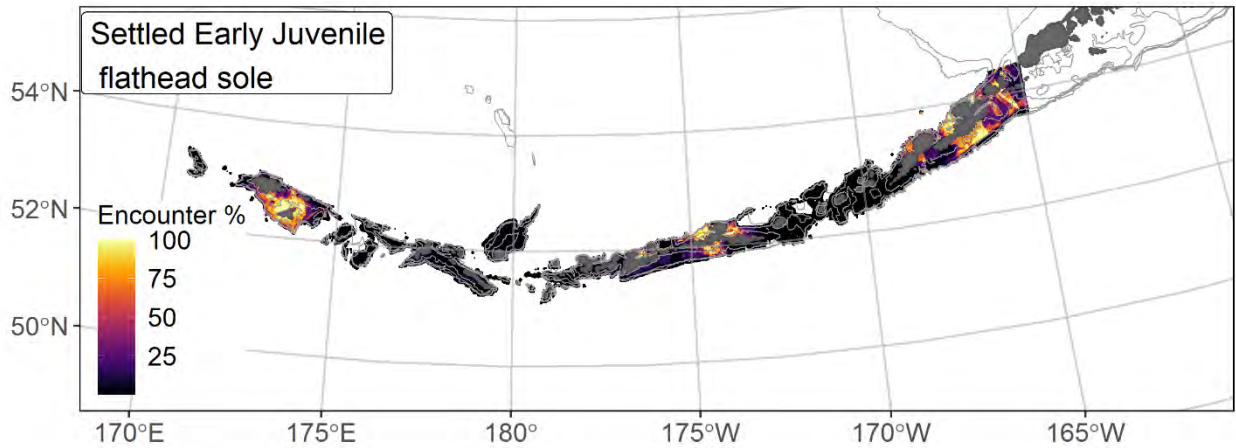
1013 Figure 14. Distribution of settled early juvenile flathead sole catches (N = 183) in 1991–2019 AFSC
 1014 RACE-GAP summer bottom trawl surveys of the Aleutian Islands with the 100 m, 300 m, and 500 m
 1015 isobaths indicated; filled red circles indicate locations in top 10% of overall abundance, open orange
 1016 circles indicate presence in remaining catches, and small blue dots indicate absence.



1017

1018 Figure 15. The top nine covariate effects (left panel) on ensemble-predicted settled early juvenile flathead sole numerical abundance across the

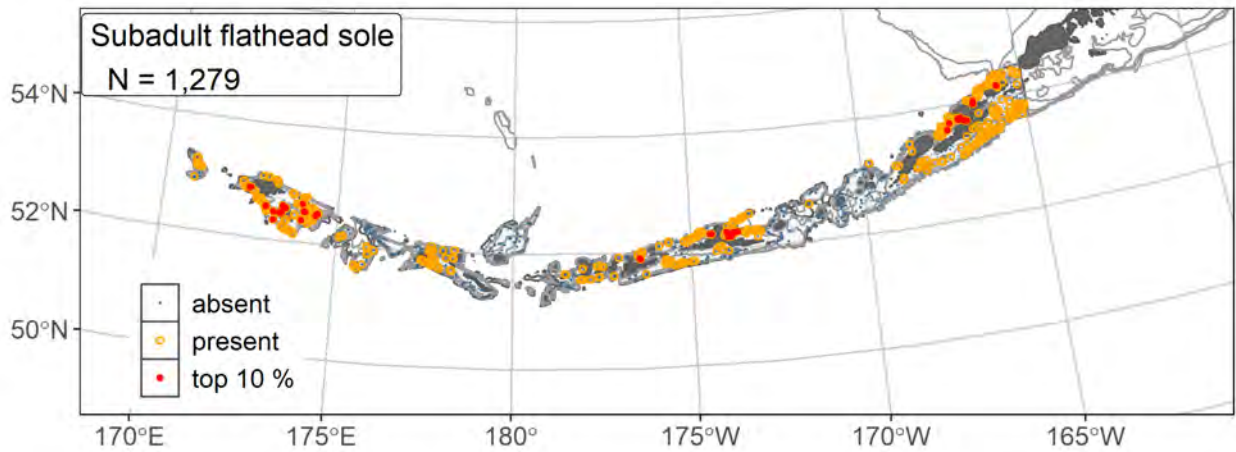
1019 Aleutian Islands (upper right panel) alongside the coefficient of variation of the ensemble predictions (lower right panel).



1020

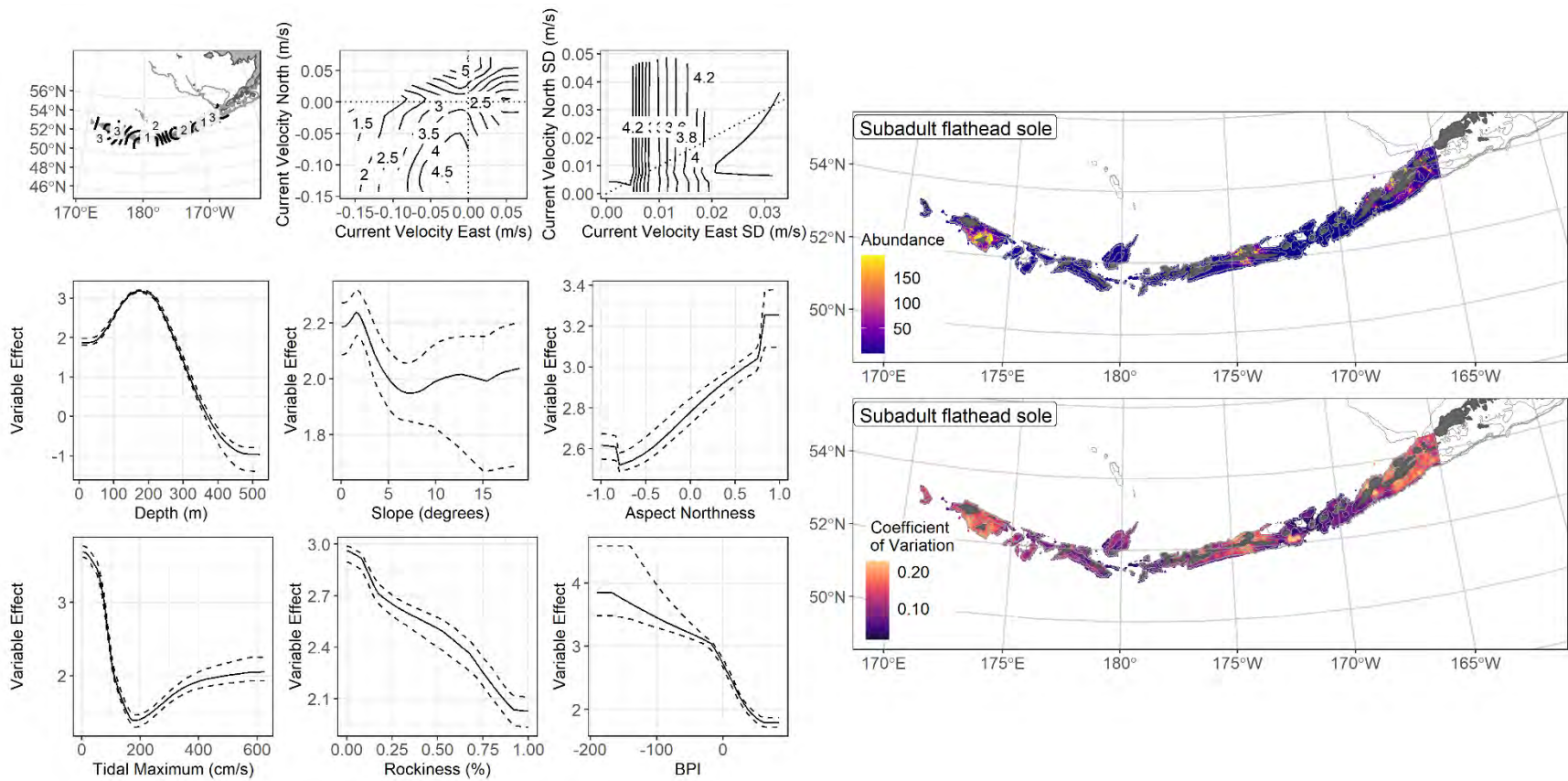
1021 Figure 16. Encounter probability of settled early juvenile flathead sole from AFSC RACE-GAP summer
 1022 bottom trawl surveys (1991–2019) of the Aleutian Islands with the 100 m, 300 m, and 500 m isobaths
 1023 indicated.

1024



1025

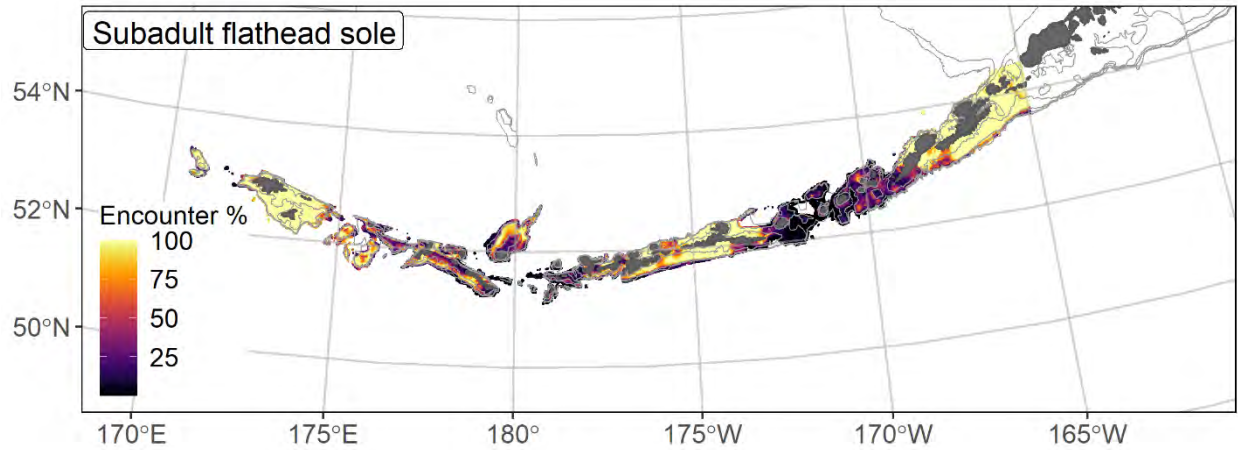
1026 Figure 17. Distribution of subadult flathead sole catches (N = 1,279) in 1991–2019 AFSC RACE-GAP
 1027 summer bottom trawl surveys of the Aleutian Islands with the 100 m, 300 m, and 500 m isobaths
 1028 indicated; filled red circles indicate locations in top 10% of overall abundance, open orange circles
 1029 indicate presence in remaining catches, and small blue dots indicate absence.



1030

1031 Figure 18. The top nine covariate effects (left panel) on ensemble-predicted subadult flathead sole numerical abundance across the Aleutian

1032 Islands (upper right panel) alongside the coefficient of variation of the ensemble predictions (lower right panel).

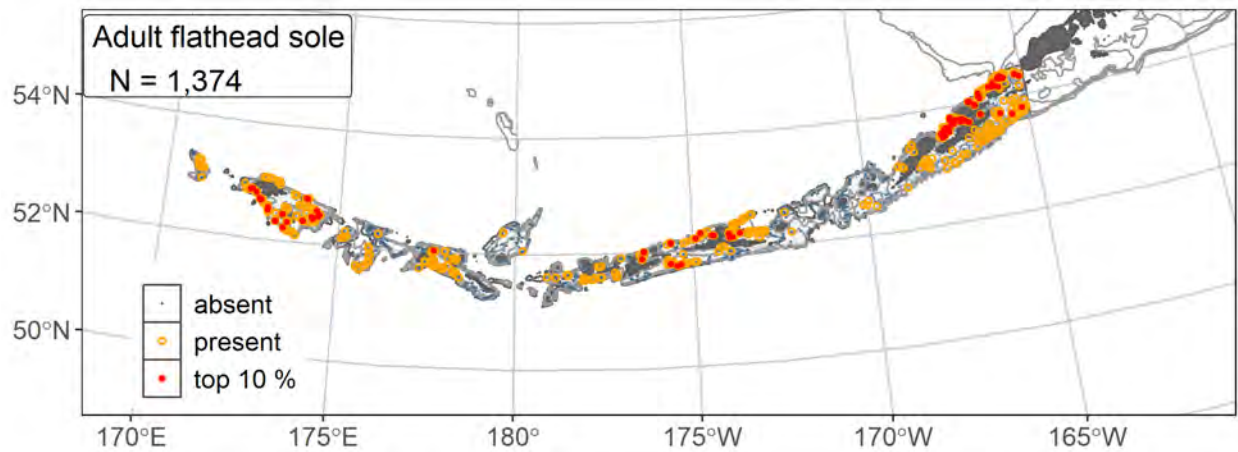


1033

1034 Figure 19. Encounter probability of subadult flathead sole from AFSC RACE-GAP summer bottom trawl

1035 surveys (1991–2019) of the Aleutian Islands with the 100 m, 300 m, and 500 m isobaths indicated.

1036



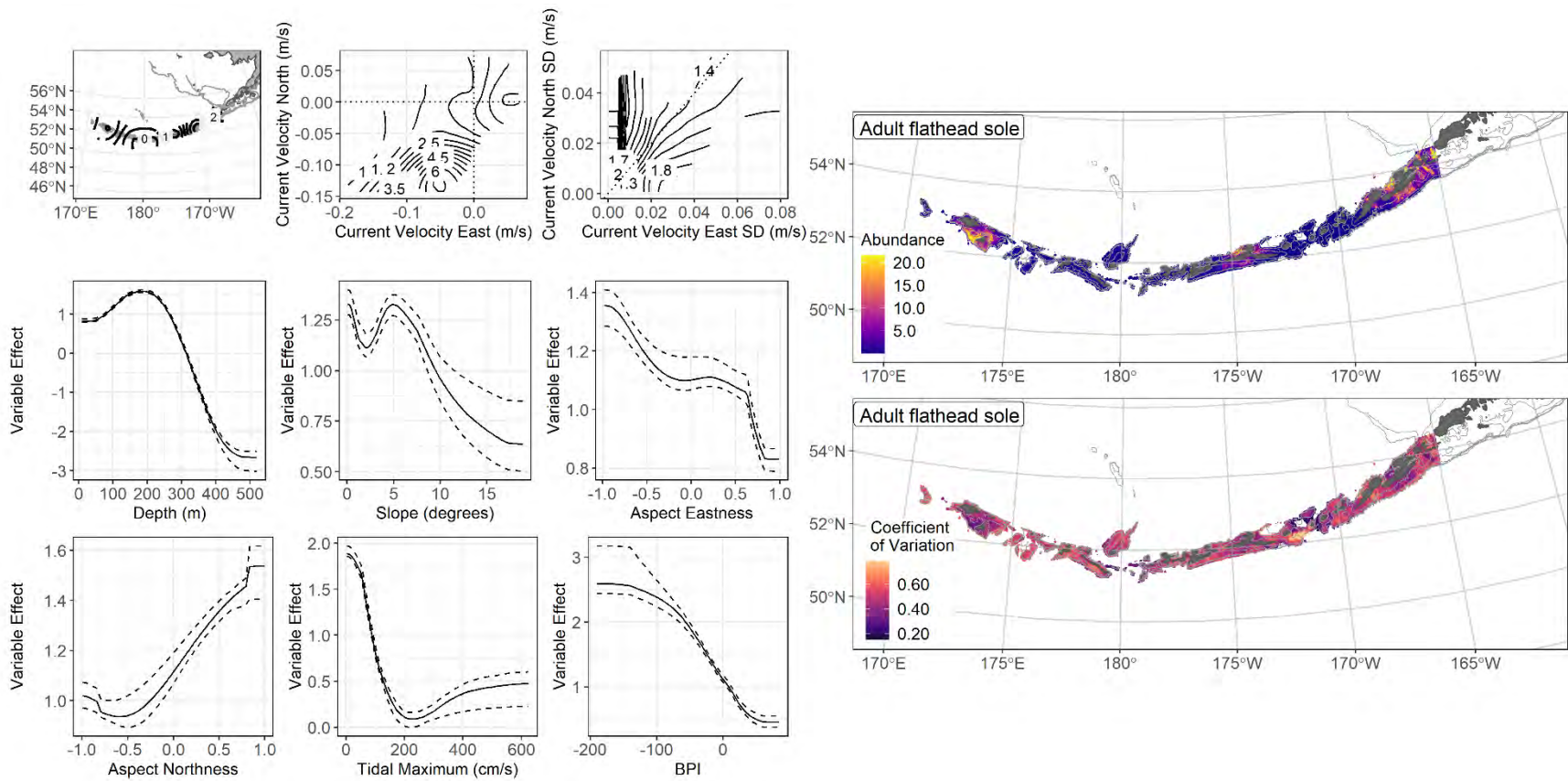
1037

1038 Figure 20. Distribution of adult flathead sole catches (N = 1,374) in 1991–2019 AFSC RACE-GAP

1039 summer bottom trawl surveys of the Aleutian Islands with the 100 m, 300 m, and 500 m isobaths

1040 indicated; filled red circles indicate locations in top 10% of overall abundance, open orange circles

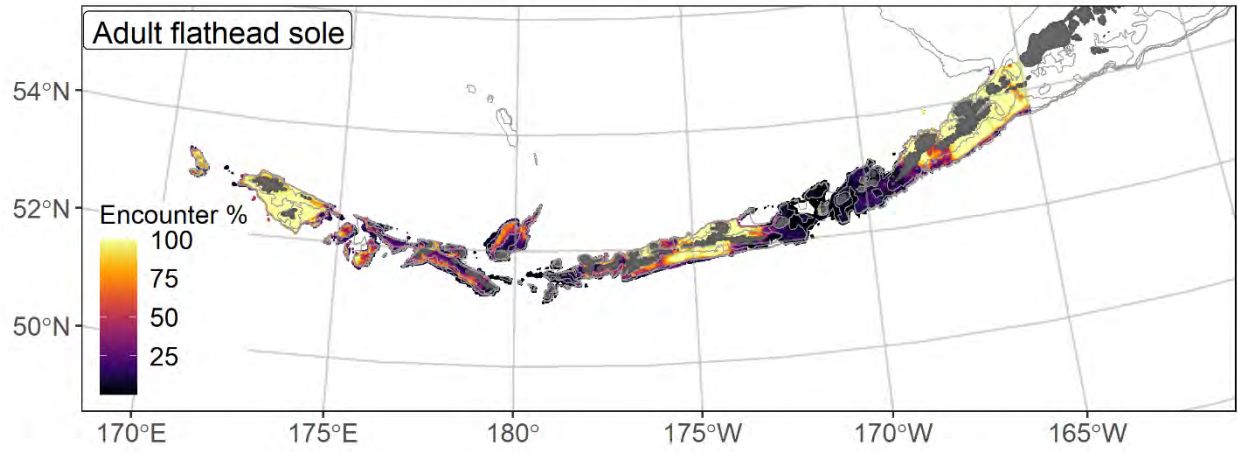
1041 indicate presence in remaining catches, and small blue dots indicate absence.



1042

1043 Figure 21. The top nine covariate effects (left panel) on ensemble-predicted adult flathead sole numerical abundance across the Aleutian Islands

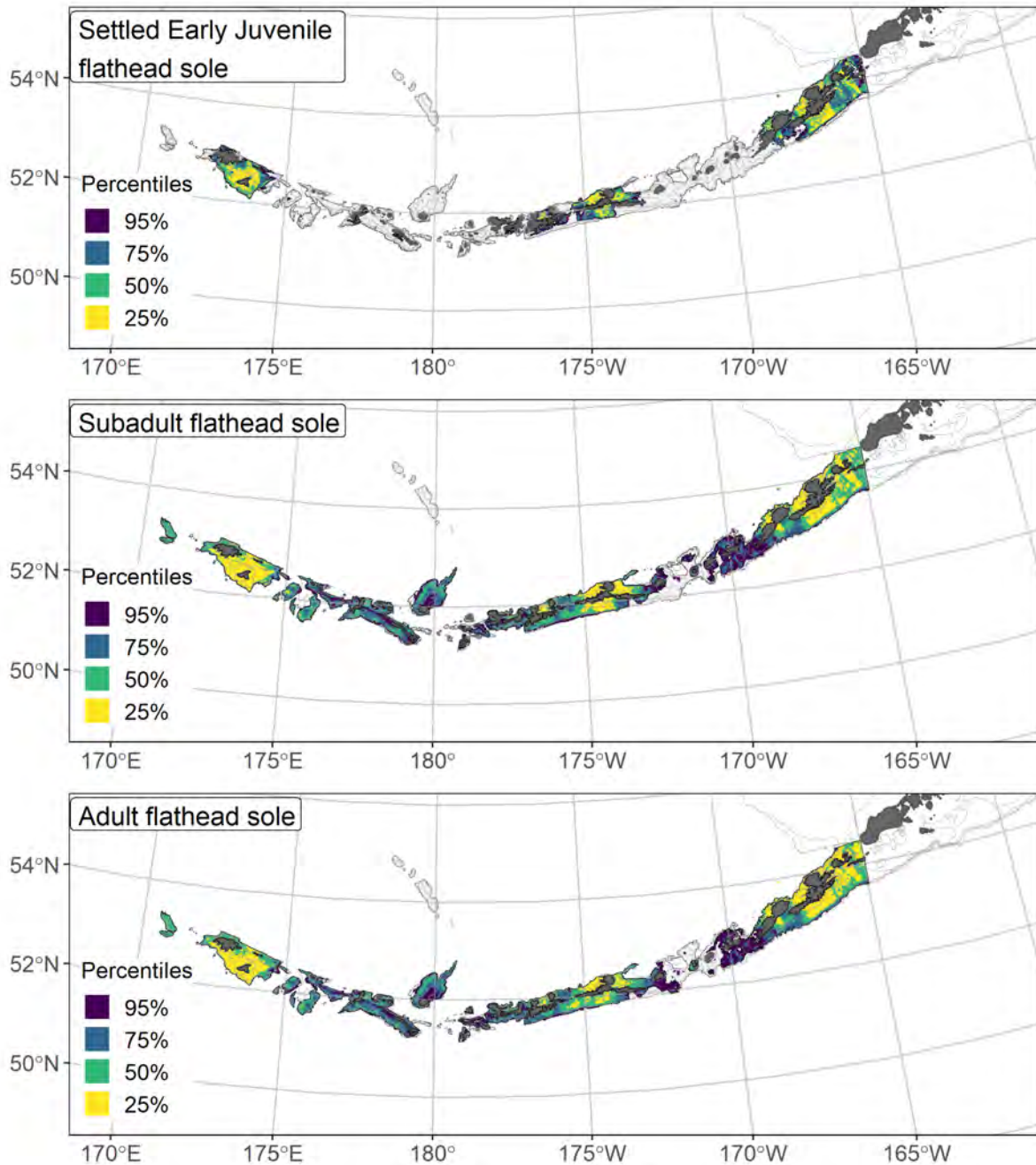
1044 (upper right panel) alongside the coefficient of variation of the ensemble predictions (lower right panel)



1045

1046 Figure 22. Encounter probability of adult flathead sole from AFSC RACE-GAP summer bottom trawl

1047 surveys (1991–2019) of the Aleutian Islands with the 100 m, 300 m, and 500 m isobaths indicated.



1048

1049 Figure 23. Essential fish habitat (EFH area) defined as the top 95% of numerical abundance predictions

1050 from a habitat-based ensemble fitted to settled early juvenile (top), subadult (middle), and adult (bottom)

1051 flathead sole distribution and abundance in AFSC RACE-GAP summer bottom trawl surveys (1991–

1052 2019) with 100 m, 300 m, and 500 m isobaths indicated; internal to the EFH map are the subareas of the

1053 top 25% (EFH hot spots), top 50% (core EFH area), and top 75% (principal EFH area) of habitat related,

1054 ensemble-predicted numerical abundance.

1055 **Greenland turbot (*Reinhardtius hippoglossoides*)**

1056 Greenland turbot (*Reinhardtius hippoglossoides*, a.k.a. Greenland halibut) is found in both the
1057 northern Pacific and northern Atlantic oceans, although it is mostly absent from the Arctic ocean north of
1058 Canada and Russia (Alton et al. 1988). Adults may be over a meter long and tend to prefer deep water
1059 along the continental slope, sometimes at depths greater than 2000m. Spawning occurs along the
1060 continental slope and in deep canyons, with eggs and larvae typically released in deep water and
1061 gradually being transported inshore (Sohn et al. 2010). Greenland turbot become sexually mature (L_{50})
1062 around 580 mm F.L., although they appear to have a complex spawning cycle and do not necessarily
1063 spawn in the first year of maturity (Tenbrink et al. 2021). Unlike most flatfish, this species is thought to
1064 forage primarily in the middle of the water column and is less dependent on benthic prey than other
1065 groundfish species (Alton et al. 1988). There is evidence that at least some individuals undertake seasonal
1066 migrations to feed in shallower water during the summer (Siwicke and Coutre 2020). In the BSAI region,
1067 Greenland turbot are managed as a single stock with a biennial assessment (Bryan et al. 2020a). Due to
1068 lack of data, only the adult life stage was modeled.

1069 **Adult Greenland turbot distribution and predicted abundance from RACE-GAP summer bottom**
1070 **trawl surveys in the Aleutian Islands–**

1071 Adult Greenland turbot were occasionally caught in the RACE-GAP summer bottom trawl survey
1072 and were usually found on the north side of the islands in deep water (Figure 24). Large catches were
1073 concentrated around the Petrel Bank area and north of Atka Island. The final ensemble contains two
1074 SDMs with the GAM_p given slightly more weight than the $paGAM$, and it demonstrated an overall good
1075 to excellent fit to the data (Table 9). The ensemble shows excellent performance when predicting
1076 presence or absence ($AUC = 0.960$) and explained most of the deviance in the observations
1077 ($PDE = 0.776$). It also achieved a lower but still good score in terms of its ability to rank catches
1078 ($\rho = 0.403$). In summary, Greenland turbot have a distinct and easily recognized distribution in the
1079 habitat, and despite only a moderate amount of data, the predictions of this ensemble fit the data well.

1080 Bottom depth was the most important covariate and accounted for 45.7% of the total deviance explained,
1081 but bottom temperature, current and geographic position also made larger than average contributions
1082 (Table 10). In general, abundance was expected to be higher in locations with high bottom depth, low
1083 temperature, weak currents, and further west in terms of longitude (Figure 25). The predicted abundance
1084 map shows that almost all Greenland turbot in the AI are predicted below the 300 m depth contour, with
1085 the highest densities occurring around Petrel Bank and Seguam Pass (Figure 25). The predicted CV of
1086 abundance was close to zero in all shallow areas where this species is always absent, and it was elevated
1087 along the slope and in the passes in the archipelago, reflecting that this species has a well-defined range
1088 but is variable within that range (Figure 25). The map of encounter probability shows a high chance of
1089 catching these species in most slope areas below 300 m, and nearly 100% in the major passes (Figure 26).

1090 **Essential fish habitat of adult Greenland turbot in the Aleutian Islands –**

1091 The habitat related abundance predictions based on RACE-GAP summer bottom trawl data
1092 (1991–2019) were translated into EFH area and subareas (Figure 27). The adult EFH area consists of hot
1093 spots around Seguam Pass and Petrel Bank, and a thin ribbon that runs along the continental slope
1094 elsewhere. The EFH area closely follows the 300 m depth contour, and very few shallow areas qualify
1095 and EFH for this species.

1096 Table 9. Constituent species distribution models (SDMs) used to construct Essential Fish Habitat (EFH)
 1097 for a) adult Greenland turbot: MaxEnt = Maximum entropy; paGAM = presence-absence generalized
 1098 additive model; hGAM = hurdle GAM; GAM_p = standard Poisson GAM; and GAM_{nb} = standard
 1099 negative-binomial GAM. Ensemble performance (ρ = Spearman's rank correlation coefficient), root-
 1100 mean-square-error (RMSE), the area under the receiver operating characteristic (AUC), and the Poisson
 1101 deviance explained (PDE) were generated from k-fold cross-validation. The "--" in a field indicates that
 1102 this SDM was not included in the final ensemble.

1103 **a) adult Greenland turbot**

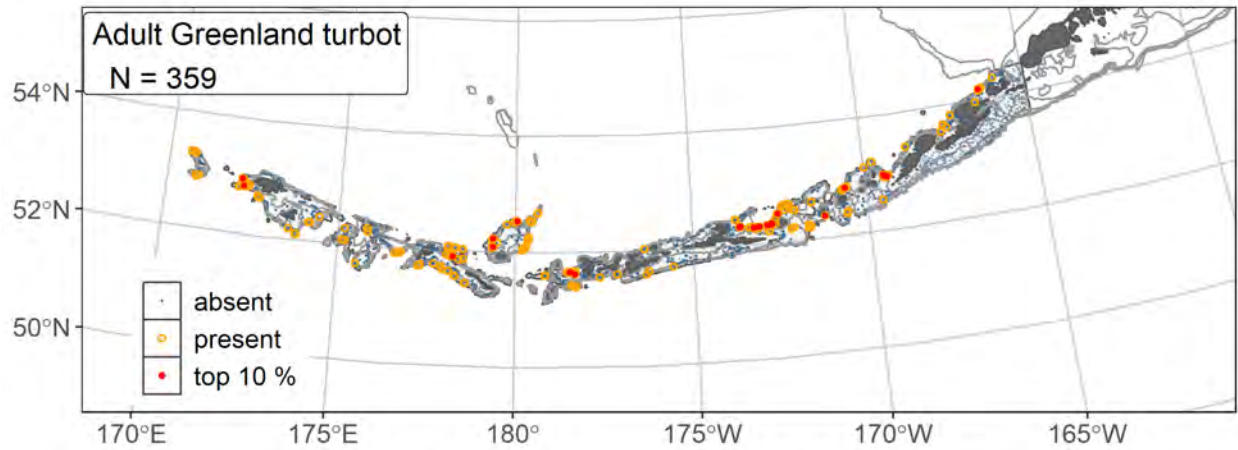
Models	RMSE	Relative Weight	ρ	AUC	PDE	EFH area (km²)
MaxEnt	--	0	--	--	--	--
paGAM	12.7	0.456	0.403	0.963	0.610	30,900
hGAM	--	0	--	--	--	--
GAM _p	11.0	0.544	0.416	0.943	0.737	18,300
GAM _{nb}	12.1	0	--	--	--	--
ensemble	6.8	1	0.403	0.960	0.776	26,500

1104

1105 Table 10. Covariates retained in the a) adult Greenland turbot species distribution model (SDM) final
 1106 ensembles, the percent contribution to the ensemble deviance explained by each, and the cumulative
 1107 percent deviance: SD = standard deviation, and BPI = bathymetric position index.

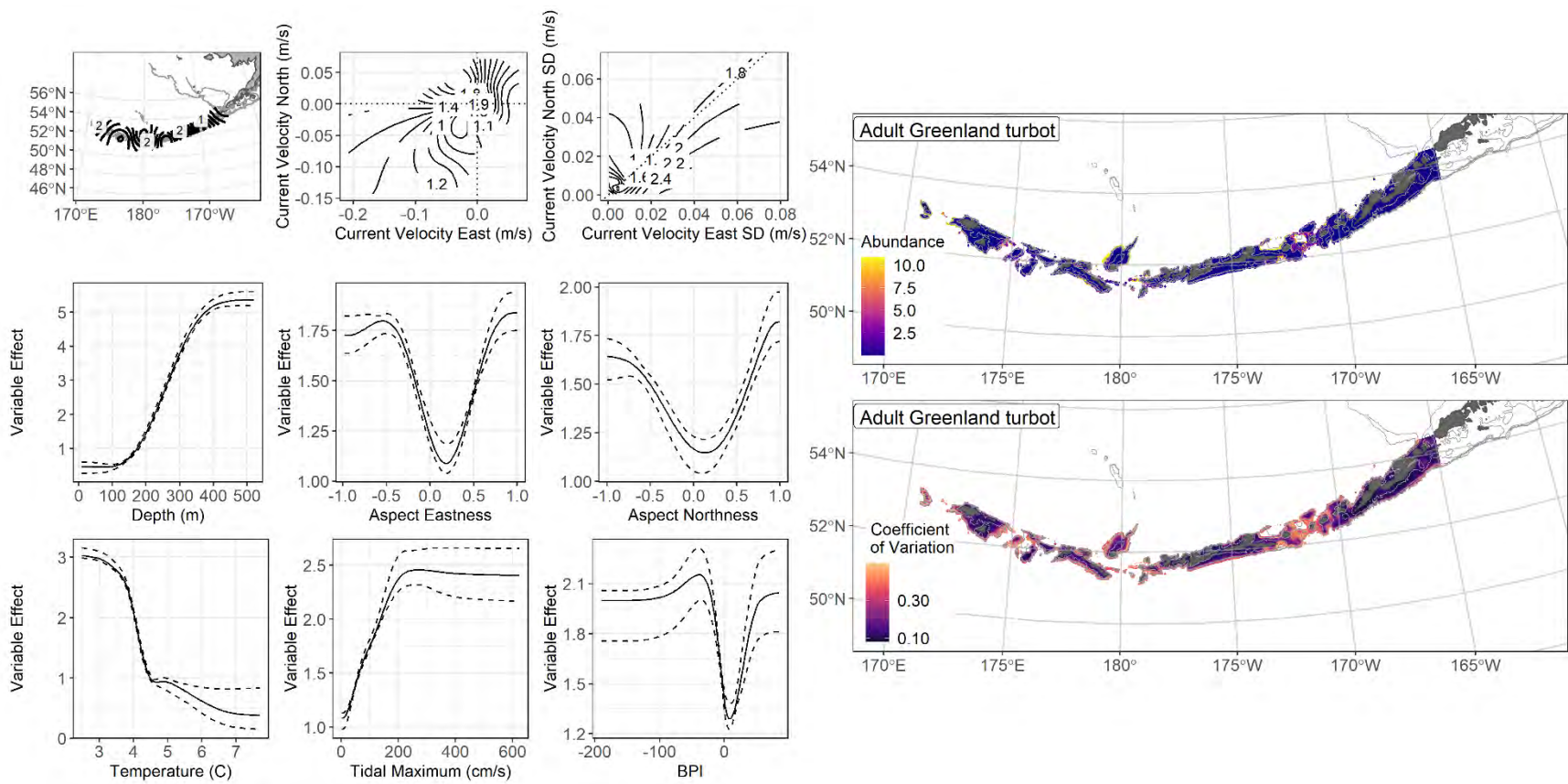
Greenland turbot a) adult	Covariate	% Contribution	Cumulative % Contribution
	bottom depth	45.7	45.7
	bottom temperature	12.7	58.3
	current	8.4	66.7
	position	8.1	74.8
	current SD	6.0	80.8
	BPI	5.5	86.3
	tidal maximum	5.4	91.7
	aspect east	2.6	94.3
	aspect north	2.6	96.9
	slope	1.0	97.9
	coral presence	0.6	98.5
	rockiness	0.5	99.0
	sponge presence	0.5	99.5
	curvature	0.4	99.9
	pennatulacean presence	0.1	100

1108



1109

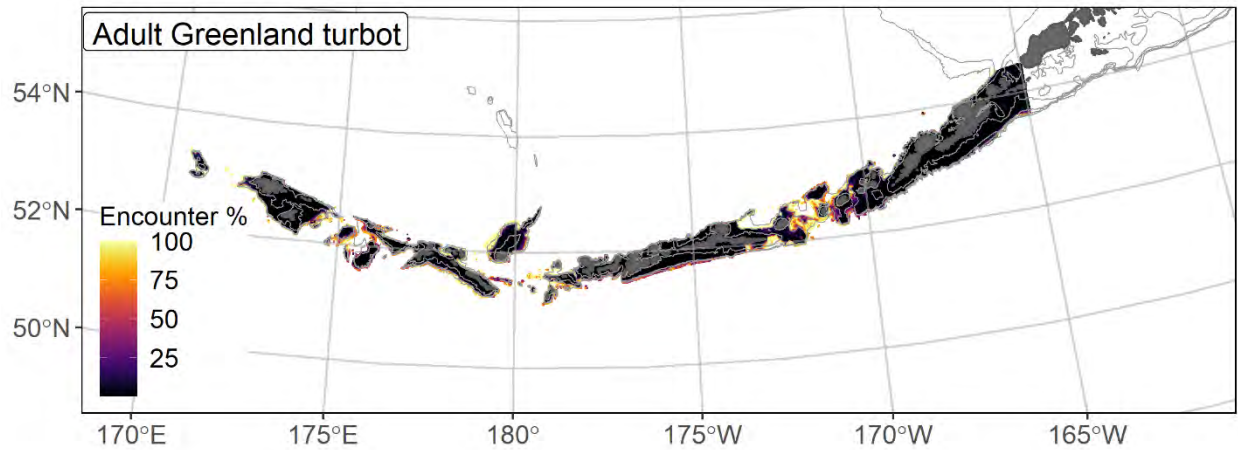
1110 Figure 24. Distribution of adult Greenland turbot catches (N = 359) in 1991–2019 AFSC RACE-GAP
 1111 summer bottom trawl surveys of the Aleutian Islands with the 100 m, 300 m, and 500 m isobaths
 1112 indicated; filled red circles indicate locations in top 10% of overall abundance, open orange circles
 1113 indicate presence in remaining catches, and small blue dots indicate absence.



1114

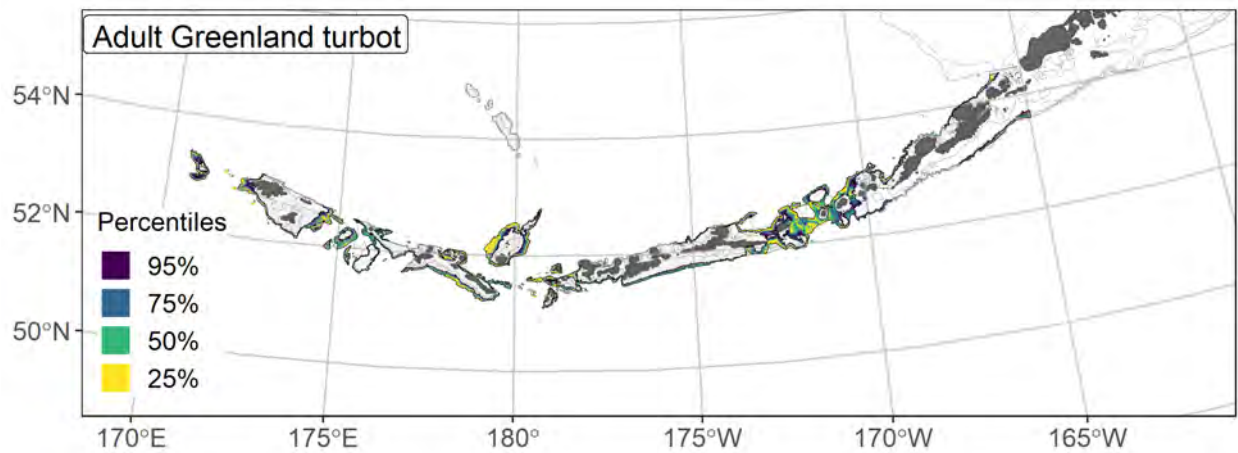
1115 Figure 25. The top nine covariate effects (left panel) on ensemble-predicted adult Greenland turbot numerical abundance across the Aleutian

1116 Islands (upper right panel) alongside the coefficient of variation of the ensemble predictions (lower right panel).



1117
 1118 Figure 26. Encounter probability of adult Greenland turbot from AFSC RACE-GAP summer bottom
 1119 trawl surveys (1991–2019) of the Aleutian Islands with the 100 m, 300 m, and 500 m isobaths indicated.

1120



1121
 1122 Figure 27. Essential fish habitat (EFH area) defined as the top 95% of numerical abundance predictions
 1123 from a habitat-based ensemble fitted to adult Greenland turbot distribution and abundance in AFSC
 1124 RACE-GAP summer bottom trawl surveys (1991–2019) with 100 m, 300 m, and 500 m isobaths
 1125 indicated; internal to the EFH map are the subareas of the top 25% (EFH hot spots), top 50% (core EFH
 1126 area), and top 75% (principal EFH area) of habitat related, ensemble-predicted numerical abundance..

1127 **Kamchatka flounder (*Atheresthes evermani*)**

1128 Kamchatka flounder (*Atheresthes evermani*) is large-bodied flatfish found from the Sea of
1129 Okhotsk through the Bering Sea and into the western GOA (Zimmermann and Goddard 1996). In U.S.
1130 waters, they occur in high concentrations in the western AI and in lower concentrations east of there
1131 (Bryan et al. 2020b). The species is morphologically similar to the more common arrowtooth flounder (*A.*
1132 *stomias*), and the two species were not routinely distinguished in assessment surveys until 1992
1133 (Bryan et al. 2018). The majority of Kamchatka flounder become sexually mature at a relatively large size
1134 ($L_{50} = 550$ mm F.L.; Stark 2012b), and can eventually grow to be 860 mm F.L. or more
1135 (Mecklenburg et al. 2005). Given its large size and predatory habits, this species is thought to be an
1136 important part of the marine food web and is a major predator of juvenile walleye pollock (*Gadus*
1137 *chalcogrammus*; Yang and Livingston 1986). This species was managed as a stock complex with
1138 arrowtooth flounder until 2011, when the start of a directed fishery for Kamchatka flounder prompted the
1139 development of separate management plans (Bryan et al. 2020b).

1140 **Subadult Kamchatka flounder distribution and predicted abundance from RACE-GAP summer**
1141 **bottom trawl surveys in the Aleutian Islands–**

1142 Subadult Kamchatka flounder catches were very common throughout the RACE-GAP summer
1143 survey areas (Figure 28), though they were less common in the eastern AI. The final ensemble contains
1144 three SDMs with the hGAM and GAM_p given more weight than the paGAM, and it demonstrated good
1145 performance across all three fit metrics (Table 11). As such, it is expected to make accurate predictions of
1146 both presence (AUC = 0.799) and abundance ($\rho = 0.566$; PDE = 0.503). Geographic position and bottom
1147 current were the most important covariates, but bottom depth, current variability, and terrain aspect were
1148 also important (Table 12). In general, high abundance was predicted for areas further east, with northerly
1149 currents, and with bottom depths between 150–300 m (Figure 29). Subadult Kamchatka flounder also
1150 tend to be associated with north facing slopes. The highest densities of this life stage occurred north of
1151 Atka and Adak Islands, as well as around Agattu Island (Figure 29). Subadults showed a preference for

1152 areas on the northern side of the islands, and seemed to occupy habitats where the 100 m depth contour
1153 runs close to the shore. The CV of abundance of variation was homogenous throughout the region
1154 (Figure 29). Predicted encounter probabilities were high in most places west of 170° W, with the
1155 exception of some shallow areas (Figure 30).

1156 **Adult Kamchatka flounder distribution and predicted abundance from RACE-GAP summer**
1157 **bottom trawl surveys in the Aleutian Islands –**

1158 Adult Kamchatka flounder in the RACE-GAP summer survey were less common than subadults,
1159 with low catches in the eastern AI (Figure 31). The final ensemble included just two SDMs that were
1160 given approximately equal weights, and it showed good to excellent performance overall (Table 11). The
1161 ensemble demonstrated good ability to predict high density catches ($\rho = 0.543$), but scored even better in
1162 terms of predicting presence (AUC = 0.897) and deviance explained (PDE = 0.718). Bottom depth was
1163 more important in the model for adults than for subadults and accounted for 39 % of the total deviance
1164 explained (Table 12). Geographic position, bottom current covariates, and terrain aspect were also
1165 important to SDM predictions. High abundance was associated with increasing bottom depth, western
1166 longitudes, southerly currents, and north facing terrain (Figure 32). The predicted abundance map for
1167 adults was much different from the map for subadults; adults were predicted to appear in high numbers
1168 around the deep passes in the island chain, including Seguam Island and to the east and west of the Rat
1169 Islands (Figure 32). The majority of adult abundance was predicted to occur at depths greater than 300 m,
1170 which may indicate that some of this life stage's habitat is outside the survey area. The predicted CV of
1171 abundance was consistently low in shallow water, where adults are usually absent, and higher in deeper
1172 water (Figure 32). Encounter probabilities displayed the same pattern, and were close to zero at most
1173 depths of less than 300 m, and 100% at depths greater than 300 m (Figure 33).

1174 **Essential fish habitat of subadult and adult Kamchatka flounder in the Aleutian Islands –**

1175 The habitat related abundance predictions based on RACE-GAP summer bottom trawl data
1176 (1992–2019) were translated into EFH area and subareas (Figure 34). Subadult Kamchatka flounder were
1177 twice as common in the trawl survey as adults, and had a larger overall EFH area. Subadult EFH hot spots
1178 occurred around Atka Island and the area between Attu and Agattu Islands, as well as Petrel Bank. The
1179 eastern part of the survey area around Unalaska Island and Unimak Pass had some areas of EFH, but with
1180 lower predicted abundance. For adults, EFH hot spots are in the deep passes that cut through the AI such
1181 as Seguam Pass and Buldir Strait. Other areas of EFH occur along the edge of the continental slope. Most
1182 shallow areas, particularly in the eastern AI, do not qualify as EFH.

1183 Table 11. Constituent species distribution models (SDMs) used to construct Essential Fish Habitat (EFH)
 1184 for a) subadult and b) adult Kamchatka flounder: MaxEnt = Maximum entropy; paGAM = presence-
 1185 absence generalized additive model; hGAM = hurdle GAM; GAM_P = standard Poisson GAM; and
 1186 GAM_{nb} = standard negative-binomial GAM. Ensemble performance (ρ = Spearman's rank correlation
 1187 coefficient), root-mean-square-error (RMSE), the area under the receiver operating characteristic (AUC),
 1188 and the Poisson deviance explained (PDE) were generated from k-fold cross-validation. The "--" in a field
 1189 indicates that this SDM was not included in the final ensemble.

1190 **a) subadult Kamchatka flounder**

Models	RMSE	Relative Weight	ρ	AUC	PDE	EFH area (km²)
MaxEnt	--	--	--	--	--	--
paGAM	26.7	0.274	0.595	0.824	0.291	77,700
hGAM	23.3	0.361	0.539	0.824	0.500	77,700
GAM _P	23.2	0.365	0.509	0.764	0.503	76,500
GAM _{nb}	28.7	0	--	--	--	--
ensemble	22.6	1	0.566	0.799	0.503	77,600

1191

1192 **b) adult Kamchatka flounder**

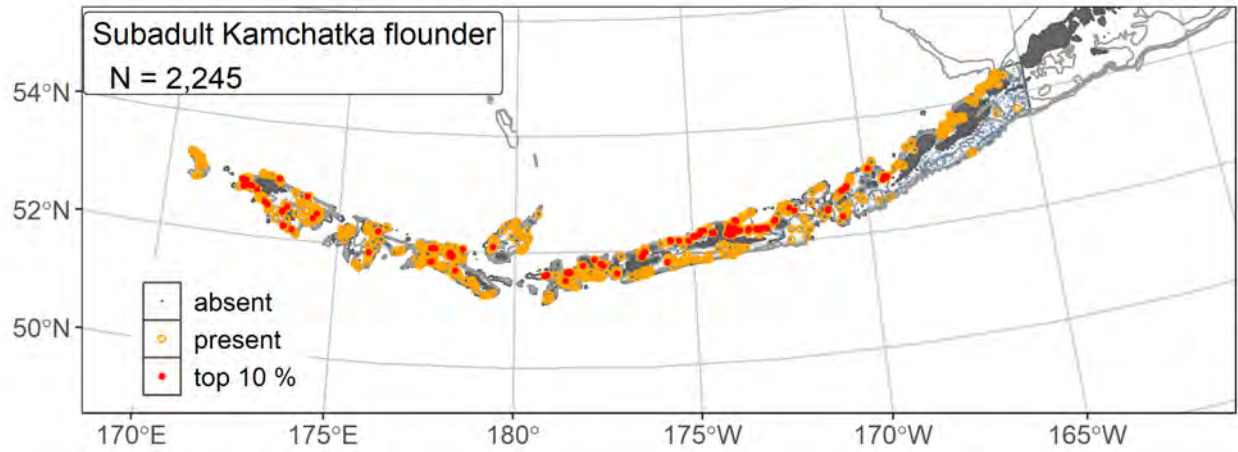
Models	RMSE	Relative Weight	ρ	AUC	PDE	EFH area (km²)
MaxEnt	--	--	--	--	--	--
paGAM	25.3	0.466	0.548	0.902	0.446	66,300
hGAM	41.5	0	--	--	--	--
GAM _P	23.6	0.534	0.469	0.837	0.744	30,800
GAM _{nb}	24.5	0	--	--	--	--
ensemble	20.8	1	0.543	0.897	0.718	57,900

1193

1194 Table 12. Covariates retained in the a) subadult and b) adult Kamchatka flounder species distribution
 1195 model (SDM) final ensembles, the percent contribution to the ensemble deviance explained by each, and
 1196 the cumulative percent deviance: SD = standard deviation, and BPI = bathymetric position index.

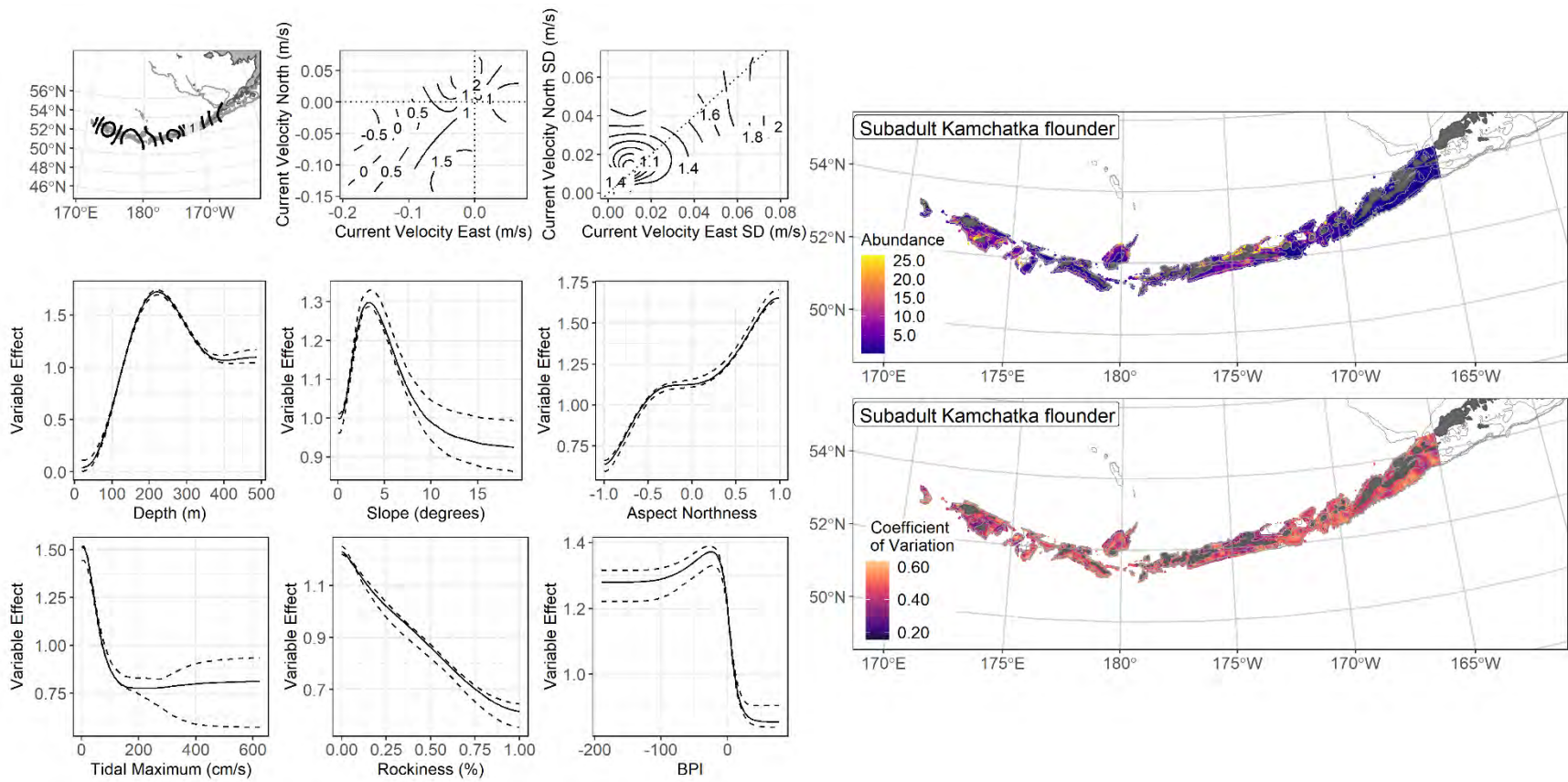
Kamchatka flounder	Covariate	% Contribution	Cumulative % Contribution
a) subadult	position	24.4	24.4
	current	22.7	47.0
	bottom depth	10.9	57.9
	current SD	10.0	67.9
	aspect north	8.8	76.6
	tidal maximum	5.2	81.8
	BPI	4.4	86.2
	slope	3.3	89.5
	rockiness	3.3	92.8
	bottom temperature	2.3	95.1
	aspect east	1.7	96.8
	coral presence	1.5	98.3
	pennatulacean presence	0.7	99.0
	curvature	0.6	99.6
	sponge presence	0.4	100
a) adult	bottom depth	39.0	39.0
	position	19.9	58.8
	current	8.1	66.9
	aspect east	5.8	72.7
	current SD	4.5	77.2
	aspect north	4.3	81.5
	coral presence	3.4	84.9
	tidal maximum	3.2	88.1
	curvature	2.9	91.0
	BPI	2.7	93.7
	slope	2.4	96.1
	bottom temperature	1.5	97.6
	sponge presence	1.2	98.8
	pennatulacean presence	0.8	99.6
	rockiness	0.4	100

1197



1198

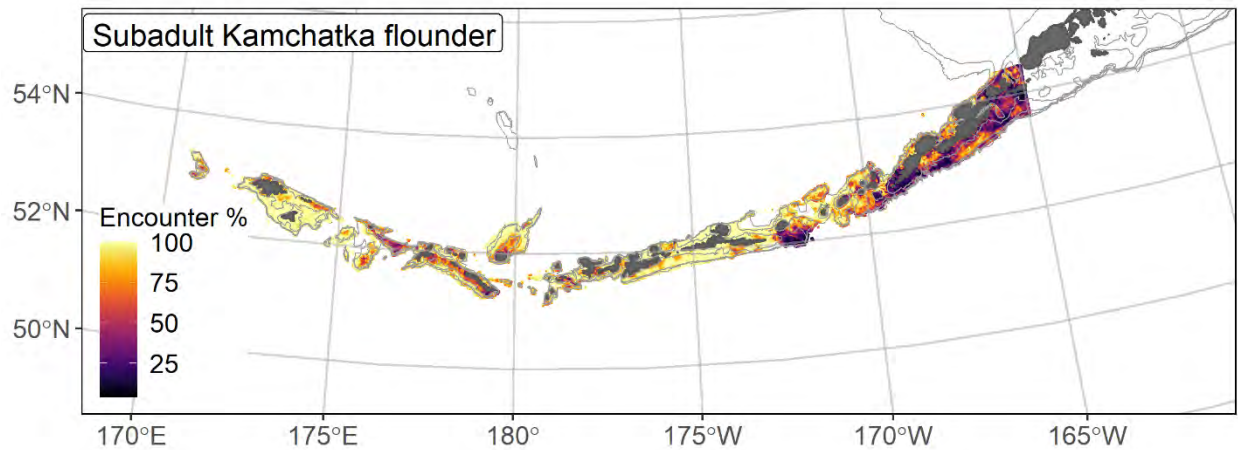
1199 Figure 28. Distribution of subadult Kamchatka flounder catches (N = 2,245) in 1992–2019 AFSC RACE-
 1200 GAP summer bottom trawl surveys of the Aleutian Islands with the 100 m, 300 m, and 500 m isobaths
 1201 indicated; filled red circles indicate locations in top 10% of overall abundance, open orange circles
 1202 indicate presence in remaining catches, and small blue dots indicate absence.



1203

1204 Figure 29. The top nine covariate effects (left panel) on ensemble-predicted subadult Kamchatka flounder numerical abundance across the

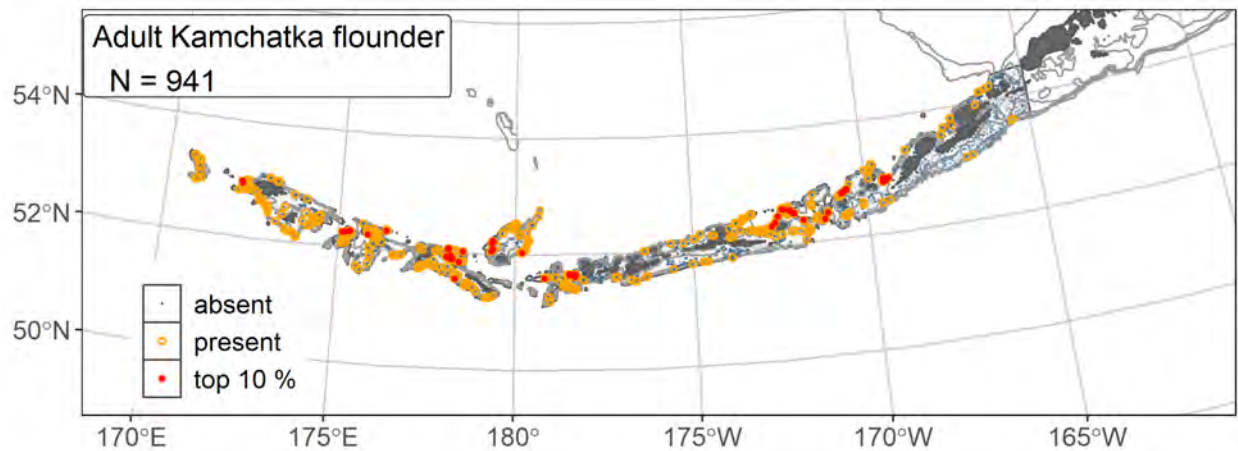
1205 Aleutian Islands (upper right panel) alongside the coefficient of variation of the ensemble predictions (lower right panel).



1206

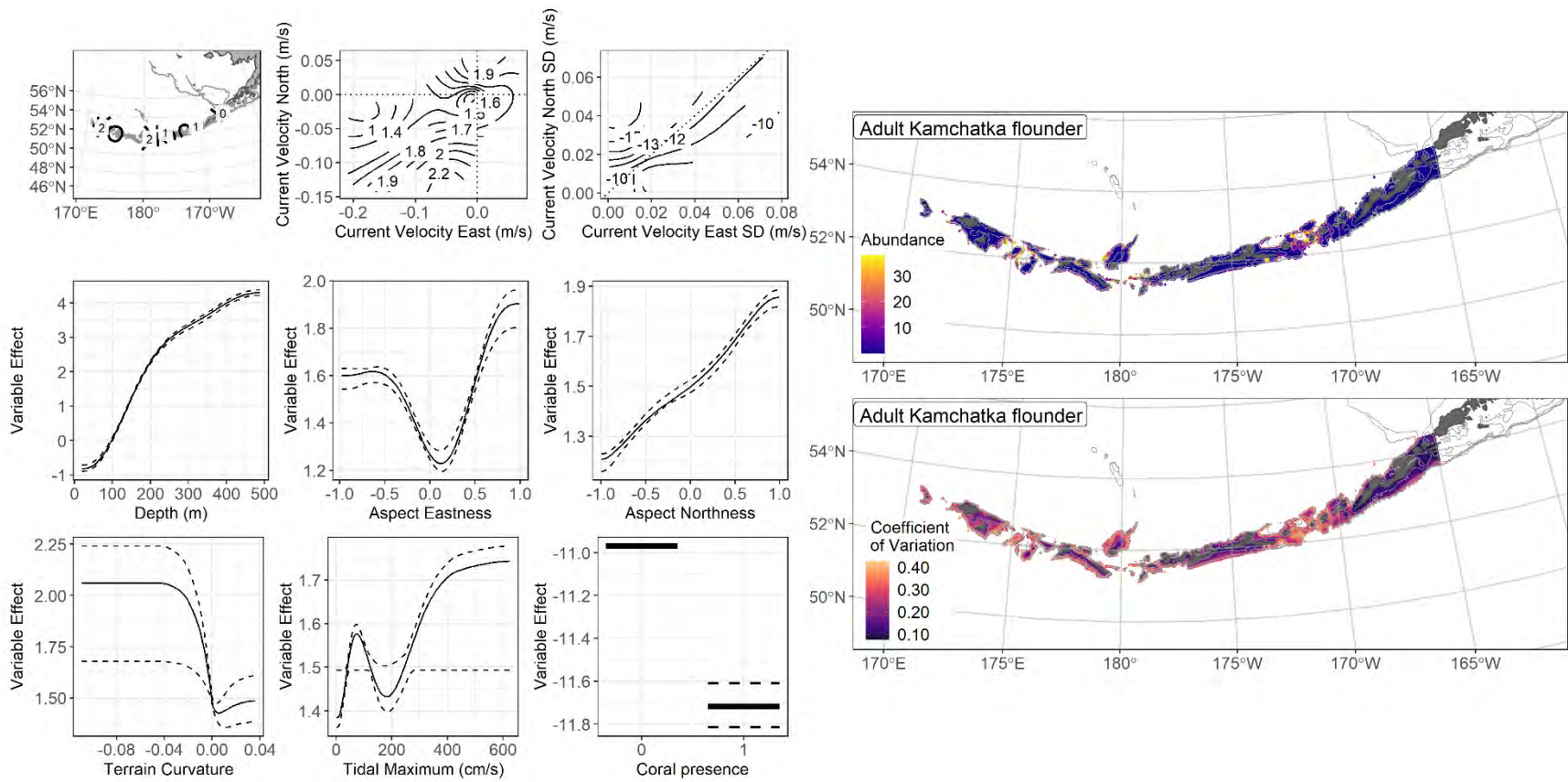
1207 Figure 30. Encounter probability of subadult Kamchatka flounder from AFSC RACE-GAP summer
 1208 bottom trawl surveys (1992–2019) of the Aleutian Islands with the 100 m, 300 m, and 500 m isobaths
 1209 indicated.

1210



1211

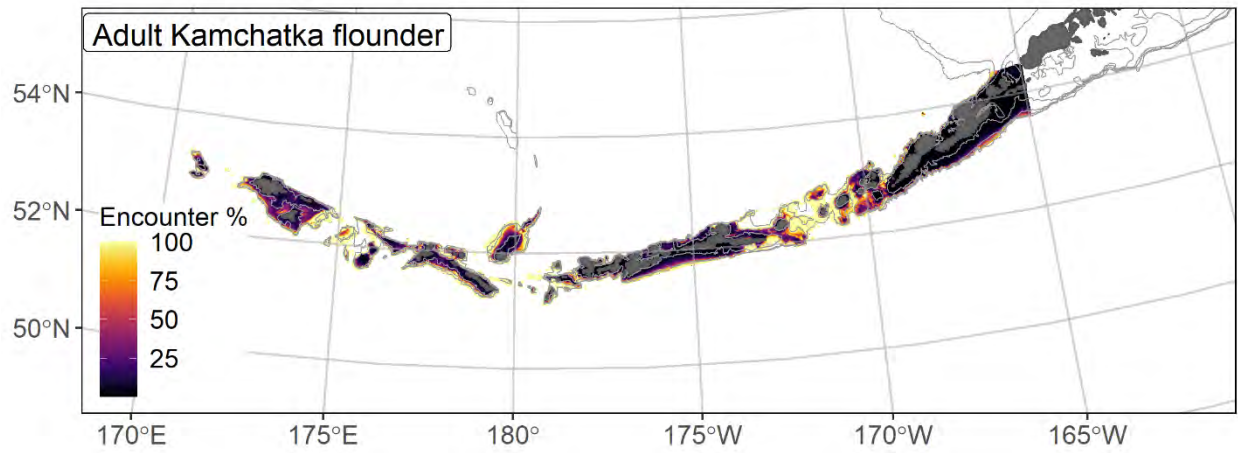
1212 Figure 31. Distribution of adult Kamchatka flounder catches (N = 941) in 1992–2019 AFSC RACE-GAP
 1213 summer bottom trawl surveys of the Aleutian Islands with the 100 m, 300 m, and 500 m isobaths
 1214 indicated; filled red circles indicate locations in top 10% of overall abundance, open orange circles
 1215 indicate presence in remaining catches, and small blue dots indicate absence.



1216

1217 Figure 32. The top nine covariate effects (left panel) on ensemble-predicted adult Kamchatka flounder numerical abundance across the Aleutian

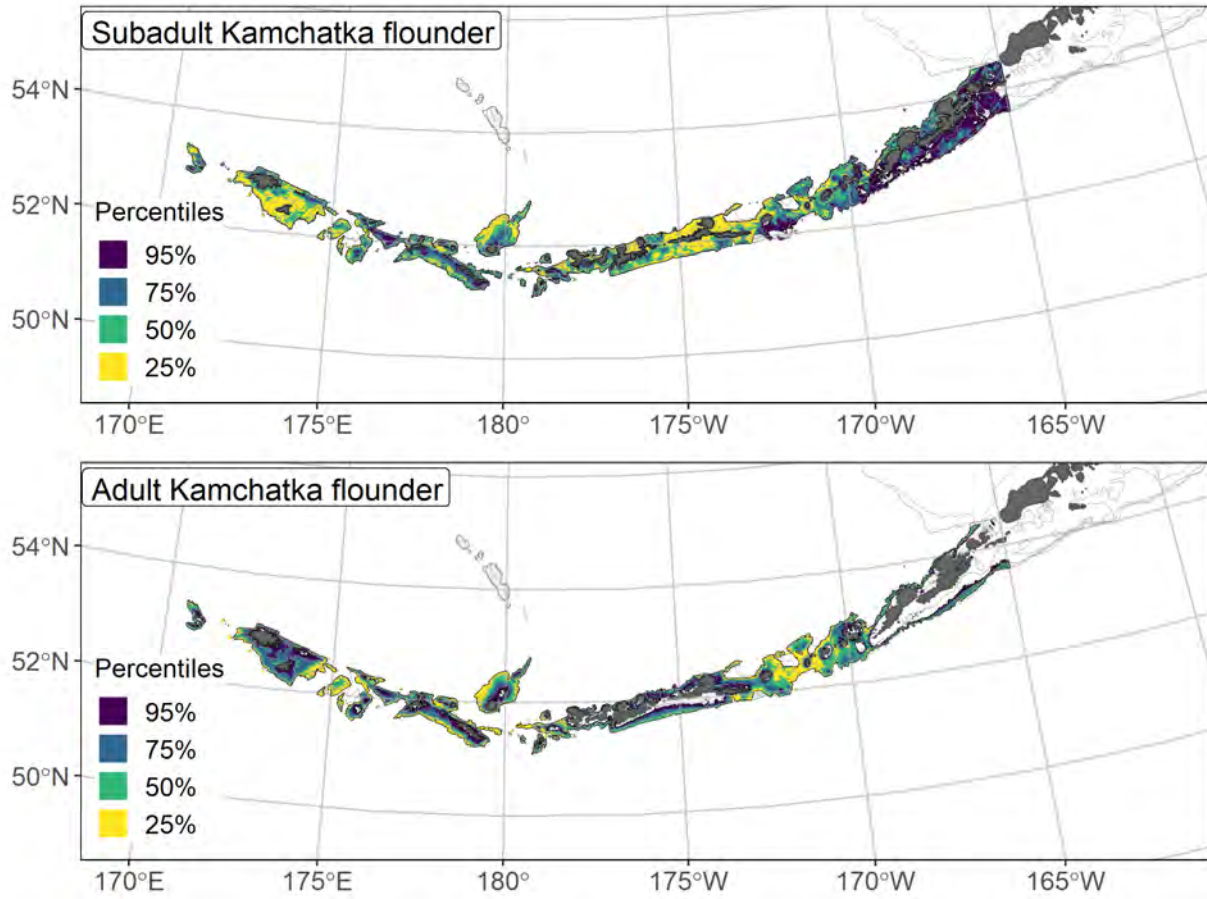
1218 Islands (upper right panel) alongside the coefficient of variation of the ensemble predictions (lower right panel).



1219

1220 Figure 33. Encounter probability of adult Kamchatka flounder from AFSC RACE-GAP summer bottom

1221 trawl surveys (1992–2019) of the Aleutian Islands with the 100 m, 300 m, and 500 m isobaths indicated.



1222
 1223 Figure 34. Essential fish habitat (EFH area) defined as the top 95% of numerical abundance predictions
 1224 from a habitat-based ensemble fitted to subadult (top) and adult (bottom) Kamchatka flounder distribution
 1225 and abundance in AFSC RACE-GAP summer bottom trawl surveys (1992–2019) with 100 m, 300 m, and
 1226 500 m isobaths indicated; internal to the EFH map are the subareas of the top 25% (EFH hot spots), top
 1227 50% (core EFH area), and top 75% (principal EFH area) of habitat related, ensemble-predicted numerical
 1228 abundance.

1229 **Northern rock sole (*Lepidopsetta polyxystra*)**

1230 Northern rock sole (*Lepidopsetta polyxystra*) is present across the north Pacific, from Puget
1231 Sound in Washington State across the AI and Bering Sea to the Kuril Islands (Orr and Matarese 2000).
1232 The species is morphologically similar to southern rock sole (*L. bilineata*) and the two were not routinely
1233 distinguished in groundfish surveys until 1996. In the Bering Sea region, the vast majority of rock soles
1234 are of *L. polyxystra*, though the species are often found together in the AI and GOA (Orr and Matarese
1235 2000). Adults may grow to as much as 690 mm T. L. (Walters and Wilderbuer 2000). Similarly, northern
1236 rock sole in the BSAI reach maturity at a smaller size (309 mm T. L.) than in the GOA (328 mm T. L.)
1237 (Stark 2012a). Spawning begins in February and peaks in the early spring (Stark 2012a). Previous
1238 research has also defined the length interval between larval transformation at 80 mm (Doyle et al. 2019)
1239 and the transition to a sub-adult habitat at 140 mm (Yeung and Cooper 2020), so the settled early juvenile
1240 life stage is modeled here. In the Bering Sea, northern rock sole supports a valuable commercial fishery,
1241 where it is managed as a mixed stock alongside the relatively uncommon southern rock sole (McGilliard
1242 et al. 2020).

1243 **Settled early juvenile northern rock sole distribution and predicted abundance from RACE-GAP**
1244 **summer bottom trawl surveys in the Aleutian Islands–**

1245 Settled early juvenile northern rock sole were relatively uncommon in the RACE-GAP summer
1246 survey of the AI compared to older life stages (Figure 35). Within the survey area, settled early juvenile
1247 northern rock sole were distributed evenly across the AI. However, given the small size of this life stage,
1248 the gear employed during the survey may not adequately sample the population, and where available,
1249 additional sources of data should be considered¹². The final ensemble contained four SDMs with
1250 approximately equal weights, and had a fair fit to the observed data (Table 13). Specifically, the ensemble

¹² A recommendation to add additional survey data types if possible to future SDM ensemble EFH mapping efforts for this species will be included as a future recommendation for research directions from the 2022 EFH 5-year Review.

1251 performed well in predicting presence or absence (AUC = 0.892), and received a fair score at predicting
1252 high or low abundance catches ($\rho = 0.250$). The ensemble scored slightly better in terms of deviance
1253 explained (PDE = 0.381), which is not uncommon for stocks with few presences and low overall density.
1254 These metrics suggest that the ensemble can predict the areas where settled early juveniles are most likely
1255 to be caught, but predicts abundance with a higher degree of uncertainty. Bottom depth was the most
1256 important covariate and accounted for 46.4% of the deviance explained by the ensemble; bottom current,
1257 terrain aspect, tidal maximum, and geographic position were also relatively important based on deviance
1258 explained (Table 14). In general, predicted abundance was high in shallow locations with southerly
1259 currents, northwest facing terrain, and weak tides (Figure 36). Settled early juvenile northern rock sole
1260 abundance was also weakly positively associated with the presence of structure forming invertebrates like
1261 sponges and corals. Predicted abundance was highest in shallow inshore areas, particularly near Attu
1262 Island in the west and Umnak Island in the east (Figure 36), though still low (<1) on average. The
1263 predicted CV of abundance was high in almost all shallow inshore areas, which is a reflection of the fact
1264 that with such low predicted abundance, any variation is high relative to the mean (Figure 36). Encounter
1265 probabilities for settled early juvenile northern rock sole were high near Attu and Umnak Islands,
1266 moderate in shallow water, and close to zero beyond the 100 m depth contour (Figure 37).

1267 **Subadult northern rock sole distribution and predicted abundance from RACE-GAP summer**
1268 **bottom trawl surveys in the Aleutian Islands –**

1269 Subadult northern rock sole catches were very common across most of the RACE-GAP summer
1270 survey area (Figure 38). They were present in especially high numbers in the western AI. The final
1271 ensemble contained four SDMs with the MaxEnt given slightly less weight than the others. The ensemble
1272 demonstrated excellent predictive performance across all three metrics $\rho = 0.731$; AUC = 0.903;
1273 PDE = 0.611) (Table 13), indicating that this ensemble is expected to make accurate predictions. Bottom
1274 depth was the most important covariate and accounted for 62.0% of the deviance explained by the
1275 ensemble, though bottom currents and geographic position were also important (Table 14). Predicted

1276 abundance was highest in shallow locations, consistent south westerly currents, and locations that were
1277 further west in the AI (Figure 39). Predicted abundance of subadult northern rock sole was high in many
1278 places in the AI, but particularly in the western parts, near Attu Island and the Rat Islands, and it tended to
1279 be lower in the eastern AI (Figure 39). The predicted CV of abundance tended to be highest in the eastern
1280 and central parts of the AI (Figure 39). These places had lower average predicted abundance, but large
1281 catches of subadult northern rock sole still occurred on occasion. Subadult northern rock sole are very
1282 common in the AI, and the encounter probability is near 100% in nearly all areas shallower than 300m,
1283 with the exception of the area around Seguam Pass and the Islands of Four Mountains (Figure 40).

1284 **Adult northern rock sole distribution and predicted abundance from RACE-GAP summer bottom**
1285 **trawl surveys in the Aleutian Islands –**

1286 Adult northern rock sole catches were very common throughout the RACE-GAP summer survey
1287 area in the AI (Figure 41). Large catches occurred across the entire AI area and were more frequent in the
1288 western parts of the island chain. The final ensemble included three SDMs, and the paGAM was weighted
1289 slightly less than the hGAM or GAM_P (Table 13). The predictions generated by the ensemble had a good
1290 to excellent fit to the data (Table 13). The ensemble performed excellently at predicting relatively high- or
1291 low-abundance catches ($\rho = 0.712$). It also showed a good fit in terms of AUC (0.880) and deviance
1292 explained (PDE = 0.464). The fact that ρ was higher than PDE suggests that the ensemble can identify
1293 areas where larger catches are expected to occur, but may not predict the exact abundance with the same
1294 accuracy. Similar to previous life stages, bottom depth, geographic position, current, and current
1295 variability were the most important covariates, and they accounted for a combined 78.7% of the deviance
1296 explained by the ensemble (Table 14). Adult northern rock sole were predicted to be abundant in shallow
1297 waters in the western AI, and to favor locations with low variability westerly bottom currents (Figure 42).
1298 The predicted CV of abundance was relatively low in most places, and the greatest uncertainty in model
1299 predictions occurred in moderately shallow areas in the eastern AI (Figure 42). Like subadults, adult

1300 northern rock sole had a 100% encounter probability in almost all areas shallower than 300 m, reflecting
1301 that they are common even outside the highest-abundance areas (Figure 43).

1302 **Essential fish habitat of settled early juvenile, subadult, and adult northern rock sole in the**
1303 **Aleutian Islands –**

1304 The habitat related abundance predictions based on RACE-GAP summer bottom trawl data
1305 (1996–2019) were translated into EFH area and subareas (Figure 44). The EFH area for settled early
1306 juvenile northern rock sole is smaller than that of the other life stages. Settled early juveniles had hot
1307 spots located in the east near Umnak Island and in the west near Attu Island. However, the settled early
1308 juvenile SDMs were based on many fewer catch records and should be used conservatively. By contrast,
1309 data were plentiful for both adult and subadult life stages. These life stages have nearly identical EFH
1310 maps, and both seem to occupy nearly all areas in the AI shallower than 300m. Both life stages also had
1311 EFH hot spots concentrated in the central and western AI.

1312 Table 13. Constituent species distribution models (SDMs) used to construct Essential Fish Habitat (EFH)
 1313 for a) settled early juvenile, b) subadult, and c) adult northern rock sole: MaxEnt = Maximum entropy;
 1314 paGAM = presence-absence generalized additive model; hGAM = hurdle GAM; GAM_P = standard
 1315 Poisson GAM; and GAM_{nb} = standard negative-binomial GAM. Ensemble performance (ρ = Spearman's
 1316 rank correlation coefficient), root-mean-square-error (RMSE), the area under the receiver operating
 1317 characteristic (AUC), and the Poisson deviance explained (PDE) were generated from k-fold cross-
 1318 validation. The "--" in a field indicates that this SDM was not included in the final ensemble.

1319 **a) settled early juvenile northern rock sole**

Models	RMSE	Relative Weight	ρ	AUC	PDE	EFH area (km ²)
MaxEnt	0.591	0.252	0.247	0.890	0.342	31,000
paGAM	0.591	0.252	0.245	0.887	0.329	33,500
hGAM	0.598	0.246	0.241	0.886	0.353	32,900
GAM _P	0.594	0.250	0.247	0.882	0.394	27,500
GAM _{nb}	0.597	0	--	--	--	--
ensemble	0.574	1	0.250	0.892	0.381	33,000

1320 **b) subadult northern rock sole**

Models	RMSE	Relative Weight	ρ	AUC	PDE	EFH area (km ²)
MaxEnt	59.3	0.158	0.720	0.904	0.350	61,400
paGAM	46.9	0.252	0.734	0.911	0.501	74,500
hGAM	43.3	0.296	0.713	0.910	0.632	60,200
GAM _P	43.5	0.294	0.704	0.884	0.626	59,300
GAM _{nb}	51.1	0	--	--	--	--
ensemble	42.6	1	0.731	0.903	0.611	69,700

1321 **c) adult northern rock sole**

Models	RMSE	Relative Weight	ρ	AUC	PDE	EFH area (km ²)
MaxEnt	--	0	--	--	--	--
paGAM	66.0	0.294	0.717	0.900	0.320	76,500
hGAM	59.9	0.357	0.693	0.900	0.478	72,100
GAM _P	60.5	0.350	0.679	0.857	0.462	74,200
GAM _{nb}	66.4	0	--	--	--	--
ensemble	59.0	1	0.712	0.880	0.464	75,000

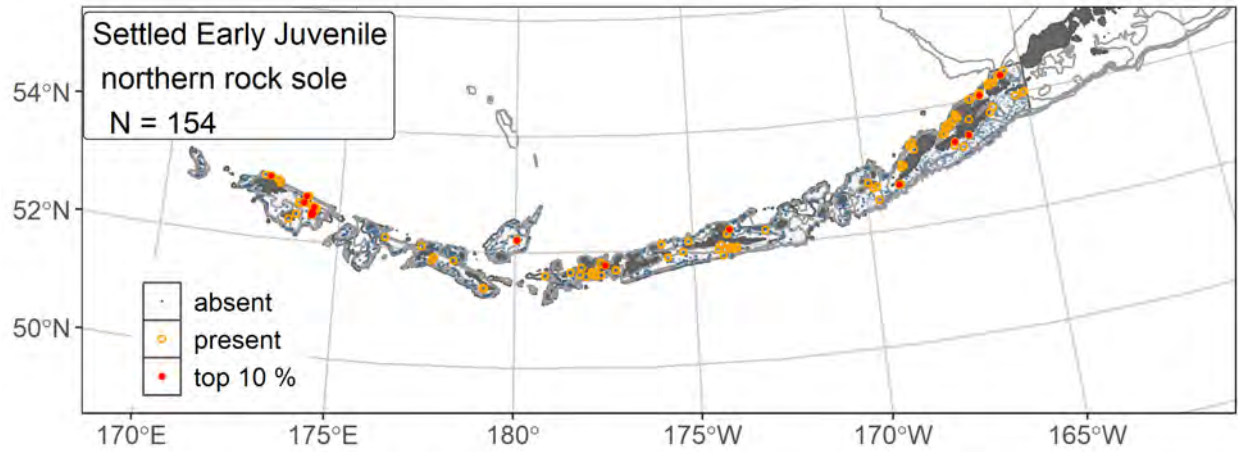
1322

1323 Table 14. Covariates retained in the a) settled early juvenile, b) subadult, and c) adult northern rock sole
 1324 species distribution model (SDM) final ensembles, the percent contribution to the ensemble deviance
 1325 explained by each, and the cumulative percent deviance: SD = standard deviation, and BPI = bathymetric
 1326 position index.

northern rock sole	Covariate	% Contribution	Cumulative % Contribution
a) settled early juvenile	bottom depth	46.4	46.4
	position	11.0	57.4
	current	10.1	67.5
	aspect east	6.4	73.9
	aspect north	5.0	78.9
	tidal maximum	5.0	84.0
	current SD	3.8	87.8
	sponge presence	2.9	90.7
	slope	2.4	93.1
	coral presence	2.3	95.4
	BPI	2.1	97.5
	bottom temperature	1.1	98.5
	rockiness	1.1	99.6
	pennatulacean presence	0.4	100
	curvature	0	100
b) subadult	bottom depth	62.0	62.0
	position	10.8	72.8
	current	6.0	78.7
	current SD	5.0	83.7
	aspect north	4.4	88.1
	tidal maximum	2.6	90.6
	BPI	2.0	92.6
	aspect east	1.8	94.5
	slope	1.7	96.2
	rockiness	1.6	97.7
	curvature	0.9	98.6
	bottom temperature	0.7	99.3
	sponge presence	0.3	99.6
	coral presence	0.3	99.9
	pennatulacean presence	0.1	100
c) adult	bottom depth	36.4	36.4
	position	22.5	58.9
	current SD	11.6	70.5
	current	8.2	78.7
	aspect north	4.2	82.9
	slope	3.9	86.8

northern rock sole	Covariate	% Contribution	Cumulative % Contribution
	tidal maximum	3.3	90.1
	aspect east	2.3	92.4
	curvature	1.6	94.0
	bottom temperature	1.6	95.6
	coral presence	1.2	96.8
	rockiness	1.1	97.9
	BPI	0.9	98.8
	sponge presence	0.6	99.4
	pennatulacean presence	0.6	100

1327



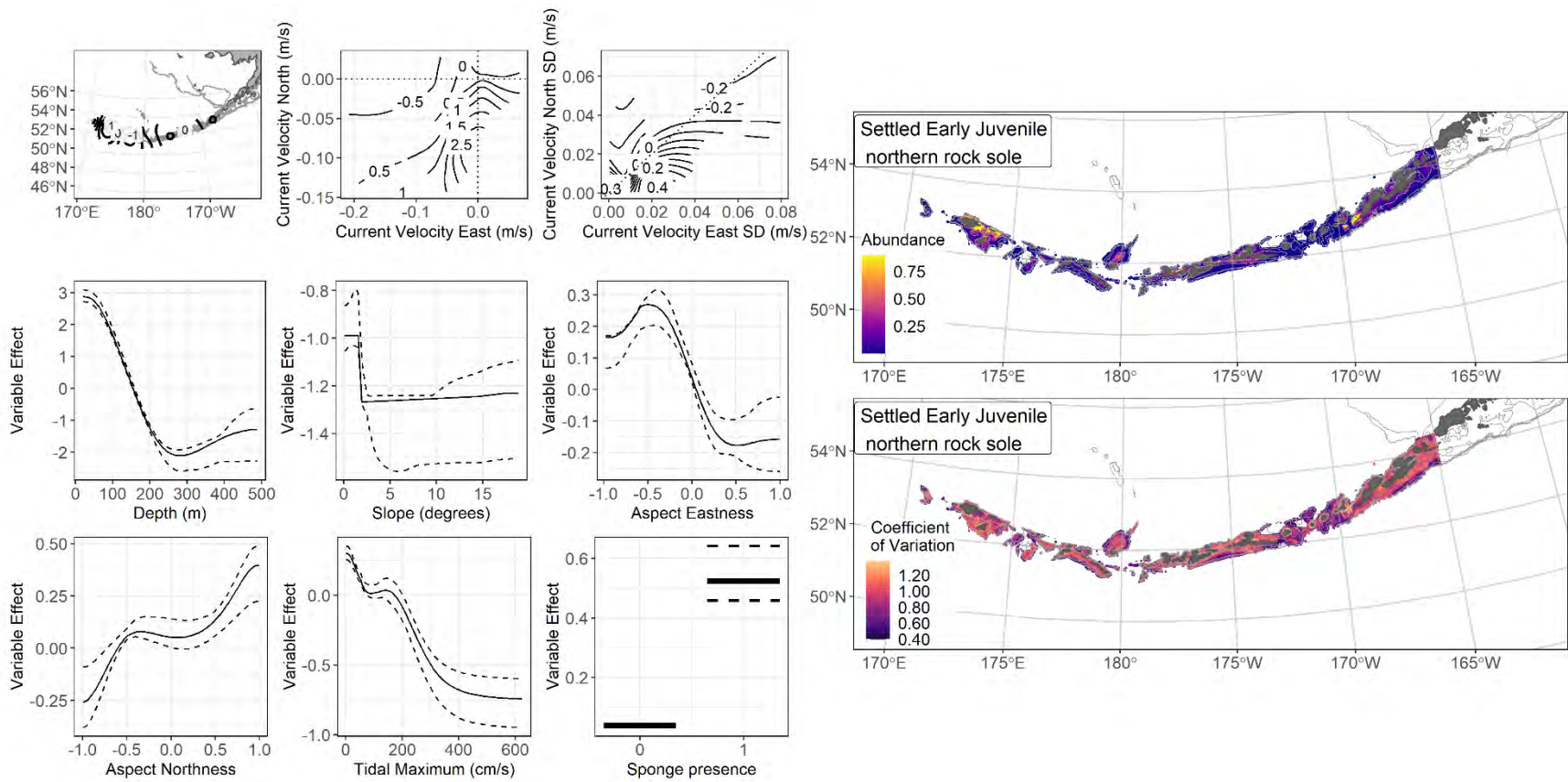
1328

1329 Figure 35. Distribution of settled early juvenile northern rock sole catches (N = 154) in 1996–2019 AFSC

1330 RACE-GAP summer bottom trawl surveys of the Aleutian Islands with the 100 m, 300 m, and 500 m

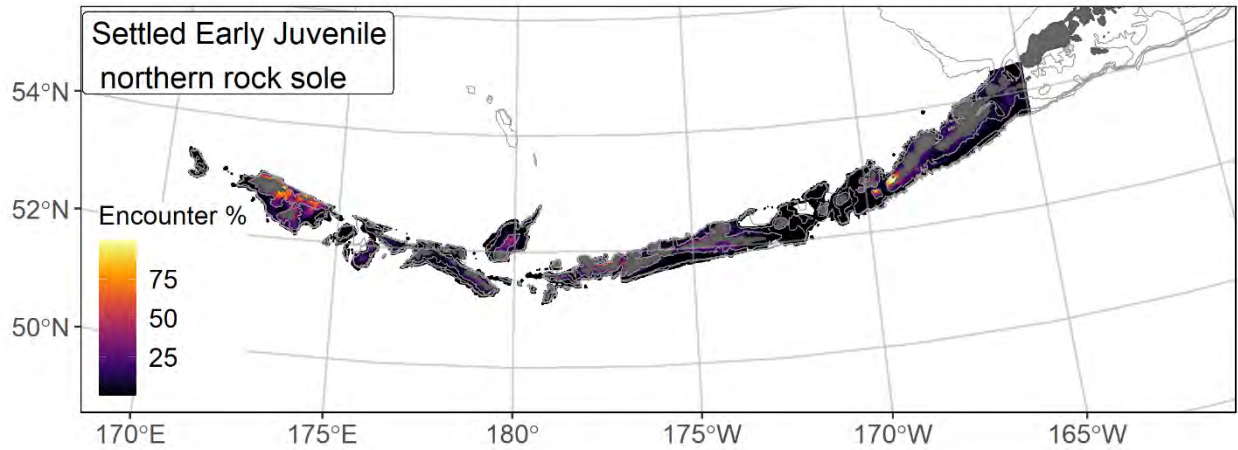
1331 isobaths indicated; filled red circles indicate locations in top 10% of overall abundance, open orange

1332 circles indicate presence in remaining catches, and small blue dots indicate absence.



1333

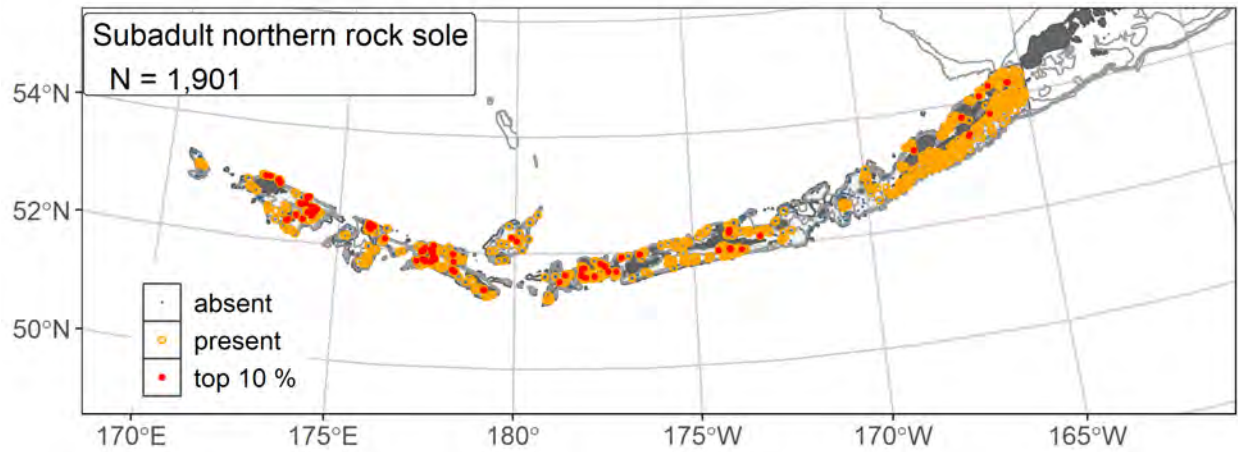
1334 Figure 36. The top nine covariate effects (left panel) on ensemble-predicted settled early juvenile northern rock sole numerical abundance across
 1335 the Aleutian Islands (upper right panel) alongside the coefficient of variation of the ensemble predictions (lower right panel).



1336

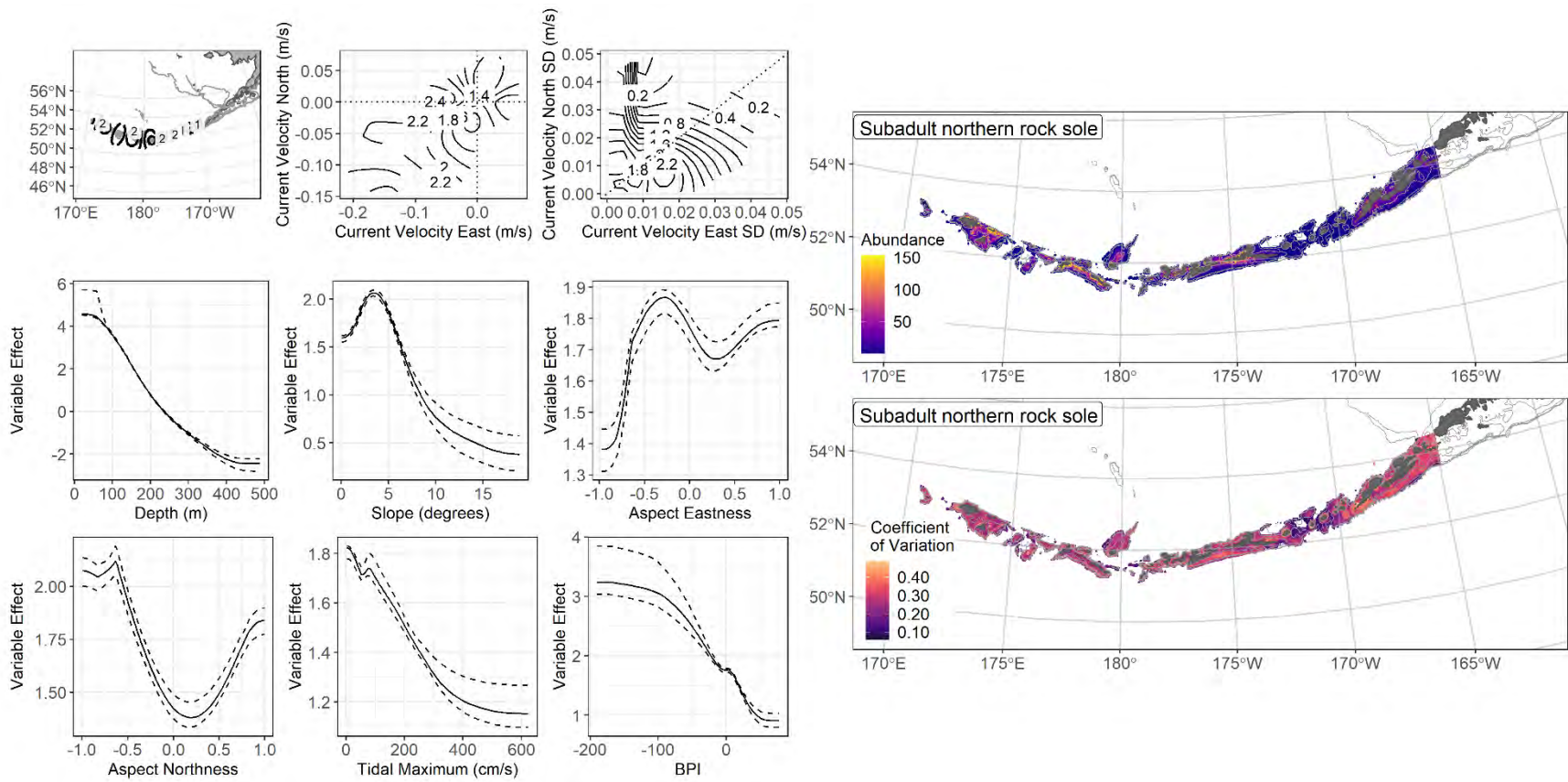
1337 Figure 37. Encounter probability of settled early juvenile northern rock sole from AFSC RACE-GAP
 1338 summer bottom trawl surveys (1996–2019) of the Aleutian Islands with the 100 m, 300 m, and 500 m
 1339 isobaths indicated.

1340



1341

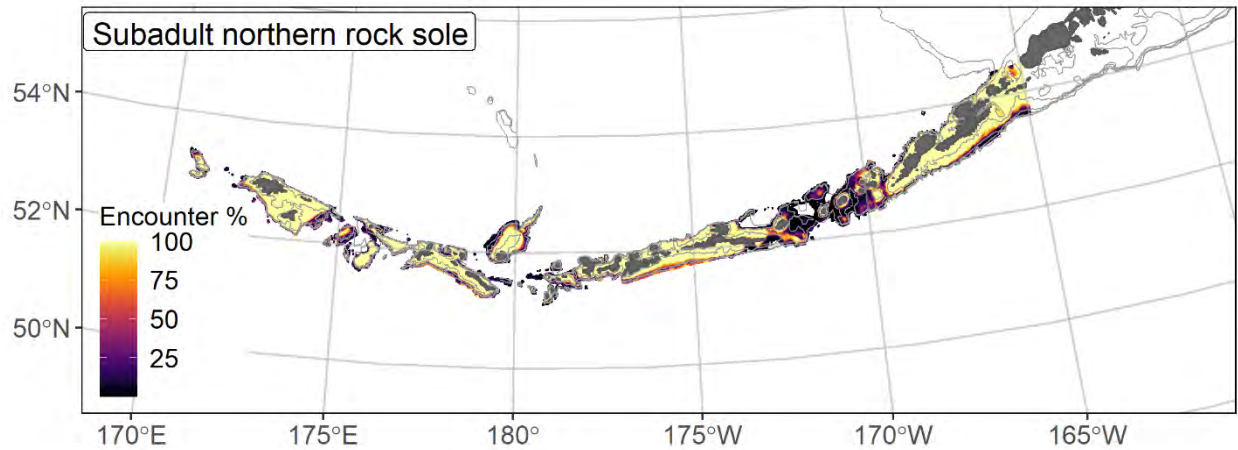
1342 Figure 38. Distribution of subadult northern rock sole catches (N = 1,901) in 1996–2019 AFSC RACE-
 1343 GAP summer bottom trawl surveys of the Aleutian Islands with the 100 m, 300 m, and 500 m isobaths
 1344 indicated; filled red circles indicate locations in top 10% of overall abundance, open orange circles
 1345 indicate presence in remaining catches, and small blue dots indicate absence.



1346

1347 Figure 39. The top nine covariate effects (left panel) on ensemble-predicted subadult northern rock sole numerical abundance across the Aleutian

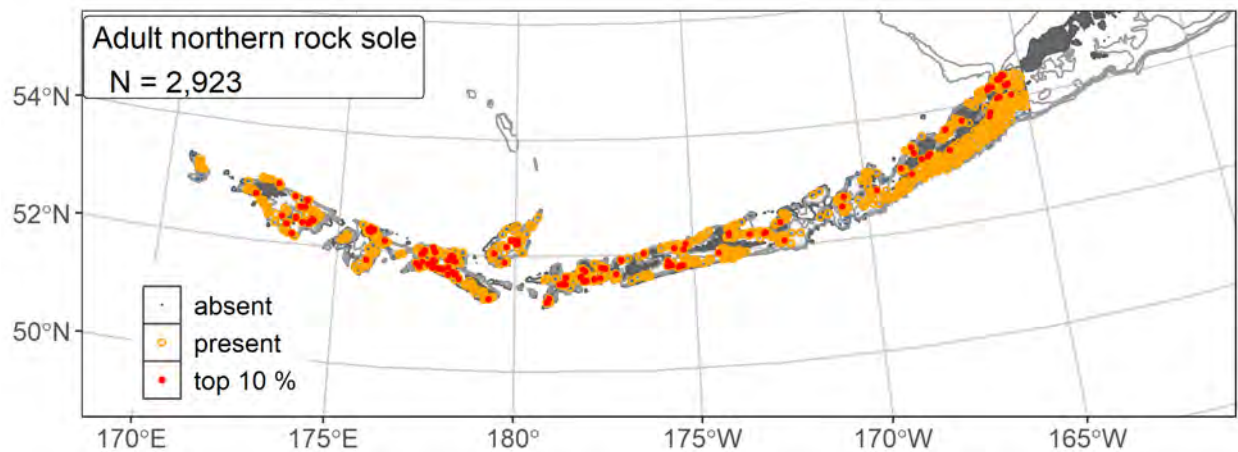
1348 Islands (upper right panel) alongside the coefficient of variation of the ensemble predictions (lower right panel).



1349

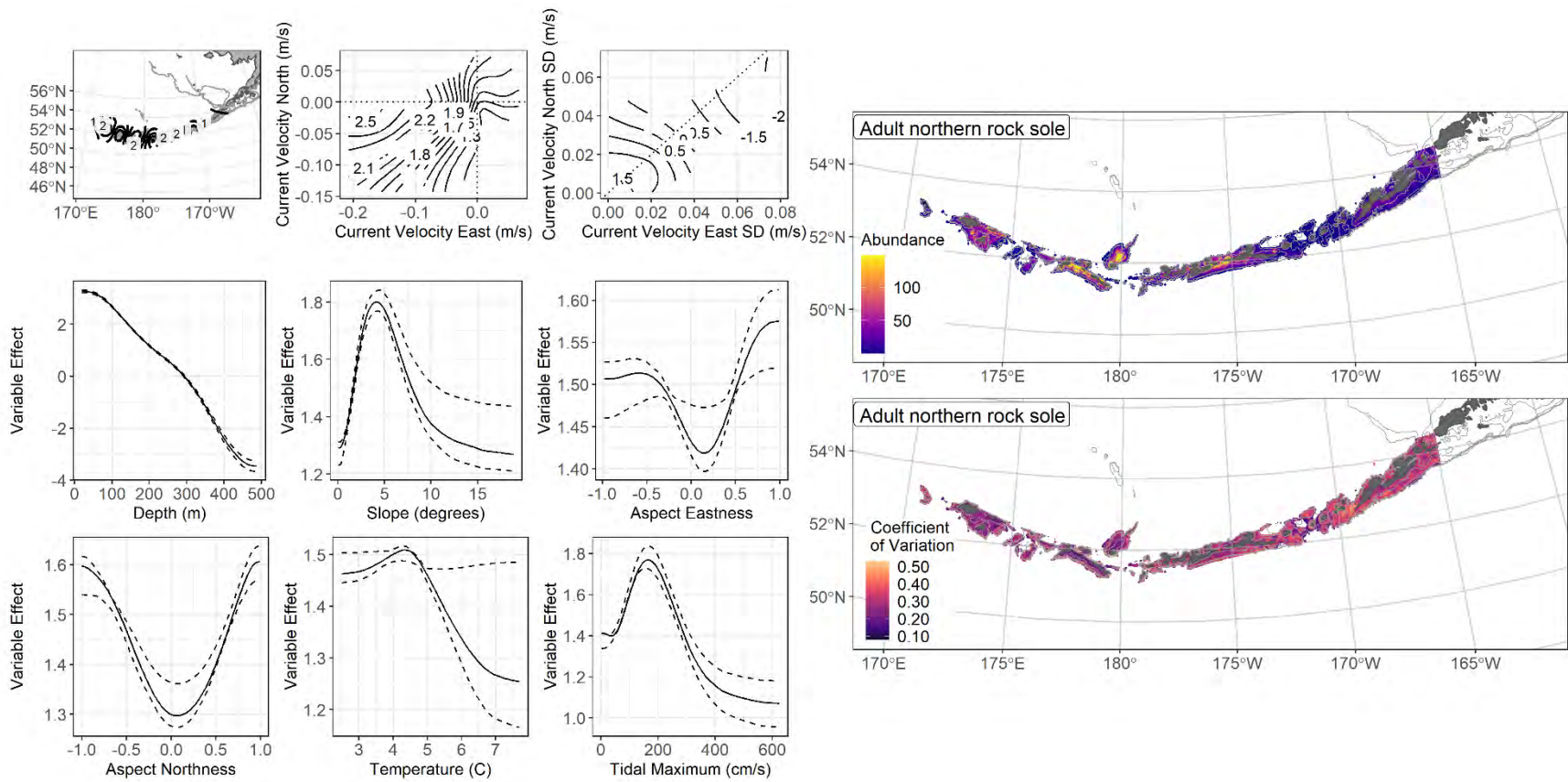
1350 Figure 40. Encounter probability of subadult northern rock sole from AFSC RACE-GAP summer bottom
 1351 trawl surveys (1996–2019) of the Aleutian Islands with the 100 m, 300 m, and 500 m isobaths indicated.

1352



1353

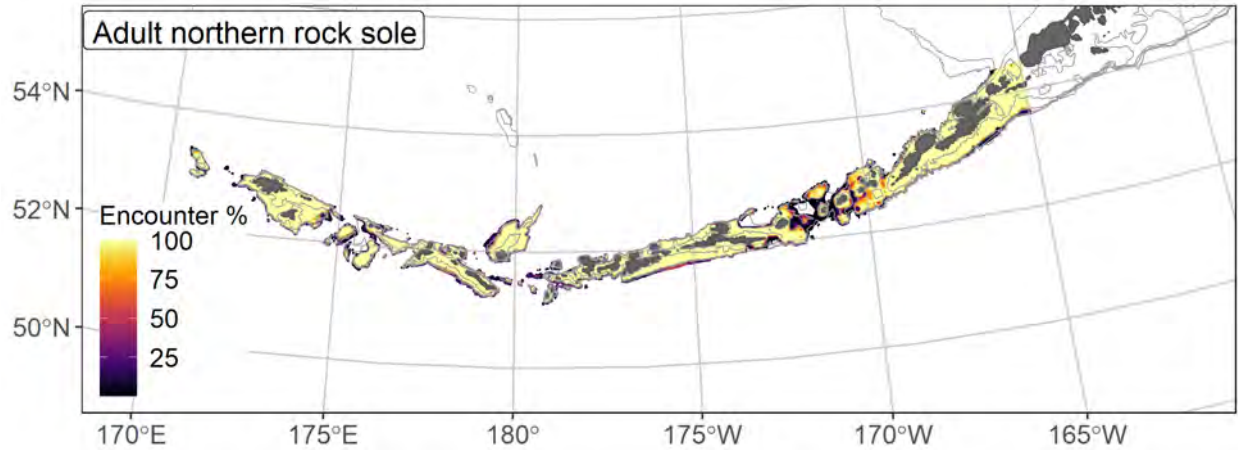
1354 Figure 41. Distribution of adult northern rock sole catches (N = 2,928) in 1996–2019 AFSC RACE-GAP
 1355 summer bottom trawl surveys of the Aleutian Islands with the 100 m, 300 m, and 500 m isobaths
 1356 indicated; filled red circles indicate locations in top 10% of overall abundance, open orange circles
 1357 indicate presence in remaining catches, and small blue dots indicate absence.



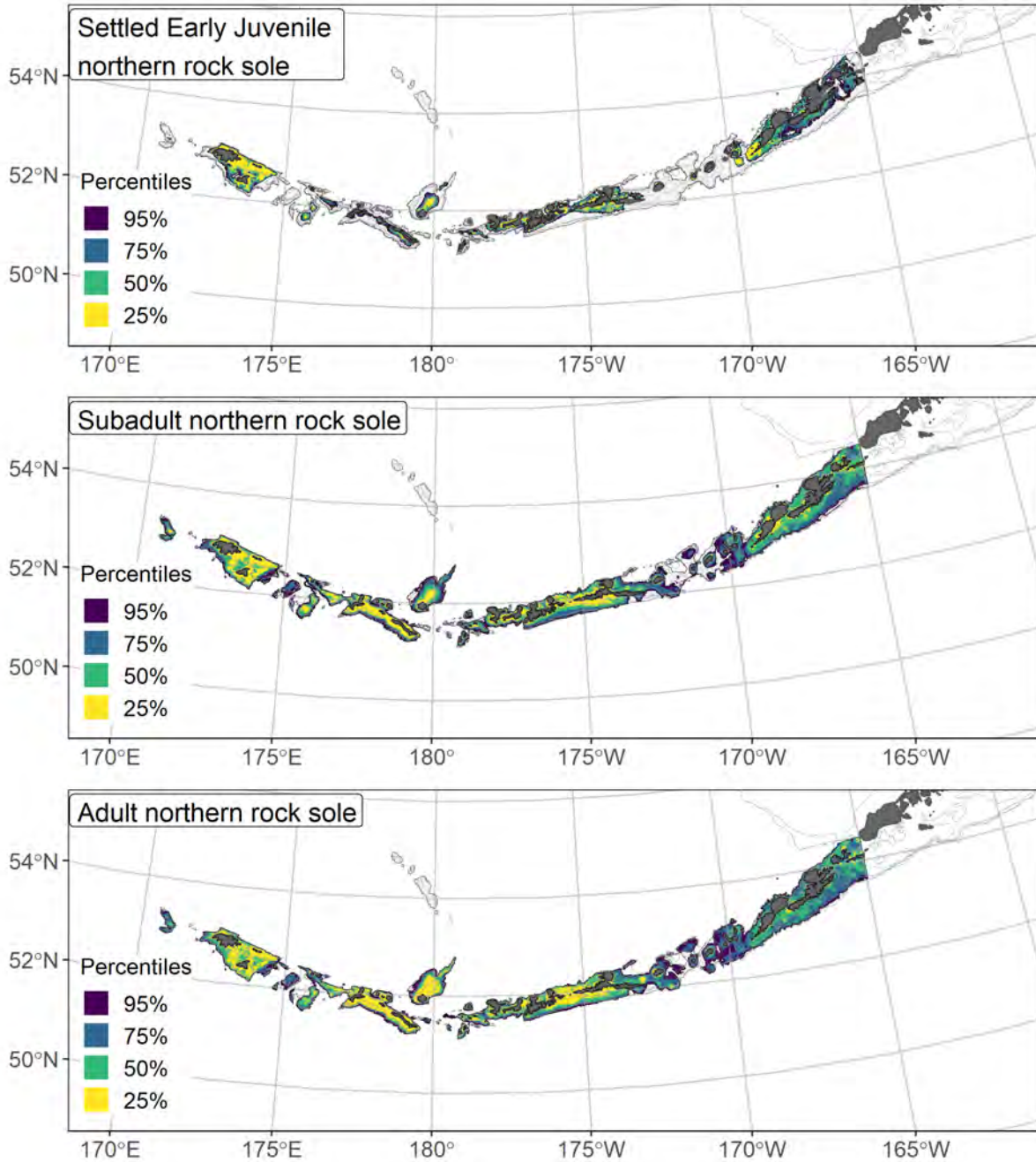
1358

1359 Figure 42. The top nine covariate effects (left panel) on ensemble-predicted adult northern rock sole numerical abundance across the Aleutian

1360 Islands (upper right panel) alongside the coefficient of variation of the ensemble predictions (lower right panel).



1361
1362 Figure 43. Encounter probability of adult northern rock sole from AFSC RACE-GAP summer bottom
1363 trawl surveys (1996–2019) of the Aleutian Islands with the 100 m, 300 m, and 500 m isobaths indicated.



1364

1365 Figure 44. Essential fish habitat (EFH area) defined as the top 95% of numerical abundance predictions

1366 from a habitat-based ensemble fitted to settled early juvenile (top), subadult (middle), and adult (bottom)

1367 northern rock sole distribution and abundance in AFSC RACE-GAP summer bottom trawl surveys

1368 (1996–2019) with 100 m, 300 m, and 500 m isobaths indicated; internal to the EFH map are the subareas

1369 of the top 25% (EFH hot spots), top 50% (core EFH area), and top 75% (principal EFH area) of habitat

1370 related, ensemble-predicted numerical abundance.

1371 **Other Flatfish Stock Complex**

1372 The Magnusson-Stevens Act mandates that EFH should be established at the lowest taxonomic
1373 level whenever possible. However, several species that lack the data necessary for a full age-structured
1374 assessment are managed as a single “other flatfish” stock complex of the BSAI region (Monnahan 2020).
1375 As a benefit to stock authors, this complex chapter includes sections for each individual species for which
1376 sufficient data was available as well as a summary of the combined multi-species stock complex. Over a
1377 dozen species of flatfish are managed in this way, but only four were common enough in the RACE-GAP
1378 summer bottom trawl survey of the AI to enable the construction of an SDM: Dover sole (*Microstomus*
1379 *pacificus*), rex sole (*Glyptocephalus zachirus*), English sole (*Parophrys vetulus*), and southern rock sole
1380 (*Lepidopsetta bilineata*). English sole are included in the adult maps only, as there was insufficient data to
1381 construct a SDM for subadults. Rex sole is the most common species of this group in the AI, and it
1382 constitutes a majority of the “other flatfish” catch in terms of biomass. Because these species are typically
1383 managed together as a stock complex, this chapter summarizes the composite abundance, encounter
1384 probabilities, and EFH of these four species in the AI. Some caution should be used in interpreting
1385 species distribution predictions for this complex. Rex sole and southern rock sole are typically caught in
1386 the eastern AI and can appear in very high densities, whereas Dover sole is primarily caught in deeper
1387 water and further west, and large catches are rare. The abundance and EFH maps for the complex tend to
1388 be most representative of the more numerous species’ distributions.

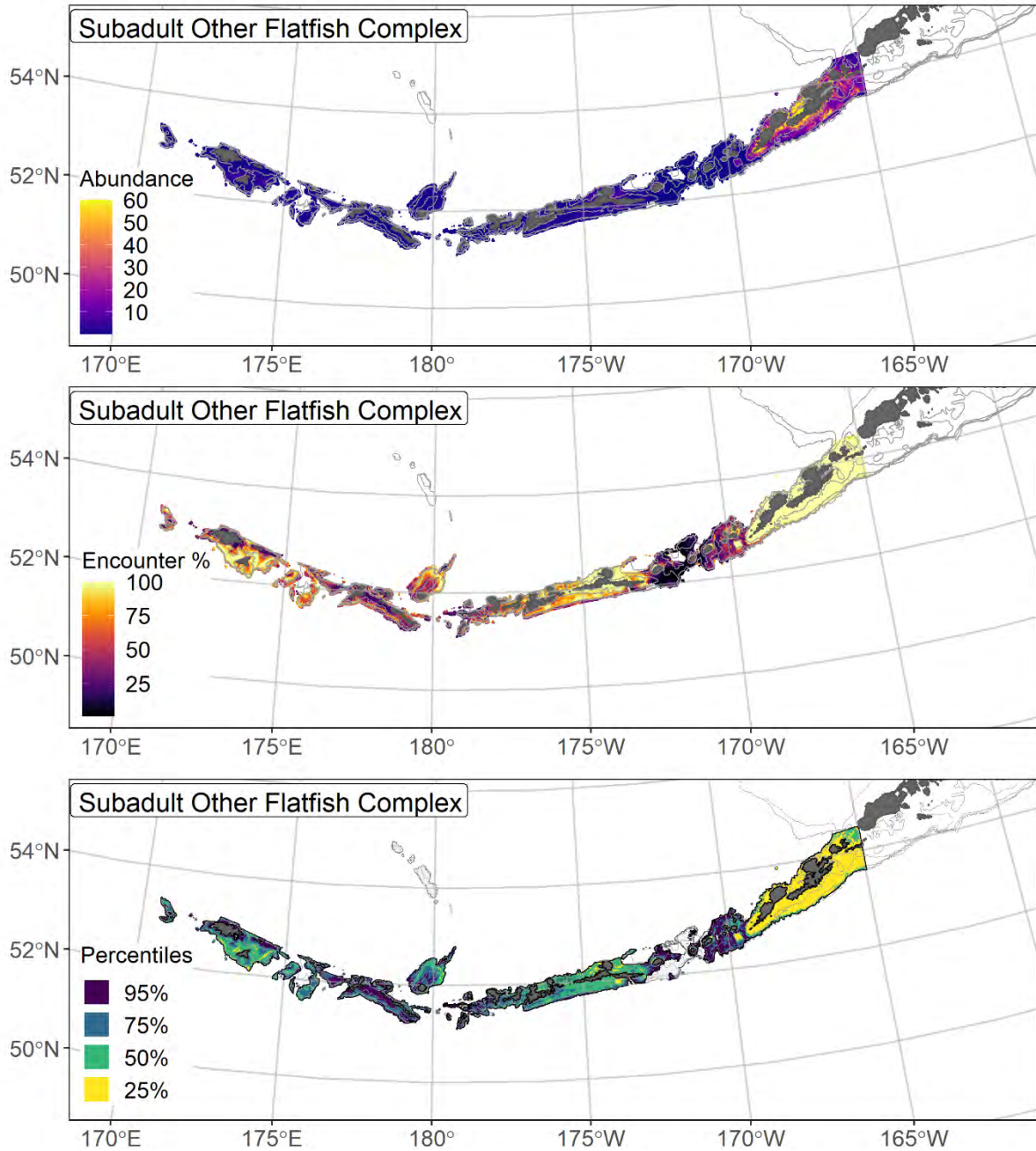
1389 **Subadult “Other Flatfish” Stock Complex abundance and distribution predicted from RACE-GAP**
1390 **summer bottom trawl surveys in the Bering Sea –**

1391 Numerical abundance predictions for Dover sole, rex sole, and southern rock sole were combined
1392 to estimate the distribution and EFH of subadults in the “other flatfish” stock complex in the AI
1393 (Figure 45). The composite abundance map was strongly influenced by rex sole and southern rock sole,
1394 and shows high numbers of flatfish in the eastern AI and around Unalaska Island. Dover sole abundance
1395 is low relative to the other species and thus is not well represented by the EFH map. The wider

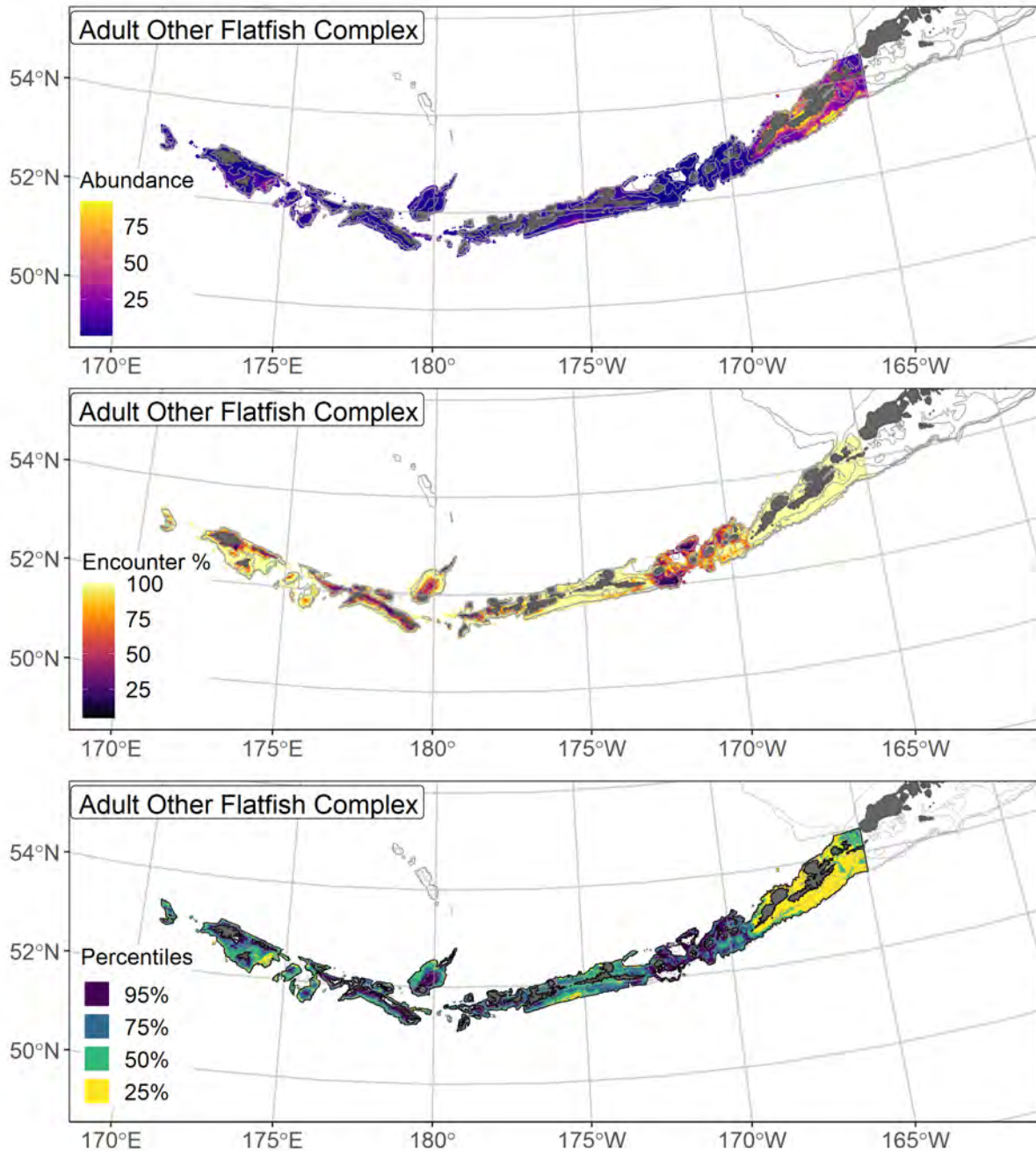
1396 distribution of all four species is more apparent in the encounter probabilities map (Figure 45). High
1397 encounter probabilities in the eastern half of the AI are primarily due to a combination of southern rock
1398 sole and rex sole. Southern rock sole are rare west of 180°, and high-probability areas around Attu Island
1399 and Petrel Bank reflect the presence of rex sole and Dover sole. The primary EFH hot spot for subadults
1400 in the whole stock complex is in the eastern AI. With the exception of some deeper habitats, most of the
1401 survey area qualifies as EFH, however this is mostly due to rex sole, which is very common throughout
1402 the region.

1403 **Adult “Other Flatfish” Stock Complex abundance and distribution predicted from RACE-GAP**
1404 **summer bottom trawl surveys in the Bering Sea –**

1405 Numerical abundance predictions for adult Dover sole, rex sole, English sole and southern rock
1406 sole were combined to estimate the distribution and EFH of the “other flatfish” stock complex in the AI
1407 (Figure 46). The abundance map for adults was very similar as that of subadults. The areas of high
1408 abundance were located in the eastern AI around Unalaska Island. Areas of high abundance close to shore
1409 consisted mostly of southern rock sole, which remain in shallow water even as adults, whereas the areas
1410 closer to the continental slope were primarily composed of rex sole, which move into deeper habitats as
1411 adults. Dover sole had a limited impact on estimated distribution of the ‘other flatfishes’ complex, as they
1412 were caught less frequently and in lower numbers than the other species in the complex. The encounter
1413 probability map followed most of the same patterns. In the eastern AI, high probabilities close to shore
1414 reflected the presence of southern rock sole and those offshore reflect the presence of rex sole. English
1415 sole overlapped with southern rock sole in the eastern AI, but its numbers were relatively small and did
1416 not have a strong impact on the overall map. However, southern rock sole are not present in the western
1417 AI, and many near shore areas show a lower encounter probability for them. As with subadults, a large
1418 EFH hot spot for adults was located in the eastern AI, representing the area of high density of southern
1419 rock sole and rex sole. In the west, most EFH for the stock complex occurred at greater depths and
1420 mirrored the distribution of rex sole.



1421
 1422 Figure 45. Composite predicted numerical abundance (top panel), encounter probability (middle panel),
 1423 and essential fish habitat (bottom panel) of subadults from the “other flatfish” stock complex for the
 1424 Aleutian Islands collected in AFSC RACE-GAP summer bottom trawl surveys (1991–2019) with 100 m,
 1425 300 m, and 500 m isobaths indicated; internal to the EFH map are the subareas of the top 25% (EFH hot
 1426 spots), top 50% (core EFH area), and top 75% (principal EFH area) of habitat related, ensemble-predicted
 1427 numerical abundance.



1428

1429 Figure 46: Composite predicted numerical abundance (top panel), encounter probability (middle panel),
 1430 and essential fish habitat (bottom panel) of adults from the “other flatfish” stock complex for the Aleutian
 1431 Islands collected in AFSC RACE-GAP summer bottom trawl surveys (1991–2019) with 100 m, 300 m,
 1432 and 500 m isobaths; internal to the EFH map are the subareas of the top 25% (EFH hot spots), top 50%
 1433 (core EFH area), and top 75% (principal EFH area) of habitat related, ensemble-predicted numerical
 1434 abundance.

1435 **Dover sole (*Microstomus pacificus*) –**

1436 Dover sole (*Microstomus pacificus*) are distributed from Baja California to the AI and into the
1437 southeastern Bering Sea (Mecklenburg et al., 2002). L_{50} in the GOA (439 mm F.L.; Abookire and
1438 Macewicz 2003) was used to separate subadult and adult life stages of Dover sole for these analyses.
1439 Adults attain a size of up to 660 mm F.L. and can be found at depths greater than 1200 m. Spawning
1440 occurs offshore and in deeper water along the edge of the continental slope, with most juveniles occurring
1441 inshore and in shallower water. This species has a spawning period from late January to early June in the
1442 GOA (Abookire, 2006). Development in Dover sole appears to exhibit significant regional and individual
1443 variation in the timing of metamorphosis and juvenile settlement (Pearcy 1977, Bailey et al., 2008). After
1444 settlement, juveniles and adults appear to migrate into deeper waters, with the oldest and largest
1445 individuals favoring greater depths. In the BSAI region, Dover sole are managed as a part of “other
1446 flatfish” stock assessment (Monnahan 2020)

1447 **Subadult Dover sole distribution and predicted abundance from RACE-GAP summer bottom trawl**
1448 **surveys in the Aleutian Islands –**

1449 Subadult Dover sole catches occurred in localized patches in the RACE-GAP summer survey
1450 areas (Figure 47). Large catches were located around Unalaksa Island, Petrel Bank, and the Rat Islands.
1451 The final ensemble contained four equally weighted SDMs and it showed a fair fit to the data (Table 15).
1452 Specifically, the ensemble showed good performance at predicting presence or absence in catches
1453 (AUC = 0.835), and fair accuracy in terms of predicting abundance and deviance explained ($\rho = 0.307$;
1454 PDE = 0.383). Overall, these metrics suggest that the ensemble provides an accurate description of where
1455 this species is found, but is less effective at predicting the abundance observed in trawl catches.
1456 Geographic position, bottom depth, and current vector and variability were the most important covariates
1457 for the model and accounted for 68.3% of the deviance explained by the model (Table 16). Although
1458 important in the ensemble, geographic position had an inconsistent pattern that is difficult to interpret.
1459 The other covariates show a stronger pattern, and the model predicts higher abundance in locations with

1460 weak currents, high current variability, and bottom depths between 200-300 m (Figure 48). Predicted
1461 abundance was highest around Petrel Bank (Figure 48). The predicted CV of abundance was highest in
1462 near the deep passes in the island chain, such as south of Buldir Island (Figure 48). Subadult Dover sole
1463 were not common in the AI trawl survey, and encounter probabilities for them were high in only a few
1464 places, including around Petrel Bank (Figure 49).

1465 **Adult Dover sole distribution and predicted abundance from RACE-GAP summer bottom trawl**
1466 **surveys in the Aleutian Islands –**

1467 Adult Dover sole catches in the RACE-GAP summer survey were not common, and the highest
1468 abundance catches were located around Petrel Bank (Figure 50). The three SDMs in the final ensemble
1469 performed similarly and were assigned equal weights, and the ensemble provided a fair to good fit overall
1470 (Table 15). Specifically, the ensemble achieves good performance in terms of predicting presence
1471 (AUC = 0.874) and in terms of deviance explained (PDE = 0.462), but only fair ability in terms of
1472 predicting relatively high or low abundance ($\rho = 0.266$). The discrepancy between the values for ρ and
1473 PDE occurred because the data have numerous observations close to zero, and this combination indicated
1474 that many of the model errors are small in absolute terms. Overall, the ensemble captured the general
1475 pattern of adult Dover sole presence and absence and demonstrated fair to good accuracy in predicting
1476 abundance. Geographic position, bottom depth, and current were the most important covariates and
1477 accounted for 85.9% of the deviance explained (Table 16). The ensemble predicted higher abundance
1478 around Petrel Bank, as well as higher abundance with increasing depth and in places with variable,
1479 southerly bottom currents (Figure 51). Predicted abundance was highest near Petrel Bank and Amchitka
1480 Pass, as well as several places along the edge of the continental slope at around 500 m depth (Figure 51).
1481 The predicted CV of abundance was elevated along these slope areas, and while the predicted mean
1482 abundance was fairly low, these locations have a higher predicted degree of variability and may hold
1483 larger numbers of this life stage (Figure 51). Ensemble-predicted encounter probabilities for adult Dover

1484 sole were often close to zero in depths shallower than 300 m, and tended to be higher with increasing
1485 depth (Figure 52).

1486 **Essential fish habitat of subadult and adult Dover sole in the Aleutian Islands –**

1487 The habitat related abundance predictions based on RACE-GAP summer bottom trawl data
1488 (1991–2019) were translated into EFH area and subareas (Figure 53). The EFH area for subadult Dover
1489 sole was larger than that of adults, and showed hot spots around Petrel Bank, on the shelf south of
1490 Unalaska Island, and some areas of the far west AI. Subadult EFH included shallower, more near shore
1491 areas, but was mostly located at moderately deep areas around 200–300 m. By contrast, the EFH area for
1492 adults was much smaller, and showed a single main hot spot around Petrel Bank and Amchitka Pass.
1493 Additional EFH for adults is located around the deep passes through the AI chain, mostly near 500 m
1494 depth. Given this pattern and life history information about Dover sole, it is likely that much of the adult
1495 population in the AI resides in deeper areas outside of the survey area.

1496 Table 15. Constituent species distribution models (SDMs) used to construct Essential Fish Habitat (EFH)
 1497 for a) subadult and b) adult *Dover* sole: MaxEnt = Maximum entropy; paGAM = presence-absence
 1498 generalized additive model; hGAM = hurdle GAM; GAM_p = standard Poisson GAM; and
 1499 GAM_{nb} = standard negative-binomial GAM. Ensemble performance (ρ = Spearman's rank correlation
 1500 coefficient), root-mean-square-error (RMSE), the area under the receiver operating characteristic (AUC),
 1501 and the Poisson deviance explained (PDE) were generated from k-fold cross-validation. The "--" in a field
 1502 indicates that this SDM was not included in the final ensemble.

1503 **a) subadult *Dover* sole**

Models	RMSE	Relative Weight	ρ	AUC	PDE	EFH area (km²)
MaxEnt	1.49	0.249	0.278	0.804	0.260	52,500
paGAM	1.48	0.253	0.305	0.834	0.343	44,200
hGAM	1.50	0.244	0.290	0.833	0.395	35,900
GAM _p	1.49	0	--	--	--	--
GAM _{nb}	1.47	0.254	0.303	0.831	0.386	37,100
ensemble	1.42	1	0.307	0.835	0.383	45,300

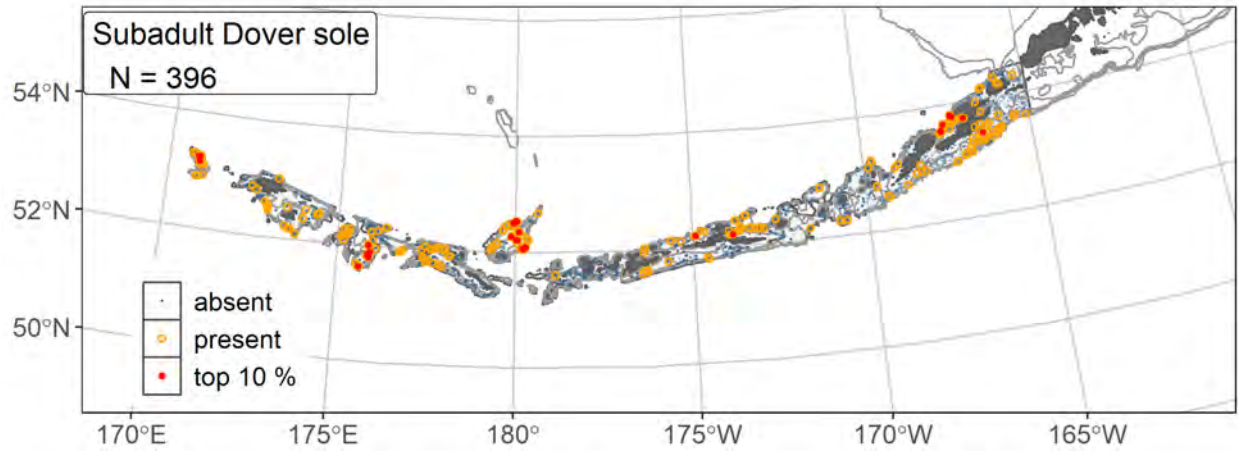
1504 **b) adult *Dover* sole**

Models	RMSE	Relative Weight	ρ	AUC	PDE	EFH area (km²)
MaxEnt	--	0	--	--	--	--
paGAM	0.904	0.355	0.268	0.877	0.398	28,900
hGAM	0.948	0.322	0.263	0.876	0.451	26,600
GAM _p	0.947	0.323	0.252	0.856	0.471	25,200
GAM _{nb}	0.973	0	--	--	--	--
ensemble	0.84	1	0.266	0.874	0.462	27,600

1505

1506 Table 16. Covariates retained in the a) subadult and b) adult Dover sole species distribution model (SDM)
 1507 final ensembles, the percent contribution to the total deviance explained by each, and the cumulative
 1508 percent deviance: SD = standard deviation, and BPI = bathymetric position index.

Dover sole	Covariate	% Contribution	Cumulative % Contribution
a) subadult	position	20.9	20.9
	current	17.8	38.7
	bottom depth	17.6	56.4
	current SD	11.9	68.3
	aspect north	6.5	74.8
	tidal maximum	6.3	81.1
	aspect east	5.9	87.0
	BPI	4.0	91.0
	bottom temperature	3.1	94.1
	slope	2.5	96.6
	curvature	1.3	97.9
	rockiness	1.0	98.9
	coral presence	0.7	99.6
	pennatulacean presence	0.4	100
a) adult	position	35.4	35.4
	bottom depth	23.8	59.3
	current	13.3	72.6
	current SD	13.3	85.9
	curvature	2.4	88.3
	aspect east	2.3	90.6
	bottom temperature	2.3	92.9
	aspect north	1.9	94.8
	BPI	1.1	95.9
	tidal maximum	1.0	96.9
	sponge presence	0.9	97.8
	slope	0.9	98.7
	coral presence	0.5	99.2
	rockiness	0.5	99.7
	pennatulacean presence	0.3	100



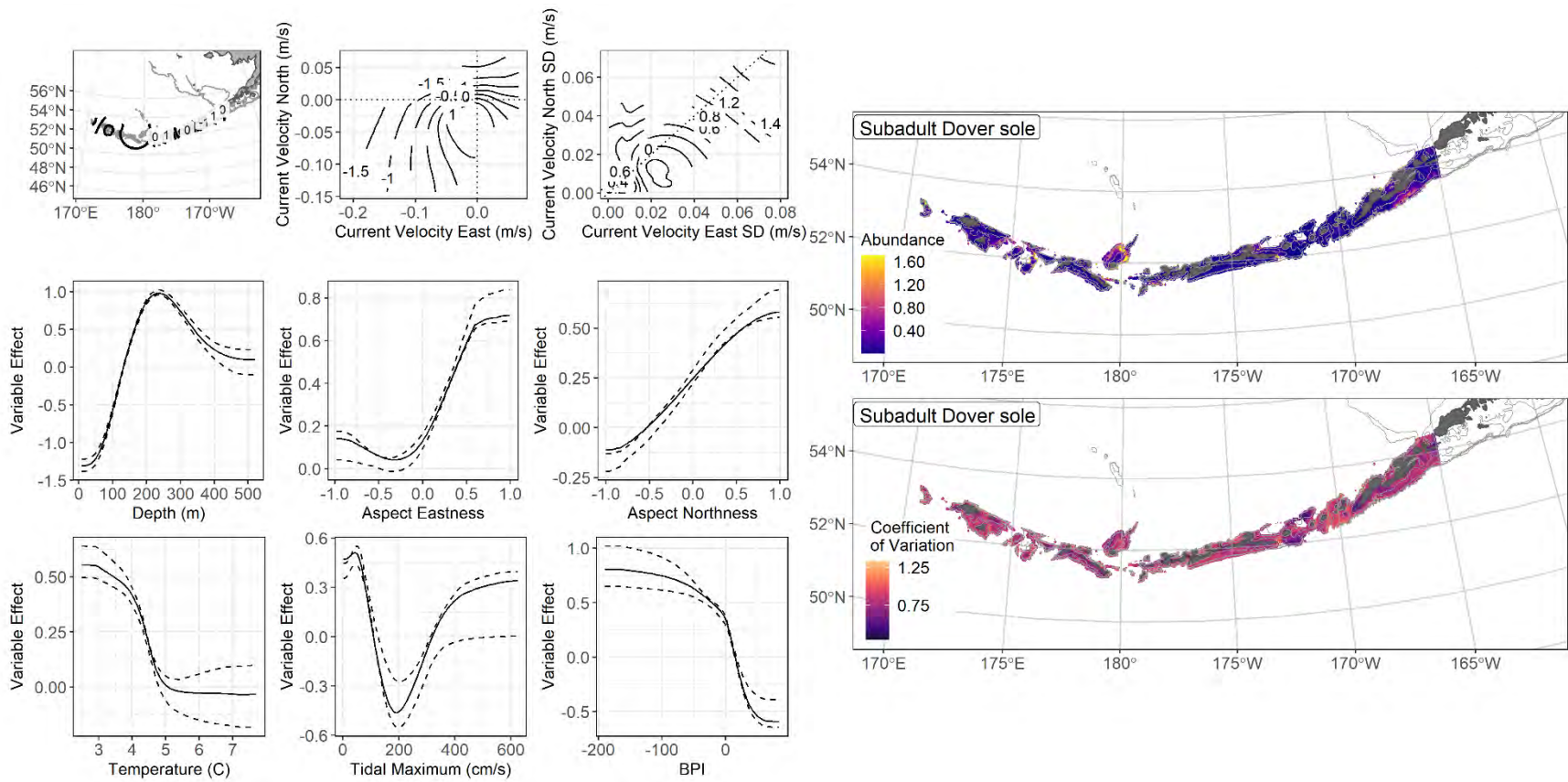
1509

1510 Figure 47. Distribution of subadult Dover sole catches (N = 396) in 1991–2019 AFSC RACE-GAP

1511 summer bottom trawl surveys of the Aleutian Islands with the 100 m, 300 m, and 500 m isobaths

1512 indicated; filled red circles indicate locations in top 10% of overall abundance, open orange circles

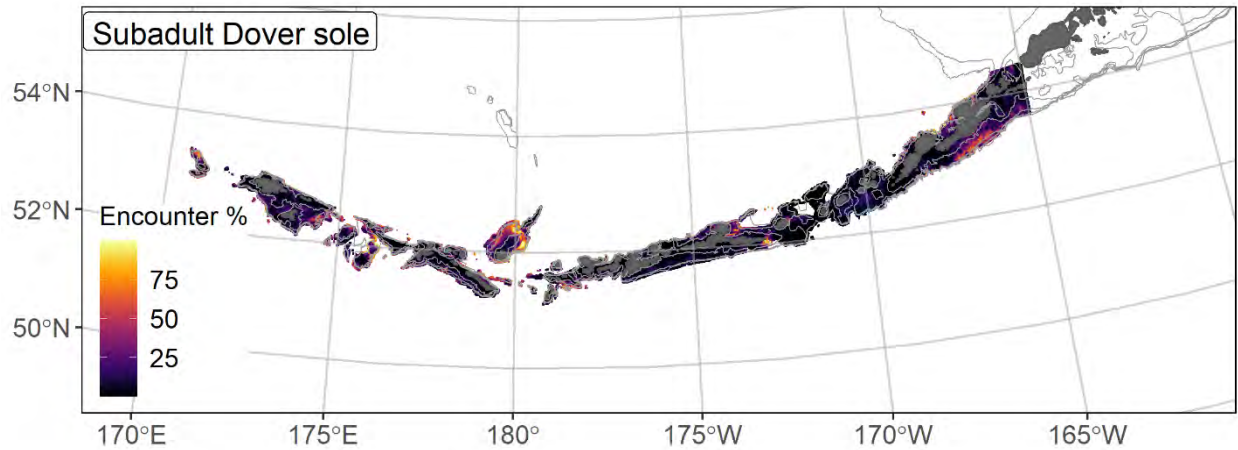
1513 indicate presence in remaining catches, and small blue dots indicate absence.



1514

1515 Figure 48. The top nine covariate effects (left panel) on ensemble-predicted subadult Dover sole numerical abundance across the Aleutian Islands

1516 (upper right panel) alongside the coefficient of variation of the ensemble predictions (lower right panel).

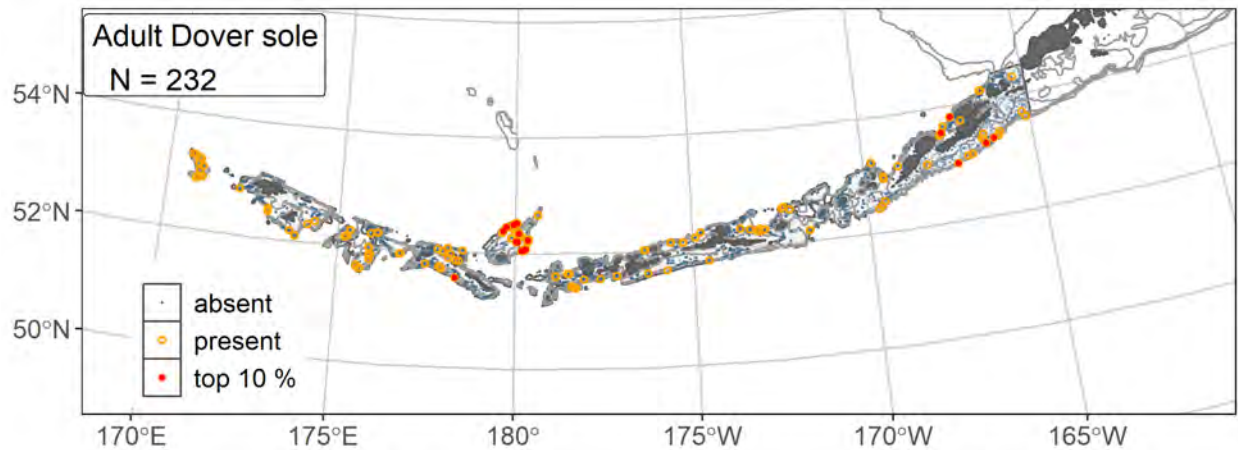


1517

1518 Figure 49. Encounter probability of subadult Dover sole from AFSC RACE-GAP summer bottom trawl

1519 surveys (1991–2019) of the Aleutian Islands with the 100 m, 300 m, and 500 m isobaths indicated.

1520



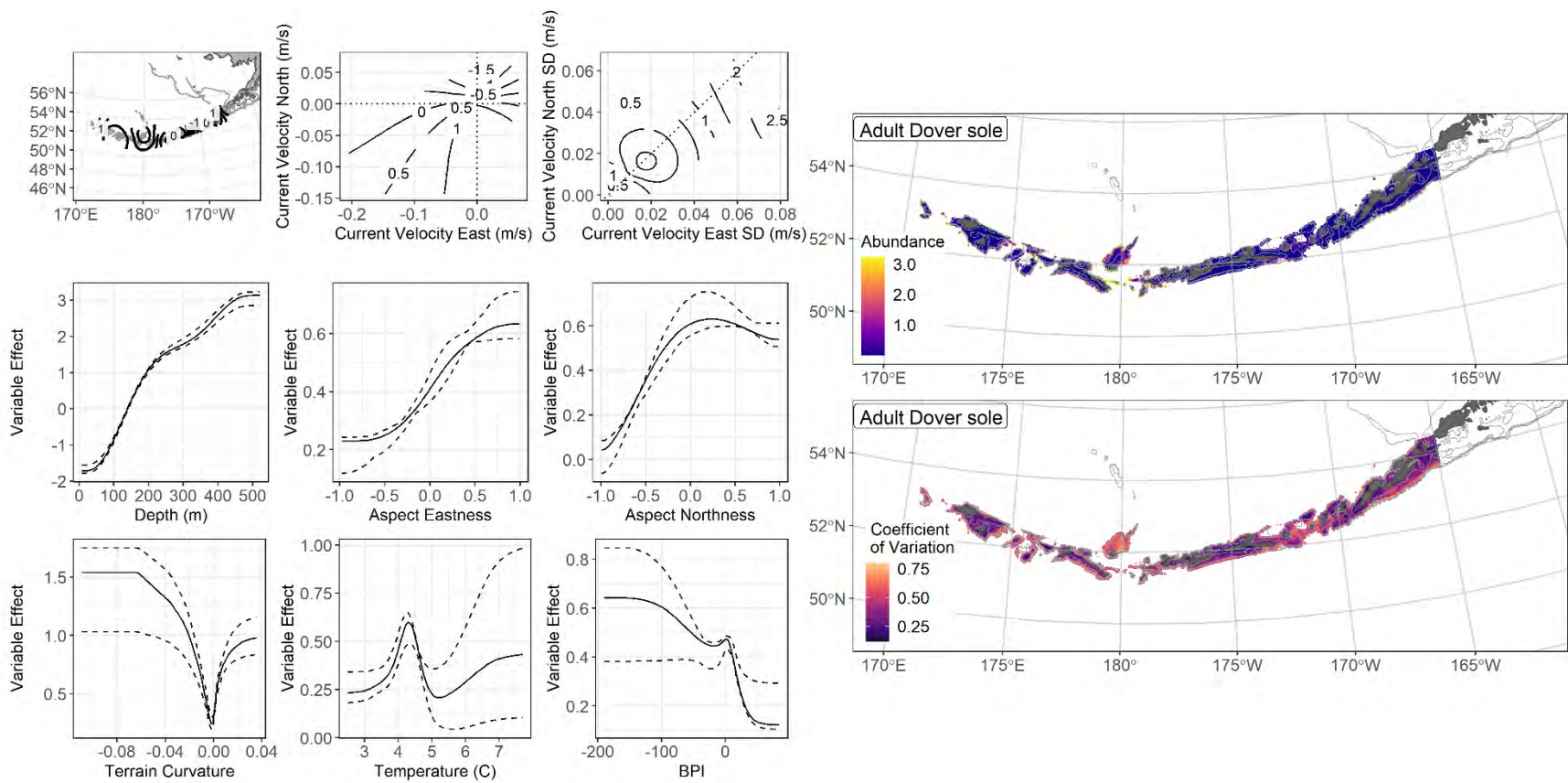
1521

1522 Figure 50. Distribution of adult Dover sole catches (N = 232) in 1991–2019 AFSC RACE-GAP summer

1523 bottom trawl surveys of the Aleutian Islands with the 100 m, 300 m, and 500 m isobaths indicated; filled

1524 red circles indicate locations in top 10% of overall abundance, open orange circles indicate presence in

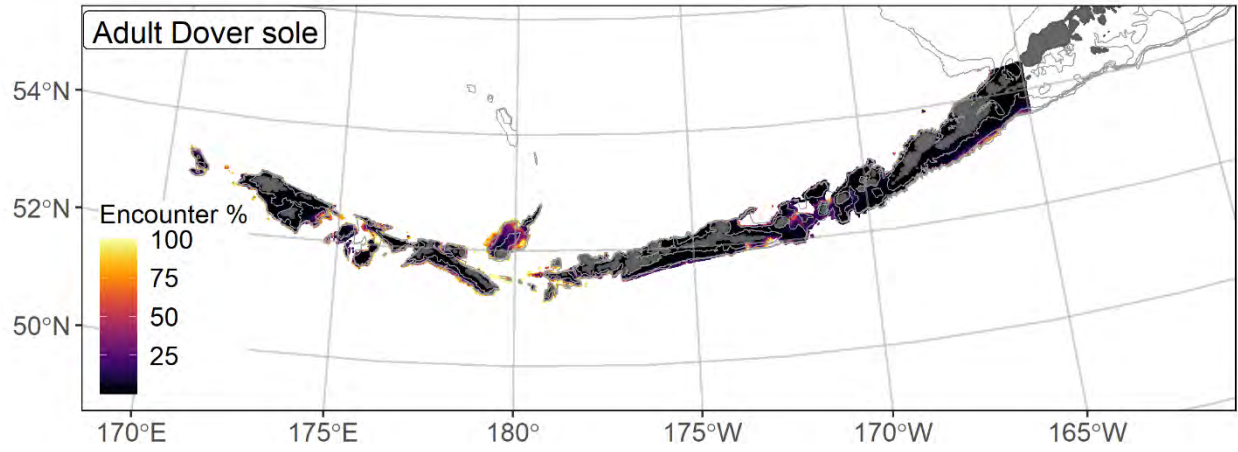
1525 remaining catches, and small blue dots indicate absence.



1526

1527 Figure 51. The top nine covariate effects (left panel) on ensemble-predicted adult Dover sole numerical abundance across the Aleutian Islands

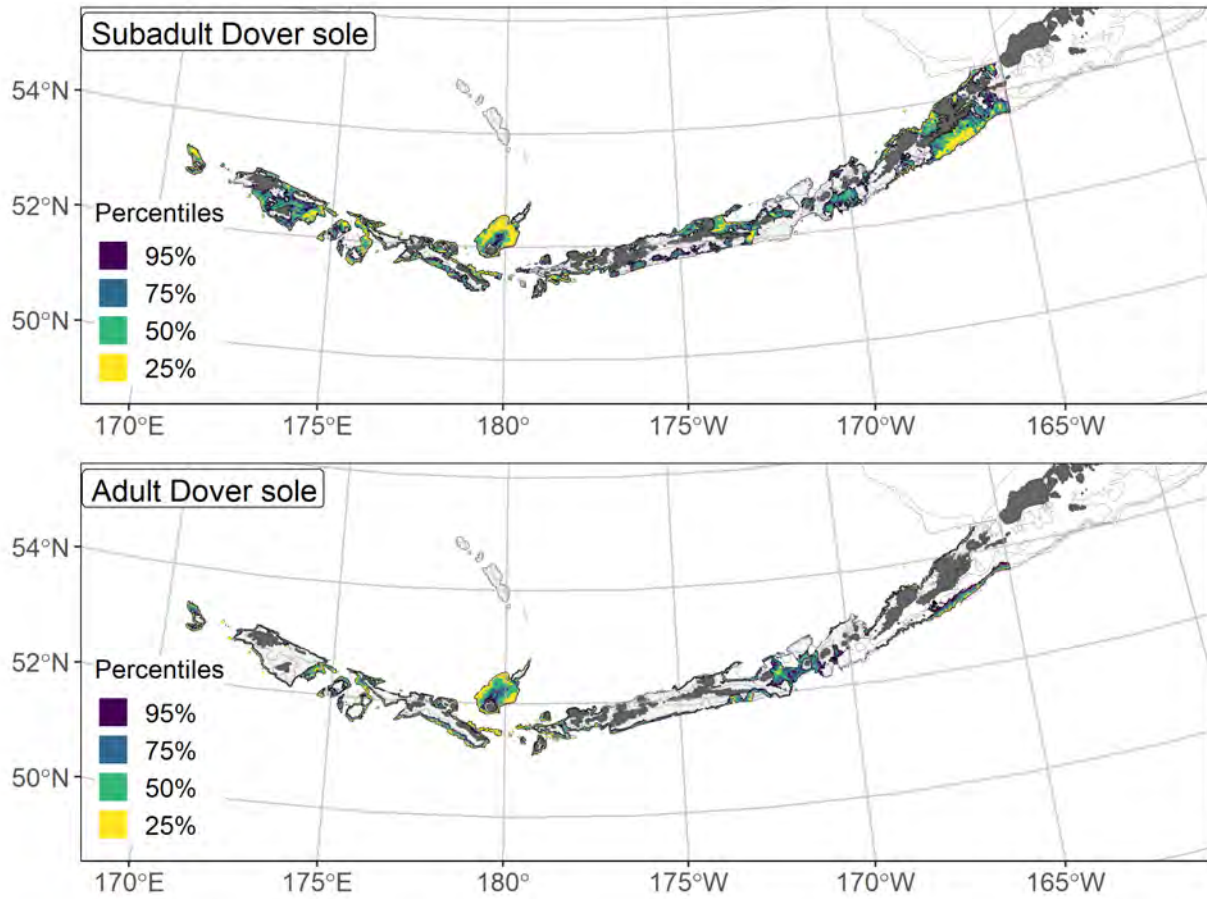
1528 (upper right panel) alongside the coefficient of variation of the ensemble predictions (lower right panel).



1529

1530 Figure 52. Encounter probability of adult Dover sole from AFSC RACE-GAP summer bottom trawl

1531 surveys (1991–2019) of the Aleutian Islands with the 100 m, 300 m, and 500 m isobaths indicated.



1532

1533 Figure 53. Essential fish habitat (EFH area) defined as the top 95% of numerical abundance predictions
 1534 from a habitat-based ensemble fitted to subadult (top) and adult (bottom) Dover sole distribution and
 1535 abundance in AFSC RACE-GAP summer bottom trawl surveys (1991–2019) with 100 m, 300 m, and
 1536 500 m isobaths indicated; internal to the EFH map are the subareas of the top 25% (EFH hot spots), top
 1537 50% (core EFH area), and top 75% (principal EFH area) of habitat related, ensemble-predicted numerical
 1538 abundance.

1539 **English sole (*Parophrys vetulus*)**

1540 English sole (*Parophrys vetulus*) is a moderately-sized flatfish that reaches an adult size of up to
1541 630 mm F. L. in RACE-GAP bottom trawl surveys. It is found from the central AI to Baja California, and
1542 in the Bering Sea (Hart 1973). Little is known about English sole life history in Alaska, but along the
1543 coasts of Oregon and Washington, the spawning season lasts from September to April (Krygier and
1544 Pearcy 1986), and juveniles spend their first year in nursery areas near estuaries before eventually
1545 spreading out along the coast (Gunderson et al. 1990). No settled early juveniles (<140 mm F.L.; Yeung
1546 and Cooper 2020) and very few subadults (<230 mm F.L.; L₅₀; Sampson and Al-Jufaily 1998) were
1547 captured in the AI bottom trawl survey and only adults had sufficient data to construct a species
1548 distribution model. In the BSAI region, English sole are managed as part of the Other Flatfish stock
1549 complex, and do not receive a species-specific fishing target (Monnahan 2020).

1550 **Adult English sole distribution and predicted abundance from RACE-GAP summer bottom trawl**
1551 **surveys in the Aleutian Islands –**

1552 Adult English sole catches in the RACE-GAP summer bottom trawl survey were very rare and
1553 almost all occurrences were near Unalaska Island (Figure 54). In fact, only 50 positive catches of English
1554 sole were recorded in the history of the survey, a count that is considered the bare minimum amount of
1555 data to construct an SDM in this project. Because of this data limitation, all findings for this species in the
1556 AI should be treated as preliminary and used with caution. The ensemble contained three SDMs with
1557 approximately equal weights, and it performed well considering the limited amount of data (Table 17).
1558 The ensemble scored well at predicting presence in trawl catches (AUC = 0.982) and the deviance
1559 explained was also excellent (PDE = 0.817). By contrast, the ensemble did not score highly in terms of
1560 predicting relative abundance ($\rho = 0.238$). These statistics should be interpreted with caution because of
1561 the limited dataset on which they are based. On one hand, the small number of English sole catches in the
1562 AI are almost all near shore around Unalaska Island, which makes presence easy to predict. On the other
1563 hand, with so few occurrences, it is hard to say if this distribution pattern should be expected to be

1564 consistent over time. Several environmental covariates were included in the ensemble for English sole
1565 catches, including tidal maximum, bottom depth, BPI, temperature, and bottom current (Table 18).
1566 English sole catches were associated with weak currents, weak tides, shallow water, and warm
1567 temperatures (Figure 55). Predicted abundance was highest near shore around Unalaska and Umnak
1568 Islands, and low below 100 m depth (Figure 55). The predicted CV of abundance was high in most places
1569 where this species is found, which is unsurprising given the small amount of data (Figure 55). Predicted
1570 encounter probabilities for adult English sole were high in a few places near Unalaska Island, and zero
1571 over most of the AI region (Figure 56).

1572 **Essential fish habitat of adult English sole in the Aleutian Islands –**

1573 The habitat related abundance predictions based on RACE-GAP summer bottom trawl data
1574 (1991–2019) were translated into EFH area and subareas (Figure 57). The EFH area for English sole is
1575 localized to the areas near shore around Unalaska and Umnak Islands, with a smaller area near Atka
1576 Island. All EFH hot spots for English sole occur close to shore, with the overall EFH extending into
1577 deeper water up to 300 m.

1578 Table 17. Constituent species distribution models (SDMs) used to construct Essential Fish Habitat (EFH)
 1579 for adult English sole: MaxEnt = Maximum entropy; paGAM = presence-absence generalized additive
 1580 model; hGAM = hurdle GAM; GAM_P = standard Poisson GAM; and GAM_{nb} = standard negative-
 1581 binomial GAM. Ensemble performance (ρ = Spearman's rank correlation coefficient), root-mean-square-
 1582 error (RMSE), the area under the receiver operating characteristic (AUC), and the Poisson deviance
 1583 explained (PDE) were generated from k-fold cross-validation. The "--" in a field indicates that this SDM
 1584 was not included in the final ensemble.

1585 **adult English sole**

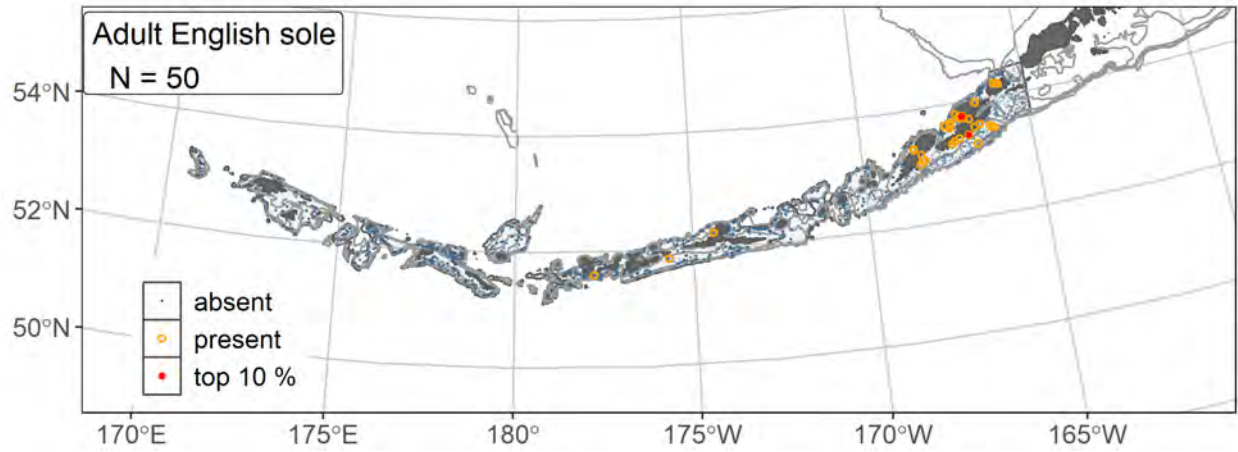
Models	RMSE	Relative Weight	ρ	AUC	PDE	EFH area (km²)
MaxEnt	1.93	0.337	0.256	0.954	0.594	6,800
paGAM	1.95	0.329	0.227	0.982	0.676	11,800
hGAM	--	0	--	--	--	--
GAM _P	1.94	0.334	0.260	0.966	0.835	4,000
GAM _{nb}	1.95	0	--	--	--	--
ensemble	1.48	1	0.238	0.982	0.817	10,300

1586

1587 Table 18. Covariates retained in the adult English sole species distribution model (SDM) final ensembles,
 1588 the percent contribution to the total deviance explained by each, and the cumulative percent deviance:
 1589 SD = standard deviation, and BPI = bathymetric position index.

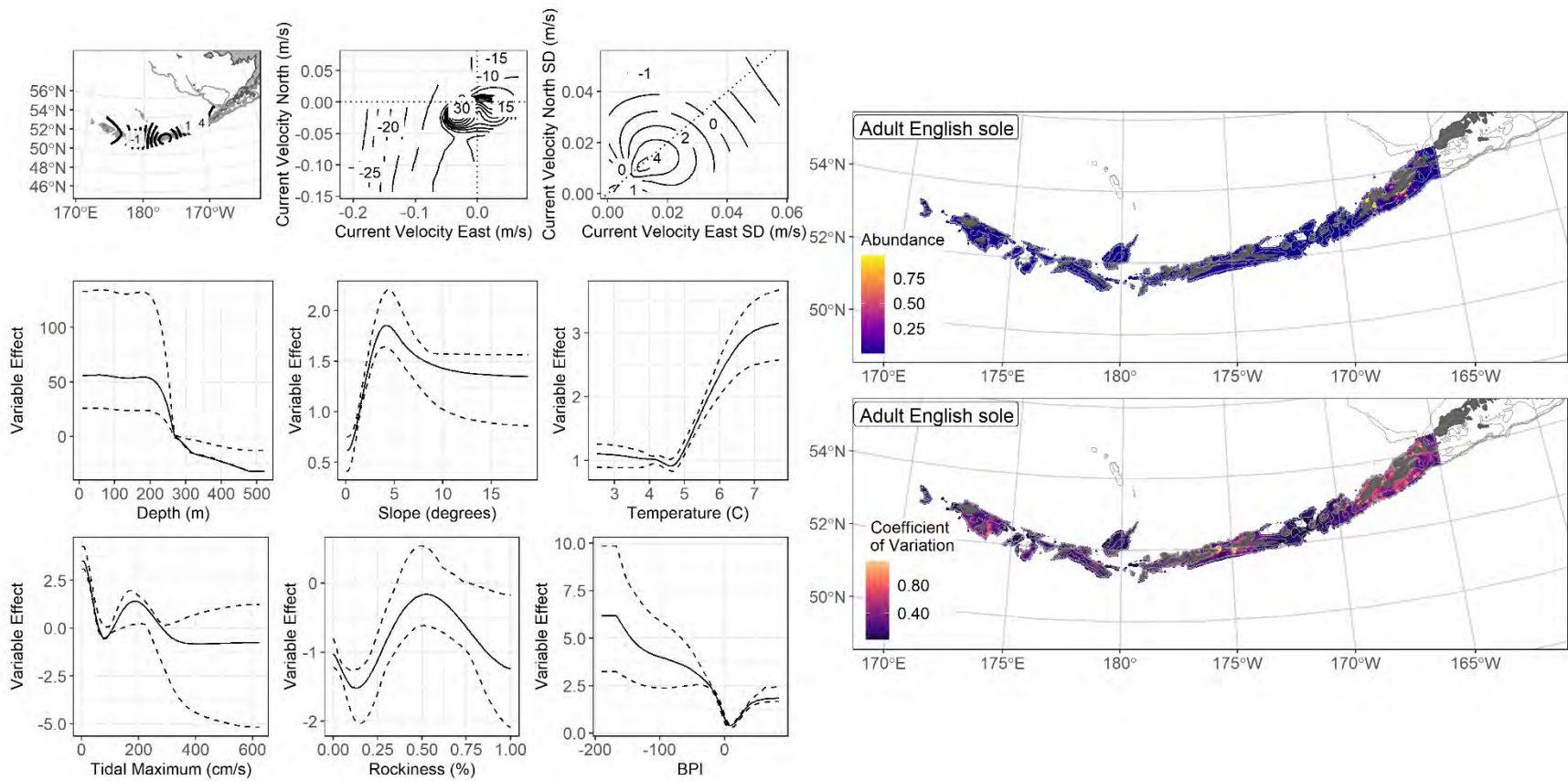
English sole adult	Covariate	% Contribution	Cumulative % Contribution
	tidal maximum	17.8	17.8
	bottom depth	14.3	32.1
	BPI	13.0	45.1
	current SD	11.8	56.9
	current	9.8	66.7
	bottom temperature	9.3	76.0
	slope	8.7	84.7
	position	6.0	90.7
	rockiness	3.1	93.8
	aspect east	2.6	96.4
	pennatulacean presence	1.5	97.9
	aspect north	0.8	98.7
	curvature	0.5	99.2
	coral presence	0.5	99.7
	sponge presence	0.3	100

1590



1591

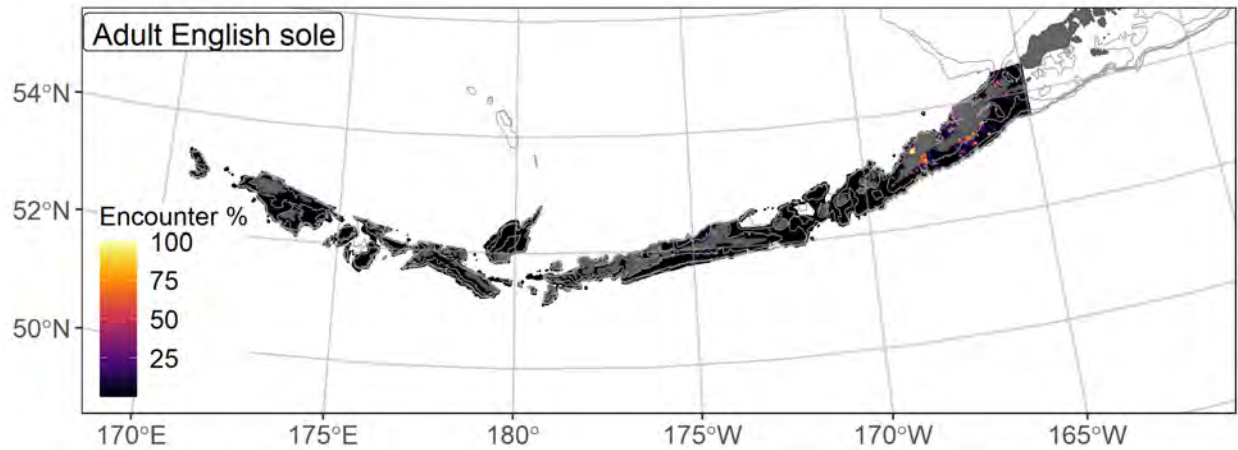
1592 Figure 54. Distribution of adult English sole catches (N = 50) in 1991–2019 AFSC RACE-GAP summer
 1593 bottom trawl surveys of the Aleutian Islands with the 100 m, 300 m, and 500 m isobaths indicated; filled
 1594 red circles indicate locations in top 10% of overall abundance, open orange circles indicate presence in
 1595 remaining catches, and small blue dots indicate absence.



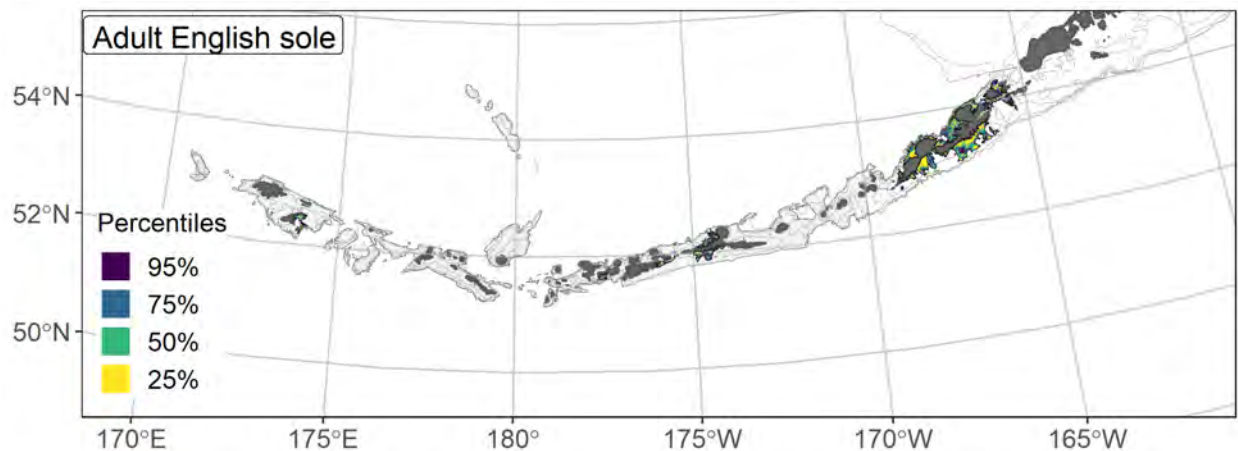
1596

1597 Figure 55. The top nine covariate effects (left panel) on ensemble-predicted adult English sole numerical abundance across the Aleutian Islands

1598 (upper right panel) alongside the coefficient of variation of the ensemble predictions (lower right panel).



1599
 1600 Figure 56. Encounter probability of adult English sole from AFSC RACE-GAP summer bottom trawl
 1601 surveys (1991–2019) of the Aleutian Islands with the 100 m, 300 m, and 500 m isobaths indicated.



1602
 1603 Figure 57. Essential fish habitat (EFH area) defined as the top 95% of numerical abundance predictions
 1604 from a habitat-based ensemble fitted to adult English sole distribution and abundance in AFSC RACE-
 1605 GAP summer bottom trawl surveys (1991–2019) with 100 m, 300 m, and 500 m isobaths indicated;
 1606 internal to the EFH map are the subareas of the top 25% (EFH hot spots), top 50% (core EFH area), and
 1607 top 75% (principal EFH area) of habitat related, ensemble-predicted numerical abundance.

1608 **Rex sole (*Glyptocephalus zachirus*)**

1609 Rex sole (*Glyptocephalus zachirus*) is a widely distributed flatfish with a native range that
1610 extends from Baja California to the western Bering Sea (Mecklenburg et al. 2002). Adults may grow to
1611 600 mm T.L. and are found from the surface to depths of 850 m (Abookire and Bailey 2007). Early
1612 juveniles settle between 70 and 140 mm T.L. (Doyle et al. 2019). The majority of rex sole reach maturity
1613 (L_{50}) at 352 mm (Abookire 2006). Spawning occurs offshore and in deeper water along the edge of the
1614 continental slope, with juveniles distributed inshore. This species has an estimated spawning period from
1615 October to May in the GOA (Abookire 2006), and an extended larval stage that can last from nine months
1616 to two years (Abookire 2006, Percy et. al. 1977). Significant regional differences in rex sole growth rates
1617 have been observed in the GOA and along the Oregon coast with Alaska populations having higher
1618 growth rates (Abookire 2006). Rex sole are managed as a part of “other flatfish” stock complex in the
1619 BSAI (Monnahan 2020).

1620 **Subadult rex sole distribution and predicted abundance from RACE-GAP summer bottom trawl**
1621 **surveys in the Aleutian Islands–**

1622 Subadult rex sole catches were common throughout the RACE-GAP summer survey areas
1623 (Figure 58), but were higher in the eastern AI. The final ensemble contained four SDMs, and the hGAM
1624 and GAM_P received slightly more weight (Table 19). The ensemble showed good performance across all
1625 three fit metrics ($\rho = 0.490$; AUC = 0.836; PDE = 0.486; Table 19). Geographic position and bottom
1626 depth accounted for 54.4% of the deviance explained by the ensemble, though current, current variability,
1627 and tidal maximum were also important (Table 20). In general, abundance was predicted to be higher at
1628 more eastern longitudes, at depths between 150-300 m, in weak currents, and at a low tidal maximum
1629 (Figure 59). Predicted abundance was high in the eastern AI, particularly south of Unalaska Island and
1630 Unimak Pass and moderate around Atka and Agattu Islands (Figure 59). The predicted CV of abundance
1631 was low in the east near Unalaska Island and somewhat higher further west (Figure 59). This predicts that
1632 estimates of high abundances in the eastern AI are likely to be reliable, while the abundance estimates in

1633 other locations may be more variable. Encounter probabilities for subadult rex sole were high in most
1634 areas between the 100 m and 300 m depth contours, particularly in the eastern AI, and are lower around
1635 the passes and sea mounts further west (Figure 60).

1636 **Adult rex sole distribution and predicted abundance from RACE-GAP summer bottom trawl**
1637 **surveys in the Aleutian Islands –**

1638 Adult rex sole catches in the RACE-GAP summer survey were evenly distributed across most of
1639 the AI, though like subadults, large catches were more common in the east near Unalaska Island and
1640 Unimak Pass (Figure 61). The final ensemble contained four SDMs, and the GAM_P and hGAM
1641 performed somewhat better than the paGAM or MaxEnt and were given higher weights (Table 19). The
1642 ensemble had a good fit to the data, scoring well on all three fit metrics ($\rho = 0.581$; AUC = 0.833;
1643 PDE = 0.457; Table 19). Geographic position and bottom depth account for a combined 48.5% of the
1644 deviance explained by the ensemble (Table 20), though current, tidal maximum, and slope aspect were
1645 also important. Like subadults, adult rex sole are predicted to be abundant in the eastern AI and are
1646 associated with areas with weak bottom currents and deeper habitats (Figure 62). Very similar to
1647 subadults, predicted abundance of adult rex sole was highest south of Unalaska Island, but occurred
1648 further offshore and in deeper water (Figure 62). The predicted CV of abundance was low in deeper areas,
1649 and higher in moderate to shallow ones, which reflects that adult rex sole are consistently found in deeper
1650 water (Figure 62). Encounter probabilities for adult rex sole are high in most places except in some
1651 shallow areas close to shore (Figure 63).

1652 **Essential fish habitat of subadult and adult rex sole in the Aleutian Islands –**

1653 The habitat related abundance predictions based on RACE-GAP summer bottom trawl data
1654 (1991–2019) were translated into EFH area and subareas (Figure 64). The EFH areas for the two life
1655 stages of rex sole were similar, with large hot spots to the south of Unalaska Island. Both life stages also
1656 had smaller hot spots further west near Atka Island and Agattu Island. Subadults were less likely to be

1657 found in waters deeper than 300 m, so areas near sea mounts or along the edge of the continental slope
1658 did not qualify as EFH. However, the greater depth range of adults allows them to occupy these areas.

1659 Table 19. Constituent species distribution models (SDMs) used to construct Essential Fish Habitat (EFH)
 1660 for a) subadult and b) adult rex sole: MaxEnt = Maximum entropy; paGAM = presence-absence
 1661 generalized additive model; hGAM = hurdle GAM; GAM_p = standard Poisson GAM; and
 1662 GAM_{nb} = standard negative-binomial GAM. Ensemble performance (ρ = Spearman's rank correlation
 1663 coefficient), root-mean-square-error (RMSE), the area under the receiver operating characteristic (AUC),
 1664 and the Poisson deviance explained (PDE) were generated from k-fold cross-validation. The "--" in a field
 1665 indicates that this SDM was not included in the final ensemble.

1666 **a) subadult rex sole**

Models	RMSE	Relative Weight	ρ	AUC	PDE	EFH area (km²)
MaxEnt	9.32	0.220	0.453	0.814	0.303	69,400
paGAM	9.06	0.223	0.497	0.843	0.393	71,000
hGAM	8.30	0.277	0.458	0.843	0.508	61,300
GAM _p	8.41	0.270	0.430	0.792	0.494	62,400
GAM _{nb}	13.31	0	--	--	--	--
ensemble	7.92	1	0.490	0.836	0.486	69,100

1667 **b) adult rex sole**

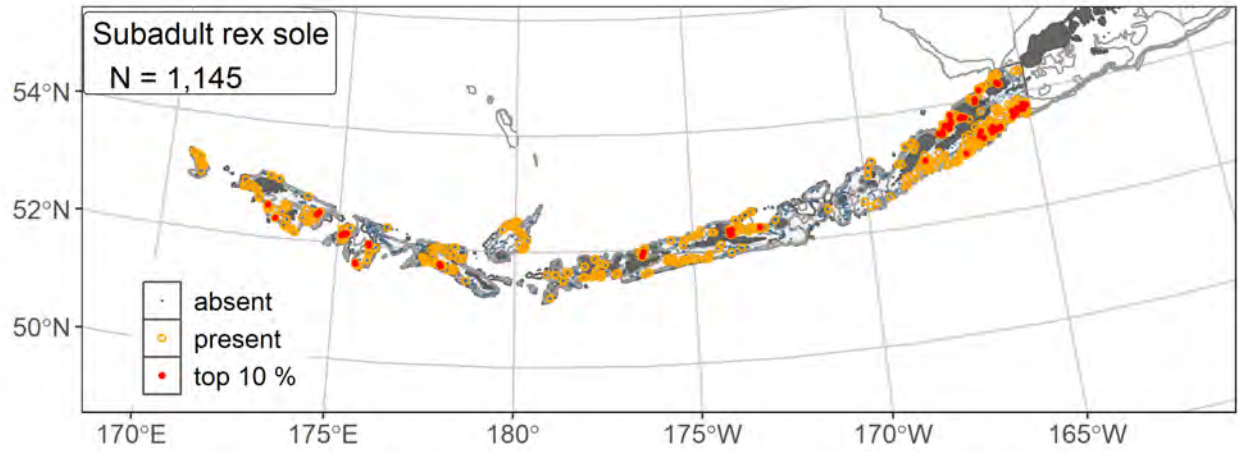
Models	RMSE	Relative Weight	ρ	AUC	PDE	EFH area (km²)
MaxEnt	26.0	0.215	0.550	0.821	0.249	74,400
paGAM	26.5	0.206	0.590	0.844	0.325	77,500
hGAM	22.2	0.293	0.549	0.844	0.477	74,200
GAM _p	22.5	0.286	0.520	0.793	0.462	76,800
GAM _{nb}	43.8	0	--	--	--	--
ensemble	22.2	1	0.581	0.833	0.457	77,200

1668

1669 Table 20. Covariates retained in the a) subadult and b) adult rex sole species distribution model (SDM)
 1670 final ensembles, the percent contribution to the ensemble deviance explained by each, and the cumulative
 1671 percent deviance: SD = standard deviation, and BPI = bathymetric position index.

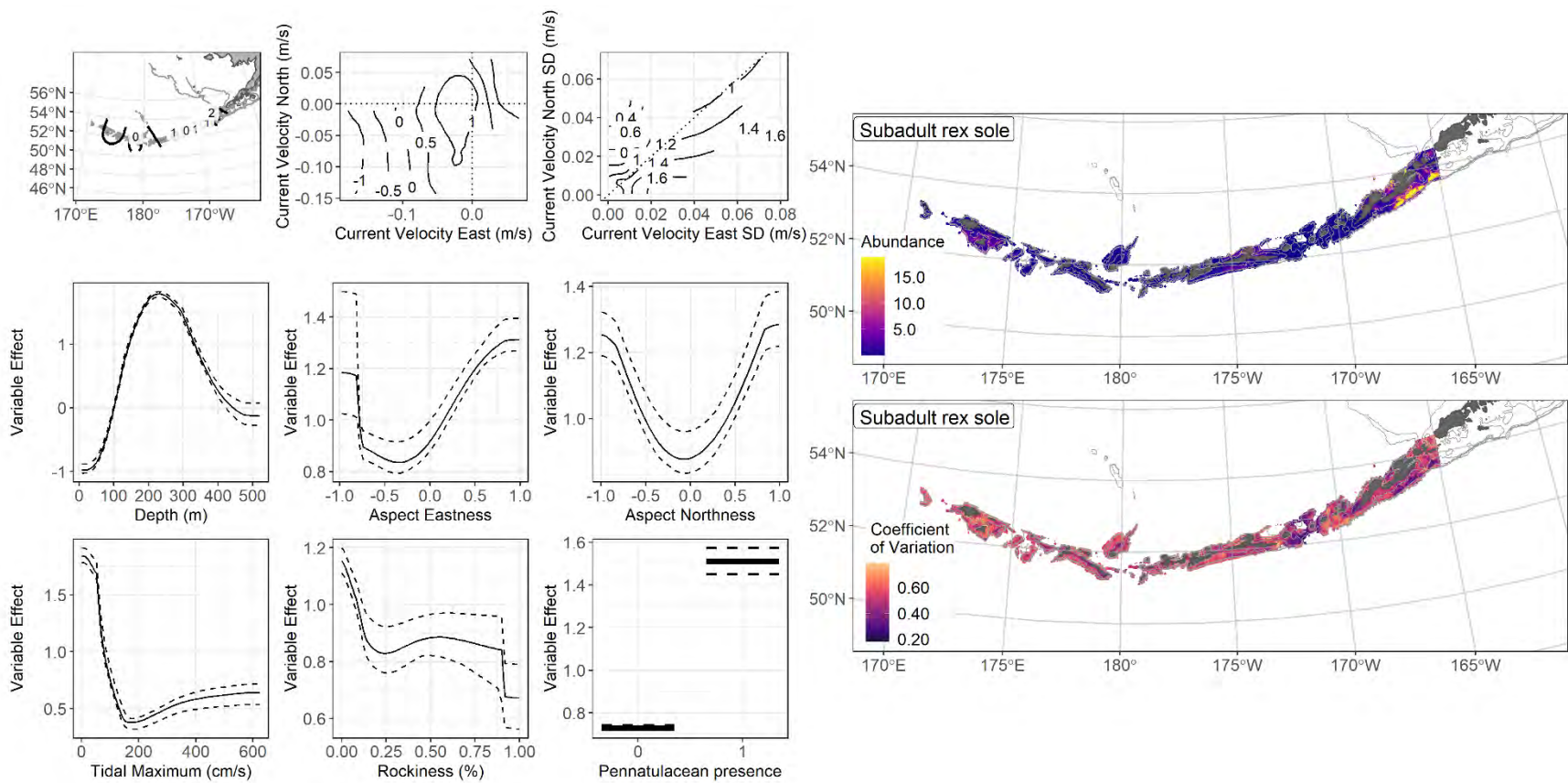
rex sole	Covariate	% Contribution	Cumulative % Contribution
a) subadult	position	27.4	27.4
	bottom depth	27.1	54.4
	current SD	7.3	61.7
	current	7.2	68.9
	tidal maximum	7.1	76.0
	aspect north	5.2	81.2
	aspect east	3.6	84.8
	rockiness	3.6	88.4
	pennatulacean presence	3.5	91.9
	BPI	3.2	95.1
	slope	2.0	97.1
	bottom temperature	1.6	98.7
	sponge presence	0.7	99.4
	curvature	0.4	99.8
coral presence	0.2	100	
a) adult	position	25.0	25.0
	bottom depth	23.5	48.5
	current	9.3	57.7
	tidal maximum	8.5	66.2
	aspect north	7.9	74.1
	current SD	7.2	81.3
	rockiness	5.2	86.5
	aspect east	5.1	91.6
	slope	3.3	94.9
	bottom temperature	1.6	96.5
	BPI	1.3	97.8
	pennatulacean presence	0.9	98.7
	coral presence	0.6	99.3
	sponge presence	0.5	99.8
curvature	0.2	100	

1672



1673

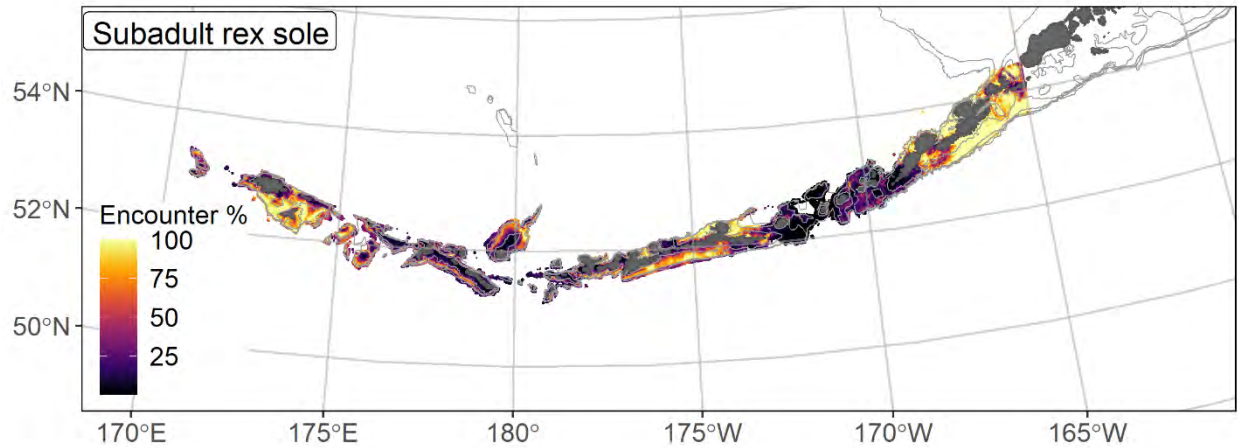
1674 Figure 58. Distribution of subadult rex sole catches (N = 1,145) in 1991–2019 AFSC RACE-GAP
 1675 summer bottom trawl surveys of the Aleutian Islands with the 100 m, 300 m, and 500 m isobaths
 1676 indicated; filled red circles indicate locations in top 10% of overall abundance, open orange circles
 1677 indicate presence in remaining catches, and small blue dots indicate absence.



1678

1679 Figure 59. The top nine covariate effects (left panel) on ensemble-predicted subadult rex sole numerical abundance across the Aleutian Islands

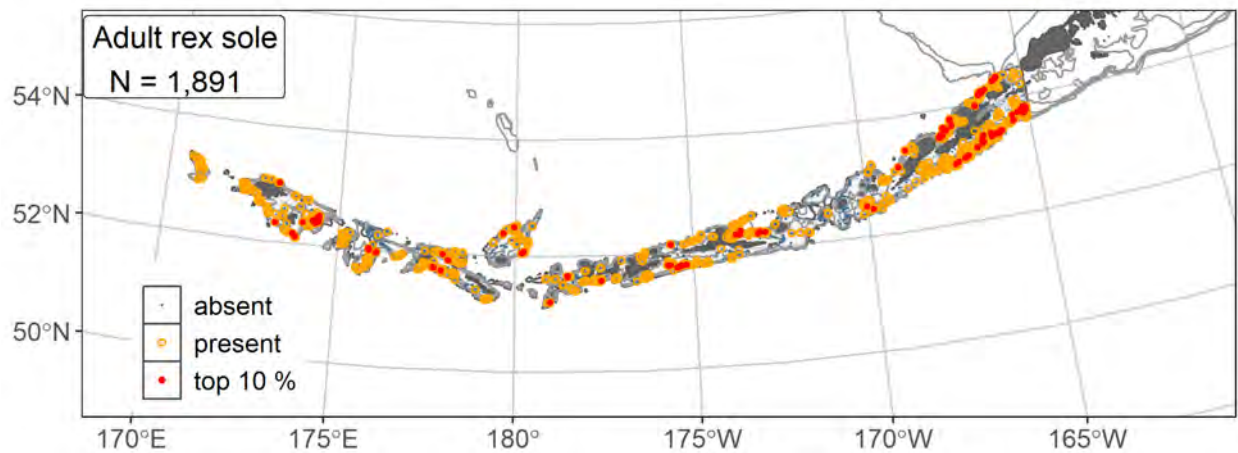
1680 (upper right panel) alongside the coefficient of variation of the ensemble predictions (lower right panel).



1681

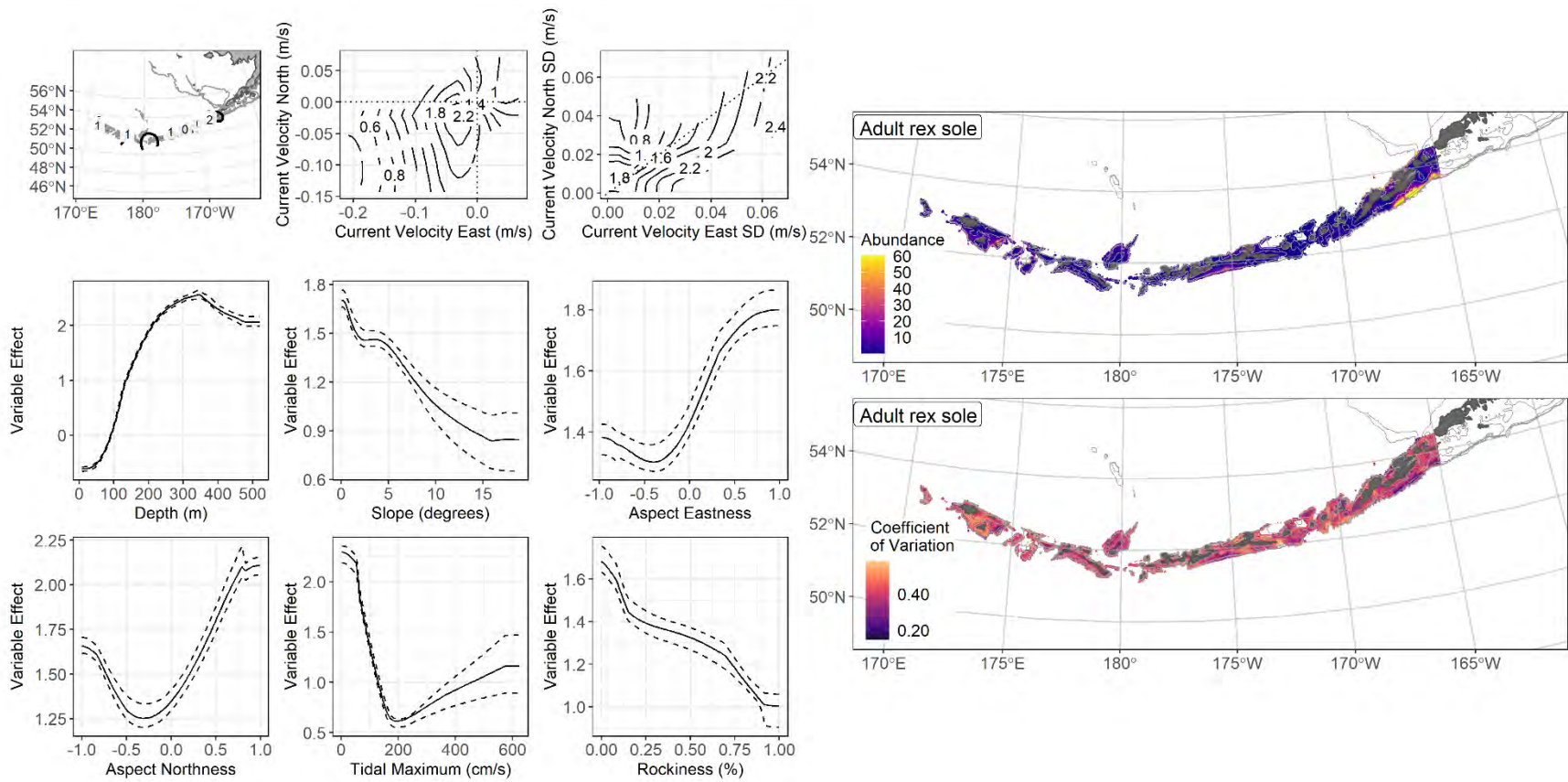
1682 Figure 60. Encounter probability of subadult rex sole from AFSC RACE-GAP summer bottom trawl
 1683 surveys (1991–2019) of the Aleutian Islands with the 100 m, 300 m, and 500 m isobaths indicated.

1684



1685

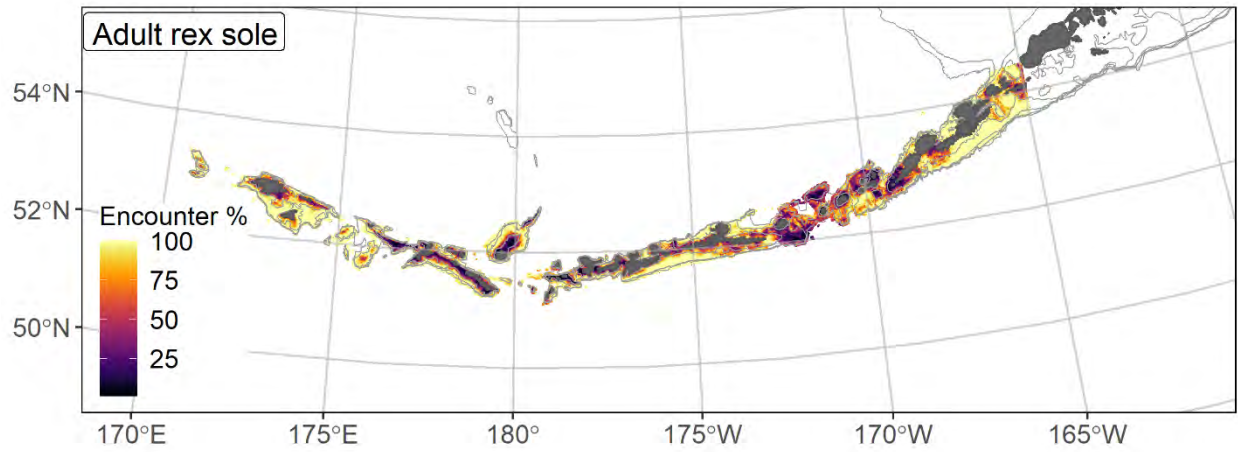
1686 Figure 61. Distribution of adult rex sole catches (N = 1,891) in 1991–2019 AFSC RACE-GAP summer
 1687 bottom trawl surveys of the Aleutian Islands with the 100 m, 300 m, and 500 m isobaths indicated; filled
 1688 red circles indicate locations in top 10% of overall abundance, open orange circles indicate presence in
 1689 remaining catches, and small blue dots indicate absence.



1690

1691 Figure 62. The top nine covariate effects (left panel) on ensemble-predicted adult rex sole numerical abundance across the Aleutian Islands (upper

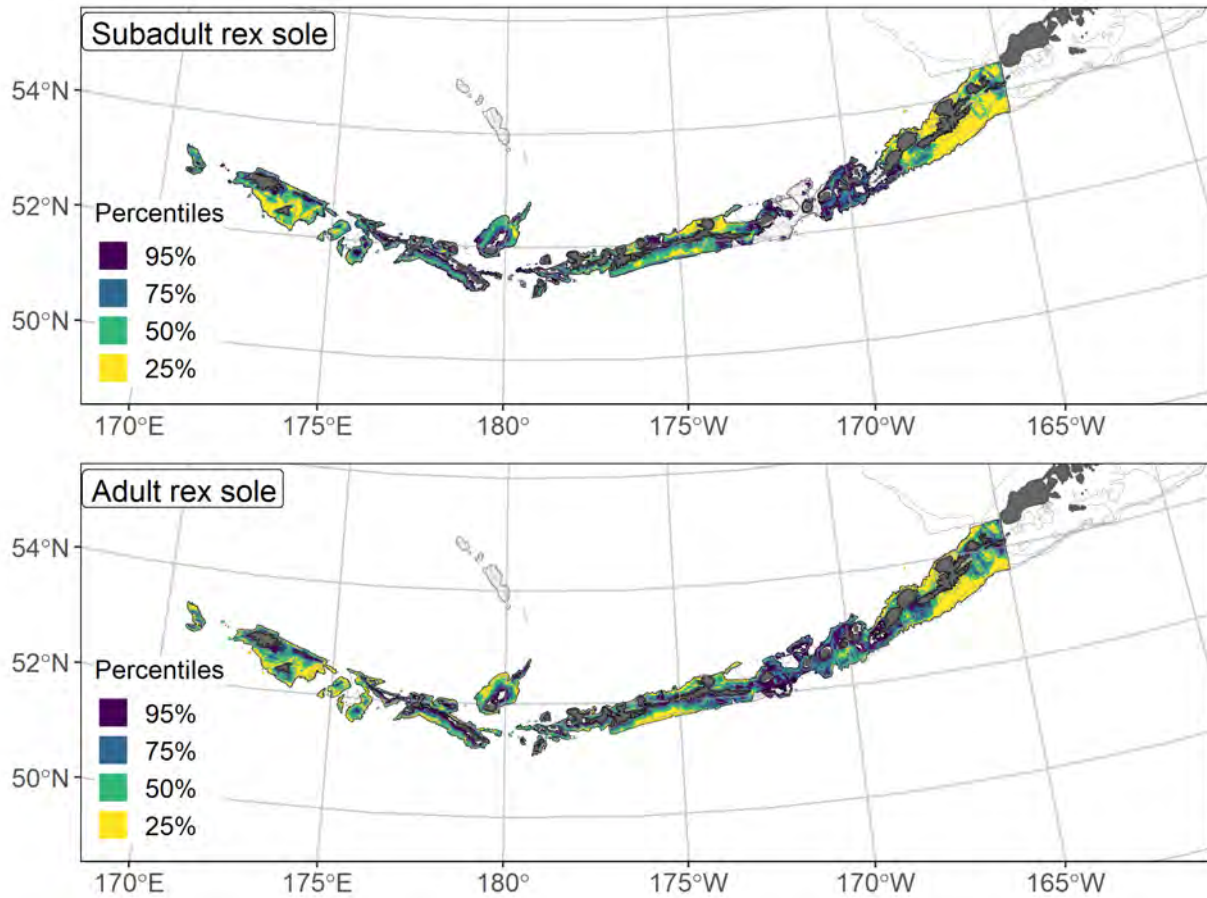
1692 right panel) alongside the coefficient of variation of the ensemble predictions (lower right panel).



1693

1694 Figure 63. Encounter probability of adult rex sole from AFSC RACE-GAP summer bottom trawl surveys

1695 (1991–2019) of the Aleutian Islands with the 100 m, 300 m, and 500 m isobaths indicated.



1696

1697 Figure 64. Essential fish habitat (EFH area) defined as the top 95% of numerical abundance predictions
 1698 from a habitat-based ensemble fitted to subadult (top) and adult (bottom) rex sole distribution and
 1699 abundance in AFSC RACE-GAP summer bottom trawl surveys (1991–2019) with 100 m, 300 m, and
 1700 500 m isobaths indicated; internal to the EFH map are the subareas of the top 25% (EFH hot spots), top
 1701 50% (core EFH area), and top 75% (principal EFH area) of habitat related, ensemble-predicted numerical
 1702 abundance.

1703 **Southern rock sole (*Lepidopsetta bilineata*)**

1704 Southern rock sole (*Lepidopsetta bilineata*) is found in coastal waters from the eastern AI to Baja
1705 California (Orr and Matarese 2000). The species is morphologically similar to northern rock sole (*L.*
1706 *polyxstra*), and the two species are often confounded in older literature. They were not routinely
1707 distinguished in groundfish surveys until 1996. There is broad overlap in the ranges of the two species in
1708 the Gulf of Alaska and the eastern Aleutian Islands. Adults may grow to as much as 580 mm T. L. (Orr
1709 and Matarese 2000), and females become mature at approximately 347 mm T.L. (L₅₀; Stark and Somerton
1710 2002). Female length at maturity was used to separate life stages for both sexes in this study. Compared
1711 to northern rock sole, there has been comparatively little research specific to southern rock sole. In the
1712 BSAI region, almost the entire catch of southern rock sole in the survey is from the eastern AI. It is
1713 managed in the BSAI in a mixed stock fishery with the more abundant and commercially valuable
1714 northern rock sole stock (McGillard et al 2020).

1715 **Subadult southern rock sole distribution and predicted abundance from RACE-GAP summer**
1716 **bottom trawl surveys in the Aleutian Islands–**

1717 Subadult southern rock sole catches from the RACE-GAP summer survey were concentrated in
1718 the eastern AI (Figure 65). Catches were less common west of 170° W. Only two SDMs were included in
1719 the ensemble and the GAM_P was weighted somewhat higher than the paGAM. The ensemble showed a
1720 good to excellent fit to the observed data (Table 21). Specifically, the ensemble demonstrated “good”
1721 ability to predict high vs low density catches ($\rho = 0.551$), and demonstrated “excellent” performance in
1722 terms of predicting presence and in terms of deviance explained (AUC = 0.969; PDE = 0.773). Together,
1723 these results suggested that the predictions of the ensemble were accurate and adequately described the
1724 distribution of this species. Bottom depth and geographic position accounted for 80.8% of the deviance
1725 explained by the ensemble (Table 22). In general, high abundance was predicted by shallow water, being
1726 further east, and weak currents (Figure 66). Predicted abundance was highest in the eastern AI,
1727 particularly around Unalaska Island (Figure 66). The predicted CV of abundance was high in many

1728 shallow areas across the AI, including areas where the ensemble predicted abundance (Figure 66).
1729 Consistent with other results, the predicted encounter probability for subadult southern rock sole was high
1730 in the eastern part of the AI survey area, and in shallow water around Atka Island (Figure 67).

1731 **Adult southern rock sole distribution and predicted abundance from RACE-GAP summer bottom**
1732 **trawl surveys in the Aleutian Islands –**

1733 Similar to the subadults, adult southern rock sole catches from the RACE-GAP summer survey
1734 were concentrated in the eastern Aleutian Islands and southern Bering Sea (Figure 68). All the largest
1735 catches occurred near Unalaska Island or Unimak Pass. The ensemble consisted of two SDMs, and the
1736 GAM_P was weighted somewhat higher than the paGAM. The ensemble showed excellent performance
1737 across all three fit metrics (Table 21). Bottom depth and geographic position alone counted for 89.8% of
1738 the deviance explained by the ensemble (Table 22). Southern rock sole were predicted to be abundant in
1739 shallow water and in eastern longitudes (Figure 69). As with subadults, predicted abundance for adult
1740 southern rock sole was highest in the eastern parts of the AI, particularly around Unalaska Island
1741 (Figure 69). The predicted CV of abundance was low in most places, higher in deeper waters in the east,
1742 as well as shallow areas in the central AI (Figure 69). This pattern reflects that the area around Unalaska
1743 has consistently high abundance, whereas catches further east are more variable. Encounter probabilities
1744 were uniformly high in the eastern AI, though a second area near shore around Atka Island also showed
1745 high probabilities (Figure 70).

1746 **Essential fish habitat of subadult and adult southern rock sole in the Aleutian Islands –**

1747 The habitat related abundance predictions based on RACE-GAP summer bottom trawl data
1748 (1996–2019) were translated into EFH area and subareas (Figure 71). Overall, the EFH areas for each life
1749 stage were very similar. Both life stages had a large hot spot in the southern Bering Sea subregion
1750 centered on Unalaska Island and an area of core EFH centered on Atka Island. These regions were
1751 marked by large, shallow continental shelf habitats, and the high performance scores for the models

1752 suggested that this association is accurate. There also appeared to be a strong longitudinal cline that is not
1753 explained by other habitat covariates, given their low weight in the ensembles (Table 6). This indicates
1754 that other covariates not included here may explain the absence of the species from similar habitats
1755 further west, such as Petrel Bank or the area around Attu Island.

1756 Table 21. Constituent species distribution models (SDMs) used to construct Essential Fish Habitat (EFH)
 1757 for a) subadult and b) adult southern rock sole: MaxEnt = Maximum entropy; paGAM = presence-
 1758 absence generalized additive model; hGAM = hurdle GAM; GAM_P = standard Poisson GAM; and
 1759 GAM_{nb} = standard negative-binomial GAM. Ensemble performance (ρ = Spearman's rank correlation
 1760 coefficient), root-mean-square-error (RMSE), the area under the receiver operating characteristic (AUC),
 1761 and the Poisson deviance explained (PDE) were generated from k-fold cross-validation. The "--" in a field
 1762 indicates that this SDM was not included in the final ensemble.

1763 **a) subadult southern rock sole**

Models	RMSE	Relative Weight	ρ	AUC	PDE	EFH area (km²)
MaxEnt	--	0	--	--	--	--
paGAM	13.5	0.440	0.549	0.970	0.680	46,100
hGAM	--	0	--	--	--	--
GAM _P	11.9	0.560	0.591	0.957	0.784	30,400
GAM _{nb}	13.4	0	--	--	--	--
ensemble	11.6	1	0.551	0.969	0.773	42,000

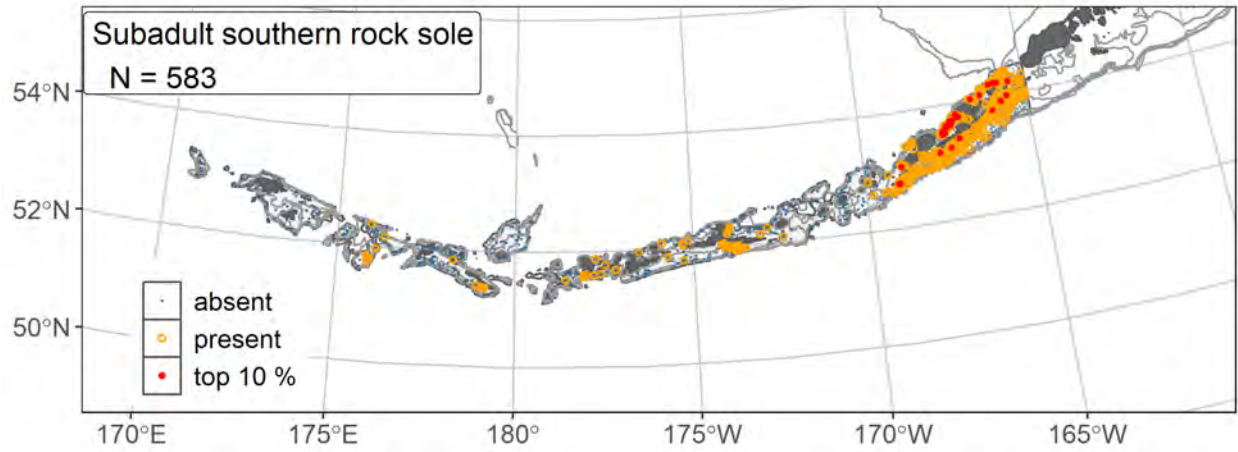
1764 **b) adult southern rock sole**

Models	RMSE	Relative Weight	ρ	AUC	PDE	EFH area (km²)
MaxEnt	--	0	--	--	--	--
paGAM	13.1	0.435	0.623	0.976	0.745	43,900
hGAM	26.7	0	--	--	--	--
GAM _P	11.5	0.565	0.626	0.965	0.822	37,200
GAM _{nb}	17.1	0	--	--	--	--
ensemble	11.6	1	0.625	0.974	0.810	42,300

1765

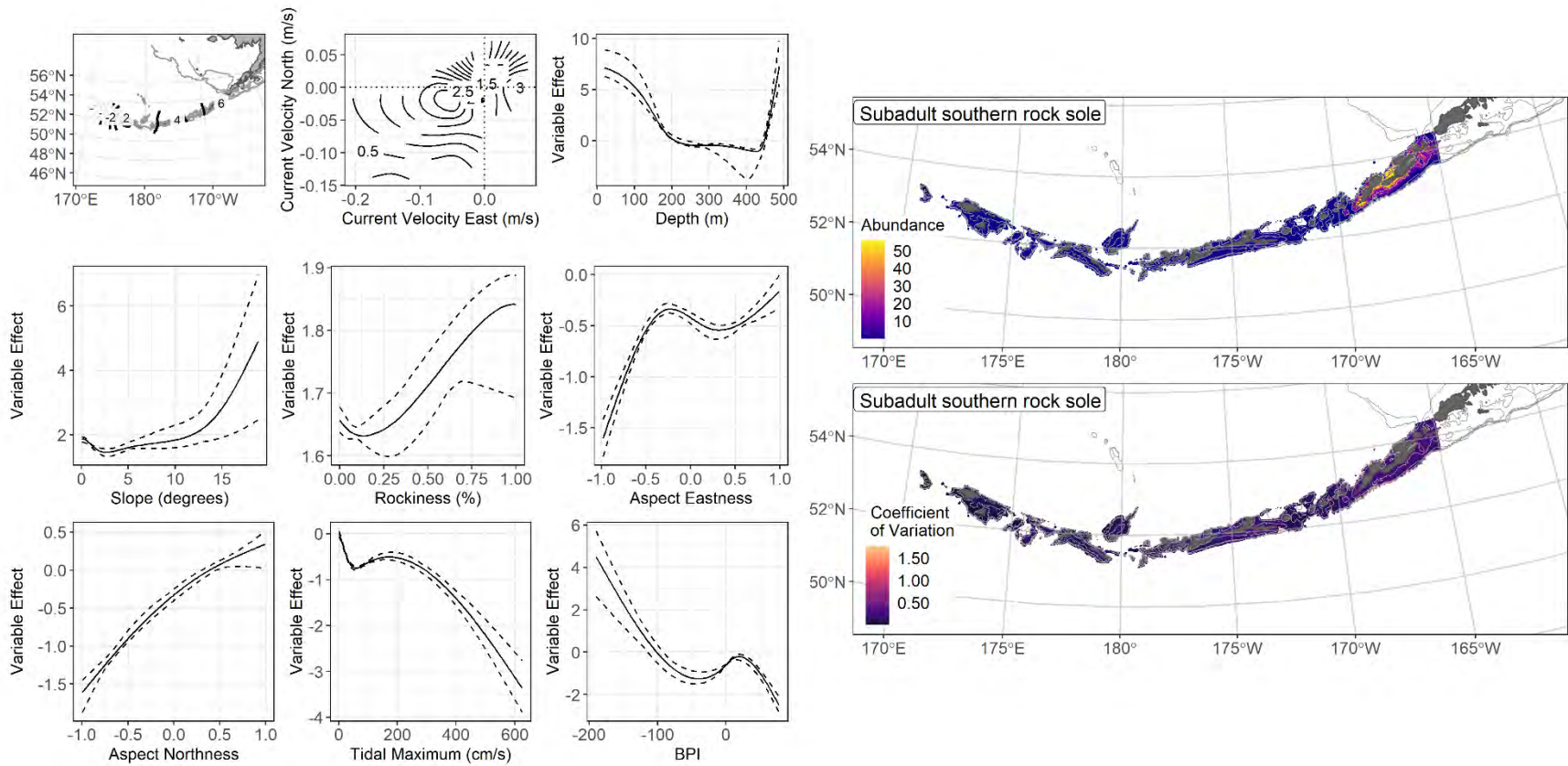
1766 Table 22. Covariates retained in the a) subadult and b) adult southern rock sole species distribution model
 1767 (SDM) final ensembles, the percent contribution to the ensemble deviance explained by each, and the
 1768 cumulative percent deviance: SD = standard deviation, and BPI = bathymetric position index.

southern rock sole	Covariate	% Contribution	Cumulative % Contribution
a) subadult	position	41.4	41.4
	bottom depth	39.3	80.8
	current	7.3	88.1
	aspect north	3.2	91.3
	tidal maximum	1.6	92.9
	BPI	1.2	94.1
	rockiness	1.1	95.2
	aspect east	1.1	96.3
	slope	1.0	97.3
	bottom temperature	1.0	98.3
	current SD	0.8	99.1
	curvature	0.5	99.6
	sponge presence	0.2	99.8
	coral presence	0.2	100
	pennatulacean presence	0	100
a) adult	position	50.4	50.4
	bottom depth	39.4	89.8
	current	3.6	93.4
	aspect north	2.1	95.5
	current SD	1.0	96.5
	BPI	0.8	97.3
	slope	0.7	98.0
	curvature	0.7	98.7
	bottom temperature	0.5	99.2
	tidal maximum	0.3	99.5
	aspect east	0.2	99.7
	sponge presence	0.1	99.8
	rockiness	0.1	99.9
	coral presence	0.1	100
	pennatulacean presence	0	100



1769

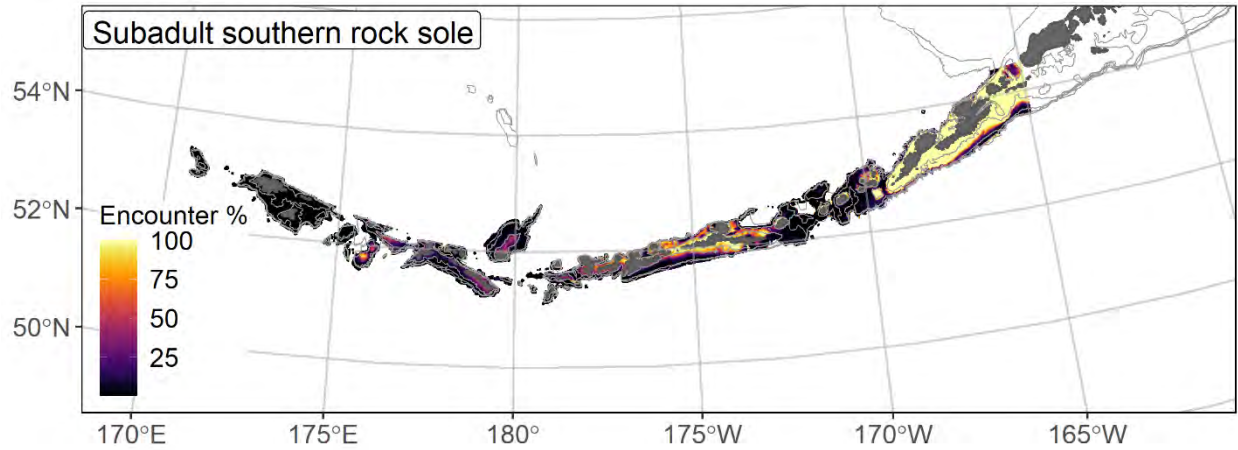
1770 Figure 65. Distribution of subadult southern rock sole catches (N = 583) in 1996–2019 AFSC RACE-
 1771 GAP summer bottom trawl surveys of the Aleutian Islands with the 100 m, 300 m, and 500 m isobaths
 1772 indicated; filled red circles indicate locations in top 10% of overall abundance, open orange circles
 1773 indicate presence in remaining catches, and small blue dots indicate absence.



1774

1775 Figure 66. The top nine covariate effects (left panel) on ensemble-predicted subadult southern rock sole numerical abundance across the Aleutian

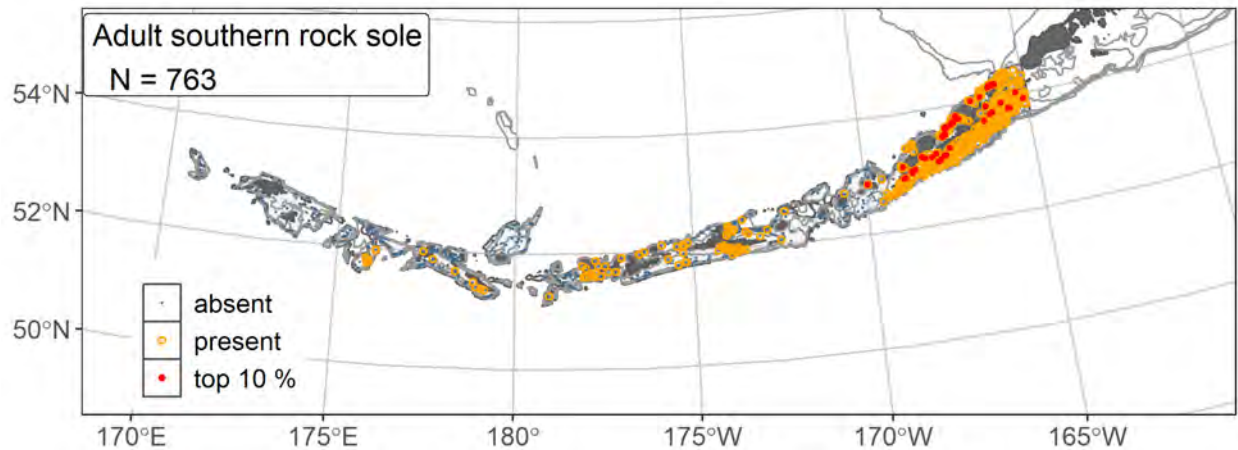
1776 Islands (upper right panel) alongside the coefficient of variation of the ensemble predictions (lower right panel).



1777

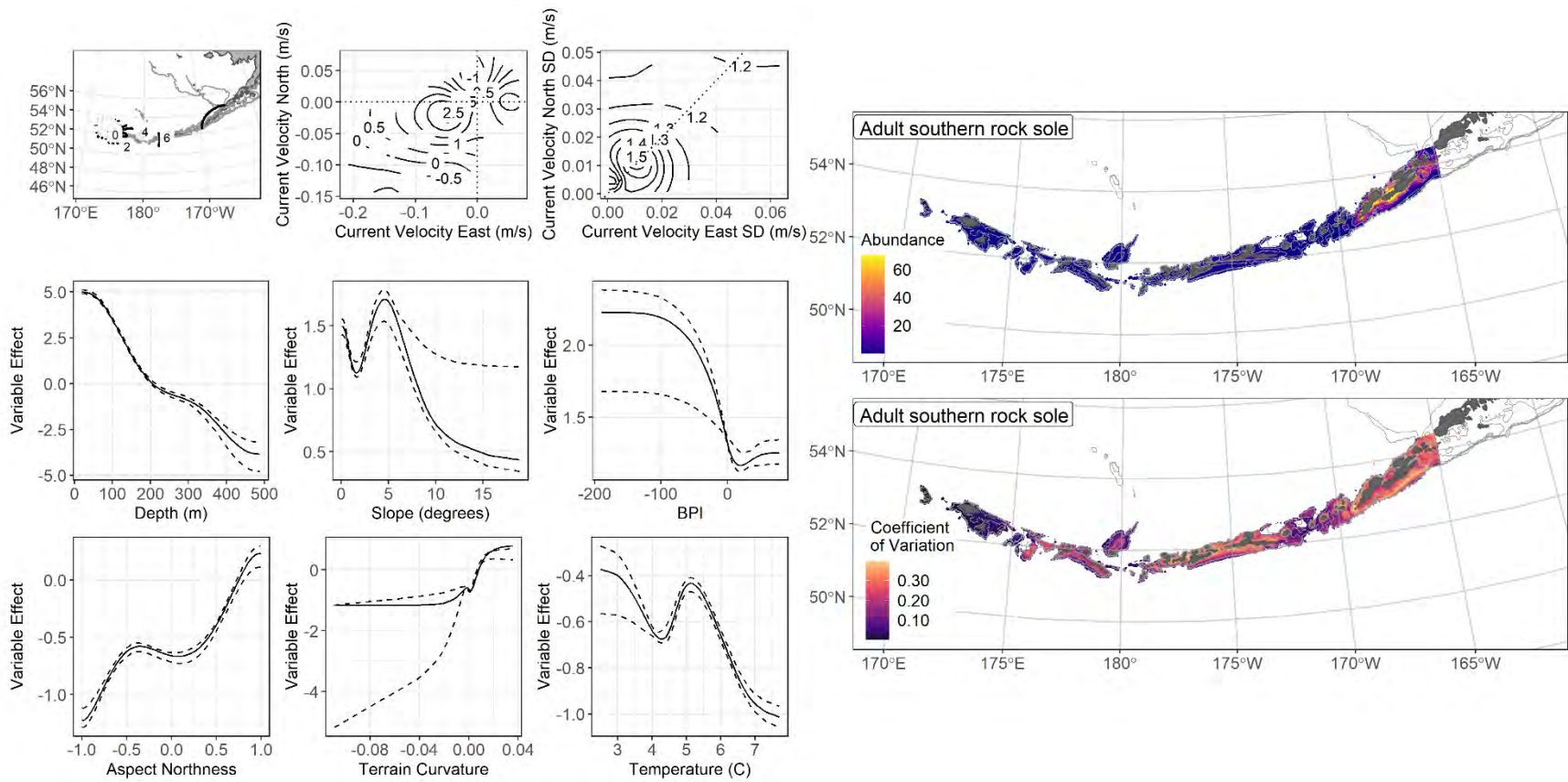
1778 Figure 67. Encounter probability of subadult southern rock sole from AFSC RACE-GAP summer bottom
 1779 trawl surveys (1996–2019) of the Aleutian Islands with the 100 m, 300 m, and 500 m isobaths indicated.

1780



1781

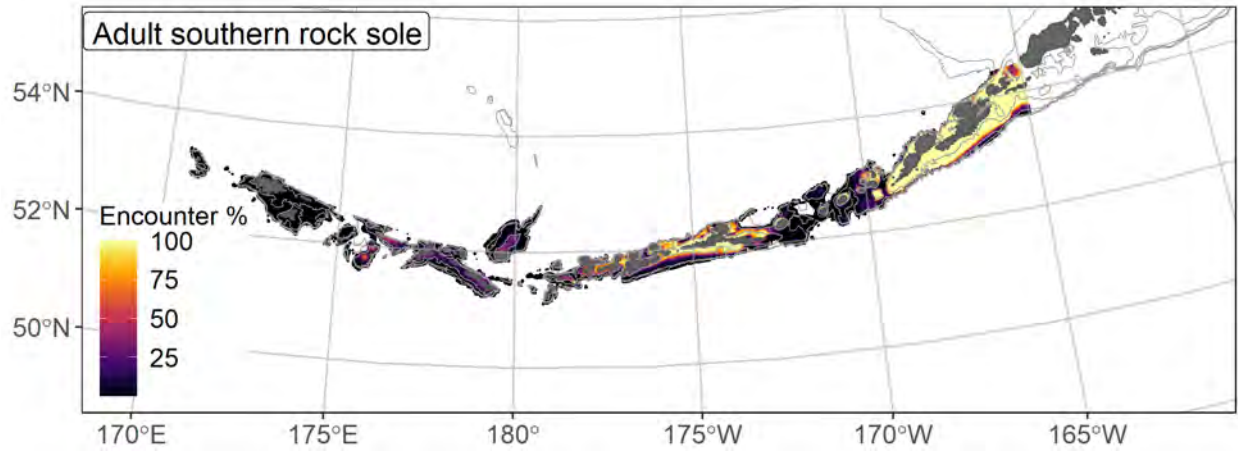
1782 Figure 68. Distribution of adult southern rock sole catches (N = 763) in 1996–2019 AFSC RACE-GAP
 1783 summer bottom trawl surveys of the Aleutian Islands with the 100 m, 300 m, and 500 m isobaths
 1784 indicated; filled red circles indicate locations in top 10% of overall abundance, open orange circles
 1785 indicate presence in remaining catches, and small blue dots indicate absence.



1786

1787 Figure 69. The top nine covariate effects (left panel) on ensemble-predicted adult southern rock sole numerical abundance across the Aleutian

1788 Islands (upper right panel) alongside the coefficient of variation of the ensemble predictions (lower right panel).



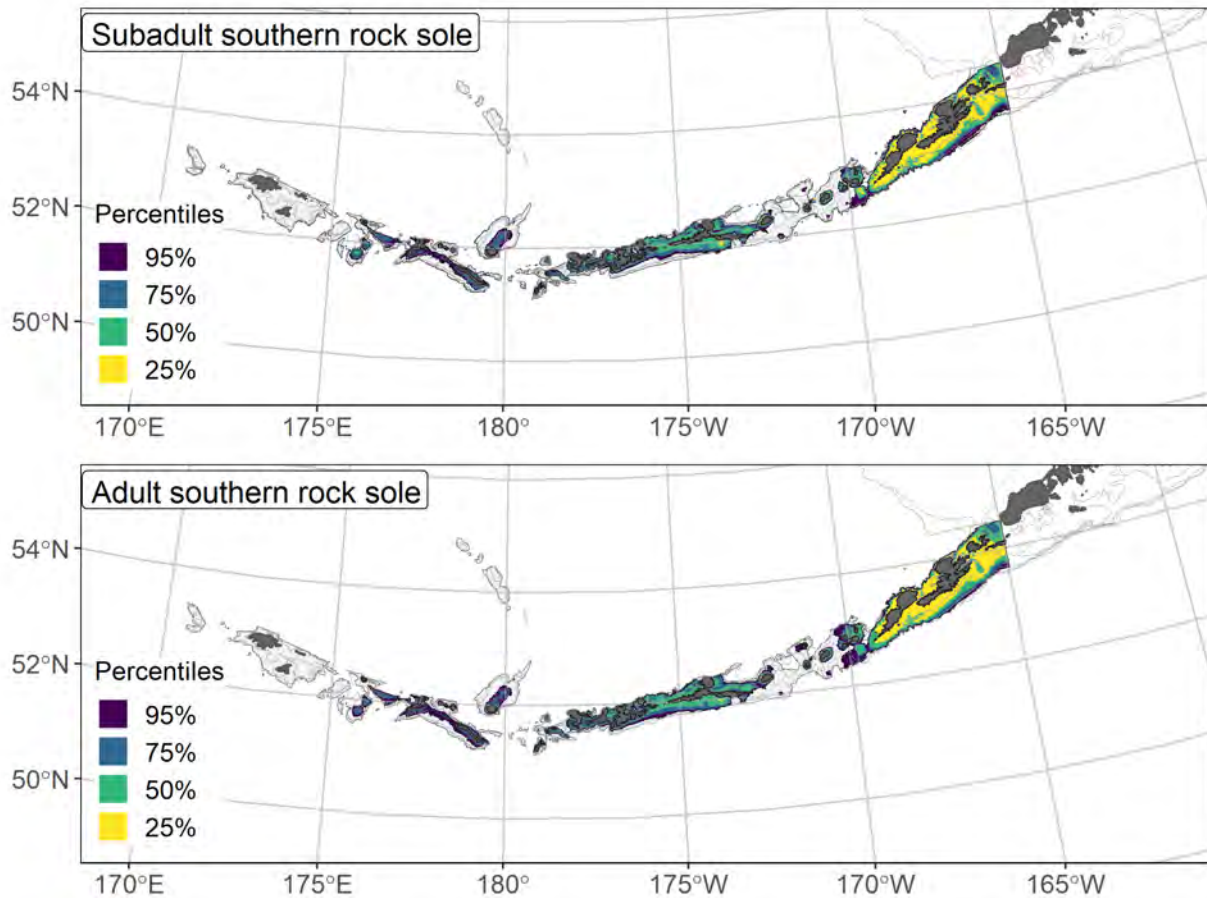
1789

1790

Figure 70. Encounter probability of adult southern rock sole from AFSC RACE-GAP summer bottom

1791

trawl surveys (1996–2019) of the Aleutian Islands with the 100 m, 300 m, and 500 m isobaths indicated.



1792

1793

Figure 71. Essential fish habitat (EFH area) defined as the top 95% of numerical abundance predictions

1794

from a habitat-based ensemble fitted to subadult (top) and adult (bottom) southern rock sole distribution

1795

and abundance in AFSC RACE-GAP summer bottom trawl surveys (1996–2019) with 100 m, 300 m, and

1796

500 m isobaths indicated; internal to the EFH map are the subareas of the top 25% (EFH hot spots), top

1797

50% (core EFH area), and top 75% (principal EFH area) of habitat related, ensemble-predicted numerical

1798

abundance.

Roundfishes

1799

1800 **Atka mackerel (*Pleurogrammus monopterygius*)**

1801 Atka mackerel (*Pleurogrammus monopterygius*) is a member of the greenling family
1802 (Hexagrammidae) that is found across the northern Pacific ocean from the Kuril Islands to the eastern
1803 GOA, with the largest concentrations found around Atka Island in the western AI (Lauth et al. 2007). The
1804 maturity schedule of Atka mackerel varies by region and growth conditions, though this study will use an
1805 intermediate value of 344 mm F.L. (L_{50} ; McDermott and Lowe 1997). Atka mackerel form nests in rocky
1806 habitat and males guard the developing eggs for several months (Lauth et al. 2007). Adult Atka mackerel
1807 are an important component in the diets of several marine mammals, particularly Stellers sea lions
1808 (Sinclair et. al. 2013), and are an important commercial stock, with most of the catch sold for export
1809 (Lowe et. al. 2019).

1810 **Subadult Atka mackerel distribution and predicted abundance from RACE-GAP summer bottom** 1811 **trawl surveys in the Aleutian Islands –**

1812 Subadult Atka mackerel catches from the RACE-GAP summer survey were common throughout
1813 the AI (Figure 72). The largest catches were located in the central and western AI. The final ensemble
1814 contains three SDMs with the GAM_{nb} given slightly less weight than the others. The ensemble had a fair
1815 to good fit to the data (Table 23). Specifically, it showed a “fair” ability to predict catches where this life
1816 stage is present ($AUC = 0.727$) and explained a fair amount of the deviance in the data ($PDE = 0.396$). It
1817 performed slightly better at predicting high or low abundance catches ($\rho = 0.542$). Atka mackerel catches
1818 were extremely variable, and taken together, these metrics suggest that the model adequately predicted
1819 subadult distribution, but it was not as useful for predicting exact abundance. Geographic position and
1820 bottom depth were the most important covariates and accounted for 69.8% of the deviance explained by
1821 the ensemble (Table 24), though tidal maximum and current variability also contributed. In general, high
1822 abundance was predicted in further west longitudes, shallow depths, and moderate tidal currents
1823 (Figure 73). Predicted abundance was highest in the areas around and west of the Rat Islands, and was

1824 predicted to be moderate almost everywhere in the AI (Figure 73). The ensemble predicted CV of
1825 abundance tended to be high in areas with average abundance (Figure 73). The ensemble predicted high
1826 encounter probabilities throughout the region (Figure 74).

1827 **Adult Atka mackerel distribution and predicted abundance from RACE-GAP summer bottom**
1828 **trawl surveys in the Aleutian Islands –**

1829 Adult Atka mackerel catches from the RACE-GAP summer survey were common throughout
1830 nearly all of the AI, with the largest catches occurring in the western AI (Figure 75). The ensemble
1831 contained four SDMs that were weighted almost equally and had a fair fit to the data (Table 23). The
1832 ensemble scored well in terms of predicting abundance ($\rho = 0.536$) and in terms of deviance explained
1833 (PDE = 0.413), but poorly in terms of predicting presence vs absence in catches (AUC = 0.650). This
1834 discrepancy is a consequence of the very patchy distribution of Atka mackerel catches. When the
1835 ensemble predicts a high average abundance at a location, it also assumes consistent presence in trawl
1836 survey catches at that location. However, Atka mackerel can be absent from many tows, and then
1837 suddenly appear in a large school. Thus, the predictions of abundance can be accurate on average while
1838 over-predicting presence in individual hauls. Bottom depth and geographic position were the two most
1839 important covariates, accounting for 63.0% of the deviance explained by the ensemble (Table 24). Bottom
1840 current, current variability, and tidal maximum also accounted for a substantial fraction of the deviance
1841 explained. Adult Atka mackerel are predicted to be abundant at shallow depths, favoring further west
1842 areas in the AI (Figure 76). Minor predictors of adult Atka mackerel abundance included southwesterly
1843 currents, moderate tidal currents, and warm temperatures. Predicted abundance was highest in the areas
1844 around and west of the Rat Islands. It was also high near Atka Island (Figure 76). The predicted CV of
1845 abundance was fairly uniform across most of the AI (Figure 76). The ensemble predicted that the
1846 encounter probability for adult Atka mackerel was nearly 100% across the entire AI (Figure 77).
1847 However, Atka mackerel did not conform to the assumption that high average abundance results in high
1848 encounter probability, and this species was absent from trawl catches more often than expected. While the

1849 map of predicted abundance is an accurate representation of average trawl catches, the map of encounter
1850 probability should be used with caution.

1851 **Essential fish habitat of subadult and adult Atka mackerel in the Aleutian Islands –**

1852 The habitat related abundance predictions based on RACE-GAP summer bottom trawl data
1853 (1991–2019) were translated into EFH area and subareas (Figure 78). The EFH area for subadult and
1854 adult Atka mackerel was almost identical, and encompassed nearly all of the survey area. The largest EFH
1855 hot spots for both life stages occurred along the islands in the central AI, with a second large area located
1856 east of Atka Island. Subadults have a slightly more western distribution with a larger hot spot in the far
1857 west near Attu Island, whereas adults have a slightly more eastern distribution, with a hot spot predicted
1858 along the edge of the AI survey area near Unimak Pass.

1859 Table 23. Constituent species distribution models (SDMs) used to construct Essential Fish Habitat (EFH)
 1860 for a) subadult and b) adult Atka mackerel: MaxEnt = Maximum entropy; paGAM = presence-absence
 1861 generalized additive model; hGAM = hurdle GAM; GAM_p = standard Poisson GAM; and
 1862 GAM_{nb} = standard negative-binomial GAM. Ensemble performance (ρ = Spearman's rank correlation
 1863 coefficient), root-mean-square-error (RMSE), the area under the receiver operating characteristic (AUC),
 1864 and the Poisson deviance explained (PDE) were generated from k-fold cross-validation. The "--" in a field
 1865 indicates that this SDM was not included in the final ensemble.

1866 **a) subadult Atka mackerel**

Models	RMSE	Relative Weight	ρ	AUC	PDE	EFH area (km²)
MaxEnt	1,140	0.348	0.486	0.813	0.327	77,600
paGAM	1,140	0.348	0.548	0.855	0.360	77,700
hGAM	--	0	--	--	--	--
GAM _p	--	0	--	--	--	--
GAM _{nb}	1,220	0.304	0.528	0.839	0.388	62,300
ensemble	1,120	1	0.542	0.727	0.396	77,700

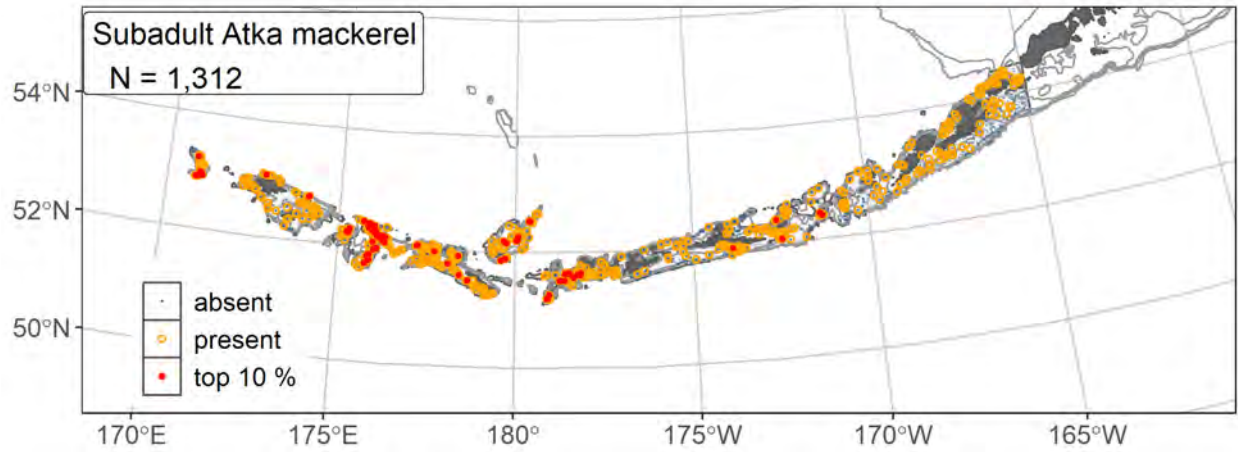
1867 **b) adult Atka mackerel**

Models	RMSE	Relative Weight	ρ	AUC	PDE	EFH area (km²)
MaxEnt	1,250	0.237	0.518	0.782	0.240	77,700
paGAM	1,260	0.236	0.551	0.801	0.219	77,700
hGAM	1,190	0.262	0.484	0.801	0.439	73,800
GAM _p	1,180	0.266	0.481	0.707	0.445	60,800
GAM _{nb}	1,330	0	--	--	--	--
ensemble	1,160	1	0.536	0.650	0.413	77,700

1868

1869 Table 24. Covariates retained in the a) subadult and b) adult Atka mackerel species distribution model
 1870 (SDM) final ensembles, the percent contribution to the ensemble deviance explained by each, and the
 1871 cumulative percent deviance: SD = standard deviation, and BPI = bathymetric position index.

Atka mackerel	Covariate	% Contribution	Cumulative % Contribution
a) subadult	bottom depth	36.0	36.0
	position	33.8	69.8
	tidal maximum	7.4	77.2
	current SD	5.2	82.4
	aspect north	3.6	86.0
	current	2.9	88.9
	slope	2.8	91.7
	aspect east	2.2	93.9
	bottom temperature	2.0	95.9
	coral presence	1.7	97.6
	sponge presence	0.7	98.3
	BPI	0.6	98.9
	pennatulacean presence	0.5	99.4
	rockiness	0.4	99.8
curvature	0.2	100	
a) adult	bottom depth	41.6	41.6
	position	21.4	63.0
	current	6.1	69.1
	tidal maximum	6.0	75.1
	current SD	5.3	80.4
	slope	3.5	83.9
	aspect east	3.4	87.3
	bottom temperature	3.4	90.7
	aspect north	3.1	93.8
	BPI	1.9	95.7
	sponge presence	1.5	97.2
	rockiness	0.9	98.1
	coral presence	0.9	99.1
	pennatulacean presence	0.8	99.9
curvature	0.1	100	



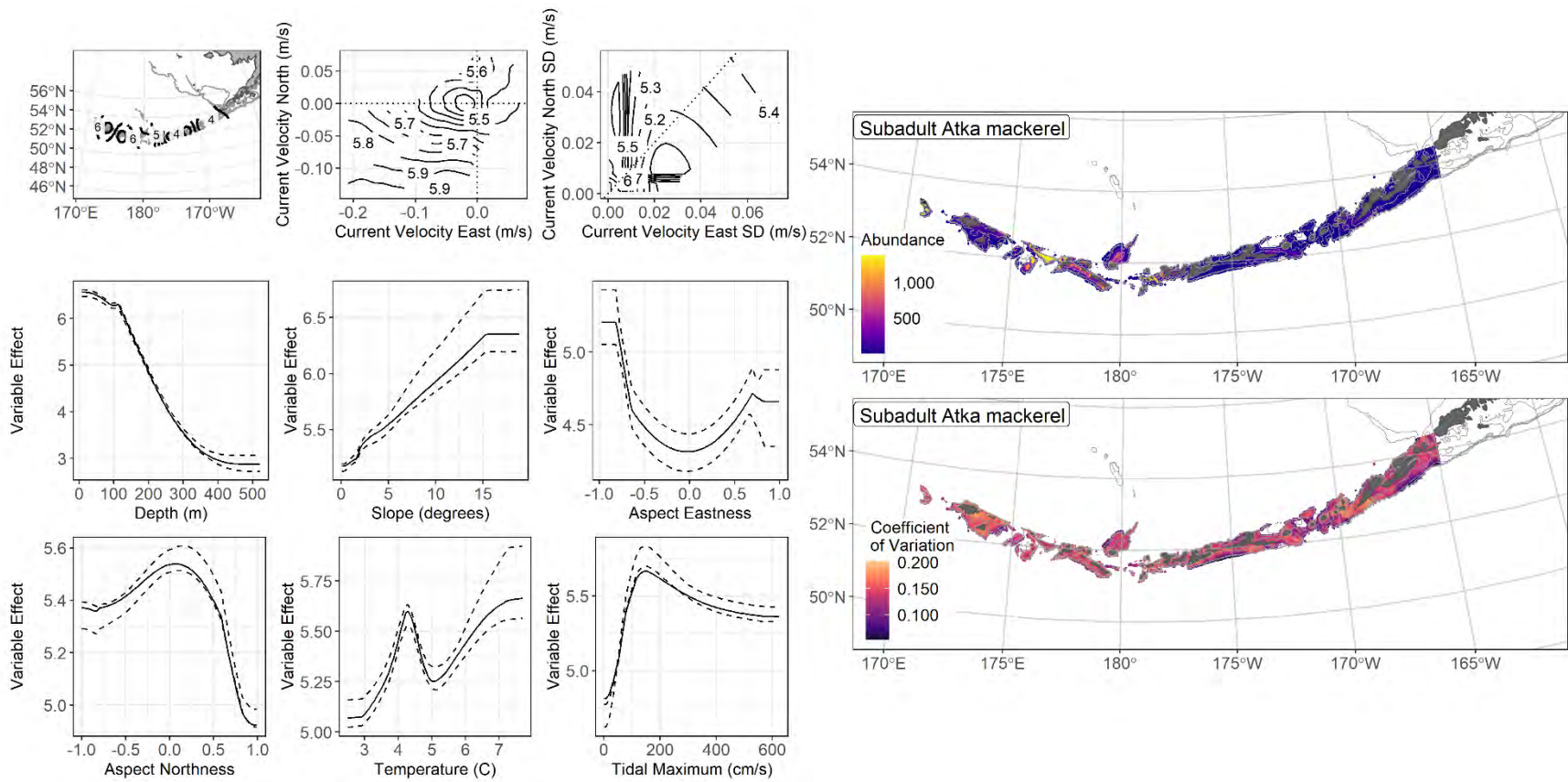
1872

1873 Figure 72. Distribution of subadult Atka mackerel catches (N = 1,312) in 1991–2019 AFSC RACE-GAP

1874 summer bottom trawl surveys of the Aleutian Islands with the 100 m, 300 m, and 500 m isobaths

1875 indicated; filled red circles indicate locations in top 10% of overall abundance, open orange circles

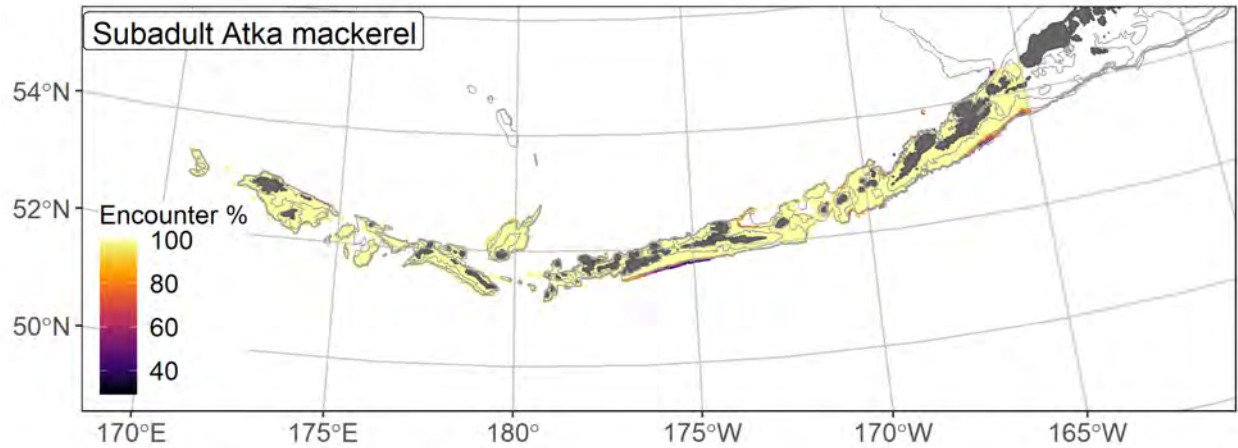
1876 indicate presence in remaining catches, and small blue dots indicate absence.



1877

1878 Figure 73. The top nine covariate effects (left panel) on ensemble-predicted subadult Atka mackerel numerical abundance across the Aleutian

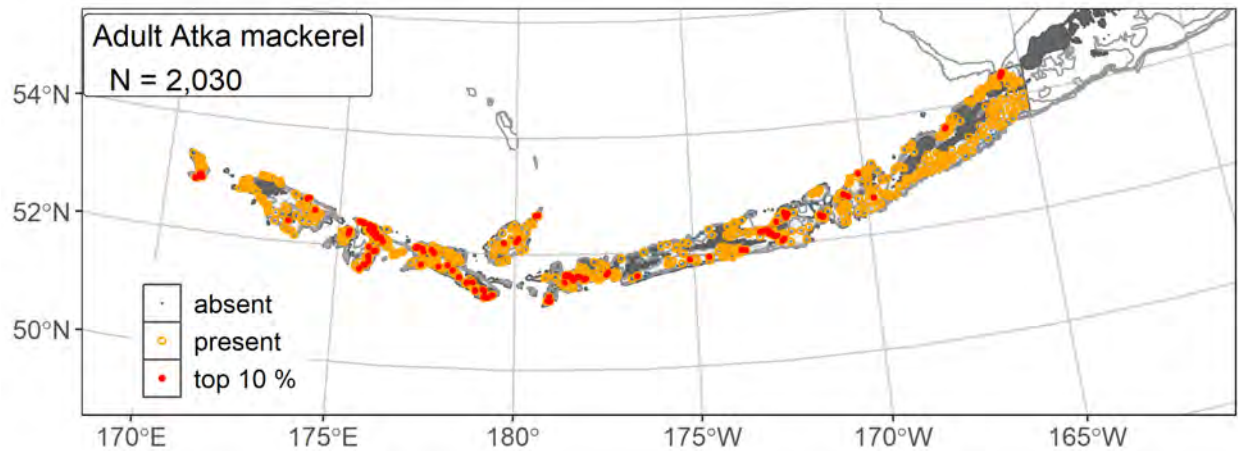
1879 Islands (upper right panel) alongside the coefficient of variation of the ensemble predictions (lower right panel).



1880

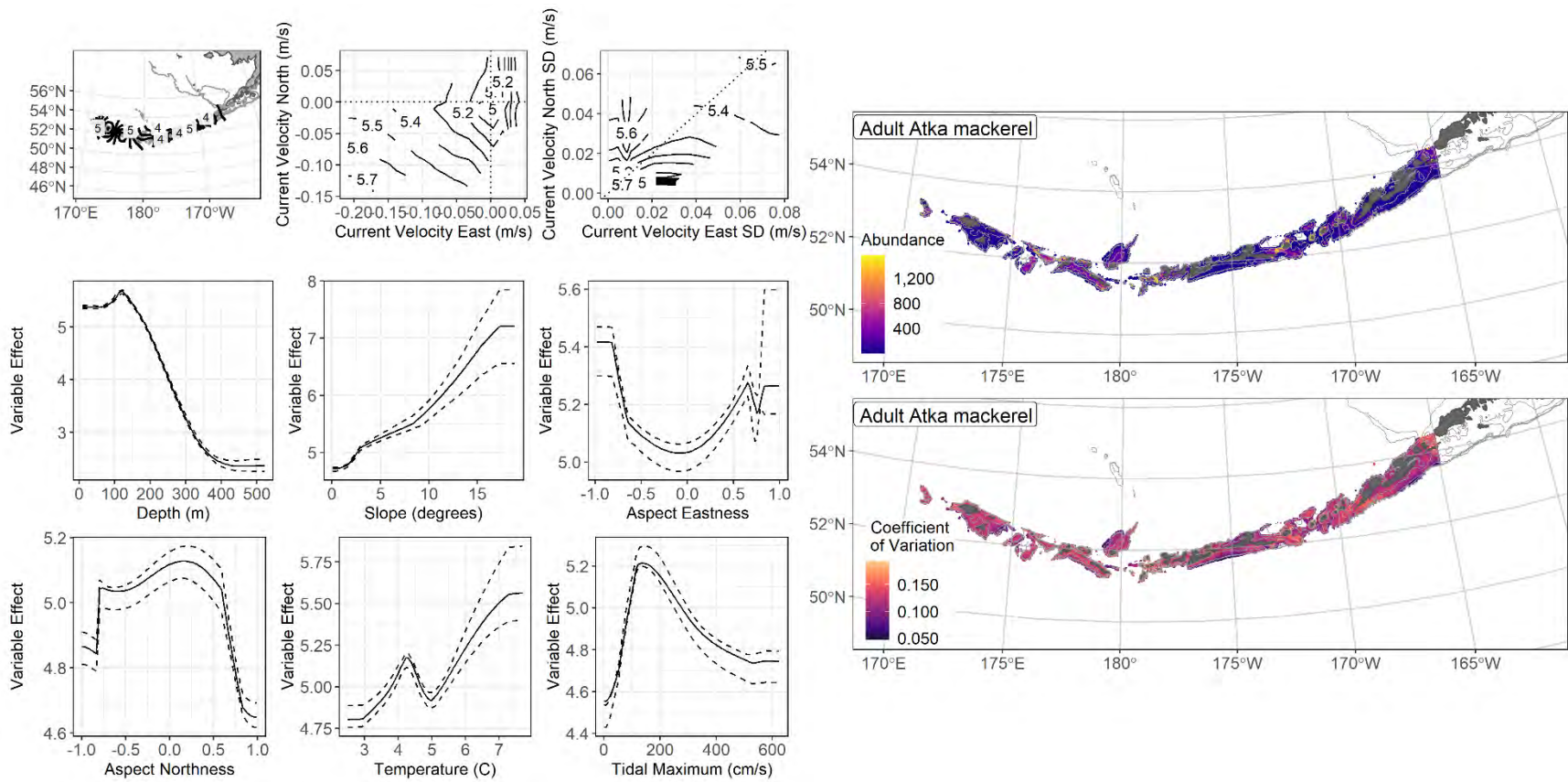
1881 Figure 74. Encounter probability of subadult Atka mackerel from AFSC RACE-GAP summer bottom
 1882 trawl surveys (1991–2019) of the Aleutian Islands with the 100 m, 300 m, and 500 m isobaths indicated.

1883



1884

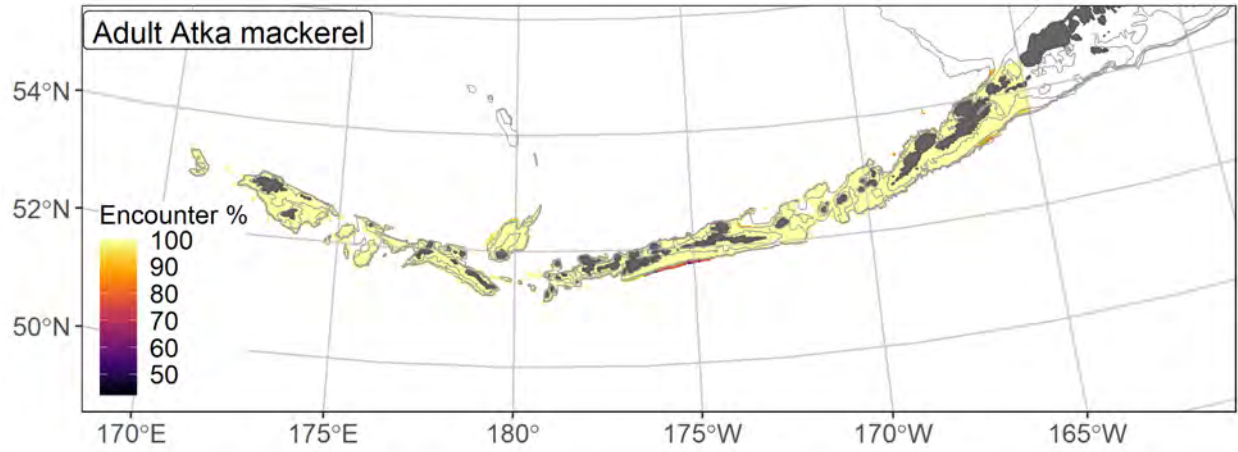
1885 Figure 75. Distribution of adult Atka mackerel catches (N = 2,030) in 1991–2019 AFSC RACE-GAP
 1886 summer bottom trawl surveys of the Aleutian Islands with the 100 m, 300 m, and 500 m isobaths
 1887 indicated; filled red circles indicate locations in top 10% of overall abundance, open orange circles
 1888 indicate presence in remaining catches, and small blue dots indicate absence.



1889

1890 Figure 76. The top nine covariate effects (left panel) on ensemble-predicted adult Atka mackerel numerical abundance across the Aleutian Islands

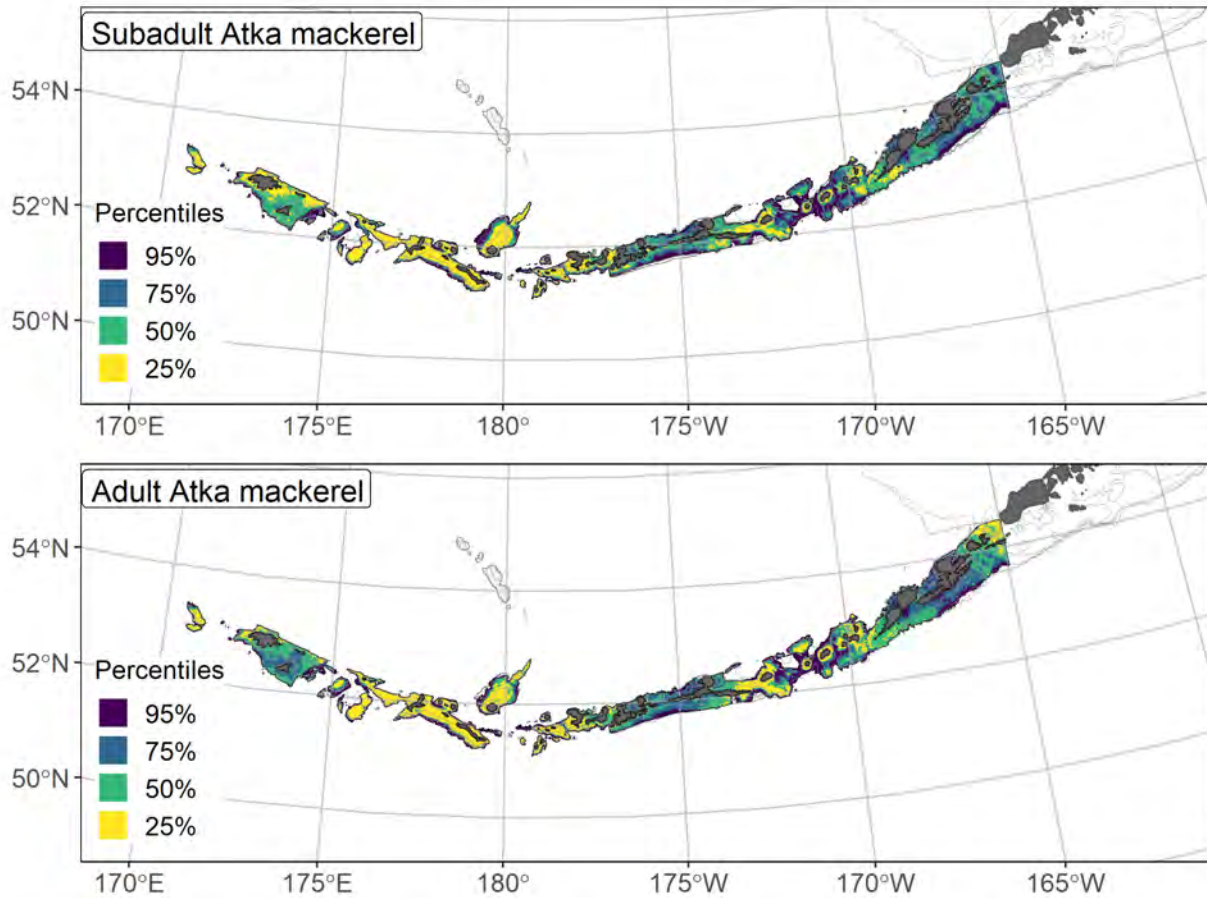
1891 (upper right panel) alongside the coefficient of variation of the ensemble predictions (lower right panel).



1892

1893 Figure 77. Encounter probability of adult Atka mackerel from AFSC RACE-GAP summer bottom trawl

1894 surveys (1991–2019) of the Aleutian Islands with the 100 m, 300 m, and 500 m isobaths indicated.



1895
 1896 Figure 78. Essential fish habitat (EFH area) defined as the top 95% of numerical abundance predictions
 1897 from a habitat-based ensemble fitted to subadult (top) and adult (bottom) Atka mackerel distribution and
 1898 abundance in AFSC RACE-GAP summer bottom trawl surveys (1991–2019) with 100 m, 300 m, and
 1899 500 m isobaths indicated; internal to the EFH map are the subareas of the top 25% (EFH hot spots), top
 1900 50% (core EFH area), and top 75% (principal EFH area) of habitat related, ensemble-predicted numerical
 1901 abundance.

1902 **Pacific cod (*Gadus macrocephalus*)**

1903 Pacific cod (*Gadus macrocephalus*) occur from the shoreline to 500 m throughout the RACE-
1904 GAP study area and support an important multi-gear commercial fishery throughout Alaskan waters
1905 (Thompson et al. 2020). Tagging studies have shown that Pacific cod move between the EBS, AI, and
1906 GOA (Shimada and Kimura 1994, Bryan et al. 2021), but genetic research indicates that there are discrete
1907 stocks in the EBS and AI (Canino et al. 2010, Spies 2012). They form aggregations during peak spawning
1908 season (Neidetcher et al. 2014) and lay demersal, adhesive eggs with a narrow thermal window for
1909 successful incubation (3–6°C). After hatching, the larvae enter an epipelagic phase and move
1910 ontogenetically toward the bottom with early juveniles (<150 mm F. L.; Laurel et al. 2009) more
1911 shallowly distributed than later life stages. Subadults settle into habitats near the bottom for several years
1912 before reaching maturity at 580 mm F.L. (L₅₀; Stark 2007). Settled early juveniles were not common in
1913 the trawl survey and there was not sufficient data to construct a SDM for this life stage. Pacific cod have
1914 been managed as a combined stock across the EBS and AI until 2013, but have had separate harvest
1915 specifications in each region since 2014.

1916 **Subadult Pacific cod distribution and predicted abundance from RACE-GAP summer bottom**
1917 **trawl surveys in the Aleutian Islands –**

1918 Subadult Pacific cod were common across the RACE-GAP summer survey of the AI
1919 (Figure 79). Large catches occurred throughout the region, and were absent only around the passes where
1920 deep water flows from the Pacific Ocean to the Bering Sea. The final ensemble contained four SDMs with
1921 approximately equal weights, and it showed a fair to good performance in terms of model fit (Table 25).
1922 Specifically, the ensemble demonstrated good accuracy at predicting relatively high or low density
1923 catches ($\rho = 0.461$), and it showed fair scores at measures of predicting presence or absence
1924 (AUC = 0.745) and in terms of deviance explained (PDE = 0.230). The good score for ρ suggested that
1925 the ensemble may predict the presence or absence of subadult Pacific cod catches, but may not accurately
1926 predict abundance. Bottom depth was the most important covariate in the ensemble and accounted for

1927 41.7% of the deviance explained by the ensemble, though geographic position, current, and slope were
1928 also important (Table 26). In general, predicted abundance was high in locations that were less than 250
1929 m depth, with westerly currents and a sloping bottom (Figure 80). Although past research suggests that
1930 temperature can be an important driver of subadult Pacific cod distribution, there is relatively little
1931 variation in summer bottom temperature in the AI (Figure 2), so temperature did not explain much of the
1932 variation in observed abundance. The predicted abundance map showed that this life stage is present
1933 across most of the AI, but the highest concentrations occurred around Atka and Adak Islands, as well as
1934 in the east near Unimak Pass (Figure 80). The predicted CV of abundance was low in most areas,
1935 reflecting that Pacific cod are consistently present in the bottom trawl catch (Figure 80). Estimated
1936 encounter probabilities for subadult Pacific cod were near 100% in all but a few areas along the 500 m
1937 depth contour (Figure 81).

1938 **Adult Pacific cod distribution and predicted abundance from RACE-GAP summer bottom trawl**
1939 **surveys in the Aleutian Islands –**

1940 Adult Pacific cod were ubiquitous in catches from the RACE-GAP summer survey area
1941 (Figure 82). There was no clear pattern to large catches, and large aggregations of Pacific cod occurred
1942 throughout the entirety of the AI. The final ensemble contained four SDMs with equal weights and
1943 demonstrated a fair to good fit to the observed data (Table 25). The fit metrics for adult Pacific cod were
1944 very similar to those for subadults, and the ensemble scored well in predicting the highest and lowest
1945 abundance catches ($\rho = 0.490$), but only fair according to other measures of fit ($AUC = 0.754$;
1946 $PDE = 0.332$). As with subadults, the values for these metrics suggest that the ensemble accurately
1947 predicts high vs. low densities, but may less accurately predict observed abundance. Bottom depth and
1948 geographic position were the most important covariates and accounted for 48.5% of the deviance
1949 explained by the ensemble, but current covariates, tidal maximum, and substrate rockiness were also
1950 important (Table 26). The model predicted high adult abundance in places with depths less than 300 m,
1951 more eastern longitudes, and areas with southwesterly currents, moderate tidal currents, and somewhat

1952 rocky substrates (Figure 83). Adult Pacific cod occurred in most places shallower than 300 m, but the
1953 highest catches were predicted for the eastern AI around the Islands of Four Mountains and near Unimak
1954 Pass (Figure 83). The predicted CV of abundance was high overall and homogenous throughout the
1955 region, reflecting that high numbers of this life stage may occur almost anywhere in the AI (Figure 83).
1956 Like subadults, the encounter probability for adults was near 100% across almost the entire AI region,
1957 save a few deeper locations along the continental slope (Figure 84).

1958 **Essential fish habitat of subadult and adult Pacific cod in the Aleutian Islands –**

1959 The habitat related abundance predictions based on RACE-GAP summer bottom trawl data
1960 (1991–2019) were translated into EFH area and subareas (Figure 85). Both life stages of Pacific cod were
1961 very common and had EFH areas that encompassed almost the entire survey area. Subadults had EFH hot
1962 spots predicted around Unimak Pass, the Andreanof Islands, and in the western AI near Attu Island. All
1963 areas shallower than 100 m were designated EFH and areas deeper than 300 m were generally not EFH.
1964 Adult Pacific cod shared an EFH hot spot with subadults near Unimak Pass, but had a large hot spot
1965 around the Islands of Four Mountains that was not shared with subadults. The area around the Islands of
1966 Four Mountains has greater bottom depths and stronger currents, which were associated with high adult
1967 abundance.

1968 Table 25. Constituent species distribution models (SDMs) used to construct Essential Fish Habitat (EFH)
 1969 for a) subadult and b) adult Pacific cod: MaxEnt = Maximum entropy; paGAM = presence-absence
 1970 generalized additive model; hGAM = hurdle GAM; GAM_p = standard Poisson GAM; and
 1971 GAM_{nb} = standard negative-binomial GAM. Ensemble performance (ρ = Spearman's rank correlation
 1972 coefficient), root-mean-square-error (RMSE), the area under the receiver operating characteristic (AUC),
 1973 and the Poisson deviance explained (PDE) were generated from k-fold cross-validation. The "--" in a field
 1974 indicates that this SDM was not included in the final ensemble.

1975 **a) subadult Pacific cod**

Models	RMSE	Relative Weight	ρ	AUC	PDE	EFH area (km ²)
MaxEnt	35.3	0.248	0.419	0.739	0.096	76,600
paGAM	35.2	0.251	0.468	0.759	0.127	77,200
hGAM	35.2	0.250	0.416	0.759	0.250	68,100
GAM _p	35.2	0.251	0.408	0.711	0.251	68,400
GAM _{nb}	35.3	0	--	--	--	--
ensemble	34.6	1	0.461	0.745	0.230	74,700

1976 **b) adult Pacific cod**

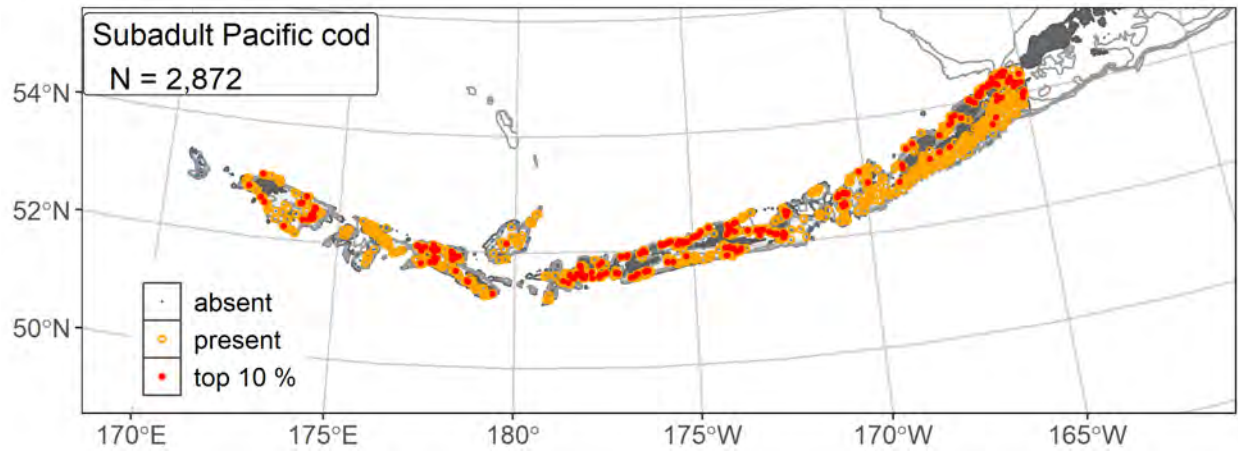
Models	RMSE	Relative Weight	ρ	AUC	PDE	EFH area (km ²)
MaxEnt	44.3	0.236	0.466	0.748	0.164	77,300
paGAM	43.6	0.243	0.492	0.772	0.151	77,600
hGAM	42.1	0.261	0.419	0.772	0.347	74,700
GAM _p	42.1	0.260	0.413	0.707	0.342	73,800
GAM _{nb}	43.1	0	--	--	--	--
ensemble	41.2	1	0.490	0.754	0.332	77,600

1977

1978 Table 26. Covariates retained in the a) subadult and b) adult Pacific cod species distribution model (SDM)
 1979 final ensembles, the percent contribution to the ensemble deviance explained by each, and the cumulative
 1980 percent deviance: SD = standard deviation, and BPI = bathymetric position index.

Pacific cod	Covariate	% Contribution	Cumulative % Contribution
a) subadult	bottom depth	41.7	41.7
	position	13.5	55.3
	current SD	11.8	67.1
	slope	6.0	73.1
	current	5.5	78.6
	tidal maximum	3.4	82.0
	BPI	3.1	85.1
	rockiness	2.9	88.0
	aspect north	2.4	90.4
	bottom temperature	2.4	92.8
	aspect east	2.0	94.8
	curvature	1.8	96.6
	pennatulacean presence	1.7	98.3
	coral presence	1.2	99.5
	sponge presence	0.5	100
b) adult	bottom depth	35.7	35.7
	position	12.8	48.5
	tidal maximum	9.5	58.0
	current SD	9.2	67.2
	current	6.6	73.8
	slope	6.5	80.3
	rockiness	6.2	86.5
	bottom temperature	3.7	90.2
	aspect east	2.0	92.2
	curvature	1.9	94.1
	coral presence	1.6	95.7
	sponge presence	1.6	97.3
	aspect north	1.5	98.8
	BPI	1.1	99.9
	pennatulacean presence	0.1	100

1981



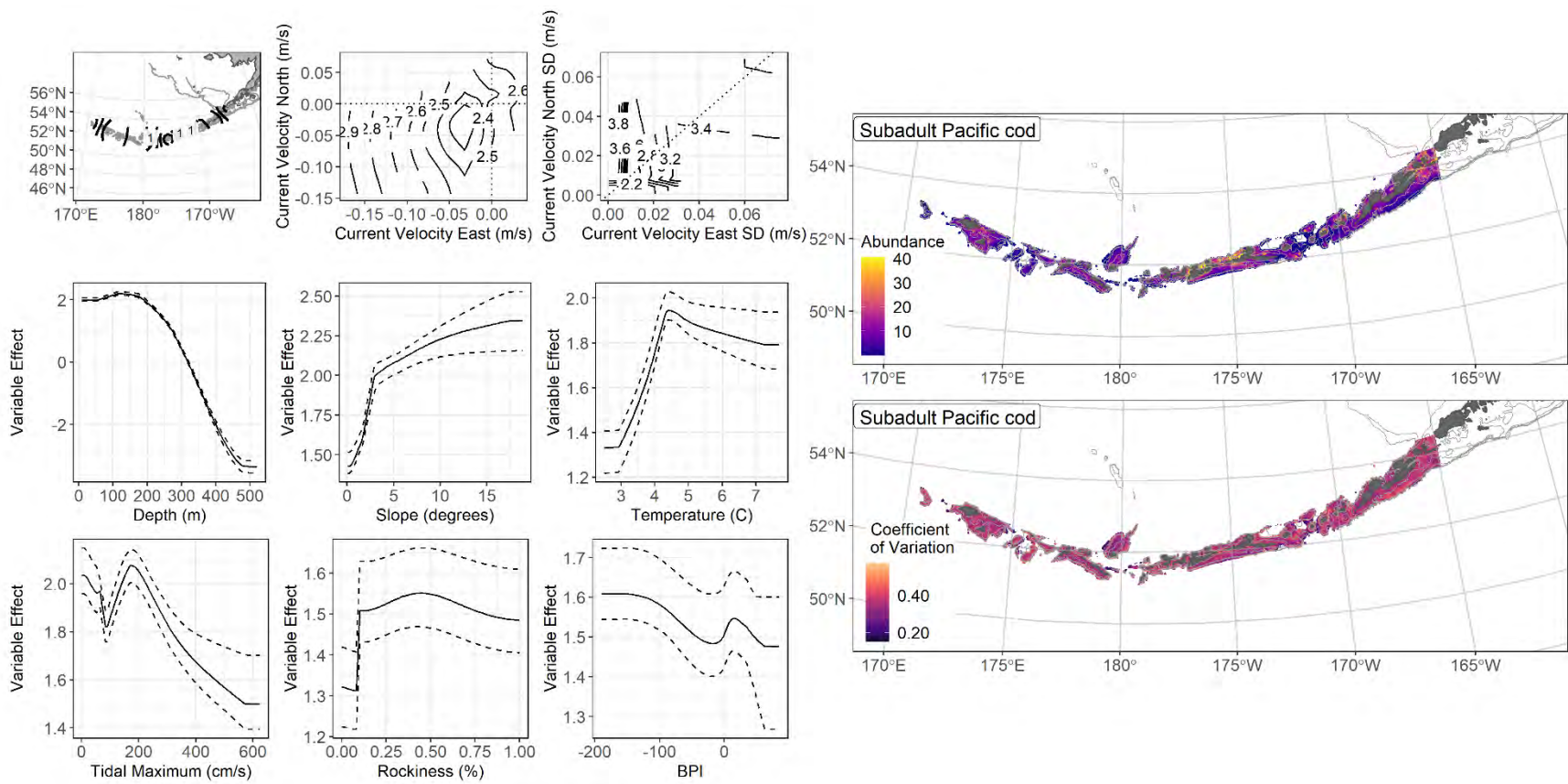
1982

1983 Figure 79. Distribution of subadult Pacific cod catches (N = 2,872) in 1991–2019 AFSC RACE-GAP

1984 summer bottom trawl surveys of the Aleutian Islands with the 100 m, 300 m, and 500 m isobaths

1985 indicated; filled red circles indicate locations in top 10% of overall abundance, open orange circles

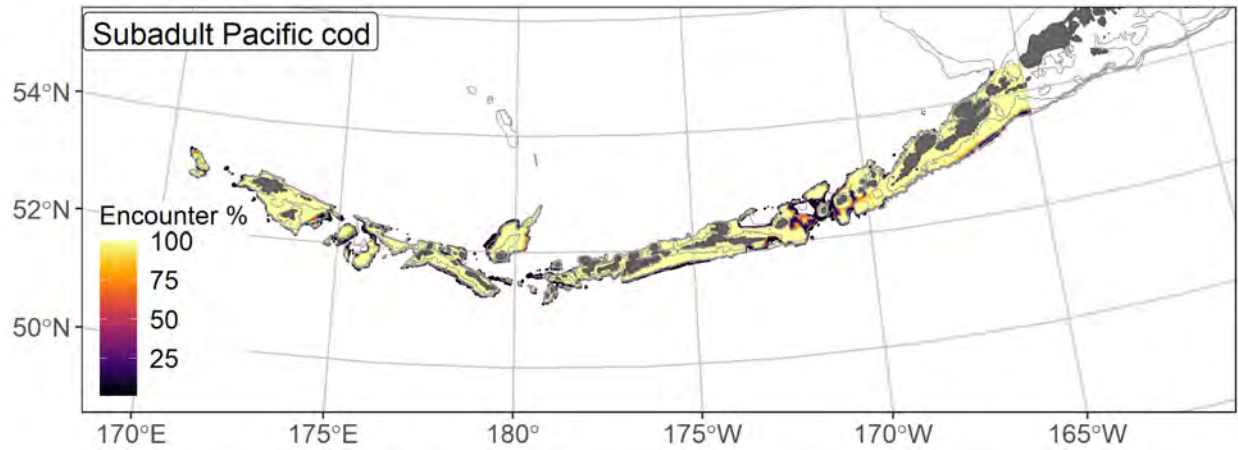
1986 indicate presence in remaining catches, and small blue dots indicate absence.



1987

1988 Figure 80. The top nine covariate effects (left panel) on ensemble-predicted subadult Pacific cod numerical abundance across the Aleutian Islands

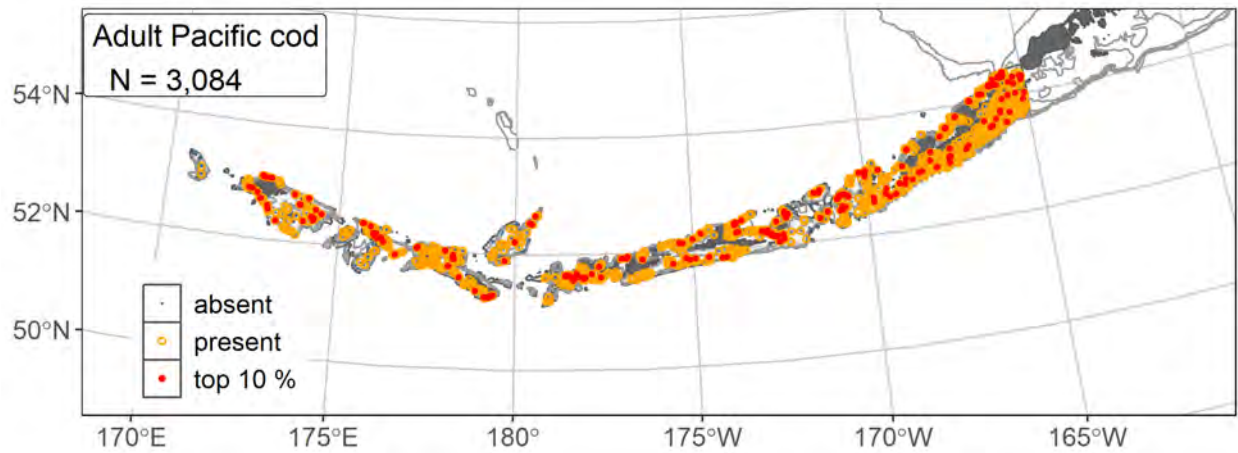
1989 (upper right panel) alongside the coefficient of variation of the ensemble predictions (lower right panel).



1990

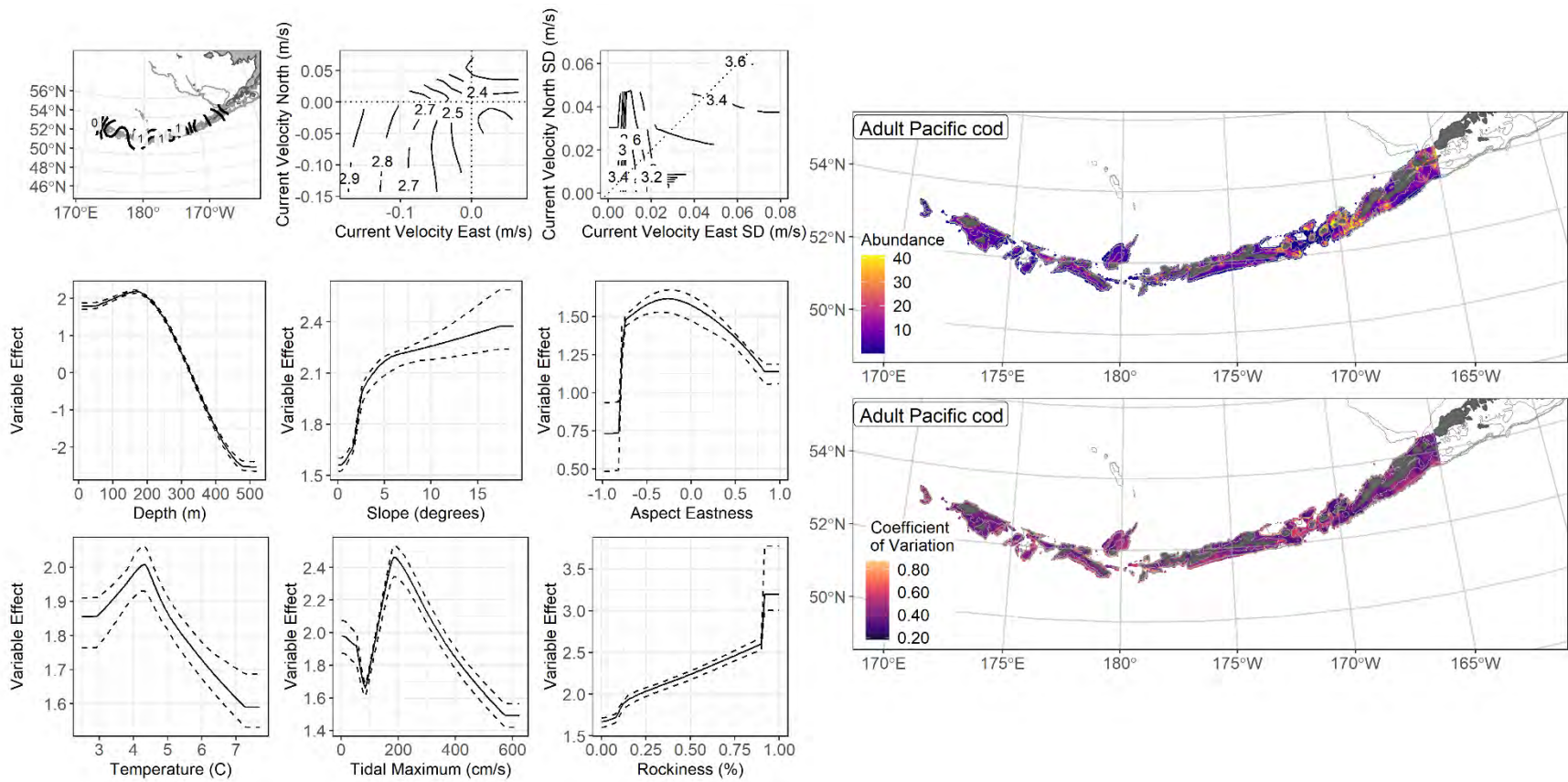
1991 Figure 81. Encounter probability of subadult Pacific cod from AFSC RACE-GAP summer bottom trawl
 1992 surveys (1991–2019) of the Aleutian Islands with the 100 m, 300 m, and 500 m isobaths indicated.

1993



1994

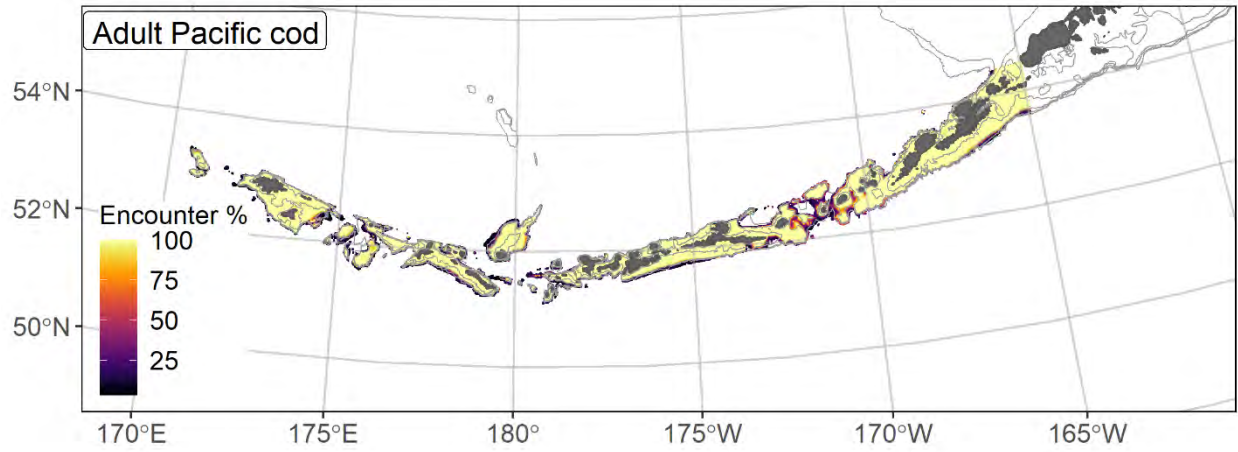
1995 Figure 82. Distribution of adult Pacific cod catches (N = 3,084) in 1991–2019 AFSC RACE-GAP
 1996 summer bottom trawl surveys of the Aleutian Islands with the 100 m, 300 m, and 500 m isobaths
 1997 indicated; filled red circles indicate locations in top 10% of overall abundance, open orange circles
 1998 indicate presence in remaining catches, and small blue dots indicate absence.



1999

2000 Figure 83. The top nine covariate effects (left panel) on ensemble-predicted adult Pacific cod numerical abundance across the Aleutian Islands

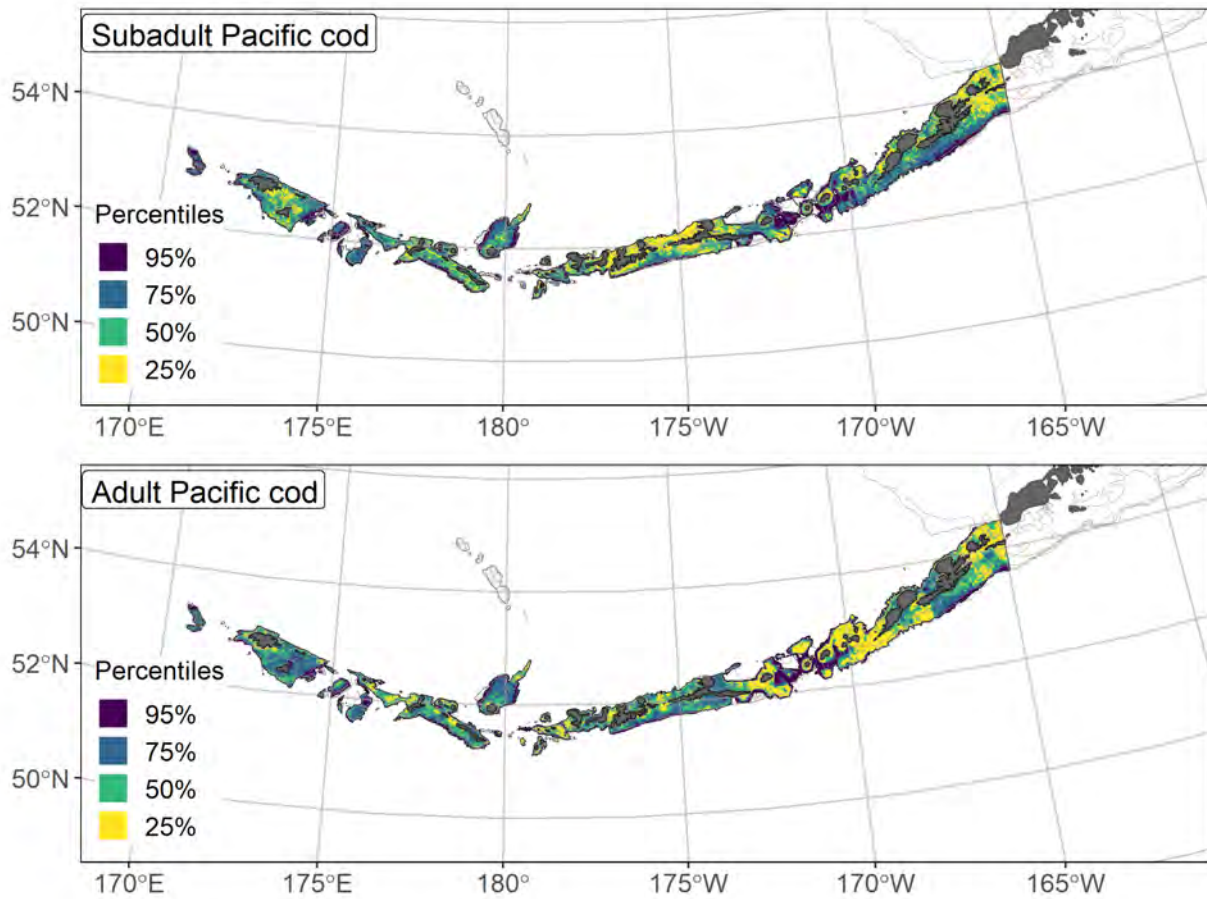
2001 (upper right panel) alongside the coefficient of variation of the ensemble predictions (lower right panel).



2002

2003 Figure 84. Encounter probability of adult Pacific cod from AFSC RACE-GAP summer bottom trawl

2004 surveys (1991–2019) of the Aleutian Islands with the 100 m, 300 m, and 500 m isobaths indicated.



2005

2006

Figure 85. Essential fish habitat (EFH area) defined as the top 95% of numerical abundance predictions

2007

from a habitat-based ensemble fitted to subadult (top) and adult (bottom) Pacific cod distribution and

2008

abundance in AFSC RACE-GAP summer bottom trawl surveys (1991–2019) with 100 m, 300 m, and

2009

500 m isobaths indicated; internal to the EFH map are the subareas of the top 25% (EFH hot spots), top

2010

50% (core EFH area), and top 75% (principal EFH area) of habitat related, ensemble-predicted numerical

2011

abundance.

2012 **Sablefish (*Anoplopoma fimbria*)**

2013 Sablefish (*Anoplopoma fimbria*) support an important commercial fishery in Alaska. Adults
2014 inhabit deep water (200–1000 m) along the shelf break and upper continental slope from Baja California
2015 to Japan (Mecklenburg et al. 2002). Spawning typically occurs in deeper waters (300–500 m) near the
2016 shelf break (Mason et al. 1983) with eggs developing at depth and larvae developing near the surface
2017 (Wing 1997), and young fish typically settle in shallow coastal waters (Kendall and Matarese 1987). After
2018 overwintering in nearshore habitats, older juveniles migrate to deeper water, reaching adult habitat in
2019 three to four years (Rutecki and Varosi 1997). For the EFH descriptions in this study, we separated the
2020 settled early juvenile (150–399 mm F.L.; Sasaki 1985, Pirtle et al. 2019), subadult (400–585 mm F.L.;
2021 Rodgveller et al. 2018), and adult life stages (>585 mm F.L.) by length. The geographic extent of this
2022 population and the potential for large-scale movement of individuals (Heifetz and Fujioka 1991,
2023 Hanselman et al. 2015) has led to sablefish being managed as a single stock across Alaska
2024 (Goethel et al. 2020). The SDMs in the present work were parameterized with catches from the AFSC
2025 RACE-GAP summer bottom trawl survey of the AI, which typically does not sample depths below 500
2026 m. Therefore, we recommend that AFSC longline survey data be integrated with AFSC RACE-GAP
2027 summer bottom trawl survey data into future EFH reviews¹³.

2028 **Subadult sablefish distribution and predicted abundance from RACE-GAP summer bottom trawl**
2029 **surveys in the Aleutian Islands –**

2030 Subadult sablefish catches in the RACE-GAP summer bottom trawl survey were common in deep
2031 water in the eastern AI, and rare west of 180° (Figure 86). The final ensemble contained four SDMs and
2032 the paGAM and GAM_P were weighted more heavily than the other two (Table 27). Overall, the ensemble
2033 showed good performance on two out of the three fit metrics ($\rho = 0.426$; PDE = 0.538) and excellent

¹³ A recommendation to add additional survey data types if possible to future SDM ensemble EFH mapping efforts for this species will be included as a future recommendation for research directions from the 2022 EFH 5-year Review.

2034 performance on the third (AUC = 0.931). The metrics suggested that the ensemble was excellent at
2035 predicting where sablefish will be caught in the trawl survey, and that it is somewhat accurate at
2036 predicting the number of fish caught. However, these findings do not extend beyond the RACE-GAP
2037 survey grid, and should be considered in context with the potential limitations of bottom trawl gear.
2038 Bottom depth, geographic position, and bottom temperature were the most important covariates and
2039 accounted for a combined 73.3% of the deviance explained by the ensemble (Table 28). The ensemble
2040 predicted that abundance would be highest in areas that are east of 180°, with deeper depths and warmer
2041 bottom temperatures (Figure 87). Predicted abundance was highest south of Unalaska Island at depths
2042 greater than 300 m, and around the western end of the Andreanof Islands (Figure 87). Predicted
2043 abundance was higher on the south side of the AI chain. The predicted CV of abundance was higher along
2044 the continental slope, reflecting that the catch in these locations can be quite variable (Figure 87).
2045 Locations shallower than 200 m typically had close to zero predicted abundance with little variation.
2046 Encounter probabilities for subadult sablefish were highest along much of the continental slope on the
2047 southern side of the Aleutian Island chain and east of 180°, as well as around amidst the Islands of Four
2048 Mountains (Figure 88).

2049 **Adult sablefish distribution and predicted abundance from RACE-GAP summer bottom trawl**
2050 **surveys in the Aleutian Islands –**

2051 Adult sablefish catches in the RACE-GAP summer survey were distributed similarly to the
2052 subadults; they were common along the continental slope areas east of 180° (Figure 89). The three models
2053 in the final ensemble were assigned close to equal weights and the ensemble did a good job of fitting the
2054 data (Table 27). Specifically, the ensemble scored excellently at predicting presence or absence
2055 (AUC = 0.949) and explaining deviance (PDE = 0.681), but only fair to good in terms of ranking the
2056 catches by abundance ($\rho = 0.403$). Given the values of these metrics, the ensemble predictions accurately
2057 describe the distribution and much of the observed abundance of adult sablefish. As with subadults,
2058 caution should be used in interpreting these predictions, as they do not account for portions of the

2059 population that are below 500 m depth, and reflect only the catch from bottom trawl gear. Bottom depth
2060 and geographic position were the most important covariates and accounted for 54.3% of the deviance
2061 explained by the ensemble (Table 28), though current and terrain curvature were also found to be
2062 important covariates. Like subadults, adult sablefish were predicted to be abundant in the eastern AI and
2063 in deep water (Figure 90). Unlike subadults, temperature was not a strong predictor of survey catches;
2064 instead the model predicted high adult abundance in places with northeastern or southwestern currents
2065 and along terrain with a concave surface. Predicted abundance was highest in several places along the
2066 continental slope east of 180° (Figure 90). Compared to subadults, adults tended to be located further
2067 west and were less abundant south of Unalaska Island. The predicted CV of abundance was highest
2068 around many of the slope areas where adults were predicted to be abundant (Figure 90). Encounter
2069 probabilities for adult sablefish followed the same pattern and were high along continental slope areas and
2070 low in shallow water (Figure 91).

2071 **Essential fish habitat of subadult and adult sablefish in the Aleutian Islands –**

2072 The habitat related abundance predictions based on RACE-GAP summer bottom trawl data
2073 (1991–2019) were translated into EFH area and subareas (Figure 92). The EFH areas for the two life
2074 stages of sablefish were almost identical. Both show EFH hot spots along most of the continental slope
2075 east of 180°, particularly south of the AI chain. The areas at the west end of the Andreanof Islands and the
2076 Islands of Four Mountains were also included in the core EFH. Subadults differ from adults in that their
2077 EFH area is more likely to extend into shallow water, particularly in the eastern AI south of Unalaska
2078 Island. It is well-established that much of the sablefish population, especially adults, is found below 500
2079 m and thus is not accessible to the bottom trawl survey. The addition of data from longline surveys would
2080 allow EFH for this species to be defined across its entire habitat.

2081

2082 Table 27. Constituent species distribution models (SDMs) used to construct Essential Fish Habitat (EFH)
 2083 for a) subadult and b) adult sablefish: MaxEnt = Maximum entropy; paGAM = presence-absence
 2084 generalized additive model; hGAM = hurdle GAM; GAM_p = standard Poisson GAM; and
 2085 GAM_{nb} = standard negative-binomial GAM. Ensemble performance (ρ = Spearman's rank correlation
 2086 coefficient), root-mean-square-error (RMSE), the area under the receiver operating characteristic (AUC),
 2087 and the Poisson deviance explained (PDE) were generated from k-fold cross-validation. The "--" in a field
 2088 indicates that this SDM was not included in the final ensemble.

2089 **a) subadult sablefish**

Models	RMSE	Relative Weight	ρ	AUC	PDE	EFH area (km²)
MaxEnt	14.4	0.181	0.418	0.918	0.139	34,300
paGAM	10.1	0.364	0.433	0.939	0.450	44,600
hGAM	19.2	0.102	0.435	0.938	-0.848	2,900
GAM _p	10.3	0.353	0.414	0.912	0.587	30,100
GAM _{nb}	11.1	0	--	--	--	--
ensemble	9.6	1	0.426	0.931	0.538	40,200

2090 **b) adult sablefish**

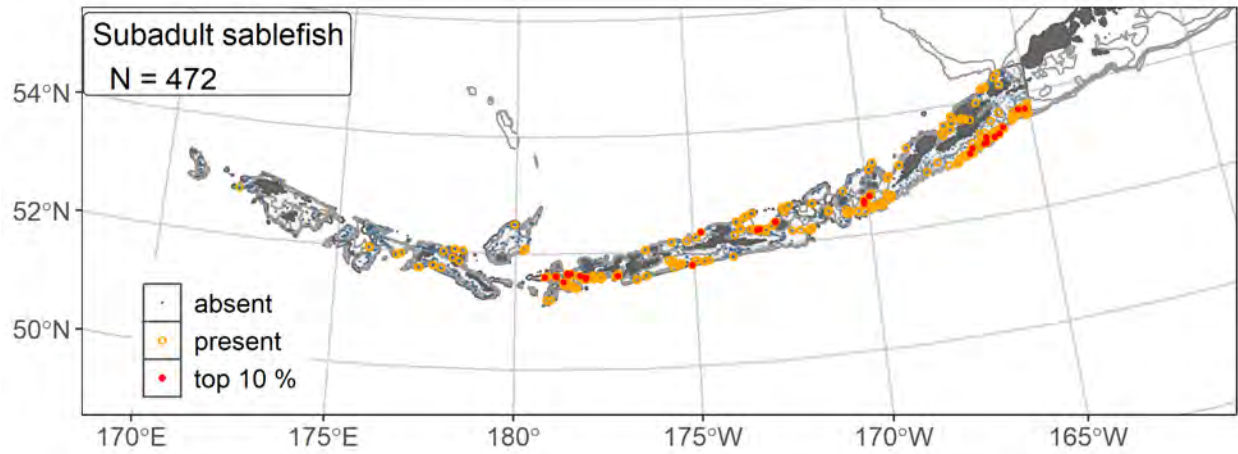
Models	RMSE	Relative Weight	ρ	AUC	PDE	EFH area (km²)
MaxEnt	--	0	--	--	--	--
paGAM	9.64	0.351	0.403	0.954	0.446	33,300
hGAM	9.94	0.330	0.394	0.954	0.675	34,700
GAM _p	10.11	0.319	0.408	0.925	0.661	23,800
GAM _{nb}	11.4	0	--	--	--	--
ensemble	8.13	1	0.426	0.949	0.681	33,900

2091

2092 Table 28. Covariates retained in the a) subadult and b) adult sablefish species distribution model (SDM)
 2093 final ensembles, the percent contribution to the ensemble deviance explained by each, and the cumulative
 2094 percent deviance: SD = standard deviation, and BPI = bathymetric position index.

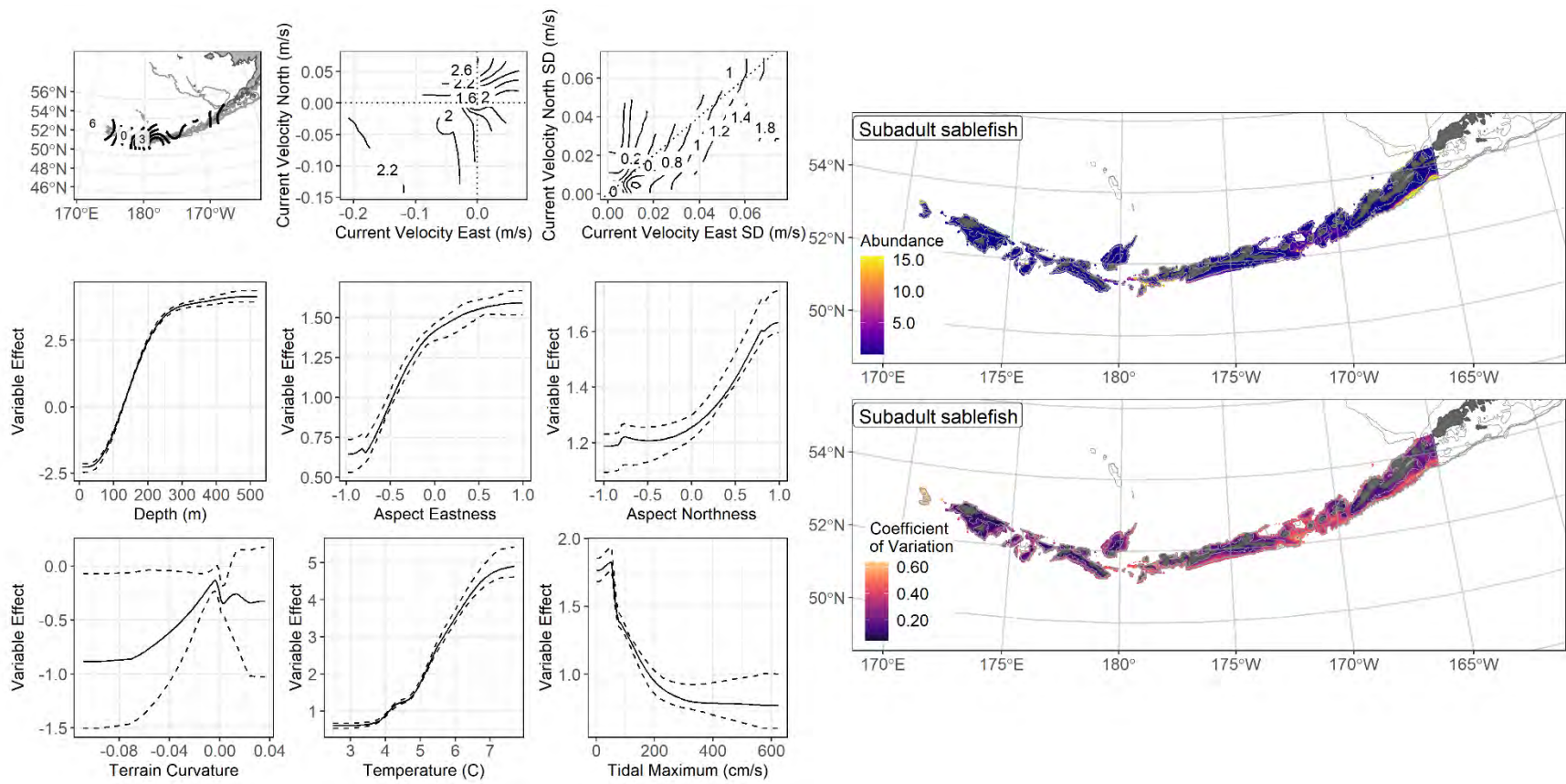
sablefish	Covariate	% Contribution	Cumulative % Contribution
a) subadult	bottom depth	32.7	32.7
	position	30.5	63.1
	bottom temperature	10.2	73.3
	current	6.4	79.7
	tidal maximum	4.2	83.9
	current SD	3.7	87.6
	aspect east	3.2	90.8
	aspect north	3.1	93.9
	curvature	1.4	95.3
	rockiness	1.4	96.7
	slope	1.1	97.8
	pennatulacean presence	0.8	98.6
	BPI	0.7	99.3
	sponge presence	0.6	99.9
coral presence	0.1	100	
a) adult	bottom depth	29.3	29.3
	position	25.0	54.3
	curvature	9.4	63.7
	current	7.2	70.9
	slope	4.5	75.4
	aspect north	4.5	79.9
	tidal maximum	4.1	84.0
	current SD	3.3	87.3
	sponge presence	2.5	89.8
	aspect east	2.2	92.0
	BPI	2.1	94.1
	coral presence	2.0	96.1
	bottom temperature	1.8	97.9
	pennatulacean presence	1.3	99.2
	rockiness	0.8	100

2095



2096

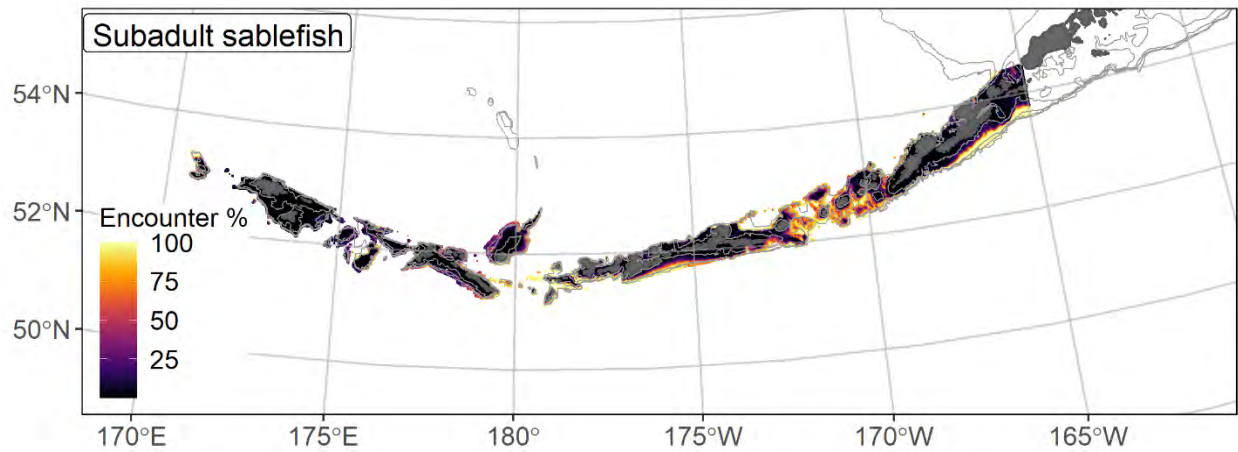
2097 Figure 86. Distribution of subadult sablefish catches (N = 472) in 1991–2019 AFSC RACE-GAP summer
 2098 bottom trawl surveys of the Aleutian Islands with the 100 m, 300 m, and 500 m isobaths indicated; filled
 2099 red circles indicate locations in top 10% of overall abundance, open orange circles indicate presence in
 2100 remaining catches.



2101

2102 Figure 87. The top nine covariate effects (left panel) on ensemble-predicted subadult sablefish numerical abundance across the Aleutian Islands

2103 (upper right panel) alongside the coefficient of variation of the ensemble predictions (lower right panel).

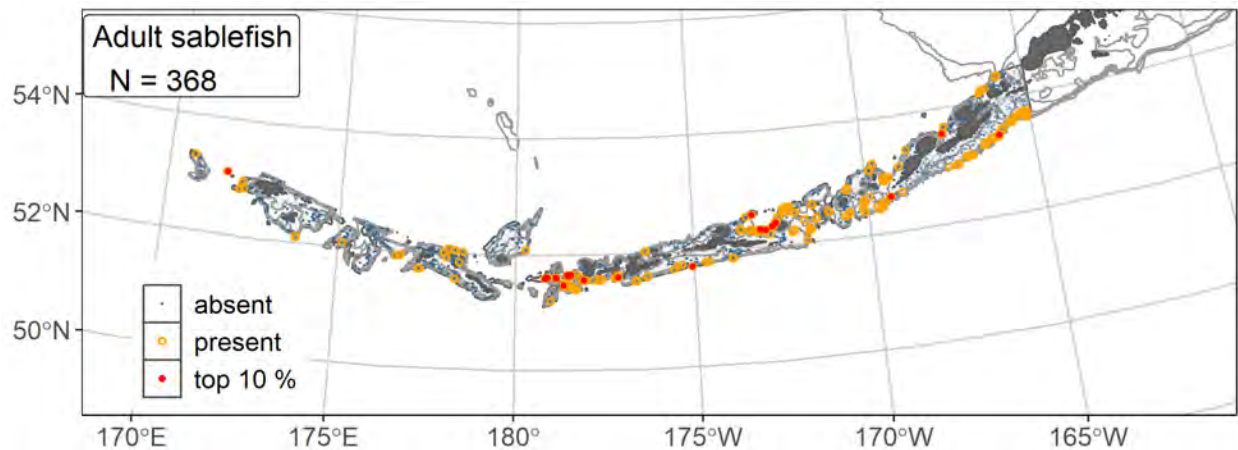


2104

2105 Figure 88. Encounter probability of subadult sablefish from AFSC RACE-GAP summer bottom trawl

2106 surveys (1991–2019) of the Aleutian Islands with the 100 m, 300 m, and 500 m isobaths indicated.

2107



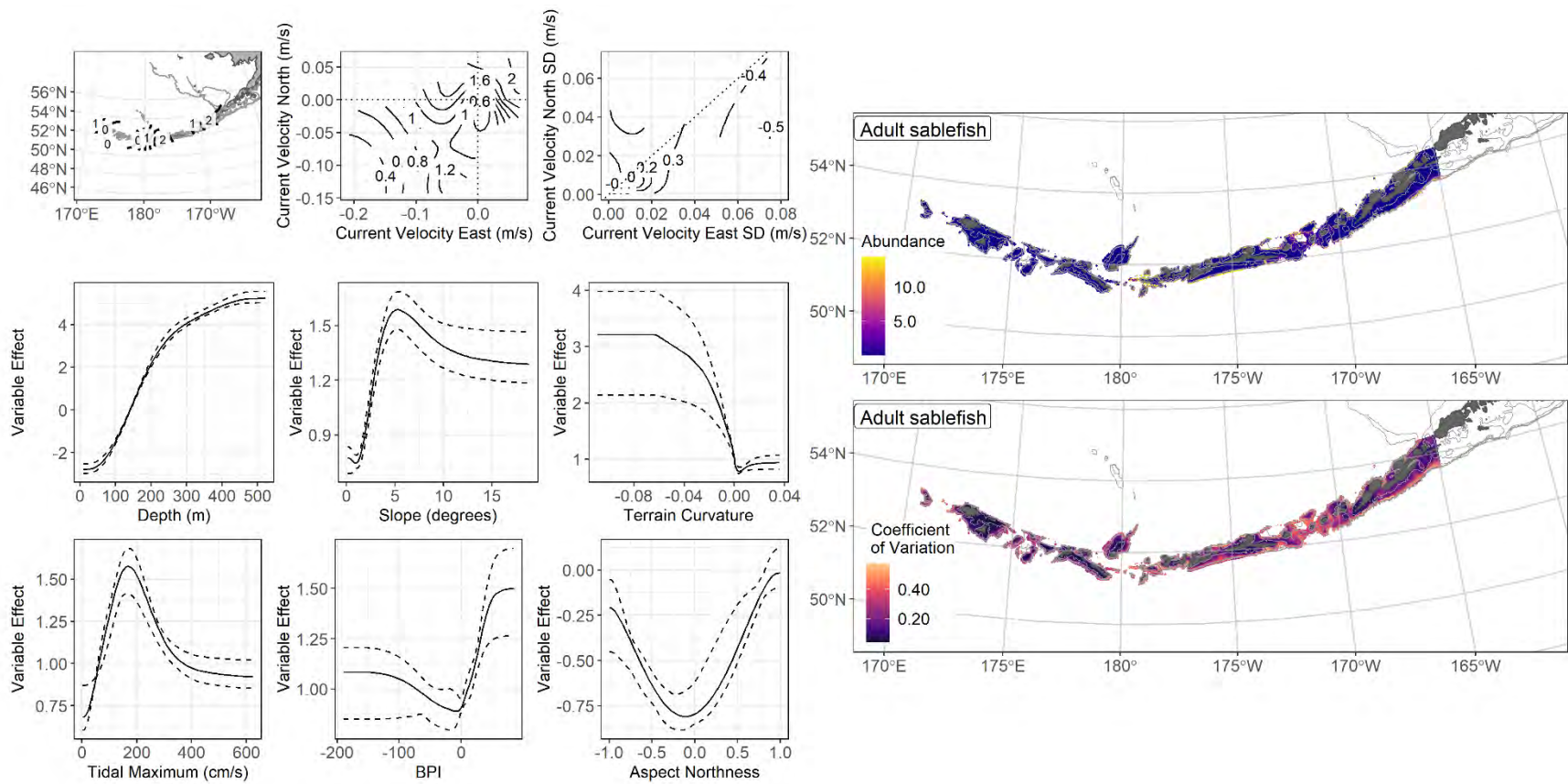
2108

2109 Figure 89. Distribution of adult sablefish catches (N = 368) in 1991–2019 AFSC RACE-GAP summer

2110 bottom trawl surveys of the Aleutian Islands with the 100 m, 300 m, and 500 m isobaths indicated; filled

2111 red circles indicate locations in top 10% of overall abundance, open orange circles indicate presence in

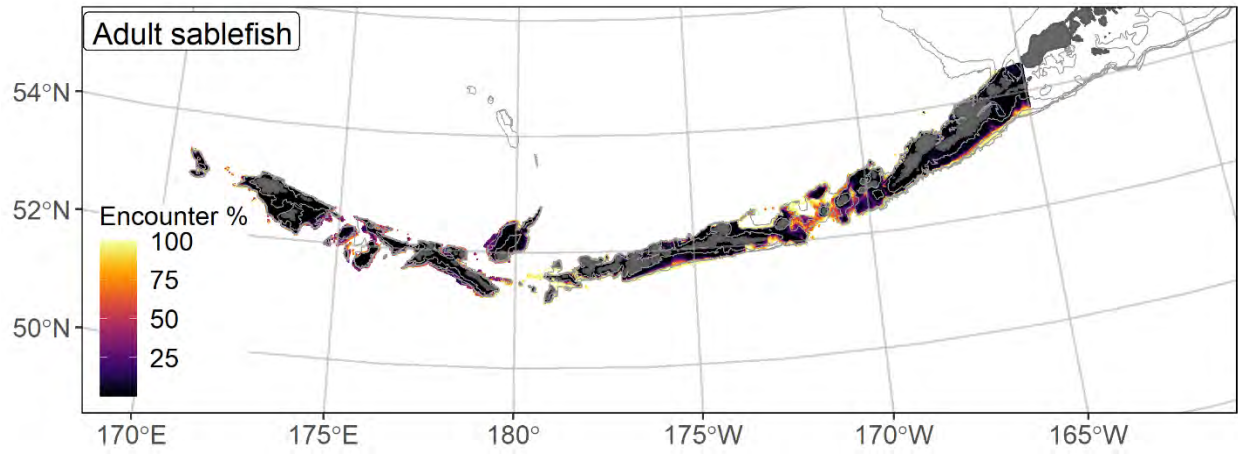
2112 remaining catches.



2113

2114 Figure 90. The top nine covariate effects (left panel) on ensemble-predicted adult sablefish numerical abundance across the Aleutian Islands

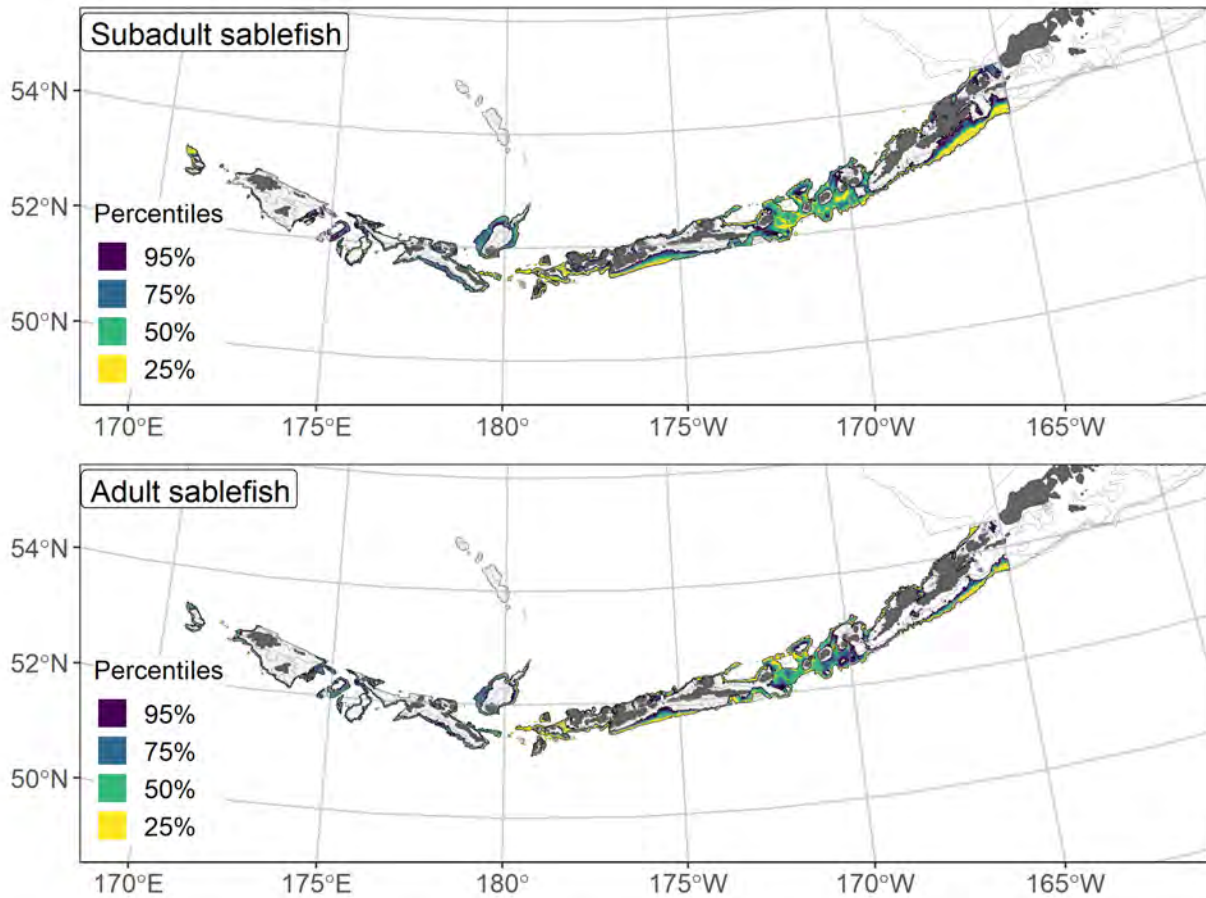
2115 (upper right panel) alongside the coefficient of variation of the ensemble predictions (lower right panel).



2116

2117 Figure 91. Encounter probability of adult sablefish from AFSC RACE-GAP summer bottom trawl

2118 surveys (1991–2019) of the Aleutian Islands with the 100 m, 300 m, and 500 m isobaths indicated.



2119

2120 Figure 92. Essential fish habitat (EFH area) defined as the top 95% of numerical abundance predictions
 2121 from a habitat-based ensemble fitted to subadult (top) and adult (bottom) sablefish distribution and
 2122 abundance in AFSC RACE-GAP summer bottom trawl surveys (1991–2019) with 100 m, 300 m, and
 2123 500 m isobaths indicated; internal to the EFH map are the subareas of the top 25% (EFH hot spots), top
 2124 50% (core EFH area), and top 75% (principal EFH area) of habitat related, ensemble-predicted numerical
 2125 abundance.

2126 **Walleye pollock (*Gadus chalcogrammus*)**

2127 Bering Sea-Aleutian Islands (BSAI) walleye pollock are ecologically important and support one
2128 of the world's largest commercial fisheries in the BSAI (Fissel et al. 2019). They spawn in March–May
2129 (Bailey 2000) with earlier spawning near shore north of Unimak Island in March and April and spawning
2130 in the Pribilof Islands later in the season (Bacheler et al. 2010); females can spawn up to 10 batches of
2131 eggs per year. Young-of-the-year pollock feed on plankton (Ciannelli et al. 2004) and provide forage for
2132 piscivores (Yang and Livingston 1986, Barnes et al. 2020). Two- to three-year-old pollock are rarely
2133 collected in bottom trawls, but are detected by mid-water acoustic summer surveys (e.g.,
2134 McCarthy et al. 2020). Younger pollock are more common in the northern portions of the RACE-GAP
2135 bottom trawl survey area and a pattern of movement to the southeast Bering Sea as they age has been
2136 noted (Buckley et al. 2009, Thorson et al. 2017). Length ranges were used to define ontogenetic stages for
2137 walleye pollock. Settled early juvenile walleye pollock lengths range from 40 mm F.L. at the end of the
2138 transformation stage (Doyle et al. 2018) to 140 mm F.L. (Pirtle et al. 2019). Subadults (141–381 mm
2139 F.L.) were assigned based on L_{50} reported by Stahl and Kruse (2008) for EBS pollock; the adult life stage
2140 was defined as fish with lengths greater than 381 mm F.L.

2141 **Settled early juvenile walleye pollock distribution and predicted abundance from RACE-GAP**
2142 **summer bottom trawl surveys in the Aleutian Islands –**

2143 Settled early juvenile walleye pollock were relatively uncommon in the RACE-GAP summer
2144 bottom trawl survey of the AI compared to older life stages (Figure 93). They occurred throughout the
2145 survey area and were most concentrated towards the eastern AI around Unalaska Island. The final
2146 ensemble contains three SDMs with approximately equal weights. The ensemble showed fair
2147 performance overall in terms of model fit (Table 29). Specifically, the model had an AUC of 0.850, which
2148 indicates a strong ability to discriminate presence from non-presence areas. However, the lower scores for
2149 ρ and PDE (0.220 and .280 respectively) suggest that this model may not accurately predict abundance
2150 and leaves most of the deviance unexplained. Overall, these metrics suggested that the model provides a

2151 somewhat accurate description of the areas where settled early juvenile pollock can be found, though it
2152 does not provide an accurate estimate of their abundance. The inclusion of small mesh trawls or similar
2153 methods in the future might provide better data and allow for better predictions¹⁴. No single covariate had
2154 a particularly large effect on model predictions of settled early juvenile pollock abundance, but bottom
2155 depth, geographic position, terrain aspect, current, and bottom temperature were the most important
2156 covariates and accounted for 78.5% of the deviance explained by the ensemble (Table 30). In general, the
2157 ensemble predicted that high abundance in shallow areas in the eastern AI, and areas with cool
2158 temperatures, weak currents, and south facing terrain (Figure 94). Predicted abundance was highest in the
2159 eastern AI, near-shore to Unalaska Island, with additional pockets of high abundance around Atka and
2160 Attu Islands (Figure 94). The predicted CV of abundance was high throughout most of the region, with
2161 the highest values occurring close to shore (Figure 94). This reflects that the catch of early juveniles is
2162 often quite variable, even inside of their usual habitat. Encounter probabilities for settled early juvenile
2163 walleye pollock were high near the areas described above, and close to zero in most places with depth
2164 greater than 200 m (Figure 95).

2165 **Subadult walleye pollock distribution and predicted abundance from RACE-GAP summer bottom**
2166 **trawl surveys in the Aleutian Islands –**

2167 Subadult walleye pollock catches were very common within RACE-GAP summer survey area
2168 (Figure 96). Large catches were distributed evenly across the AI. The final ensemble contained four
2169 SDMs with equal weights, and demonstrated fair to good predictive performance ($\rho = 0.403$, Table 29).
2170 The AUC of 0.752 suggests a fair ability to identify where subadults will be caught, and the PDE of 0.388
2171 shows that the model explains a fair amount of the observed deviance. Considering that subadult walleye
2172 pollock catches are quite variable, these metrics show that the ensemble predictions capture the general
2173 distribution of pollock in trawl catches but may not be precise. Bottom depth was the most important

¹⁴ A recommendation to add additional survey data types if possible to future SDM ensemble EFH mapping efforts for this species will be included as a future recommendation for research directions from the 2022 EFH 5-year Review.

2174 covariate and it accounted for 39.7 % of the deviance explained by the model, but geographic position,
2175 tidal maximum, rockiness, current variables, and temperature also contributed (Table 30). Based on the
2176 covariates, subadult walleye pollock are more likely to be found in water 100-200 m in depth, locations in
2177 the western AI, weaker tides, rocky terrain, and warmer temperatures (Figure 97). The estimated
2178 abundance of the subadult life stage was high in far west around Attu Island and in the east around
2179 Unalaska Island, with lower abundance predicted in between. As with early juveniles, predicted subadult
2180 abundance is highest in shallow areas and almost all subadults are predicted to occur above the 300 m
2181 depth contour (Figure 97). The predicted CV of abundance was uniformly high throughout the entire
2182 region (Figure 97). Subadult walleye pollock are very common in the AI, and the estimated encounter
2183 probability was near 100% in almost all areas, except in deeper water at the edge of the continental slope
2184 (Figure 98).

2185 **Adult walleye pollock distribution and predicted abundance from RACE-GAP summer bottom**
2186 **trawl surveys in the Aleutian Islands –**

2187 Adult walleye pollock catches were ubiquitous throughout the RACE-GAP summer survey area
2188 in the AI (Figure 99). Large catches occurred across the entire AI, and tended to occur further from shore
2189 compared to earlier life stages. The four SDMs included in the ensemble were assigned approximately
2190 equal weights and the predictions generated by the ensemble model had a good fit to the data ($\rho = 0.510$,
2191 Table 29). The AUC of 0.713 was only “fair,” but this may be influenced by the fact that there were
2192 almost no areas in the AI where adult walleye pollock were consistently absent. The PDE was somewhat
2193 lower at 0.298, which corresponds to a “fair” amount of the deviance. Overall, the abundance of adult
2194 walleye pollock in the AI was highly variable and the fit metrics for the model ensemble suggest that
2195 predictions about distribution were accurate but abundance estimates were less accurate. Bottom depth,
2196 geographic position, and current were the most important covariates and explained 70.1% of the deviance
2197 explained by the ensemble (Table 30). The ensemble predicted that adult walleye pollock were more
2198 abundant in the eastern AI, and that they preferred areas from 200-300 m in depth with southerly currents

2199 (Figure 100). Adult walleye pollock appear in greater numbers than the other life stages, and were
2200 predicted to occur in especially high densities near Unimak Pass and in the eastern AI (Figure 100).
2201 However, even in the western AI, where adult abundance was comparatively lower, average catches of
2202 50-100 pollock per haul could still be expected in many areas. Despite the very high abundance predicted
2203 in the east, the CV of abundance there is not higher than average, conveying that the eastern AI had
2204 reliably high abundance, whereas predictions for the other areas were more variable (Figure 100). The
2205 lowest predicted encounter probability for walleye pollock of any location in the AI summer bottom trawl
2206 survey was 84%, demonstrating that this species was common throughout the region (Figure 101).

2207 **Essential fish habitat of settled early juvenile, subadult, and adult walleye pollock in the Aleutian**
2208 **Islands –**

2209 The habitat related abundance predictions based on RACE-GAP summer bottom trawl data
2210 (1991–2019) were translated into EFH area and subareas (Figure 102). The EFH area for settled early
2211 juvenile walleye pollock is smaller than that of the other life stages. The largest section of EFH for this
2212 life stage was centered around Unalaska Island, though additional hot spots were predicted near Atka
2213 Island and Attu Island. Most of the EFH for this life stage occurred in relatively shallow water, and it was
2214 absent from areas with greater than 300 m depth. Both the subadult and adult life stages included nearly
2215 the whole survey area as EFH, but the details of their respective maps differ in some important ways.
2216 Subadult EFH showed a similar pattern to the early juveniles, with notable hot spots occurring near the
2217 same islands described above. However, subadults showed an increased depth range, with some parts of
2218 the EFH extending out towards the continental slope and deeper water. By contrast, the adult EFH map
2219 showed hot spots and core EFH areas concentrated in the east near Unalaska Island and Unimak Pass and
2220 in deeper water along the slope. Shallow near shore areas were generally not predicted to be part of the
2221 core EFH (50%) or hot spots. Given the similarity of the early juvenile and subadult EFH maps, it is
2222 curious that the adult population does not have a similar hot spot in the western AI. It is possible that
2223 adults in that region migrate elsewhere in the island chain, or descend into waters deeper than 500 m,

2224 thereby avoiding the survey. The ensembles for settled early juveniles showed marginal predictive
2225 performance and should be interpreted with caution, but the agreement between subadult and early
2226 juvenile maps suggested that the ensemble did not make unreasonable predictions.

2227 **Settled early juvenile walleye pollock Level 3 Essential Fish Habitat Information – Habitat-Related**
2228 **Vital Rates**

2229 Laboratory-reared early juvenile walleye pollock displayed temperature dependent growth
2230 following the below equation (Laurel et al. 2016):

2231
$$GR = 0.2023 + 0.0092 * T + 0.0335 * T^2 - 0.0019 * T^3$$

2232 Where *GR* is the growth rate (% body weight (g) per day (d)), and *T* is the temperature. The raster product
2233 of early juvenile walleye pollock predicted abundance and their spatially explicit temperature-dependent
2234 growth resulted in an EFH Level 3 map of habitat-related population (abundance) growth potential. The
2235 growth rate of early juvenile walleye pollock had a theoretical maximum at around 11°C
2236 (Laurel et al. 2016), however the summer bottom temperature in the AI had a more limited range than
2237 other regions, from around 3–7 °C (Figure 2). In the resulting map of temperature dependent growth, the
2238 highest growth areas were about 40% higher than the lowest growth areas (Figure 103). Notably, some of
2239 the areas with the highest temperature dependent growth rate occurred in the eastern AI, which is a major
2240 EFH hot spot. This was observed in the map of growth potential and abundance, which showed that only
2241 a few locations have both high growth potential and high predicted abundance (Figure 103).Some areas
2242 with high temperatures and hence high potential growth rates were not accompanied by high settled
2243 juvenile abundance, suggesting that temperature is not the only driver of walleye pollock distribution.
2244 However, the higher growth potential predicted in the eastern AI suggests that this section of EFH may be
2245 of greater importance to the overall health of the walleye pollock population compared to other EFH areas
2246 further west in the islands.

2247 A second vital rate, summer lipid accumulation rate (LAR) was determined from laboratory
2248 reared early juvenile walleye pollock according to the below equation (Copeman et al. 2017):

2249
$$LAR = 11.6 * \exp \left[-0.5 \left(\frac{T - 14.37}{6.39} \right)^2 \right]$$

2250 where *LAR* is the lipid accumulation rate (% lipids per % body weight per day) and *T* is the temperature
2251 (°C). The map of temperature dependent LAR (Figure 104) was nearly identical to that of the temperature
2252 dependent growth rate (Figure 104). This is unsurprising, since both are based on temperature. While
2253 Copeman et al. (2017) found that the optimal temperature for lipid accumulation (13-14 °C) was higher
2254 than the optimal growth rate temperature of 11°C (Laurel et al. 2016), both temperatures are much higher
2255 than are routinely found in the AI region, and this difference has little impact.

2256 Table 29. Constituent species distribution models (SDMs) used to construct Essential Fish Habitat (EFH)
 2257 for a) settled early juvenile, b) subadult, and c) adult walleye pollock: MaxEnt = Maximum entropy;
 2258 paGAM = presence-absence generalized additive model; hGAM = hurdle GAM; GAM_P = standard
 2259 Poisson GAM; and GAM_{nb} = standard negative-binomial GAM. Ensemble performance (ρ = Spearman's
 2260 rank correlation coefficient), root-mean-square-error (RMSE), the area under the receiver operating
 2261 characteristic (AUC), and the Poisson deviance explained (PDE) were generated from k-fold cross-
 2262 validation. The "--" in a field indicates that this SDM was not included in the final ensemble.

2263 **a) settled early juvenile walleye pollock**

Models	RMSE	Relative Weight	ρ	AUC	PDE	EFH area (km ²)
MaxEnt	4.82	0.333	0.220	0.835	0.280	59,000
paGAM	4.80	0.336	0.233	0.854	0.350	53,600
hGAM	--	--	--	--	--	--
GAM _P	5.19	0	--	--	--	--
GAM _{nb}	4.84	0.330	0.232	0.850	0.407	38,500
ensemble	4.76	1	0.235	0.857	0.368	55,100

2264 **b) subadult walleye pollock**

Models	RMSE	Relative Weight	ρ	AUC	PDE	EFH area (km ²)
MaxEnt	336.9	0.252	0.409	0.758	0.041	77,700
paGAM	336.7	0.252	0.435	0.774	0.087	77,700
hGAM	341.8	0.245	0.332	0.774	0.423	66,300
GAM _P	342.1	0	--	--	--	--
GAM _{nb}	337.1	0.251	0.366	0.727	0.276	69,800
ensemble	323.5	1	0.403	0.752	0.388	77,700

2265 **c) adult walleye pollock**

Models	RMSE	Relative Weight	ρ	AUC	PDE	EFH area (km ²)
MaxEnt	476.4	0.233	0.499	0.778	-0.122	77,700
paGAM	467.5	0.242	0.563	0.806	0.077	77,700
hGAM	448.5	0.263	0.337	0.806	0.343	77,700
GAM _P	448.4	0.263	0.317	0.632	0.334	77,600
GAM _{nb}	666.6	0	--	--	--	--
ensemble	444.8	1	0.510	0.713	0.298	77,700

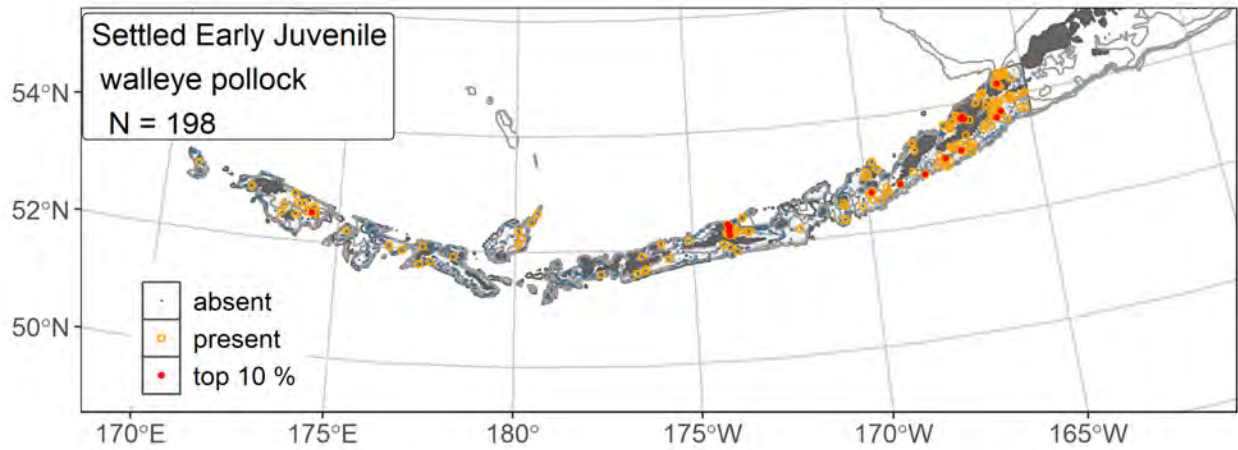
2266

2267 Table 30. Covariates retained in the a) settled early juvenile, b) subadult, and c) adult walleye pollock
 2268 species distribution model (SDM) final ensembles, the percent contribution to the ensemble deviance
 2269 explained by each, and the cumulative percent deviance: SD = standard deviation, and BPI = bathymetric
 2270 position index.

walleye pollock	Covariate	% Contribution	Cumulative % Contribution
a) settled early juvenile	position	22.0	22.0
	bottom depth	21.9	43.9
	aspect north	13.9	57.9
	current	11.8	69.7
	bottom temperature	8.8	78.5
	rockiness	5.5	84.0
	current SD	4.2	88.2
	BPI	3.3	91.5
	aspect east	2.8	94.3
	tidal maximum	2.0	96.3
	pennatulacean presence	2.0	98.3
	curvature	0.8	99.1
	sponge presence	0.5	99.6
	coral presence	0.3	99.9
	slope	0.1	100
b) subadult	bottom depth	39.7	39.7
	position	14.9	54.5
	tidal maximum	7.5	62.0
	rockiness	6.2	68.2
	current SD	5.4	73.6
	current	5.2	78.8
	bottom temperature	4.6	83.4
	slope	4.0	87.4
	BPI	3.4	90.8
	curvature	3.0	93.8
	aspect north	1.9	95.7
	coral presence	1.4	97.1
	pennatulacean presence	1.3	98.4
	aspect east	1.2	99.6
	sponge presence	0.4	100
c) adult	bottom depth	34.9	34.9
	position	25.6	60.4
	current	9.7	70.1
	aspect north	4.3	74.4
	current SD	3.9	78.3
	bottom temperature	3.9	82.2

walleye pollock	Covariate	% Contribution	Cumulative % Contribution
	tidal maximum	3.7	85.9
	sponge presence	2.7	88.6
	aspect east	2.4	91.0
	rockiness	2.4	93.4
	slope	1.9	95.3
	curvature	1.8	97.1
	BPI	1.8	98.9
	coral presence	0.8	99.7
	pennatulacean presence	0.3	100

2271



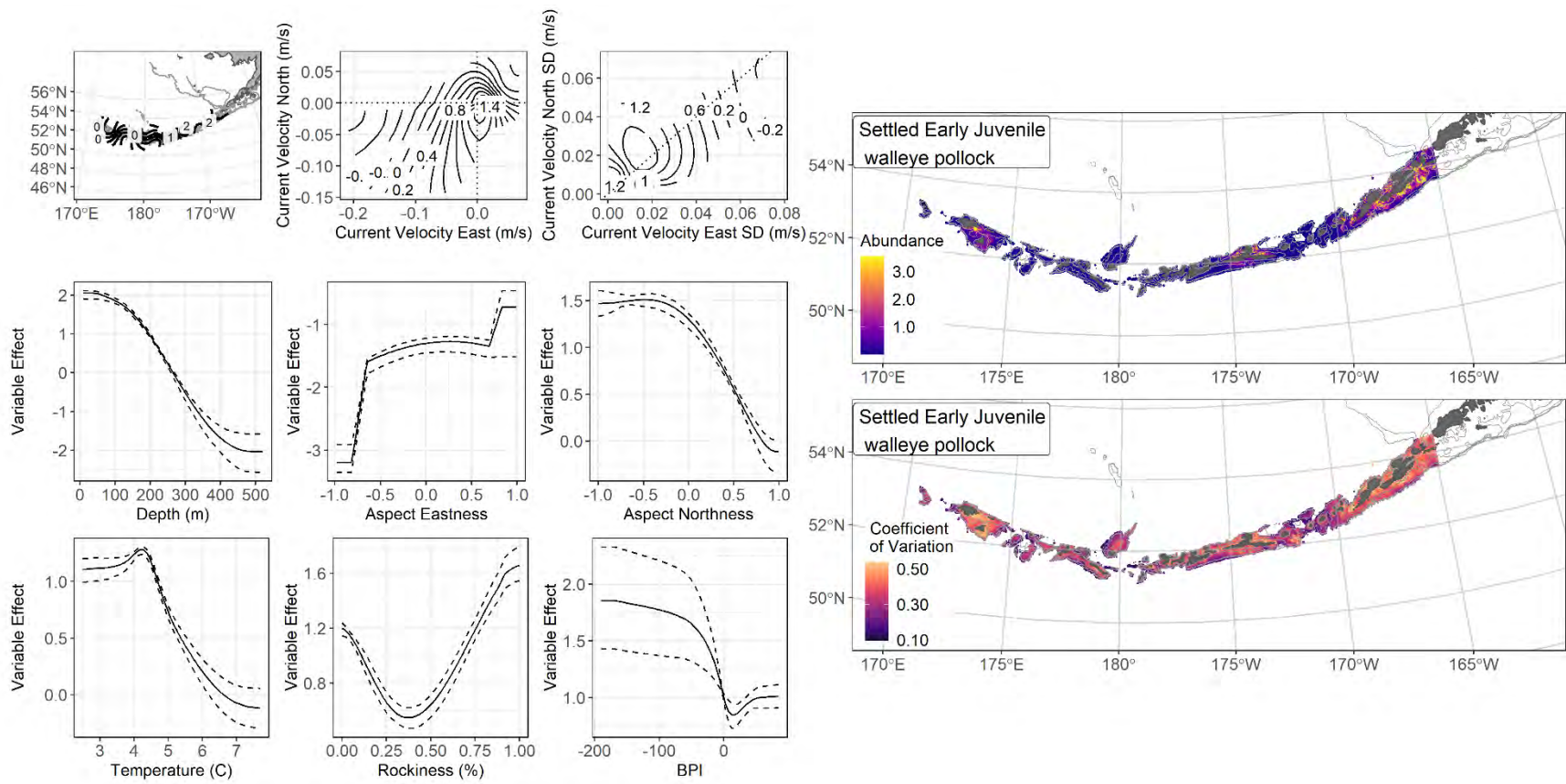
2272

2273 Figure 93. Distribution of settled early juvenile walleye pollock catches (N = 198) in 1991–2019 AFSC

2274 RACE-GAP summer bottom trawl surveys of the Aleutian Islands with the 100 m, 300 m, and 500 m

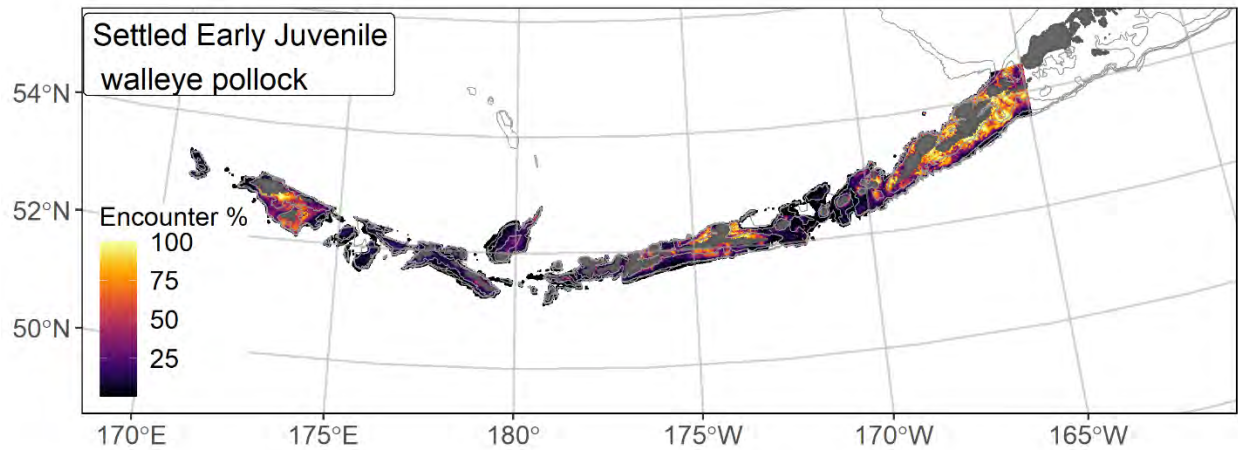
2275 isobaths indicated; filled red circles indicate locations in top 10% of overall abundance, open orange

2276 circles indicate presence in remaining catches, and small blue dots indicate absence.



2277

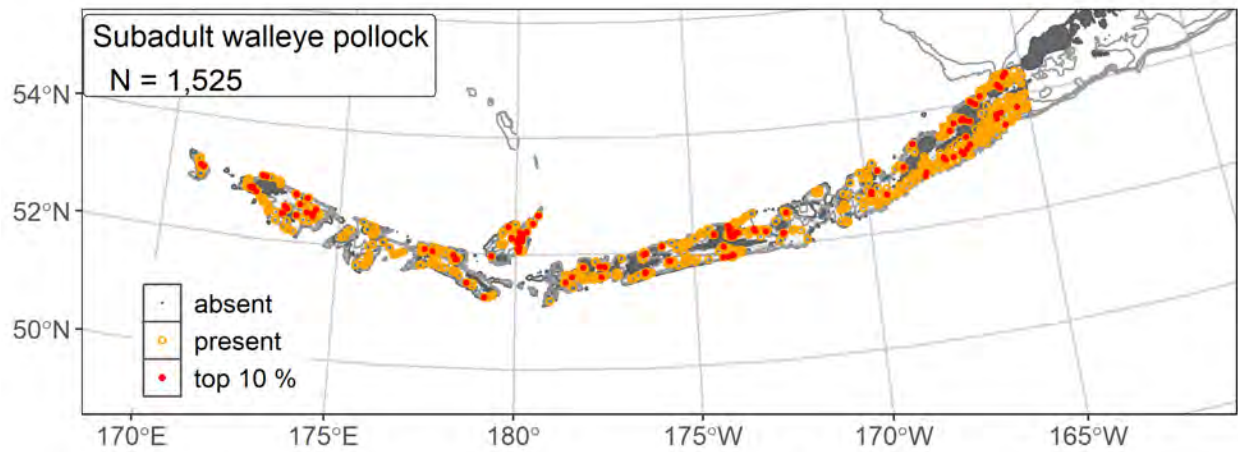
2278 Figure 94. The top nine covariate effects (left panel) on ensemble-predicted settled early juvenile walleye pollock numerical abundance across the
 2279 Aleutian Islands (upper right panel) alongside the coefficient of variation of the ensemble predictions (lower right panel).



2280

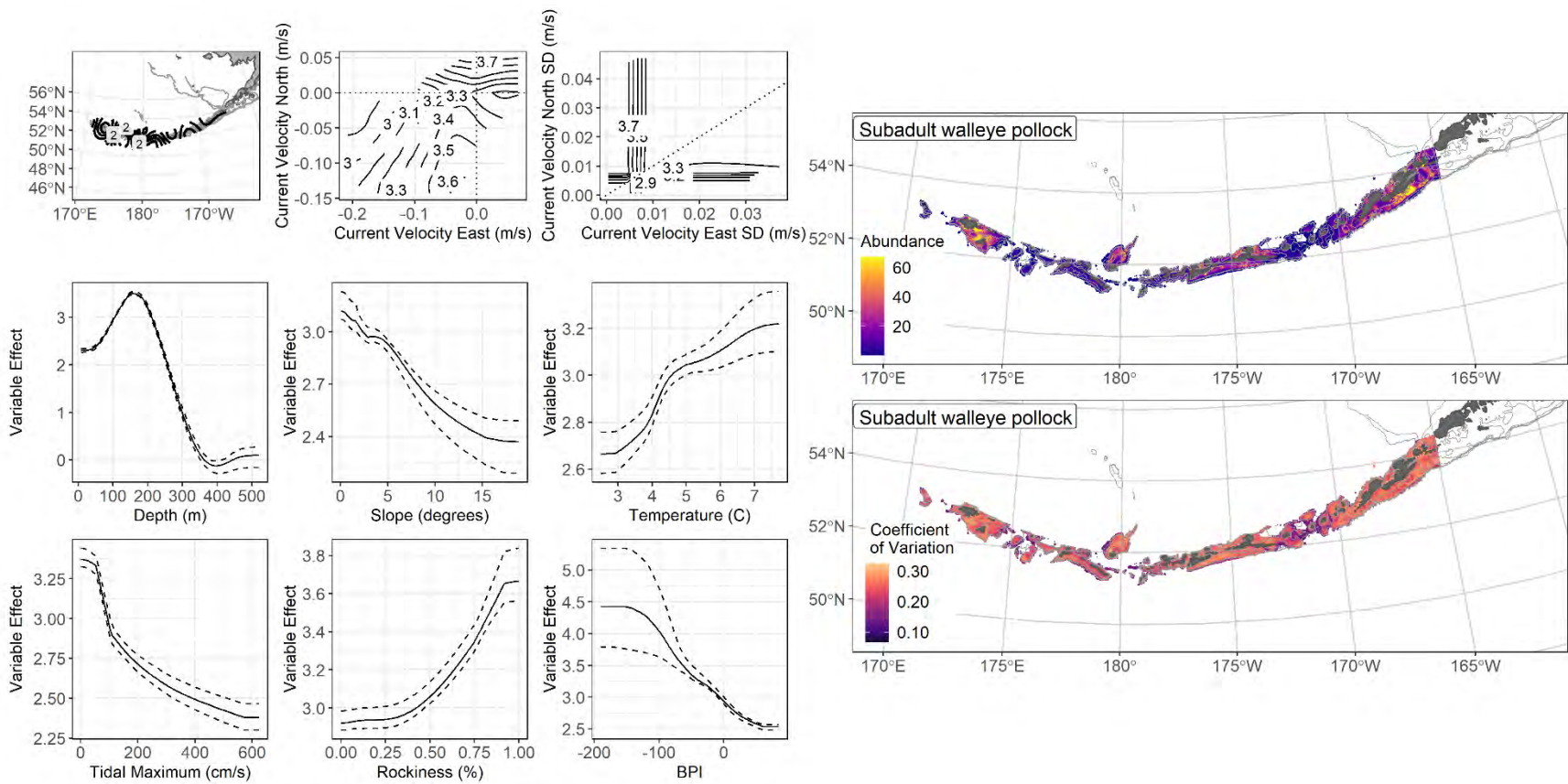
2281 Figure 95. Encounter probability of settled early juvenile walleye pollock from AFSC RACE-GAP
 2282 summer bottom trawl surveys (1991–2019) of the Aleutian Islands with the 100 m, 300 m, and 500 m
 2283 isobaths indicated.

2284



2285

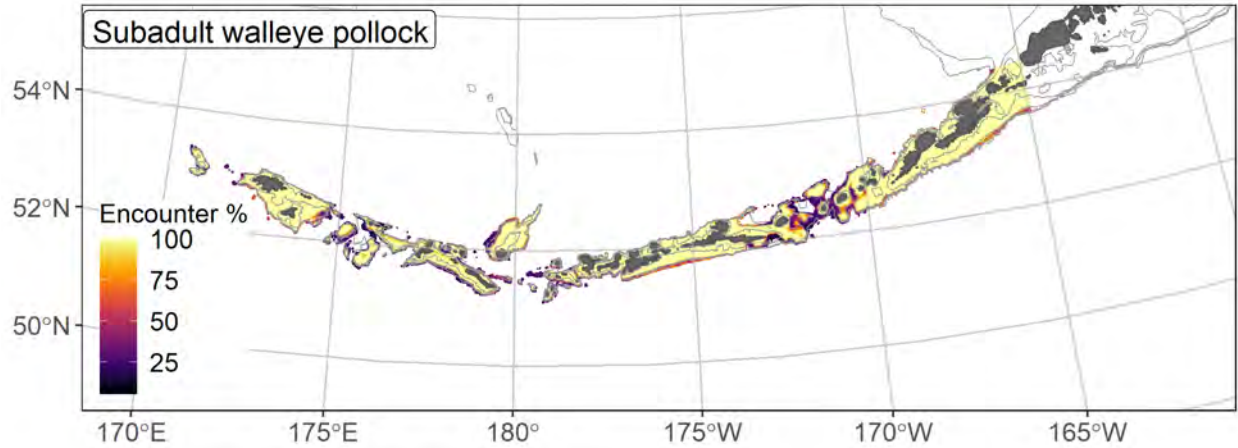
2286 Figure 96. Distribution of subadult walleye pollock catches (N = 1,525) in 1991–2019 AFSC RACE-GAP
 2287 summer bottom trawl surveys of the Aleutian Islands with the 100 m, 300 m, and 500 m isobaths
 2288 indicated; filled red circles indicate locations in top 10% of overall abundance, open orange circles
 2289 indicate presence in remaining catches, and small blue dots indicate absence.



2290

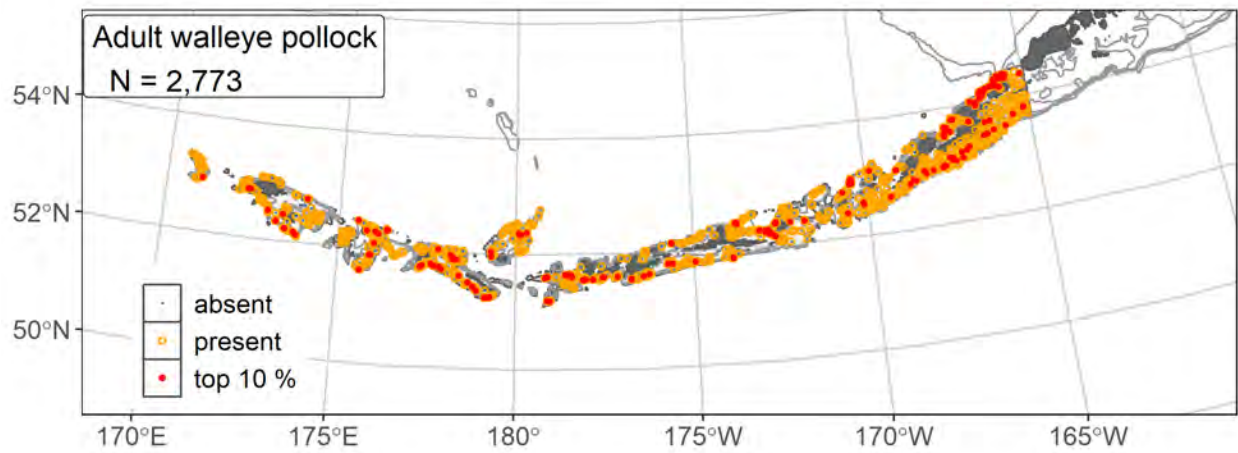
2291 Figure 97. The top nine covariate effects (left panel) on ensemble-predicted subadult walleye pollock numerical abundance across the Aleutian

2292 Islands (upper right panel) alongside the coefficient of variation of the ensemble predictions (lower right panel).

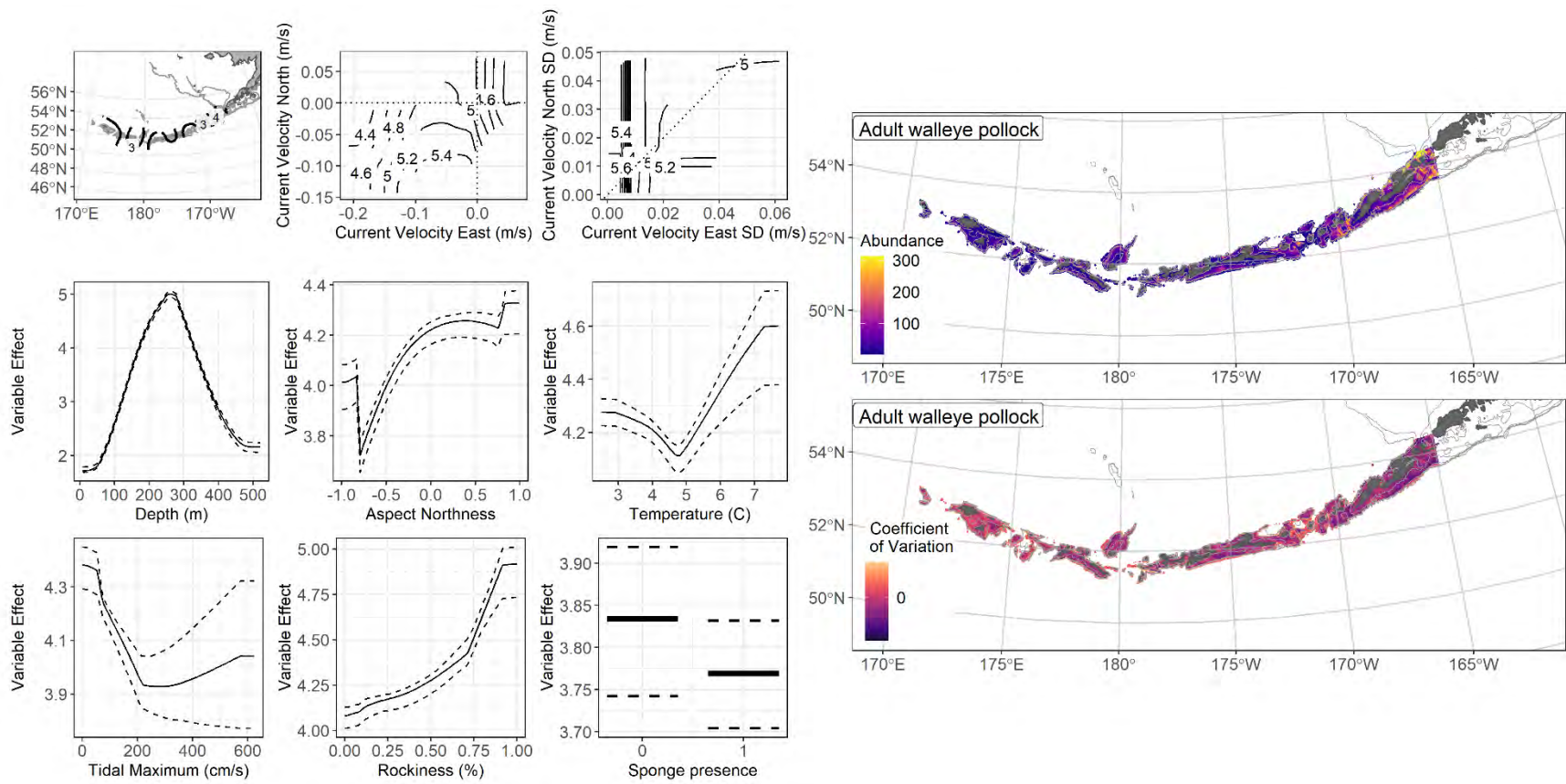


2293
2294 Figure 98. Encounter probability of subadult walleye pollock from AFSC RACE-GAP summer bottom
2295 trawl surveys (1991–2019) of the Aleutian Islands with the 100 m, 300 m, and 500 m isobaths indicated.

2296



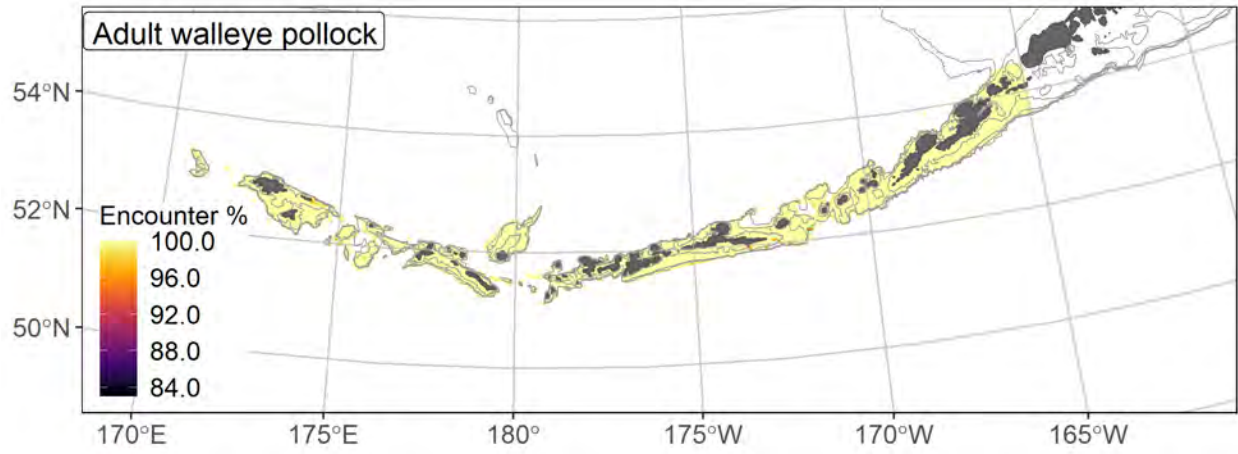
2297
2298 Figure 99. Distribution of adult walleye pollock catches (N = 2,773) in 1991–2019 AFSC RACE-GAP
2299 summer bottom trawl surveys of the Aleutian Islands with the 100 m, 300 m, and 500 m isobaths
2300 indicated; filled red circles indicate locations in top 10% of overall abundance, open orange circles
2301 indicate presence in remaining catches, and small blue dots indicate absence.



2302

2303 Figure 100. The top nine covariate effects (left panel) on ensemble-predicted adult walleye pollock numerical abundance across the Aleutian

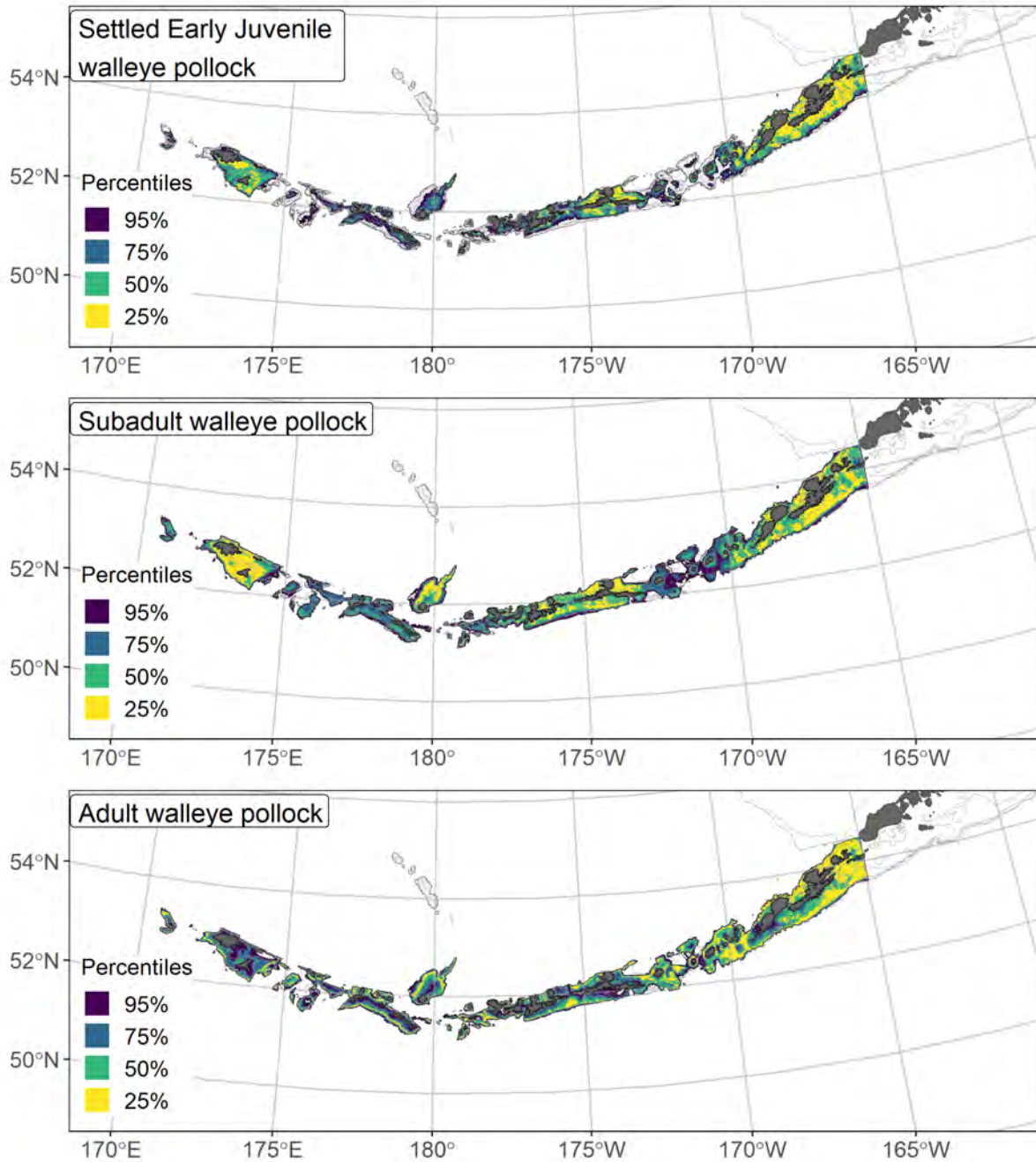
2304 Islands (upper right panel) alongside the coefficient of variation of the ensemble predictions (lower right panel)



2305

2306 Figure 101. Encounter probability of adult walleye pollock from AFSC RACE-GAP summer bottom

2307 trawl surveys (1991–2019) of the Aleutian Islands with the 100 m, 300 m, and 500 m isobaths indicated.



2308

2309 Figure 102. Essential fish habitat (EFH area) defined as the top 95% of numerical abundance predictions

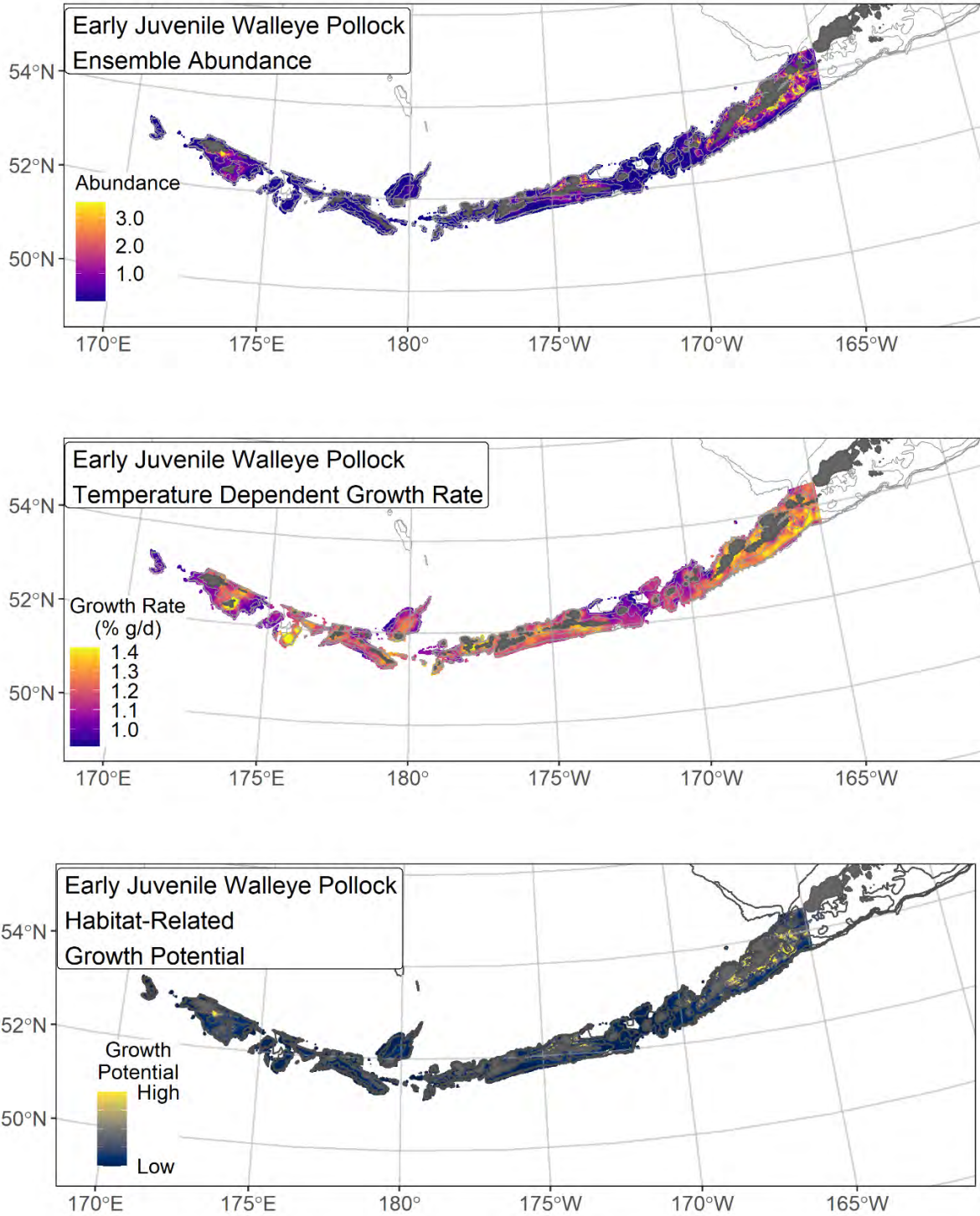
2310 from a habitat-based ensemble fitted to settled early juvenile (top), subadult (middle), and adult (bottom)

2311 walleye pollock distribution and abundance in AFSC RACE-GAP summer bottom trawl surveys (1991–

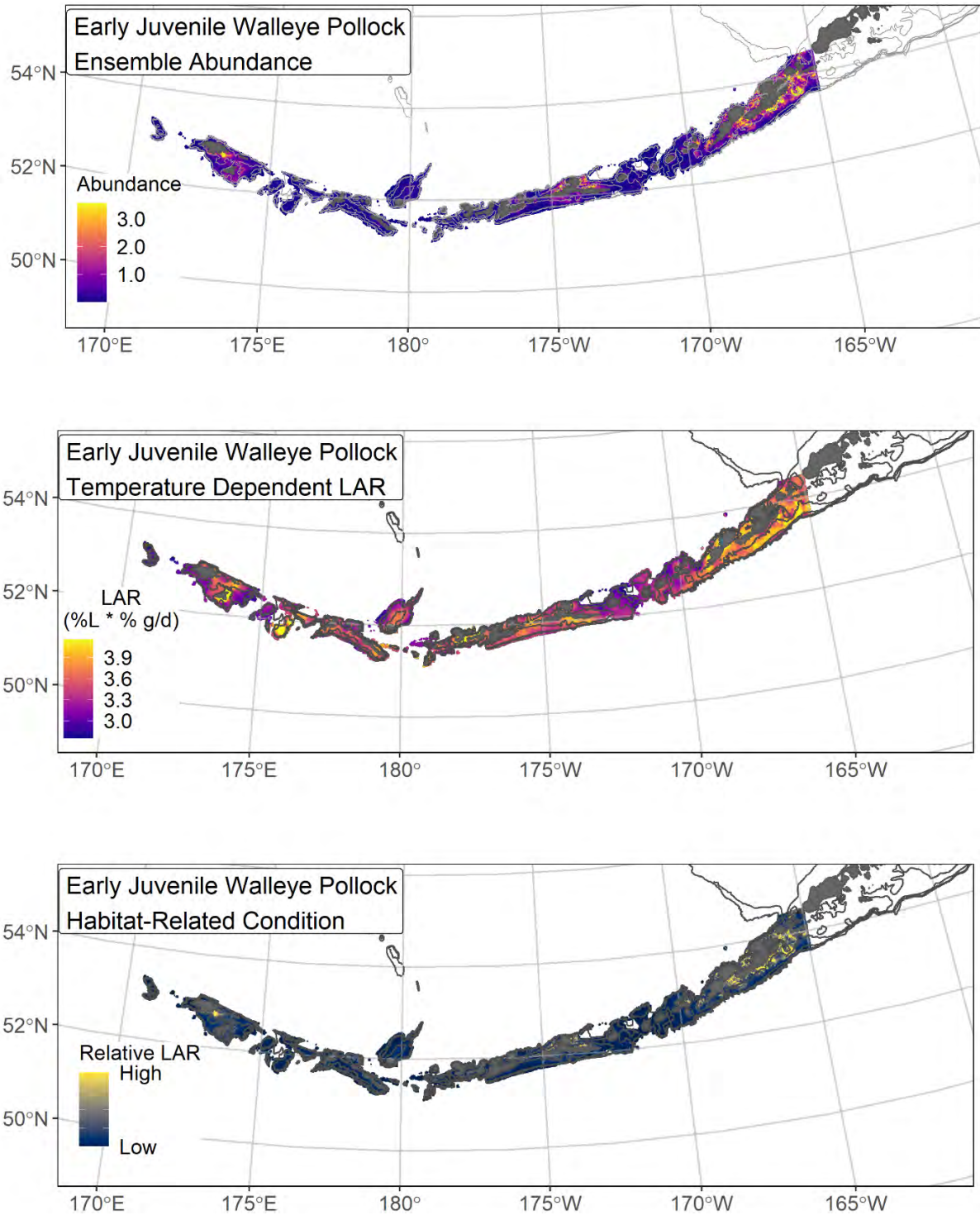
2312 2019) with 100 m, 300 m, and 500 m isobaths indicated; internal to the EFH map are the subareas of the

2313 top 25% (EFH hot spots), top 50% (core EFH area), and top 75% (principal EFH area) of habitat related,

2314 ensemble-predicted numerical abundance.



2315
 2316 Figure 103. Early juvenile walleye pollock ensemble-predicted abundance from RACE-GAP summer
 2317 bottom trawl surveys of the AI (1991–2019; top panel), temperature-dependent growth rate (% body
 2318 weight (g) per day; center panel), and habitat-related growth potential (bottom panel; this is the raster
 2319 product of ensemble-predicted abundance and spatially-explicit, temperature-dependent growth rate).



2320
 2321 Figure 104. Early juvenile walleye pollock ensemble-predicted abundance from RACE-GAP summer
 2322 bottom trawl surveys of the AI (1991–2019; top panel), temperature-dependent lipid accumulation rate
 2323 (LAR; % lipids per % body weight (g) per day; center panel), and habitat-related lipid condition (bottom
 2324 panel; the raster product of ensemble-predicted abundance and temperature-dependent growth rate).

Rockfishes

2325

2326 **Northern rockfish (*Sebastes polyspinis*)**

2327 Northern rockfish (*Sebastes polyspinis*) are common in Alaska waters from British Columbia to
2328 the Kuril Islands and Kamchatka Peninsula (Clausen and Heifetz 2002). They are the second most
2329 common rockfish species in the BSAI and are most abundant along the shelf break. Like other members
2330 of the genus *Sebastes*, northern rockfish are long-lived, ovoviviparous, and may skip mating during years
2331 with unfavorable conditions (Conrath 2019). Northern rockfish in the AI reach maturity at 277 mm F.L.
2332 (L_{50} ; Tenbrink and Spencer 2013), which is somewhat smaller than specimens from the GOA. Catches of
2333 northern rockfish in the BSAI have historically occurred as bycatch in other fisheries (i.e. Pacific ocean
2334 perch, Atka mackerel), but in recent years targeted fishing of northern rockfish has increased (Spencer
2335 and Ianelli 2019).

2336 **Subadult northern rockfish distribution and predicted abundance from RACE-GAP summer** 2337 **bottom trawl surveys in the Aleutian Islands –**

2338 Subadult northern rockfish catches were common across the area covered by the RACE-GAP
2339 summer bottom trawl survey (Figure 105). Large catches occurred mostly in the western AI, and
2340 consisted of thousands of northern rockfish per tow. The final ensemble contained three equally weighted
2341 SDMs and its predictions demonstrated good performance (Table 31). The ensemble scored well across
2342 all three metrics ($\rho = 0.432$; AUC = 0.824; PDE = 0.508) indicating that its predictions are accurate.
2343 Geographic position, bottom depth, and current accounted for 75.2% of the deviance explained by the
2344 ensemble (Table 32). Predicted, abundance increased further west in the AI, as well as in shallow depths
2345 and southerly currents (Figure 106). Predicted abundance was increased in the western AI, and was
2346 particularly high around Attu Island, the sea mounts near Buldir Strait, and Stalemate Bank (Figure 106).
2347 The CV of abundance was homogenous across the entire survey area (Figure 106). This species and life
2348 stage were common across the AI survey area, and a high encounter probability was predicted everywhere
2349 except in some habitats deeper than 300 m (Figure 107).

2350 **Adult northern rockfish distribution and predicted abundance from RACE-GAP summer bottom**
2351 **trawl surveys in the Aleutian Islands –**

2352 Adult northern rockfish catches in the RACE-GAP summer survey were very common in all parts
2353 of the AI (Figure 108). Like subadults, the highest density catches were concentrated in the western AI.
2354 The four SDMs present in the final ensemble were assigned equal weights, and the resulting model
2355 showed mixed predictive performance (Table 31). Specifically, the ensemble achieved good scores at
2356 predicting abundance ($\rho = 0.568$; PDE = 0.479), but performed poorly in terms of predicting presence and
2357 absence (AUC = 0.676). The wide ranging magnitude of adult northern rockfish catches (from 0 to
2358 thousands) resulted in high average abundances which the ensemble assumed to be locations with
2359 consistent presence. However, this assumption did not hold in this case and the ensemble over-predicted
2360 observed presence in trawl catches. The most important covariates were geographic position and bottom
2361 depth which explained 80.1% of the deviance explained in the ensemble (Table 32). According to the
2362 model, abundance is expected to increase from east to west, in depths between 100 and 200 m, and with
2363 strong but variable southerly currents (Figure 109). Predicted abundance was high overall, particularly
2364 around sea mounts in Buldir Strait and Stalemate Bank (Figure 109), but areas with relatively low
2365 abundance still averaged a hundred or more fish per haul. The predicted CV of abundance was elevated in
2366 many deeper areas that were near locations with high abundance, reflecting some uncertainty as to
2367 whether high abundance is driven mainly by geographic location or by depth (Figure 109). Adult northern
2368 rockfish were ubiquitous in the AI, and the nearly 100% encounter probability predicted in most places
2369 was consistent with their high numbers and wide distribution (Figure 110).

2370 **Essential fish habitat of subadult and adult northern rockfish in the Aleutian Islands –**

2371 The habitat related abundance predictions based on RACE-GAP summer bottom trawl data
2372 (1991–2019) were translated into EFH area and subareas (Figure 111). Both life stages of northern
2373 rockfish were very common throughout the AI. The EFH maps for the two life stages were nearly
2374 identical, and both covered almost the entirety of the region. In the EFH hot spots around Buldir Strait

2375 and Stalemate Bank, a single haul often encountered several thousand northern rockfish, and in areas of
2376 lower abundance it was common to catch dozens per tow. Most of the EFH hot spots were located at
2377 shallow depths in the western AI, and lower abundance EFH areas were usually in deeper water along the
2378 continental slope.

2379 Table 31. Constituent species distribution models (SDMs) used to construct Essential Fish Habitat (EFH)
 2380 for a) subadult and b) adult northern rockfish: MaxEnt = Maximum entropy; paGAM = presence-absence
 2381 generalized additive model; hGAM = hurdle GAM; GAM_p = standard Poisson GAM; and
 2382 GAM_{nb} = standard negative-binomial GAM. Ensemble performance (ρ = Spearman's rank correlation
 2383 coefficient), root-mean-square-error (RMSE), the area under the receiver operating characteristic (AUC),
 2384 and the Poisson deviance explained (PDE) were generated from k-fold cross-validation. The "--" in a field
 2385 indicates that this SDM was not included in the final ensemble.

2386 **a) subadult northern rockfish**

Models	RMSE	Relative Weight	ρ	AUC	PDE	EFH area (km²)
MaxEnt	297.9	0.302	0.405	0.816	0.263	74,500
paGAM	277.8	0.347	0.433	0.837	0.388	76,900
hGAM	--	--	--	--	--	--
GAM _p	--	--	--	--	--	--
GAM _{nb}	275.9	0.352	0.399	0.807	0.591	53,200
ensemble	271.1	1	0.432	0.824	0.508	76,000

2387 **b) adult northern rockfish**

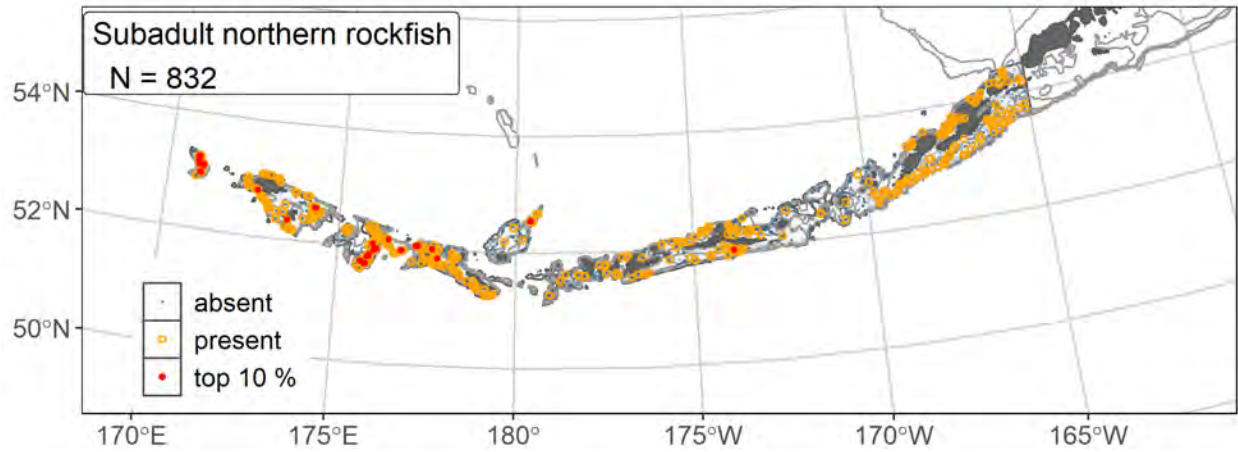
Models	RMSE	Relative Weight	ρ	AUC	PDE	EFH area (km²)
MaxEnt	828.5	0.235	0.510	0.779	0.204	77,700
paGAM	821.9	0.239	0.572	0.813	0.262	77,700
hGAM	784.5	0.262	0.466	0.813	0.532	71,900
GAM _p	781.0	0.264	0.449	0.668	0.533	58,600
GAM _{nb}	955.3	0	--	--	--	--
ensemble	746.6	1	0.568	0.676	0.265	77,700

2388

2389 Table 32. Covariates retained in the a) subadult and b) adult northern rockfish species distribution model
 2390 (SDM) final ensembles, the percent contribution to the ensemble deviance explained by each, and the
 2391 cumulative percent deviance: SD = standard deviation, and BPI = bathymetric position index.

northern rockfish	Covariate	% Contribution	Cumulative % Contribution
a) subadult	bottom depth	43.5	43.5
	position	25.3	68.9
	current	6.3	75.2
	current SD	4.2	79.4
	tidal maximum	3.9	83.3
	coral presence	3.3	86.6
	aspect east	2.7	89.3
	rockiness	2.7	92.0
	slope	2.5	94.5
	aspect north	2.4	96.9
	bottom temperature	1.5	98.4
	sponge presence	1.5	99.9
	pennatulacean presence	0.1	100
	curvature	0	100
a) adult	bottom depth	37.3	37.3
	position	25.5	62.9
	current SD	11.0	73.9
	current	6.2	80.1
	rockiness	3.3	83.4
	slope	2.7	86.1
	aspect east	2.3	88.4
	tidal maximum	2.2	90.6
	bottom temperature	2.1	92.7
	coral presence	2.1	94.8
	aspect north	1.6	96.4
	BPI	1.6	98.0
	sponge presence	1.0	99.0
	curvature	0.7	99.7
	pennatulacean presence	0.3	100

2392



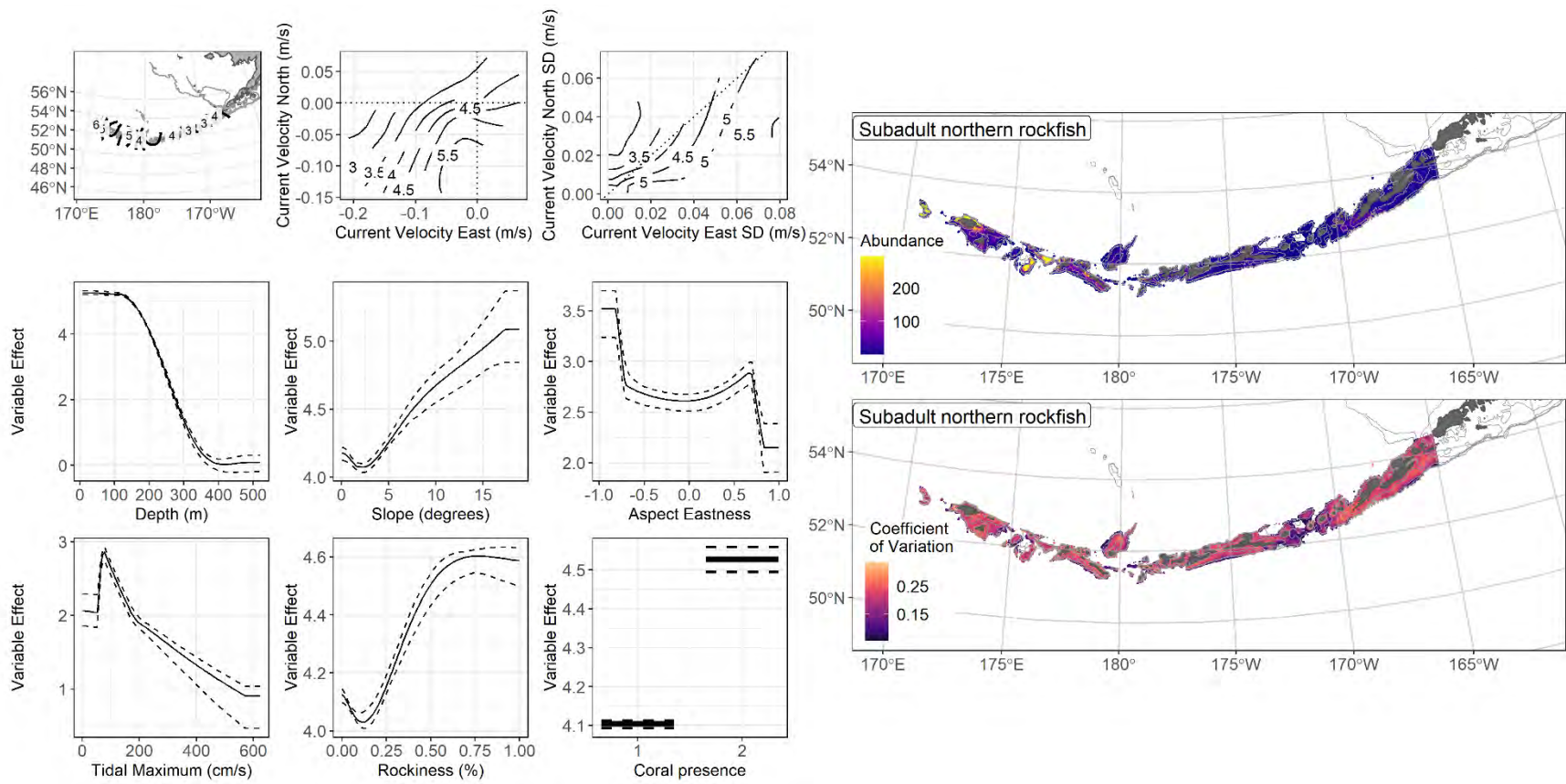
2393

2394 Figure 105. Distribution of subadult northern rockfish catches (N = 832) in 1991–2019 AFSC RACE-

2395 GAP summer bottom trawl surveys of the Aleutian Islands with the 100 m, 300 m, and 500 m isobaths

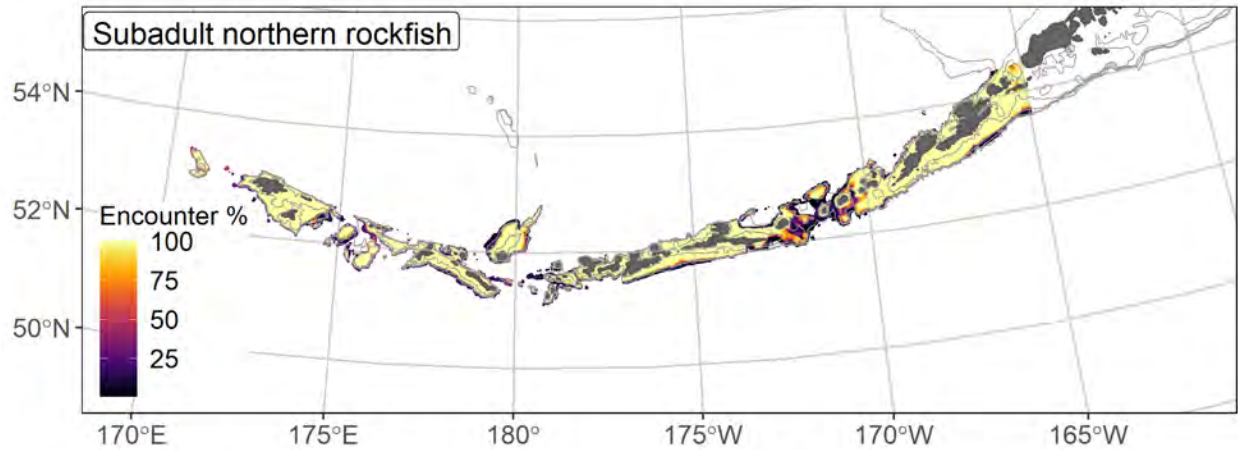
2396 indicated; filled red circles indicate locations in top 10% of overall abundance, open orange circles

2397 indicate presence in remaining catches, and small blue dots indicate absence.

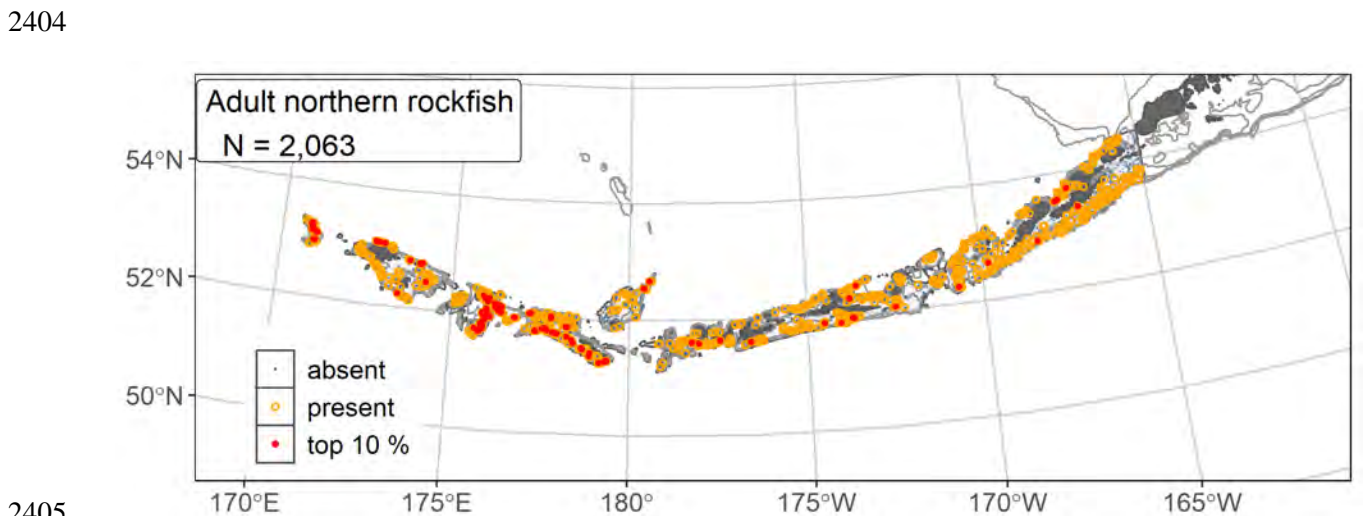


2398

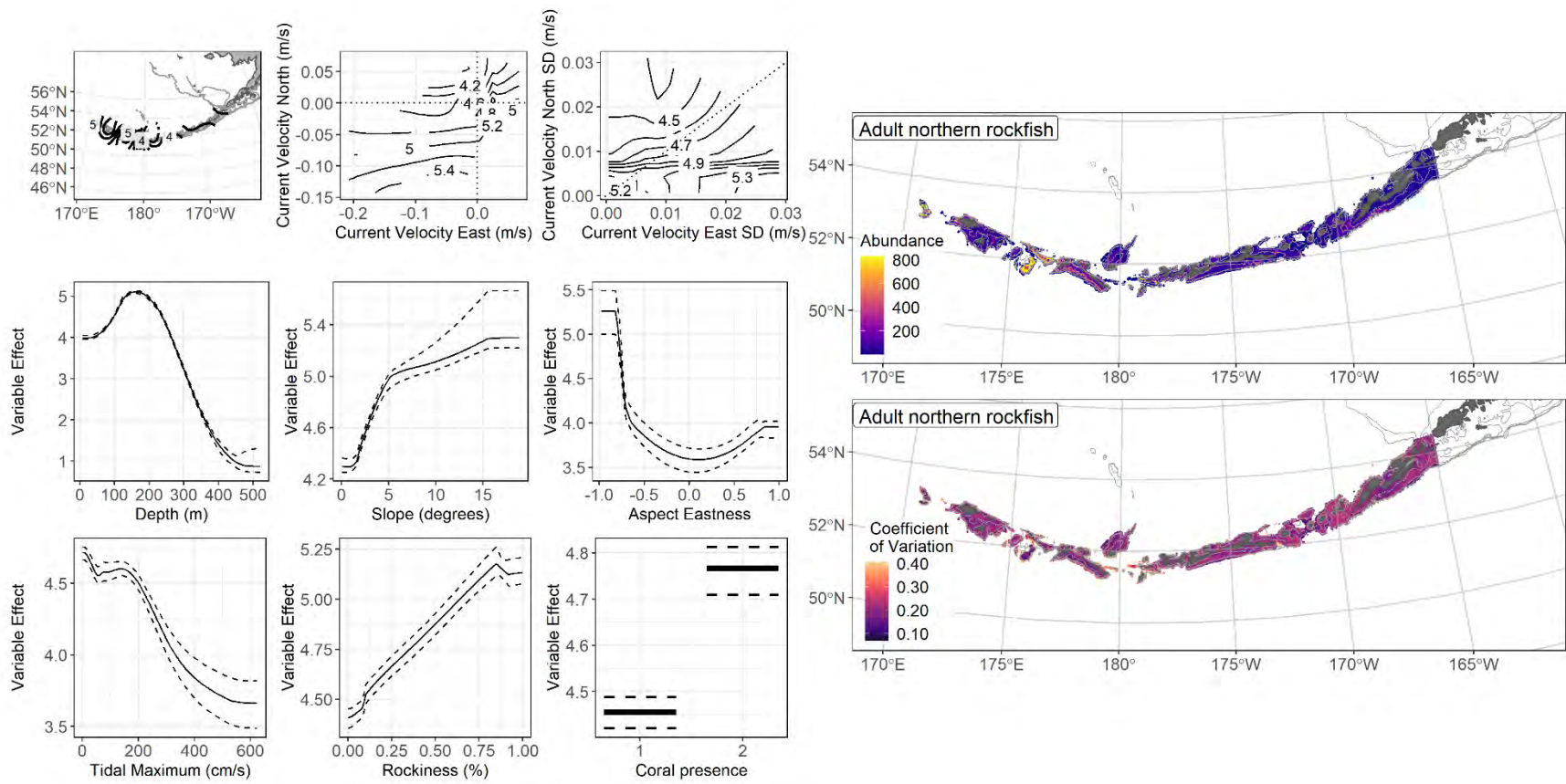
2399 Figure 106. The top nine covariate effects (left panel) on ensemble-predicted subadult northern rockfish numerical abundance across the Aleutian
 2400 Islands (upper right panel) alongside the coefficient of variation of the ensemble predictions (lower right panel).



2401
 2402 Figure 107. Encounter probability of subadult northern rockfish from AFSC RACE-GAP summer bottom
 2403 trawl surveys (1991–2019) of the Aleutian Islands with the 100 m, 300 m, and 500 m isobaths indicated.



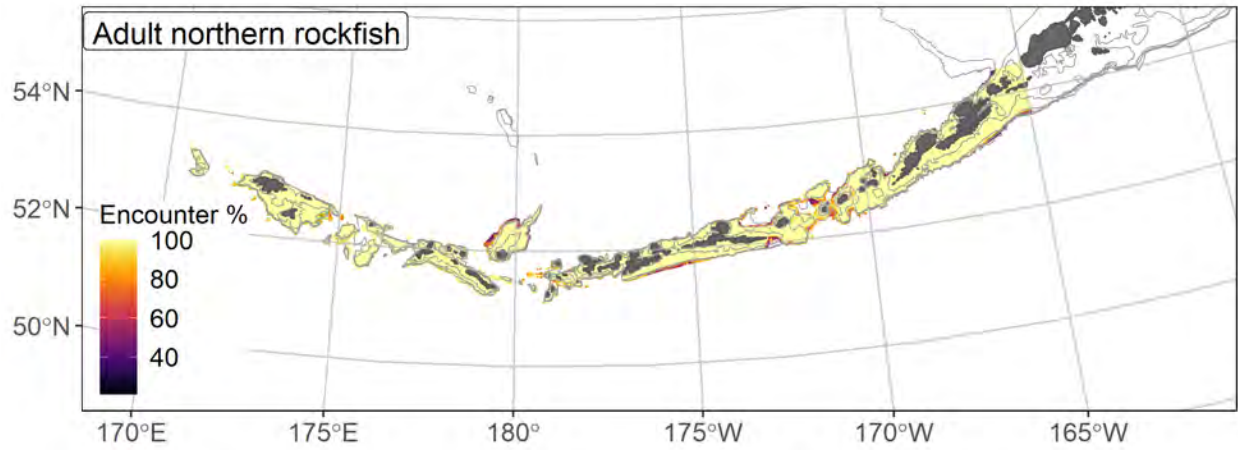
2405
 2406 Figure 108. Distribution of adult northern rockfish catches (N = 2,063) in 1991–2019 AFSC RACE-GAP
 2407 summer bottom trawl surveys of the Aleutian Islands with the 100 m, 300 m, and 500 m isobaths
 2408 indicated; filled red circles indicate locations in top 10% of overall abundance, open orange circles
 2409 indicate presence in remaining catches, and small blue dots indicate absence.



2410

2411 Figure 109. The top nine covariate effects (left panel) on ensemble-predicted adult northern rockfish numerical abundance across the Aleutian

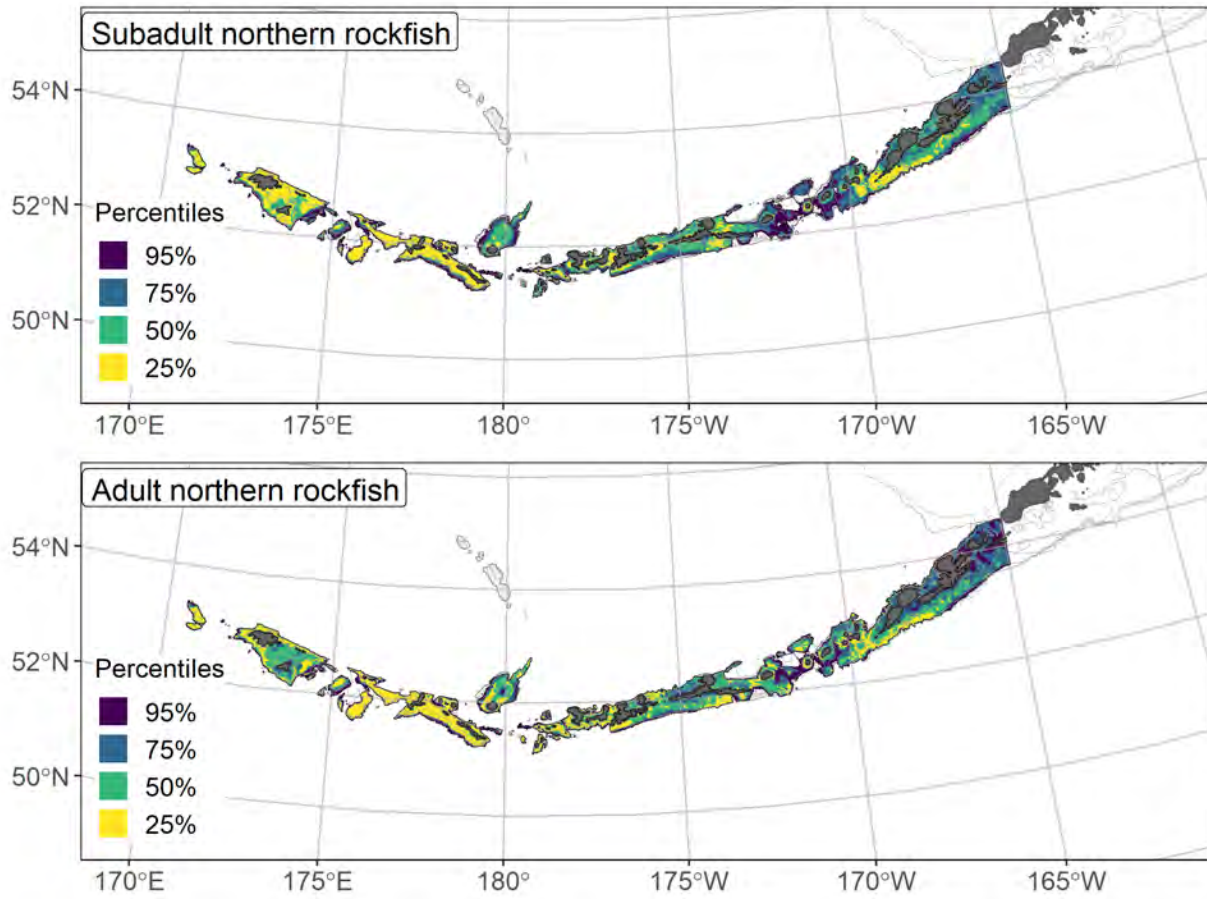
2412 Islands (upper right panel) alongside the coefficient of variation of the ensemble predictions (lower right panel).



2413

2414 Figure 110. Encounter probability of adult northern rockfish from AFSC RACE-GAP summer bottom

2415 trawl surveys (1991–2019) of the Aleutian Islands with the 100 m, 300 m, and 500 m isobaths indicated.



2416

2417 Figure 111. Essential fish habitat (EFH area) defined as the top 95% of numerical abundance predictions
 2418 from a habitat-based ensemble fitted to subadult (top) and adult (bottom) northern rockfish distribution
 2419 and abundance in AFSC RACE-GAP summer bottom trawl surveys (1991–2019) with 100 m, 300 m, and
 2420 500 m isobaths indicated; internal to the EFH map are the subareas of the top 25% (EFH hot spots), top
 2421 50% (core EFH area), and top 75% (principal EFH area) of habitat related, ensemble-predicted numerical
 2422 abundance.

2423 **Pacific ocean perch (*Sebastes alutus*)**

2424 Pacific ocean perch (*Sebastes alutus*, POP) are distributed across the North Pacific including the
2425 Bering Sea ranging from Baja California to Japan, and are the most common and commercially important
2426 rockfish species in the BSAI region (Mecklenburg et al. 2002). Seasonal differences in depth distributions
2427 were noted by Love et al. (2002) and compare favorably with the depths where POP are typically
2428 encountered on RACE-GAP summer bottom trawl surveys of the EBS (150–300 m). In fall and winter,
2429 adults inhabit deeper depths (300–420 m) until around May. Juveniles have been found in shallow (37 m)
2430 inshore waters gradually moving to deeper habitats with age (Carlson and Straty 1981). These rockfish
2431 display pronounced diel vertical movements (Brodeur 2001) and often form dense, localized schools off
2432 bottom (Hanselman et al. 2001, Hulson et al. 2017). Species in the genus *Sebastes* are ovoviviparous,
2433 with internal fertilization and the release of live young. After birthing, early juvenile POP (50–200 mm
2434 F.L.) settle into nursery habitat until they grow large enough to begin occupying their primary habitat
2435 (Pirtle et al. 2019). At approximately 250 mm, subadults become sexually mature and are thought to
2436 undertake another habitat transition towards deeper waters (Carlson and Straty 1981, Rooper et al. 2007,
2437 Rooper 2008).

2438 **Settled early juvenile Pacific ocean perch distribution and predicted abundance from RACE-GAP**
2439 **summer bottom trawl surveys in the Aleutian Islands–**

2440 Settled early juvenile POP were common across most areas covered in the RACE-GAP summer
2441 survey of the Aleutian Islands (Figure 112). Large catches were less common in the eastern AI, but were
2442 evenly distributed otherwise. POP do not transition to a subadult lifestyle until the relatively large size of
2443 200 mm, and the bottom trawl survey was able to sample a large number of them. However, it is possible
2444 that the current data missed smaller individuals, and additional data sources might be useful for this life

2445 stage¹⁵. The final ensemble contained four SDMs with approximately equal weights, and it showed fair
2446 performance when compared to the data (Table 33). Specifically, the ensemble showed good ability at
2447 predicting presence and absence (AUC = 0.803), and it had fair accuracy at predicting abundance and
2448 accounting for variation ($\rho = 0.368$; PDE = 0.371). Overall, this indicates that the ensemble is able to
2449 identify the areas POP are most likely to be found, but may not accurately predict the number caught.
2450 Considering that POP catches are highly variable and can involve a small handful of individuals or a
2451 school of thousands, some uncertainty in numbers is to be expected and these predictions should still
2452 provide useful information. Geographic position, bottom depth, and bottom currents were the most
2453 important covariates and accounted for 55.0% of the deviance explained in the ensemble (Table 34). This
2454 shows that a wide range of variables influenced predictions the settled early juvenile distribution of this
2455 species. In general, predicted abundance was high in locations that were further west, with 100–300 m
2456 depths, with westerly currents, and with corals and sponges (Figure 113). Predicted abundance was
2457 highest in areas of moderate depth, like Seguam Pass and Stalemate Bank (Figure 113). The predicted CV
2458 of abundance was higher near areas of high abundance, which reflected the high variation found in large
2459 POP catches (Figure 113). Encounter probabilities for settled early juvenile POP were high in most places
2460 shallower than 300 m, and tended to be somewhat lower in the eastern AI (Figure 114).

2461 **Subadult Pacific ocean perch distribution and predicted abundance from RACE-GAP summer**
2462 **bottom trawl surveys in the Aleutian Islands –**

2463 Subadult POP catches were common and evenly distributed within the RACE-GAP summer
2464 survey area (Figure 115). They were present in high density in many places in the eastern AI. The final
2465 ensemble contains four SDMs with equal weights and it demonstrated a fair fit to the observed data as
2466 measured by all three metrics ($\rho = 0.397$; AUC = 0.781; PDE = 0.396; Table 33). Taken together, this

¹⁵ A recommendation to add additional survey data types if possible to future SDM ensemble EFH mapping efforts for this species will be included as a future recommendation for research directions from the 2022 EFH 5-year Review.

2467 suggested that this ensemble was fairly accurate, but some errors should be expected. Geographic position
2468 and bottom depth were the most important covariates but accounted for only 51.5% of the deviance
2469 explained, and a variety of other covariates were also important to ensemble predictions (Table 34). Like
2470 the early juveniles, moderate depths and rocky substrates had a strong positive effect on model
2471 predictions (Figure 116). Overall abundance of this life stage was predicted to be lowest in the eastern AI,
2472 and highest around the sea mounts near Seguam Pass, Buldir Strait, and Stalemate Bank (Figure 116).
2473 The predicted coefficient of variation was fairly low in most places and did not display any obvious
2474 pattern (Figure 116). Subadult POP are very common in the AI, and the encounter probability was near
2475 100% in almost all surveyed areas, except the deepest locations along the edge of the continental slope
2476 (Figure 117).

2477 **Adult Pacific ocean perch distribution and predicted abundance from RACE-GAP summer bottom**
2478 **trawl surveys in the Aleutian Islands –**

2479 Adult Pacific ocean perch catches were universally common throughout the RACE-GAP summer
2480 survey area in the AI (Figure 118). Large catches occurred across the entire AI area, but were somewhat
2481 more frequent in the western parts of the island chain. The final ensemble included three SDMs with the
2482 paGAM weighted slightly less than the hGAM or GAM_P, and the predictions showed a good fit, though
2483 the metrics suggested some complications (Table 33). Specifically, the ensemble performed well in terms
2484 of deviance explained (PDE = 0.519) and excellently in terms of predicting areas of relatively high or low
2485 abundance ($\rho = 0.740$). However, it showed poor ability at predicting catches where POP would be
2486 present (AUC = 0.685) which likely reflects a failure to accurately predict the minority of catches where
2487 POP were absent. In summary, this ensemble performed well at predicting abundance on average, and
2488 very well at identifying the highest abundance catches, but it underestimated the frequency of absences in
2489 catches. Bottom depth alone accounted for 71.5% of the deviance explained by the ensemble, while
2490 geographic position, slope, and bottom current made smaller contributions (Table 34). The model
2491 predicted high abundance in places with moderate depth (200–300 m) and a high slope (Figure 119). POP

2492 were concentrated along the upper edge of the continental slope, usually just above the 300 m depth
2493 contour (Figure 119). The predicted CV of abundance was highest in areas of high abundance along the
2494 edge of the continental slope, reflecting that schools of POP vary greatly in size (Figure 119). The lowest
2495 encounter probability predicted by the ensemble was 97%, illustrating that adult POP can be found
2496 everywhere in the AI, even if not everywhere attracted large aggregations (Figure 120).

2497 **Essential fish habitat of settled early juvenile, subadult, and adult Pacific ocean perch in the**
2498 **Aleutian Islands –**

2499 The habitat related abundance predictions based on RACE-GAP summer bottom trawl data
2500 (1991–2019) were translated into EFH area and subareas (Figure 121). The EFH areas for all three life
2501 stages encompassed nearly the entire survey area, reflecting that POP were very common in the AI
2502 region. Settled early juveniles had EFH hot spots east of Atka Island, and around sea mounts in many
2503 areas. The EFH areas for subadults were similar, but was shifted further offshore. Adult EFH followed a
2504 distinct pattern compared to the other life stages. The EFH hot spots for adults occurred further offshore
2505 and closely tracked the 300 m depth contour.

2506 Table 33. Constituent species distribution models (SDMs) used to construct Essential Fish Habitat (EFH)
 2507 for a) settled early juvenile, b) subadult, and c) adult Pacific ocean perch: MaxEnt = Maximum entropy;
 2508 paGAM = presence-absence generalized additive model; hGAM = hurdle GAM; GAM_P = standard
 2509 Poisson GAM; and GAM_{nb} = standard negative-binomial GAM. Ensemble performance (ρ = Spearman's
 2510 rank correlation coefficient), root-mean-square-error (RMSE), the area under the receiver operating
 2511 characteristic (AUC), and the Poisson deviance explained (PDE) were generated from k-fold cross-
 2512 validation. The "--" in a field indicates that this SDM was not included in the final ensemble.

2513 **a) settled early juvenile Pacific ocean perch**

Models	RMSE	Relative Weight	ρ	AUC	PDE	EFH area (km ²)
MaxEnt	71.7	0.254	0.393	0.829	0.193	65,500
paGAM	71.9	0.252	0.378	0.817	0.165	76,000
hGAM	72.9	0.246	0.280	0.817	0.347	59,100
GAM _P	72.6	0.248	0.280	0.729	0.382	52,700
GAM _{nb}	74.7	0	--	--	--	--
ensemble	68.9	1	0.368	0.806	0.371	70,100

2514 **b) subadult Pacific ocean perch**

Models	RMSE	Relative Weight	ρ	AUC	PDE	EFH area (km ²)
MaxEnt	186	0.246	0.423	0.805	0.187	73,900
paGAM	185	0.249	0.425	0.808	0.188	77,700
hGAM	183	0.254	0.292	0.807	0.390	74,600
GAM _P	184	0.251	0.307	0.714	0.418	66,200
GAM _{nb}	207	0	--	--	--	--
ensemble	174	1	0.397	0.781	0.396	77,600

2515 **c) adult Pacific ocean perch**

Models	RMSE	Relative Weight	ρ	AUC	PDE	EFH area (km ²)
MaxEnt	--	0	--	--	--	--
paGAM	1,690	0.302	0.731	0.887	0.335	77,700
hGAM	1,560	0.354	0.692	0.887	0.549	77,700
GAM _P	1,580	0.344	0.675	0.700	0.542	77,500
GAM _{nb}	--	0	--	--	--	--
ensemble	1,520	1	0.740	0.685	0.519	77,700

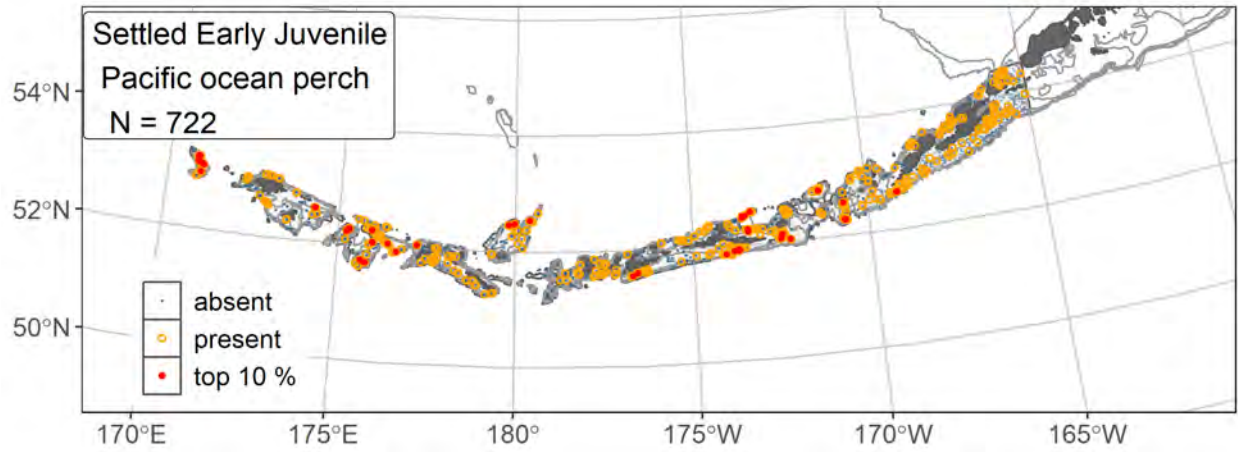
2516

2517 Table 34. Covariates retained in the a) settled early juvenile, b) subadult, and c) adult Pacific ocean perch
 2518 species distribution model (SDM) final ensembles, the percent contribution to the ensemble deviance
 2519 explained by each, and the cumulative percent deviance: SD = standard deviation, and BPI = bathymetric
 2520 position index.

Pacific ocean perch	Covariate	% Contribution	Cumulative % Contribution
a) settled early juvenile	bottom depth	28.8	28.8
	position	13.4	42.2
	current	12.9	55.0
	sponge presence	7.3	62.3
	coral presence	6.2	68.6
	current SD	5.0	73.6
	aspect east	4.9	78.5
	aspect north	4.6	83.2
	bottom temperature	4.4	87.5
	rockiness	4.1	91.6
	tidal maximum	3.6	95.2
	BPI	2.5	97.7
	slope	1.6	99.3
	curvature	0.5	99.9
	pennatulacean presence	0.1	100
b) subadult	bottom depth	37.7	37.7
	position	13.9	51.5
	rockiness	7.5	59.0
	aspect east	6.5	65.6
	current	5.3	70.9
	current SD	4.8	75.7
	BPI	4.8	80.5
	sponge presence	4.7	85.2
	coral presence	4.0	89.2
	aspect north	2.8	92.0
	bottom temperature	2.5	94.5
	tidal maximum	2.4	96.9
	slope	1.9	98.8
	curvature	1.2	100
	pennatulacean presence	0	100
c) adult	bottom depth	71.5	71.5
	position	7.9	79.4
	current	6.8	86.2
	slope	4.3	90.6

Pacific ocean perch	Covariate	% Contribution	Cumulative % Contribution
	BPI	2.8	93.3
	current SD	1.5	94.9
	sponge presence	1.2	96.1
	rockiness	0.9	97.1
	aspect north	0.8	97.8
	aspect east	0.6	98.5
	coral presence	0.6	99.1
	bottom temperature	0.3	99.4
	tidal maximum	0.3	99.7
	pennatulacean presence	0.2	99.8
	curvature	0.2	100

2521



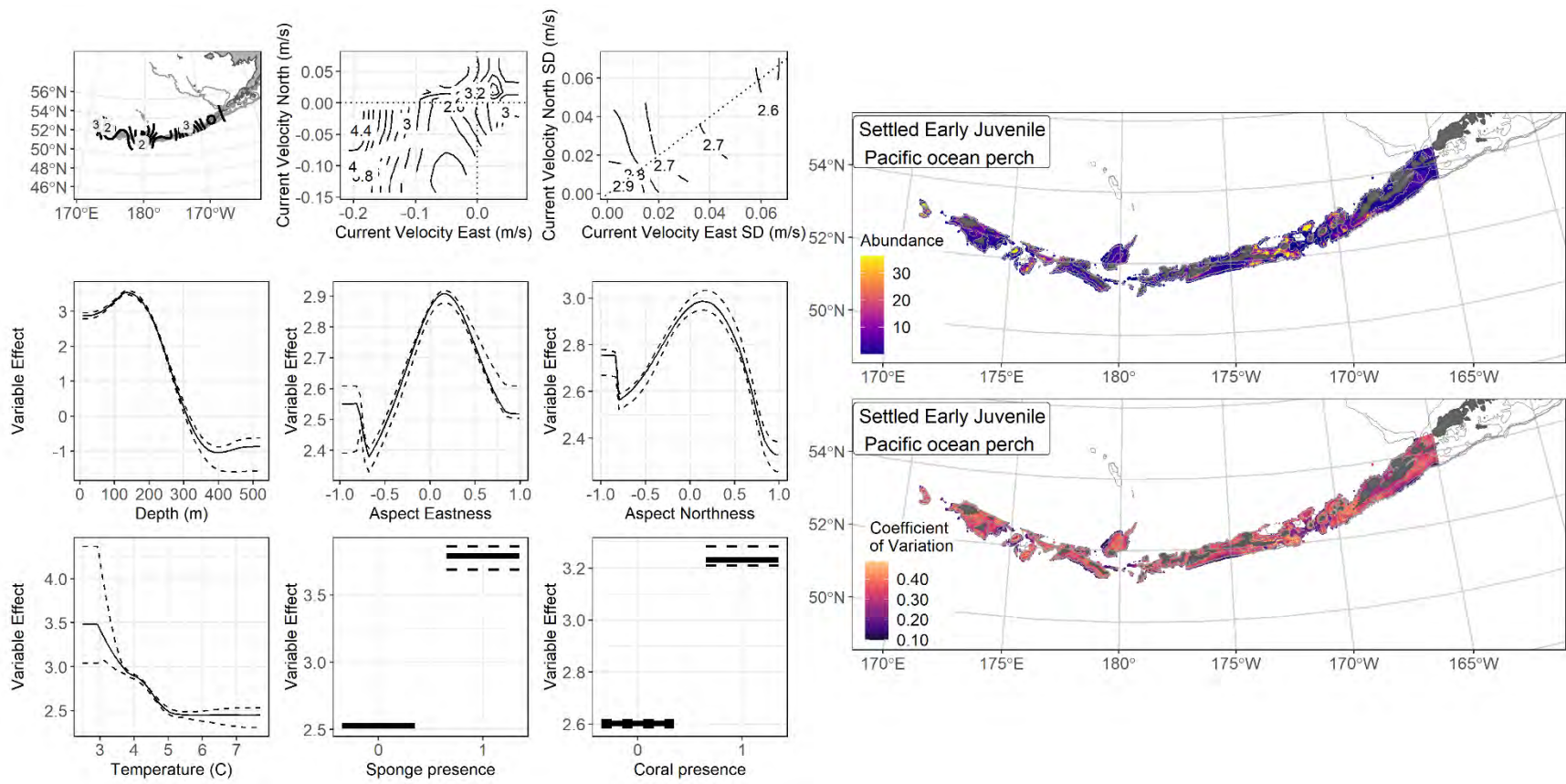
2522

2523 Figure 112. Distribution of settled early juvenile Pacific ocean perch catches (N = 722) in 1991–2019

2524 AFSC RACE-GAP summer bottom trawl surveys of the Aleutian Islands with the 100 m, 300 m, and

2525 500 m isobaths indicated; filled red circles indicate locations in top 10% of overall abundance, open

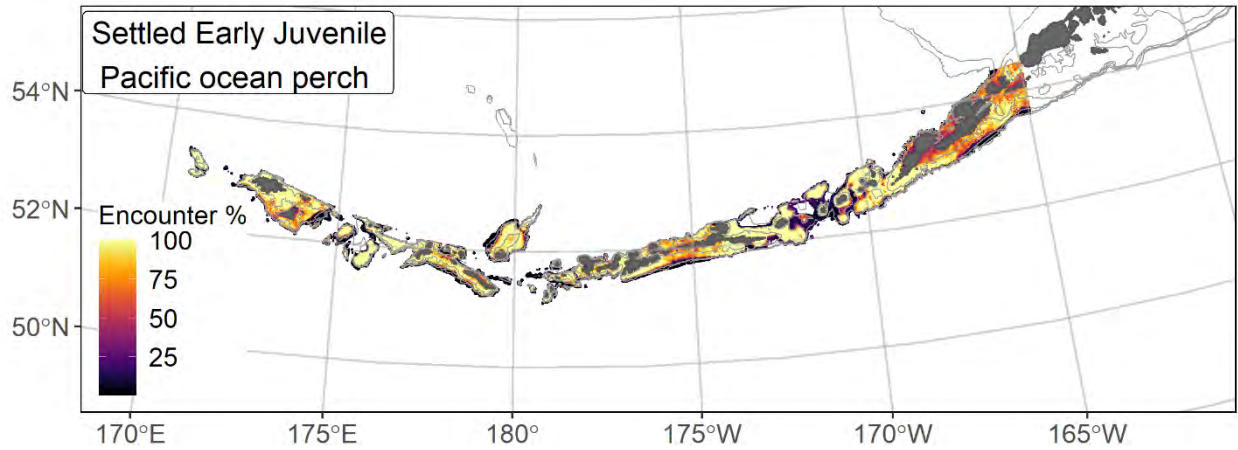
2526 orange circles indicate presence in remaining catches, and small blue dots indicate absence.



2527

2528 Figure 113. The top nine covariate effects (left panel) on ensemble-predicted settled early juvenile Pacific ocean perch numerical abundance

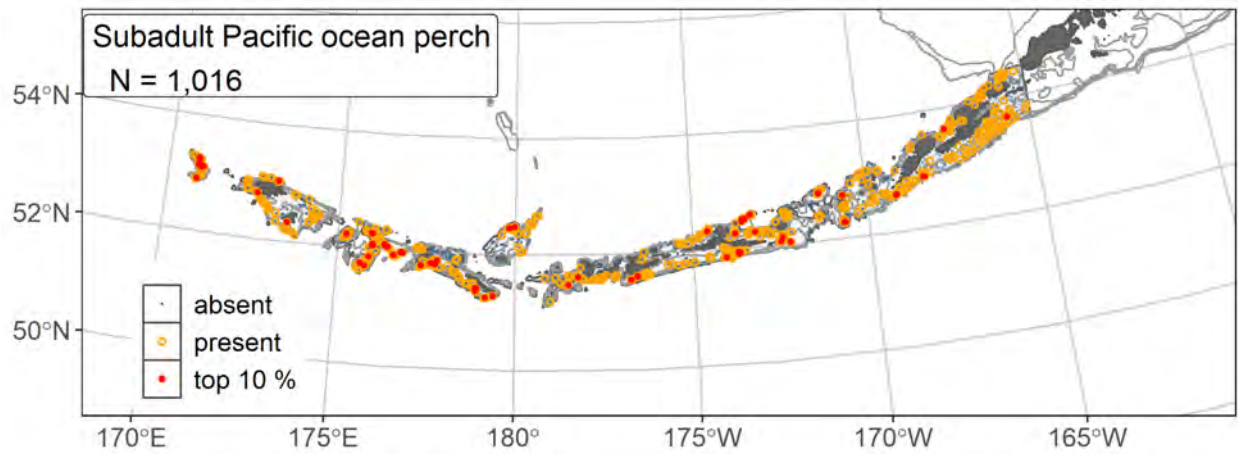
2529 across the Aleutian Islands (upper right panel) alongside the coefficient of variation of the ensemble predictions (lower right panel).



2530

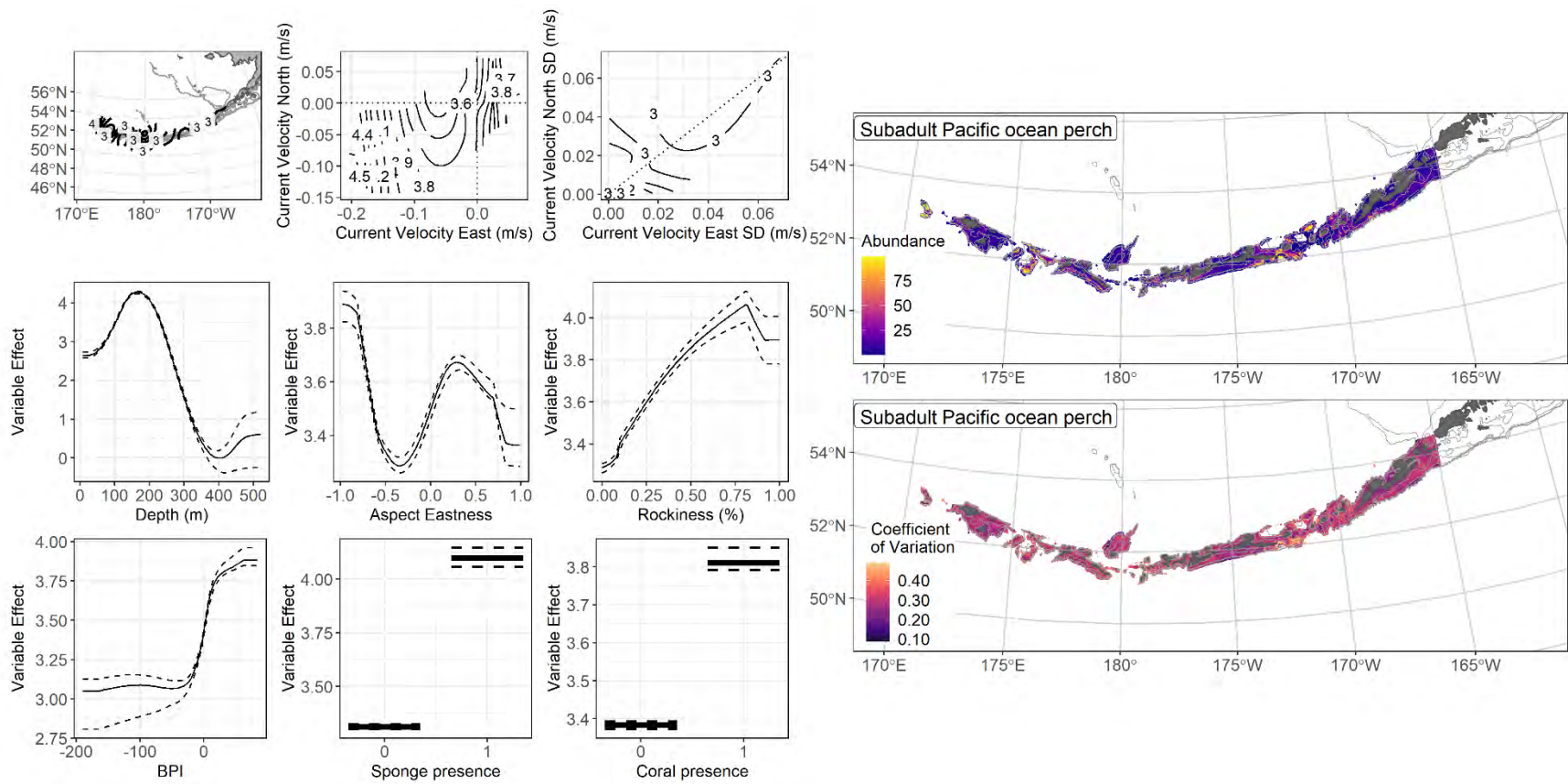
2531 Figure 114. Encounter probability of settled early juvenile Pacific ocean perch from AFSC RACE-GAP
 2532 summer bottom trawl surveys (1991–2019) of the Aleutian Islands with the 100 m, 300 m, and 500 m
 2533 isobaths indicated.

2534



2535

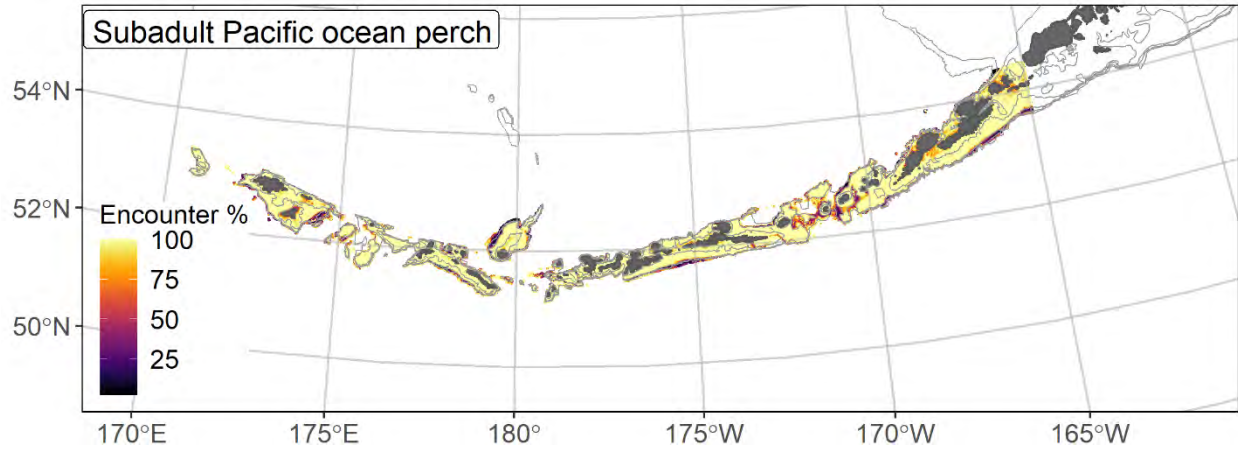
2536 Figure 115. Distribution of subadult Pacific ocean perch catches (N = 1,016) in 1991–2019 AFSC RACE-
 2537 GAP summer bottom trawl surveys of the Aleutian Islands with the 100 m, 300 m, and 500 m isobaths
 2538 indicated; filled red circles indicate locations in top 10% of overall abundance, open orange circles
 2539 indicate presence in remaining catches, and small blue dots indicate absence.



2540

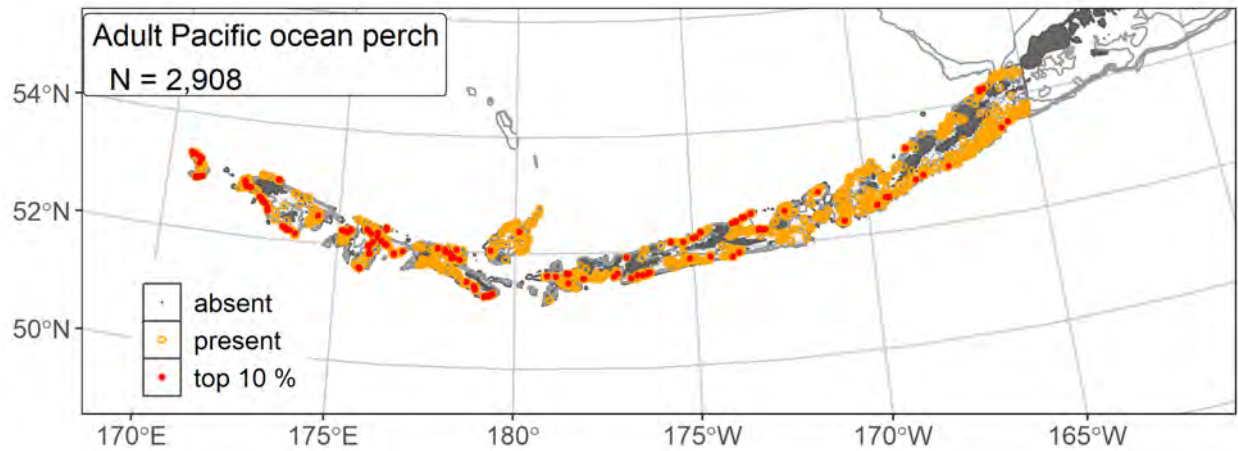
2541 Figure 116. The top nine covariate effects (left panel) on ensemble-predicted subadult Pacific ocean perch numerical abundance across the

2542 Aleutian Islands (upper right panel) alongside the coefficient of variation of the ensemble predictions (lower right panel).

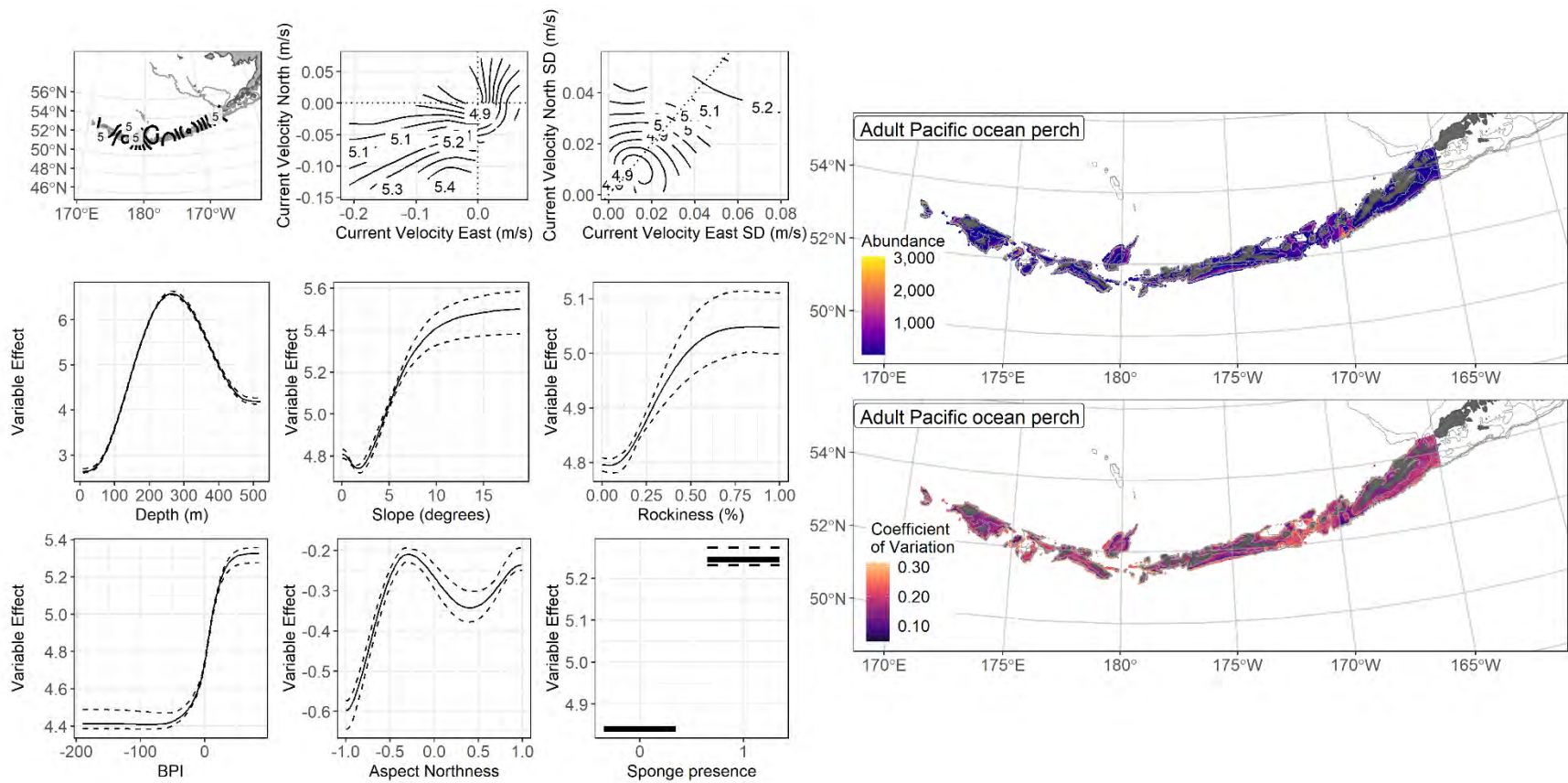


2543
2544 Figure 117. Encounter probability of subadult Pacific ocean perch from AFSC RACE-GAP summer
2545 bottom trawl surveys (1991–2019) of the Aleutian Islands with the 100 m, 300 m, and 500 m isobaths
2546 indicated.

2547



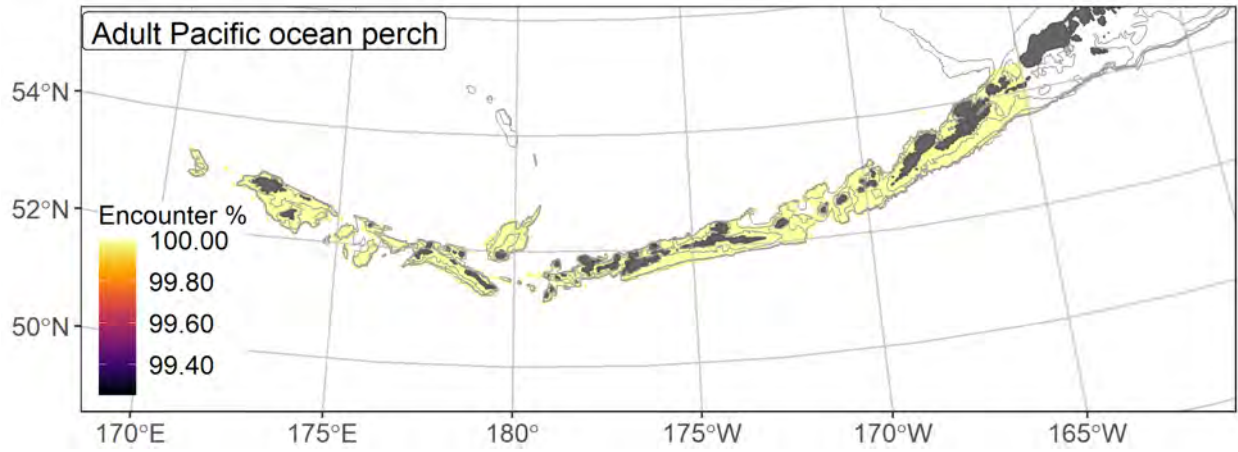
2548
2549 Figure 118. Distribution of adult Pacific ocean perch catches (N = 2,908) in 1991–2019 AFSC RACE-
2550 GAP summer bottom trawl surveys of the Aleutian Islands with the 100 m, 300 m, and 500 m isobaths
2551 indicated; filled red circles indicate locations in top 10% of overall abundance, open orange circles
2552 indicate presence in remaining catches, and small blue dots indicate absence.



2553

2554 Figure 119. The top nine covariate effects (left panel) on ensemble-predicted adult Pacific ocean perch numerical abundance across the Aleutian

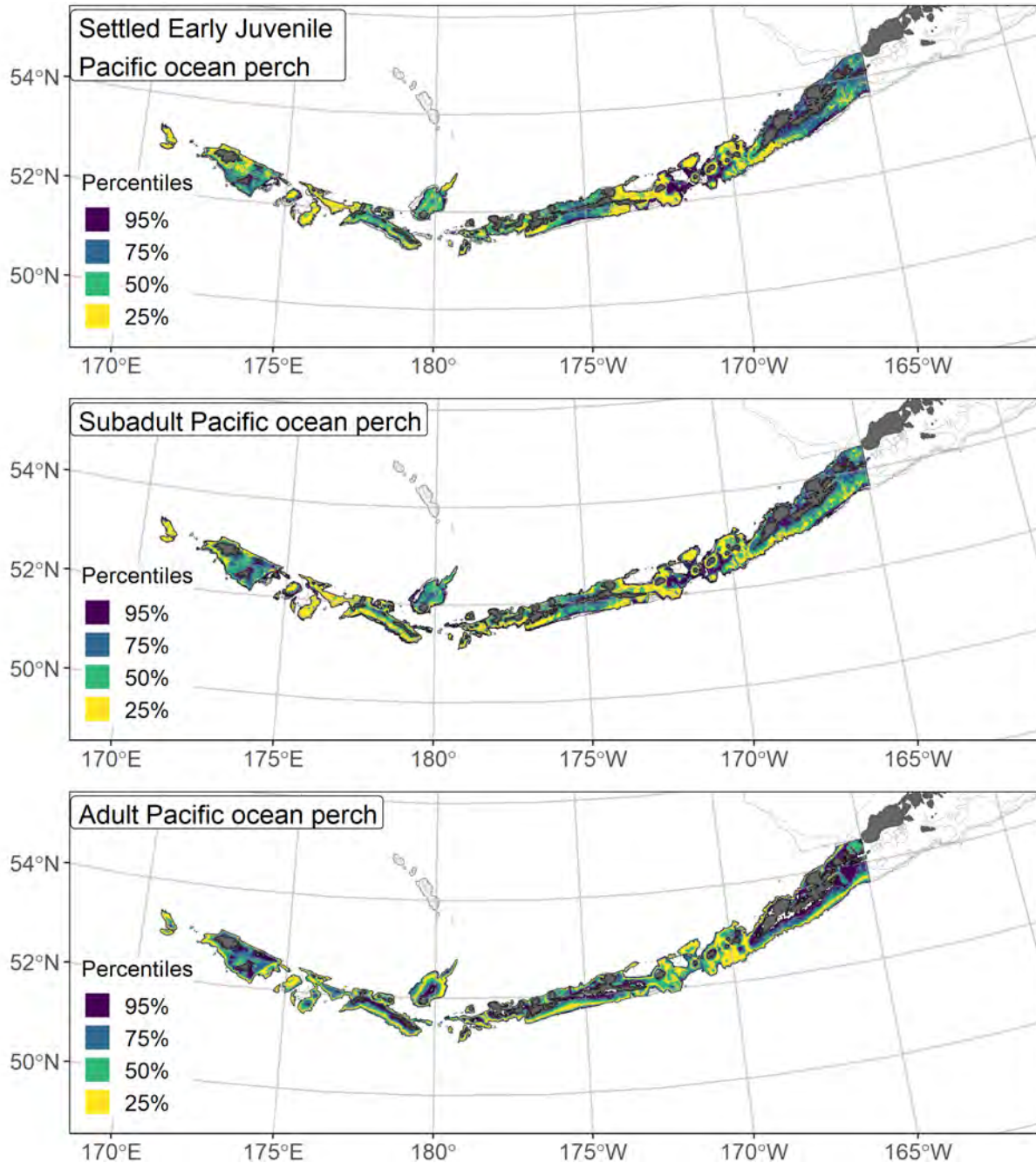
2555 Islands (upper right panel) alongside the coefficient of variation of the ensemble predictions (lower right panel)



2556

2557 Figure 120. Encounter probability of adult Pacific ocean perch from AFSC RACE-GAP summer bottom

2558 trawl surveys (1991–2019) of the Aleutian Islands with the 100 m, 300 m, and 500 m isobaths indicated.



2559
 2560 Figure 121. Essential fish habitat (EFH area) defined as the top 95% of numerical abundance predictions
 2561 from a habitat-based ensemble fitted to settled early juvenile (top), subadult (middle), and adult (bottom)
 2562 Pacific ocean perch distribution and abundance in AFSC RACE-GAP summer bottom trawl surveys
 2563 (1991–2019) with 100 m, 300 m, and 500 m isobaths indicated; internal to the EFH map are the subareas
 2564 of the top 25% (EFH hot spots), top 50% (core EFH area), and top 75% (principal EFH area) of habitat
 2565 related, ensemble-predicted numerical abundance.

2566 **Shortraker rockfish (*Sebastes borealis*)**

2567 Shortraker rockfish (*Sebastes borealis*) range from Japan to California including the Bering Sea
2568 (Mecklenburg et al. 2002). With a maximum size of 1130 mm, this is the largest species of rockfish
2569 encountered in the Alaska trawl surveys, and aging studies suggest they can live up to 157 years, making
2570 them one of the oldest animal species on earth. They are most abundant on the continental slope at depths
2571 between 300 and 500 m (Rooper 2008) though they range from 25 to 1,200 m. Shortraker rockfish
2572 become mature at a length of 499 mm (F.L. Conrath 2017), and like other species in the genus, they show
2573 internal fertilization and egg development leading to the release of live larvae. Shortraker rockfish are
2574 seasonal synchronous spawners with the onset of egg development occurring later in the summer and
2575 parturition taking place from March through May (Conrath 2017). Although not as commercially
2576 important as species like Pacific ocean perch (*S. alutus*), the slow development and late maturity of
2577 shortraker rockfish makes them potentially vulnerable to overfishing and they have received a separate
2578 assessment in the BSAI region since 2004 (Shotwell et al. 2020b).

2579 **Subadult shortraker rockfish distribution and predicted abundance from RACE-GAP summer**
2580 **bottom trawl surveys in the Aleutian Islands–**

2581 Subadult shortraker rockfish were common along many of the continental slope areas covered in
2582 the RACE-GAP summer survey of the Aleutian Islands (Figure 122). All large catches occurred in deep
2583 water around the 300 m depth contour, and were more common on the south side of the island chain. The
2584 final ensemble contains three SDMs with the paGAM given less weight than the others, and it
2585 demonstrated good to excellent accuracy when compared to the observed data (Table 35). In particular,
2586 the ensemble performed excellently at predicting presence/absence (AUC = 0.978) and explained a
2587 majority of the deviance (0.857). The ensemble scored less well according to its Spearman correlation,
2588 which scored in the range considered good ($\rho = 0.471$). The high PDE and AUC scores suggest that the
2589 model is very accurate at predicting bottom trawl catches. Bottom depth was the most important covariate
2590 in the ensemble and accounted for 47.0 % of the deviance explained, though geographic position, current,

2591 and slope were also somewhat important (Table 36). In general, predicted abundance was high in
2592 locations with more than 350 m depth, with weak or south westerly currents, and with a sloping bottom
2593 (Figure 123). Most shortraker rockfish were predicted deeper than 300 m, with the highest abundance
2594 occurring in scattered patches along the 500 m depth contour (Figure 123). The predicted CV of
2595 abundance mirrored the abundance map, with more variation in deep water and zero in shallow areas
2596 where the species almost never occurs (Figure 123). Encounter probabilities for subadults were high in
2597 most places below the 300 m depth contour, and very low in shallower areas (Figure 124).

2598 **Adult shortraker rockfish distribution and predicted abundance from RACE-GAP summer bottom**
2599 **trawl surveys in the Aleutian Islands –**

2600 Adult shortraker rockfish catches from the RACE-GAP summer survey followed the same pattern
2601 as subadults and were restricted to areas deeper than 300 m along the continental slope (Figure 125). The
2602 final ensemble contained three SDMs with equal weight, and demonstrated a good to excellent fit to the
2603 observed data (Table 35). The pattern observed in the adult metrics was similar to that of subadults; the
2604 ensemble scored excellently at predicting presence/absence (AUC = 0.961) and on measures of deviance
2605 explained (PDE = 0.767), and it achieved a good rating in terms of Spearman correlation ($\rho = 0.482$).
2606 Overall, this suggested that the ensemble predictions are accurate both in predicting which catches will
2607 contain shortraker rockfish and roughly how many will be caught. Like subadults, bottom depth,
2608 geographic position, bottom currents, and slope were the most important covariates (Table 36). Similar to
2609 subadults, the ensemble predicted that adult abundance will be high in locations with deeper water,
2610 southwesterly currents, and a sloped bottom (Figure 126). The predicted abundance map showed that
2611 adults mostly occupy habitats below the 300 m depth contour, with the highest densities found even
2612 deeper, particularly around Amchitka Pass (Figure 126). The predicted CV of abundance was highest just
2613 above the 300 m depth contour where this life stage is sometimes absent (Figure 126). Similar to the
2614 abundance map, the map of encounter probability showed a fairly high chance of catching shortraker
2615 rockfish below 300 m, and a very low chance above that (Figure 127).

2616 **Essential fish habitat of subadult and adult shortraker rockfish in the Aleutian Islands –**

2617 The habitat related abundance predictions based on RACE-GAP summer bottom trawl data
2618 (1991–2019) were translated into EFH area and subareas (Figure 128). Both life stages displayed the
2619 same pattern in their abundance and EFH, and it is difficult to point to any differences between the two.
2620 The EFH encompassed most of the area between the 300 m and 500 m depth contours, with intermittent
2621 hot spots along the continental slope south of the AI and around the deeper passes between the islands.
2622 Given its depth preferences and other observations of this species, it seems likely that much of its
2623 essential habitat exists in depth strata beyond what is covered in the bottom trawl survey. While this
2624 project has produced high quality models for both life stages, additional sources of data such as longline
2625 surveys could help extend these findings for of shortraker rockfish¹⁶.

¹⁶ A recommendation to add additional survey data types if possible to future SDM ensemble EFH mapping efforts for this species will be included as a future recommendation for research directions from the 2022 EFH 5-year Review.

2626 Table 35. Constituent species distribution models (SDMs) used to construct Essential Fish Habitat (EFH)
 2627 for a) subadult and b) adult shortraker rockfish: MaxEnt = Maximum entropy; paGAM = presence-
 2628 absence generalized additive model; hGAM = hurdle GAM; GAM_P = standard Poisson GAM; and
 2629 GAM_{nb} = standard negative-binomial GAM. Ensemble performance (ρ = Spearman's rank correlation
 2630 coefficient), root-mean-square-error (RMSE), the area under the receiver operating characteristic (AUC),
 2631 and the Poisson deviance explained (PDE) were generated from k-fold cross-validation. The "--" in a field
 2632 indicates that this SDM was not included in the final ensemble.

2633 **a) subadult shortraker rockfish**

Models	RMSE	Relative Weight	ρ	AUC	PDE	EFH area (km²)
MaxEnt	--	0	--	--	--	--
paGAM	14.2	0.267	0.452	0.981	0.733	25,900
hGAM	11.8	0.387	0.513	0.981	0.868	21,400
GAM _P	12.5	0.345	0.509	0.965	0.857	21,000
GAM _{nb}	15.8	0	--	--	--	--
ensemble	8.7	1	0.471	0.978	0.857	23,100

2634 **b) adult shortraker rockfish**

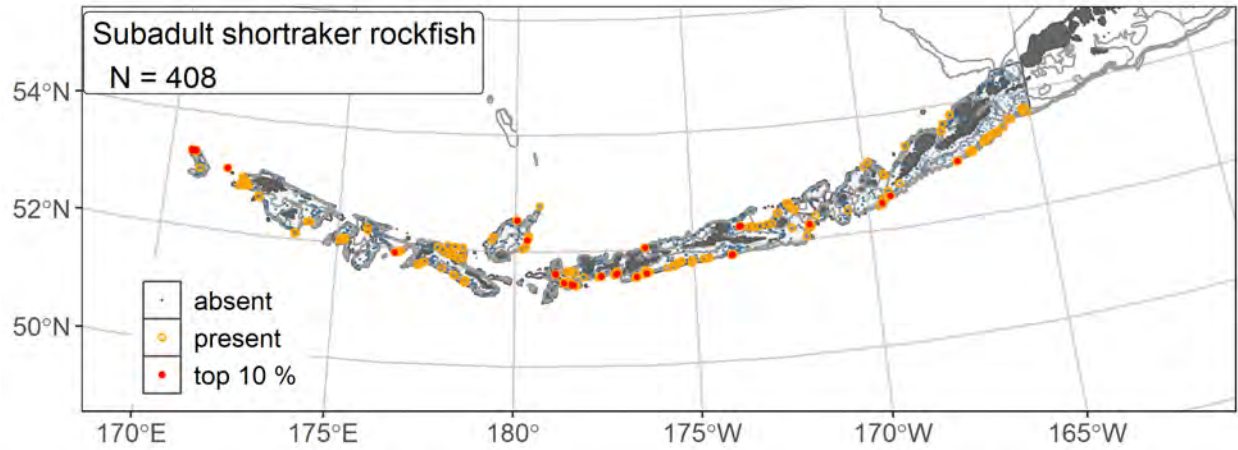
Models	RMSE	Relative Weight	ρ	AUC	PDE	EFH area (km²)
MaxEnt	--	--	--	--	--	--
paGAM	9.56	0.263	0.482	0.967	0.583	29,300
hGAM	8.12	0.365	0.485	0.966	0.767	25,600
GAM _P	8.05	0.372	0.491	0.951	0.766	25,300
GAM _{nb}	9.58	0	--	--	--	--
ensemble	5.85	1	0.482	0.961	0.767	27,000

2635

2636 Table 36. Covariates retained in the a) subadult and b) adult shortraker rockfish species distribution model
 2637 (SDM) final ensembles, the percent contribution to the ensemble deviance explained by each, and the
 2638 cumulative percent deviance: SD = standard deviation, and BPI = bathymetric position index.

Shortraker rockfish	Covariate	% Contribution	Cumulative % Contribution
a) subadult	bottom depth	47.0	47.0
	position	21.3	68.3
	current	9.0	77.3
	current SD	7.6	84.9
	slope	4.9	89.8
	rockiness	3.0	92.8
	aspect east	1.5	94.3
	aspect north	1.3	95.6
	tidal maximum	1.3	96.9
	BPI	1.0	97.9
	curvature	0.9	98.8
	bottom temperature	0.4	99.2
	coral presence	0.3	99.5
	sponge presence	0.3	99.8
	pennatulacean presence	0.2	100
b) adult	bottom depth	36.9	36.9
	position	22.5	59.3
	current SD	9.1	68.4
	current	7.1	75.5
	slope	5.6	81.1
	aspect east	4.8	85.9
	BPI	3.4	89.3
	aspect north	2.6	91.9
	tidal maximum	2.4	94.3
	rockiness	2.4	96.7
	bottom temperature	1.1	97.8
	sponge presence	1.1	98.9
	curvature	0.7	99.6
	coral presence	0.3	99.9
	pennatulacean presence	0.1	100

2639



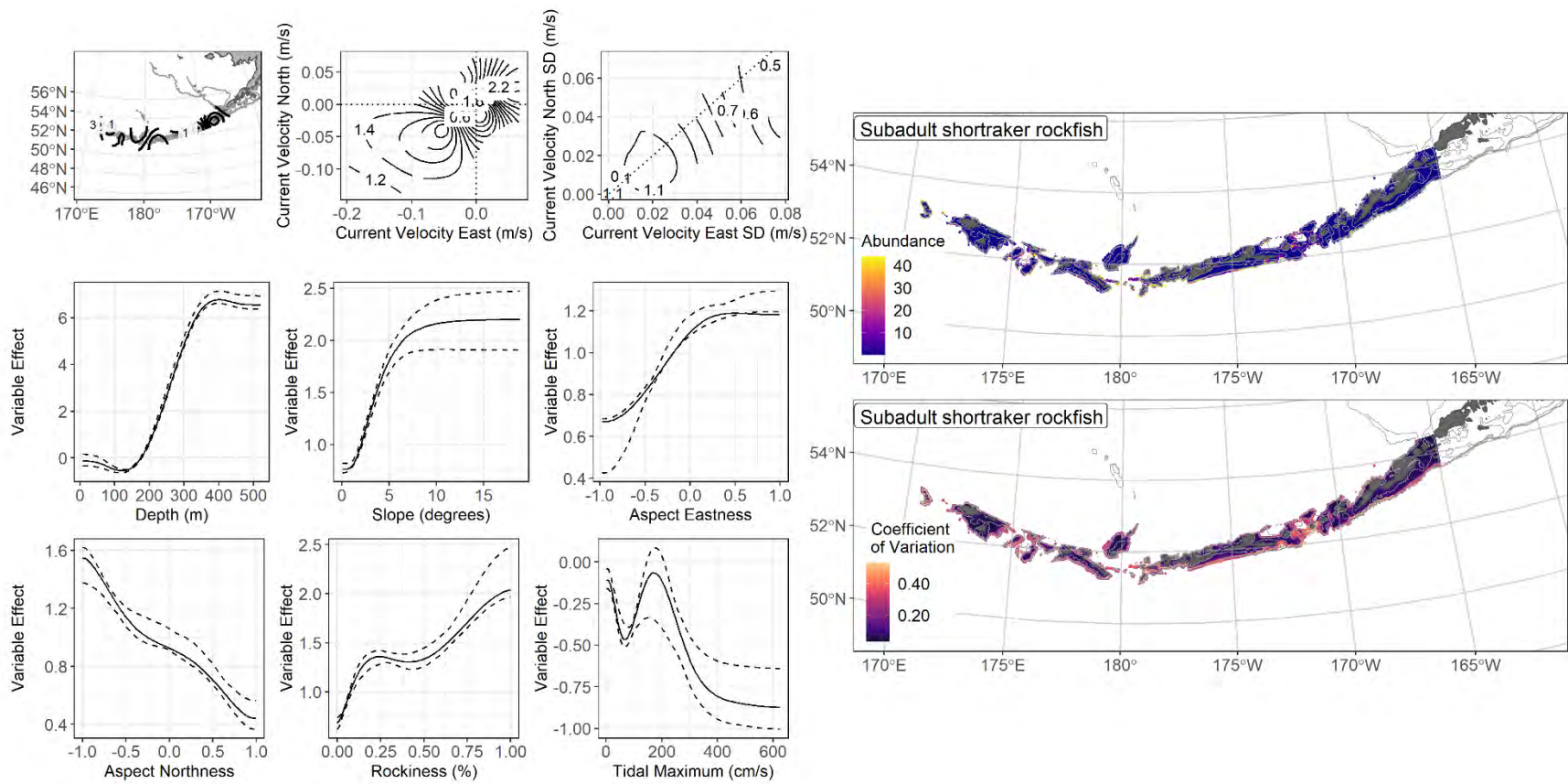
2640

2641 Figure 122. Distribution of subadult shorttraker rockfish catches (N = 408) in 1991–2019 AFSC RACE-

2642 GAP summer bottom trawl surveys of the Aleutian Islands with the 100 m, 300 m, and 500 m isobaths

2643 indicated; filled red circles indicate locations in top 10% of overall abundance, open orange circles

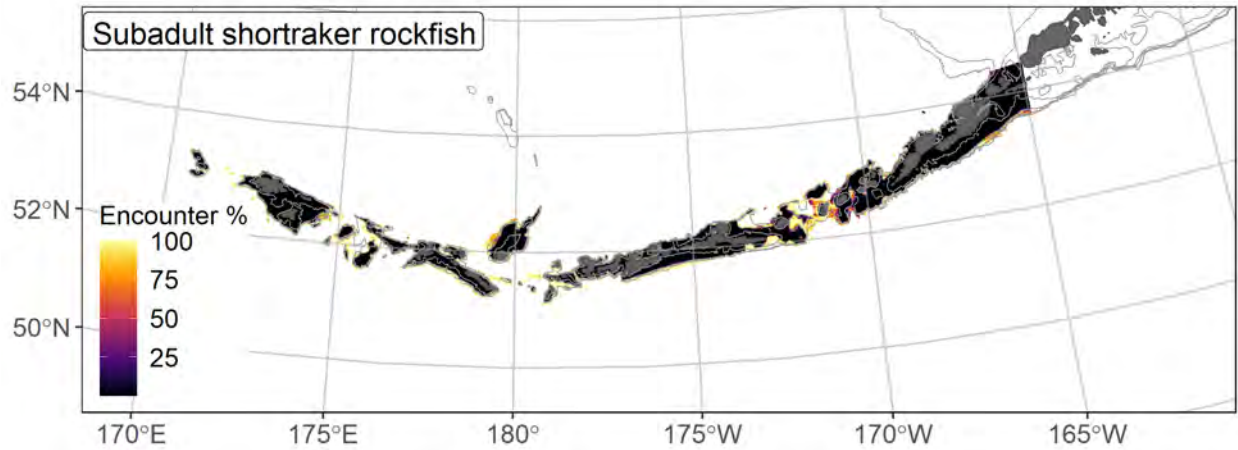
2644 indicate presence in remaining catches, and small blue dots indicate absence.



2645

2646 Figure 123. The top nine covariate effects (left panel) on ensemble-predicted subadult shorttraker rockfish numerical abundance across the Aleutian

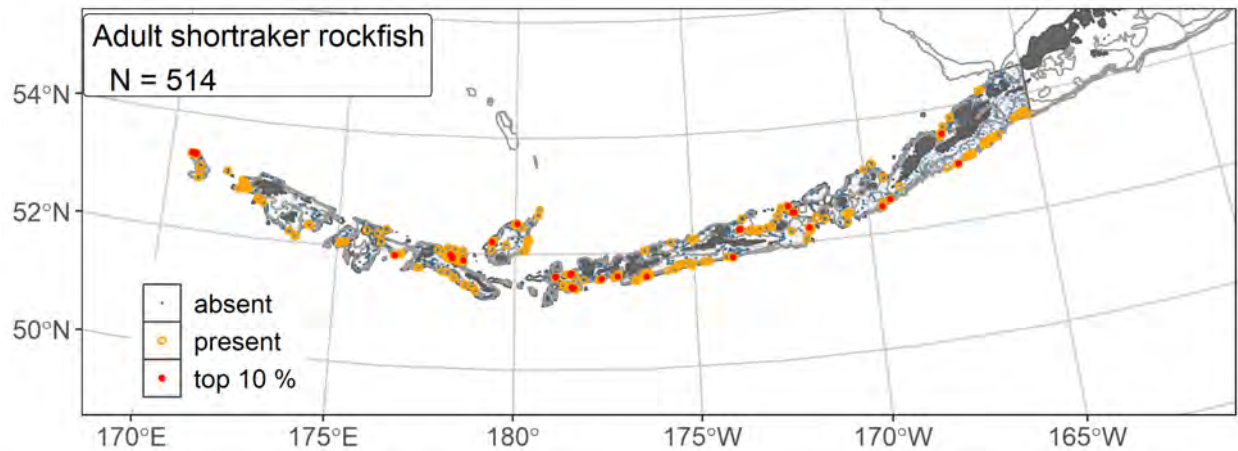
2647 Islands (upper right panel) alongside the coefficient of variation of the ensemble predictions (lower right panel).



2648

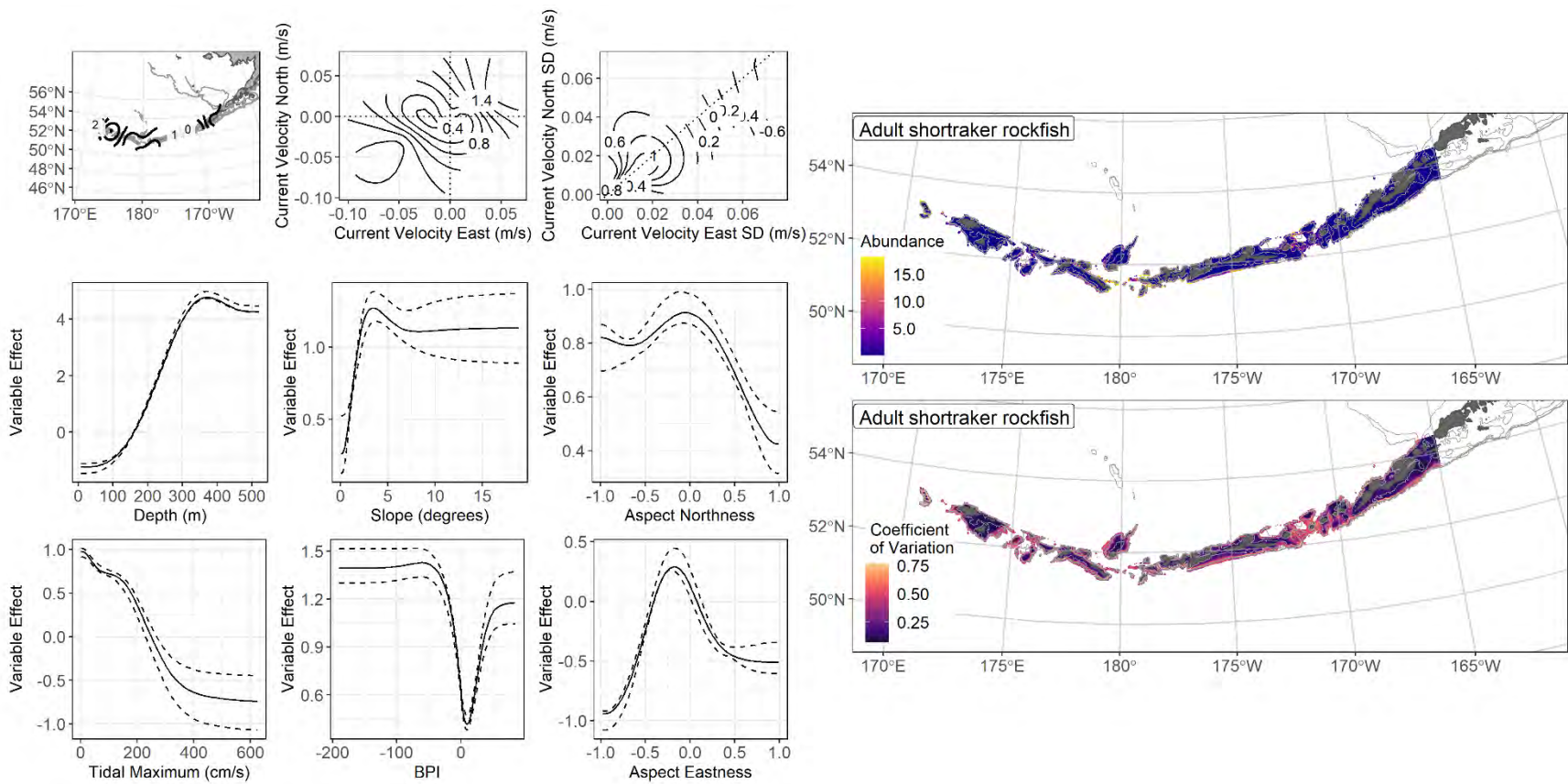
2649 Figure 124. Encounter probability of subadult shorttraker rockfish from AFSC RACE-GAP summer
 2650 bottom trawl surveys (1991–2019) of the Aleutian Islands with the 100 m, 300 m, and 500 m isobaths
 2651 indicated.

2652



2653

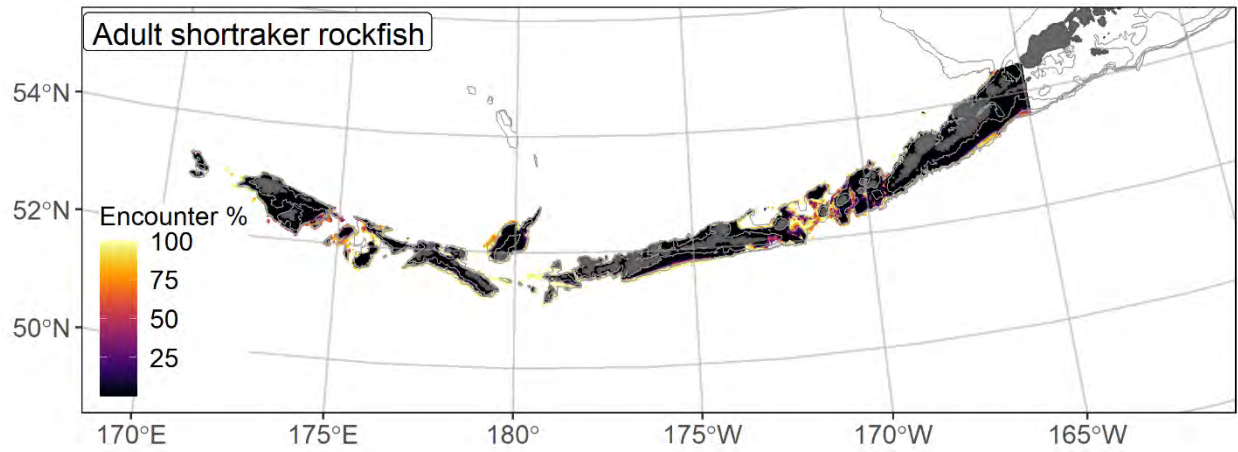
2654 Figure 125. Distribution of adult shorttraker rockfish catches (N = 514) in 1991–2019 AFSC RACE-GAP
 2655 summer bottom trawl surveys of the Aleutian Islands with the 100 m, 300 m, and 500 m isobaths
 2656 indicated; filled red circles indicate locations in top 10% of overall abundance, open orange circles
 2657 indicate presence in remaining catches, and small blue dots indicate absence.



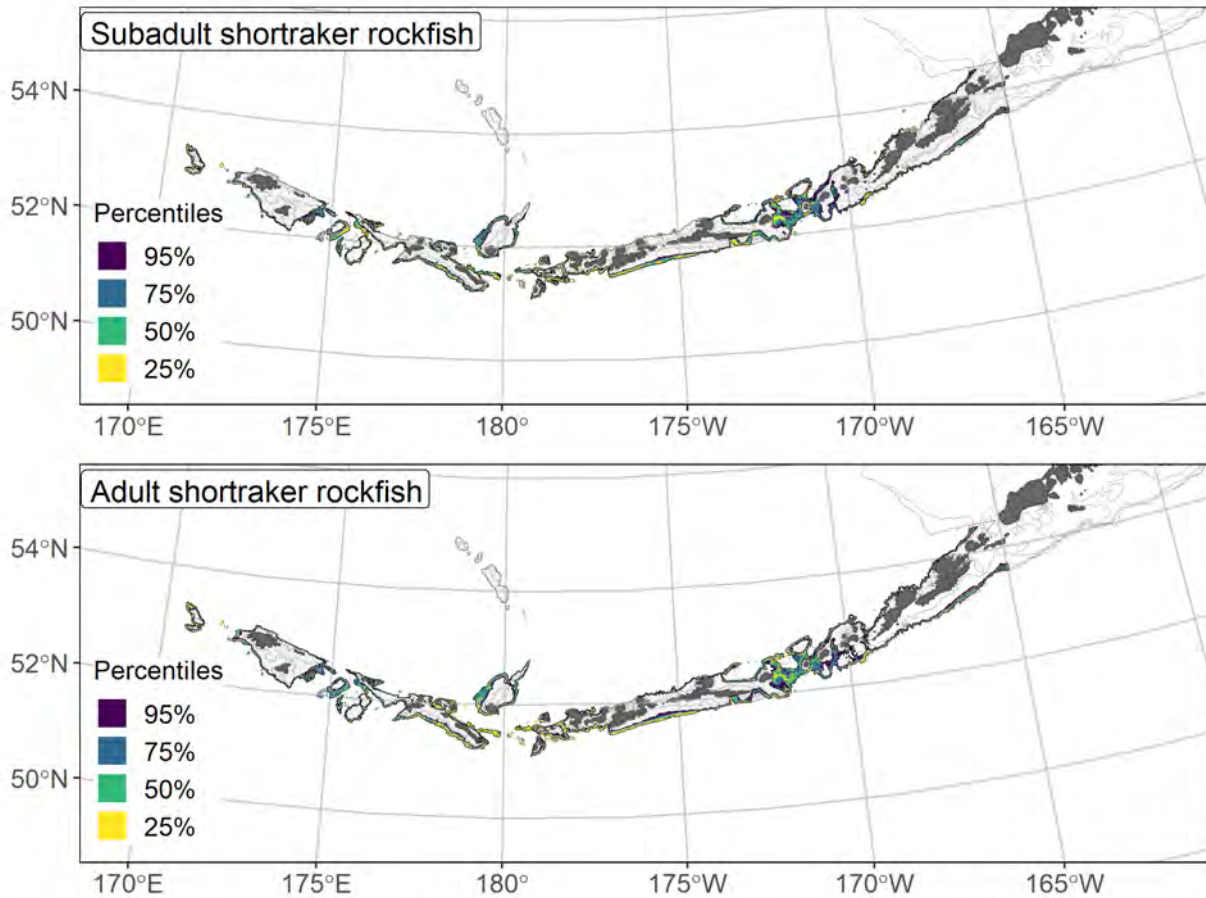
2658

2659 Figure 126. The top nine covariate effects (left panel) on ensemble-predicted adult shorttraker rockfish numerical abundance across the Aleutian

2660 Islands (upper right panel) alongside the coefficient of variation of the ensemble predictions (lower right panel).



2661
 2662 Figure 127. Encounter probability of adult shorttraker rockfish from AFSC RACE-GAP summer bottom
 2663 trawl surveys (1991–2019) of the Aleutian Islands with the 100 m, 300 m, and 500 m isobaths indicated.



2664

2665 Figure 128. Essential fish habitat (EFH area) defined as the top 95% of numerical abundance predictions
 2666 from a habitat-based ensemble fitted to subadult (top) and adult (bottom) shorttraker rockfish distribution
 2667 and abundance in AFSC RACE-GAP summer bottom trawl surveys (1991–2019) with 100 m, 300 m, and
 2668 500 m isobaths indicated; internal to the EFH map are the subareas of the top 25% (EFH hot spots), top
 2669 50% (core EFH area), and top 75% (principal EFH area) of habitat related, ensemble-predicted numerical
 2670 abundance.

2671 **Complex: Rougheye/Blackspotted rockfish (*Sebastes aleutianus*/*Sebastes melanostictus*)**

2672 Rougheye rockfish (*Sebastes aleutianus*) and blackspotted rockfish (*S. melanostictus*) are
2673 distributed along the outer continental shelf and upper continental slope of the northeastern Pacific and
2674 across the North Pacific from Japan to Point Conception, California and including the Bering Sea
2675 (Kramer and O’Connell 1988). They are some of the largest rockfish species and both reach maximum
2676 lengths over 700 mm. The two species co-occur throughout their range and overlap extensively
2677 (Gharrett et al. 2005) though blackspotted rockfish extend farther into the western Aleutian Islands and
2678 towards Russia and Japan (Orr and Hawkins 2008). Blackspotted rockfish also tend to occupy deeper
2679 water than rougheye rockfish, but they frequently co-occur between 300–500 m along the upper
2680 continental slope in the Gulf of Alaska (Ito 1999). While the two species reach maturity at approximately
2681 the same length (blackspotted $L_{50} = 453$ mm, rougheye $L_{50} = 450$ mm), rougheye rockfish exhibit faster
2682 growth and reach this length at a younger age (Conrath 2017). Due to high field misidentification rates,
2683 these two species are presently managed as a complex in the BSAI and GOA regions (Spencer et al.
2684 2020), and this project models them with a single ensemble.

2685 **Subadult rougheye/blackspotted rockfish distribution and predicted abundance from RACE-GAP**
2686 **summer bottom trawl surveys in the Aleutian Islands–**

2687 Subadult rougheye/blackspotted rockfish were common in many areas covered in the RACE-
2688 GAP summer survey of the Aleutian Islands, with most catches occurring at depths greater than 300 m
2689 (Figure 129). The final ensemble contained three SDMs with approximately equal weights, and it
2690 performed well with respect to the observed data (Table 37). All three fit metrics scored in the range that
2691 is considered “good” ($\rho = 0.535$; AUC = 0.882; PDE = 0.504), indicating that this ensemble is reliable
2692 and makes accurate predictions. Bottom depth, geographic position, current, and current variability were
2693 the most important covariates and accounted for 75.6% of the deviance explained by the ensemble
2694 (Table 38). In general, predicted abundance was high in locations around 300 m depth, with weak but
2695 variable currents (Figure 130). The abundance map predicted that most rougheye and blackspotted

2696 rockfishes will be found along the edge of the continental slope, between the 300 m and 500 m depth
2697 contours (Figure 130). The highest abundance occurred in scattered patches that are near the passes
2698 through the island chain. The predicted CV of abundance mirrored the abundance map, with more
2699 variation in deep water and zero in shallow areas where the species almost never occurred (Figure 130).
2700 Encounter probabilities for subadults were high in most places below the 300 m depth contour,
2701 particularly on the south side of the AI and in the passes, and were very low in shallower areas
2702 (Figure 131).

2703 **Adult rougheye/blackspotted rockfish distribution and predicted abundance from RACE-GAP**
2704 **summer bottom trawl surveys in the Aleutian Islands –**

2705 Adult rougheye/blackspotted rockfish catches from the RACE-GAP summer survey followed the
2706 same pattern as subadults and were most common at around 300 m depth along the continental slope
2707 (Figure 132). Large catches were scattered across the AI, but a notable cluster occurred north of the Rat
2708 Islands. The final ensemble contained three SDMs with equal weights and it demonstrated a good to
2709 excellent fit to the observed data (Table 37). Specifically, it scored excellently in terms of predicting
2710 presence (AUC = 0.934) and deviance explained (PDE = 0.787), and performed well at predicting relative
2711 abundance ($\rho = 0.516$). Overall, this suggests that these predictions are accurate and accounted for a
2712 majority of the variation in observed catches. Bottom depth, geographic position, current variability, and
2713 bottom temperature were the most important covariates and accounted for 75.2% of the deviance
2714 explained by the ensemble (Table 38). Similar to subadults, the ensemble predicted an ideal bottom depth
2715 of around 300 m, but the confidence interval is much wider in adults, which suggested a more uncertain
2716 relationship with depth (Figure 133). Also, adults are associated with colder water, while bottom
2717 temperature was not an important predictor of subadult abundance. The predicted abundance map showed
2718 that rougheye/blackspotted rockfishes occupied habitats below the 300 m depth contour, with the highest
2719 densities found around Seguam Pass and the Rat Islands (Figure 133). The predicted CV of abundance
2720 was similar to the map of abundance, demonstrating that most of the variation in catch is confined to

2721 those slope areas where this species was common (Figure 133). The map of encounter probability showed
2722 a high chance of catching these species below 300 m and around the various passes that cut through the
2723 archipelago (Figure 134).

2724 **Essential fish habitat of subadult and adult rougheye/blackspotted rockfish in the Aleutian Islands**

2725 –

2726 The habitat related abundance predictions based on RACE-GAP summer bottom trawl data
2727 (1991–2019) were translated into EFH area and subareas (Figure 135). The subadult EFH map
2728 encompassed nearly twice the overall area of the adult map, primarily because the subadult EFH included
2729 shallower water. While EFH hot spots for subadults all occurred in water from about 250-500 m deep, the
2730 EFH area extended into some shallower areas in the eastern AI. By contrast, the EFH for adults was
2731 strictly confined to deeper water and did not extend shallower than 300 m. This pattern would be
2732 consistent with many other species in this region that tend to migrate towards deeper habitats as they
2733 grow larger. It seems likely that much of the EFH for adults and possibly subadults is below 500 m, and
2734 additional data from other sources such as the long-line survey may help extend these findings¹⁷.

¹⁷ A recommendation to add additional survey data types if possible to future SDM ensemble EFH mapping efforts for this species will be included as a future recommendation for research directions from the 2022 EFH 5-year Review.

2735 Table 37. Constituent species distribution models (SDMs) used to construct Essential Fish Habitat (EFH)
 2736 for a) subadult and b) adult rougheye/blackspotted rockfish: MaxEnt = Maximum entropy;
 2737 paGAM = presence-absence generalized additive model; hGAM = hurdle GAM; GAM_P = standard
 2738 Poisson GAM; and GAM_{nb} = standard negative-binomial GAM. Ensemble performance (ρ = Spearman's
 2739 rank correlation coefficient), root-mean-square-error (RMSE), the area under the receiver operating
 2740 characteristic (AUC), and the Poisson deviance explained (PDE) were generated from k-fold cross-
 2741 validation. The "--" in a field indicates that this SDM was not included in the final ensemble.

2742 **a) subadult rougheye/blackspotted rockfish**

Models	RMSE	Relative Weight	ρ	AUC	PDE	EFH area (km ²)
MaxEnt	--	0	--	--	--	--
paGAM	11.6	0.328	0.549	0.895	0.417	71,600
hGAM	11.5	0.330	0.507	0.894	0.505	62,400
GAM _P	11.3	0.342	0.515	0.859	0.515	21,300
GAM _{nb}	12.1	0	--	--	--	--
ensemble	11.0	1	0.535	0.882	0.504	67,200

2743 **b) adult rougheye/blackspotted rockfish**

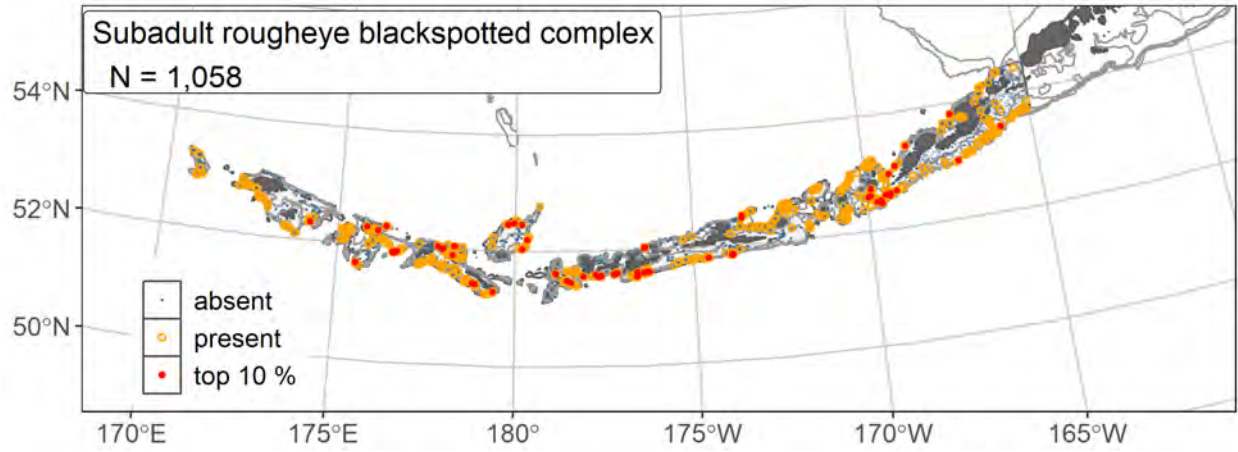
Models	RMSE	Relative Weight	ρ	AUC	PDE	EFH area (km ²)
MaxEnt	--	--	--	--	--	--
paGAM	26.9	0.302	0.517	0.936	0.426	57,500
hGAM	25.3	0.342	0.518	0.935	0.782	29,100
GAM _P	24.8	0.356	0.511	0.911	0.786	25,800
GAM _{nb}	26.0	0	--	--	--	--
ensemble	18.4	1	0.516	0.934	0.787	35,800

2744

2745 Table 38. Covariates retained in the a) subadult and b) adult roughey/blackspotted rockfish species
 2746 distribution model (SDM) final ensembles, the percent contribution to the ensemble deviance explained
 2747 by each, and the cumulative percent deviance: SD = standard deviation, and BPI = bathymetric position
 2748 index.

roughey/ blackspotted rockfish	Covariate	% Contribution	Cumulative % Contribution
a) subadult	bottom depth	41.2	41.2
	position	15.8	57.0
	current	9.5	66.5
	current SD	9.1	75.6
	aspect east	4.4	80.0
	aspect north	4.1	84.1
	slope	3.5	87.6
	rockiness	2.6	90.2
	BPI	2.6	92.8
	tidal maximum	2.3	95.1
	curvature	1.8	96.9
	coral presence	1.4	98.3
	sponge presence	0.9	99.2
	bottom temperature	0.8	100
	pennatulacean presence	0	100
b) adult	bottom depth	44.3	44.3
	position	13.4	57.6
	current SD	12.1	69.7
	bottom temperature	5.5	75.2
	current	5.0	80.2
	BPI	3.5	83.7
	aspect east	3.4	87.1
	slope	3.3	90.4
	aspect north	2.5	92.9
	curvature	2.5	95.4
	rockiness	2.2	97.6
	sponge presence	1.1	98.7
	tidal maximum	0.8	99.5
	coral presence	0.4	99.9
	pennatulacean presence	0.1	100

2749



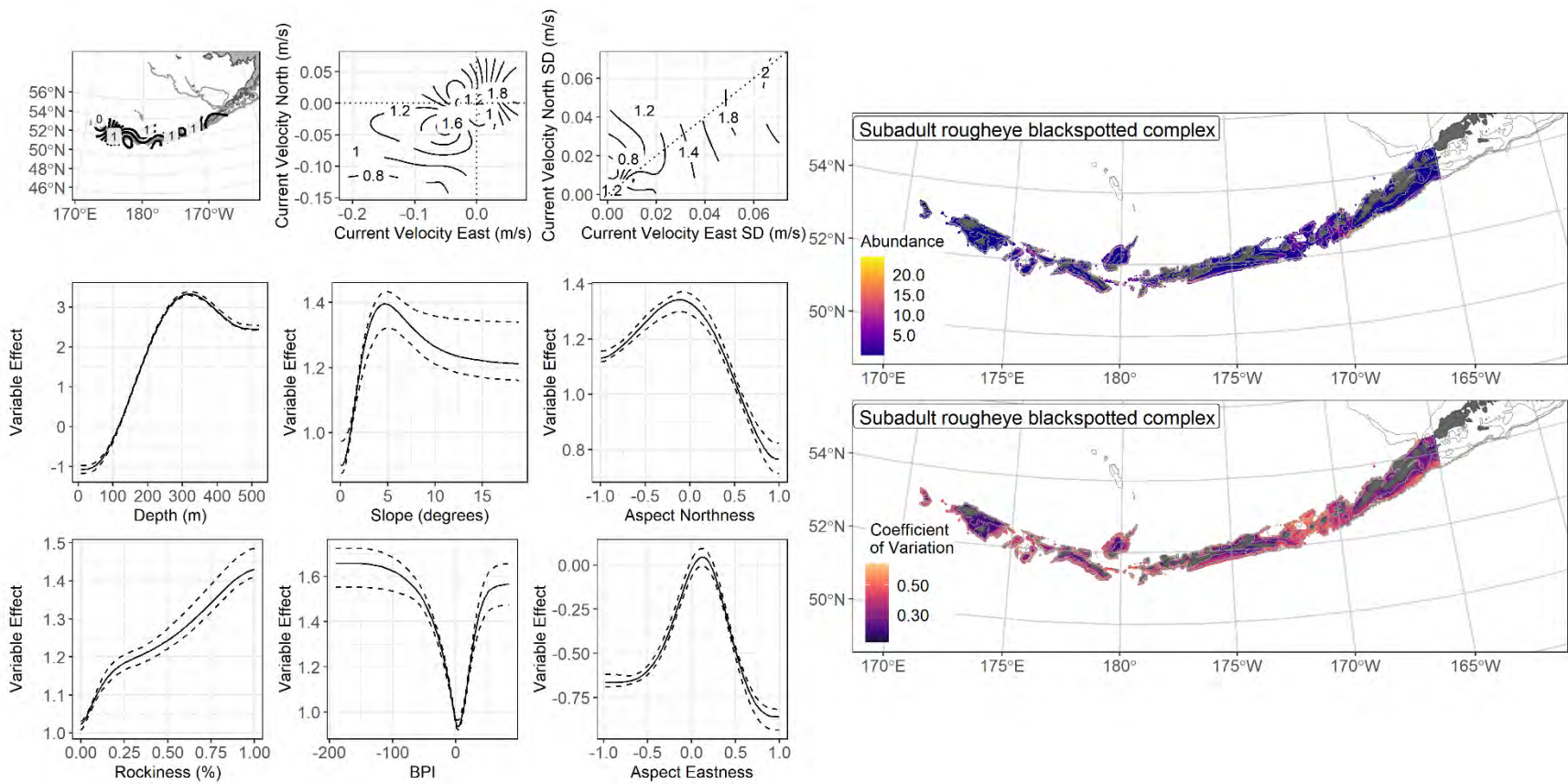
2750

2751 Figure 129. Distribution of subadult roughey/blackspotted rockfish catches (N = 1,058) in 1991–2019

2752 AFSC RACE-GAP summer bottom trawl surveys of the Aleutian Islands with the 100 m, 300 m, and

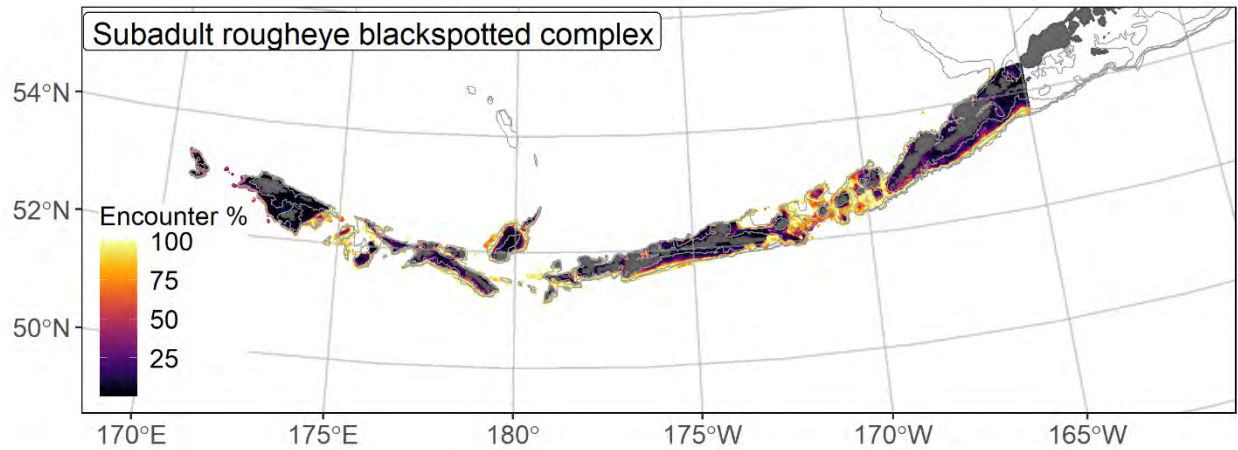
2753 500 m isobaths indicated; filled red circles indicate locations in top 10% of overall abundance, open

2754 orange circles indicate presence in remaining catches, and small blue dots indicate absence.



2755

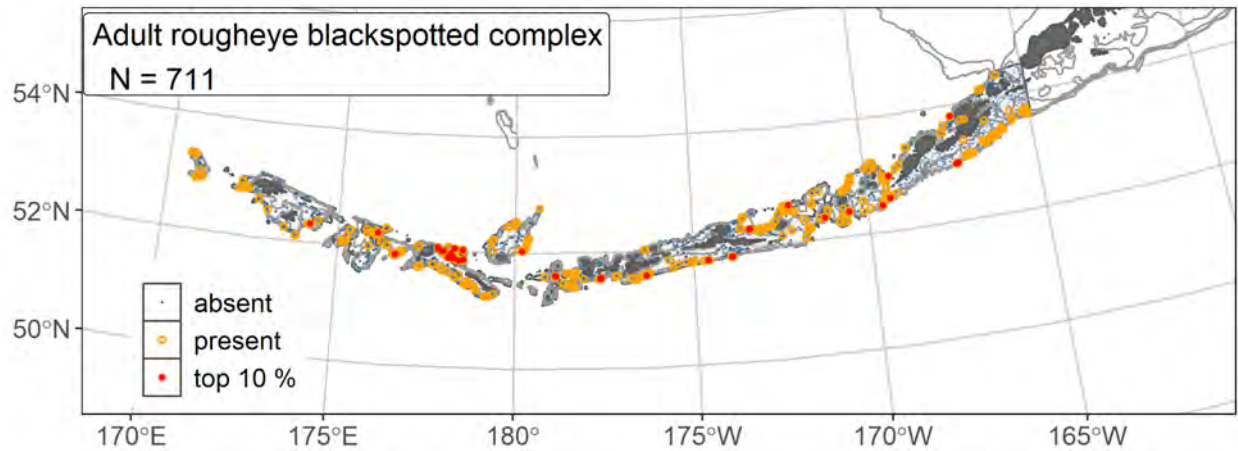
2756 Figure 130. The top nine covariate effects (left panel) on ensemble-predicted subadult roughey/blackspotted rockfish numerical abundance across
 2757 the Aleutian Islands (upper right panel) alongside the coefficient of variation of the ensemble predictions (lower right panel).



2758

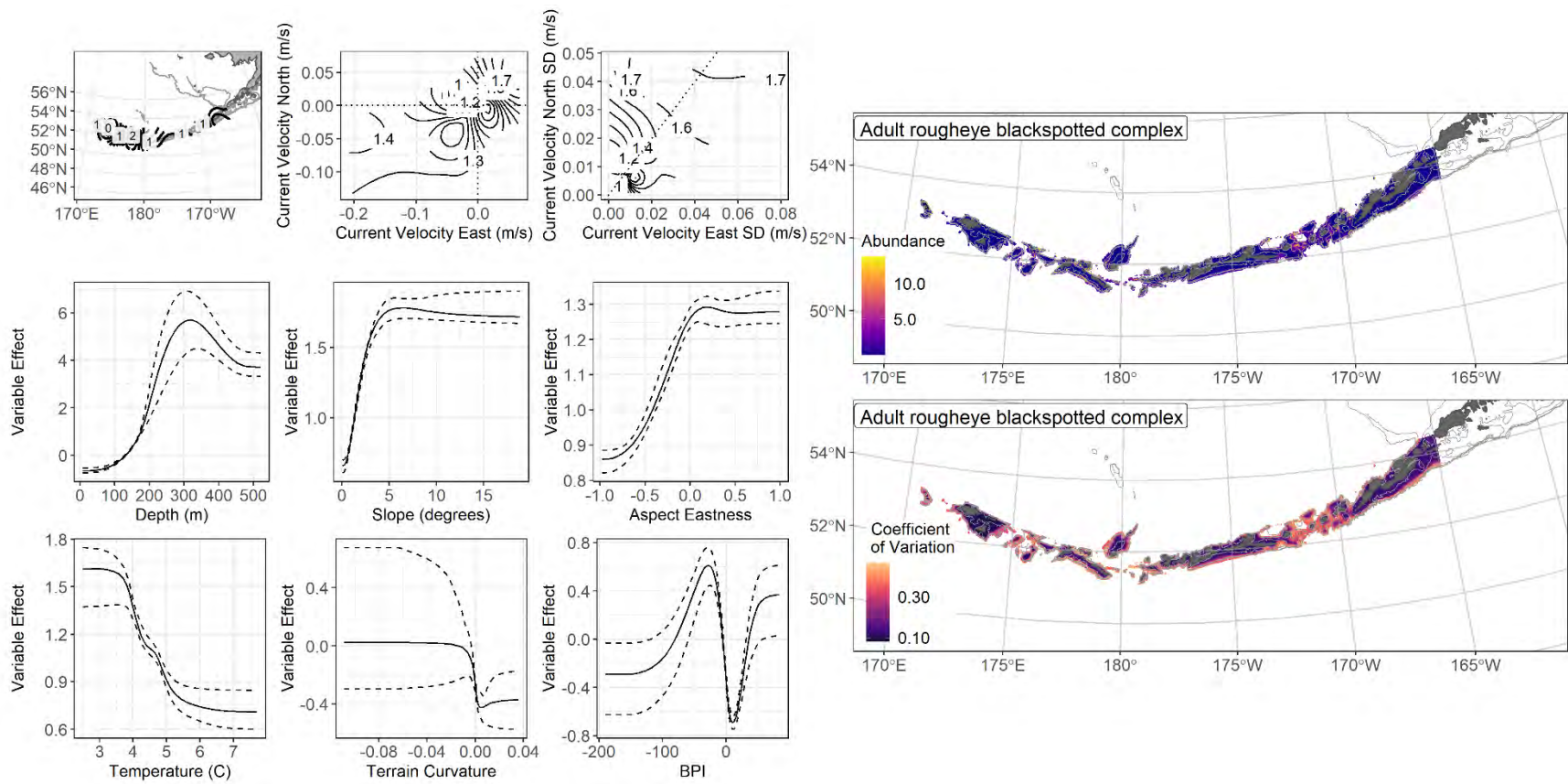
2759 Figure 131. Encounter probability of subadult roughey/blackspotted rockfish from AFSC RACE-GAP
 2760 summer bottom trawl surveys (1991–2019) of the Aleutian Islands with the 100 m, 300 m, and 500 m
 2761 isobaths indicated.

2762



2763

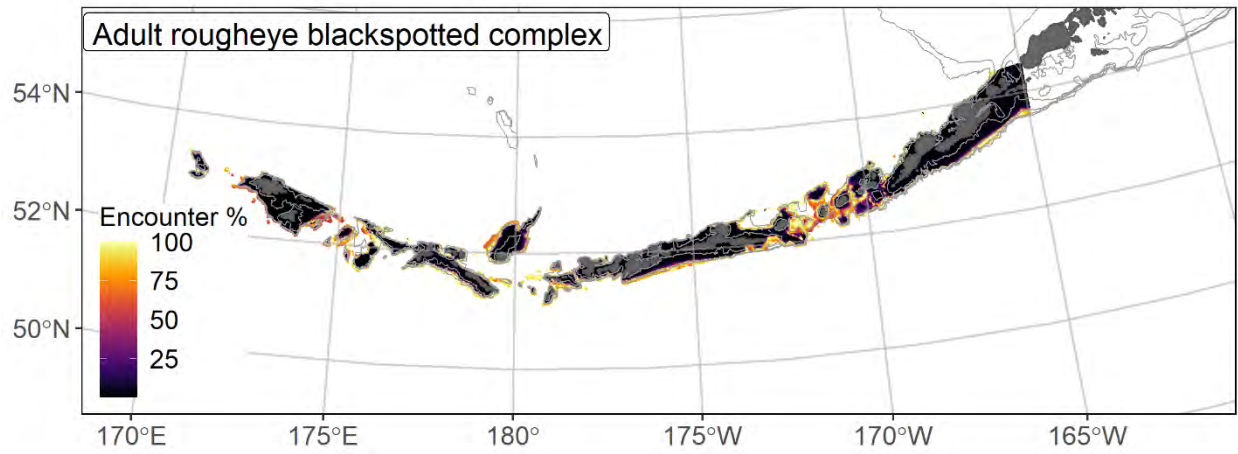
2764 Figure 132. Distribution of adult roughey/blackspotted rockfish catches (N = 711) in 1991–2019 AFSC
 2765 RACE-GAP summer bottom trawl surveys of the Aleutian Islands with the 100 m, 300 m, and 500 m
 2766 isobaths indicated; filled red circles indicate locations in top 10% of overall abundance, open orange
 2767 circles indicate presence in remaining catches, and small blue dots indicate absence.



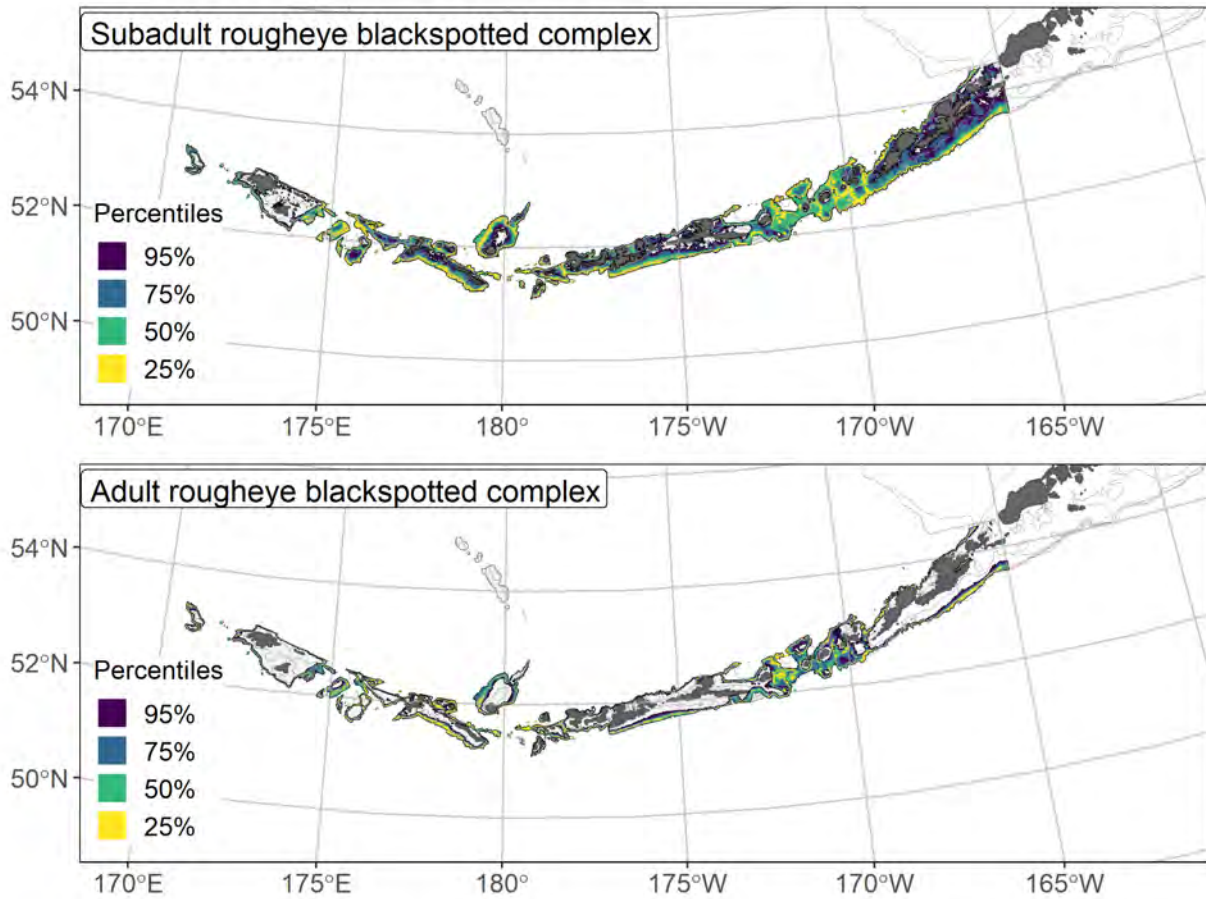
2768

2769 Figure 133. The top nine covariate effects (left panel) on ensemble-predicted adult roughey/blackspotted rockfish numerical abundance across the

2770 Aleutian Islands (upper right panel) alongside the coefficient of variation of the ensemble predictions (lower right panel).



2771
 2772 Figure 134. Encounter probability of adult rougheye/blackspotted rockfish from AFSC RACE-GAP
 2773 summer bottom trawl surveys (1991–2019) of the Aleutian Islands with the 100 m, 300 m, and 500 m
 2774 isobaths indicated.



2775
 2776 Figure 135. Essential fish habitat (EFH area) defined as the top 95% of numerical abundance predictions
 2777 from a habitat-based ensemble fitted to subadult (top) and adult (bottom) roughey/blackspotted rockfish
 2778 distribution and abundance in AFSC RACE-GAP summer bottom trawl surveys (1991–2019) with 100 m,
 2779 300 m, and 500 m isobaths indicated; internal to the EFH map are the subareas of the top 25% (EFH hot
 2780 spots), top 50% (core EFH area), and top 75% (principal EFH area) of habitat related, ensemble-predicted
 2781 numerical abundance.

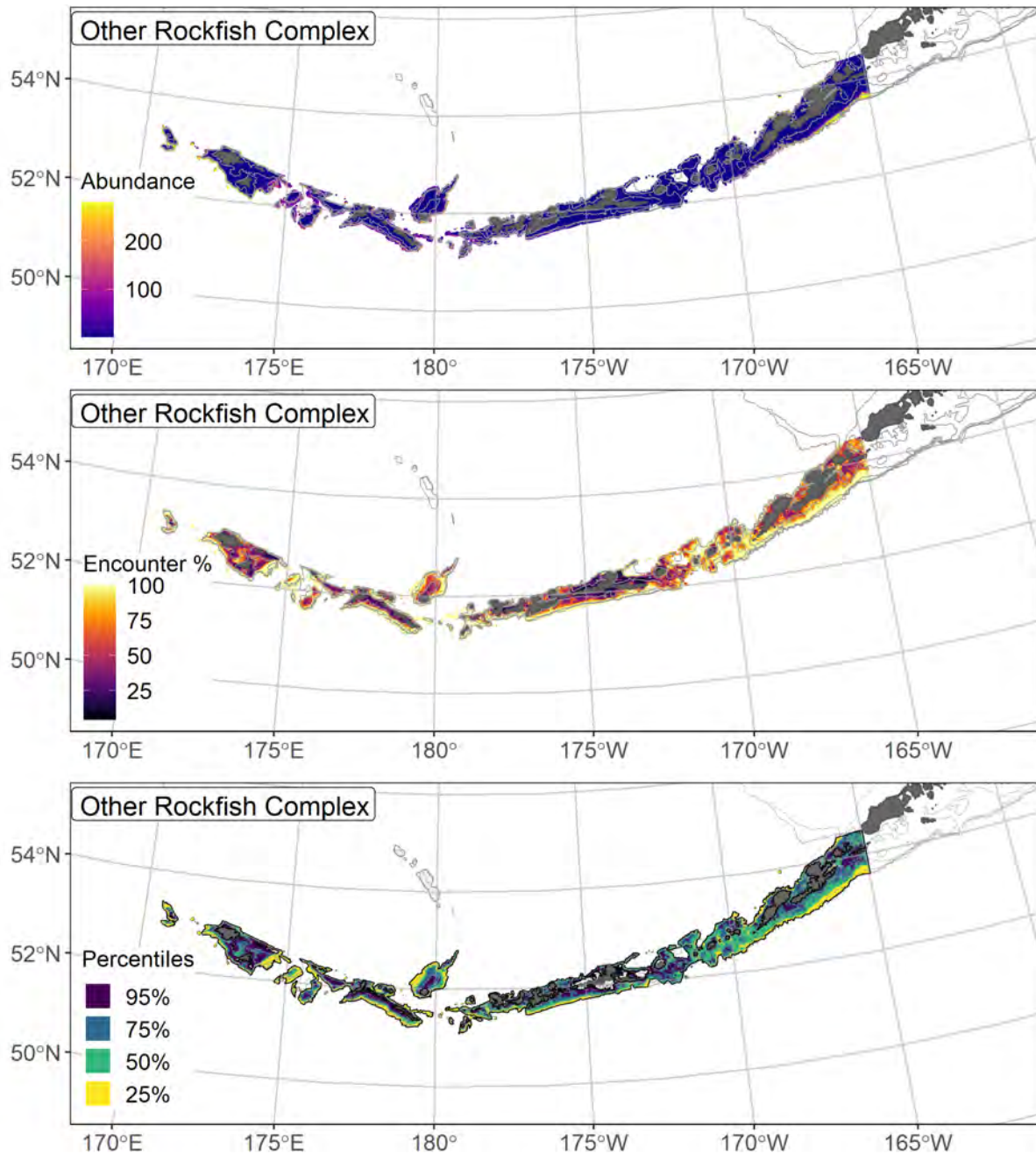
2782 **Stock Complex: Other Rockfishes**

2783 Several species that lack the data necessary for a full age structured assessment are managed
2784 under the “other rockfish” stock complex of the BSAI region (Sullivan et al 2020). In practice, this
2785 consists of data from seven rockfish species which occur often enough in the fishery to be of concern, but
2786 only three were common enough in the RACE-GAP summer bottom trawl survey of the AI to enable the
2787 construction of an SDM: dusky rockfish (*Sebastes variabilis*), harlequin rockfish (*Sebastes variegatus*),
2788 and shortspine thornyhead (*Sebastolobus alascanus*). Additionally, insufficient data were available to
2789 construct a model for subadult harlequin rockfish, so both adult and subadult life stages were combined to
2790 make a single set of maps for the “other rockfish” stock complex. In the AI, shortspine thornyhead (SST)
2791 accounted for 90% of the survey catch of species in this complex and the resulting maps are somewhat
2792 biased towards areas with high abundance of this species. However, as all three species occupied similar
2793 environments, this imbalance is unlikely to have an adverse effect on EFH predictions. Of larger concern
2794 is that because adults are much more common than subadults, the resulting maps may not adequately
2795 reflect the habitats necessary to young life stages of these rockfish species.

2796 **“Other Rockfish” Stock Complex abundance and distribution predicted from RACE-GAP summer**
2797 **bottom trawl surveys in the Bering Sea–**

2798 Numerical abundance predictions for three rockfish species were combined to estimate the
2799 abundance and EFH of the “other rockfish” stock complex in the AI (Figure 136). The composite
2800 abundance map was strongly influenced by SST, and the resulting map shows high numbers of rockfishes
2801 predicted along the continental slope south of Unalaska Island. This was slightly different from the main
2802 areas of abundance for adult dusky and harlequin rockfishes, which occurred a little further west along the
2803 slope. Additionally, subadult and adult dusky rockfish were sometimes found in shallower water closer to
2804 shore, which was not apparent from the map. While the abundance map was strongly weighted towards
2805 SST, the encounter probability map was less influenced by a single high density species. Notably, this
2806 map showed high encounter probabilities in many shallower areas in the eastern AI, which better reflected

2807 the distribution of dusky rockfish. The EFH map for the complex predicted hot spots along most of the
2808 continental slope areas throughout the region. This was consistent with the distributions of adults from all
2809 three species and subadult shortspine thornyhead. Many inshore areas in the eastern AI were part of the
2810 core EFH area, which reflected data from subadult dusky rockfish. As subadult dusky rockfish were less
2811 common in the western AI, most shallow areas in the west were not part of the EFH area.



2812

2813 Figure 136: Composite predicted numerical abundance (top panel), encounter probability (middle panel),
 2814 and essential fish habitat (bottom panel) for the “other rockfish” stock complex in the Aleutian Islands
 2815 collected in the AFSC RACE-GAP summer bottom trawl surveys (1991–2019) with 100 m, 300 m, and
 2816 500 m isobaths indicated. EFH is defined as the top 95% of numerical abundance predictions above a
 2817 presence threshold, and integral to the EFH map are the top 25% (EFH hot spots), top 50% (core EFH
 2818 area), and top 75% (principal EFH area) of habitat related, ensemble-predicted numerical abundance.

2819 **Dusky rockfish (*Sebastes variabilis*)**

2820 Dusky rockfish (*Sebastes variabilis*) is a moderately large (up to 590 mm) rockfish that is found
2821 from the Oregon coast across the Aleutian Islands, and as far as Hokkaido Japan (Orr and Blackburn,
2822 2004). It is one of the more common rockfish species in the BSAI region, though it is primarily found in
2823 the Aleutian Islands and Gulf of Alaska, and only rarely in the Bering Sea (Sullivan et al. 2020). Like
2824 other members of the genus *Sebastes*, dusky rockfish are long lived and may skip spawning during years
2825 with unfavorable conditions (Conrath, 2019). Dusky rockfish become mature (L_{50}) beginning around
2826 365 mm F.L., and display traits such as internal fertilization and live birth that are common to other
2827 members of the genus *Sebastes* (Chilton 2010). Prior to 1996, this species was often mixed with catches
2828 of the dark rockfish (*S. ciliatus*), which is similar in morphology but darker in coloration. For a time,
2829 catches of these species were recorded as “light dusky” or “dark dusky,” which allowed for the true
2830 species to be retroactively determined from the RACE-GAP survey data after the species were officially
2831 described by Orr and Blackburn (2004). In the BSAI region, dusky rockfish are managed as the second
2832 most abundant species in the “other rockfish complex” (Sullivan et al. 2020).

2833 **Subadult dusky rockfish distribution and predicted abundance from RACE-GAP summer bottom**
2834 **trawl surveys in the Aleutian Islands–**

2835 Subadult dusky rockfish catches were somewhat common in the eastern AI near Unimak Pass and
2836 Unalaska Island, but were less common further west (Figure 137). The final ensemble contained three
2837 SDMs and the hGAM was given slightly less weight than the others (Table 5). When compared with
2838 observed data, the ensemble showed fair performance (Table 39). Specifically, the ensemble scored well
2839 in predicting presence or absence in catches ($AUC = 0.880$), but scored only fair at predicting abundance
2840 ($\rho = 0.203$) and in terms of deviance explained ($PDE = 0.335$). Taken together, this suggested that
2841 predictions about presence or absence are likely to be accurate, but that predictions of abundance were
2842 more uncertain. This is explained in part by the limited amount of data available (108 positive records),
2843 and so the outputs of the ensemble should be used with caution. Geographic position, bottom depth, and

2844 bottom currents were the most important covariates and accounted for 77.8% of the deviance explained
2845 by the ensemble (Table 40). Ensemble predictions showed high abundance in the eastern AI, shallower
2846 depths, and places with south to southeasterly currents, but the confidence intervals around many of the
2847 covariates were very wide and do not support strong conclusions (Figure 138). Predicted abundance was
2848 highest around Unalaska Island, though localized areas of high abundance are also predicted near Umnak
2849 and Amchitka Islands (Figure 138). This pattern is supported by the survey catch records which show
2850 some high density catches in those areas (Figure 138). The map of the predicted CV of abundance was
2851 difficult to interpret, but was consistent with the high uncertainty around the estimated covariate effects
2852 (Figure 138). Encounter probabilities for subadult dusky rockfish were low in most places across the AI,
2853 but they were common near shore around Unalaska Island, in pockets around the Fox Islands and
2854 Amchitka Island (Figure 139).

2855 **Adult dusky rockfish distribution and predicted abundance from RACE-GAP summer bottom**
2856 **trawl surveys in the Aleutian Islands –**

2857 Adult dusky rockfish catches in the RACE-GAP summer survey were distributed throughout the
2858 Aleutian Islands, but were most concentrated in the east near Unalaska Island (Figure 140). The four
2859 SDMs retained in the final ensemble were equally weighted and performed slightly better than the
2860 subadult ensemble when compared to the data (Table 39). All three metrics scored in the range considered
2861 fair ($\rho = 0.272$; AUC = 0.782; PDE = 0.392), and taken together they suggest that the ensemble's
2862 predictions were somewhat accurate, but caution is still advised when using the following maps.
2863 Geographic position, bottom depth, bottom currents, and slope were responsible for 62.8% of the
2864 deviance explained by the ensemble (Table 40), though current variability, temperature, and rocky terrain
2865 also made minor contributions. The model predicted high abundance in locations further east that have
2866 bottom depths between 100-200 m, a slope of at least 5°, and strong southerly currents (Figure 141). The
2867 predicted abundance map for adults was similar to subadults in that it predicted areas of high abundance
2868 south of Unalaska Island and Umnak Island. However, the areas of high abundance were further off shore

2869 and the overall abundance of adults in the survey was much higher than that of subadults (Figure 141).
2870 The predicted CV of abundance was highest in the eastern AI around locations of high abundance
2871 (Figure 141). Encounter probabilities for adult dusky rockfish were high in the eastern AI, and in a few
2872 other places where the preferred depth and other conditions were present (Figure 142).

2873 **Essential fish habitat of subadult and adult dusky rockfish in the Aleutian Islands –**

2874 The habitat related abundance predictions based on RACE-GAP summer bottom trawl data
2875 (1996–2019) were translated into EFH area and subareas (Figure 143). The EFH area for subadults was
2876 much smaller than that of adults, and was concentrated east of 170° W. Smaller pockets of EFH were
2877 present around the inshore areas of other islands further west in the chain, such as Amchitka Island. The
2878 adult EFH was much larger, though its primary hot spot also occurred in the eastern AI, east of 170° W.
2879 The adult EFH extended into areas with greater depths, and covered much of the area around the Islands
2880 of Four Mountains and Andreanof Islands, before becoming sparser further west.

2881

2882 Table 39. Constituent species distribution models (SDMs) used to construct Essential Fish Habitat (EFH)
 2883 for a) subadult and b) adult dusky rockfish: MaxEnt = Maximum entropy; paGAM = presence-absence
 2884 generalized additive model; hGAM = hurdle GAM; GAM_p = standard Poisson GAM; and
 2885 GAM_{nb} = standard negative-binomial GAM. Ensemble performance (ρ = Spearman's rank correlation
 2886 coefficient), root-mean-square-error (RMSE), the area under the receiver operating characteristic (AUC),
 2887 and the Poisson deviance explained (PDE) were generated from k-fold cross-validation. The "--" in a field
 2888 indicates that this SDM was not included in the final ensemble.

2889 **a) subadult dusky rockfish**

Models	RMSE	Relative Weight	ρ	AUC	PDE	EFH area (km²)
MaxEnt	--	0	--	--	--	--
paGAM	1.38	0.447	0.206	0.889	0.302	29,800
hGAM	2.03	0.113	0.183	0.887	0.210	17,500
GAM _p	1.43	0	--	--	--	--
GAM _{nb}	1.38	0.441	0.202	0.873	0.338	23,500
ensemble	1.39	1	0.203	0.880	0.335	27,400

2890 **b) adult dusky rockfish**

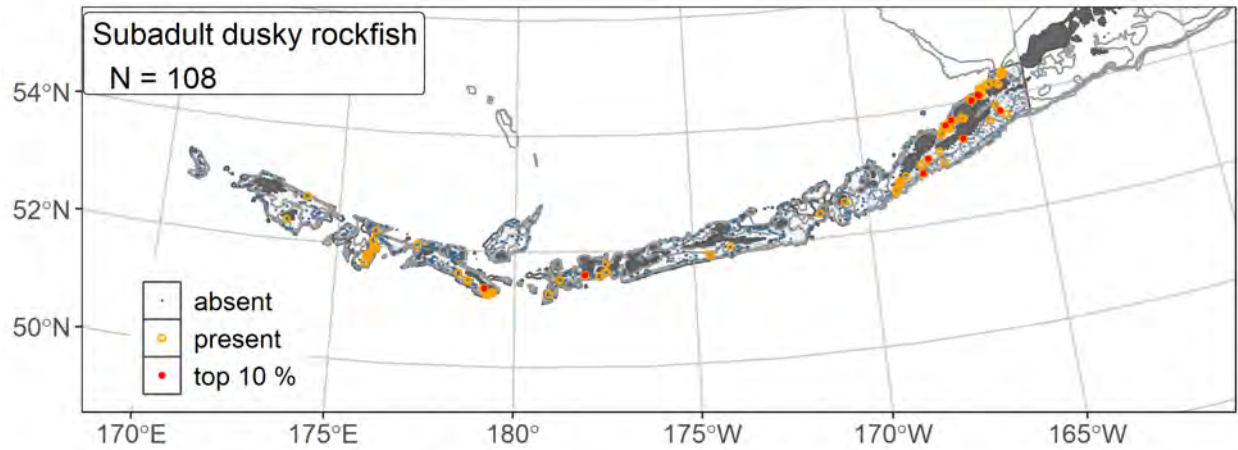
Models	RMSE	Relative Weight	ρ	AUC	PDE	EFH area (km²)
MaxEnt	9.71	0.255	0.262	0.773	0.215	66,800
paGAM	9.69	0.257	0.277	0.789	0.229	68,600
hGAM	10.09	0.237	0.223	0.788	0.438	45,500
GAM _p	9.91	0	--	--	--	--
GAM _{nb}	9.71	0.251	0.250	0.758	0.372	53,300
ensemble	9.39	1	0.272	0.782	0.392	65,300

2891

2892 Table 40. Covariates retained in the a) subadult and b) adult dusky rockfish species distribution model
 2893 (SDM) final ensembles, the percent contribution to the ensemble deviance explained by each, and the
 2894 cumulative percent deviance: SD = standard deviation, and BPI = bathymetric position index.

dusky rockfish	Covariate	% Contribution	Cumulative % Contribution
a) subadult	position	35.5	35.5
	bottom depth	26.3	61.8
	current	16.0	77.8
	slope	4.2	82.0
	tidal maximum	4.2	86.2
	sponge presence	4.1	90.3
	current SD	3.6	93.9
	aspect east	2.7	96.6
	rockiness	0.8	97.4
	bottom temperature	0.7	98.1
	coral presence	0.5	98.6
	aspect north	0.5	99.1
	curvature	0.5	99.6
	BPI	0.4	100
pennatulacean presence	0	100	
a) adult	position	18.5	18.5
	bottom depth	16.2	34.8
	current	16.0	50.8
	slope	12.0	62.8
	current SD	9.4	72.2
	bottom temperature	5.1	77.4
	rockiness	4.6	82.0
	aspect east	4.4	86.4
	BPI	3.9	90.3
	aspect north	3.3	93.6
	tidal maximum	3.0	96.6
	curvature	1.9	98.5
	sponge presence	0.8	99.3
	coral presence	0.6	99.9
	pennatulacean presence	0.1	100

2895



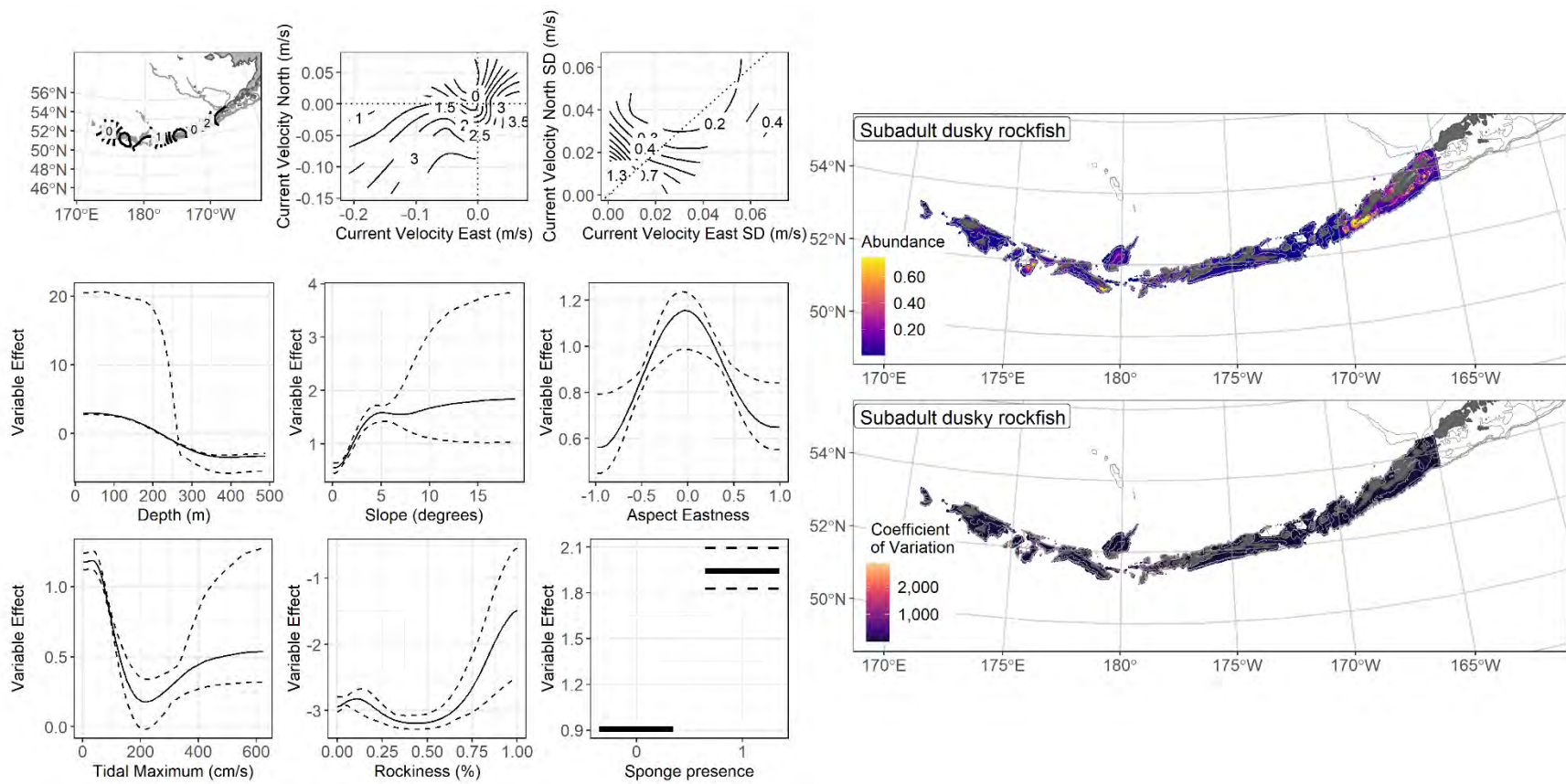
2896

2897 Figure 137. Distribution of subadult dusky rockfish catches (N = 108) in 1996–2019 AFSC RACE-GAP

2898 summer bottom trawl surveys of the Aleutian Islands with the 100 m, 300 m, and 500 m isobaths

2899 indicated; filled red circles indicate locations in top 10% of overall abundance, open orange circles

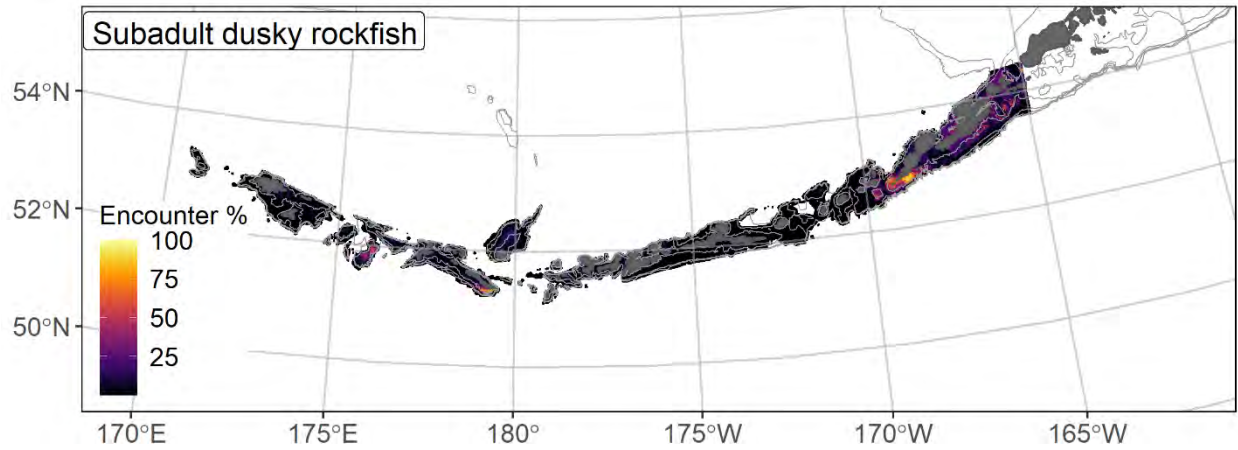
2900 indicate presence in remaining catches, and small blue dots indicate absence.



2901

2902 Figure 138. The top nine covariate effects (left panel) on ensemble-predicted subadult dusky rockfish numerical abundance across the Aleutian

2903 Islands (upper right panel) alongside the coefficient of variation of the ensemble predictions (lower right panel).



2904

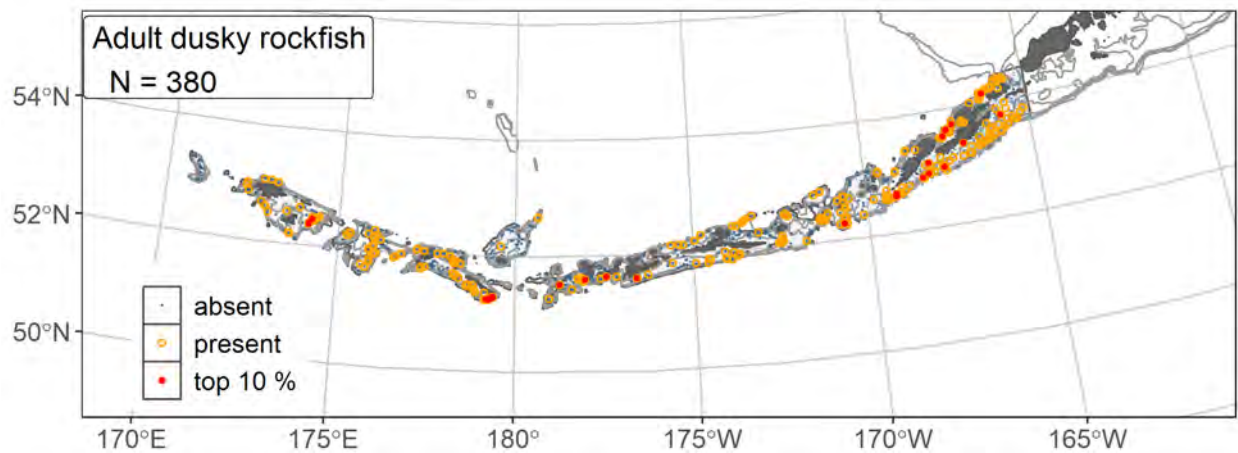
2905

Figure 139. Encounter probability of subadult dusky rockfish from AFSC RACE-GAP summer bottom

2906

trawl surveys (1996–2019) of the Aleutian Islands with the 100 m, 300 m, and 500 m isobaths indicated.

2907



2908

2909

Figure 140. Distribution of adult dusky rockfish catches (N = 221) in 1996–2019 AFSC RACE-GAP

2910

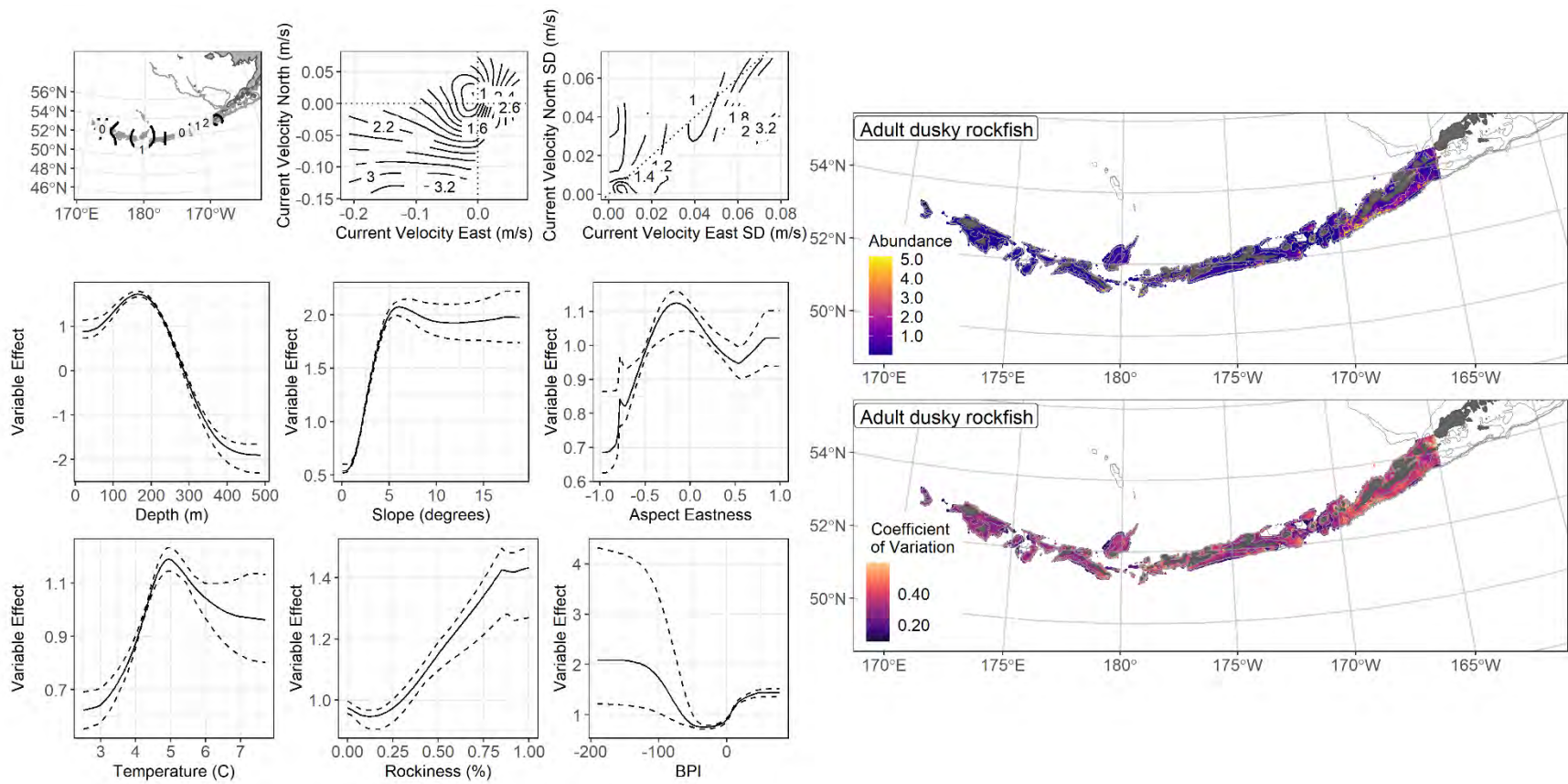
summer bottom trawl surveys of the Aleutian Islands with the 100 m, 300 m, and 500 m isobaths

2911

indicated; filled red circles indicate locations in top 10% of overall abundance, open orange circles

2912

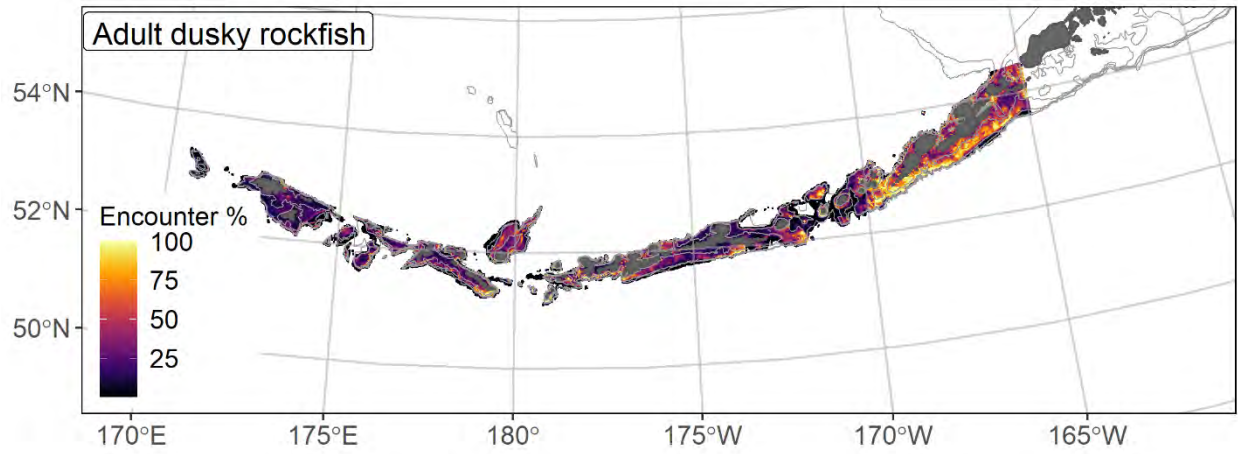
indicate presence in remaining catches, and small blue dots indicate absence.



2913

2914 Figure 141. The top nine covariate effects (left panel) on ensemble-predicted adult dusky rockfish numerical abundance across the Aleutian

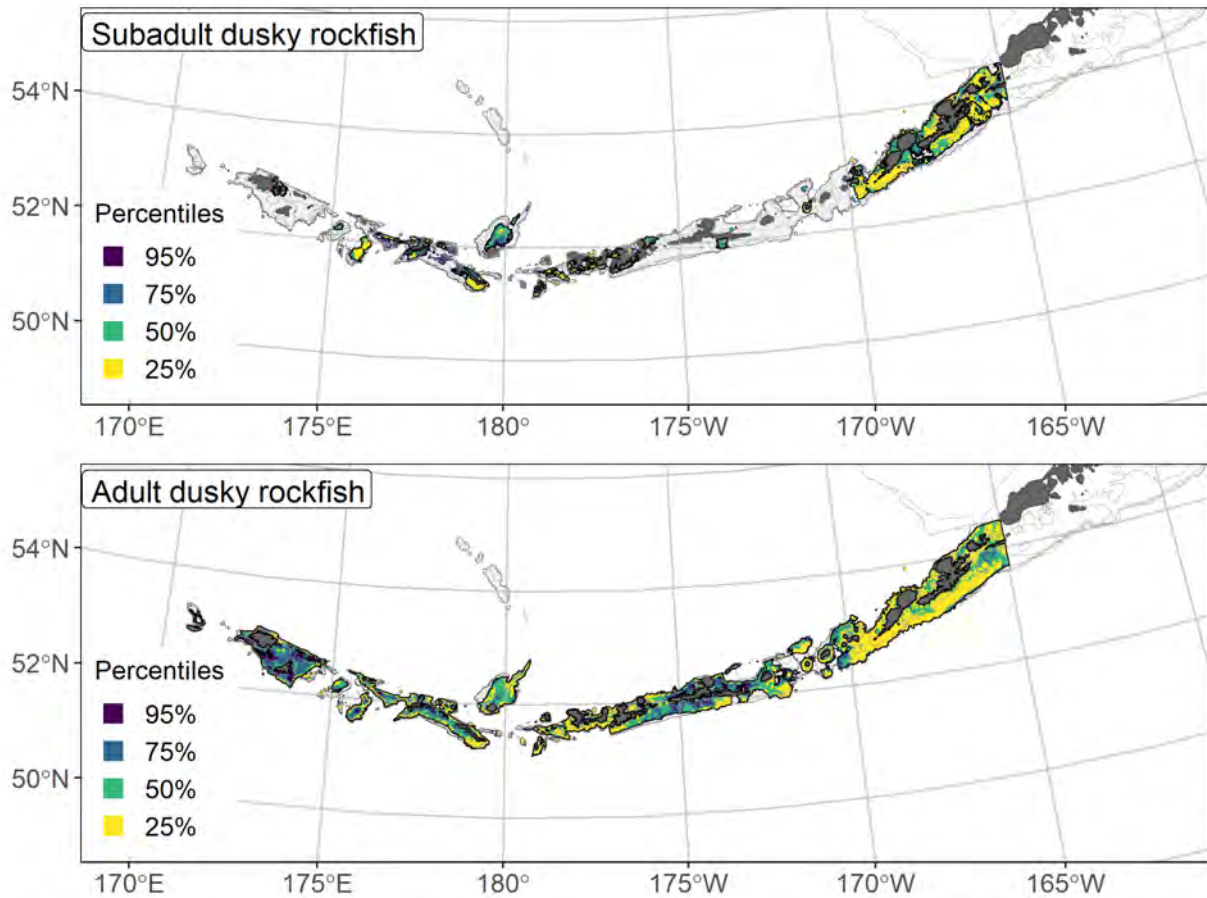
2915 Islands (upper right panel) alongside the coefficient of variation of the ensemble predictions (lower right panel).



2916

2917 Figure 142. Encounter probability of adult dusky rockfish from AFSC RACE-GAP summer bottom trawl

2918 surveys (1996–2019) of the Aleutian Islands with the 100 m, 300 m, and 500 m isobaths indicated.



2919

2920 Figure 143. Essential fish habitat (EFH area) defined as the top 95% of numerical abundance predictions
 2921 from a habitat-based ensemble fitted to subadult (top) and adult (bottom) dusky rockfish distribution and
 2922 abundance in AFSC RACE-GAP summer bottom trawl surveys (1996–2019) with 100 m, 300 m, and
 2923 500 m isobaths indicated; internal to the EFH map are the subareas of the top 25% (EFH hot spots), top
 2924 50% (core EFH area), and top 75% (principal EFH area) of habitat related, ensemble-predicted numerical
 2925 abundance.

2926 **Harlequin rockfish (*Sebastes variegatus*)**
2927 Harlequin rockfish (*Sebastes variegatus*) is found from the Oregon coast to the western Aleutian
2928 Islands (Love et al. 2002). Harlequin rockfish is one of the smaller species of rockfish and females
2929 become mature at a length of 188 mm F.L. (L_{50} ; Tenbrink and Helser 2021) and achieves a maximum
2930 length of 420 mm F.L. (Rooper 2008). This species becomes mature at a relatively young age for seabastid
2931 rockfishes (4.5 years), but can still live as long as 75 years (Kastelle et al. 2020). One complication for the
2932 assessment of this species is that it is often associated with habitat that is untrawlable using standard
2933 RACE-GAP survey gear, including areas that are rocky or have a high density of structure forming
2934 invertebrates such as corals (Conrath et al. 2019). In multiple studies harlequin rockfish were found to be
2935 closely associated with the bottom or amidst rocks (Johnson et al. 2003, Jones et al. 2012). Harlequin
2936 rockfish is managed as part of the “other rockfish” stock complex in both the BSAI and GOA regions,
2937 though the species is poorly sampled by the trawl survey in the AI and is uncommon in the Bering Sea
2938 (Sullivan et al. 2020). In the GOA, it is the most common species in the “other rockfish” stock by survey
2939 catch (Tribuzio and Echave 2019). The subadult life stage was present in fewer than 50 hauls in the
2940 RACE-GAP Aleutian Islands trawl survey and therefore, results are only available for the adult life stage.

2941 **Adult harlequin rockfish distribution and predicted abundance from RACE-GAP summer bottom**
2942 **trawl surveys in the Aleutian Islands–**

2943 Adult harlequin rockfish from the RACE-GAP summer survey were sparsely distributed across
2944 the AI and with no particular area showing higher catches (Figure 144). Catches occurred primarily in
2945 shallow water around 100 m deep. The final ensemble contained three equally weighted SDMs that
2946 showed a poor to fair fit to the data (Table 41). Specifically, the ensemble scored well on predicting
2947 presence or absence (AUC = 0.860), and explained a fair amount of the deviance in the data
2948 (PDE = 0.404). However, it scored poorly on measures of its ability to predict relative high or low
2949 abundance catches ($\rho = 0.178$). This pattern in the fit metrics can sometimes occur in species with limited
2950 data (111 positive catches 1991-2019) and many observations near zero. The high score on AUC

2951 suggested that this ensemble was capable of identifying the most likely locations adult harlequin rockfish
2952 would be found. However, the combination of limited data, low value for ρ , and the preference of this
2953 species for untrawlable areas (Johnson et al. 2012), suggests that these predictions should be used with
2954 caution. There was no dominant covariate that influenced model predictions. Geographic position, bottom
2955 depth, bottom currents, BPI, slope angle and slope aspect accounted for 81.6 % of the deviance explained
2956 (Table 42). In general, high abundance was predicted in either the eastern or western AI (but not the
2957 center), at bottom depths from 100–300 m, where there were high variability currents, and with steep,
2958 south facing slopes. (Figure 145). A positive BPI, which describes locations that are relatively higher than
2959 their surroundings such as along the slope/shelf transition, was also correlated with increased abundance.
2960 Predicted abundance was highest along the edge of the continental slope, particularly south of Unalaska
2961 and Umnak Islands (Figure 145). The CV of abundance for the predictions was high along the edge of the
2962 continental slope, and was zero in shallower water where the species was almost never found
2963 (Figure 145). Predicted encounter probability was high only around those areas described above as having
2964 high abundance (Figure 146). However, these probabilities reflect the likelihood of encounter in a trawl
2965 survey, which is likely to underestimate their density in complex, rocky habitats.

2966 **Essential fish habitat of adult harlequin rockfish in the Aleutian Islands –**

2967 The habitat related abundance predictions based on RACE-GAP summer bottom trawl data
2968 (1991–2019) were translated into EFH area and subareas (Figure 147). Despite the relatively uncommon
2969 presence of harlequin rockfish in trawl catches, the EFH area covered approximately 75% of the AI. Most
2970 of the area south of the archipelago along the edge of the continental slope was designated as EFH hot
2971 spots for harlequin rockfish. Shallow, inshore areas were typically not EFH. The constituent SDMs
2972 disagreed about the size of the EFH area, and the GAM_{nb} predicted an area that is only a quarter of the
2973 size of the others (Table 41), which suggests that the EFH for this species should be interpreted with some
2974 caution.

2975 Table 41. Constituent species distribution models (SDMs) used to construct Essential Fish Habitat (EFH)
 2976 for adult harlequin rockfish: MaxEnt = Maximum entropy; paGAM = presence-absence generalized
 2977 additive model; hGAM = hurdle GAM; GAM_p = standard Poisson GAM; and GAM_{nb} = standard
 2978 negative-binomial GAM. Ensemble performance (ρ = Spearman's rank correlation coefficient), root-
 2979 mean-square-error (RMSE), the area under the receiver operating characteristic (AUC), and the Poisson
 2980 deviance explained (PDE) were generated from k-fold cross-validation. The "--" in a field indicates that
 2981 this SDM was not included in the final ensemble.

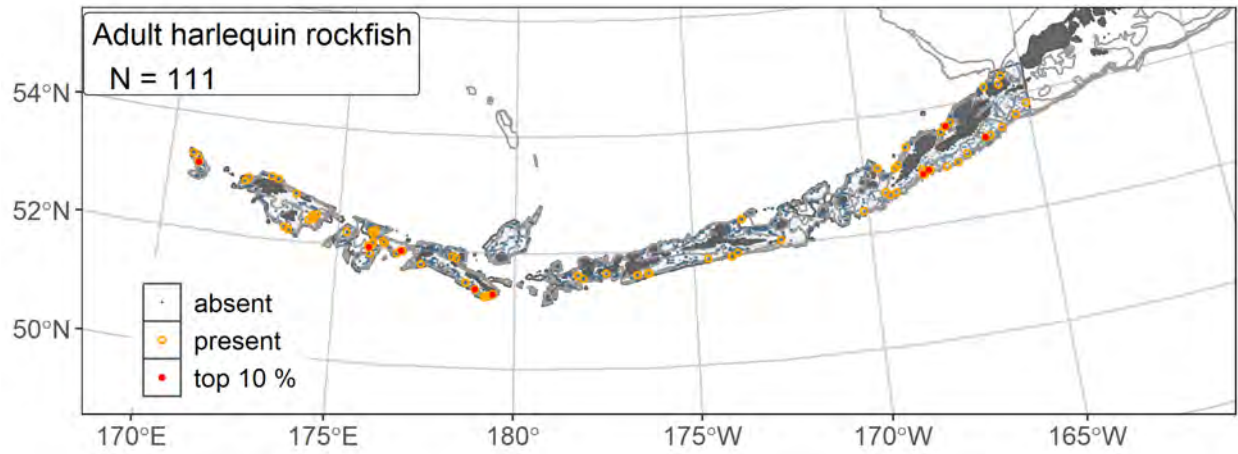
Models	RMSE	Relative Weight	ρ	AUC	PDE	EFH area (km²)
MaxEnt	23.6	0.331	0.176	0.857	0.236	60,100
paGAM	23.6	0.333	0.172	0.847	0.291	66,900
hGAM	--	0	--	--	--	--
GAM _p	--	0	--	--	--	--
GAM _{nb}	23.5	0.336	0.167	0.832	0.485	15,000
ensemble	23.3	1	0.178	0.860	0.404	62,600

2982

2983 Table 42. Covariates retained in the adult harlequin rockfish species distribution model (SDM) final
 2984 ensemble, the percent contribution to the ensemble deviance explained by each, and the cumulative
 2985 percent deviance: BPI = bathymetric position index.

harlequin rockfish	Covariate	% Contribution	Cumulative % Contribution
a) adults	position	19.1	19.1
	current	15.2	34.3
	bottom depth	11.7	46.0
	BPI	11.1	57.2
	aspect north	10.6	67.8
	current SD	8.3	76.1
	slope	8.0	84.1
	rockiness	3.2	87.3
	aspect east	2.9	90.2
	coral presence	2.5	92.7
	bottom temperature	2.1	94.8
	tidal maximum	1.9	96.7
	sponge presence	1.7	98.4
	curvature	1.5	99.9
	pennatulacean presence	0.1	100

2986



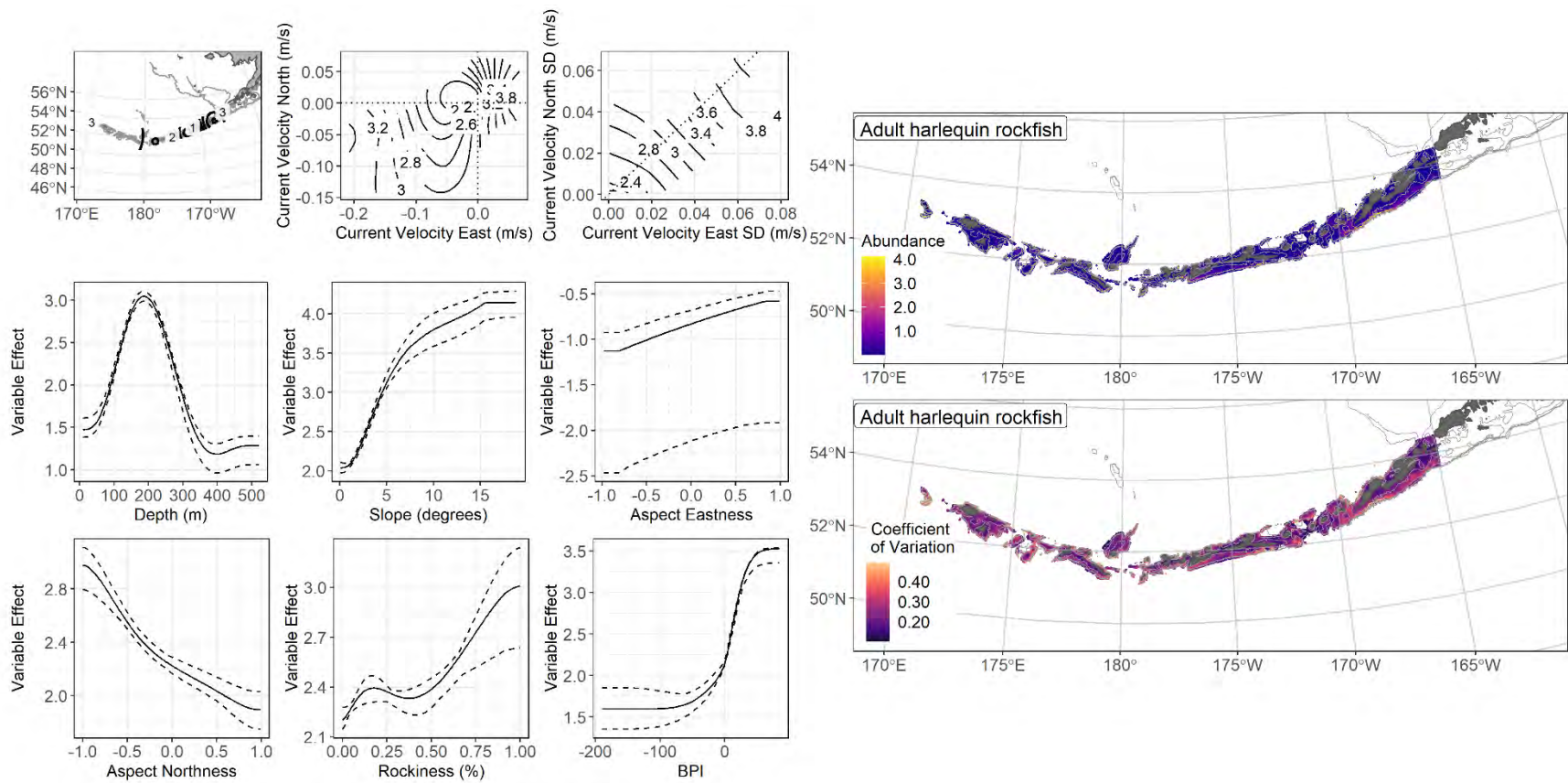
2987

2988 Figure 144. Distribution of adult harlequin rockfish catches (N = 111) in 1991–2019 AFSC RACE-GAP

2989 summer bottom trawl surveys of the Aleutian Islands with the 100 m, 300 m, and 500 m isobaths

2990 indicated; filled red circles indicate locations in top 10% of overall abundance, open orange circles

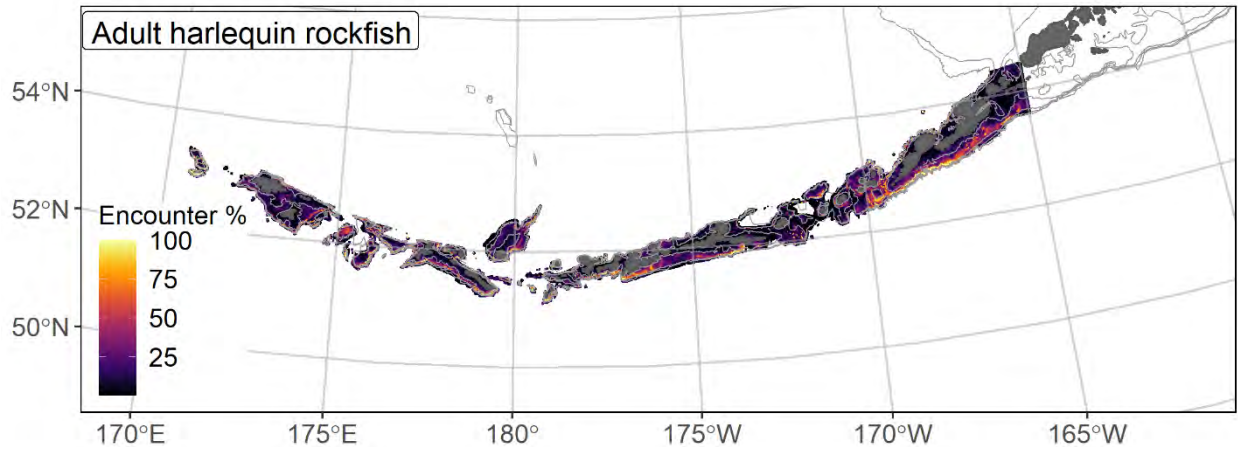
2991 indicate presence in remaining catches, and small blue dots indicate absence.



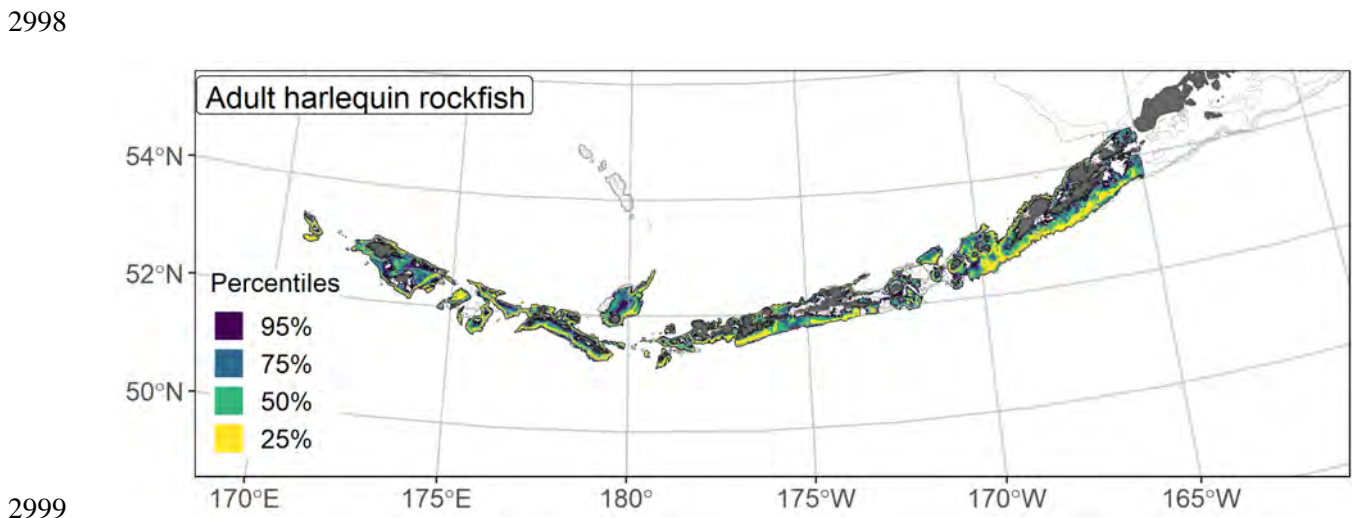
2992

2993 Figure 145. The top nine covariate effects (left panel) on ensemble-predicted adult harlequin rockfish numerical abundance across the Aleutian

2994 Islands (upper right panel) alongside the coefficient of variation of the ensemble predictions (lower right panel).



2995
 2996 Figure 146. Encounter probability of adult harlequin rockfish from AFSC RACE-GAP summer bottom
 2997 trawl surveys (1991–2019) of the Aleutian Islands with the 100 m, 300 m, and 500 m isobaths indicated.



2999
 3000 Figure 147. Essential fish habitat (EFH area) defined as the top 95% of numerical abundance predictions
 3001 from a habitat-based ensemble fitted to adult harlequin rockfish distribution and abundance in AFSC
 3002 RACE-GAP summer bottom trawl surveys (1991–2019) with 100 m, 300 m, and 500 m isobaths
 3003 indicated; internal to the EFH map are the subareas of the top 25% (EFH hot spots), top 50% (core EFH
 3004 area), and top 75% (principal EFH area) of habitat related, ensemble-predicted numerical abundance.

3005 **Shortspine thornyhead (*Sebastolobus alascanus*)**

3006 Shortspine thornyhead (*Sebastolobus alascanus*; SST) are encountered from Russia and Japan to
3007 the northern Bering Sea (Navarin Canyon) and through the Aleutian Islands to Baja California
3008 (Love et al. 2002, Mecklenburg et al. 2002). They inhabit a wide band of depths throughout their range
3009 (20–1,500 m) but are most abundant in Alaska between 150 and 500 m. Although related to sebastid
3010 rockfishes, thornyheads lack a swim bladder and release pelagic eggs as opposed to live young (Pearson
3011 and Gunderson 2003). Shortspine thornyheads can grow to a maximum length of 750 mm and live up to
3012 100 years (Kastelle et al 2000). Larvae have a prolonged pelagic phase of up to 15 months and juveniles
3013 are often found over mud bottoms 100–600 m before migrating into deeper depths as they mature. The
3014 L_{50} for both sexes has been reported as 215 mm F.L. (Pearson and Gunderson 2003) and we used this
3015 length to separate subadult and adult SST for this study. In the BSAI region, SST is managed as part of
3016 the “other rockfish” stock complex, where it is typically one of the top two components
3017 (Sullivan et al. 2020).

3018 **Subadult shortspine thornyhead distribution and predicted abundance from RACE-GAP summer**
3019 **bottom trawl surveys in the Aleutian Islands–**

3020 Subadult SST catches in the RACE-GAP summer trawl survey were split between the slope areas
3021 south of Unalaska Island in the east, and several deep water sites in the western AI (Figure 148 The final
3022 ensemble only contained two SDMs, and the GAM_P received about twice as much weight as the paGAM.
3023 The ensemble displayed good to excellent predictive performance (Table 43). Specifically, the ensemble
3024 received excellent scores for predictions of presence/absence (AUC = 0.978) and deviance explained
3025 (PDE = 0.753), and it performed well, though not excellently, at predicting relative abundance
3026 ($\rho = 0.457$). Given the near perfect score on AUC and the high portion of the deviance explained, this
3027 ensemble appeared to make very accurate predictions. Bottom depth was the most important covariate
3028 and accounted for 41.4% of the deviance explained by the ensemble (Table 44). Geographic position,
3029 current, and slope aspect also made substantial contributions. The model predicted higher subadult

3030 abundance at greater depths, in areas with weak bottom currents, and on the southern side of the island
3031 chain (Figure 149). Predicted abundance was highest in the east, along the slope south of Unalaska Island,
3032 though localized areas of high abundance were predicted further west (Figure 149). Invariably, high
3033 abundance occurred along the continental slope, often at the very edge of the survey area. The map of the
3034 predicted CV of abundance showed high variation in most deep slope areas (Figure 149). Encounter
3035 probabilities for subadult SST demonstrated the same pattern, with high probabilities in many slope areas
3036 (Figure 150).

3037 **Adult shortspine thornyhead distribution and predicted abundance from RACE-GAP summer**
3038 **bottom trawl surveys in the Aleutian Islands –**

3039 Adult SST catches in the RACE-GAP summer survey were more common than subadults. The
3040 geographic distribution of adult catches was similar to subadults with most catches taken in from 300–500
3041 m (Figure 151). The final ensemble combined the three SDMs, with the paGAM given about half the
3042 weight of the others and it showed an excellent fit to the data (Table 43). All three fit metrics were rated
3043 as excellent ($\rho = 0.615$; AUC = 0.938; PDE = 0.744), suggesting that this ensemble was very effective at
3044 predicting the presence and abundance of adult SST in bottom trawl catches. Geographic position and
3045 bottom depth were the most important covariates and accounted for 68.7% of the deviance explained by
3046 the ensemble (Table 44). In general, the model predicted that abundance would be higher in places with
3047 deeper bottom depths and in locations that were either in the eastern or western AI (Figure 152). Adult
3048 SST abundance was predicted to be highest along the continental slope south of Unalaska Island, and in
3049 general was often quite high within limited geographic patches (Figure 152). The predicted CV of
3050 abundance was highest along the slope near the 500 m depth contour (Figure 152). Encounter
3051 probabilities were high along most of the slope areas of sufficient depth (Figure 153).

3052 **Essential fish habitat of subadult and adult shortspine thornyhead in the Aleutian Islands –**

3053 The habitat related abundance predictions based on RACE-GAP summer bottom trawl data
3054 (1991–2019) were translated into EFH area and subareas (Figure 154). The EFH of both life stages was
3055 located in deep water along the continental slope, particularly south of Unalaska Island. Almost all of the
3056 EFH area for subadults was located in waters more than 300 m deep. The EFH for adults was
3057 considerably larger than that of subadults, but it followed the same general patterns. Around Unalaska
3058 Island and Attu Island, the EFH for adults extended into shallow water closer to shore. Given the
3059 observed and predicted depth distribution of this species, it seems likely that much of the habitat for SST
3060 is deeper than 500 m and hence outside the range of the RACE-GAP survey. Additional data sources,
3061 such as from longline surveys, might more effectively characterize this species' habitat¹⁸.

¹⁸ A recommendation to add additional survey data types if possible to future SDM ensemble EFH mapping efforts for this species will be included as a future recommendation for research directions from the 2022 EFH 5-year Review.

3062 Table 43. Constituent species distribution models (SDMs) used to construct Essential Fish Habitat (EFH)
 3063 for a) subadult and b) adult shortspine thornyhead: MaxEnt = Maximum entropy; paGAM = presence-
 3064 absence generalized additive model; hGAM = hurdle GAM; GAM_P = standard Poisson GAM; and
 3065 GAM_{nb} = standard negative-binomial GAM. Ensemble performance (ρ = Spearman's rank correlation
 3066 coefficient), root-mean-square-error (RMSE), the area under the receiver operating characteristic (AUC),
 3067 and the Poisson deviance explained (PDE) were generated from k-fold cross-validation. The "--" in a field
 3068 indicates that this SDM was not included in the final ensemble.

3069 **a) subadult shortspine thornyhead**

Models	RMSE	Relative Weight	ρ	AUC	PDE	EFH area (km²)
MaxEnt	--	--	--	--	--	--
paGAM	14.2	0.342	0.449	0.982	0.596	22,400
hGAM	--	--	--	--	--	--
GAM _P	10.2	0.658	0.469	0.969	0.774	22,400
GAM _{nb}	--	--	--	--	--	--
ensemble	8.57	1	0.457	0.978	0.753	23,200

3070 **b) adult shortspine thornyhead**

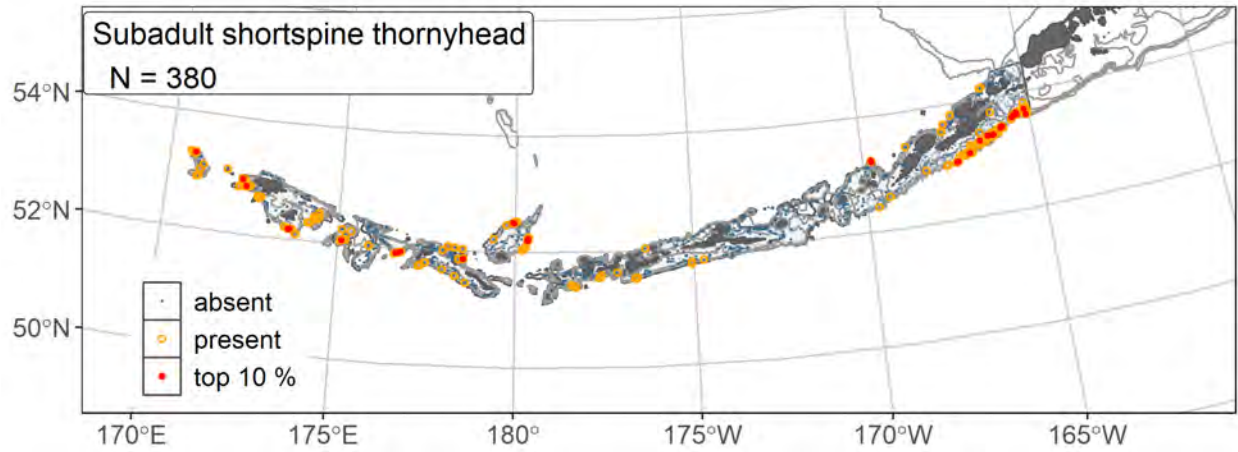
Models	RMSE	Relative Weight	ρ	AUC	PDE	EFH area (km²)
MaxEnt	--	--	--	--	--	--
paGAM	35.1	0.219	0.624	0.947	0.632	60,400
hGAM	27.3	0.395	0.612	0.947	0.753	45,800
GAM _P	27.1	0.386	0.605	0.930	0.741	55,900
GAM _{nb}	--	--	--	--	--	--
ensemble	25.8	1	0.615	0.938	0.744	54,600

3071

3072 Table 44. Covariates retained in the a) subadult and b) adult shortspine thornyhead species distribution
 3073 model (SDM) final ensembles, the percent contribution to the ensemble deviance explained by each, and
 3074 the cumulative percent deviance: SD = standard deviation, and BPI = bathymetric position index.

Shortspine thornyhead	Covariate	% Contribution	Cumulative % Contribution
a) subadult	bottom depth	41.4	41.4
	position	24.3	65.7
	current	9.8	75.6
	aspect north	8.1	83.7
	current SD	3.9	87.6
	BPI	3.5	91.1
	curvature	1.9	93.0
	aspect east	1.5	94.5
	slope	1.4	95.9
	tidal maximum	1.2	97.1
	pennatulacean presence	1.2	98.3
	rockiness	1.1	99.4
	bottom temperature	0.3	99.7
	sponge presence	0.3	100
coral presence	0	100	
a) adult	bottom depth	37.6	37.6
	position	31.2	68.7
	aspect north	7.8	76.5
	current SD	6.6	83.1
	current	4.9	88.0
	aspect east	4.4	92.4
	bottom temperature	2.5	94.9
	slope	1.6	96.5
	curvature	1.1	97.6
	tidal maximum	0.7	98.3
	rockiness	0.5	98.8
	BPI	0.4	99.2
	sponge presence	0.4	99.6
	pennatulacean presence	0.2	99.8
coral presence	0.2	100	

3075



3076

3077

Figure 148. Distribution of subadult shortspine thornyhead catches (N = 380) in 1991–2019 AFSC

3078

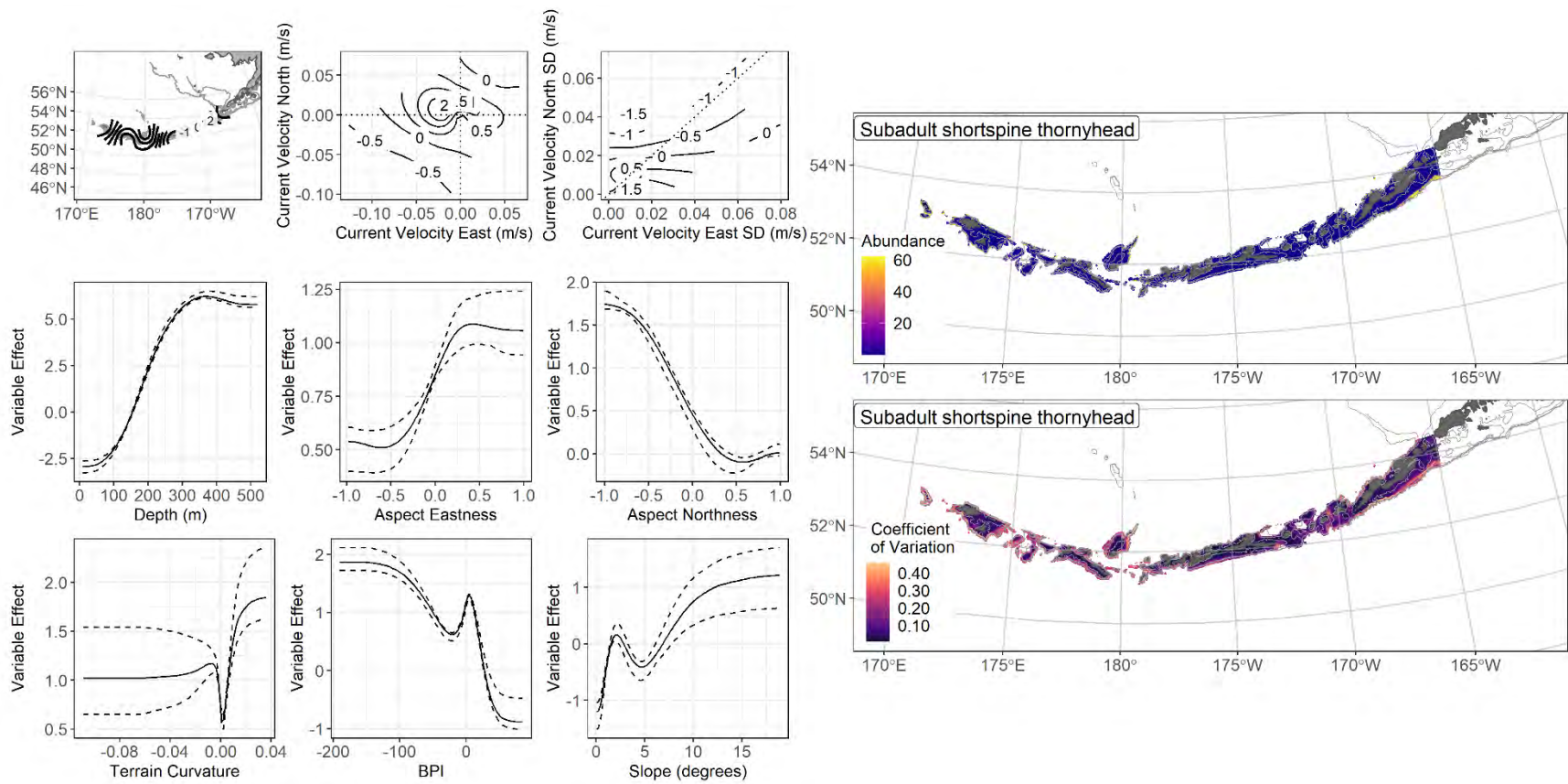
RACE-GAP summer bottom trawl surveys of the Aleutian Islands with the 100 m, 300 m, and 500 m

3079

isobaths indicated; filled red circles indicate locations in top 10% of overall abundance, open orange

3080

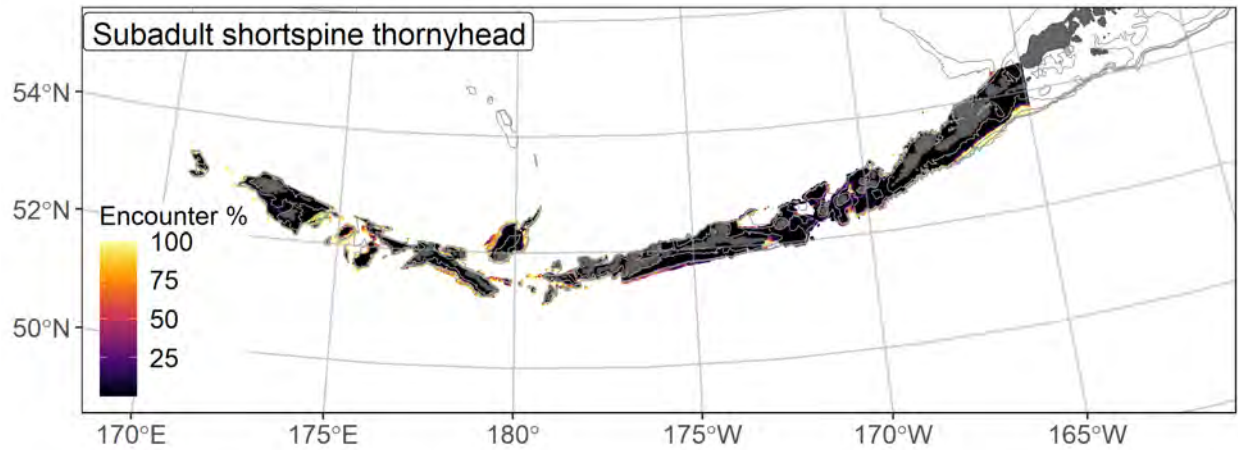
circles indicate presence in remaining catches.



3081

3082 Figure 149. The top nine covariate effects (left panel) on ensemble-predicted subadult shortspine thornyhead numerical abundance across the

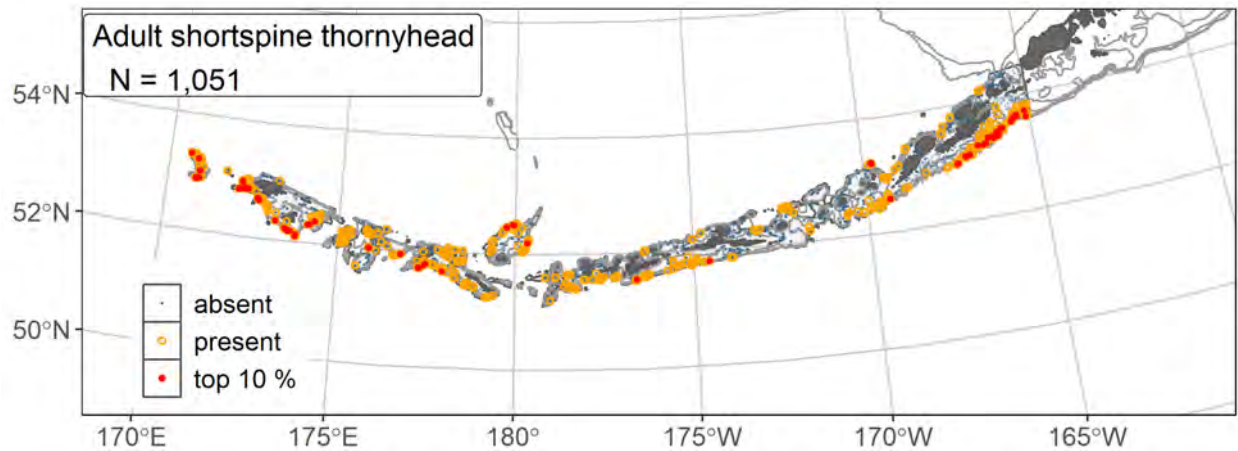
3083 Aleutian Islands (upper right panel) alongside the coefficient of variation of the ensemble predictions (lower right panel).



3084

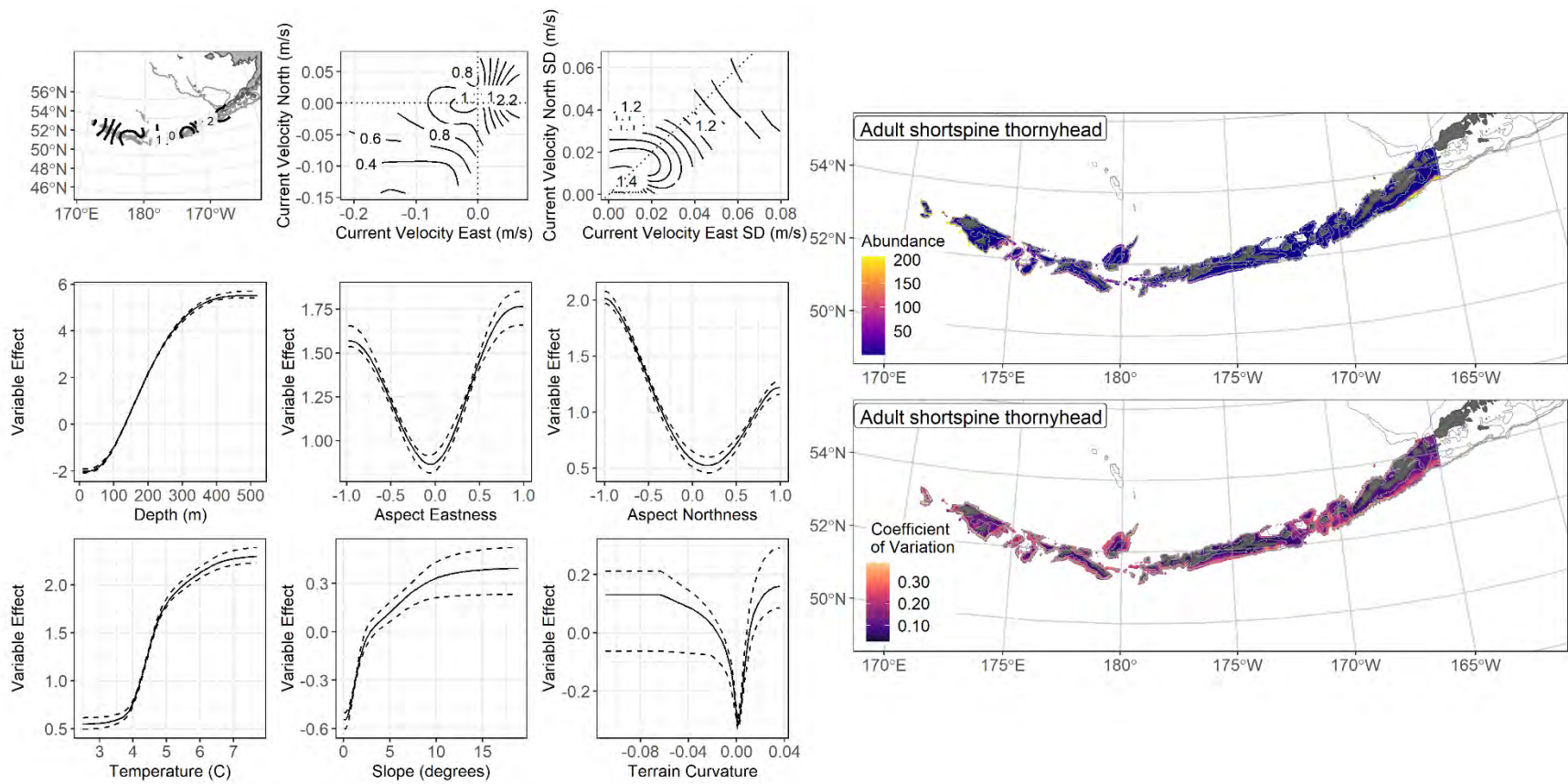
3085 Figure 150. Encounter probability of subadult shortspine thornyhead from AFSC RACE-GAP summer
 3086 bottom trawl surveys (1991–2019) of the Aleutian Islands with the 100 m, 300 m, and 500 m isobaths
 3087 indicated.

3088



3089

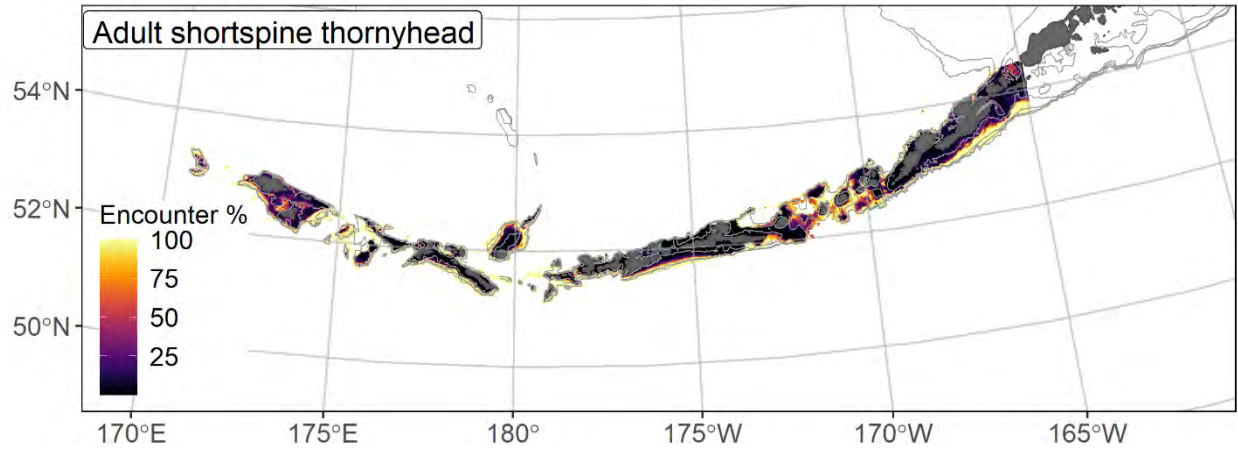
3090 Figure 151. Distribution of adult shortspine thornyhead catches (N = 1,051) in 1991–2019 AFSC RACE-
 3091 GAP summer bottom trawl surveys of the Aleutian Islands with the 100 m, 300 m, and 500 m isobaths
 3092 indicated; filled red circles indicate locations in top 10% of overall abundance, open orange circles
 3093 indicate presence in remaining catches.



3094

3095 Figure 152. The top nine covariate effects (left panel) on ensemble-predicted adult shortspine thornyhead numerical abundance across the Aleutian

3096 Islands (upper right panel) alongside the coefficient of variation of the ensemble predictions (lower right panel).

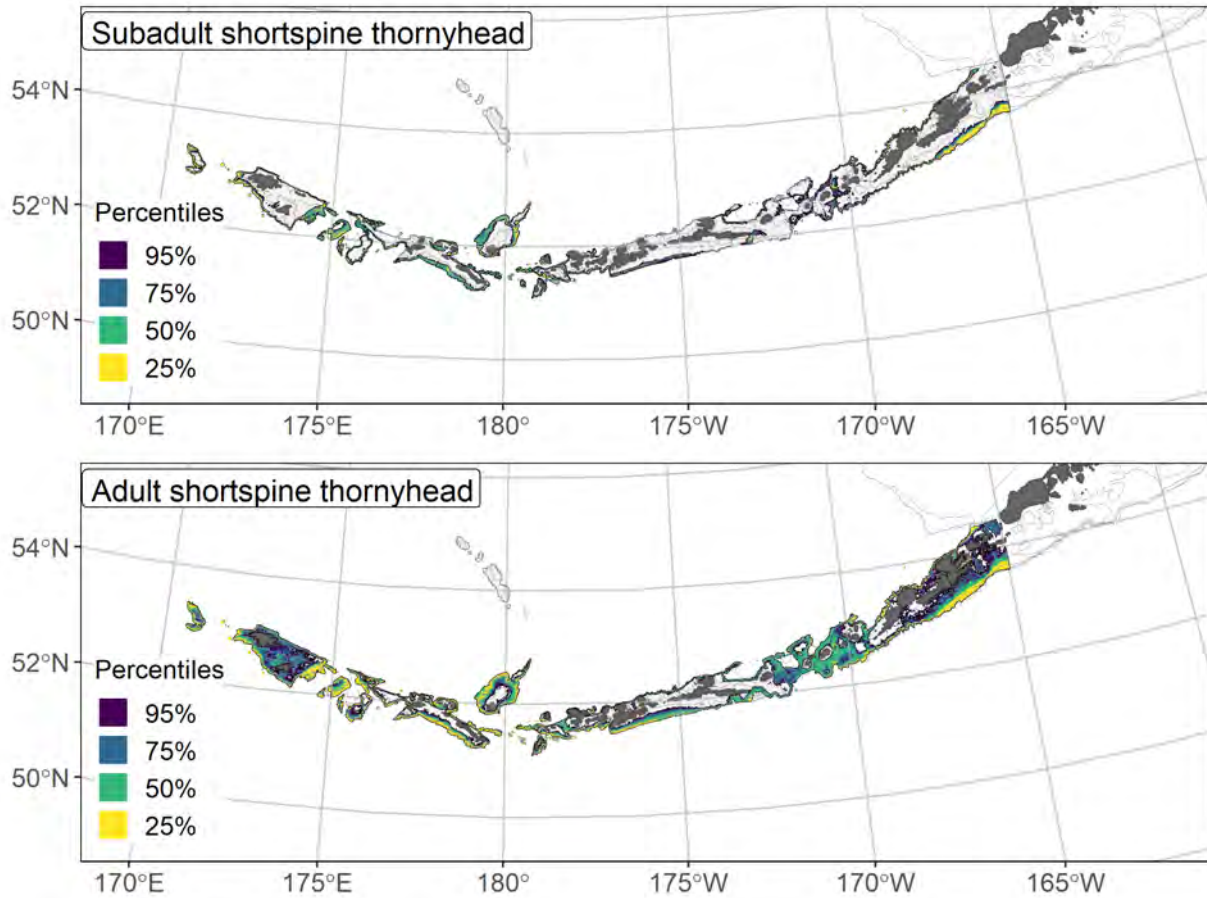


3097

3098 Figure 153. Encounter probability of adult shortspine thornyhead from AFSC RACE-GAP summer

3099 bottom trawl surveys (1991–2019) of the Aleutian Islands with the 100 m, 300 m, and 500 m isobaths

3100 indicated.



3101
 3102 Figure 154. Essential fish habitat (EFH area) defined as the top 95% of numerical abundance predictions
 3103 from a habitat-based ensemble fitted to subadult (top) and adult (bottom) shortspine thornyhead
 3104 distribution and abundance in AFSC RACE-GAP summer bottom trawl surveys (1991–2019) with 100 m,
 3105 300 m, and 500 m isobaths indicated; internal to the EFH map are the subareas of the top 25% (EFH hot
 3106 spots), top 50% (core EFH area), and top 75% (principal EFH area) of habitat related, ensemble-predicted
 3107 numerical abundance.

3108

Skates - Stock Complex

3109 Aleutian Islands skates are managed in aggregate as part of the skate stock complex of the BSAI region
3110 (Ormseth 2020). In the Bering Sea, Alaska skate (*Bathyraja parmifera*) is the dominant species, but it is
3111 less abundant in the AI. For the BSAI management region, Alaska skate receives a separate assessment
3112 although harvest specifications are made for the complex as a whole. . For this project, four species of
3113 skates were prevalent enough in the RACE-GAP summer bottom trawl surveys to allow for the
3114 development of SDMs: Alaska skate, Aleutian skate (*B. aleutica*), mud skate (*B. taranetzi*), and
3115 whiteblotched skate (*B. maculata*). A fifth species, the leopard skate (*B. panthera*) likely has sufficient
3116 data to develop a SDM and will be investigated during the 2027 EFH cycle. All four of the species
3117 currently included were modelled with both subadult and adult life stages. Because these species are
3118 typically managed together as a stock complex, this chapter summarizes the composite abundance,
3119 encounter probabilities, and EFH of these four species in the AI as a single complex. Stock assessments
3120 have identified whiteblotched skate as the dominant species in the AI representing over 50% of the total
3121 skate biomass (Ormseth 2020), which is apparent in the complex maps below.

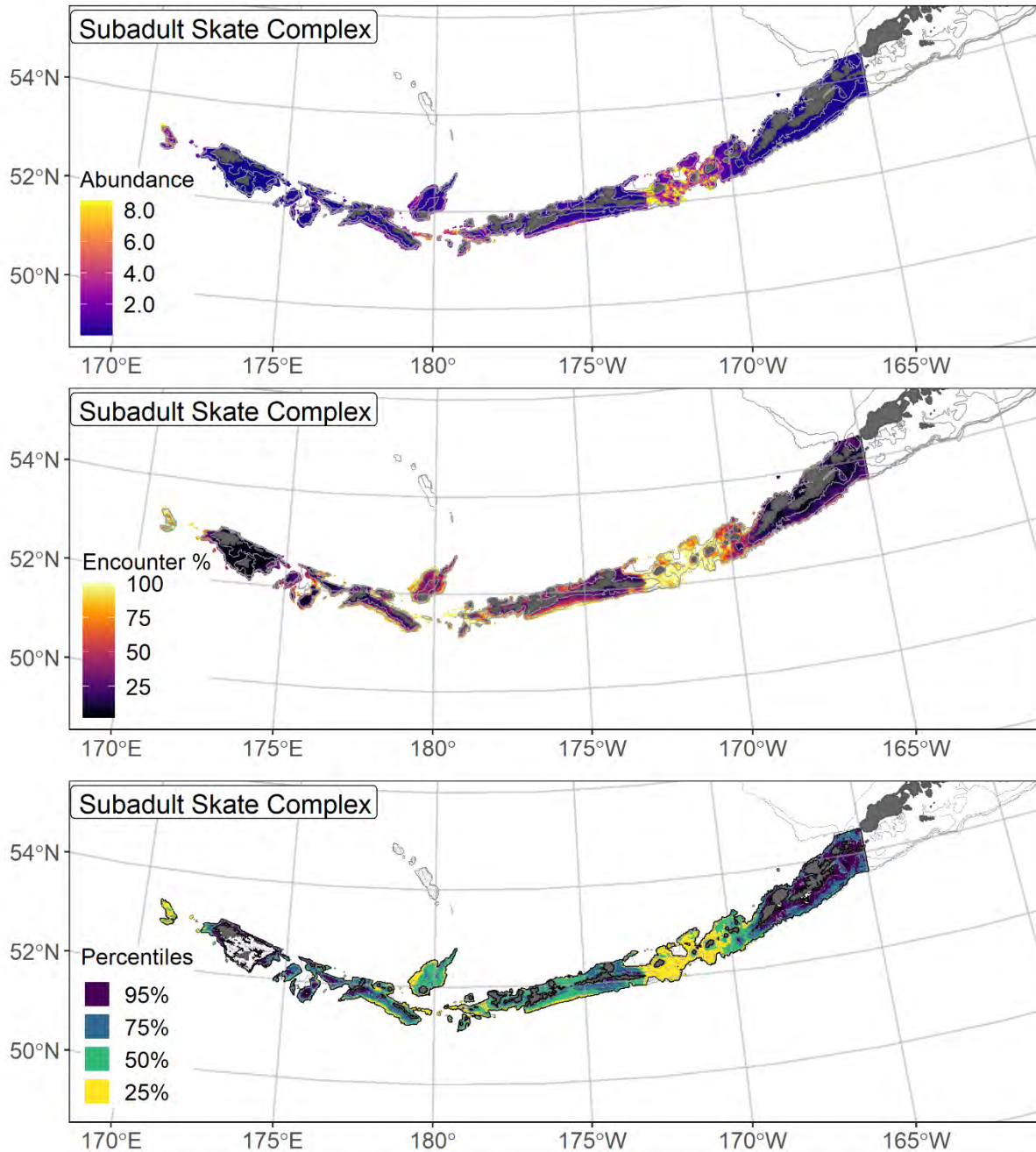
3122 **Subadult Skate Stock Complex abundance and distribution predicted from RACE-GAP summer** 3123 **bottom trawl surveys in the Bering Sea–**

3124 Numerical abundance predictions for four species of subadult skates were combined to estimate
3125 the abundance and EFH of the subadult skate stock complex in the AI (Figure 155). The composite
3126 abundance map was strongly influenced by whiteblotched and mud skates, and the resulting map showed
3127 high numbers of skates around Seguam Pass and the Islands of Four Mountains. Amchitka Pass and
3128 Stalemate Bank were predicted to have moderately high skate abundance, and Amchitka Pass contained
3129 EFH hot spots for all four species. Some areas of high abundance also occurred along the continental
3130 slope south of Adak Island, which was important habitat for mud skates and Aleutian skates. Subadult
3131 Alaska skate were rarely encountered in the AI and made a minimal contribution to the complex map.
3132 Encounter probabilities for subadults in the skate complex were high in the areas described above, and

3133 generally tended to be high in most areas with a moderate depth. The EFH areas for subadults in this
3134 complex followed the same pattern, with most of the core EFH and EFH hot spot subareas located further
3135 from shore along the continental slope.

3136 **Adult Skate Stock Complex abundance and distribution predicted from RACE-GAP summer**
3137 **bottom trawl surveys in the Bering Sea –**

3138 Numerical abundance predictions for four species of adult skates were combined to estimate the
3139 abundance and EFH of the adult skate stock complex in the AI (Figure 156). The map for the adult skate
3140 complex in the AI was very similar to the map for subadults. This map was consistent with the SDMs for
3141 the individual species which also predicted only minor differences in habitat usage between adults and
3142 subadults. The composite abundance map was dominated by whiteblotched skates, and the resulting
3143 complex map was very similar to the map of whiteblotched skate abundance (Figure 182). Notably, this
3144 included the area around Seguam Pass and to the east. Some areas of high abundance also occurred
3145 further to the west along the slope. Alaska skate abundance was more influential in the adult skate
3146 complex map, as it was more likely to be found in shallower water as an adult, unlike Aleutian and mud
3147 skates. Encounter probabilities for adults in the skate complex were high in Seguam Pass, as well as some
3148 areas around Petrel Bank, Amchitka Pass, and Stalemate Bank. Unlike subadults, adult encounter
3149 probability was not notably higher in the deeper water along the continental slope. This was likely an
3150 effect of the species included in the complex, as older Alaska and whiteblotched skates were more
3151 common in these shallower habitats, whereas adult Aleutian skate and mud skate were common in deeper
3152 waters but were less abundant in the survey. The EFH map for adults in this complex reflected the areas
3153 of high abundance described above.



3154

3155 Figure 155. Composite predicted numerical abundance (top panel), encounter probability (middle panel),

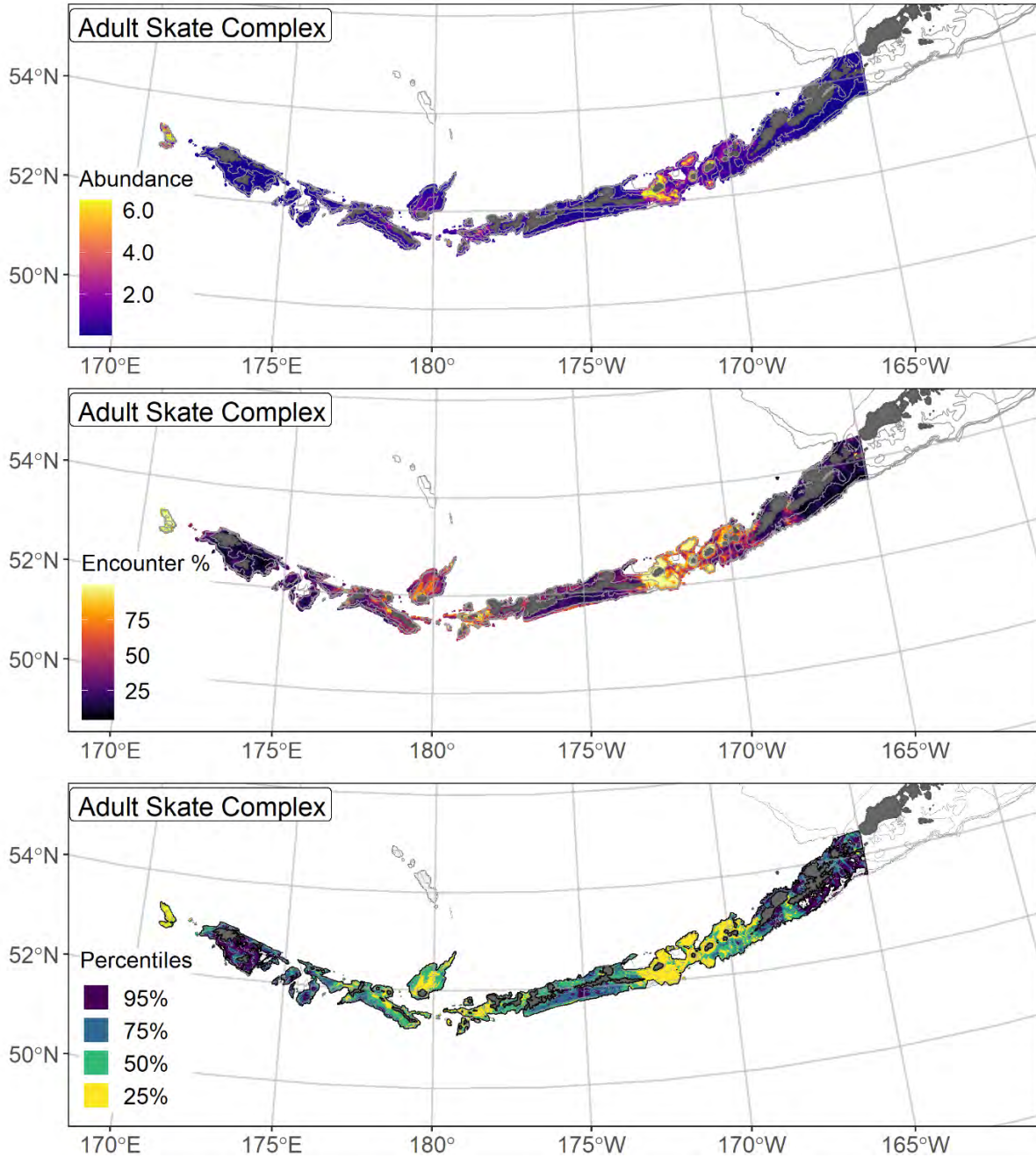
3156 and essential fish habitat (bottom panel) of subadult skates from the Aleutian Islands collected in AFSC

3157 RACE-GAP summer bottom trawl surveys (1991–2019) with 100 m, 300 m, and 500 m isobaths

3158 indicated. EFH defined as the top 95% of numerical abundance predictions above a presence threshold,

3159 and integral to the EFH map are the shapes of the top 25% (EFH hot spots), top 50% (core EFH area), and

3160 top 75% (principal EFH area) of habitat-related, ensemble-predicted numerical abundance.



3161
 3162 Figure 156. Composite predicted numerical abundance (top panel), encounter probability (middle panel),
 3163 and essential fish habitat (bottom panel) of adult skates from Aleutian Islands collected in AFSC RACE-
 3164 GAP summer bottom trawl surveys (1991–2019) with 100 m, 300 m, and 500 m isobaths indicated. EFH
 3165 defined as the top 95% of numerical abundance predictions above a presence threshold, and integral to the
 3166 EFH map are the shapes of the top 25% (EFH hot spots), top 50% (core EFH area), and top 75%
 3167 (principal EFH area) of habitat-related, ensemble-predicted numerical abundance.

3168 **Alaska skate (*Bathyraja parmifera*)**

3169 The Alaska skate (*Bathyraja parmifera*) is a large, shallow water skate (Ebert 2005,
3170 Stevenson et al. 2007) that is common throughout shallow to moderate depths in the AI RACE-GAP
3171 summer bottom trawl surveys. Hoff (2008) determined that reproductive activity for this species in the
3172 EBS occurs primarily at several defined nursery areas. Similar locations have not been located in the AI
3173 region, but this species prefers areas between 150 m and 300 m in depth near the slope/shelf interface in
3174 the EBS. The Alaska skate grows to fairly large sizes and attains a maximum length of at least 1350 mm
3175 (Stevenson et al. 2007). Subadults (≤ 930 mm T.L.) were distinguished from adults (> 930 mm T.L.)
3176 based on L_{50} (Matta and Gunderson 2007). The Aleutian Islands are also home to the endemic leopard
3177 skate (*Bathyraja panthera*), which is similar in appearance to Alaska skate. Prior to 2006, the survey data
3178 reflects a mix of these two species, and therefore only data for Alaska skate from 2006-2019 are modeled
3179 here. Alaska skate are managed in a complex with several other species and while they are the dominant
3180 species in the BSAI, they are a smaller component of the more diverse skate assemblage found in the
3181 Aleutian Islands (Ormseth 2020).

3182 **Subadult Alaska skate distribution and predicted abundance from RACE-GAP summer bottom**
3183 **trawl surveys in the Aleutian Islands–**

3184 Subadult Alaska skate catches from the RACE-GAP summer survey of the AI were somewhat
3185 rare (N=102, Figure 157). The highest density catches were located in the central AI. The final ensemble
3186 contained three SDMs with approximately equal weights, and it demonstrated poor to fair performance
3187 overall (Table 45). The ensemble performed well at discriminating presence and absence (AUC = 0.791),
3188 but had a poor fit to the abundance data ($\rho = 0.192$) and explained only a fair amount of the deviance
3189 (PDE = 0.241). The ability of the SDMs to fit the data was probably impaired by the relatively small
3190 amount of data available, since records before 2006 are confounded with *B. panthera*. Geographic
3191 position, bottom depth, bottom current, and slope, and slope aspect were the most important covariates
3192 and accounted for 90.8% of the deviance explained by the ensemble (Table 46). In general, high

3193 abundance was predicted by being located in the central part of the AI, in shallow depths, with weak
3194 bottom currents, and steep terrain oriented towards the northeast (Figure 158). Predicted abundance was
3195 low overall, but was highest in the central part of the islands, between Atka and Adak Islands, and tended
3196 to be higher on the northern side of the islands facing the Bering Sea. The CV of abundance for ensemble
3197 predictions was highest in the east near Unalaska Island and Unimak Pass. Predicted encounter
3198 probability was generally low except around the central AI (Figure 159).

3199 **Adult Alaska skate distribution and predicted abundance from RACE-GAP summer bottom trawl**
3200 **surveys in the Aleutian Islands –**

3201 Adult Alaska skate catches from the RACE-GAP summer survey were uncommon throughout
3202 much of the Aleutian Islands, with the highest density catches located in the central AI (Figure 160). The
3203 final ensemble contained four SDMS which were weighted about equally and displayed fair predictive
3204 ability overall (Table 45). More specifically, the ensemble was a good predictor of the presence of adult
3205 Alaska skate in a catch (AUC = 0.817), showed a fair fit to the observed abundance data ($\rho = 0.251$), and
3206 provided a fair reduction in the overall deviance (PDE = 0.265). Together, these metrics indicated that the
3207 ensemble can provide general predictions about the presence of adults, but they may not accurately
3208 estimate abundance. Due to taxonomic issues with Alaska and leopard skates, only seven survey years of
3209 data were available, and these findings should be considered temporary until additional data are available.
3210 A variety of covariates were important to the model, including geographic position, bottom depth, current,
3211 current variability, slope, and BPI (Table 46). Adult Alaska skates were predicted to be abundant at
3212 shallow depths near 180° longitude (Figure 161). The ensemble also predicted high abundance in areas
3213 with variable northerly currents and terrain with valleys or similar features. Predicted abundance was
3214 highest in the central AI and above the 100 m depth contour. The predicted CV of abundance was mostly
3215 uniform. Adult Alaska skates encounter probability was usually highest close to shore and close to zero in
3216 most places greater than 300 m depth (Figure 162).

3217 **Essential fish habitat of subadult and adult Alaska skate in the Aleutian Islands –**

3218 The habitat related abundance predictions based on RACE-GAP summer bottom trawl data
3219 (2006–2019) were translated into EFH area and subareas (Figure 163). The EFH area for subadult Alaska
3220 skate encompassed most shallow areas between 174° W and 179° E. EFH hot spots occurred around
3221 Petrel Bank and the Andreanof Islands. The adult EFH area was larger and included all the areas of the
3222 subadult life stage, as well as the regions around Attu Island and Unalaska Island. In summary, while both
3223 life stages showed a strong association with shallow water, subadults are confined to a subset of the
3224 suitable terrain, whereas adults appear to occupy almost all areas less than 200 m deep.

3225 Table 45. Constituent species distribution models (SDMs) used to construct Essential Fish Habitat (EFH)
 3226 for a) subadult and b) adult Alaska skate: MaxEnt = Maximum entropy; paGAM = presence-absence
 3227 generalized additive model; hGAM = hurdle GAM; GAM_p = standard Poisson GAM; and
 3228 GAM_{nb} = standard negative-binomial GAM. Ensemble performance (ρ = Spearman's rank correlation
 3229 coefficient), root-mean-square-error (RMSE), the area under the receiver operating characteristic (AUC),
 3230 and the Poisson deviance explained (PDE) were generated from k-fold cross-validation. The "--" in a field
 3231 indicates that this SDM was not included in the final ensemble.

3232 **a) subadult Alaska skate**

Models	RMSE	Relative Weight	ρ	AUC	PDE	EFH area (km²)
MaxEnt	--	0	--	--	--	--
paGAM	0.431	0.338	0.197	0.797	0.208	25,900
hGAM	0.439	0.326	0.188	0.792	0.250	25,700
GAM _p	0.433	0	--	--	--	--
GAM _{nb}	0.431	0.337	0.186	0.781	0.223	27,300
ensemble	0.423	1	0.192	0.791	0.241	26,500

3233 **b) adult Alaska skate**

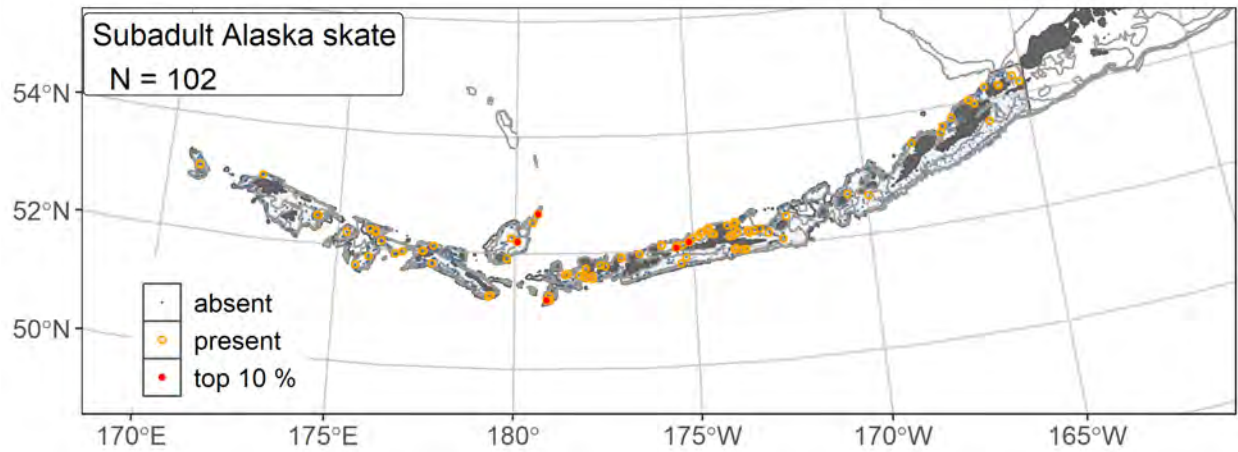
Models	RMSE	Relative Weight	ρ	AUC	PDE	EFH area (km²)
MaxEnt	0.664	0.258	0.254	0.821	0.250	44,600
paGAM	0.659	0.262	0.248	0.814	0.235	48,100
hGAM	0.707	0.228	0.221	0.798	0.235	43,500
GAM _p	0.672	0	--	--	--	--
GAM _{nb}	0.671	0.252	0.235	0.798	0.250	45,300
ensemble	0.650	1	0.251	0.817	0.265	48,600

3234

3235 Table 46. Covariates retained in the a) subadult and b) adult Alaska skate species distribution model
 3236 (SDM) final ensembles, the percent contribution to the ensemble deviance explained by each, and the
 3237 cumulative percent deviance: SD = standard deviation, and BPI = bathymetric position index.

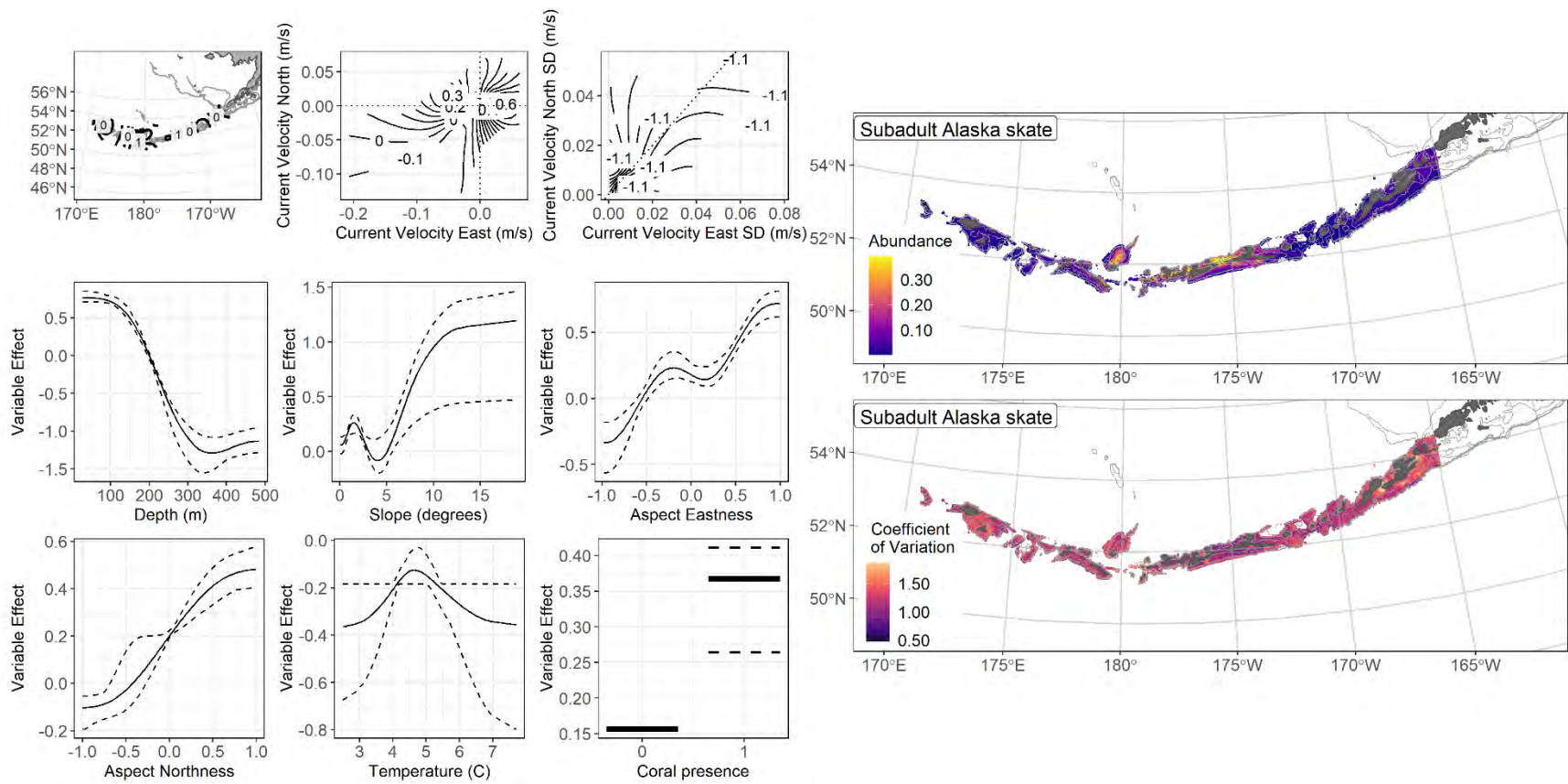
Alaska skate	Covariate	% Contribution	Cumulative % Contribution
a) subadult	position	34.0	34.0
	bottom depth	17.4	51.4
	aspect east	11.1	62.5
	current	9.8	72.3
	aspect north	9.6	81.9
	slope	8.9	90.8
	current SD	2.1	92.9
	coral presence	1.9	94.8
	bottom temperature	1.6	96.4
	pennatulacean presence	1.0	97.4
	rockiness	0.9	98.3
	curvature	0.7	99.0
	BPI	0.7	99.7
	sponge presence	0.3	100
tidal maximum	0	100	
a) adult	bottom depth	28.8	28.8
	position	9.5	38.2
	current	8.7	46.9
	current SD	7.6	54.5
	BPI	7.6	62.2
	slope	7.5	69.7
	tidal maximum	4.7	74.4
	coral presence	4.1	78.5
	aspect east	4.0	82.5
	curvature	3.8	86.3
	aspect north	3.5	89.8
	pennatulacean presence	3.0	92.7
	bottom temperature	2.6	95.3
	rockiness	2.3	97.7
	sponge presence	2.3	100

3238



3239

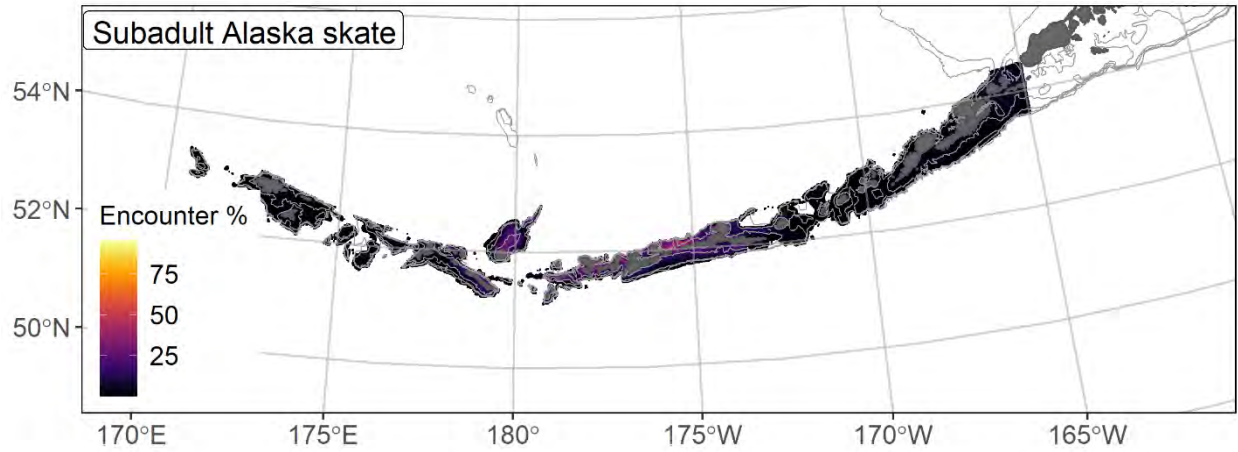
3240 Figure 157. Distribution of subadult Alaska skate catches (N = 102) in 2006–2019 AFSC RACE-GAP
 3241 summer bottom trawl surveys of the Aleutian Islands with the 100 m, 300 m, and 500 m isobaths
 3242 indicated; filled red circles indicate catches in top 10% of overall abundance, open orange circles indicate
 3243 presence in remaining catches, and small blue dots indicate absence.



3244

3245 Figure 158. The top nine covariate effects (left panel) on ensemble-predicted subadult Alaska skate numerical abundance across the Aleutian

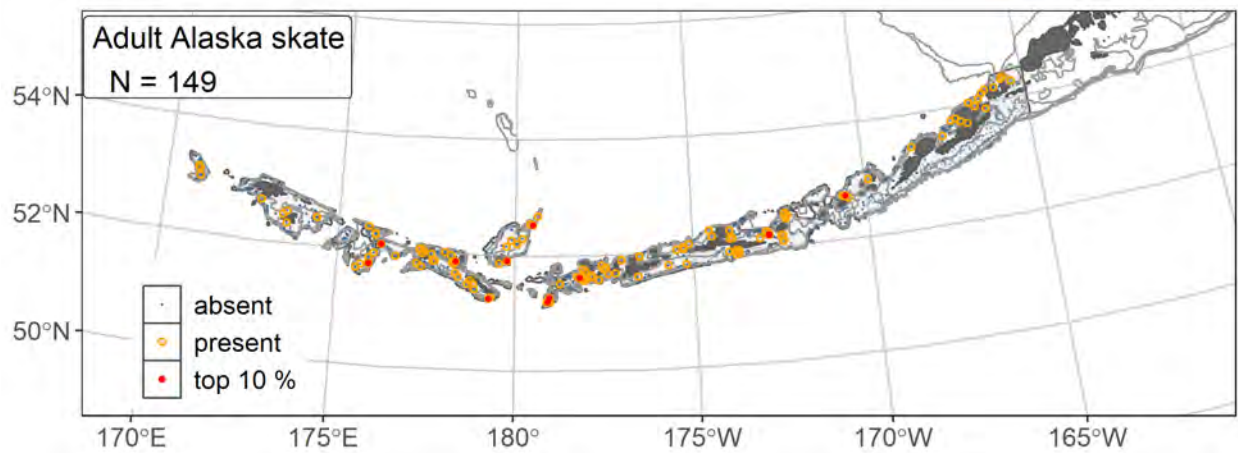
3246 Islands (upper right panel) alongside the coefficient of variation of the ensemble predictions (lower right panel).



3247

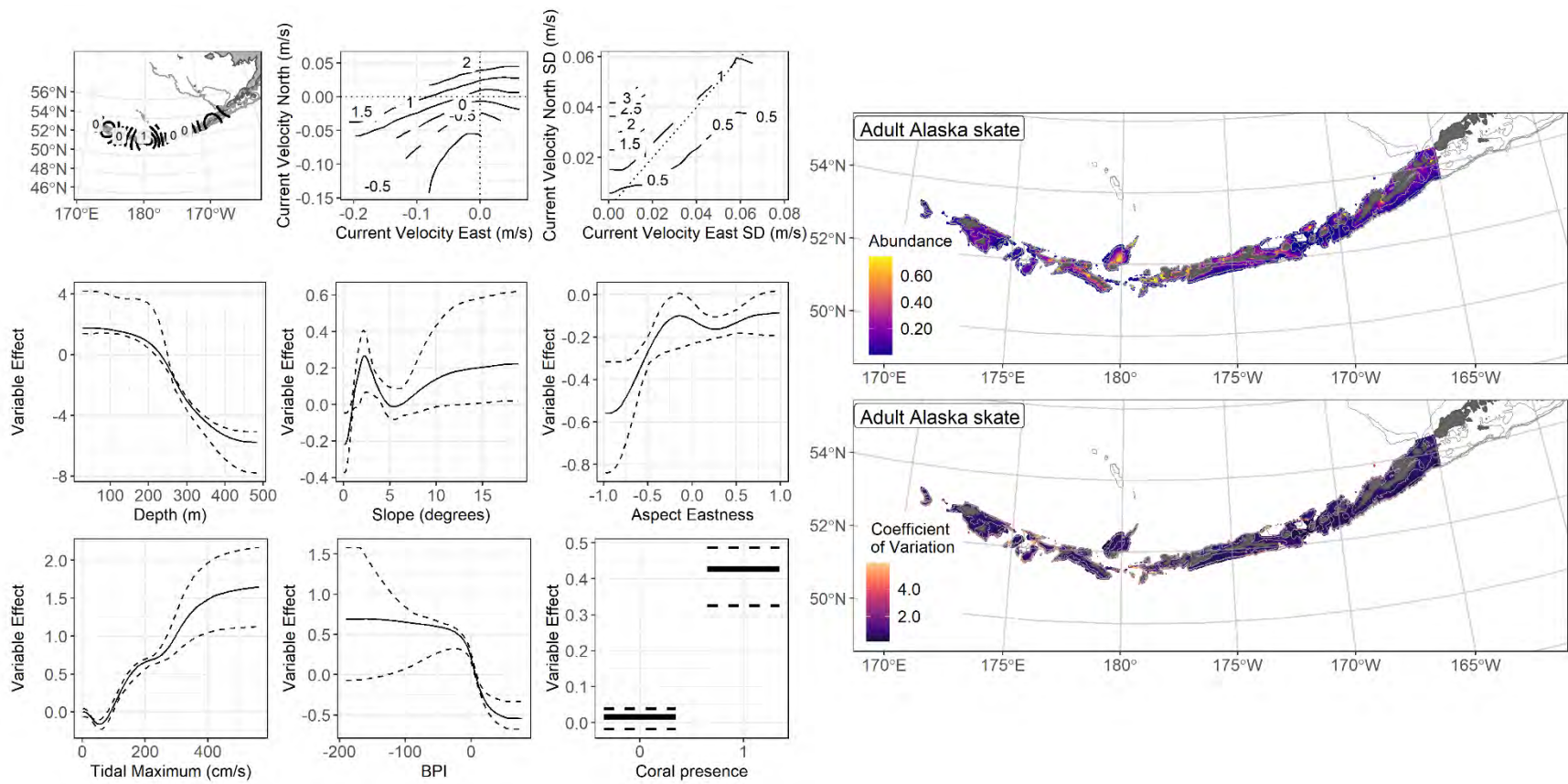
3248 Figure 159. Encounter probability of subadult Alaska skate from AFSC RACE-GAP summer bottom
 3249 trawl surveys (2006–2019) of the Aleutian Islands with the 100 m, 300 m, and 500 m isobaths indicated.

3250



3251

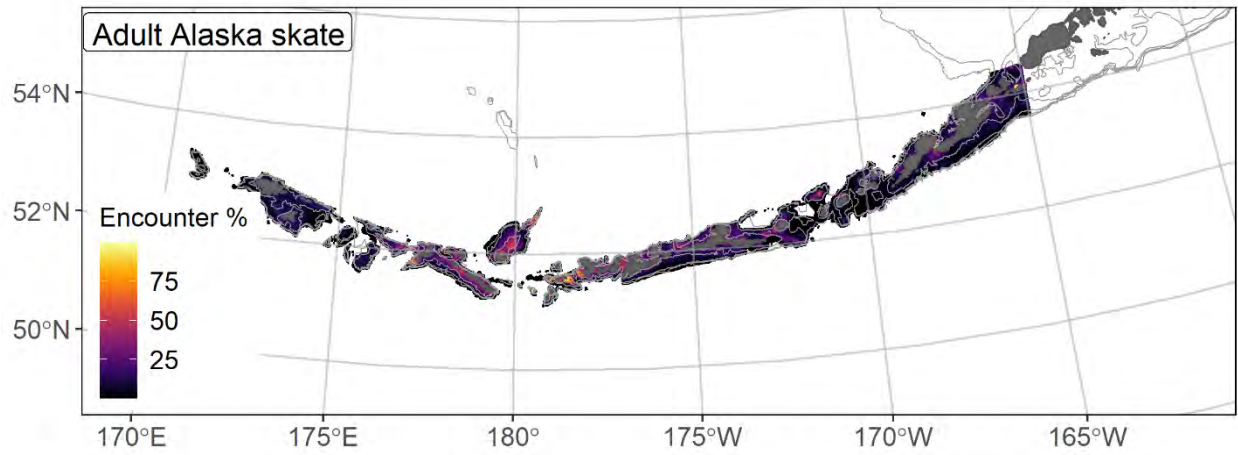
3252 Figure 160. Distribution of adult Alaska skate catches (N = 149) in 2006–2019 AFSC RACE-GAP
 3253 summer bottom trawl surveys of the Aleutian Islands with the 100 m, 300 m, and 500 m isobaths
 3254 indicated; filled red circles indicate catches in top 10% of overall abundance, open orange circles indicate
 3255 presence in remaining catches, and small blue dots indicate absence.



3256

3257 Figure 161. The top nine covariate effects (left panel) on ensemble-predicted adult Alaska skate numerical abundance across the Aleutian Islands

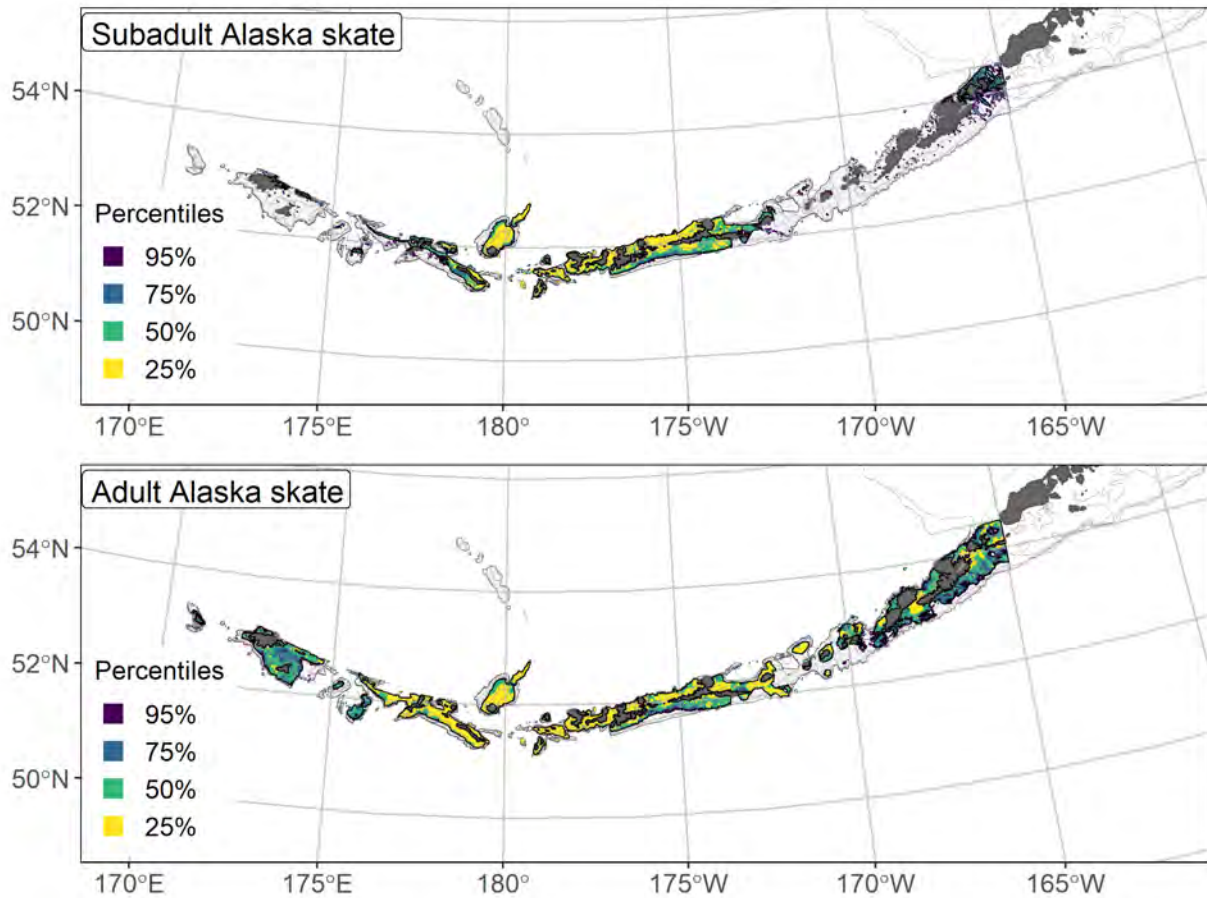
3258 (upper right panel) alongside the coefficient of variation of the ensemble predictions (lower right panel).



3259

3260 Figure 162. Encounter probability of adult Alaska skate from AFSC RACE-GAP summer bottom trawl

3261 surveys (2006–2019) of the Aleutian Islands with the 100 m, 300 m, and 500 m isobaths indicated.



3262
 3263 Figure 163. Essential fish habitat (EFH area) defined as the top 95% of numerical abundance predictions
 3264 from a habitat-based ensemble fitted to subadult (top) and adult (bottom) Alaska skate distribution and
 3265 abundance in AFSC RACE-GAP summer bottom trawl surveys (2006–2019) with 100 m, 300 m, and
 3266 500 m isobaths indicated; internal to the EFH map are the subareas of the top 25% (EFH hot spots), top
 3267 50% (core EFH area), and top 75% (principal EFH area) of habitat related, ensemble-predicted numerical
 3268 abundance.

3269 **Aleutian skate (*Bathyraja aleutica*)**

3270 The Aleutian skate (*Bathyraja aleutica*) is a large (161 cm T.L. maximum length) species that
3271 ranges from the Gulf of Alaska and Aleutian Islands into the Bering Sea. This species is found over a
3272 wide range of depths (29–950 m; Stevenson et al. 2007), and in the RACE-GAP bottom trawl surveys of
3273 the AI, they are found at moderate depths in most of the island chain (Hoff 2009). Aleutian skates mature
3274 slowly and do not reproduce until attaining a large size (> 1320 mm T.L.), depositing their egg sacs in
3275 distinct nursery grounds (Ebert et al. 2007, Haas et al. 2016). Aleutian skates are among the most
3276 abundant skates in RACE-GAP AI bottom trawl surveys and are managed in aggregate as part of the
3277 skate complex across the BSAI region (Ormseth 2020). Aleutian skates were not routinely identified to
3278 species until 1999, so these models exclude data collected before that year.

3279 **Subadult Aleutian skate distribution and predicted abundance from RACE-GAP summer bottom**
3280 **trawl surveys in the Aleutian Islands–**

3281 Subadult Aleutian skate catches were somewhat common and evenly distributed across the
3282 RACE-GAP summer survey areas (Figure 164). There was no particular spatial pattern to large catches,
3283 and the majority of hauls in which the species was present contained a single individual. The final
3284 ensemble contained three SDMs with equal weights, and it demonstrated poor to fair performance
3285 (Table 47). The ensemble showed fair performance in two of the three metrics ($\rho = 0.242$, AUC = 0.744),
3286 but displayed poor performance in terms of deviance explained (PDE = 0.186). Taken together, this
3287 suggests that the ensemble was only able to predict some general patterns in the presence and abundance
3288 of subadult Aleutian skates, and it did not explain much of the variation in observed abundance.
3289 Geographic position and bottom depth were the most important covariates and accounted for 52.0% of the
3290 deviance explained (Table 48), though current covariates and bottom temperature also contributed. In
3291 general, high abundance was predicted by in deeper water and with warmer temperatures (Figure 165).
3292 Though important to the models, geographic position and current did not show a clear trend. Predicted
3293 abundance was highest in the areas west and south of Adak Island, though subadult Aleutian skates were

3294 predicted in lesser abundance along most slope areas (Figure 165). The predicted CV of abundance was
3295 fairly uniform across most of the AI region (Figure 165). Although not rare, encounter probabilities for
3296 Aleutian skate were fairly low, except in the region near Adak Island, reflecting that this species was not
3297 caught in large numbers (Figure 166).

3298 **Adult Aleutian skate distribution and predicted abundance from RACE-GAP summer bottom**
3299 **trawl surveys in the Aleutian Islands –**

3300 Adult Aleutian skate catches were somewhat common and evenly distributed across the RACE-
3301 GAP summer survey areas (Figure 167). The slopes around Attu Island produced several large catches,
3302 but other areas in the AI region showed no obvious pattern. The final ensemble consisted of three SDMs
3303 with equal weights, but showed a poor fit to the data (Table 47). The ensemble managed to produce fair
3304 estimates of presence and relative abundance ($AUC = 0.759$, $\rho = 0.203$), but performed poorly with
3305 respect to deviance explained ($PDE = 0.173$). Overall, this model provided a preliminary picture of
3306 Aleutian skate distribution, but it should be used with caution until more data and better predictions are
3307 available. Aleutian skates are known to inhabit deep water environments (Hoff 2009), but the RACE-
3308 GAP survey of the AI only covered depths up to 500 m, meaning that a portion of this population might
3309 not have been adequately sampled in the current dataset. Bottom depth, current, geographic position, and
3310 tidal maximum were the most important covariates, accounting for 78.9% of the deviance explained in the
3311 ensemble (Table 48). Aleutian skates were predicted to be abundant in both moderate and deeper water at
3312 various locations, and with easterly currents and a low tidal maximum (Figure 168). Predicted abundance
3313 was highest around Attu Island, though several pockets of above average abundance existed elsewhere
3314 (Figure 168). The predicted CV of abundance was uniform across most of the AI region (Figure 168).
3315 Encounter probabilities for Aleutian skate were fairly low throughout the region (Figure 169).

3316 **Essential fish habitat of subadult and adult Aleutian skate in the Aleutian Islands –**

3317 The habitat related abundance predictions based on RACE-GAP summer bottom trawl data
3318 (1999–2019) were translated into EFH area and subareas (Figure 170). The EFH area for subadult
3319 Aleutian skate was larger than that of adults, and had a large continuous hot spot along the continental
3320 slope south of Adak Island. Subadults were also distinguished by having a large section of EFH core
3321 habitat near Unimak Pass. By contrast, the EFH for adults was discontinuous, with several patches
3322 scattered around the AI. Some areas were EFH for both life stages, such as the area around Attu Island.
3323 Both life stages showed a bimodal relationship with bottom depth with a peak in predicted abundance at
3324 the edge of the sampled depth range (Figure 165 and Figure 168). It is possible that a portion of the
3325 population for each life stage is located deeper than 500 m and is not sampled by the RACE-GAP bottom
3326 trawl survey.

3327 Table 47. Constituent species distribution models (SDMs) used to construct Essential Fish Habitat (EFH)
 3328 for a) subadult and b) adult Aleutian skate: MaxEnt = Maximum entropy; paGAM = presence-absence
 3329 generalized additive model; hGAM = hurdle GAM; GAM_p = standard Poisson GAM; and
 3330 GAM_{nb} = standard negative-binomial GAM. Ensemble performance (ρ = Spearman's rank correlation
 3331 coefficient), root-mean-square-error (RMSE), the area under the receiver operating characteristic (AUC),
 3332 and the Poisson deviance explained (PDE) were generated from k-fold cross-validation. The "--" in a field
 3333 indicates that this SDM was not included in the final ensemble.

3334 **a) subadult Aleutian skate**

Models	RMSE	Relative Weight	ρ	AUC	PDE	EFH area (km²)
MaxEnt	--	0	--	--	--	--
paGAM	0.625	0.334	0.251	0.755	0.151	56,200
hGAM	0.626	0.333	0.228	0.746	0.183	56,300
GAM _p	0.626	0.333	0.230	0.732	0.192	48,000
GAM _{nb}	0.626	0	--	--	--	--
ensemble	0.610	1	0.242	0.744	0.186	54,400

3335 **b) adult Aleutian skate**

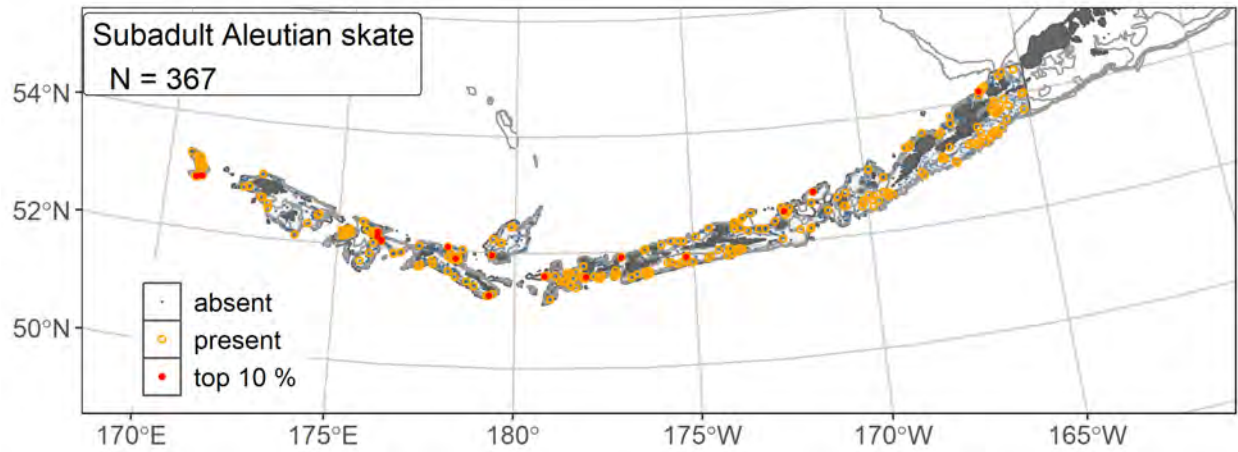
Models	RMSE	Relative Weight	ρ	AUC	PDE	EFH area (km²)
MaxEnt	0.361	0.329	0.187	0.741	0.117	27,200
paGAM	0.358	0.335	0.188	0.743	0.151	22,700
hGAM	--	0	--	--	--	--
GAM _p	0.358	0.335	0.192	0.742	0.188	21,200
GAM _{nb}	0.358	0	--	--	--	--
ensemble	0.351	1	0.203	0.759	0.173	24,200

3336

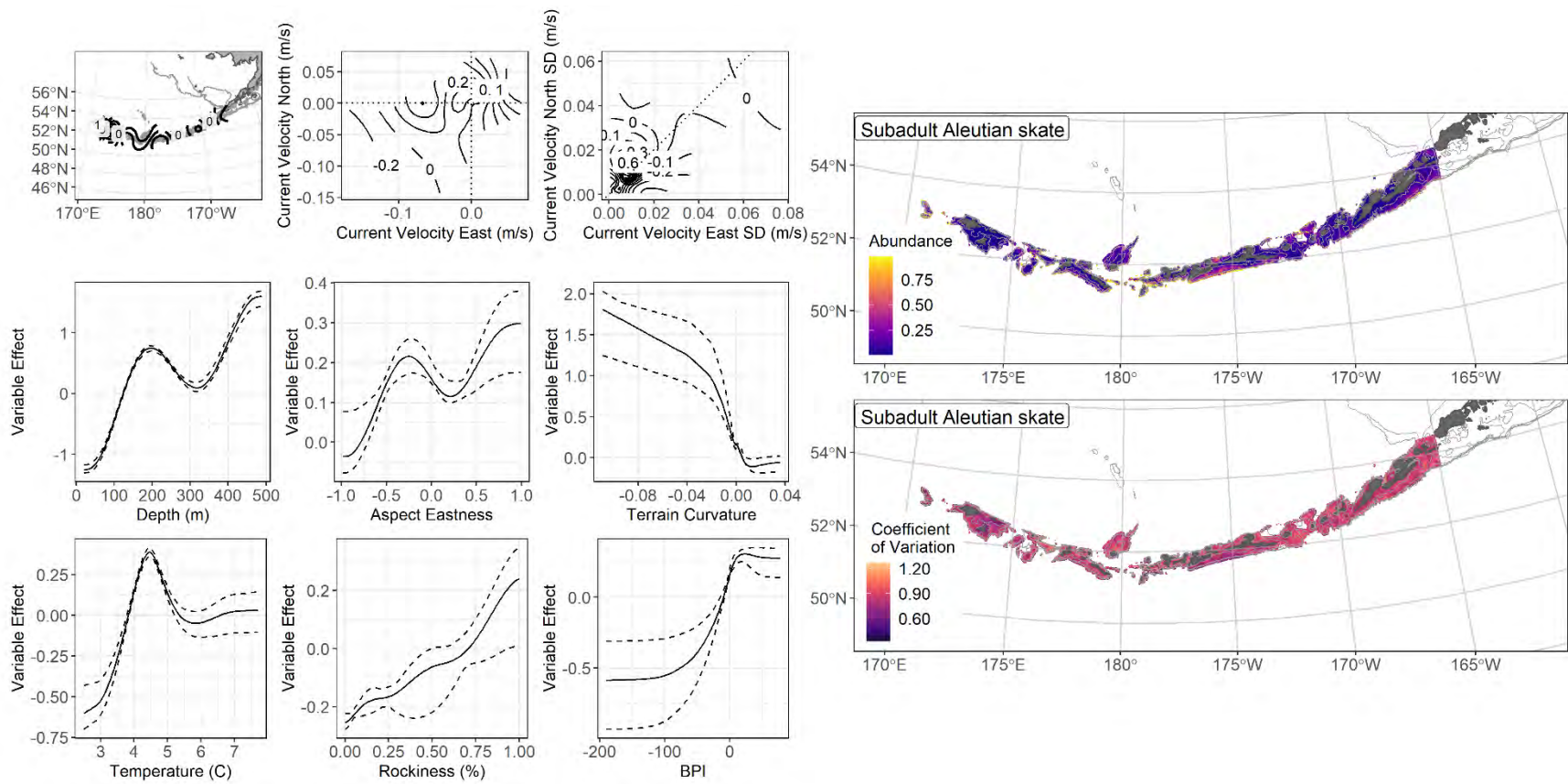
3337 Table 48. Covariates retained in the a) subadult and b) adult Aleutian skate species distribution model
 3338 (SDM) final ensembles, the percent contribution to the ensemble deviance explained by each, and the
 3339 cumulative percent deviance: SD = standard deviation, and BPI = bathymetric position index.

Aleutian skate	Covariate	% Contribution	Cumulative % Contribution
a) subadult	position	28.7	28.7
	bottom depth	23.3	52.0
	current	10.8	62.8
	current SD	10.4	73.2
	bottom temperature	6.3	79.5
	curvature	4.6	84.1
	BPI	3.7	87.8
	rockiness	3.0	90.8
	aspect east	2.9	93.7
	tidal maximum	2.5	96.2
	slope	2.1	98.3
	aspect north	0.7	99.0
	coral presence	0.6	99.6
	sponge presence	0.3	99.9
pennatulacean presence	0.1	100	
a) adult	bottom depth	25.6	25.6
	current	24.8	50.5
	position	18.2	68.7
	tidal maximum	10.2	78.9
	current SD	5.6	84.5
	rockiness	4.6	89.1
	aspect north	2.2	91.3
	aspect east	2.1	93.4
	BPI	2.0	95.4
	bottom temperature	1.5	96.9
	pennatulacean presence	1.1	98.0
	curvature	1.1	99.1
	slope	0.7	99.8
	coral presence	0.2	100

3340



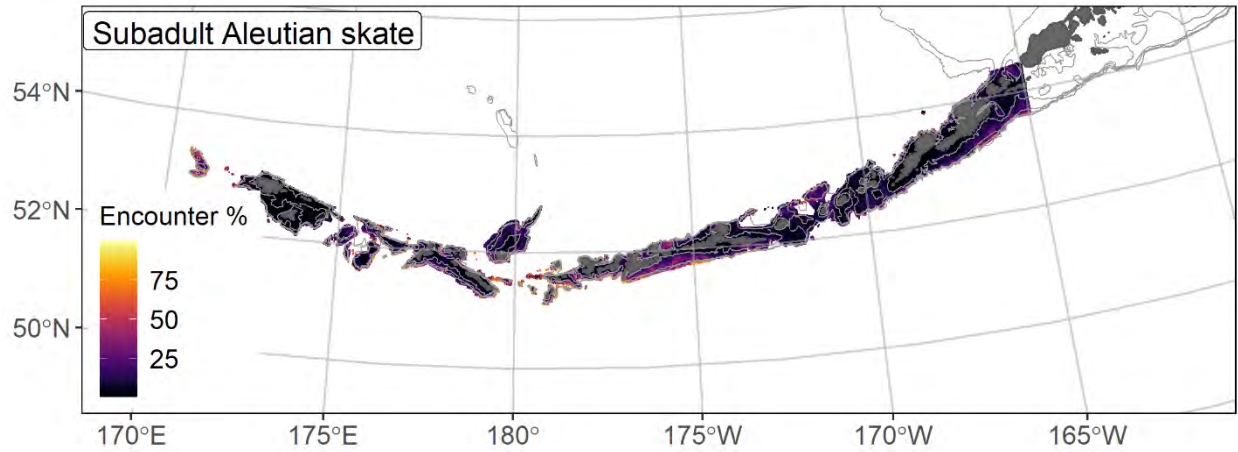
3341
3342 Figure 164. Distribution of subadult Aleutian skate catches (N = 367) in 1999–2019 AFSC RACE-GAP
3343 summer bottom trawl surveys of the Aleutian Islands with the 100 m, 300 m, and 500 m isobaths
3344 indicated; filled red circles indicate locations in top 10% of overall abundance, open orange circles
3345 indicate presence in remaining catches, and small blue dots indicate absence.



3346

3347 Figure 165. The top nine covariate effects (left panel) on ensemble-predicted subadult Aleutian skate numerical abundance across the Aleutian

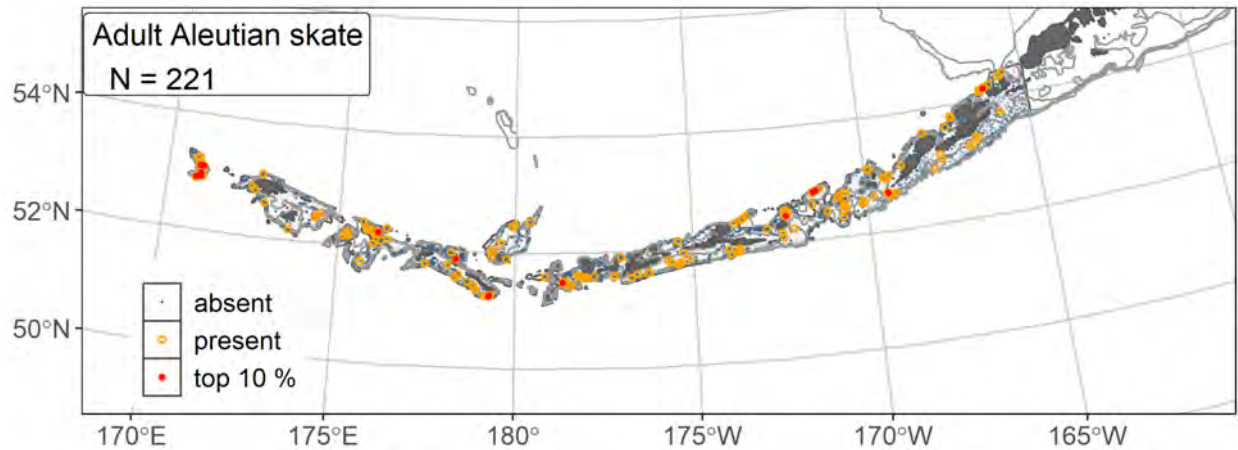
3348 Islands (upper right panel) alongside the coefficient of variation of the ensemble predictions (lower right panel).



3349

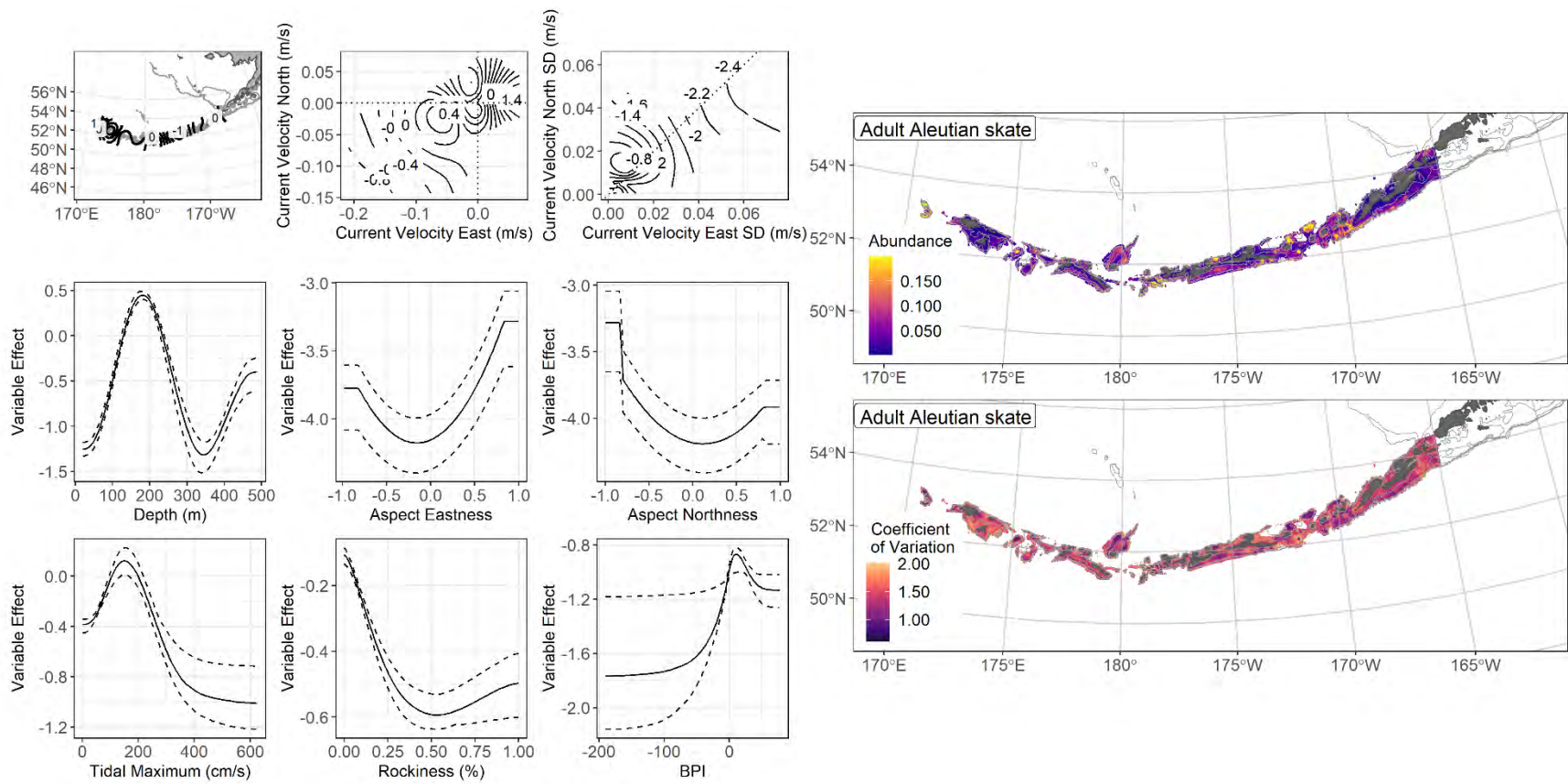
3350 Figure 166. Encounter probability of subadult Aleutian skate from AFSC RACE-GAP summer bottom
 3351 trawl surveys (1999–2019) of the Aleutian Islands with the 100 m, 300 m, and 500 m isobaths indicated.

3352



3353

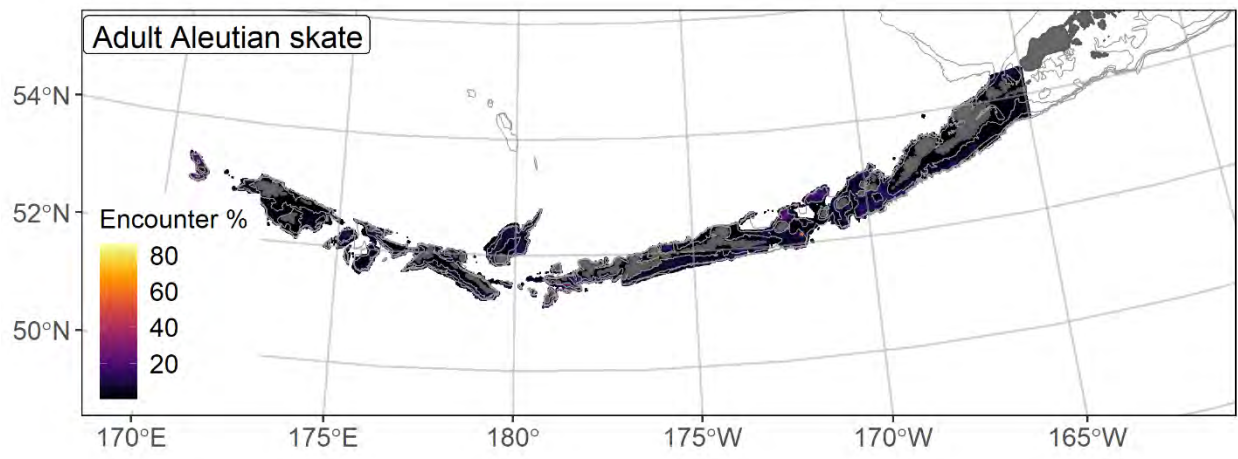
3354 Figure 167. Distribution of adult Aleutian skate catches (N = 221) in 1999–2019 AFSC RACE-GAP
 3355 summer bottom trawl surveys of the Aleutian Islands with the 100 m, 300 m, and 500 m isobaths
 3356 indicated; filled red circles indicate locations in top 10% of overall abundance, open orange circles
 3357 indicate presence in remaining catches, and small blue dots indicate absence.



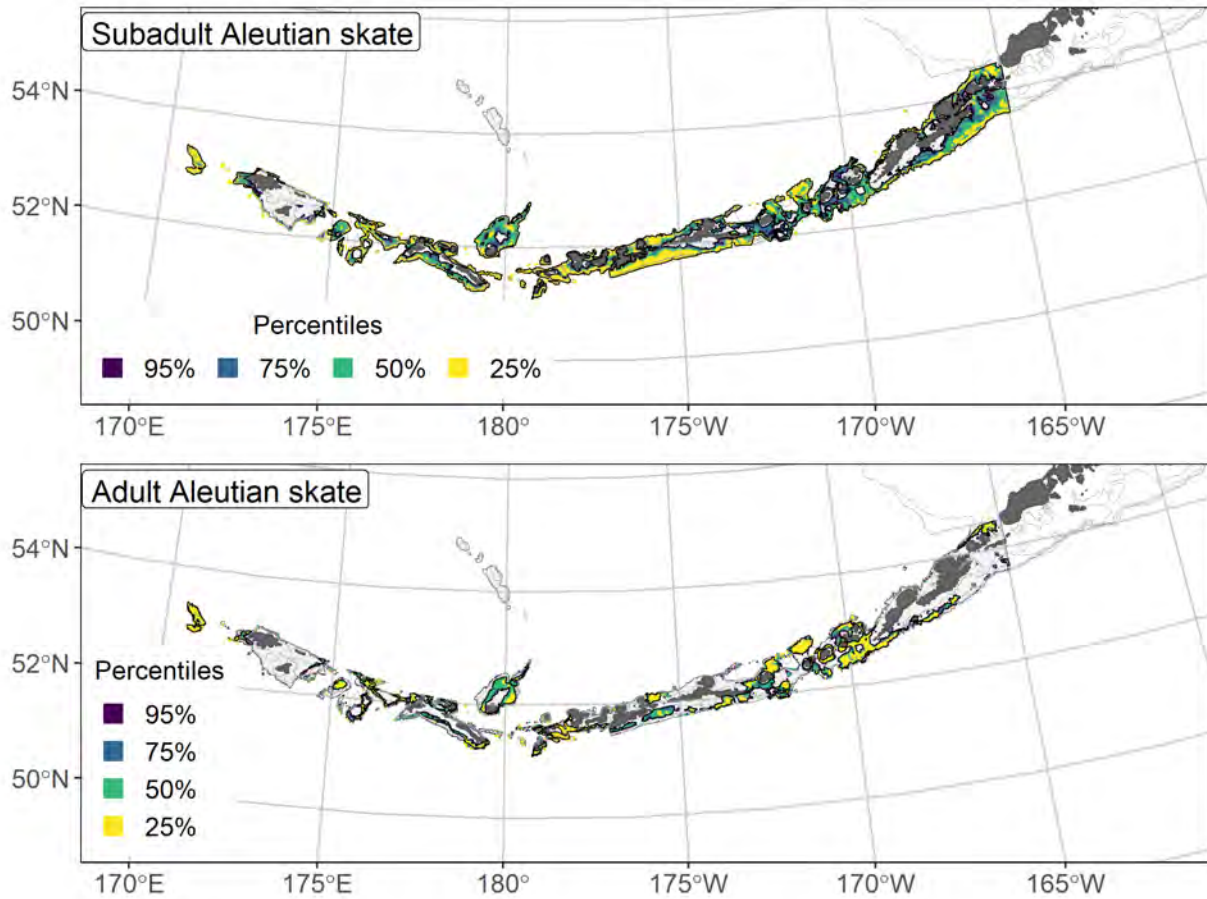
3358

3359 Figure 168. The top nine covariate effects (left panel) on ensemble-predicted adult Aleutian skate numerical abundance across the Aleutian Islands

3360 (upper right panel) alongside the coefficient of variation of the ensemble predictions (lower right panel).



3361
 3362 Figure 169. Encounter probability of adult Aleutian skate from AFSC RACE-GAP summer bottom trawl
 3363 surveys (1999–2019) of the Aleutian Islands with the 100 m, 300 m, and 500 m isobaths indicated.



3364

3365 Figure 170. Essential fish habitat (EFH area) defined as the top 95% of numerical abundance predictions
 3366 from a habitat-based ensemble fitted to subadult (top) and adult (bottom) Aleutian skate distribution and
 3367 abundance in AFSC RACE-GAP summer bottom trawl surveys (1999–2019) with 100 m, 300 m, and
 3368 500 m isobaths indicated; internal to the EFH map are the subareas of the top 25% (EFH hot spots), top
 3369 50% (core EFH area), and top 75% (principal EFH area) of habitat related, ensemble-predicted numerical
 3370 abundance.

3371 **Mud skate (*Bathyraja taranetzi*)**

3372 The mud skate (*Bathyraja taranetzi*) is the smallest species of skate commonly found in Alaskan
3373 waters with a maximum T.L. of 700 mm (Ebert 2005). This species is widely distributed across the north
3374 Pacific and ranges from the western Gulf of Alaska to the Kuril Islands (Stevenson et al. 2007). In RACE-
3375 GAP summer bottom trawl survey catches from the AI, mud skate ranks sixth in skate biomass (Ormseth
3376 2020). Mud skate reach maturity around 595 mm T.L. (Ebert 2005), and Balanov et al. (2021) report the
3377 presence of a mud skate nursery area similar to those located for Alaska skate (*B. parmifera*; Hoff 2008),
3378 though no such locations have been identified in US waters. The preferred habitat for this species is
3379 primarily along the continental slope at depths greater than 200 m (Stevenson et al. 2007). Mud skates are
3380 managed in aggregate as part of the skate complex across the BSAI region (Ormseth 2020). Most skates
3381 of the genus *Bathyraja* were not routinely identified to species until 1999, so these models exclude data
3382 collected before that year.

3383 **Subadult mud skate distribution and predicted abundance from RACE-GAP summer bottom trawl**
3384 **surveys in the Aleutian Islands–**

3385 Subadult mud skates catches were common across the RACE-GAP summer survey areas, with
3386 the largest catches being found in the central AI, approximately between 180° and 170° W (Figure 171).
3387 The final ensemble contained three SDMs with approximately equal weights, and it showed good to
3388 excellent performance when compared to the data (Table 49). Specifically, the ensemble demonstrated
3389 good performance at predicting catches with high vs low abundance ($\rho = 0.456$) and excellent
3390 performance with respect to predicting presence absence (AUC = 0.903) and deviance explained
3391 (PDE = 0.621). The discrepancy between the values for ρ and PDE suggested that many of the errors in
3392 ensemble predictions were minor and that the ensemble predictions are accurate considering the non-
3393 normal distribution of count data. Geographic position, bottom depth, and bottom currents were the most
3394 important covariates and accounted for 61.5 % of the deviance explained, though bottom current variables
3395 and substrate rockiness also contributed (Table 50). In general, high abundance was predicted by

3396 proximity to the central AI, greater bottom depth, and moderate south to southwesterly currents
3397 (Figure 172). Cooler temperatures and a less rocky substrate were also associated with high abundance.
3398 Predicted abundance was highest in the eastern and central Aleutian Islands, particularly around Seguam
3399 Pass, Amchitka Pass, and along the continental slope south of Atka Island (Figure 172). The predicted CV
3400 of abundance was high along slope areas near centers of higher abundance, reflecting variation in high
3401 abundance areas (Figure 172). Encounter probabilities for mud skate were low near shore and high along
3402 continental slope areas described above (Figure 173).

3403 **Adult mud skate distribution and predicted abundance from RACE-GAP summer bottom trawl**
3404 **surveys in the Aleutian Islands –**

3405 Adult mud skate catches were much less common than subadults in the RACE-GAP summer
3406 survey in the AI (Figure 174). Despite being encountered less frequently, the geographic distribution of
3407 adults was very similar to that of subadults, and the greatest number and largest catches occurred in the
3408 eastern and central AI. The final ensemble consisted of four SDMs that were weighted about equally, and
3409 they had a fair fit to the data overall (Table 49). Specifically, the ensemble performed well at
3410 discriminating presence or absence in trawl catches (AUC = 0.817) and showed fair ability to distinguish
3411 between high and low catches and to explain ensemble deviance ($\rho = 0.282$; PDE = 0.258). The
3412 predictions of this ensemble provided a good description of mud skate occurrences in the AI, but
3413 predictions of abundance are likely to contain errors. Bottom depth, geographic position, and slope aspect
3414 were the most important covariates, accounting for 59.1% of the ensemble deviance explained (Table 50),
3415 though bottom current variability, slope angle, and bottom temperature also contributed. Adult mud
3416 skates were predicted to be abundant in deeper waters in the central Aleutians, and were often found on
3417 slopes that ascend in a northerly direction, such as those on the south side of the AI (Figure 175). Like
3418 subadults, adult mud skate were not predicted over rocky substrates, but unlike subadults, they were
3419 associated with areas without strong bottom currents. Predicted abundance was highest in the central part
3420 of the Aleutians, particularly around Amchitka Pass and along the continental slope south of Adak Island

3421 (Figure 175). The predicted CV of abundance was lowest along the continental slope where adult mud
3422 skates were frequently encountered, and higher near shore (Figure 175). Encounter probabilities for adult
3423 mud skate were fairly low throughout the AI region, except in a few places near Adak Island as described
3424 above (Figure 176). Given the association between adult mud skates and deep water and the continental
3425 slope, it is possible that some of the population is located outside of the survey area.

3426 **Essential fish habitat of subadult and adult mud skate in the Aleutian Islands –**

3427 The habitat related abundance predictions based on RACE-GAP summer bottom trawl data
3428 (1999–2019) were translated into EFH area and subareas (Figure 177). The EFH areas for subadult and
3429 adult mud skates were similar, and both life stages have EFH hot spots around Seguam Pass, Amchitka
3430 Pass, and south of Adak Island. In general, subadult EFH included areas in the eastern and central
3431 Aleutian Islands that are deeper than 100 m and along the continental slope. While the EFH maps for the
3432 two life stages were very similar, adults showed a stronger association with greater bottom depths. Like
3433 other species in this genus, and it is possible that part of the population was located too deep for the
3434 RACE-GAP bottom trawl survey to observe.

3435 Table 49. Constituent species distribution models (SDMs) used to construct Essential Fish Habitat (EFH)
 3436 for a) subadult and b) adult mud skate: MaxEnt = Maximum entropy; paGAM = presence-absence
 3437 generalized additive model; hGAM = hurdle GAM; GAM_p = standard Poisson GAM; and
 3438 GAM_{nb} = standard negative-binomial GAM. Ensemble performance (ρ = Spearman's rank correlation
 3439 coefficient), root-mean-square-error (RMSE), the area under the receiver operating characteristic (AUC),
 3440 and the Poisson deviance explained (PDE) were generated from k-fold cross-validation. The "--" in a field
 3441 indicates that this SDM was not included in the final ensemble.

3442 **a) subadult mud skate**

Models	RMSE	Relative Weight	ρ	AUC	PDE	EFH area (km ²)
MaxEnt	--	0	--	--	--	--
paGAM	2.47	0.320	0.459	0.907	0.508	39,600
hGAM	2.47	0.321	0.451	0.906	0.622	31,300
GAM _p	2.33	0.359	0.451	0.895	0.628	30,100
GAM _{nb}	2.47	0	--	--	--	--
ensemble	2.08	1	0.456	0.903	0.621	34,200

3443 **b) adult mud skate**

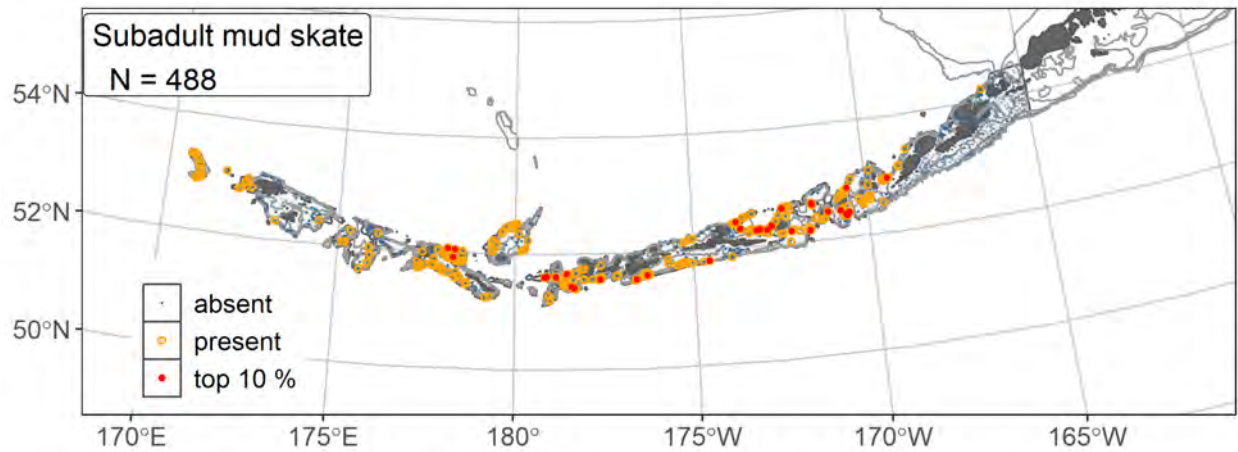
Models	RMSE	Relative Weight	ρ	AUC	PDE	EFH area (km ²)
MaxEnt	0.432	0.245	0.258	0.792	0.204	35,900
paGAM	0.428	0.250	0.276	0.811	0.234	38,800
hGAM	0.425	0.254	0.274	0.811	0.254	36,000
GAM _p	0.427	0.251	0.279	0.814	0.269	32,300
GAM _{nb}	0.429	0	--	--	--	--
ensemble	0.414	1	0.282	0.817	0.258	36,700

3444

3445 Table 50. Covariates retained in the a) subadult and b) adult mud skate species distribution model (SDM)
 3446 final ensembles, the percent contribution to the ensemble deviance explained by each, and the cumulative
 3447 percent deviance: SD = standard deviation, and BPI = bathymetric position index.

mud skate	Covariate	% Contribution	Cumulative % Contribution
a) subadult	bottom depth	34.9	34.9
	position	26.7	61.5
	current SD	7.7	69.2
	current	6.7	75.9
	rockiness	6.4	82.3
	slope	3.8	86.1
	bottom temperature	3.5	89.6
	curvature	2.9	92.5
	aspect north	2.3	94.8
	aspect east	1.6	96.4
	BPI	1.5	97.9
	sponge presence	0.8	98.7
	pennatulacean presence	0.6	99.3
	coral presence	0.4	99.7
	tidal maximum	0.3	100
a) adult	bottom depth	23.5	23.5
	aspect north	19.8	43.3
	position	15.8	59.1
	current SD	9.8	68.9
	bottom temperature	6.4	75.3
	slope	6.2	81.5
	rockiness	4.7	86.2
	current	4.3	90.5
	aspect east	2.5	93.0
	BPI	2.5	95.6
	tidal maximum	1.5	97.1
	sponge presence	1.3	98.4
	curvature	1.2	99.6
	pennatulacean presence	0.3	99.9
	coral presence	0.1	100

3448



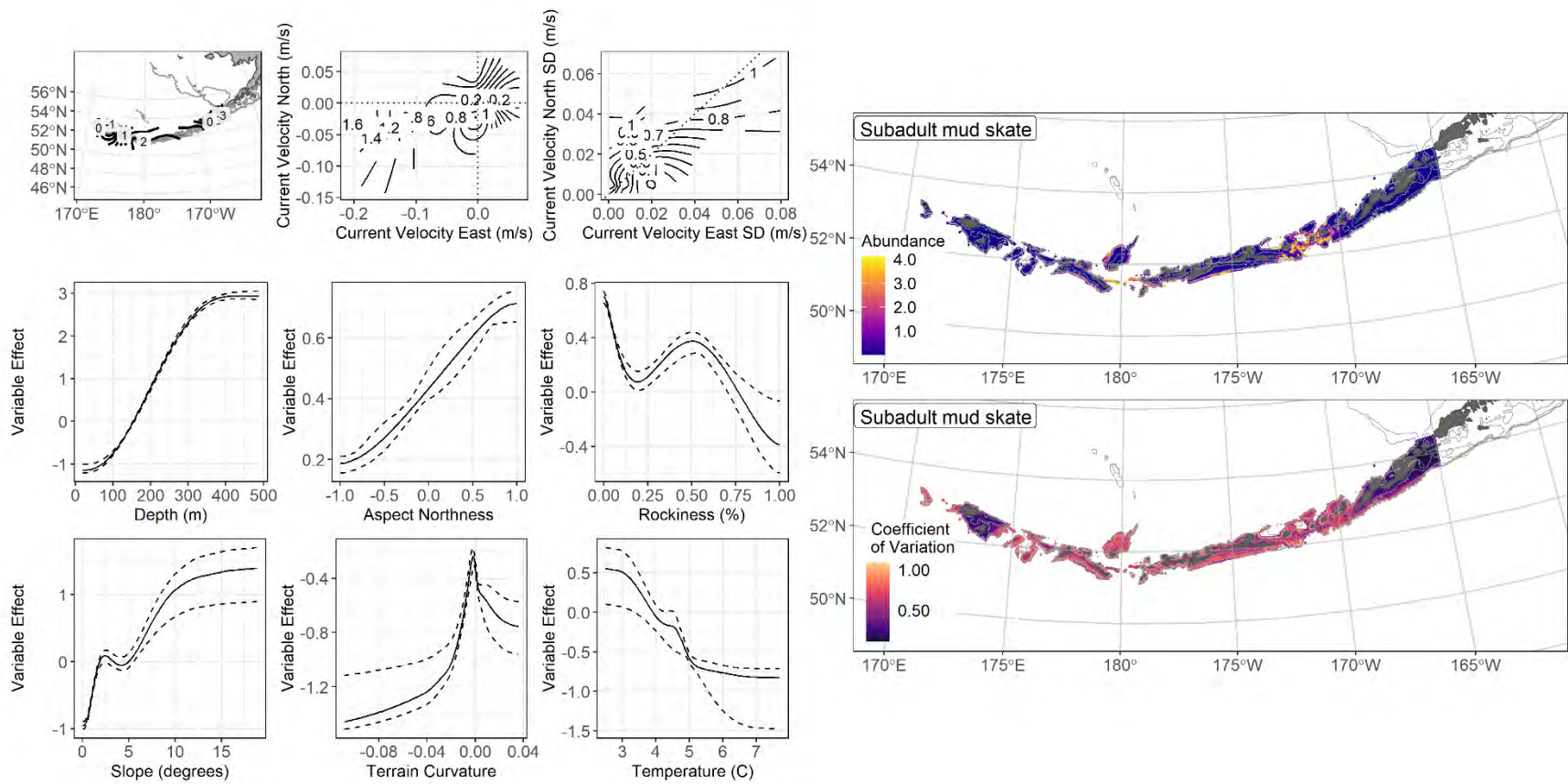
3449

3450 Figure 171. Distribution of subadult mud skate catches (N = 488) in 1999–2019 AFSC RACE-GAP

3451 summer bottom trawl surveys of the Aleutian Islands with the 100 m, 300 m, and 500 m isobaths

3452 indicated; filled red circles indicate locations in top 10% of overall abundance, open orange circles

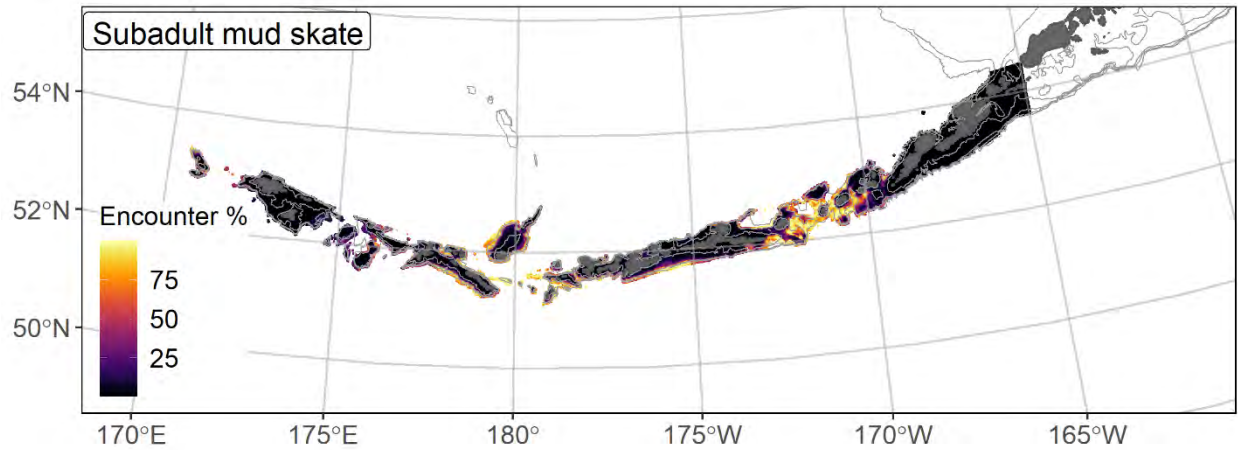
3453 indicate presence in remaining catches, and small blue dots indicate absence.



3454

3455 Figure 172. The top nine covariate effects (left panel) on ensemble-predicted subadult mud skate numerical abundance across the Aleutian Islands

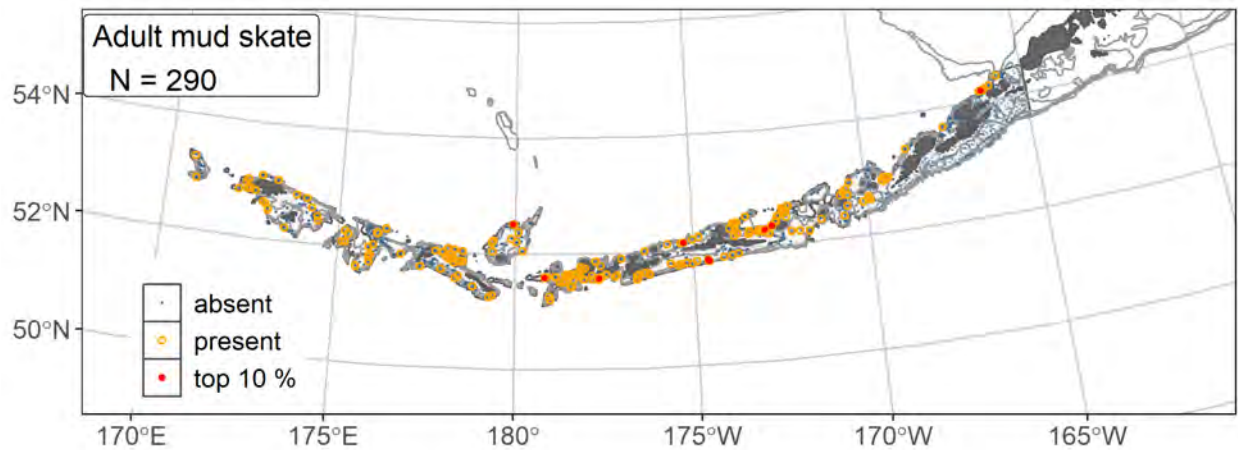
3456 (upper right panel) alongside the coefficient of variation of the ensemble predictions (lower right panel).



3457

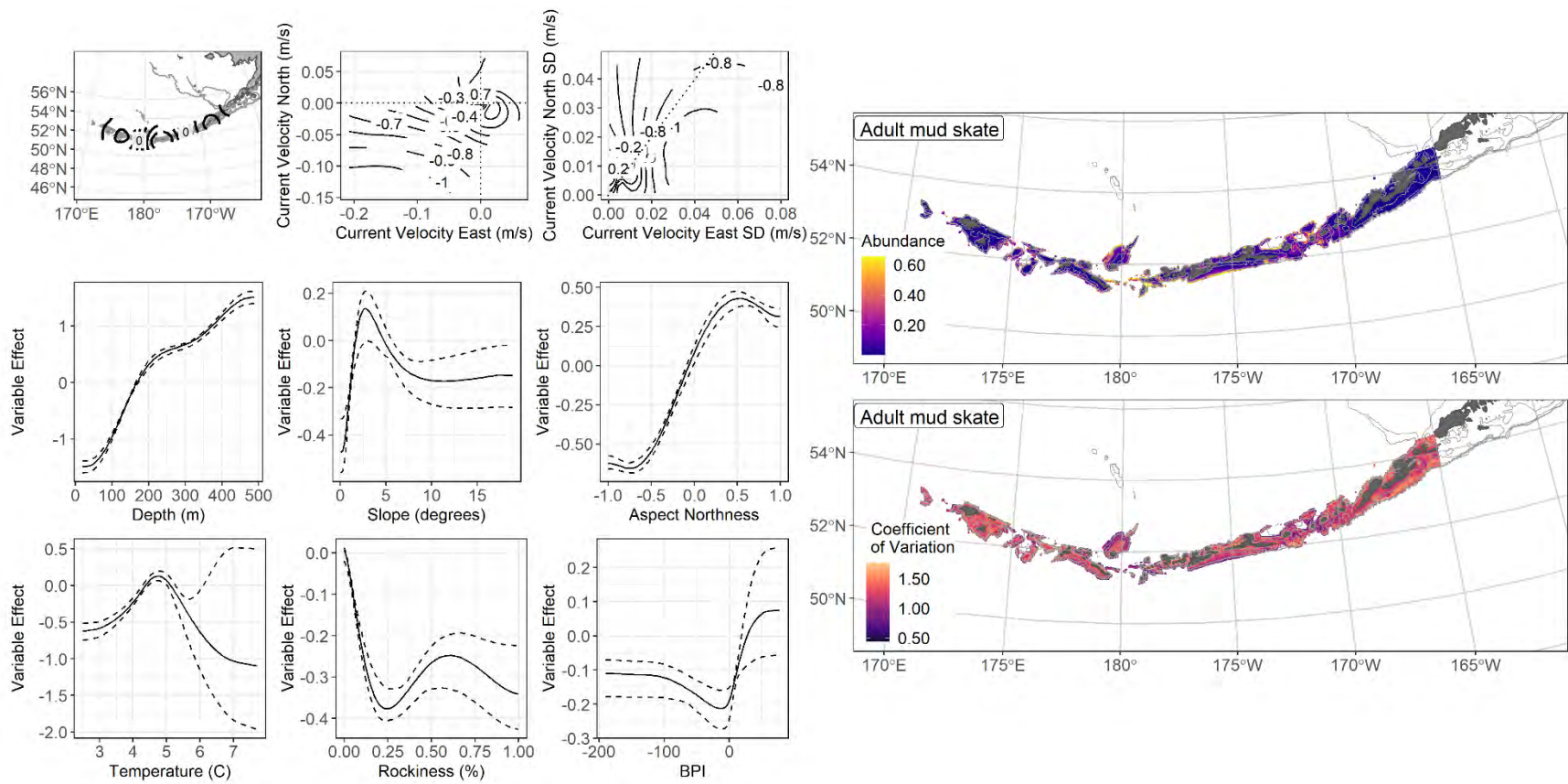
3458 Figure 173. Encounter probability of subadult mud skate from AFSC RACE-GAP summer bottom trawl
 3459 surveys (1999–2019) of the Aleutian Islands with the 100 m, 300 m, and 500 m isobaths indicated.

3460



3461

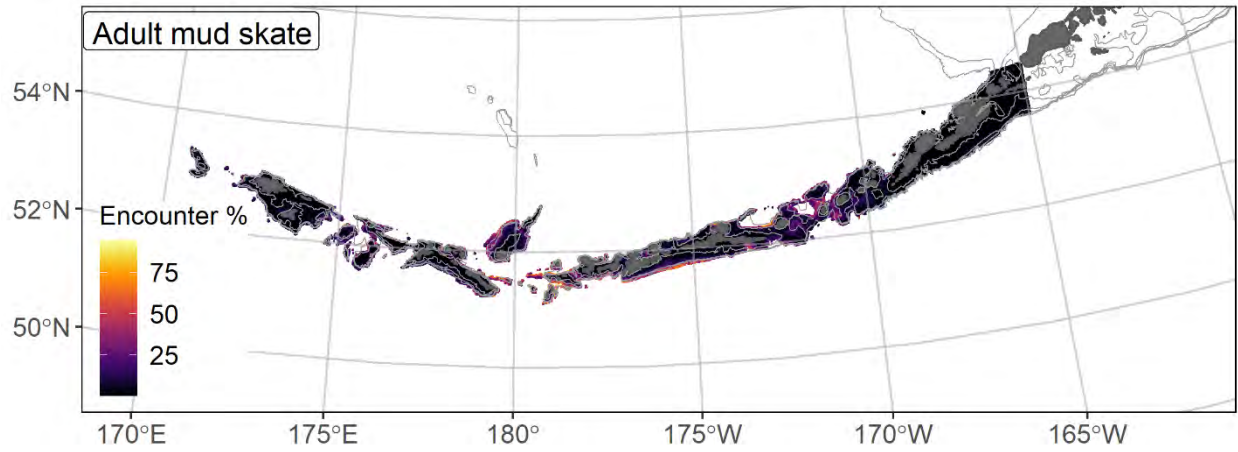
3462 Figure 174. Distribution of adult mud skate catches (N = 290) in 1999–2019 AFSC RACE-GAP summer
 3463 bottom trawl surveys of the Aleutian Islands with the 100 m, 300 m, and 500 m isobaths indicated; filled
 3464 red circles indicate locations in top 10% of overall abundance, open orange circles indicate presence in
 3465 remaining catches, and small blue dots indicate absence.



3466

3467 Figure 175. The top nine covariate effects (left panel) on ensemble-predicted adult mud skate numerical abundance across the Aleutian Islands

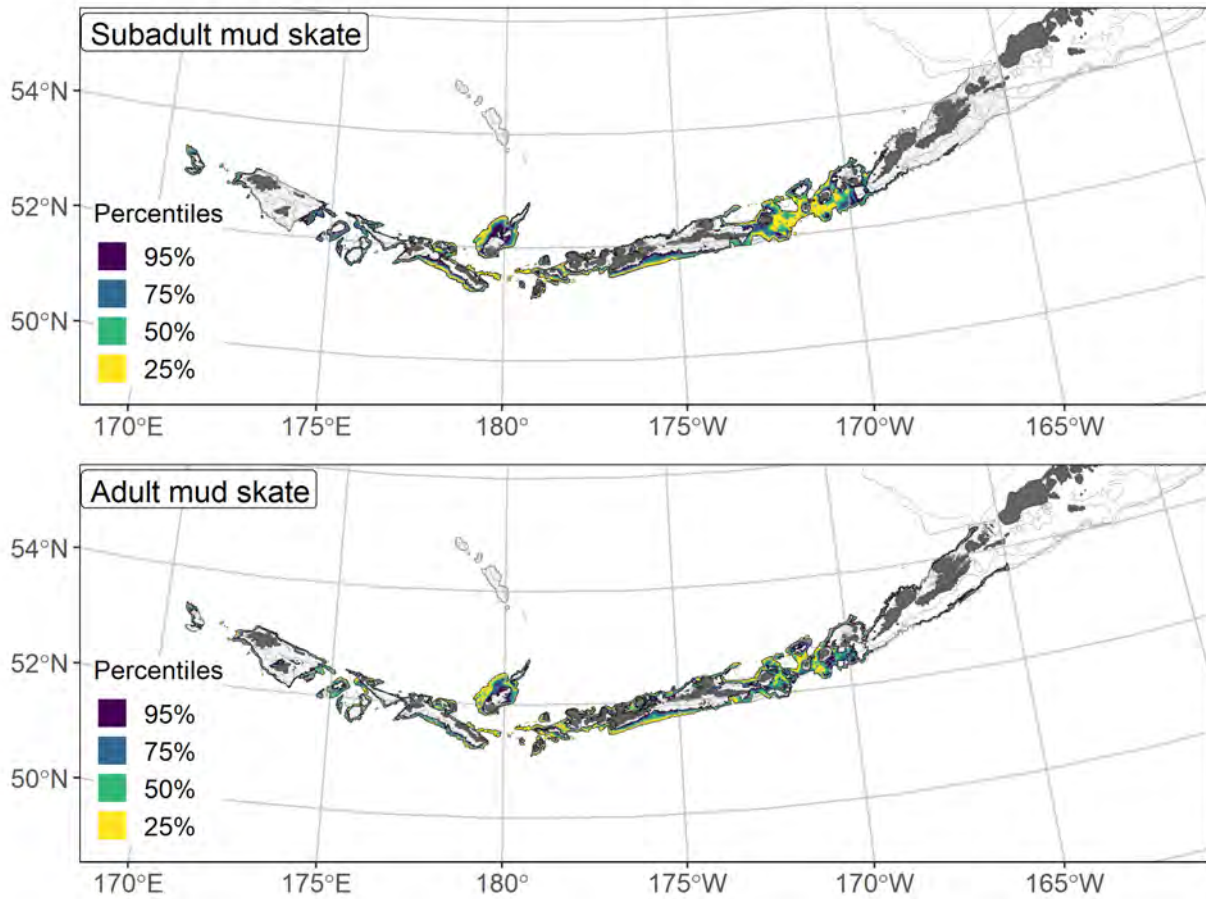
3468 (upper right panel) alongside the coefficient of variation of the ensemble predictions (lower right panel).



3469

3470 Figure 176. Encounter probability of adult mud skate from AFSC RACE-GAP summer bottom trawl

3471 surveys (1999–2019) of the Aleutian Islands with the 100 m, 300 m, and 500 m isobaths indicated.



3472
 3473 Figure 177. Essential fish habitat (EFH area) defined as the top 95% of numerical abundance predictions
 3474 from a habitat-based ensemble fitted to subadult (top) and adult (bottom) mud skate distribution and
 3475 abundance in AFSC RACE-GAP summer bottom trawl surveys (1999–2019) with 100 m, 300 m, and
 3476 500 m isobaths indicated; internal to the EFH map are the subareas of the top 25% (EFH hot spots), top
 3477 50% (core EFH area), and top 75% (principal EFH area) of habitat related, ensemble-predicted numerical
 3478 abundance.

3479 **Whiteblotched skate (*Bathyraja maculata*)**

3480 Whiteblotched skate (*Bathyraja maculata*) is moderately large skate that can be found from the
3481 western Gulf of Alaska to the Kuril Islands (Stevenson 2007). Whiteblotched skate is the dominant
3482 species of skate in the Aleutian Islands, representing over 50% of total skate biomass in the region
3483 (Ormseth 2018). Like many species in the genus *Bathyraja*, this one is predominantly found along the
3484 continental slope, or near the interface between slope and shelf areas. It can reach an adult length of
3485 1200 mm T.L. (Mecklenburg et al. 2002) and like many skates, has a long juvenile phase with an average
3486 L_{50} of 964 mm T.L. across both sexes (Ebert 2005). As an adult, this species is a major predator in the
3487 region and derives a significant amount of its diet from important commercial fish species like Atka
3488 mackerel and walleye pollock (Yang 2007). Skates from the genus *Bathyraja* were not commonly
3489 identified to species in RACE-GAP trawl surveys until 1999, so data on whiteblotched skate before then
3490 is lacking. There is no directed fishery for skates, and all skates in the BSAI region are managed as part of
3491 a single multi-species complex (Ormseth 2018).

3492 **Subadult whiteblotched skate distribution and predicted abundance from RACE-GAP summer**
3493 **bottom trawl surveys in the Aleutian Islands–**

3494 Subadult whiteblotched skate catches were common in some areas covered by the RACE-GAP
3495 summer survey areas (Figure 178). Notably, they were prevalent in Seguam and Amchitka Passes, as well
3496 as around Stalemate Bank. The final ensemble contained three SDMs with approximately equal weights,
3497 and it showed good to excellent performance when compared to the data (Table 51). Specifically, the
3498 ensemble demonstrated good performance at distinguishing areas of high and low abundance ($\rho = 0.482$)
3499 and excellent performance with respect to predicting presence absence (AUC = 0.937) and explaining
3500 deviance explained (PDE = 0.667). Geographic position alone accounted for 47.7% of the deviance
3501 explained by the ensemble, though current, current variability, bottom temperature, and tidal maximum
3502 were also relatively important (Table 52). In general, the ensemble predicted high abundance in the
3503 eastern AI, in areas with strong northerly to northeasterly currents, and areas with strong tides

3504 (Figure 179). Predicted abundance was highest around Seguam Pass, though an additional area of high
3505 abundance occurred in the far west at Stalemate Bank (Figure 179). The predicted CV of abundance was
3506 highest around the passes through the island chain and low elsewhere (Figure 179). Encounter
3507 probabilities for subadult whiteblotched skate were high around Seguam Pass and Stalemate Bank,
3508 moderate around Amchitka Pass, and low elsewhere (Figure 180).

3509 **Adult whiteblotched skate distribution and predicted abundance from RACE-GAP summer bottom**
3510 **trawl surveys in the Aleutian Islands –**

3511 Adult whiteblotched skate catches in the RACE-GAP summer survey were distributed similarly
3512 to subadults; they were common around Seguam Pass, Amchitka Pass, and Stalemate Bank (Figure 181).
3513 The final ensemble contained three SDMs and the GAM_P and hGAM performed somewhat better than the
3514 paGAM, and were weighted slightly higher (Table 51). Overall, the ensemble showed good to excellent
3515 predictive skill across the fit metrics (Table 51). Specifically, the ensemble demonstrated good
3516 performance at distinguishing areas of high vs low abundance ($\rho = 0.495$) and was excellent at predicting
3517 presence or absence (AUC = 0.916) and deviance explained (PDE = 0.728). The particularly high value
3518 for the deviance explained suggested that most of the variation in adult whiteblotched skate catches was
3519 accounted for in the ensemble. Geographic position was responsible for the majority of the deviance
3520 explained in the ensemble (59.9%; Table 52), though bottom depth, current conditions, and tidal
3521 maximum made minor contributions. Like subadults, adult whiteblotched skates were predicted to be
3522 abundant around the passes in the AI, and occupied a distinct set of areas, consistent with the high value
3523 placed on geographic position in the model (Figure 182). Predicted abundance was highest in and around
3524 Seguam Pass and Stalemate Bank, with more moderate abundances predicted in Amchitka Pass
3525 (Figure 182). The predicted CV of abundance was highest around the passes through the island chain and
3526 low elsewhere (Figure 182). Encounter probabilities for adult whiteblotched skate followed the same
3527 pattern as abundance, with encounters being likely in Seguam Pass, Stalemate Bank, and Amchitka Pass,
3528 and unlikely in other places (Figure 183).

3529 **Essential fish habitat of subadult and adult whiteblotched skate in the Aleutian Islands –**

3530 The habitat related abundance predictions based on RACE-GAP summer bottom trawl data
3531 (1999–2019) were translated into EFH area and subareas (Figure 184). The EFH areas for the two life
3532 stages of whiteblotched skate were almost identical. The largest hot spot for both life stages was in
3533 Seguam Pass, with smaller hot spots at Stalemate Bank and Amchitka Pass. The ensembles for both life
3534 stages assigned a large portion of the deviance explained to latitude and longitude, and it is difficult to say
3535 which habitat covariates drove the association between this species and these locations.

3536 Table 51. Constituent species distribution models (SDMs) used to construct Essential Fish Habitat (EFH)
 3537 for a) subadult and b) adult whiteblotched skate: MaxEnt = Maximum entropy; paGAM = presence-
 3538 absence generalized additive model; hGAM = hurdle GAM; GAM_P = standard Poisson GAM; and
 3539 GAM_{nb} = standard negative-binomial GAM. Ensemble performance (ρ = Spearman's rank correlation
 3540 coefficient), root-mean-square-error (RMSE), the area under the receiver operating characteristic (AUC),
 3541 and the Poisson deviance explained (PDE) were generated from k-fold cross-validation. The "--" in a field
 3542 indicates that this SDM was not included in the final ensemble.

3543 **a) subadult whiteblotched skate**

Models	RMSE	Relative Weight	ρ	AUC	PDE	EFH area (km²)
MaxEnt	--	0	--	--	--	--
paGAM	2.86	0.328	0.483	0.940	0.558	40,500
hGAM	2.81	0.339	0.477	0.940	0.669	31,700
GAM _P	2.84	0.333	0.484	0.928	0.677	27,700
GAM _{nb}	4.10	0	--	--	--	--
ensemble	2.50	1	0.482	0.937	0.667	35,800

3544 **b) adult whiteblotched skate**

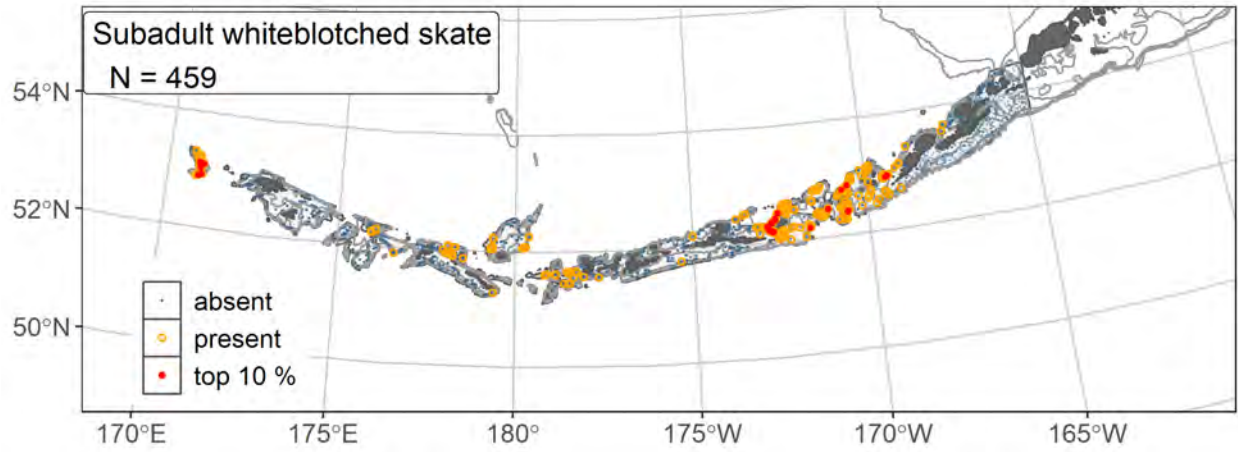
Models	RMSE	Relative Weight	ρ	AUC	PDE	EFH area (km²)
MaxEnt	--	0	--	--	--	--
paGAM	2.63	0.266	0.500	0.922	0.612	42,100
hGAM	2.26	0.358	0.492	0.922	0.730	36,200
GAM _P	2.21	0.376	0.287	0.907	0.729	31,700
GAM _{nb}	2.46	0	--	--	--	--
ensemble	2.04	1	0.495	0.916	0.728	37,600

3545

3546 Table 52. Covariates retained in the a) subadult and b) adult whiteblotched skate species distribution
 3547 model (SDM) final ensembles, the percent contribution to the ensemble deviance explained by each, and
 3548 the cumulative percent deviance: SD = standard deviation, and BPI = bathymetric position index.

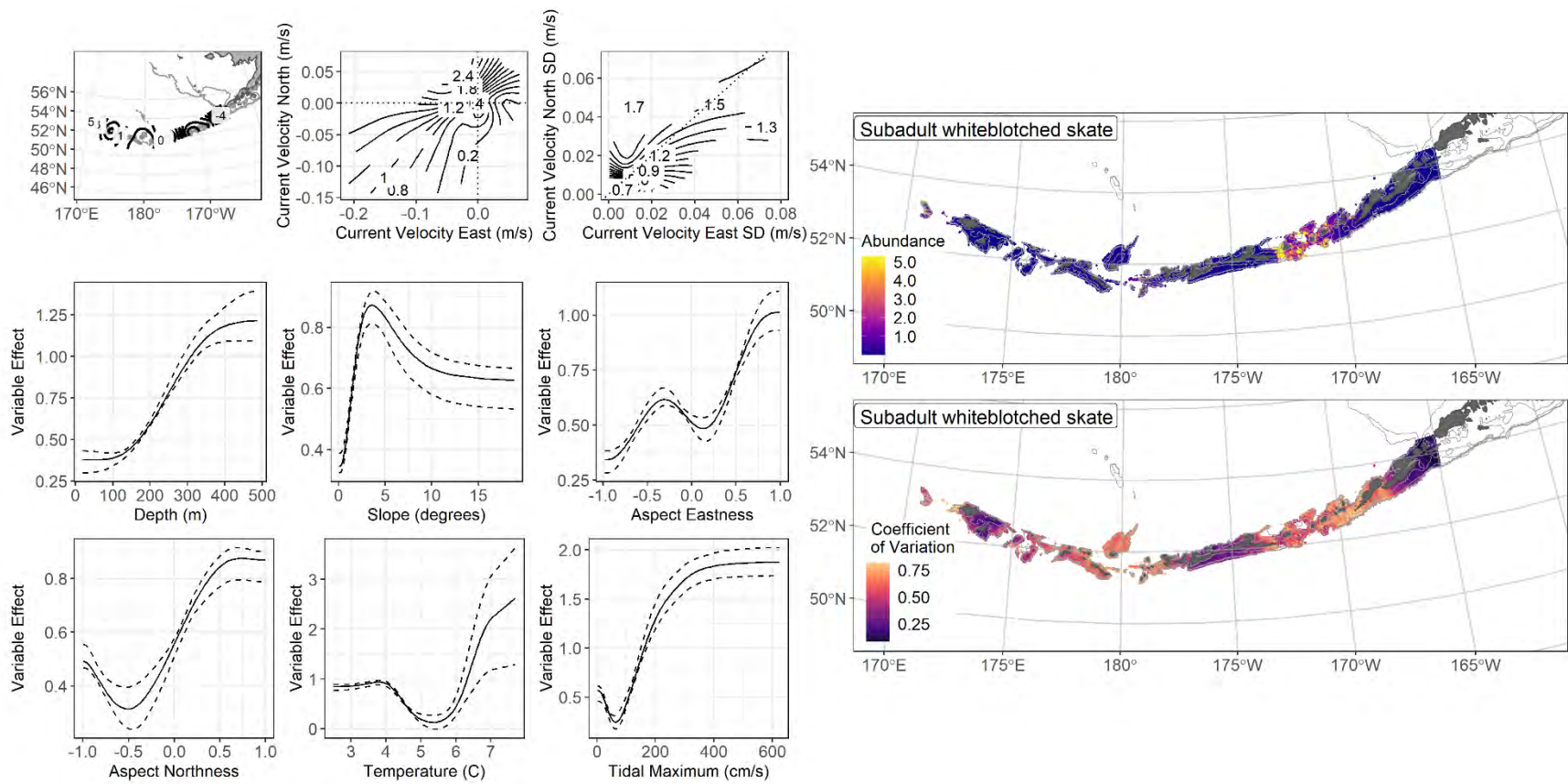
whiteblotched skate	Covariate	% Contribution	Cumulative % Contribution
a) subadult	position	47.7	47.7
	current	14.6	62.3
	tidal maximum	7.6	69.9
	current SD	6.3	76.2
	bottom temperature	5.2	81.4
	slope	4.3	85.7
	aspect east	3.6	89.3
	bottom depth	3.5	92.8
	aspect north	2.3	95.1
	curvature	2.1	97.2
	sponge presence	1.0	98.2
	BPI	0.8	99.0
	rockiness	0.6	99.6
	coral presence	0.4	100
a) adult	position	58.9	58.9
	bottom depth	6.3	65.2
	current SD	5.9	71.1
	current	4.7	75.8
	tidal maximum	4.7	80.5
	aspect north	3.9	84.4
	bottom temperature	3.0	87.4
	aspect east	2.8	90.2
	slope	2.5	92.7
	curvature	1.8	94.5
	BPI	1.5	96.0
	rockiness	1.3	97.3
	coral presence	1.0	98.3
	pennatulacean presence	0.9	99.2
sponge presence	0.8	100	

3549



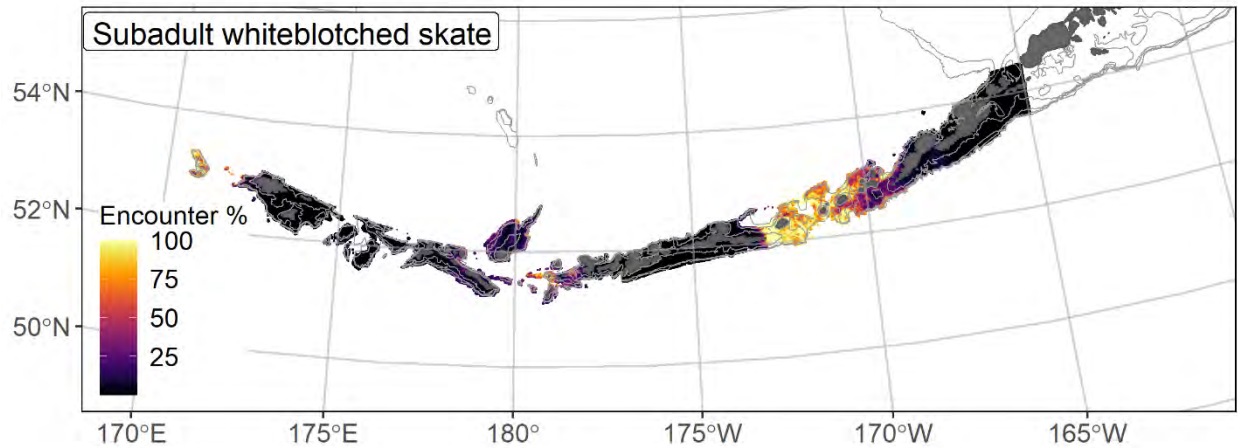
3550

3551 Figure 178. Distribution of subadult whiteblotched skate catches (N = 459) in 1999–2019 AFSC RACE-
 3552 GAP summer bottom trawl surveys of the Aleutian Islands with the 100 m, 300 m, and 500 m isobaths
 3553 indicated; filled red circles indicate locations in top 10% of overall abundance, open orange circles
 3554 indicate presence in remaining catches, and small blue dots indicate absence.



3555

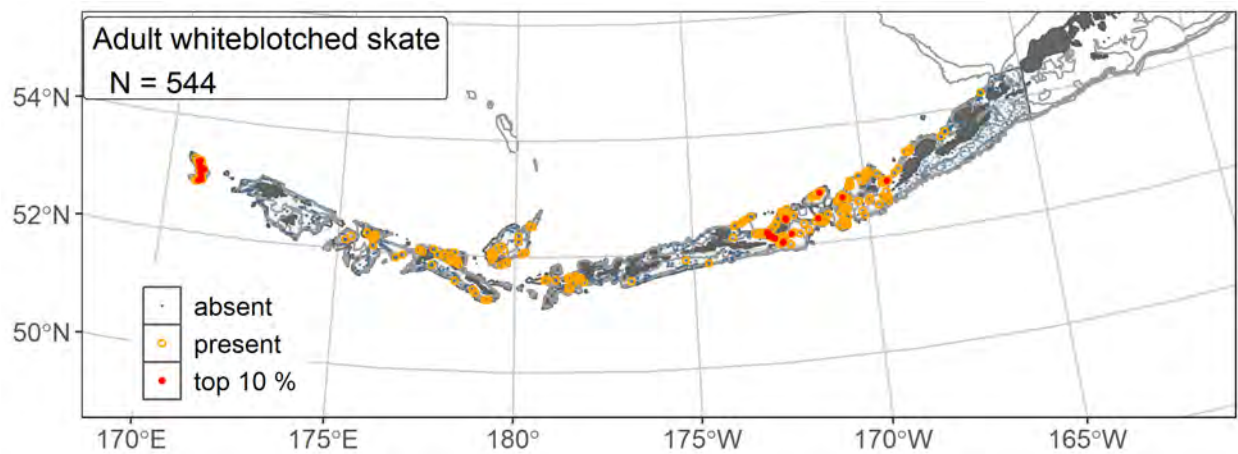
3556 Figure 179. The top nine covariate effects (left panel) on ensemble-predicted subadult whiteblotched skate numerical abundance across the
 3557 Aleutian Islands (upper right panel) alongside the coefficient of variation of the ensemble predictions (lower right panel).



3558

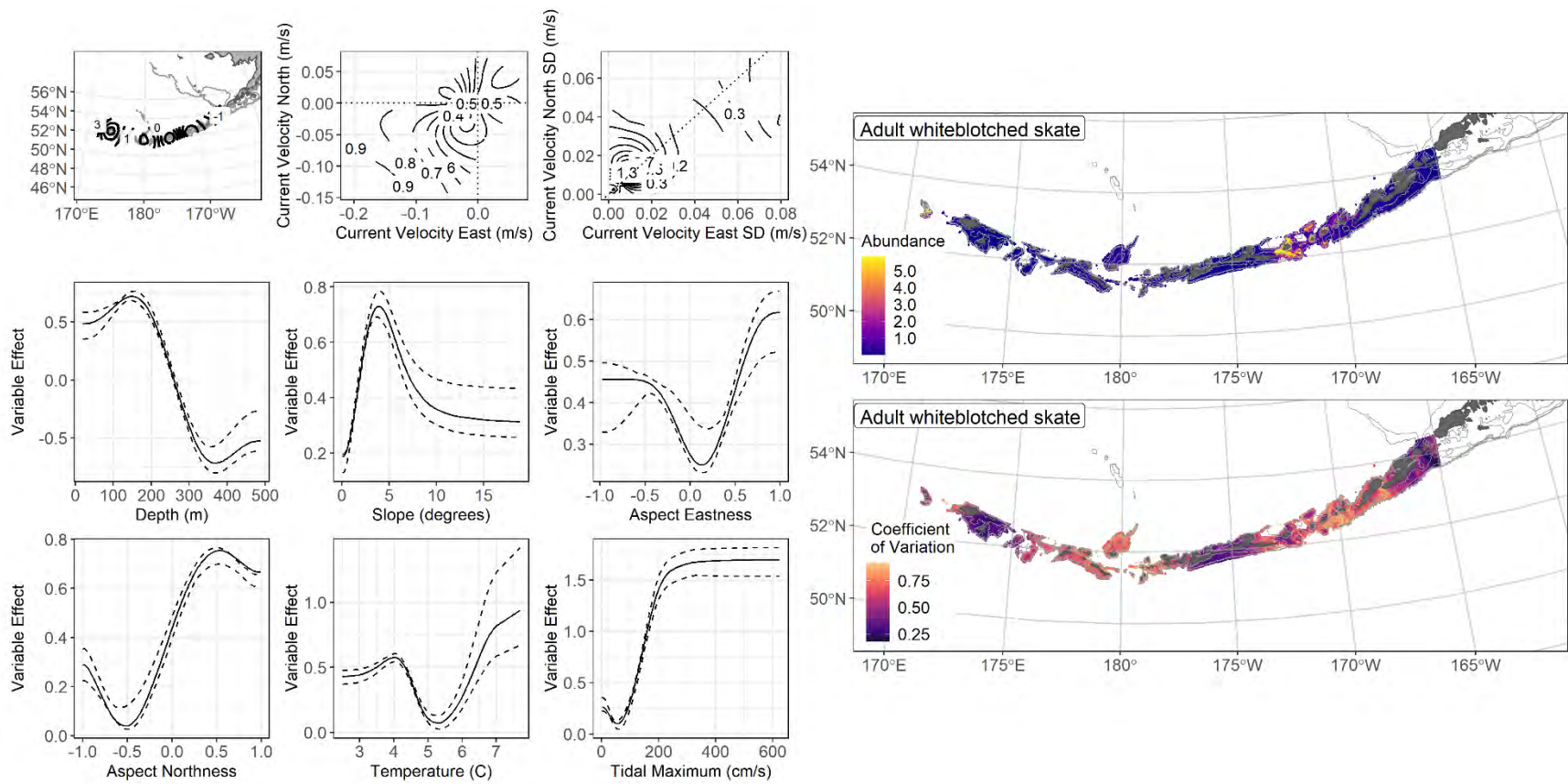
3559 Figure 180. Encounter probability of subadult whiteblotched skate from AFSC RACE-GAP summer
 3560 bottom trawl surveys (1999–2019) of the Aleutian Islands with the 100 m, 300 m, and 500 m isobaths
 3561 indicated.

3562



3563

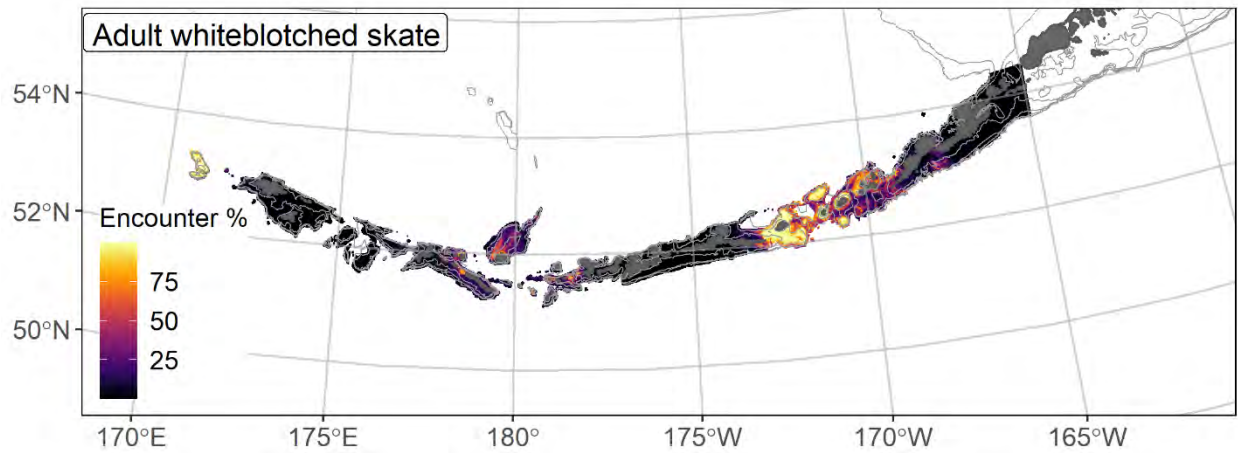
3564 Figure 181. Distribution of adult whiteblotched skate catches (N = 544) in 1999–2019 AFSC RACE-GAP
 3565 summer bottom trawl surveys of the Aleutian Islands with the 100 m, 300 m, and 500 m isobaths
 3566 indicated; filled red circles indicate locations in top 10% of overall abundance, open orange circles
 3567 indicate presence in remaining catches, and small blue dots indicate absence.



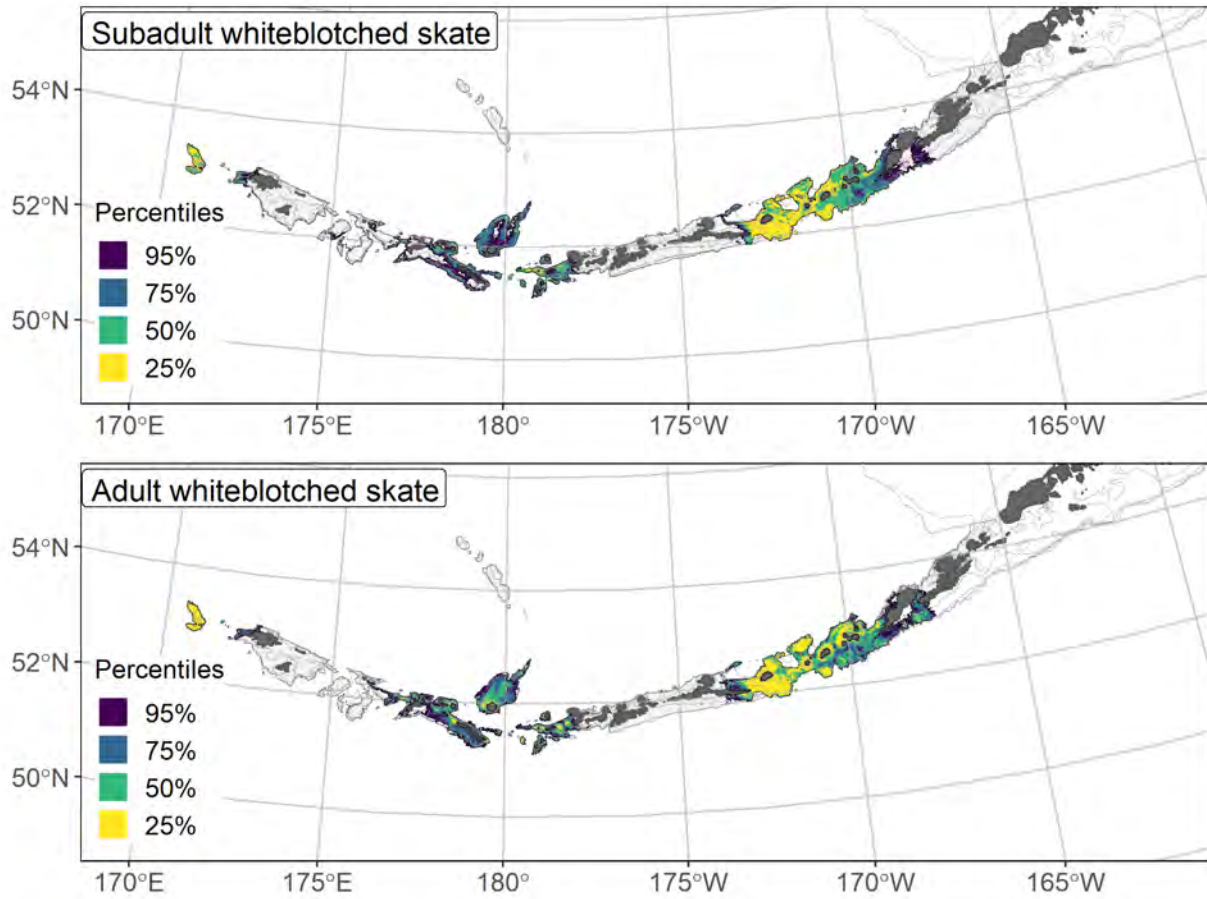
3568

3569 Figure 182. The top nine covariate effects (left panel) on ensemble-predicted adult whiteblotched skate numerical abundance across the Aleutian

3570 Islands (upper right panel) alongside the coefficient of variation of the ensemble predictions (lower right panel).



3571
3572 Figure 183. Encounter probability of adult whiteblotched skate from AFSC RACE-GAP summer bottom
3573 trawl surveys (1999–2019) of the Aleutian Islands with the 100 m, 300 m, and 500 m isobaths indicated.



3574

3575

Figure 184. Essential fish habitat (EFH area) is the top 95% of numerical abundance predictions from a

3576

habitat-based ensemble fitted to subadult (top) and adult (bottom) whiteblotched skate distribution and

3577

abundance in AFSC RACE-GAP summer bottom trawl surveys (1999–2019) with 100 m, 300 m, and

3578

500 m isobaths indicated; internal to the EFH map are the subareas of the top 25% (EFH hot spots), top

3579

50% (core EFH area), and top 75% (principal EFH area) of habitat related, ensemble-predicted numerical

3580

abundance.

Invertebrates

3581

3582 **Golden king crab (*Lithodes aequispinus*)**

3583 Golden king crab (*Lithodes aequispinus*) are found from the coast of British Columbia across the
3584 North Pacific to Japan. For management purposes, the Aleutian Islands population is divided into two
3585 sub-stocks separated at the 174° W meridian (Siddeck et al. 2019). Golden king crab are typically found
3586 in deep water (>300 m; Somerton and Otto 1981) and often prefer high-relief rocky or coral habitats.
3587 These characteristics make this species more difficult to harvest by trawl gear, and prior to the mid-1980s,
3588 the fishery for golden king crab was limited. However, declines in other king crab species have resulted in
3589 increased interest in this species and prompted advances in its management (Olsen et al. 2018). The
3590 reproductive cycle is thought to last approximately 24 months and at any time of year, ovigerous females
3591 can be found carrying egg clutches in highly disparate developmental states (Otto and Cummiskey 1985).
3592 Eggs are relatively large compared to other king crab species and appear to be carried by the females for
3593 an extended period before hatching. Larvae do not appear to remain at depth and owing to the large yolk
3594 reserves, can develop into juveniles without additional feeding (Shirley and Zhou, 1997). Long molting
3595 cycles also contribute to difficulty in assigning ages to this species. These life history complexities and
3596 the lack of a fishery independent crab survey have made golden king crab populations difficult to assess
3597 using standard age-based stock assessment tools (Sideek et al. 2019).

3598 **Golden king crab (all life stages combined) distribution and predicted abundance from RACE-GAP** 3599 **summer bottom trawl surveys in the Aleutian Islands–**

3600 Golden king crab from the RACE-GAP summer survey were distributed across the Aleutian
3601 Islands beginning at 169° W and extending across the archipelago (Figure 185). Catches occurred
3602 primarily along the continental slope and were highest in the area around Seguam Pass. The final
3603 ensemble contained three SDMs with approximately equal weights and achieved a good fit to the data
3604 (Table 53). The ensemble was generally able to predict relatively high or low abundance areas
3605 ($\rho = 0.558$), distinguish between presence and absence locations (AUC = 0.888), and was able to account

3606 for a good portion of the observed deviance ($PDE = 0.478$). Bottom depth, geographic position, and
3607 bottom current were the most important covariates and accounted for 54.6 % of the deviance explained in
3608 the ensemble, but other covariates such as maximum tidal current, temperature, rockiness, and slope
3609 aspect were also important (Table 54). In general, higher abundance was predicted with increasing depth,
3610 northeasterly currents, strong tidal movement, low temperatures, and rocky terrain (Figure 186). Predicted
3611 abundance was highest in the area between Atka and Unalaska Islands, with pockets of high density
3612 predicted further to the west (Figure 186). The CV of abundance was high near areas where predicted
3613 abundance was high, which reflected uncertainty in the numbers caught in high abundance areas
3614 (Figure 186). Encounter probability was high in the passes through the island chain, which was consistent
3615 with the modelled covariate effects for deep water and stronger currents (Figure 187).

3616 **Essential fish habitat of golden king crab in the Aleutian Islands –**

3617 The habitat related abundance predictions based on RACE-GAP summer bottom trawl data
3618 (1991–2019) were translated into EFH area and subareas (Figure 188). The EFH area encompassed most
3619 of the survey area along the continental slope at depths greater than 300 m. Hot spots occurred at Seguam
3620 Pass, Amchitka Pass, and Buldir Strait. The RACE-GAP summer bottom trawl surveys used trawl gear
3621 that is not ideally suited for surveying crab species, so this EFH description should be used with caution.
3622 However, the ensemble showed good performance across multiple metrics so this map should be a useful
3623 resource until additional data sources can be incorporated into the EFH process.

3624 Table 53. Constituent species distribution models (SDMs) used to construct Essential Fish Habitat (EFH)
 3625 for golden king crab: MaxEnt = Maximum entropy; paGAM = presence-absence generalized additive
 3626 model; hGAM = hurdle GAM; GAM_p = standard Poisson GAM; and GAM_{nb} = standard negative-
 3627 binomial GAM. Ensemble performance (ρ = Spearman's rank correlation coefficient), root-mean-square-
 3628 error (RMSE), the area under the receiver operating characteristic (AUC), and the Poisson deviance
 3629 explained (PDE) were generated from k-fold cross-validation. The "--" in a field indicates that this SDM
 3630 was not included in the final ensemble.

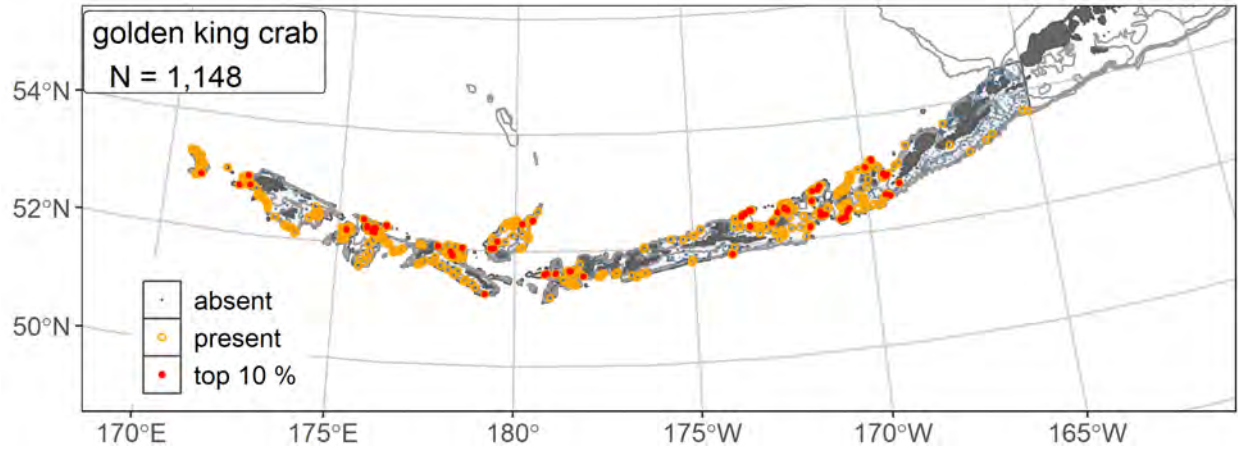
Models	RMSE	Relative Weight	ρ	AUC	PDE	EFH area (km²)
MaxEnt	--	0	--	--	--	--
paGAM	6.59	0.340	0.575	0.902	0.267	48,400
hGAM	6.65	0.333	0.542	0.902	0.471	50,300
GAM _p	6.72	0.327	0.521	0.862	0.462	52,600
GAM _{nb}	6.75	0	--	--	--	--
ensemble	6.19	1	0.558	0.888	0.478	52,300

3631

3632 Table 54. Covariates retained in the golden king crab species distribution model (SDM) final ensemble,
 3633 the percent contribution to the ensemble deviance explained by each, and the cumulative percent
 3634 deviance: SD = standard deviation, and BPI = bathymetric position index.

Golden king crab	Covariate	% Contribution	Cumulative % Contribution
a) all life stages	bottom depth	24.7	24.7
	position	17.4	42.0
	current	12.6	54.6
	tidal maximum	6.7	61.3
	current SD	6.5	67.8
	bottom temperature	5.6	73.4
	aspect north	5.5	78.8
	rockiness	5.5	84.3
	aspect east	3.8	88.1
	curvature	3.6	91.7
	slope	3.2	94.9
	coral presence	2.2	97.1
	sponge presence	1.8	98.9
	BPI	1.1	100
	pennatulacean presence	0	100

3635



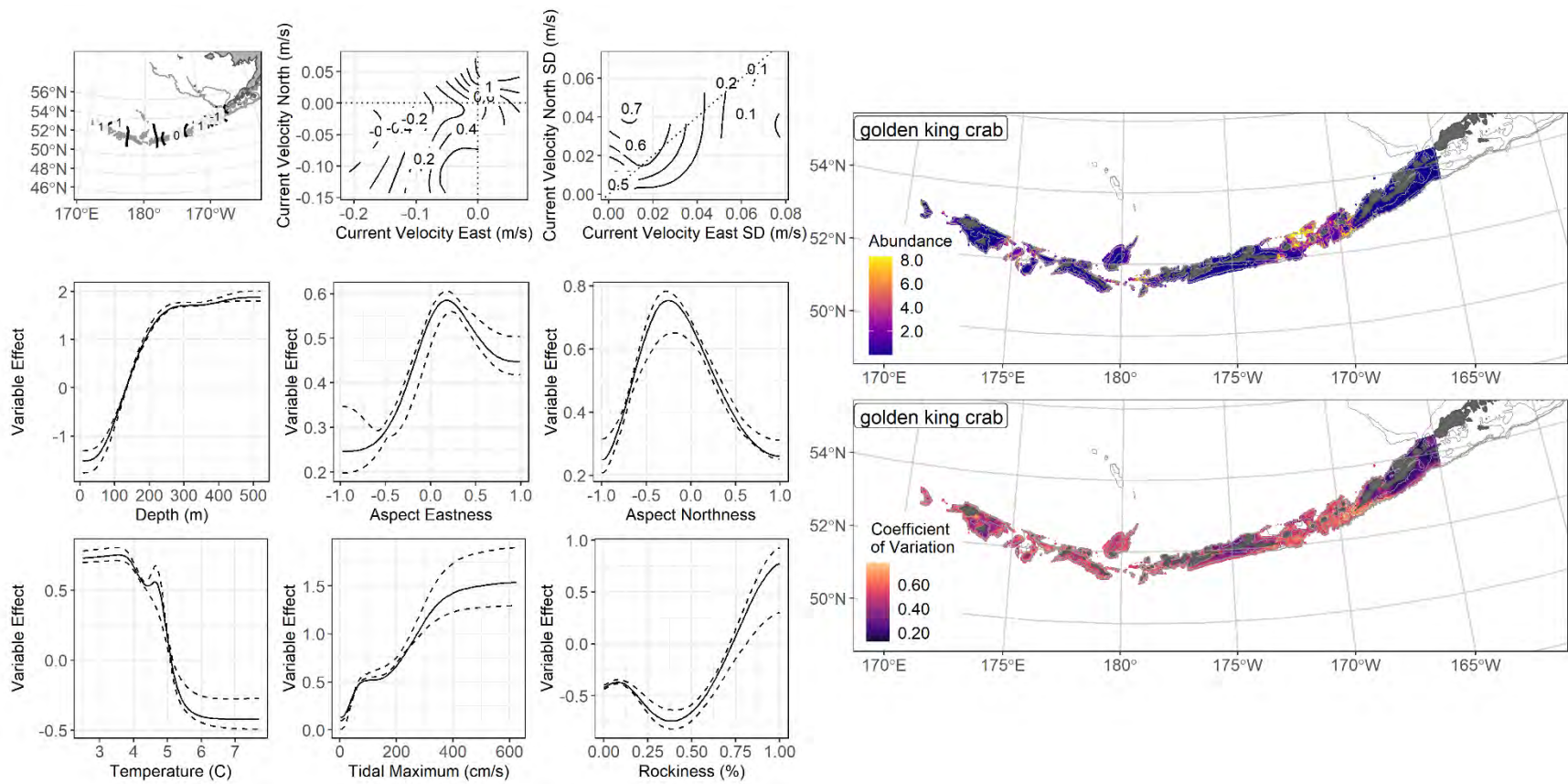
3636

3637 Figure 185. Distribution of golden king crab catches (N = 1,148) in 1991–2019 AFSC RACE-GAP

3638 summer bottom trawl surveys of the Aleutian Islands with the 100 m, 300 m, and 500 m isobaths

3639 indicated; filled red circles indicate locations in top 10% of overall abundance, open orange circles

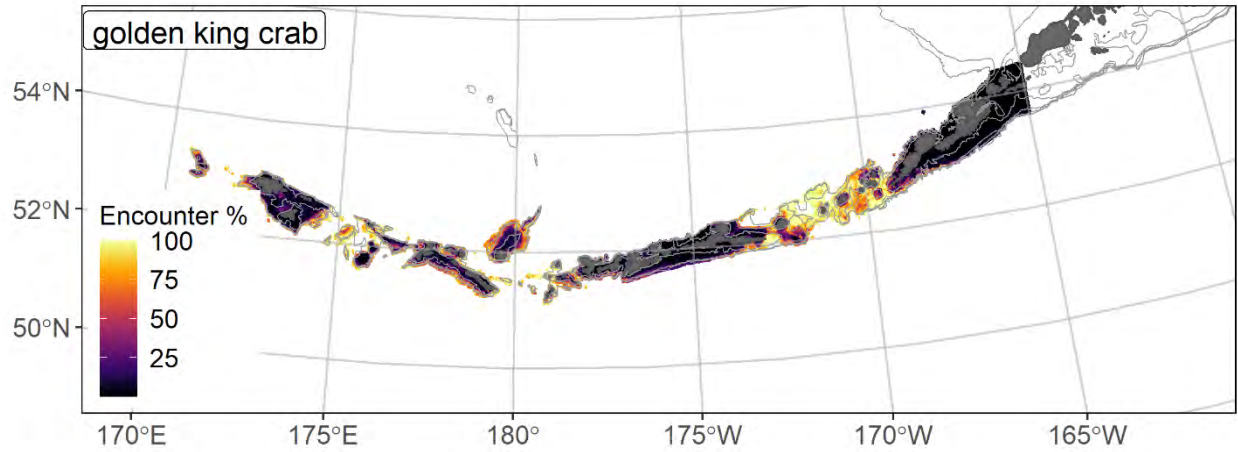
3640 indicate presence in remaining catches, and small blue dots indicate absence.



3641

3642 Figure 186. The top nine covariate effects (left panel) on ensemble-predicted golden king crab numerical abundance across the Aleutian Islands

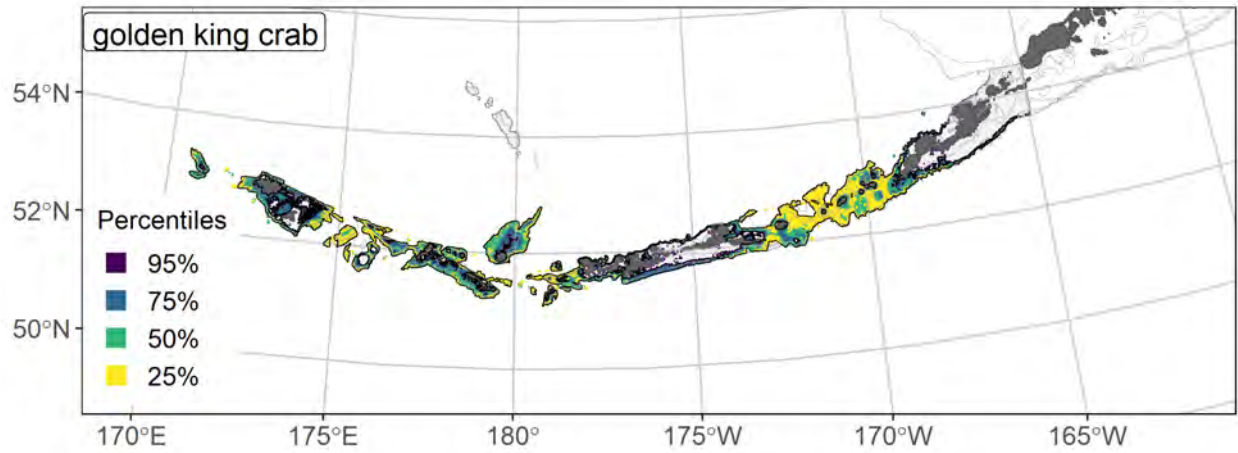
3643 (upper right panel) alongside the coefficient of variation (CV) of the ensemble predictions (lower right panel).



3644

3645 Figure 187. Encounter probability of golden king crab from AFSC RACE-GAP summer bottom trawl
 3646 surveys (1991–2019) of the Aleutian Islands with the 100 m, 300 m, and 500 m isobaths indicated.

3647



3648

3649 Figure 188. Essential fish habitat (EFH area) defined as the top 95% of numerical abundance predictions
 3650 from a habitat-based ensemble fitted to golden king crab distribution and abundance in AFSC RACE-
 3651 GAP summer bottom trawl surveys (1991–2019) with 100 m, 300 m, and 500 m isobaths indicated;
 3652 internal to the EFH map are the subareas of the top 25% (EFH hot spots), top 50% (core EFH area), and
 3653 top 75% (principal EFH area) of habitat related, ensemble-predicted numerical abundance.

3654 **Red king crab (*Paralithodes camtschaticus*)**

3655 Red king crab (*Paralithodes camtschaticus*) are found from the coast of British Columbia across
3656 the North Pacific to Japan (Zheng and Siddeek 2019). In the AI, they are primarily found in the west, with
3657 the largest concentrations found in the shallow waters of Petrel Bank (Daly 2020). Red king crab growth
3658 rates are strongly influenced by temperature and they can take over 9 years to reach maturity after larval
3659 settlement, depending on stock (Loher et al. 2001). Concern has been raised about the potential response
3660 of red king crab (and other crustaceans to potential ocean acidification, as a significant reduction in pH
3661 had a strong negative effect on larval survival in a laboratory study (Long et al. 2013). The red king crab
3662 fishery in the AI has been closed since the 2003/2004 season due to uncertainty on the status of pre-
3663 recruit legal males and low catch rates during cooperative industry-ADFG surveys (Daly 2020). For this
3664 study, we did not separate red king crabs into life stages and modeled all crabs caught in AI RACE-GAP
3665 bottom trawls as a single, composite life stage.

3666 **Red king crab (all life stages combined) distribution and predicted abundance from RACE-GAP**
3667 **summer bottom trawl surveys in the Aleutian Islands–**

3668 Red king crab from the RACE-GAP summer survey were sparsely distributed across the eastern
3669 AI and were more concentrated near Petrel Bank and further to the west (Figure 189). Catches occurred
3670 primarily in shallow water around 100 m deep. The final ensemble contained two SDMs with
3671 approximately equal weights and achieved a poor to fair fit to the observed data (Table 55), potentially
3672 due to the scarcity of red king crab in the survey (only 83 catches from 1991–2019). While the model
3673 showed a fair ability to discriminate catches where this species was present or absent (AUC = 0.820) and
3674 a similarly explained a fair amount of the deviance (PDE = 0.274), it showed a poor ability to predict high
3675 or low abundance catches ($p = 0.138$). These scores, along with the small number of positive catches,
3676 suggest that this model should be used with caution. Geographic position, bottom depth, tidal current, and
3677 bottom currents were the most important covariates and accounted for 81.6 % of the deviance explained
3678 (Table 56). In general, high abundance was predicted further west, in shallow depths, with a low tidal

3679 maximum, and southwesterly ocean currents (Figure 190). Predicted abundance was highest around Petrel
3680 Bank, with additional pockets of high abundance predicted around the Rat Islands and near Unalaska
3681 Island (Figure 190). The predicted CV of abundance was high in shallow areas such as between Adak and
3682 Atka, where environmental conditions suggested suitable habitat exists but where there were few
3683 observed catches (Figure 190). Predicted encounter probability was high only around those pockets
3684 described above, reflecting the fairly limited distribution of red king crab in the AI region (Figure 191).

3685 **Essential fish habitat of red king crab in the Aleutian Islands –**

3686 The habitat related abundance predictions based on RACE-GAP summer bottom trawl data
3687 (1991–2019) were translated into EFH area and subareas (Figure 192). The EFH area encompassed most
3688 of the survey area around Petrel Bank and shallow areas further west. A second area of EFH is located
3689 near Unalaska. Given the poor scores from the fit metrics, the low amount of data, and the difficulty in
3690 sampling crabs using trawl gear, this EFH description should be used with some caution.

3691 Table 55. Constituent species distribution models (SDMs) used to construct Essential Fish Habitat (EFH)
 3692 for red king crab: MaxEnt = Maximum entropy; paGAM = presence-absence generalized additive model;
 3693 hGAM = hurdle GAM; GAM_p = standard Poisson GAM; and GAM_{nb} = standard negative-binomial
 3694 GAM. Ensemble performance (ρ = Spearman's rank correlation coefficient), root-mean-square-error
 3695 (RMSE), the area under the receiver operating characteristic (AUC), and the Poisson deviance explained
 3696 (PDE) were generated from k-fold cross-validation. The "--" in a field indicates that this SDM was not
 3697 included in the final ensemble.

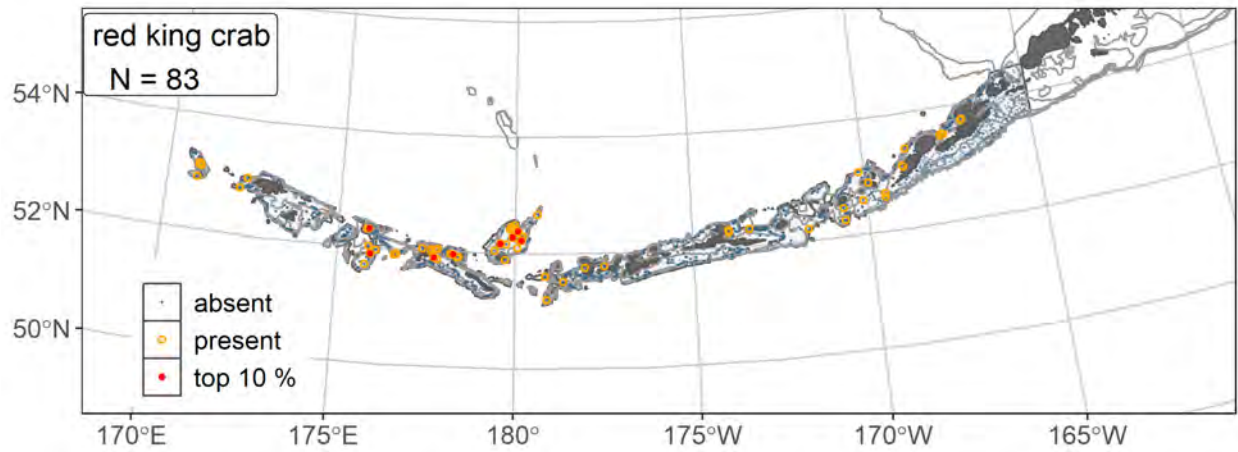
Models	RMSE	Relative Weight	ρ	AUC	PDE	EFH area (km²)
MaxEnt	--	--	--	--	--	--
paGAM	1.55	0.503	0.135	0.812	0.205	36,400
hGAM	--	--	--	--	--	--
GAM _p	1.69	0	--	--	--	--
GAM _{nb}	1.56	.497	0.136	0.814	0.297	21,600
ensemble	1.55	1	0.138	0.820	0.274	28,900

3698

3699 Table 56. Covariates retained in the red king crab species distribution model (SDM) final ensemble, the
 3700 percent contribution to the ensemble deviance explained by each, and the cumulative percent deviance:
 3701 BPI = bathymetric position index.

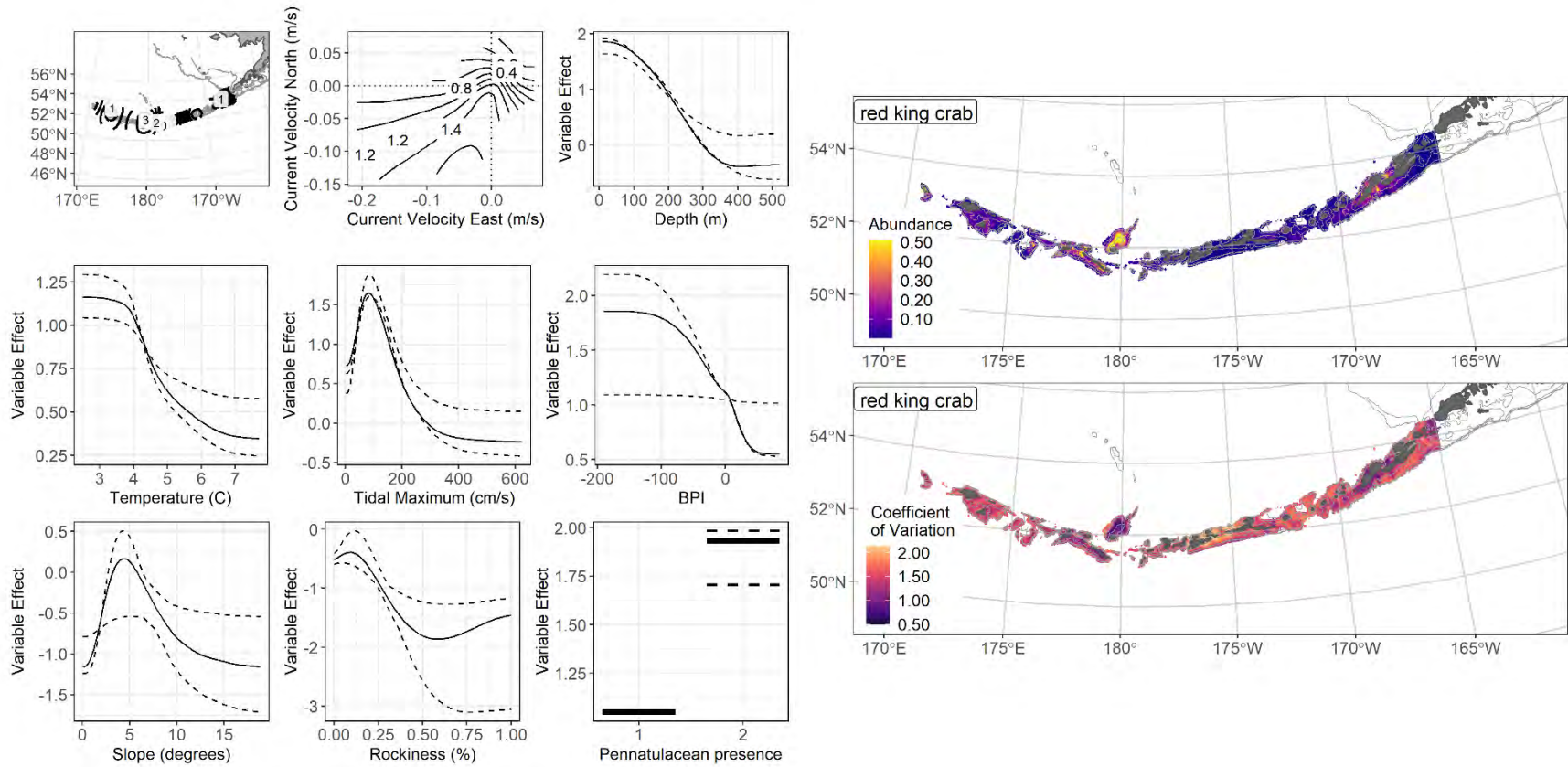
Golden king crab	Covariate	% Contribution	Cumulative % Contribution
a) all life stages	position	47.4	47.4
	bottom depth	18.8	66.2
	tidal maximum	8.1	74.3
	current	7.3	81.6
	BPI	5.9	87.5
	slope	4.1	91.6
	bottom temperature	3.0	94.6
	rockiness	2.2	96.8
	pennatulacean presence	1.6	98.4
	aspect north	1.1	99.5
	sponge presence	0.5	100

3702



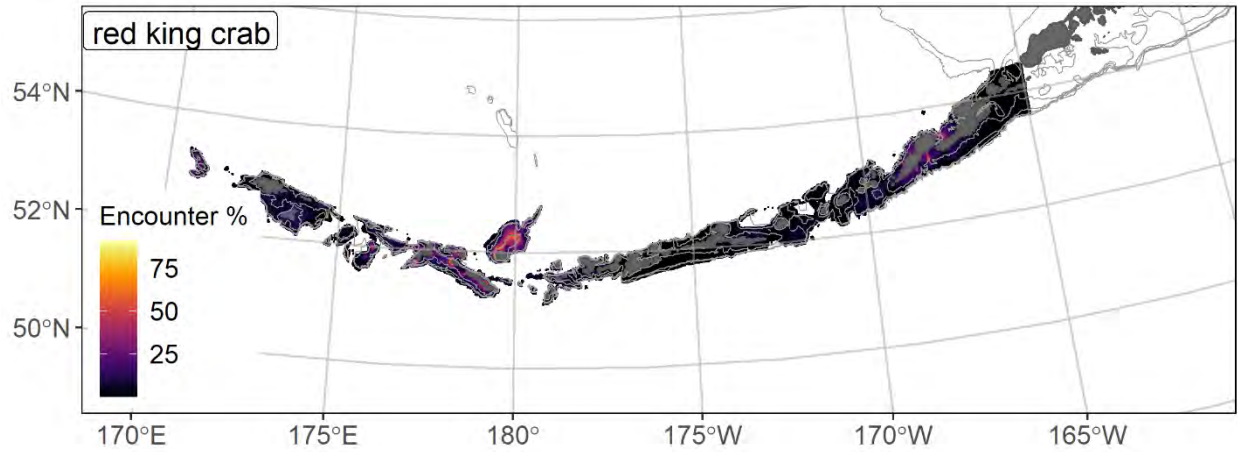
3703

3704 Figure 189. Distribution of red king crab catches (N = 83) in 1991–2019 AFSC RACE-GAP summer
 3705 bottom trawl surveys of the Aleutian Islands with the 100 m, 300 m, and 500 m isobaths indicated; filled
 3706 red circles indicate catches in top 10% of overall abundance, open orange circles indicate presence in
 3707 remaining catches, .



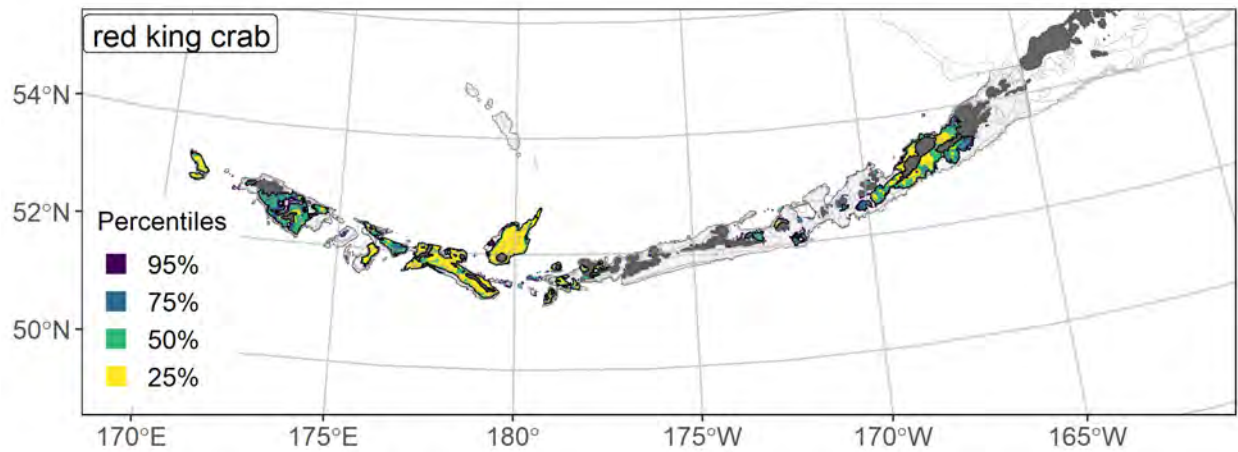
3708

3709 Figure 190. The top nine covariate effects (left panel) on ensemble-predicted red king crab numerical abundance across the Aleutian Islands (upper
 3710 right panel) alongside the coefficient of variation of the ensemble predictions (lower right panel).



3711
 3712 Figure 191. Encounter probability of red king crab from AFSC RACE-GAP summer bottom trawl
 3713 surveys (1991–2019) of the Aleutian Islands with the 100 m, 300 m, and 500 m isobaths indicated.

3714



3715
 3716 Figure 192. Essential fish habitat (EFH area) is the top 95% of numerical abundance predictions from a
 3717 habitat-based ensemble fitted to red king crab distribution and abundance in AFSC RACE-GAP summer
 3718 bottom trawl surveys (1991–2019) with 100 m, 300 m, and 500 m isobaths indicated; internal to the EFH
 3719 map are the subareas of the top 25% (EFH hot spots), top 50% (core EFH area), and top 75% (principal
 3720 EFH area) of habitat related, ensemble-predicted numerical abundance.

3721 **Octopus (*Enteroctopus dofleini*)**

3722 The giant Pacific octopus (*Enteroctopus dofleini*) is the most common octopod encountered in the
3723 RACE-GAP summer bottom trawl survey of the AI (Ormseth et al. 2018). True to its name, this species is
3724 the largest species of octopus in the world and can be over two meters long. Giant Pacific octopus are
3725 terminal spawners that die after mating (males) and the hatching of eggs (females; Jorgensen 2009). Peak
3726 spawning occurs in the winter and early spring (Brewer 2016), and females release between 40,000 to
3727 240,000 eggs (Conrath and Connors 2014). While weight at 50% maturity is available for this species
3728 (Brewer and Norcross 2012), all life stages are combined for this project. Data on sex-specific octopus
3729 weights are not regularly collected in either the commercial fisheries or the RACE-GAP bottom trawl
3730 surveys, and estimates of octopus biomass are considered unreliable at this time (Ormseth et al. 2018). In
3731 2011, FMPs were amended to provide for separate management of the sharks, skates, sculpins, and
3732 octopuses that previously comprised the “other species” complex managed in BSAI through 2010
3733 (Ormseth et al. 2018).

3734 **Giant Pacific octopus (all life stages combined) distribution and predicted abundance from RACE-**
3735 **GAP summer bottom trawl surveys in the Aleutian Islands–**

3736 Giant Pacific octopus catches from the RACE-GAP summer survey were common throughout the
3737 AI (Figure 193). Most catches occurred at moderate depths from 100-300 m, and were slightly more
3738 common further west. The final ensemble contained four equally weighted SDMs that fitted the data
3739 poorly (Table 57), and should be used with some caution. While the ensemble achieved a fair degree of
3740 accuracy in predicting catches with relatively low or high density ($\rho = 0.219$), it performed poorly by
3741 other metrics (AUC = 0.687; PDE = 0.107). It is unclear why the ensemble did not perform better, but
3742 stock managers have also reported difficulty estimating octopus population numbers and biomass. As this
3743 species typically hides in the substrate and rocky areas, it is possible that trawl gear is not an efficient
3744 method of sampling for octopods. The most important covariate in the ensemble was the presence of
3745 sponges, though this accounted for only 23.6% of the explained deviance, and a variety of covariates such

3746 as bottom depth, geographic position, bottom temperature, currents, and tidal maximum are required to
3747 account for the rest (Table 58). Octopus abundance was predicted to be high in places where sponges
3748 were present, bottom temperatures were warm, and the depth was approximately 150 m (Figure 194).
3749 Predicted abundance was high in areas with moderate depth and in patches near Atka, Adak, and the Rat
3750 Islands (Figure 194). These patches are similar to the distribution of sponges in the AI. The predicted CV
3751 of abundance did not display any clear patterns, and was high throughout (Figure 194). The predicted
3752 encounter probability map showed a few places with high values but many places where the encounter
3753 probability is 20-40% (Figure 195). This reflected that octopus are rarely caught in large numbers. Given
3754 the issues discussed above, it is difficult to determine if this indicated the actual population density of the
3755 species is usually low or if they are difficult to sample using trawl gear.

3756 **Essential fish habitat of giant Pacific octopus (all life stages combined) in the Aleutian Islands –**

3757 The habitat related abundance predictions based on RACE-GAP summer bottom trawl data
3758 (1991–2019) were translated into EFH area and subareas (Figure 196). Despite the low overall abundance
3759 of giant Pacific octopus in the survey, they were present in many areas of the AI and the predicted EFH
3760 area was large. EFH hot spots were located in the central and western AI and correspond to locations
3761 where sponges are likely to be present. The ensemble predicted a very close association between this
3762 species and sponges, which seems like a promising target for future research. However, given the poor
3763 model fit and the sampling issues inherent to this species, this EFH map should be treated with some
3764 caution.

3765 Table 57. Constituent species distribution models (SDMs) used to construct Essential Fish Habitat (EFH)
 3766 for giant Pacific octopus: MaxEnt = Maximum entropy; paGAM = presence-absence generalized additive
 3767 model; hGAM = hurdle GAM; GAM_p = standard Poisson GAM; and GAM_{nb} = standard negative-
 3768 binomial GAM. Ensemble performance (ρ = Spearman's rank correlation coefficient), root-mean-square-
 3769 error (RMSE), the area under the receiver operating characteristic (AUC), and the Poisson deviance
 3770 explained (PDE) were generated from k-fold cross-validation. The "--" in a field indicates that this SDM
 3771 was not included in the final ensemble.

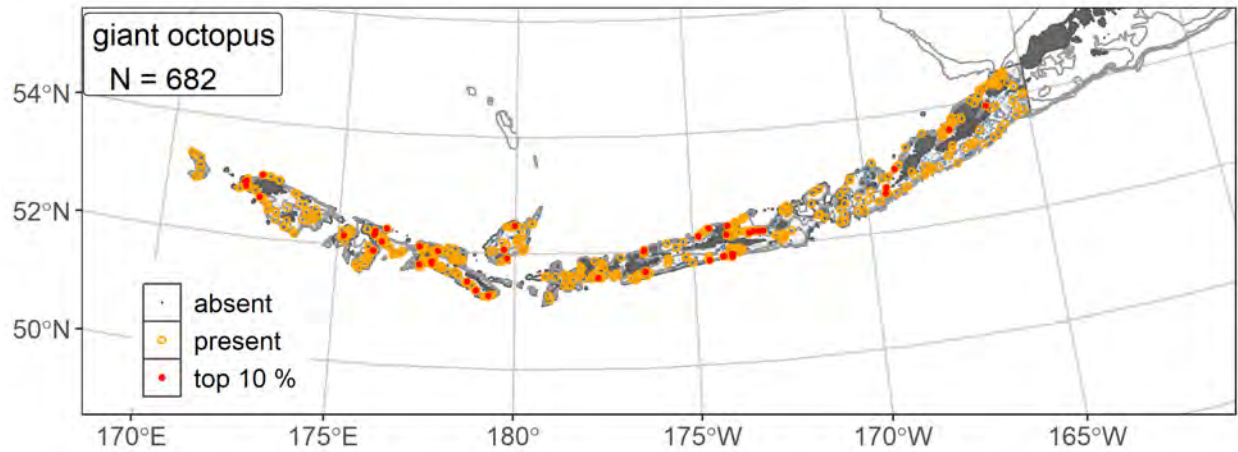
Models	RMSE	Relative Weight	ρ	AUC	PDE	EFH area (km²)
MaxEnt	0.82	0.250	0.218	0.688	0.084	71,000
paGAM	0.81	0.251	0.217	0.686	0.090	74,500
hGAM	0.82	0.249	0.205	0.683	0.112	71,000
GAM _p	0.82	0	--	--	--	--
GAM _{nb}	0.82	0.250	0.207	0.676	0.104	69,000
ensemble	0.81	1	0.219	0.687	0.107	72,800

3772

3773 Table 58. Covariates retained in the giant Pacific octopus species distribution model (SDM) final
 3774 ensemble, the percent contribution to the ensemble deviance explained by each, and the cumulative
 3775 percent deviance: BPI = bathymetric position index.

Giant Pacific octopus	Covariate	% Contribution	Cumulative % Contribution
a) all life stages	sponge presence	23.6	23.6
	bottom temperature	13.3	36.9
	bottom depth	9.8	46.7
	position	9.3	56.1
	current SD	7.6	63.7
	tidal maximum	7.2	70.9
	current	5.9	76.8
	aspect east	5.3	82.1
	aspect north	5.3	87.4
	curvature	3.5	90.9
	coral presence	2.5	93.4
	pennatulacean presence	2.2	95.6
	rockiness	1.6	97.2
	BPI	1.6	98.8
	slope	1.2	100

3776



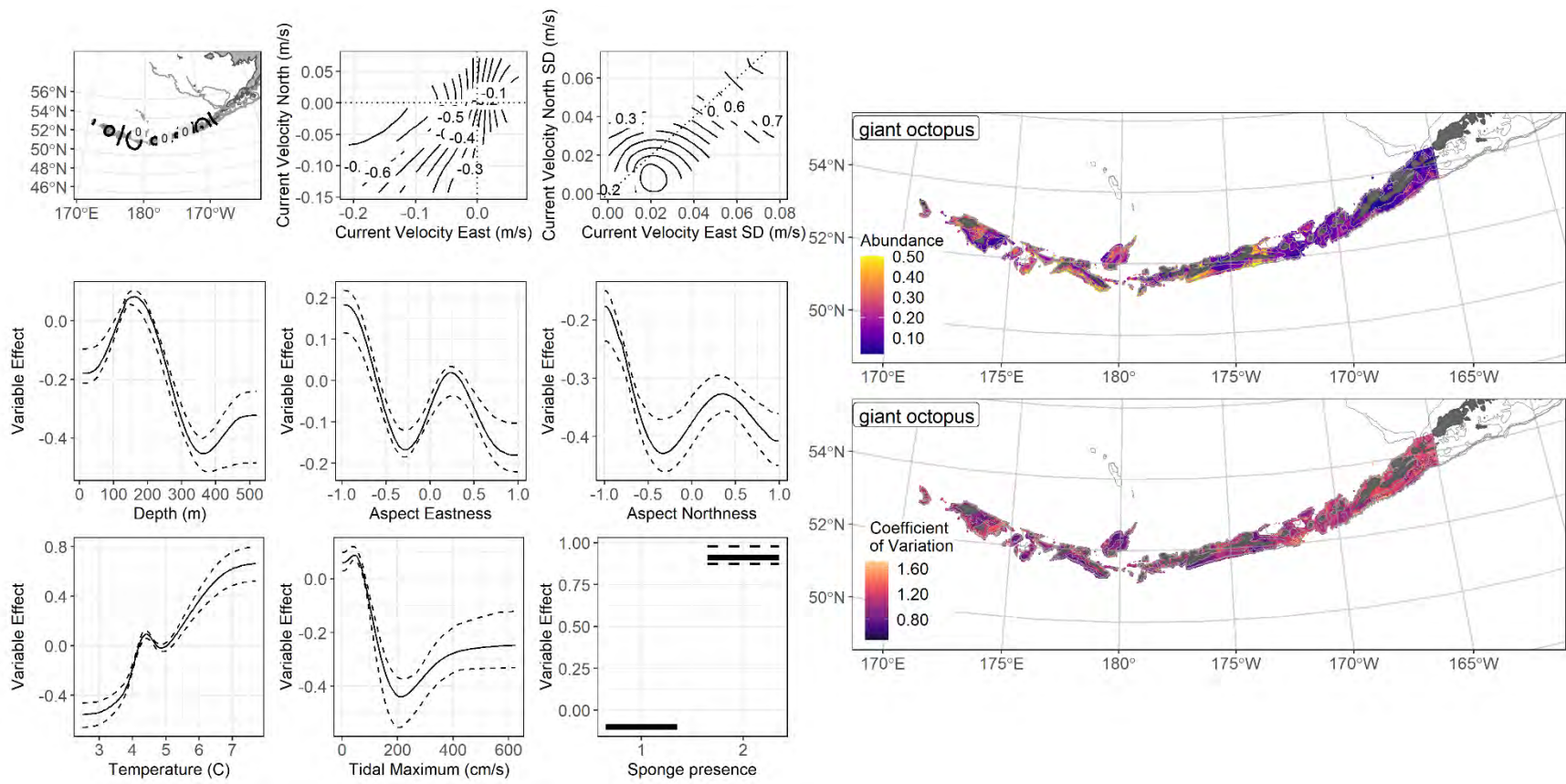
3777

3778 Figure 193. Distribution of giant Pacific octopus catches (N = 682) in 1991–2019 AFSC RACE-GAP

3779 summer bottom trawl surveys of the Aleutian Islands with the 100 m, 300 m, and 500 m isobaths

3780 indicated; filled red circles indicate locations in top 10% of overall abundance, open orange circles

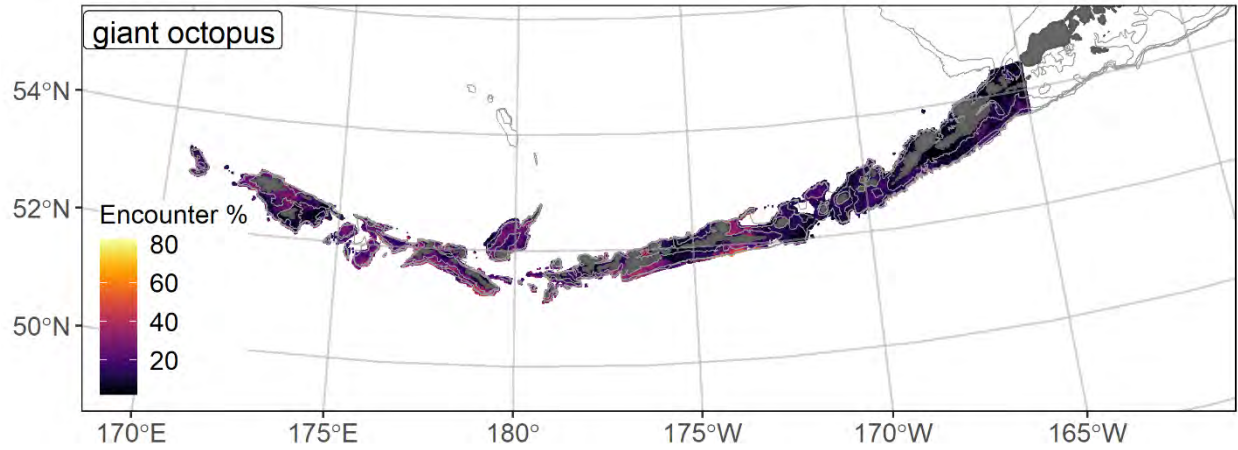
3781 indicate presence in remaining catches, and small blue dots indicate absence.



3782

3783 Figure 194. The top nine covariate effects (left panel) on ensemble-predicted giant Pacific octopus numerical abundance across the Aleutian

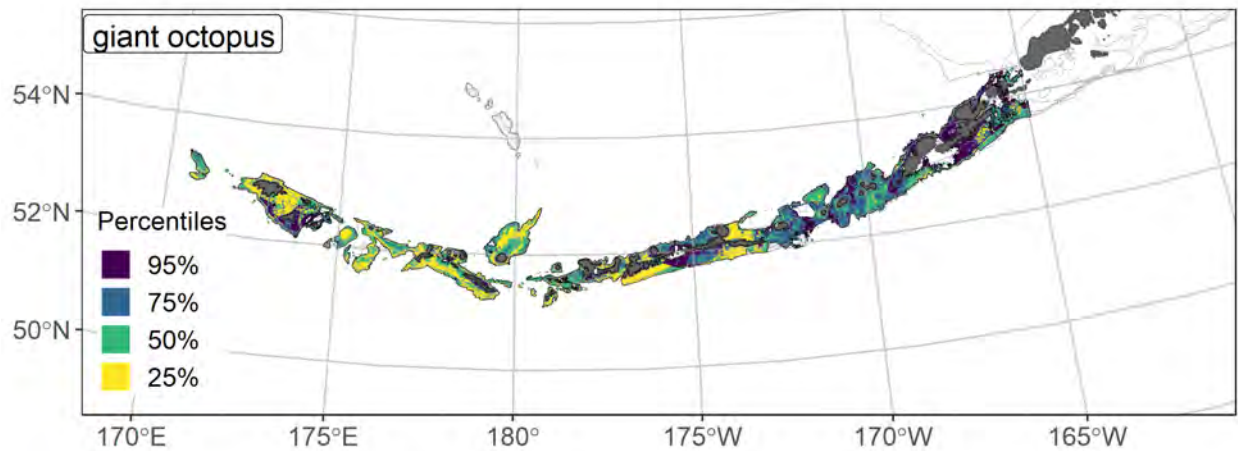
3784 Islands (upper right panel) alongside the coefficient of variation of the ensemble predictions (lower right panel).



3785

3786 Figure 195. Encounter probability of giant Pacific octopus from AFSC RACE-GAP summer bottom trawl
 3787 surveys (1991–2019) of the Aleutian Islands with the 100 m, 300 m, and 500 m isobaths indicated.

3788



3789

3790 Figure 196. Essential fish habitat (EFH area) defined as the top 95% of numerical abundance predictions
 3791 from a habitat-based ensemble fitted to giant Pacific octopus distribution and abundance in AFSC RACE-
 3792 GAP summer bottom trawl surveys (1991–2019) with 100 m, 300 m, and 500 m isobaths indicated;
 3793 internal to the EFH map are the subareas of the top 25% (EFH hot spots), top 50% (core EFH area), and
 3794 top 75% (principal EFH area) of habitat related, ensemble-predicted numerical abundance.

3795
3796
3797
3798
3799
3800
3801
3802
3803
3804
3805
3806
3807
3808

Future Recommendations

The EFH Final Rule requires that Fishery Management Councils and NMFS must periodically review the EFH components of FMPs and revise or amend these components with respect to new information at least every 5 years ([50 CFR 600.815\(a\)\(10\)](#)) with an overarching consideration that the science related to this effort meets the standards of best available science (NMFS National Standard 2 – Scientific Information 50 CFR 600.315). In the present work, we have adhered to these mandates as we have described and mapped EFH for FMP species in Alaska, using species distribution models (SDMs); incorporating modeling refinements and additional data sources where appropriate. While completing this work, and through conversation and review with stock assessment authors, other species experts, Plan Team members, the SSC, and additional stakeholders, we have also identified future refinements and recommendations that could be considered for future EFH 5-year Reviews. These recommendations fall into three areas: prioritizing and improving EFH for select species, increasing the scope and applicability of EFH research, and improving process.

3809

PRIORITIZE AND IMPROVE EFH FOR SELECT SPECIES

3810
3811
3812
3813
3814
3815
3816
3817
3818

The existing methodology for describing EFH works well for most species. For others, approaches need to be modified in order to better capture drivers of density and generate habitat descriptions. These approaches may involve incorporating new datasets (for fish distribution, environmental covariates, or life history parameters), or the development of modeling approaches that are amenable to their distributions (e.g., modeling at a broader spatial scale). For some of these species, the need for model improvements has been discussed in the results chapters for the current EFH Review cycle; in the future it is important to have processes in place (both modeling approaches and communication approaches) for these species. These may include agreed-upon differences in the modeling approach depending on the data needs and model ensemble performance in previous cycles.

3819
3820
3821
3822
3823
3824
3825
3826
3827
3828

3829
3830
3831
3832
3833
3834
3835
3836
3837
3838
3839
3840
3841

Leverage existing species distribution data

Data for species and life stages that are not well-sampled in the RACE GAP summer bottom trawl surveys may need to be augmented with data from other sources. In this study we combined additional surveys and data sources inshore of the RACE GAP survey area in a single, presence-only SDM (MaxEnt) to more comprehensively describe and map the EFH for the settled early juvenile life stage of 11 groundfish species. Data sets for EFH species, in particular the settled early juvenile life stage of groundfishes and crabs in nearshore areas, should be further developed to improve EFH descriptions and maps for species in nursery habitats, and to improve our understanding of how management decisions affecting nearshore and coastal nursery habitats may affect fishery productivity (e.g., Thorson et al. 2021).

Data other than the RACE-GAP summer bottom trawl survey that could be included in EFH descriptions include data from the North Pacific Observer program, the AFSC and IPHC longline surveys, and MACE acoustic surveys (e.g., McGowan et al. 2019, Monnahan et al. 2021). In these and other instances, it is important at a minimum to estimate fishing-power corrections between gears, and in some cases might be helpful to identify differences in vertical availability or selectivity ratios (Kotwicki et al. 2017, 2018; Monnahan et al. 2021; see “Develop methodology for combining disparate datasets” section below). The stock assessment author review of the EFH descriptions and identification (maps) (component 1) for the 2022 EFH 5-year Review suggested that the addition of longline survey data may be particularly helpful for arrowtooth flounder, blackspotted and rougheye rockfishes, shortraker rockfish, shortspine thornyhead, sablefish, and Pacific sleeper sharks. In addition, tagging studies and genetic data may be helpful and most useful for fitting process models, which can, in turn, inform SDMs for EFH species (Thorson et al. 2021). These data sources are summarized in Table 59. SDMs that take advantage of multiple data sources may improve the resolution and reliability of existing EFH descriptions.

3842 Incorporating existing datasets into future EFH descriptions and maps may also expand the
3843 spatial scope of EFH areas. For example, in the present work we combined nearshore surveys with
3844 offshore surveys in the Gulf of Alaska (GOA) to develop more comprehensive coverage of EFH species
3845 and life stages in nearshore areas (see above). There is also a potential for a multiscale approach to EFH
3846 that includes paired maps of nearshore and offshore areas, where nearshore maps could be of finer spatial
3847 resolution than the offshore maps depending on available data (e.g., Grüss et al. 2021b). With enough
3848 detailed information from other surveys, it may also be possible to identify biological processes occurring
3849 at a subregional scale, such as differences in growth or reproductive output. Dover sole (McGilliard et al.
3850 2019) and rex sole (McGilliard and Palsson 2017) in the GOA are other examples of species where
3851 additional survey data may help better distinguish subregional growth differences. Additional information
3852 can not only improve Level 3 EFH information, but is useful for stock assessments, especially for species
3853 with spatial management (e.g., sablefish; Hanselman et al. 2019). The spatial scope of EFH descriptions
3854 and maps will also expand with surveys of untrawlable habitats, including camera surveys.

3855 Combining data between the RACE-GAP bottom trawl surveys and other sources in the SDM
3856 ensemble framework presented by this study will require additional research as well as some collaborative
3857 guidelines for deciding on criteria for survey and data source inclusion (including non-standard surveys).
3858 These criteria may result in the elimination of some datasets from the current RACE GAP summer bottom
3859 trawl survey collection. For example, the Eastern Bering Sea slope survey was only conducted in 2002,
3860 2004, 2008, 2010, 2012, and 2016 and may not improve the EFH definitions for Bering Sea species. It
3861 will take some modeling effort to determine parameters like gear efficiency ratios that can be used for
3862 combining data in SDMs.

3863 Some species have distributions that occupy a narrow subarea within the trawl survey area, or
3864 have limited data, and thus likely require alternative SDM approaches. For these species, it may be
3865 sensible to adopt species-specific modeling approaches where possible to accommodate some of these
3866 idiosyncrasies. Species like sablefish and shortraker rockfish in the EBS have “long and skinny

3867 distributions”, which result in poor model fits; species with limited data in a particular region have
 3868 relatively low ensemble performance, compared to other species modeled in the present study, and would
 3869 benefit from additional survey data to improve ensemble outcomes. In the case of some species at the
 3870 edge of their distribution, expanding the spatial scope of the modeled area may yield better EFH
 3871 information (e.g., Atka mackerel EFH in the EBS might be improved by modeling the Bering Sea and
 3872 Aleutian Islands together); in other cases additional survey data from the same location may be needed
 3873 (e.g., EBS sablefish from longline surveys).

3874 Table 59: Data sources to consider incorporating for species distribution.

Data source	Type of data (presence/absence, density, etc)	Species for which these data are important	Path to SDMs
North Pacific Observer Program	Presence/absence (PA), density, age and length distributions	Commercially targeted species (e.g., pollock, cod, sablefish, yellowfin sole, etc.)	PA and density data can be used directly; age and length distributions can inform IBMs
IPHC longline surveys	PA, density, age and length distributions	Arrowtooth flounder, blackspotted and roughey rockfishes, shortraker rockfish, shortspine thornyhead, sablefish, and Pacific sleeper shark, skates	PA and density data can be used directly; age and length distributions can inform IBMs
AFSC longline surveys	PA, density, age and length distributions	Arrowtooth flounder, blackspotted and roughey rockfishes, shortraker rockfish, shortspine thornyhead, sablefish, and Pacific sleeper shark, skates	PA and density data can be used directly; age and length distributions can inform IBMs
MACE acoustic surveys	PA, density	Prey species, groundfish with more midwater distributions (e.g., pollock)	Include directly in SDMs after estimating gear efficiency ratios
Tagging studies	Movement parameters and nonlocal effects	Sablefish, Pacific cod, arrowtooth flounder, Pacific ocean perch	Parameterize IBMs to inform species distribution models
Genetic data	PA, density	Blackspotted rockfish, Atka mackerel	Include directly in SDMs after estimating gear efficiency ratios and/or spatial sampling precision

3875

Leverage environmental data

3876

3877

3878

3879

3880

3881

3882

3883

3884

3885

The suite of habitat-related covariates used to parameterize SDMs in the present work was extensive, covering static and dynamic metrics ranging from bathymetry and seafloor terrain features, to long-term averaged, observed bottom temperatures and modeled tidal and bottom currents. Ongoing work is exploring the utility of fitting bottom temperature or other covariates over annual time scales, which may provide insight as to how well models with long-term averaged covariates explain historical species distributions (e.g., Barnes et al. *in review*). Covariates from climatological models (e.g., Bering10K ROMS or GOA 3K ROMS NPZ) can be used for hindcasting and forecasting population responses over a variety of climate scenarios and time scales (Thorson et al. 2020b; Rooper et al. 2021, Barnes et al. *in review*). In addition, covariates utilized in the present work should be evaluated *post hoc* to determine if some of the present suite of predictors could be eliminated in the next EFH Review.

3886

3887

3888

3889

3890

3891

3892

3893

3894

3895

As of this EFH report, environmental habitat covariates have included geographic position, bottom temperature, depth, bathymetry derived terrain metrics, tidal and bottom currents, sediment grain size, seafloor rockiness, and the presence of structure-forming invertebrates. Several other covariates may impact groundfish and crab distributions, including (1) irradiance spatially interpolated from net sensors; (2) average (across years and/or seasons) surface chlorophyll from satellites, perhaps broken into size or functional groups; (3) average storm frequency as proxy for turbulent mixing; (4) average mixed layer depth or other stratification variables; (5) spatially interpolated empirical data or modeled values for secondary producers (copepods and euphausiids) from RPP/MACE/EMA programs and ROMS. Surface chlorophyll covariates were produced for the 2017 EFH report. These data were used for pelagic early life stages in 2017 and could be adapted to future SDMs for pelagic and demersal life stages.

3896

3897

3898

New dynamic covariates can also be explored for inclusion in the SDMs in the future (e.g., prey fields, remote sensing data sets, the Cold Pool or El Niño Southern Oscillation indices, etc.). Many of the covariates in the current report are fixed characteristics of the physical habitat, including substrate and

3899 depth. However, for more mobile and/or more pelagic species, important physical habitat may also
3900 include areas with high productivity, prey density, and temperature. We recommend the careful
3901 consideration and inclusion of important covariates as they are available in future EFH Reviews. Many of
3902 these data are currently available, though some work will be required to properly prepare them for use in
3903 SDMs (Table 60). We encourage further evaluation of SDMs with dynamic covariates to leverage high-
3904 resolution temporal and spatiotemporal data and improve the accuracy of EFH information. In these
3905 cases, we would likely need to average predictions of density across some larger number of years.

3906 Existing data should be updated based on ongoing work, including covariate data and species
3907 distribution data. For example, bathymetry for the EBS has been updated and should be included in the
3908 next EFH report. Some datasets (e.g., trawl data from the Northern Bering Sea prior to 2010) may be used
3909 to extend the temporal scope of EFH. Summarizing and communicating data limitations will help
3910 prioritize data gaps to fill. Existing data may be used in new ways to inform ecological differences
3911 between regions; for example covariate effects may vary across regions and this information could be
3912 useful for stock assessments and for regional management.

3913 **Leverage life history information and process studies**

3914 The data necessary for using SDMs to describe and map EFH are species-specific response
3915 variables (i.e., presence-absence or abundance) and habitat-related predictors (covariates) such as bottom
3916 depth or bottom temperature. Because the MSA EFH Regulations specify that EFH descriptions are both
3917 species- and life stage-specific, life history updates are an integral part of incorporating new data and
3918 applying best available science to the EFH components of FMPs. Striving to improve life history data and
3919 EFH information for ecologically distinct and underrepresented life stages is an ongoing priority.

3920 In this report, species-specific length-based life stage definitions were employed to separate
3921 settled early juveniles from subadult stages and subadults from adult stages. We recommend that future
3922 EFH work leverages existing data sources and process studies, including novel approaches, to continually

3923 improve the available life history information. The next EFH 5-year Review should apply the crab
3924 maturity data regularly collected on Bering Sea RACE-GAP bottom trawl surveys to inform life stage-
3925 specific SDMs for these ecologically important species in the BSAI King and Tanner Crabs FMP. This
3926 effort should involve collaboration with scientists from the AFSC Kodiak Laboratory and the Alaska
3927 Department of Fish and Game (ADFG), both of which have crab size measurements and maturity data.
3928 These data could be used to apportion crab catches to mature and immature life stages in the EBS and to
3929 describe and map those life stages for the next EFH 5-year Review.

3930 Existing process studies on species physiology, behavior, and diets can be used to improve the
3931 selection of habitat covariates, inform life history and behavioral parameters, generally improve SDMs,
3932 and inform mechanistic models that can be used to link environment drivers and ecosystem processes. For
3933 example, process studies may inform which life stage of a given species is most likely to be influenced by
3934 a given environmental process. Life stage specific parameters can be integrated to obtain growth
3935 parameters at the population level. They can also inform IBMs that account for life stage-specific habitat
3936 needs and behaviors (e.g., foraging, water column position, movement between areas). In 2020, the SSC
3937 recommended several pathways by which IBMs could be used to improve habitat information, including
3938 through mapping of pelagic early life stage habitat (EFH), the incorporation of ecosystem model outputs
3939 in IBMs, and the use of IBMs to estimate the value of different spawning locations. IBMs can also be
3940 used to integrate life stage information and better assess the impacts of human activities (e.g., fishing) at
3941 the population scale. Process modeling studies can also incorporate existing IBMs (e.g., Gibson et al.
3942 2019, sablefish; Hinckley et al. 2019, Pacific cod; Daly et al. 2020, red king crab), where life history and
3943 behavioral parameters can be updated with new process studies from the laboratory and field and
3944 advancements to the modeling environment (e.g., ROMS).

3945 Structural equation models (SEMs) can help better identify environmental drivers and link them
3946 mechanistically to population impacts (Thorson et al. 2021). Spatial demographic models accounting for
3947 movement rates among areas can help address issues of non-local habitat impacts, impacts of

3948 management decisions on non-surveyed age classes, and provide another way to evaluate the combined
3949 effects of fishing and habitat impacts at the population scale. Process-based approaches are helpful to
3950 describe and map EFH, inform ecosystem-based fisheries management (EBFM) (e.g., Goldstein et al.
3951 2020), and determine the population-level impacts of management decisions (e.g., Thorson et al. 2021).

3952

3953

Combine disparate datasets

3954 In the present studies, our primary response variable was numerical abundance generated from the
3955 fishery-independent RACE-GAP summer bottom trawl surveys. We also modeled settled early juvenile
3956 life stage distribution from a variety of inshore and offshore fishery-independent surveys utilizing various
3957 sampling modes (e.g., RACE-GAP large mesh bottom trawls, ADFG small mesh bottom trawls, and
3958 beach seines) employing MaxEnt modeling of presence as a vehicle to combine these disparate data
3959 sources in analyses. There is a growing body of research that could be harnessed in the future to better
3960 quantitatively combine data from disparate data sources and fishery-dependent collections, thereby
3961 expanding the scope and seasonal availability of species response variables to the SDMs. We recommend
3962 that combining disparate data sources be a priority area of research development for future EFH Reviews.

3963 One of the refinements we implemented in the present work was to move away from single
3964 models for species-specific SDMs to an ensemble modeling approach. Ensemble models have been
3965 shown to improve performance (better model fits; Rooper et al., 2017b). Of the five constituent models
3966 estimated and considered for the final ensembles in the present work, four were GAMs and the fifth was a
3967 MaxEnt model describing the probability of the presence of suitable habitat for each species in a given
3968 location. One recommendation for future EFH reviews is to expand the variety and types of models
3969 considered in the ensemble approach (e.g., random forest or spatio-temporal models) to expand the range
3970 of fitting capabilities across the wide array of distribution patterns encountered in our data sets. As
3971 mentioned above, taking a modeling approach that facilitates combining data from disparate data sources

3972 should also be considered since it would expand the number and types of response variables available to
3973 the EFH descriptions in both space and time.

3974 There are several datasets that could be used to either improve existing EFH information within
3975 the survey areas, or to expand the spatial and temporal extent over which we provide EFH information
3976 (e.g., North Pacific Observer data, AFSC longline survey, ADFG small-mesh bottom trawl survey, etc.).
3977 Additional work is needed to be able to combine these disparate datasets in the same SDMs including the
3978 estimation of sampling efficiency ratios for surveys with different gear efficiencies (e.g., O’Leary et al.
3979 2021).

3980 **Consider diverse constituent models**

3981 SDM approaches are still under development and should be reviewed regularly. As of the present report,
3982 MaxEnt models do not directly model absences (Phillips and Dudík 2008) and so may overpredict
3983 occupancy based on covariates in the detection areas into areas where a species was not detected. GAM
3984 approaches explicitly account for presence/absence and do so in a more ecologically realistic way by
3985 modeling presence and absence as a binomial process. In this EFH Review, we presented presence-
3986 absence GAMs, hurdle GAMs, standard GAMs using the Poisson distribution, as well as GAMs using the
3987 negative binomial distribution to account for overdispersion. In the future, we propose to explore
3988 alternatives for modeling distributions. For species with limited data, random forests, boosted regression
3989 trees, and other approaches may be more appropriate to include in model ensembles. Our current
3990 ensemble framework can be readily expanded to test and incorporate additional constituent SDMs.

3991

3992 **INCREASE SCOPE AND APPLICABILITY OF EFH RESEARCH**

3993 Ongoing discussions with the SSC and stock assessment authors have identified conceptual frameworks
3994 that should be considered in the future for developing, evaluating, and utilizing EFH descriptions and
3995 maps. Considering how EFH is defined in terms of scale and ecological function could improve the utility

3996 of this concept for management. The present working definition of EFH equates the area containing 95%
3997 of the total estimated occupied habitat with EFH (NMFS 2005), and core habitat as the area containing
3998 50% of occupied habitat. In the present work, occupancy was defined as areas with >5% probability of an
3999 encounter based on the RACE GAP bottom trawl survey data. However, this definition may not be as
4000 ecologically meaningful for highly mobile species, or those with a high degree of uncertainty in the
4001 estimate of their population density. For example, the distribution of highly mobile predators might be
4002 more strongly impacted by prey availability than by environmental conditions. It may also not be a useful
4003 metric if a shrinking proportion of their population is available to the bottom trawl survey, as is the case
4004 for species with poleward-shifting distributions. As models describing and predicting species distribution
4005 and abundance (density or biomass) become more tightly and realistically linked to habitat and
4006 environmental change, there may be opportunity to reconsider how EFH is defined, potentially arriving at
4007 a more objective and constrained (less open to interpretation) definition that could be universally
4008 applicable across species and regions.

4009 **Describe prey species habitat**

4010 Many groundfish species are predators of smaller forage species and likely respond to changes in the
4011 density of euphausiids and other prey species. They may also be adequate samplers not only of available
4012 forage for predators, but also of prey biomass (Ng et al. 2021). Approaching groundfish density from the
4013 perspective of prey availability aligns with EFH component 7 in the FMPs (Prey Species: “FMPs should
4014 list the major prey species for the species in the fishery management unit and discuss the location of prey
4015 species' habitat”; [50 CFR 600.815\(a\)\(7\)](#)), which includes predator-prey dynamics. Several data sources
4016 are available for capturing predator-prey interactions spatially, including data on forage density from
4017 midwater acoustic surveys done by the Midwater Assessment and Conservation Engineering (MACE)
4018 division and stomach content data from Resource Ecology and Ecosystem Modeling (REEM). For
4019 midwater predators especially, data from midwater acoustic surveys may provide useful information on
4020 prey fields and therefore distribution. As prey fields shift on short time scales, the appropriate modeling

4021 approach will likely be a dynamic approach as opposed to the static EFH maps drawn based on temporal
4022 averages.

4023 Stomach contents, behavioral studies, genetics, and other datasets can be used to identify areas of
4024 prey abundance, and diet proportions can be analyzed to provide new SDM predictors (Thorson et al.
4025 2021; Grüss et al. 2020, Grüss et al. 2021b). Predator stomach contents can be fit with environmental
4026 covariates, providing a more mechanistic approach for modeling trophic interactions. We recommend that
4027 future studies further explore the potential for predator diets to serve as indices of prey abundance and
4028 distribution, including through an SDM framework to develop maps of prey habitat (i.e., EFH component
4029 7 - “location of prey species habitat”). This effort may in turn help identify areas of importance for their
4030 EFH species predators.

4031 **Expand to EFH Levels 3 and 4 where appropriate**

4032 In the present EFH Review, growth, lipid accumulation, and energy loss are the vital rate parameters
4033 included to explore Level 3 EFH (habitat-related vital rates). In the future, we recommend adding other
4034 vital rates such as lipid consumption or fecundity, as well as Level 4 rates like habitat-related productivity
4035 or recruitment. Currently we have Level 2 EFH information for crab species in the EBS and AI; Level 3
4036 information for crab species could be obtained with growth rate information from surveys carried out by
4037 ADFG and the AFSC Kodiak Laboratory (see the “Add life stages” section above).

4038 **Continue to advance and apply dynamic SDM methods**

4039 Ongoing research indicates that dynamic models that capture interannual shifts in density and in habitat
4040 covariates describe historical habitat better than static models (Barnes et al. *in review*). Other work shows
4041 that many biological processes affecting fish distributions occur on a seasonal timescale, or even a weekly
4042 basis (e.g., Thorson et al. 2020a). In 2020, the SSC asked about the implications of higher or lower
4043 sampling frequency for EFH descriptions; considering more dynamic models in the model ensemble

4044 would help address this. Continuing to evaluate the impacts of model complexity (including time-varying
 4045 covariates) on model fit will be necessary to ensure that EFH maps capture relevant processes.

4046 Many of the habitat covariates identified for further exploration are dynamic in nature and require
 4047 a modeling approach that accounts for this. For example, areas of high productivity or high prey density
 4048 may be important for higher trophic levels, but their location will shift over time in response to
 4049 environmental drivers, including currents, light, and the timing of ice retreat. Therefore, dynamic SDMs
 4050 applied over shorter time spans should be considered as an option for presenting dynamic maps alongside
 4051 static SDM EFH maps (based on long term averages) in the next EFH Review. Pairing temporally
 4052 dynamic and static (long term) approaches to describe and map EFH will improve understanding of how
 4053 species habitat availability and spatial stock structure shift in space and time, which is needed to improve
 4054 climate-responsive approaches to EBFM.

4055

4056 Table 60: Existing environmental datasets to explore as covariates in future EFH analysis.

Covariate	Source	Current status	Future direction	Data processing needed
Light levels (irradiance)	Bering Sea ROMS model. Vertical profiles of light levels (PAR) available from RPA (EcoFOCI PMEL, EMA) data. Contacts: Jeanette Gann, Phyllis Stabeno.	Water column irradiance could be calculated from ROMS light attenuation and other variables but is not currently a diagnostic output of the ROMS model. In Access database for EMA Bering surveys (2003-present); PMEL mooring survey data also available.	Use light fields to define suitable habitat for visual predators.	If it is to be used as a covariate, irradiance will have to be added as a diagnostic output to future versions of the Bering Sea ROMS model. Then it can be used to calculate other values.

Covariate	Source	Current status	Future direction	Data processing needed
Bottom light levels (optical depth)	Net sensors on bottom trawls (vertical profiles and on bottom in situ irradiance-RACE GAP); vertical profiles of light levels (PAR) available from RPA (EcoFOCI PMEL, EMA) data. Contacts: Jeanette Gann, Phyllis Stabeno.	Available for recent years (EBS: 2004-present, NBS: 2010-present, GOA: 2005-present, AI: 2006-present) (Rohan et al. 2020, Rohan et al. 2021)	Use light fields to define suitable habitat for visual predators. Optical depth (depth \times diffuse attenuation coefficient) can be used to identify areas where predators can find prey	Data may require additional kriging; interpolation for years/areas where data are absent
Surface total chlorophyll estimates (satellite)	Satellite data (when cloud cover and sea ice are not interfering). Contact: Jens Nielsen (CICOES).	Includes all phytoplankton together. Data have been organized for including as covariates as of 2017 EFH report.	Test phytoplankton as covariate in SDMs	No further processing needed.
Surface total chlorophyll estimates (discrete/ in situ)	CTD cast data from discrete sampling stations; includes fluorometer for chl a from RPA cruises. Contacts: Jeanette Gann, Colleen Harpold.	Bering Sea data stored in Access; GOA and AI data may not be available yet.	Use as coarser measure of productivity	Unknown
Ice algae	Not available yet	Not yet available	Likely related to sea ice; food resource for crabs and other benthic invertebrates	Unknown
Size-fractionated surface chlorophyll (discrete / in situ)	Taxonomic data collection in progress. Contacts: Lisa Eisner; Jeanette Gann	Bering Sea data stored in Access; GOA and AI data may not be available yet (PI: Lisa Eisner; contact Jeanette Gann with database inquiries)	Larger phytoplankton may be better food (e.g., diatoms) so size fractions might better indicate food availability / quality. There will be a seasonal shift to smaller sizes but persistent hotspots probably have many sizes.	Unknown

Covariate	Source	Current status	Future direction	Data processing needed
Size-fractionated surface chlorophyll (satellite)	Contact: Jens Nielsen	Satellite algorithm still in development. Included in ESR for Eastern Bering Sea.	Larger phytoplankton may be better food (e.g., diatoms) so size fractions might better indicate food availability / quality.	Additional interpolation may be necessary.
Size-fractionated and size-specific or vertically integrated chlorophyll samples (spring and fall)	Contacts: Lisa Eisner, PhD student Jeanette Gann	TBD following collaboration discussion. In Access database for EMA Bering surveys (2003-present); PMEL mooring survey data also available.	Larger phytoplankton may be better food (e.g., diatoms) so size fractions might better indicate food availability / quality.	Additional interpolation may be necessary.
Storm frequency (proxy for turbulent mixing)	May be available from wind speeds (Contact: Pelland) or in ESRs.	Unknown	Turbulent mixing may influence food availability and productivity.	Unknown
Timing and size of spring bloom	Derived from variables described above	Nielsen in ESR for Eastern Bering Sea	For a spatially-varying response, an annual index can still generate interesting differences in distribution among years (Thorson 2019)	Annual indices ready to use for EBS; may be available for other regions.
Average mixed layer depth	PMEL moorings (seasonal coverage) and oceanographic surveys (PMEL, RPA). Contact: Jeanette Gann, Jens Nielsen, Phyllis Stabeno.	In Access database for EMA Bering surveys (2003-present); PMEL mooring survey data also available.	Mixed layer depth may impact food availability and productivity; may be useful for Component 1 descriptions.	Unknown
Cold Pool Index (CPI)	Net sensors on bottom trawls. CTD data from RPA ecosystem and mooring surveys. Also ROMS model output. Contact: Kearney.	CPI is fairly standard (O'Leary et al. 2020) but has not been used in EFH so far. Data ready for use.	Use CPI as covariate to improve EFH Component 1 descriptions.	May require additional interpolation.

Covariate	Source	Current status	Future direction	Data processing needed
Secondary producers (other forage including copepods and euphausiids)	RPP/MACE/EMA surveys- zooplankton water column net tows (Contact: Dave Kimmel) and diets in forage fish (Contacts: Dave Kimmel, Alex Andrews). Gut contents from stomach sampling on trawl surveys. ROMS modeled values (e.g., GOA NPZ 3K ROMS small and large copepod fields; Contact K Coyle)	Data available	Use prey data to develop prey habitat descriptions for Component 7.	May require additional interpolation and/or diet data to determine important taxa or sizes.
Secondary producers: euphausiids	MACE product from midwater acoustic survey (Contact: Patrick Ressler)	Used annually for Ecosystem Status Reports.	Use prey survey data to explore EFH for predators, e.g., euphausiid data can be used as covariate for midwater foragers like walleye pollock	May require additional interpolation. Acoustic data may need additional manipulation.
Secondary producers: stomach contents as direct measure of foraging success	REEM stomach contents data	Data available	Can be used in a spatial model to interpolate (examples: Ng et al. 2021; Grüss et al. 2020; Grüss et al. 2021b); methods exist to fit with environmental covariates using GAMs and GLMs	Data may require additional kriging or similar

4057

4058
4059
4060
4061
4062
4063
4064
4065
4066
4067
4068

IMPROVE PROCESS AND COMMUNICATION

Improving methodological approaches and clearly communicating them is a high priority. Review and input by the Council’s SSC, Plan Teams, the stock assessment authors, and other stakeholders is an important part of the iterative EFH 5-year Review process. Expert peer-reviews in particular can help identify cases where changes are needed to account for species with lower quality data or low availability to the surveys where species data has been used to model and map EFH. Additionally, the EFH process involves communicating model results to a broad stakeholder audience and adapting models when appropriate based on feedback. For example, a species with poor model fits or low stock assessment author confidence in the EFH map might be evaluated using a different SDM, or certain data requirements might be identified early that would lead to that species being modeled differently. Each EFH 5-year Review is an opportunity to improve the process and communication.

4069
4070
4071
4072
4073
4074
4075
4076
4077
4078
4079
4080
4081
4082

We are proud of the process and communication improvements that we implemented during this EFH 5-year Review to improve coordination and collaboration between SDM EFH analysts and stock assessment authors. We have implemented SSC suggestions from 2021 about communicating methods and results, including providing descriptions of ensemble modeling methods and probability thresholds, clear descriptions of data including data transformations and timeframes, and summaries of skill testing results. We (AKRO and AFSC) hosted a stock assessment author summit in January 2021 to discuss and co-develop the review process of the current and new EFH descriptions and maps. We set a timeline that worked for all parties and agreed on the content to be reviewed and the methods, which was well communicated and executed in an approachable process for the reviewers. In past EFH 5-year Reviews, current EFH descriptions and maps in the FMPs were provided to stock assessment authors with the new EFH maps for review. In this EFH Review, as the SDM ensemble EFH methods represent a significant advancement over the 2017 SDM EFH approach, and expert peer-review is an important part of the iterative EFH 5-year Review process; we provided the stock assessment authors with the complete set of regional SDM ensemble EFH methods (3 regions) and species results chapters (118 chapters). Stock

4083 assessment authors are considered subject matter experts, whose input was used to ground truth EFH
4084 information, including improving the modeling methodology in general and for their species. We
4085 recommend that an agreement be reached at the beginning of next 5-year review regarding the process
4086 and scope for stock-assessment author review, in a way that remains feasible for the EFH analytical team.

4087 **Communicate confidence in EFH designations**

4088 In 2021, the SSC recommended that analysts define thresholds for excluding or denoting areas where
4089 uncertainty is high (e.g., report the ratio of estimated response to uncertainty). This would allow scientists
4090 to communicate areas where confidence in the EFH designations was high vs. low. Propagating
4091 uncertainty through the existing EFH maps in this way is unclear, and may lead to “patchy” maps that are
4092 more difficult to communicate with stakeholders and regional managers. Additionally, the coefficients of
4093 variation (CVs) from cross-validation that we reported in the present results largely track abundance
4094 predictions from SDMs, as areas with high abundance tend to have high uncertainty when abundance is
4095 Poisson-distributed. Future studies should evaluate uncertainty and find ways to communicate uncertainty
4096 in SDM predictions; determine where uncertainty in untrawled/untrawable areas differs from that in
4097 trawled/trawable areas; and evaluate how these designations might be successfully communicated and
4098 addressed in EFH descriptions.

4099 **Develop thresholds for EFH mapping and test them**

4100 Another aspect where the EFH 5-year Review process and communication can be strengthened is the
4101 scientific guidance that informs the various thresholds applied to map EFH from SDMs and evaluate
4102 these EFH maps with the fishing effects model (SASI model; Smeltz et al. 2019) and subsequent analysis
4103 of stock level impacts by the stock assessment authors (Simpson et al. 2017). Also, with respect to
4104 conceptual frameworks that should be considered in the future for developing, evaluating, and utilizing
4105 EFH descriptions and maps within the EFH Regulations (see above section “Increase Scope and

4106 Applicability of EFH Research”). We recommend forming a Work Group to develop and communicate
4107 scientific guidance on both of these aspects to the SSC prior to the start of the next EFH 5-year Review.

4108 **Add more opportunities for communication**

4109 Monitoring research, process research, and model development should be coordinated in order to target
4110 knowledge gaps about the relationship between habitat, fishing, and fishery productivity. This
4111 coordination should occur across divisions and include conversations with researchers who work outside
4112 the existing EFH areas, in cases where species ranges are suspected to be shifting. Ongoing conversations
4113 with stakeholders about management priorities and risk tolerance and tradeoffs, will help frame process
4114 and modeling studies (Thorson et al. 2021). With consistent stakeholder involvement, simulation
4115 approaches such as management strategy evaluation (MSE; Smith 1994, Punt et al. 2016) can be used to
4116 compare the performance of different management strategies and data collection practices (like survey
4117 frequency) under various degrees of uncertainty, including process and model uncertainty.

4118 **Streamline workflows and reproducibility**

4119 Further improving communication around data and code can be achieved with currently available tools.
4120 For the next EFH 5-year Review, we recommend augmenting the existing review process with more best
4121 practices for open data science, sharing code with reviewers and collaborators and creating more
4122 reproducible workflows to streamline the EFH process (e.g., Lowndes et al. 2017). These changes should
4123 include producing reproducible code, making covariate/raster data available through NCEI ERDDAP and
4124 AKFIN, and automating the generation of EFH reports and presentation slides using Markdown to
4125 streamline the creation of EFH products. Reproducible code practices should include the production of an
4126 R package for the EFH SDMs, so that scientists with species distribution data can easily test model
4127 improvements and new data sources instead of waiting for EFH analysts to carry out these comparisons.
4128 When data or modeling approaches need to be modified for select species (first section of this chapter),
4129 they can be adjusted just for those species while others are only updated with new data each EFH cycle.

4130 Tracking comments and changes to the models, making code available to stock assessment authors, and
4131 automating some of the map and report generation processes will improve transparency and speed up the
4132 generation of EFH products.

4133 **CONCLUSIONS**

4134 We have identified several areas where Essential Fish Habitat research can be advanced in the coming
4135 EFH 5-year Review cycles (Table 61). Further work in these areas will identify better SDMs or SDM
4136 ensembles for defining EFH, especially for species with less available trawl data. Advancements in many
4137 of the areas we describe here are connected to other topics; for example the development of approaches
4138 for quantifying and describing uncertainty in EFH maps (see the “Modeling” section) will also improve
4139 Process and Communication, providing a straightforward way of communicating uncertainty to stock
4140 assessment authors and the Council.

4141 The studies recommended here will take longer than one EFH 5-year Review cycle, so some care
4142 should be taken to identify priorities for data collection, data setup, and model development. We identify
4143 next steps needed for projects involving new covariates in Table 60 and areas where cross-disciplinary
4144 collaboration will be especially helpful in Table 61. Cross-divisional collaborations will expand the suite
4145 of covariate data that can be incorporated into EFH models and provide a basis for ongoing discussions
4146 about ecosystem structure and function as they relate to EFH. Modeling advancements will provide ways
4147 to use existing data, account for processes that affect multiple life stages, and account for environmental
4148 drivers mechanistically. Finally, discussions with stakeholders and modelers can form a strong foundation
4149 for the design of simulation studies that assess the impacts of management decisions on EFH species.

4150 Table 61: Summary table of future recommendations for EFH research to advance EFH component 1
 4151 descriptions and maps, and how EFH component 1 outputs are evaluated and applied to management.

Area of research	Improvement/advancement	Taxa with potential EFH improvement
Prioritize and improve EFH for select species	Leverage existing species distribution data to expand spatial scope and improve predictions in existing EFH maps	Species where higher-quality EFH information is needed (current maps contradict expert experience; model fits are relatively low compared to other species modeled)
	Leverage environmental data	All (especially species where higher-quality EFH information is needed)
	Improve life history information with best available science	All (especially crab species)
	Expand and improve existing SDM EFH mapping to include species and life stages in the nearshore (e.g., at appropriate spatial resolutions)	Many EFH species and their prey that inhabit nearshore habitats
	Develop methodology for combining disparate datasets	Species where higher-quality EFH information is needed
	Develop process studies to inform EFH descriptions and maps (e.g., vital rates, movement, population dynamics)	All
	Consider diverse constituent models	Species where higher-quality EFH information is needed; especially those with EFH level 1 information only
Increase scope and applicability of EFH research	Describe prey species habitat (EFH component 7)	Most groundfish, especially those with diets more specialized on forage
	Expand to EFH Levels 3 and 4	All
	Continue to advance and apply dynamic SDM methods in development to map and forecast shifts in EFH and spatial stock structure to improve climate responsive approaches to EFH and EBFM	All
Improve process and communication	Communicate confidence in EFH designations/boundaries	All
	Develop thresholds for mapping EFH with SDMs and SDM EFH applied to the Fishing Effects analysis (e.g., thresholds applied), through research and an expert work group, and communicate this guidance to the SSC prior to the launch of the next EFH 5-year Review.	All
	Add more opportunities for communication	All
	Streamline workflows and reproducibility	All

4152

ACKNOWLEDGEMENTS

4153

4154 We thank Lyle Britt, Wayne Palsson, and Stan Kotwicki of the NMFS AFSC Groundfish Assessment
4155 Program for their strong support of this work. We wish to thank Gretchen Harrington, Kim Rand, Jim
4156 Thorson, and Molly Zaleski for their insightful reviews of this report. This work was greatly improved by
4157 the time and energy invested by all of the stock assessment authors and stock experts who contributed to
4158 the review of these documents. This project was funded by the AKRO/AFSC Essential Fish Habitat
4159 Research Funds.

4160

4161

REFERENCES

- 4162 Abookire, A. A. 2006. Reproductive biology, spawning season, and growth of female rex sole
4163 (*Glyptocephalus zachirus*) in the Gulf of Alaska. Fish. Bull. 104(3):350-359.
- 4164 Abookire, A. A., and B. J. Macewicz. 2003. Latitudinal variation in reproductive biology and growth of
4165 female Dover sole (*Microstomus pacificus*) in the North Pacific, with emphasis on the Gulf of
4166 Alaska stock. J. Sea Res. 57:198-208.
- 4167 Abookire, A. A., and K. M. Bailey. 2007. The distribution of life cycle stages of two deep-water
4168 pleuronectids, Dover sole (*Microstomus pacificus*) and rex sole (*Glyptocephalus zachirus*), at the
4169 northern extent of their range in the Gulf of Alaska. J. Sea Res. 50:187-197.
- 4170 Alton, M. S., R. G. Bakkala, G. E. Walters, and P. T. Munro. 1988. Greenland Turbot *Reinhardtius*
4171 *hippoglossoides* of the Eastern Bering Sea and Aleutian Islands Region. NOAA Technical Report
4172 NMFS 71: pp 38.
- 4173 Araujo, M. B., and M. New. 2007. Ensemble forecasting of species distributions. Trends Eco. Evo.,
4174 22(1):42:47. <https://doi.org/10.1016/j.tree.2006.09.010>
- 4175 Bachelier, N. M., L. Ciannelli, K. M. Bailey, and J. T. Duffy-Anderson. 2010. Spatial and temporal
4176 patterns of walleye pollock (*Theragra chalcogramma*) spawning in the eastern Bering Sea
4177 inferred from egg and larval distributions. Fish. Oceanogr. 19(2):107-120.
- 4178 Bailey, K. M. 2000. Shifting control of recruitment of walleye pollock *Theragra chalcogramma* after a
4179 major climatic and ecosystem change. Mar. Ecol. Prog. Ser. 198:215-224.
- 4180 Bailey, K. M., A. A. Abookire, and J. T. Duffy-Anderson. 2008. Ocean transport paths for the early life
4181 history stages of offshore-spawning flatfishes: a case study in the Gulf of Alaska. Fish Fisher.
4182 9:44-66.
- 4183 Balanov, A. A., V. V. Panchenko, and A. B. Savin. 2020. The First Record of a Spawning Ground of the
4184 Mud Skate *Bathyraja taranetzi* (Dolganov, 1983) and the Okhotsk Skate *B. violacea* (Suvorov,
4185 1935) in Pacific Waters off the Northern Kuril Islands. Russ. J. Mar. Biol. 46:501–505.
- 4186 Barnes, C. L., A. H. Beaudreau, M. W. Dorn, K. K. Holsman, and F. J. Mueter. 2020. Development of a
4187 predation index to assess trophic stability in the Gulf of Alaska. Ecol. App. 30(7):e02141. doi:
4188 10.1002/eap.2141.
- 4189 Barnes C. L., J. T. Thorson, J. L. Pirtle, C. N. Rooper, E. A. Laman, K. K. Holsman, K. Y. Aydin, and T.
4190 E. Essington. *In prep*. Effects of model complexity on describing and forecasting species
4191 responses to changing climate. Ecography.
- 4192 Barry, S. C., and A. H. Welsh 2002. Generalized additive modeling and zero inflated count data. Ecol.
4193 Model. 157:179-188.
- 4194 Best, D. J., and D. E. Roberts. 1975. Algorithm AS 89: the upper tail probabilities of Spearman's rho.
4195 Appl. Stat. 24:377-379.
- 4196 Boldt, J. L., T. W. Buckley, C. N. Rooper, and K. Aydin. 2012 Factors influencing cannibalism and
4197 abundance of walleye pollock (*Theragra chalcogramma*) on the eastern Bering Sea shelf, 1982-
4198 2006. Fish. Bull. 110(3):293–306.
- 4199 Brewer, R.S. and B.L. Norcross. 2012. Long-term retention of internal elastomer tags in a wild population
4200 of North Pacific giant octopus (*Enteroctopus dofleini*), Fish. Res. 134-136: 17-20.
4201 <https://doi.org/10.1016/j.fishres.2012.07.020>

- 4202 Brewer, R.S. 2016. Population biology and ecology of the North Pacific Giant Octopus in the eastern
4203 Bering Sea. PhD thesis, Univ. Alaska Fairbanks.
- 4204 Brodeur, R. D. 2001. Habitat-specific distribution of Pacific ocean perch (*Sebastes alutus*) in Pribilof
4205 Canyon, Bering Sea. *Continent. Shelf Res.* 21:207-224.
- 4206 Bryan, M. D., S. J. Barbeaux, J. Ianelli, S. Zador, and J. Hoff. 2020a. Assessment of Greenland turbot in
4207 the Bering Sea and Aleutian Islands. *In* Stock Assessment and Fishery Evaluation Report for the
4208 Groundfish Resources of the Bering Sea/Aleutian Islands Regions. North Pacific Fishery
4209 Management Council 1007 West Third, Suite 400 Anchorage, AK 99501.
- 4210 Bryan, M. D., K. Shotwell, S. Zador, and J. Ianelli. 2020b. Assessment of the Kamchatka flounder stock
4211 in the Bering sea/Aleutian islands. *In* Stock Assessment and Fishery Evaluation Report for the
4212 Groundfish Resources of the Bering Sea and Aleutian Islands. North Pacific Fishery Management
4213 Council 1007 West Third, Suite 400 Anchorage, AK 99501.
- 4214 Bryan, D. R., S. F. McDermott, J. K. Nielsen, D. Fraser, and K. M. Rand. 2021. Seasonal migratory
4215 patterns of Pacific cod (*Gadus macrocephalus*) in the Aleutian Islands. *Anim. Biotelemetry*
4216 9(1):24. <https://doi.org/10.1186/s40317-021-00250-2>
- 4217 Buckley, T. W., A. Greig, and J. L. Boldt. 2009. Describing summer pelagic habitat over the continental
4218 shelf in the eastern Bering Sea, 1982-2006. NOAA Tech. Memo. NMFS-AFSC-196.
- 4219 Canino, M. F., I. B. Spies, K. M. Cunningham, L. Hauser, and W. S. Grant. 2010. Multiple ice-age
4220 refugia in Pacific cod, *Gadus macrocephalus*, *Mol. Ecol.* 19:4339-4351.
- 4221 Carlson, H. R., and R. R. Straty. 1981. Habitat and nursery grounds of Pacific rockfish, *Sebastes* spp., in
4222 rocky coastal areas of Southeastern Alaska. *Mar. Fish. Rev.* 43:13-19.
- 4223 Ciannelli, L., R. D. Brodeur, and J. M. Napp. 2004. Foraging impact on zooplankton by age-0 walleye
4224 pollock (*Theragra chalcogramma*) around a front in the southeast Bering Sea. *Mar. Biol.*
4225 144(3):515-526.
- 4226 Ciannelli, L., P. Fauchald, K. S. Chan, V. N. Agostini, and G. E. Dingsør. 2008. Spatial fisheries ecology:
4227 recent progress and future prospects. *J. Mar. Sys.* 71(3-4):223-236.
- 4228 Chilton, E. A. 2010. Maturity and growth of female dusky rockfish (*Sebastes variabilis*) in the central
4229 Gulf of Alaska. *Fish. Bull.* 108(1):70-78.
- 4230 Clausen, D. M., and J. Heifetz. 2002. The northern rockfish, *Sebastes polyspinis*, in Alaska: Commercial
4231 fishery, distribution, and biology. *Mar. Fish. Rev.* 64:1-28.
- 4232 Cochran, W. G. 1977. *Sampling Techniques*. 3rd ed. Wiley Series in Probability and Mathematical
4233 Statistics - Applied. John Wiley & Sons. N.Y., NY 428 p.
- 4234 Conrath, C. L. 2017. Maturity, spawning omission, and reproductive complexity of deepwater rockfish.
4235 *Trans. Am. Fish. Soc.* 146:495-507.
- 4236 Conrath, C. L. 2019. Reproductive potential of light dusky rockfish (*Sebastes variabilis*) and northern
4237 rockfish (*S. polyspinis*) in the Gulf of Alaska. *Fish. Bull.* 117:140-150.
- 4238 Conrath, C. L., and M. E. Conners. 2014. Aspects of the reproductive biology of the North Pacific giant
4239 octopus (*Enteroctopus dofleini*) in the Gulf of Alaska. *Fish. Bull.* 112(4):253-260.
- 4240 Cooper, D. W., K. R. Maslenikov, and D. R. Gunderson. 2007. Natural mortality rate, annual fecundity,
4241 and maturity at length for Greenland halibut (*Reinhardtius hippoglossoides*) from the
4242 northeastern Pacific Ocean. *Fish. Bull.* 105(2):296-304.

- 4243 Cooper, D. W., S. F. McDermott, and J. N. Ianelli. 2010. Spatial and temporal variability in Atka
4244 mackerel female maturity at length and age. *Mar. Coast. Fish.* 2:329-338.
- 4245 Copeman, L. A., B. J. Laurel, M. Spencer, and A. Sremba. 2017. Temperature impacts on lipid allocation
4246 among juvenile gadid species at the Pacific Arctic-Boreal interface: an experimental laboratory
4247 approach. *Mar. Ecol. Prog. Ser.* 566:183-198.
- 4248 Cragg, J. G. 1971. Some statistical models for limited dependent variables with application to the demand
4249 for durable goods. *Econometrica.* 39:829-844.
- 4250 Danielson, S., E. Curchitser, K. Hedstrom, T. Weingartner, and P. Stabeno. 2011. On ocean and sea ice
4251 modes of variability in the Bering Sea. *J. Geophys. Res.* 116:. doi: 10.1029/2011JC007389.
- 4252 Daly, B., C. Parada, T. Loher, S. Hinckley, A. J. Hermann, and D. Armstrong. 2020. Red king crab larval
4253 advection in Bristol Bay: Implications for recruitment variability. *Fish Oceanogr.* 29:505– 525.
4254 <https://doi.org/10.1111/fog.12492>
- 4255 Daly, B., C. Parada, T. Loher, S. Hinckley, A. J. Hermann, and D. Armstrong. 2020. Red king crab larval
4256 advection in Bristol Bay: Implications for recruitment variability. *Fish Oceanogr.* 29:505– 525.
4257 <https://doi.org/10.1111/fog.12492>
- 4258 Debenham, C., J. Moss, and R. Heintz. 2019. Ecology of age-0 arrowtooth flounder (*Atheresthes stomias*)
4259 inhabiting the Gulf of Alaska. *Deep-Sea Res. II* 165:140-149.
- 4260 Diggle, P. J., and P. J. Ribeiro Jr. 2002. Bayesian inference in Gaussian model-based geostatistics. *Geo.*
4261 *Environ. Model.* 6(2):129-146.
- 4262 Dolan, M. F. J., A. J. Grehan, J. C. Guinan, and C. Brown, C. 2008. Modelling the local distribution of
4263 cold-water corals in relation to bathymetric variables: Adding spatial context to deep-sea video
4264 data. *Deep-Sea Research Part I-Oceanographic Research Papers*, 55(11), 1564-1579.
4265 <https://doi.org/10.1016/j.dsr.2008.06.010>.
- 4266 Dolan, M. F. J., and V. L. Lucieer. 2014. Variation and Uncertainty in Bathymetric Slope Calculations
4267 Using Geographic Information Systems. *Marine Geodesy*, 37(2), 187-219.
4268 <https://doi.org/10.1080/01490419.2014.902888>.
- 4269 Doyle, M. J., C. Debenham, S. J. Barbeaux, T. W. Buckley, J. L. Pirtle, I. B. Spies, W. T. Stockhausen, S.
4270 K. Shotwell, M. T. Wilson, and D. W. Cooper. 2018. A full life history synthesis of Arrowtooth
4271 flounder ecology in the Gulf of Alaska: Exposure and sensitivity to potential ecosystem change. *J.*
4272 *Sea Res.* 142:28-51. <https://doi.org/10.1016/j.seares.2018.08.001>
- 4273 Doyle, M. J., S. L. Stromb, K. O. Coyle, A. J. Hermann, C. Ladd, A. C. Matarese, S. K. Shotwell, and R.
4274 R. Hopcroft. 2019. Early life history phenology among Gulf of Alaska fish species: Strategies,
4275 synchronies, and sensitivities. *Deep-Sea Res. II* 165:41-73.
- 4276 Duchon, J. (1977) Splines minimizing rotation-invariant semi-norms in Solobev spaces. *In* W. Shemp and
4277 K. Zeller (eds) *Construction theory of functions of several variables*. Springer, Berlin. 85-100.
- 4278 Du Preez, C., and V. Tunnicliffe. 2011. Shortspine thornyhead and rockfish (Scorpaenidae) distribution in
4279 response to substratum, biogenic structures and trawling. *Mar. Ecol. Prog. Ser.* 425: 217-231. doi:
4280 10.3354/meps09005.
- 4281 Ebert, D. A. 2005. Reproductive biology of skates, *Bathyraja* (Ishiyama), along the eastern Bering Sea
4282 continental slope. *J. Fish Biol.* 66(3):618-649.
- 4283 Ebert, D. A., W. D. Smith, D. L. Haas, S. M. Ainsley, and G. M. Cailliet. 2007. Life history and
4284 population dynamics of Alaskan skates: providing essential biological information for effective

- 4285 management of bycatch and target species. Final Report to the North Pacific Research Board,
4286 Project 510.
- 4287 Egbert, G. D., and S. Y. Erofeeva. 2002. Efficient inverse modeling of barotropic ocean tides. *J.*
4288 *Atmosph. Ocean. Tech.* 19(2):183-204. doi: 10.1175/1520-0426(2002)019.
- 4289 Elith, J., S. J. Phillips, T. Hastie, M. Dudík, Y. E. Chee, and C. J. Yates. 2011. A statistical explanation
4290 of MaxEnt for ecologists. *Divers. Distrib.* 17:43-57.
- 4291 Fissel, B., M. Dalton, B. Garber-Yonts, A. Haynie, S. Kasperski, J. Lee, D. Lew, C. Seung, K. Sparks, M.
4292 Szymkowiak, and S. Wise. 2020. Economic Status of the Groundfish Fisheries Off Alaska 2019.
4293 **In** Stock Assessment and Fishery Evaluation Report for the Groundfish Fisheries of the Gulf of
4294 Alaska and Bering Sea/Aleutian Islands Area. North Pacific Fishery Management Council 1007
4295 West Third, Suite 400 Anchorage, AK 99501.
- 4296 Fithian, W., J. Elith, T. Hastie, and D. A. Keith. 2015. Bias correction in species distribution models:
4297 pooling survey and collection data for multiple species. *Meth. Ecol. Evol.* 6:424-438. doi:
4298 10.1111/2041-210X.12242
- 4299 Fisheries Leadership and Sustainability Forum. 2016. Regional EFH Profile: North Pacific. National
4300 Essential Fish Habitat Summit, 2016. [https://www.fisheriesforum.org/our-work/special-](https://www.fisheriesforum.org/our-work/special-projects/efh-summit/efh-profiles/)
4301 [projects/efh-summit/efh-profiles/](https://www.fisheriesforum.org/our-work/special-projects/efh-summit/efh-profiles/).
- 4302 Gharrett, A. J., A. P. Matala, E. L. Peterson, A. K. Gray, Z. Li, and J. Heifetz. 2005. Two genetically
4303 distinct rougheye rockfish sibling species differ phenotypically? *Trans. Am. Fish. Soc.* 135:792-
4304 800.
- 4305 Gibson, G. A., W. T., Stockhausen, K. O. Coyle, S. Hinckley, C. Parada, A. J. Hermann, M. Doyle, and
4306 C. Ladd. 2019. An individual-based model for sablefish: Exploring the connectivity between
4307 potential spawning and nursery grounds in the Gulf of Alaska. *Deep-Sea Res. Pt. II.* 165:89-112.
- 4308 Goethel, D. R., D. H. Hanselman, C. J., Rodgveller, K. H. Fenske, S. K. Shotwell, K. B. Echave, P. W.
4309 Malecha, K. A. Siwicke, and C. R. Lunsford. 2020. Assessment of the sablefish stock in Alaska.
4310 **In** Stock assessment and fishery evaluation report for the groundfish resources of the GOA and
4311 BS/AI. North Pacific Fishery Management Council 1007 West Third, Suite 400 Anchorage, AK
4312 99501.
- 4313 Grüss, A., J. T. Thorson, G. Carroll, E. L. Ng, K. K. Holsman, K. Aydin, S. Kotwicki, H. N. Morzaria-
4314 Luna, C. H. Ainsworth, and K. A. Thompson. 2020. Spatio-temporal analyses of marine predator
4315 diets from data-rich and data-limited systems. *Fish Fisher.* 21(4):718-739.
4316 <https://doi.org/10.1111/faf.12457>
- 4317 Grüss, A., J. L. Pirtle, J. T. Thorson, M. R. Lindeberg, A. D. Neff, S. G. Lewis, and T. E. Essington.
4318 2021a. Modeling nearshore fish habitats using Alaska as a regional case study. *Fish. Res.* 238.
4319 doi: 10.1016/j.fishres.2021.105905.
- 4320 Grüss, A., J. T. Thorson, C. C. Stawitz, J. C. P. Reum, S. K. Rohan, and C. L. Barnes. 2021b. Synthesis of
4321 interannual variability in spatial demographic processes supports the strong influence of cold-
4322 pool extent on eastern Bering Sea walleye pollock (*Gadus chalcogrammus*). *Prog. Oceanogr.*
4323 194:102569. <https://doi.org/10.1016/j.pocean.2021.102569>
- 4324 Guisan, A., S. Weiss, and A. Weiss. 1999. GLM versus CCA spatial modeling of plant species
4325 distribution. *Plant Ecol.* 143:107-122.
- 4326 Guisan, A., N. E. Zimmermann, J. Elith, C. H. Graham, S. Phillips, and A. T. Peterson. 2007. What
4327 matters for predicting the occurrences of trees: techniques, data, or species' characteristics?. *Ecol.*
4328 *Monogr.* 77:615-630. <https://doi.org/10.1890/06-1060.1>.

- 4329 Gunderson, D. R., D. A. Armstrong, Y. B. Shi, and R. A. McConnaughey. 1990. Patterns of estuarine use
4330 by juvenile English sole (*Parophrys vetulus*) and Dungeness crab (*Cancer magister*). *Estuaries*,
4331 13(1):59-71.
- 4332 Haas, D. L., D. A. Ebert, and G. M. Cailliet. 2016. Comparative age and growth of the Aleutian skate,
4333 *Bathyraja aleutica*, from the eastern Bering Sea and Gulf of Alaska. *Env. Biol. Fish.* 99:813-828.
- 4334 Hanselman, D. H., T. J. Quinn II, C. Lunsford, J. Heifetz, and D. M. Clausen. 2001. Spatial implications
4335 of adaptive cluster sampling on Gulf of Alaska rockfish. **In** Proceedings of the 17th Lowell-
4336 Wakefield Symposium: Spatial Processes and Management of Marine Populations, pp. 303-325.
4337 Univ. Alaska Sea Grant Program, Fairbanks, AK.
- 4338 Hanselman, D. H., J. Heifetz, K. B. Echave, and S. C. Dressel. 2015. Move it or lose it: movement and
4339 mortality of sablefish tagged in Alaska. *Can. J. Fish. Aquat. Sci.* 72(2):238-251.
- 4340 Hanselman, D. H., C. J. Rodgveller, K. H. Fenske, S. K. Shotwell, K. B. Echave, P. W. Malecha, C. R.
4341 Lunsford. 2019. Assessment of the sablefish stock in Alaska. **In** Stock Assessment and Fishery
4342 Evaluation Report for the Groundfish Resources of the Gulf of Alaska. North Pacific Fishery
4343 Management Council 1007 West Third, Suite 400 Anchorage, AK 99501.
- 4344 Hart, J. L. 1973. Pacific Fishes of Canada. Canadian Government Publishing Centre, Supply and Services
4345 Canada, Ottawa, Canada KIA OS9
- 4346 Hastie, T. J., and R. J. Tibshirani. 1990. Generalized Additive Models. *Monogr. Stat. Appl. Prob.* 43. 338
4347 p.
- 4348 Hastie, T., R. J. Tibshirani, and J. H. Friedman. 2009. The Elements of Statistical Learning: Data Mining,
4349 Inference, and Prediction. Second edition. Springer, Berlin, Germany.
- 4350 Hawley, J. H. 1931. Hydrographic Manual; U.S. Department of Commerce, U.S. Coast and Geodetic
4351 Survey, Special Publication No. 143; U.S. Government Printing Office: Washington, DC, USA.
- 4352 Heifetz, J., and J. T. Fujioka. 1991. Movement dynamics of tagged sablefish in the northeastern Pacific.
4353 *Fish. Res.* 11:355-374.
- 4354 Heifetz, J., B. L. Wing, R. Stone, P. Malecha, and D. Courtney. 2005. Corals of the Aleutian Islands.
4355 *Fish. Oceanogr.* 14(s1):131-138. doi: 10.1111/j.1365-2419.2005.00371.x.
- 4356 Hinckley, S., W. Stockhausen, K. Coyle, B. Laurel, G. Gibson, C. Parada, A. Hermann, M. Doyle, and T.
4357 Hurst. 2019. Connectivity between spawning and nursery areas for Pacific cod (*Gadus*
4358 *macrocephalus*) in the Gulf of Alaska. *Deep-Sea Res. Pt. II.* 165-113-126.
- 4359 Hoff, G. R. 2007. Reproduction of the Alaska skate (*Bathyraja parmifera*) with regard to nursery sites,
4360 embryo development and predation. PhD dissertation, University of Washington, Seattle.
- 4361 Hoff, G. R. 2008. A nursery site of the Alaska skate (*Bathyraja parmifera*) in the eastern Bering Sea.
4362 *Fish. Bull.* 106(3):233-244.
- 4363 Hoff, G. R. 2009. Embryo developmental events and the egg case of the Aleutian skate *Bathyraja aleutica*
4364 (Gilbert) and the Alaska skate *Bathyraja parmifera* (Bean). *J. Fish. Biol.* 74(3):438-501.
- 4365 Horn, B. K. P. 1981. Hill shading and the reflectance map. *Proc. IEEE.* 69:14-47.
- 4366 Hosmer, D. W., and S. Lemeshow. 2005. Assessing the Fit of the Model. **In** Applied Logistic Regression,
4367 Second Edition edn, pp. 143-202. John Wiley and Sons, Inc., Hoboken, NJ, USA, 07030.
- 4368 Howell, K. L., R. Holt, I. P. Endrino, and H. Stewart. 2011. When the species is also a habitat: comparing
4369 the predictively modelled distributions of *Lophelia pertusa* and the reef habitat it forms. *Biol.*
4370 *Conserv.* 144, 2656–2665.

- 4371 Hulson, P. J. F., D. H. Hanselman, C. R. Lunsford, and B. Fissel. 2017. Assessment of the Pacific ocean
4372 perch stock in the Gulf of Alaska. *In* Stock assessment and fishery evaluation report for the
4373 groundfish resources of the Gulf of Alaska. North Pacific Fishery Management Council 1007
4374 West Third, Suite 400 Anchorage, AK 99501.
- 4375 Ito, D. H. 1999. Assessing shorttraker and rougheye rockfishes in the GOA: addressing a problem of
4376 habitat specificity and sampling capability. Ph.D. Dissertation, Univ. Washington, Seattle. 205
4377 pp.
- 4378 Johnson, S. W., M. L. Murphy, and D. J. Csepp. 2003. Distribution, habitat, and behavior of rockfishes,
4379 *Sebastes spp.*, in nearshore waters of southeastern Alaska: observations from a remotely operated
4380 vehicle. *Env. Bio. Fish.* 66(3):259-270.
- 4381 Johnson, S. W., A. D. Neff, J. F. Thedinga, M. R. Lindeberg, and J. M. Maselko. 2012. Atlas of nearshore
4382 fishes of Alaska: A synthesis of marine surveys from 1998 to 2011. NOAA Tech. Memo. NMFS-
4383 AFSC-239. 261 pp.
- 4384 Jones, D., C. D., Wilson, A. de Robertis, C. N. Rooper, T. C. Weber, and J. L. Butler. 2012. Evaluation of
4385 rockfish abundance in untrawlable habitat: combining acoustic and complementary sampling
4386 tools. *Fish. Bull.* 110:332-343.
- 4387 Jorgensen, E.M. 2009. Field guide to squids and octopods of the eastern North Pacific and Bering Sea.
4388 Alaska Sea Grant Pub. No. SG-ED-65, 100pp.
- 4389 Kestelle, C. R., D. K. Kimura, and S. R. Jay. 2000. Using 210Pb/226Ra disequilibrium to validate
4390 conventional ages in Scorpaenids (genera *Sebastes* and *Sebastolobus*). *Fish. Res.* 46(1-3):299-
4391 312.
- 4392 Kestelle, C., T. Helsler, T. TenBrink, C. Hutchinson, B. Goetz, C. Gburski, and I. Benson. 2020. Age
4393 validation of four rockfishes (genera *Sebastes* and *Sebastolobus*) with bomb-produced
4394 radiocarbon. *Mar. and Freshwater Res.*, 71(10):1355-1366.
- 4395 Kendall, A. W., and A. C. Matarese. 1987. Biology of eggs, larvae, and epipelagic juveniles of sablefish,
4396 *Anoplopoma fimbria*, in relation to their potential use in management. *Mar. Fish. Rev.* 49:1-13.
- 4397 Kotwicki, S., R.R. Lauth, K. Williams, and S. E. Goodman. 2017. Selectivity ratio: A useful tool for
4398 comparing size selectivity of multiple survey gears. *Fish. Res.* 191:76–86.
4399 <https://doi.org/10.1016/j.fishres.2017.02.012>
- 4400 Kotwicki, S., P. H. Ressler, J. N. Ianelli, A. E. Punt, and J.K. Horne 2018. Combining data from bottom-
4401 trawl and acoustic-trawl surveys to estimate an index of abundance for semipelagic species. *Can.*
4402 *J. Fish. Aquat. Sci.* 75:60–71. <https://doi.org/10.1139/cjfas-2016-0362>
- 4403 Kramer, D. E., and V. M. O’Connell. 1988. A Guide to Northeast Pacific Rockfishes: Genera *Sebastes*
4404 and *Sebastolobus*. *In* Alaska Sea Grant Advisory Bulletin 25.
- 4405 Krygier, E. E. and W. G. Pearcy. 1986. The role of estuarine and offshore nursery areas for young English
4406 sole, *Parophrys vetulus* Girard, of Oregon. *Fish. Bull.* 84(1):119-132.
- 4407 Laman, E. A., S. Kotwicki, and C. N. Rooper. 2015. Correlating environmental and biogenic factors with
4408 abundance and distribution of Pacific ocean perch (*Sebastes alutus*) in the Aleutian Islands,
4409 Alaska. *Fish. Bull.* 113(3):270-289. doi:10.7755/FB.113.3.4.
- 4410 Laman, E. A., C. N. Rooper, K. Turner, S. Rooney, D.W. Cooper, and M. Zimmermann. 2017. Model-
4411 based essential fish habitat definitions for Bering Sea groundfish species. U.S. Dep. Commer.,
4412 NOAA Tech. Memo. NMFS-AFSC-357, 265 p.

- 4413 Laman, E. A., C. N. Rooper, K. Turner, S. Rooney, D.W. Cooper, and M. Zimmermann. 2018. Using
4414 species distribution models to describe essential fish habitat in Alaska. *Can. J. Fish. Aquat. Sci.*
4415 <https://doi.org/10.1139/cjfas-2017-0181>.
- 4416 Laurel, B. J., C. H. Ryer, B. Knoth, and A. W. Stoner. 2009. Temporal and ontogenetic shifts in habitat
4417 use of juvenile Pacific cod (*Gadus macrocephalus*). *J. Exp. Mar. Biol. Ecol.* 377(1):28-35.
- 4418 Laurel, B. J., M. Spencer, P. Iseri, and L. A. Copeman. 2016. Temperature-dependent growth and
4419 behavior of juvenile Arctic cod (*Boreogadus saida*) and co-occurring North Pacific gadids. *Polar*
4420 *Biology* 39:1127-1135. doi 10.1007/s00300-015-1761-5
- 4421 Lauth, R. R., S. W. McEntire, and H. H. Zenger. 2007. Geographic Distribution, Depth Range, and
4422 Description of Atka Mackerel *Pleurogrammus monopterygius* Nesting Habitat in Alaska. *AK*
4423 *Fish. Res. Bull.* 12:165-186.
- 4424 Legendre, P. and L. Legendre. 2012. *Numerical Ecology*, Volume 24 - 3rd Edition. Elsevier.
4425 <https://www.elsevier.com/books/numerical-ecology/legendre/978-0-444-53868-0>
- 4426 Loher, T., D. A. Armstrong, and B. G. Stevens. 2001. Growth of juvenile red king crab (*Paralithodes*
4427 *camtschaticus*) in Bristol Bay (Alaska) elucidated from field sampling and analysis of trawl-
4428 survey data. *Fish. Bull.* 99:572-587.
- 4429 Long, W. C., K. M. Swiney, C. Harris, H. N. Page, and R. J. Foy. 2013. Effects of Ocean Acidification on
4430 Juvenile Red King Crab (*Paralithodes camtschaticus*) and Tanner Crab (*Chionoecetes bairdi*)
4431 Growth, Condition, Calcification, and Survival. *PLOS One* 8: pp. 10.
- 4432 Love, M. S., M. Yoklavich, and L. Thorsteinson. 2002. *The rockfishes of the Northeast Pacific*.
4433 University of California Press, Berkeley and Los Angeles. 404 pgs.
- 4434 Lowe, S., J. Ianelli, W. Paulson, and B. Fissel. 2019. Assessment of the Atka mackerel stock in the
4435 Bering Sea and Aleutian Islands. *In* Stock Assessment and Fishery Evaluation Report for the
4436 Groundfish Resources of the Bering sea and Aleutian islands. North Pacific Fishery Management
4437 Council 1007 West Third, Suite 400 Anchorage, AK 99501.
- 4438 Lowndes, J. S. S., B. D. Best, C. Scarborough, J. C. Afflerbach, M. R. Frazier, C. C. O'Hara, N. Jiang,
4439 and B. S. Halpern. 2017. Our path to better science in less time using open data science tools.
4440 *Nat. Ecol. Evol.* 1:1-7. <https://doi.org/10.1038/s41559-017-0160>
- 4441 Malecha, P. W., R. P. Stone, and J. Heifetz. 2005. Living substrate in Alaska: Distribution, abundance,
4442 and species associations. *In* Barnes, P. W. and Thomas, J. P., eds. *Benthic habitats and the effects*
4443 *of fishing*. Amer. Fish. Soc., Symposium 41, Bethesda, Maryland, p. 289-299.
- 4444 Marliave, J., and W. Challenger. 2009. Monitoring and evaluating rockfish conservation areas in British
4445 Columbia. *Can. J. Fish. Aquat. Sci.* 66(6):995-1006. doi: 10.1139/F09-056.
- 4446 Mason, J. C., R. J. Beamish, and G. A. McFarlane. 1983. Sexual maturity, fecundity, spawning, and early
4447 life history of sablefish (*Anoplopoma fimbria*) off the Pacific coast of Canada. *Can. J. Fish.*
4448 *Aquat. Sci.* 40: 2126-2134.
- 4449 Matta, M. E., and D. R. Gunderson. 2007. Age, growth, maturity, and mortality of the Alaska skate,
4450 *Bathyraja parmifera*, in the eastern Bering Sea. *Env. Biol. Fish.* 80(2-3):309-323.
- 4451 McCarthy, A., T. Honkalehto, N. Lauffenburger, and A. De Robertis. 2020. Results of the acoustic-trawl
4452 survey of walleye pollock (*Gadus chalcogrammus*) on the U.S. Bering Sea Shelf in June - August
4453 2018 (DY1807). AFSC Processed Rep. 2020-07, 83 p. Alaska Fish. Sci. Cent., NOAA, Natl. Mar.
4454 Fish. Serv., 7600 Sand Point Way NE, Seattle WA 98115.

- 4455 McCullagh, P., and J. A. Nelder. 1989. *Generalized Linear Models* (2nd edition), Chapman and Hall,
4456 London, UK. 511 pp. ISBN 0-412-31760-5
- 4457 McDermott, S. F., and S. A. Lowe. 1997. The reproductive cycle and sexual maturity of Atka mackerel,
4458 *Pleurogrammus monoptyerygius*, in Alaska waters. *Fish. Bull.*, U.S. 95:321-333.
- 4459 McGilliard, C. R., and W. Palsson. 2017. Assessment of the rex sole stock in the Gulf of Alaska. *In* Stock
4460 Assessment and Fishery Evaluation Report for the Groundfish Resources of the Gulf of Alaska.
4461 pp. 657–742. North Pacific Fishery Management Council 1007 West Third, Suite 400 Anchorage,
4462 AK 99501.
- 4463 McGilliard, C. R., W. Palsson, A. Havron, and S. Zador. 2019. Assessment of the deepwater flatfish stock
4464 complex in the Gulf of Alaska. *In* Stock Assessment and Fishery Evaluation Report for the
4465 Groundfish Resources of the Gulf of Alaska. North Pacific Fishery Management Council 1007
4466 West Third, Suite 400 Anchorage, AK 99501.
- 4467 McGilliard, C. R., J. Ianelli, A. E. Punt, T. Wilderbuer, D. Nichol, and R. Haehn. 2020. Assessment of the
4468 Northern Rock Sole Stock in the Bering Sea and Aleutian Islands. *In* Stock assessment and
4469 Fishery Evaluation Report for the Groundfish Resources of the Bering Sea and Aleutian Islands.
4470 North Pacific Fishery Management Council 1007 West Third, Suite 400 Anchorage, AK 99501.
- 4471 McGowan, D. W., J. K. Horne, J. T. Thorson, and M. Zimmermann. 2019. Influence of environmental
4472 factors on capelin distributions in the Gulf of Alaska. *Deep-Sea Res. Part II: Topical Studies in*
4473 *Oceanography, Understanding Ecosystem Processes in the Gulf of Alaska: Volume 2* 165, 238–
4474 254. <https://doi.org/10.1016/j.dsr2.2017.11.018>
- 4475 Mecklenburg, C. W., T. A. Mecklenburg, and L. K. Thorsteinson, L. K. 2002. *Fishes of Alaska*.
4476 American Fisheries Society: Bethesda, MD. 1037 pp.
- 4477 Mienis, F., H. C. de Stigter, M. White, G. Duineveld, H. de Haas, and T. C. E. van Weering. 2007.
4478 Hydrodynamic controls on cold-water coral growth and carbonate-mound development at the SW
4479 and SE Rockall Trough Margin, NE Atlantic Ocean. *Deep Sea Research Part I: Oceanographic*
4480 *Research Papers*, 54(9), 1655-1674. <https://doi.org/http://dx.doi.org/10.1016/j.dsr.2007.05.013>.
- 4481 Monnahan, C. C. 2020. Assessment of the other flatfish stock complex in the Bering Sea and Aleutian
4482 Islands. *In* Stock Assessment and Fishery Evaluation Report for the Groundfish Resources of the
4483 Bering Sea/Aleutian Islands Regions. North Pacific Fishery Management Council 1007 West
4484 Third, Suite 400 Anchorage, AK 99501.
- 4485 Monnahan, C. C., and R. Haehn. 2020. Assessment of the flathead sole-Bering flounder stock complex in
4486 the Bering Sea and Aleutian Islands. *In* Stock Assessment and Fishery Evaluation Report for the
4487 Groundfish Resources of the Bering Sea and Aleutian Islands. North Pacific Fishery Management
4488 Council 1007 West Third, Suite 400 Anchorage, AK 99501.
- 4489 Monnahan, C. C., J. T. Thorson, S. Kotwicki, N. Lauffenburger, J. N. Ianelli, and A. E. Punt. 2021.
4490 Incorporating vertical distribution in index standardization accounts for spatiotemporal
4491 availability to acoustic and bottom trawl gear for semi-pelagic species. *ICES J. Mar. Sci.*
4492 78:1826–1839. <https://doi.org/10.1093/icesjms/fsab085>
- 4493 Moser, H. G. 1996. *The Early Stages of Fishes in the California Current Region*. CalCOFI Atlas No. 33.
4494 Allen Press, Inc. Lawrence, Kansas. 1505 p.
- 4495 National Marine Fisheries Service (NMFS). 2005. Volume I: Final Environmental Impact Statement for
4496 Essential Fish Habitat Identification and Conservation in Alaska.
4497 <https://repository.library.noaa.gov/view/noaa/17391>.

- 4498 Neidetcher, S. K., T. P. Hurst, L. Ciannelli, and E. A. Loggerwell. 2014. Spawning phenology and
 4499 geography of Aleutian Islands and eastern Bering Sea Pacific cod (*Gadus macrocephalus*). Deep-
 4500 Sea Res. II: Topical Studies in Oceanography 109:204-214.
 4501 <http://cx.doi.org/10.1016/j.dsr2.2013.12.006i>
- 4502 Ng, E. L., J. J. Deroba, T. E. Essington, A. Grüss, B. E. Smith, and J. T. Thorson. 2021. Predator stomach
 4503 contents can provide accurate indices of prey biomass. ICES J. Mar. Sci. 78(3):1146–1159.
 4504 <https://doi.org/10.1093/icesjms/fsab026>
- 4505 O’Leary, C. A., J. T. Thorson, J. N. Ianelli, and S. Kotwicki. 2020. Adapting to climate-driven
 4506 distribution shifts using model-based indices and age composition from multiple surveys in the
 4507 walleye pollock (*Gadus chalcogrammus*) stock assessment. Fish. Oceanogr. 29(6):541–557.
 4508 <https://doi.org/10.1111/fog.12494>
- 4509 O’Leary, C. A., S. Kotwicki, G. R. Hoff, J. T. Thorson, V. V. Kulik, J. N. Ianelli, R. R. Lauth, D. G.
 4510 Nicol, J. Conner, and A. E. Punt. 2021. Estimating spatiotemporal availability of transboundary
 4511 fishes to fishery-independent surveys. J. Appl. Ecol. doi:10.1111/1365-2664.13914.
- 4512 Olson, A.P., C. E. Siddon, and G. L. Eckert. 2018. Spatial variability in size at maturity of golden king
 4513 crab (*Lithodes aequispinus*) and implications for fisheries management. R. Soc. open science,
 4514 5(3):171802.
- 4515 Ormseth, O. A. 2020. Assessment of the skate stock complex in the Bering Sea and Aleutians Islands. **In**
 4516 Stock Assessment and Fishery Evaluation Report for the Groundfish Resources of the Bering
 4517 Sea/Aleutian Islands Regions. North Pacific Fishery Management Council 1007 West Third,
 4518 Suite 400 Anchorage, AK 99501.
- 4519 Ormseth, O. A., M. E. Conners, K. Aydin, and C. Conrath. 2018. Assessment of the Octopus Stock
 4520 Complex in the Bering Sea and Aleutian Islands. **In** Stock Assessment and Fishery Evaluation
 4521 Report for the Groundfish Resources of the Bering Sea/Aleutian Islands Regions. North Pacific
 4522 Fishery Management Council 1007 West Third, Suite 400 Anchorage, AK 99501.
- 4523 Orr, J. W., and A. C. Matarese. 2000. Revision of the genus *Lepidopsetta* Gill, 1862 (Teleostei:
 4524 Pleuronectidae) based on larval and adult morphology, with a description of a new species from
 4525 the North Pacific Ocean and Bering Sea. Fish. Bull. 98: 539-582.
- 4526 Orr, J. W., and J. E. Blackburn. 2004. The dusky rockfishes (Teleostei: Scorpaeniformes) of the North
 4527 Pacific Ocean: resurrection of *Sebastes variabilis* (Pallas, 1814) and a redescription of *Sebastes*
 4528 *ciliatus* (Tilesius, 1813). Fish. Bull., 102(2):328-348.
- 4529 Orr, J. W., and S. Hawkins. 2008. Species of the rougheye rockfish complex: resurrection of *Sebastes*
 4530 *melanostictus* (Matsubara, 1934) and a redescription of *Sebastes aleutianus* (Jordan and
 4531 Evermann, 1898) (Teleostei: Scorpaeniformes). Fish. Bull. 106:111-134.
- 4532 Otto, R. S. and P. A. Cummiskey. 1985, January. Observations on the reproductive biology of golden
 4533 king crab (*Lithodes aequispina*) in the Bering Sea and Aleutian Islands. In Proc. Int. King Crab
 4534 Symp (pp. 123-136).
- 4535 Pardoe, I. 2012 Applied Regression Modeling, 2nd ed. John Wiley & Sons Inc, Hoboken, NJ, USA. 325
 4536 pp. DOI:10.1002/9781118345054
- 4537 Percy, W. G., M. J. Hosie, and S. L. Richardson. 1977. Distribution and duration of pelagic life of larvae
 4538 of Dover sole, *Microstomus pacificus*; rex sole, *Glyptocephalus zachirus*; and petrale sole,
 4539 *Eopsetta jordani*, in waters off Oregon. Fish. Bull. 75:173–183.

- 4540 Pearson, K. E. and D. R. Gunderson. 2003. Reproductive biology and ecology of shortspine thornyhead
4541 rockfish, *Sebastobus alascanus*, and longspine thornyhead rockfish, *S. altivelis*, from the
4542 northeastern Pacific Ocean. *Env. Biol. Fish.* 67(2):117-136.
- 4543 Phillips, S. J., and M. Dudík. 2008. Modeling of species distributions with Maxent: New extensions and a
4544 comprehensive evaluation. *Ecography* 31(2):161–175. [https://doi.org/10.1111/j.0906-
4545 7590.2008.5203.x](https://doi.org/10.1111/j.0906-7590.2008.5203.x)
- 4546 Phillips S. J., R. P. Anderson, and R. E. Schapire. 2006. Maximum entropy modeling of species
4547 geographic distributions. *Ecol. Model.* 190(3-4):231-59.
- 4548 Phillips, S. J., R. P. Anderson, M. Dudík, R. E. Schapire, and M. E. Blair. 2017. Opening the black box:
4549 an open-source release of Maxent. *Ecography* 40:887-893.
- 4550 Pirtle, J. L., T. C. Weber, C. D. Wilson, and C. N. Rooper. 2015. Assessment of trawlable and
4551 untrawlable seafloor using multibeam-derived metrics. *Methods Oceanogr.* 12:18–35.
- 4552 Pirtle, J. L., S. K. Shotwell, M. Zimmermann, J. A. Reid, and N. Golden. 2019. Habitat suitability models
4553 for groundfish in the Gulf of Alaska. *Deep-Sea Res. Pt. II.* <https://doi:10.1016/j.dsr2.2017.12.005>.
- 4554 Politou, C. Y., G. Tserpes, and J. Dokos. 2008. Identification of deepwater pink shrimp abundance
4555 distribution patterns and nursery grounds in the eastern Mediterranean by means of generalized
4556 additive modeling. *Hydrobiol.* 612(1):99-107. doi: 10.1007/s10750-008-9488-8.
- 4557 Porter, S. M. 2005. Temporal and spatial distribution and abundance of flathead sole (*Hippoglossoides*
4558 *elassodon*) eggs and larvae in the western Gulf of Alaska. *Fish. Bull.* 103:648-658.
- 4559 Potts, J., and J. Elith. 2006. Comparing species abundance models. *Ecol. Model.* 199:153-163.
- 4560 Punt, A. E., D. S. Butterworth, C. L. de Moor, J. A. A. De Oliveira, and M. Haddon. 2016. Management
4561 strategy evaluation: best practices. *Fish Fisher.* 17:303–334. <https://doi.org/10.1111/faf.12104>
- 4562 R Core Development Team. 2020. R: A Language and Environment for Statistical Computing. R
4563 Foundation for Statistical Computing. Vienna, Austria.
- 4564 Richwine, K. A., K. R. Smith, and R. A. McConnaughey. 2018. Surficial sediments of the eastern Bering
4565 Sea continental shelf: EBSSD-2 database documentation. U.S. Dep. Commer., NOAA Tech.
4566 Memo. NMFS-AFSC-377, 48 p.
- 4567 Rodgveller, C. J., K. B. Echave, P-J. F. Hulson, and K. M. Coutré. 2018. Age-at-maturity and fecundity
4568 of female sablefish sampled in December of 2011 and 2015 in the Gulf of Alaska. U.S. Dep.
4569 Commer., NOAA Tech. Memo. NMFS-AFSC-371, 31 p.
- 4570 Rohan, S. K., S. Kotwicki, L. L. Britt, E. A. Laman, and K. Aydin. 2020. Deriving apparent optical
4571 properties from light measurements obtained using bottom-trawl-mounted archival tags. U.S.
4572 Dep. Commer., NOAA Tech. Memo. NMFS-AFSC-403, 91 p.
- 4573 Rohan, S. K., S. Kotwicki, K. A. Kearney, J. A. Schulien, E. A. Laman, E. D. Cokelet, D. A. Beauchamp,
4574 L. L. Britt, K. Y. Aydin, and S. G. Zador. 2021. Using bottom trawls to monitor subsurface water
4575 clarity in marine ecosystems. *Prog. Oceanogr.* 194:102554.
4576 <https://doi.org/10.1016/j.pocean.2021.102554>
- 4577 Rooney, S., E. A. Laman, C. N. Rooper, K. Turner, D. W. Cooper, and M. Zimmermann. 2018. Model-
4578 based essential fish habitat definitions for Gulf of Alaska groundfish species. U.S. Dep. Commer.,
4579 NOAA Tech. Memo. NMFS-AFSC-373, 370 p.
- 4580 Rooper, C. N. 2008. An ecological analysis of rockfish (*Sebastes* spp.) assemblages in the North Pacific
4581 Ocean along broad-scale environmental gradients. *Fish. Bull.* 106:1-11.

- 4582 Rooper, C. N., J. L. Boldt, and M. Zimmermann. 2007. An assessment of juvenile Pacific ocean perch
4583 (*Sebastes alutus*) habitat use in a deepwater nursery. *Estuar. Coastal Shelf Sci.* 75:371-380.
- 4584 Rooper, C. N., G. R. Hoff, and A. DeRobertis. 2010. Assessing habitat utilization and rockfish (*Sebastes*
4585 spp.) biomass on an isolated rocky ridge using acoustics and stereo image analysis. *Can. J. Fish.*
4586 *Aquat. Sci.* 67(10):1658-1670. doi: 10.1139/F10-088.
- 4587 Rooper, C. N., Zimmermann, M., Prescott, M. M., and Hermann, A. J. 2014. Predictive models of coral
4588 and sponge distribution, abundance, and diversity in bottom trawl surveys of the Aleutian Islands,
4589 Alaska. *Mar. Ecol. Prog. Ser.* 503:157-176. doi: 10.3354/meps10710.
- 4590 Rooper, C. N., M. F., Sigler, P. Goddard, P. Malecha, R. Towler, K. Williams, R. Wilborn, and M.
4591 Zimmermann. 2016. Validation and improvement of species distribution models for structure
4592 forming invertebrates in the eastern Bering Sea with an independent survey. *Mar. Ecol. Prog. Ser.*
4593 551:117-130. doi: 10.3354/meps11703.
- 4594 Rooper, C. N., R. Wilborn, P. Goddard, K. Williams, R. Towler, and G. R. Hoff. 2017a. Validation of
4595 deep-sea coral and sponge distribution models in the Aleutian Islands, Alaska. *ICES J. Mar. Sci.*
4596 75(1):199-209.
- 4597 Rooper, C. N., M. Zimmermann, and M. M. Prescott. 2017b. Comparison of modeling methods to predict
4598 spatial distribution of deep-sea coral and sponge in the Gulf of Alaska. *Deep-Sea Res. Part I:*
4599 *Oceanogr. Res. Papers* 126:148-161. doi: 10.1016/j.dsr.2017.07.002.
- 4600 Rooper C. N., I. Ortiz, A. J. Hermann, N. (E. A.) Laman, W. Cheng, K. Kearney, and K. Aydin. 2021.
4601 Predicted shifts of groundfish distribution in the eastern Bering Sea under climate change, with
4602 implications for fish populations and fisheries management. *ICES J. Mar. Sci.* doi:
4603 10.1093/icesjms/fsaa215.
- 4604 Rutecki, T. L., and E. R. Varosi. 1997. Distribution, age, and growth of juvenile sablefish, *Anoplopoma*
4605 *fimbria*, in Southeast Alaska. **In** Saunders, M., Wilkins, M. (Eds.), *Biology and Management of*
4606 *Sablefish (Anoplopoma fimbria)*. U.S. Dep. Commer., NOAA Tech.
- 4607 Sasaki, T., D.H. Japan. In Hanselman, J. Heifetz, K.B. Echave, and S.C. Dressel. 1985. Studies on the 446
4608 Sablefish Resources in the North Pacific Ocean. *Far Seas Fishery Laboratory. Bull* 22 (2): 1-447.
- 4609 Sampson, D. B., and S. M. Al-Jufaily. 1999. Geographic variation in the maturity and growth schedules
4610 of English sole along the U.S. West Coast. *J. Fish Biol.* 54:1-17.
4611 <https://doi.org/10.1006/jfbi.1998.0841>.
- 4612 Scharf, H. R., X. Lu, P. J. Williams, and M. B. Hooten. Online Early (2019). Hierarchical approaches for
4613 flexible and interpretable binary regression models. arXiv preprint arXiv:1905.05242.
- 4614 Schmidt, J., I. S. Evans, and J. Brinkmann. 2003. Comparison of polynomial models for land surface
4615 curvature calculation. *International Journal of Geographical Information Science*, 17(8), 797-814.
4616 <https://doi.org/10.1080/13658810310001596058>. *Int. J. Geogr. Inf. Sci.* 17:797-814.
- 4617 Shimada, A. M., and D. K. Kimura. 1994. Seasonal Movements of Pacific Cod, *Gadus Macrocephalus*, in
4618 the Eastern Bering Sea and Adjacent Waters Based on Tag-Recapture Data. *Fish. Bull.* 82: 800-
4619 816.
- 4620 Shirley, T.C. and S. Zhou. 1997. Lecithotrophic development of the golden king crab *Lithodes*
4621 *aequispinus* (Anomura: Lithodidae). *J. of Crus. Bio.* 17(2):207-216.
- 4622 Shotwell, S. K., I. Spies, L. Britt, M. Bryan, D. H. Hanselman, D. G. Nichol, J. Hoff, W. Palsson, T. K.
4623 Wildebuer, and S. Zador. 2020a. Assessment of the arrowtooth flounder stock in the Eastern
4624 Bering Sea and Aleutian Islands. **In** Stock assessment and fishery evaluation report for the

- 4625 groundfish resources of the BSAI. North Pacific Fishery Management Council 1007 West Third,
4626 Suite 400 Anchorage, AK 99501.
- 4627 Shotwell, K. S., I. B. Spies, K. Echave, I. Ortiz, J. Sullivan, P. D. Spencer, and W. Palsson. 2020b.
4628 Assessment of the shorttraker rockfish stock in the Bering Sea and Aleutian Islands. *In* Stock
4629 Assessment and Fishery Evaluation Report for the Groundfish Resources of the Bering
4630 Sea/Aleutian Islands Regions. North Pacific Fishery Management Council 1007 West Third,
4631 Suite 400 Anchorage, AK 99501
- 4632 Sinclair, E. H., D. S. Johnson, T. K. Zeppelin, and T. S. Gelatt. 2013. Decadal variation in the diet of
4633 western stock Steller sea lions (*Eumetopias jubatus*). U.S. Dep. Commer., NOAA Tech. Memo.,
4634 NMFS-AFSC-248, 67 p.
- 4635 Sibson, R. 1981. A Brief Description of Natural Neighbor Interpolation, Chapter 2 *In* V. Barnett (ed.),
4636 Interpolating Multivariate Data. John Wiley and Sons, Chichester, West Sussex, UK, PO19 8SQ.
4637 pp. 21-36.
- 4638 Siddeek, M. S. M., J. Zheng, C. Siddon, B. Daly, M.J. Westphal, and L. Hulbert. Aleutian Islands Golden
4639 King Crab Model-Based Stock Assessment. *In* Stock Assessment and Fishery Evaluation Report
4640 for the king and tanner crab fisheries of the Bering Sea and Aleutian Islands Regions. North
4641 Pacific Fishery Management Council 1007 West Third, Suite 400 Anchorage, AK 99501.
- 4642 Sigler, M. F., M. P. Eagleton, T. E. Helser, J. V. Olson, J. L. Pirtle, C. N. Rooper, S. C. Simpson, and R.
4643 P. Stone. 2017. Alaska Essential Fish Habitat Research Plan: A Research Plan for the National
4644 Marine Fisheries Service's Alaska Fisheries Science Center and Alaska Regional Office. AFSC
4645 Processed Rep. 2015-05, 22 p. Alaska Fish. Sci. Cent., NOAA, Natl. Mar. Fish. Serv., 7600 Sand
4646 Point Way NE, Seattle WA 98115.
- 4647 Sigler, M. F., C. N. Rooper, G. R. Hoff, R. P. Stone, R. A. McConnaughey, and T. K. Wilderbuer. 2015.
4648 Faunal features of submarine canyons on the eastern Bering Sea slope. *Mar. Ecol. Prog. Ser.*
4649 526:21-40.
- 4650 Simpson, S. C., M. P. Eagleton, J. V. Olson, G. A. Harrington, and S. R. Kelly. 2017. Final Essential
4651 Fish Habitat (EFH) 5-year Review, Summary Report: 2010 through 2015. U.S. Dep. Commer.,
4652 NOAA Tech. Memo. NMFS-F/AKR-15, 115p.
- 4653 Siwicke, K. A., and K. Coutre. 2020. Periodic movements of Greenland turbot *Reinhardtius*
4654 *hippoglossoides* in the eastern Bering Sea and Aleutian Islands. *Fish. Res.* 229, 13 p.
- 4655 Smith, A. D. M. 1994. Management strategy evaluation – the light on the hill, in: In 'Population
4656 Dynamics for Fisheries Management.
- 4657 Sohn, D., L. Ciannelli, J T. Duffy-Anderson. 2010. Distribution and drift pathways of Greenland halibut
4658 (*Reinhardtius hippoglossoides*) during early life stages in the eastern Bering Sea and Aleutian
4659 Islands. *Fish. Oceanogr.* 19:339-353.
- 4660 Somerton, D. A., and R. S. Otto. 1986. Distribution and reproductive biology of the golden king crab,
4661 *Lithodes aequispina*, in the eastern Bering Sea. *Fish. Bull.*, 84(3):571-584.
- 4662 Spencer, P. D., and J. Ianelli. 2019. Assessment of the northern rockfish stock in the Bering Sea/Aleutian
4663 Islands. *In* Stock Assessment and Fishery Evaluation Report for the Groundfish Resources of the
4664 Bering Sea and Aleutian Islands. North Pacific Fishery Management Council 1007 West Third,
4665 Suite 400 Anchorage, AK 99501.
- 4666 Spencer, P. D., J. N. Ianelli, and W. Palsson. 2020. Assessment of the blackspotted and rougheye rockfish
4667 stock in the Bering Sea and Aleutian Islands. *In* Stock Assessment and Fishery Evaluation Report

- 4668 for the Groundfish Resources of the Bering Sea/Aleutian Islands Regions. North Pacific Fishery
4669 Management Council 1007 West Third, Suite 400 Anchorage, AK 99501.
- 4670 Spies, I. 2012. Landscape genetics reveals population subdivision in Bering Sea and Aleutian Islands
4671 Pacific cod. *Trans. Am. Fish. Soc.* 141:1557-1573.
- 4672 Spies, I., R., G. G. Thompson, I. Ortiz, E. Siddon, and W. A. Palsson. 2020. Assessment of the Pacific
4673 cod stock in the Aleutian Islands. *In* Stock assessment and fishery evaluation report for the
4674 groundfish resources of the Bering Sea and Aleutian Islands. North Pacific Fishery Management
4675 Council 1007 West Third, Suite 400 Anchorage, AK 99501.
- 4676 Stabeno, P. J., J. D. Schumacher, and K. Ohtani. 1999. The physical oceanography of the Bering Sea. *In*
4677 Loughlin T. R., and K. Ohtani (eds) *Dynamics of the Bering Sea: A Summary of Physical,*
4678 *Chemical, and Biological Characteristics, and a Synopsis of Research on the Bering Sea,* North
4679 Pacific Marine Science Organization (PICES), University of Alaska Sea Grant, AK-SG-99-03.
4680 Fairbanks, Alaska, p. 1-59.
- 4681 Stabeno, P. J., R. K. Reed, and J. M. Napp. 2002. Transport through Unimak Pass, Alaska. *Deep-Sea Res.*
4682 *II* 49:5919-5930.
- 4683 Stahl, J.P. and G. H. Kruse. 2008. Spatial and temporal variability in size at maturity of walleye pollock
4684 in the eastern Bering Sea. *Trans. Amer. Fish. Soc.*, 137(5):1543-1557.
- 4685 Stark, J. W., and D. A. Somerton. 2002. Maturation, spawning and growth of rock soles off Kodiak
4686 Island in the Gulf of Alaska. *J. Fish. Bio.* 61:417-431.
- 4687 Stark, J. W., 2007. Geographic and seasonal variations in maturation and growth of female Pacific cod
4688 (*Gadus macrocephalus*) in the Gulf of Alaska and Bering Sea. *Fish. Bull.* 105(3):396-407.
- 4689 Stark, J. W. 2012a. Contrasting maturation and growth of northern rock sole in the Eastern Bering Sea
4690 and Gulf of Alaska for the purpose of stock management. *N. Amer. J. Fish. Manage.* 32:93-99.
- 4691 Stark, J. W. 2012b. Female maturity, reproductive potential, relative distribution, and growth compared
4692 between arrowtooth flounder (*Atheresthes stomias*) and Kamchatka flounder (*A. evermanni*)
4693 indicating concerns for management. *J. Appl. Ichthyol.* 28:226-230.
- 4694 Stauffer, G. 2004. NOAA protocols for groundfish bottom trawl surveys of the Nation's fishery
4695 resources. U. S. Dep. Commer., NOAA Tech. Memo. NMFS-F/SPO-65, 205 p.
- 4696 Stevenson, D. E., J. W. Orr, G. R. Hoff, and J. D. McEachran. 2007. *Sharks, skates and ratfish of Alaska.*
4697 Fairbanks, AK: Alaska Sea Grant, University of Alaska.
- 4698 Stewart, I. J., and Hicks, A. C. 2018. Interannual stability from ensemble modelling. *Canadian Journal of*
4699 *Fisheries and Aquatic Sciences*, 75: 2109–2113.
- 4700 Stone, R., H. Lehnert, and H. Reiswig. 2011. A guide to the deep-water sponges of the Aleutian Island
4701 archipelago. NOAA Professional Paper NMFS 12. Available from
4702 <https://spo.nmfs.noaa.gov/content/guide-deepwater-sponges-aleutian-island-archipelago>
4703 (accessed 29 August 2021).
- 4704 Sullivan, J., I. Spies, P. Spencer, A. Kingham, T. Tenbrink, and W. Palsson. 2020. Assessment of the
4705 Other Rockfish stock complex in the Bering Sea/Aleutian Islands. *In* Stock Assessment and
4706 Fishery Evaluation Report for the Groundfish Resources of the Bering Sea and Aleutian Islands.
4707 North Pacific Fishery Management Council 1007 West Third, Suite 400 Anchorage, AK 99501.

- 4708 Tenbrink, T. T., and P. D. Spencer. 2013. Reproductive biology of Pacific ocean perch and northern
4709 rockfish in the Aleutian Islands. *N. Amer. J. Fish. Manage.* 33(2):373-383.
- 4710 Tenbrink, T. T., and T. K. Wilderbuer. 2015. Updated maturity estimates for flatfishes (Pleuronectidae) in
4711 the eastern Bering Sea, with implications for fishery management. *Mar. Coast. Fish.* 7:474-482.
4712 <https://doi.org/10.1080/19425120.2015.1091411>
- 4713 TenBrink, T., T. Helser, T. Wilderbuer, M. Bryan. *In Review*. Greenland turbot (*Reinhardtius*
4714 *hippoglossoides*) biology in the eastern Bering Sea: reproduction and spatio-temporal size
4715 structure.
- 4716 Tenbrink, T. T., and T. E. Helser. 2021. Reproductive biology, size, and age structure of harlequin
4717 rockfish: spatial analysis of life history traits. *Mar. Coast. Fish.* 13(5):463-477.
4718 <https://doi.org/10.1002/mcf2.10172>
- 4719 Tenbrink, T. T., and T. E. Helser. *In preparation*. Assessment of the other rockfish stock complex in the
4720 Gulf of Alaska. *In* Stock Assessment and Fishery Evaluation Report for the Groundfish
4721 Resources of the Gulf of Alaska. North Pacific Fishery Management Council 1007 West Third,
4722 Suite 400 Anchorage, AK 99501.
- 4723 Thompson, G. G., J. Conner, S. Kalei Shotwell, B. Fissel, T. Hurst, B. Laurel, L. Rogers, and E. Siddon.
4724 2020. Assessment of the Pacific cod stock in the Eastern Bering Sea. *In* Stock Assessment and
4725 Fishery Evaluation Report for the Groundfish Resources of the Bering Sea/Aleutian Islands
4726 Regions. North Pacific Fishery Management Council 1007 West Third, Suite 400 Anchorage, AK
4727 99501.
- 4728 Thorson, J. T., J. N. Ianelli, and S. Kotwicki. 2017. The relative influence of temperature and size-
4729 structure on fish distribution shifts: A case-study on walleye pollock in the Bering Sea. *Fish Fish.*
4730 18(6):1073-1084.
- 4731 Thorson, J. T. 2019. Measuring the impact of oceanographic indices on species distribution shifts: The
4732 spatially varying effect of cold-pool extent in the eastern Bering Sea. *Limnol. Oceanogr.*
4733 64(6):2632–2645. <https://doi.org/10.1002/lno.11238>
- 4734 Thorson, J. T., C. F. Adams, E. N. Brooks, L. B. Eisner, D. G. Kimmel, C. N. Legault, L. A. Rogers, and
4735 E. M. Yasumiishi. 2020a. Seasonal and interannual variation in spatio-temporal models for index
4736 standardization and phenology studies. *ICES J. Mar. Sci.* 77:1879–1892.
4737 <https://doi.org/10.1093/icesjms/fsaa074>
- 4738 Thorson, J. T., W. Cheng, A. J. Hermann, J. N. Ianelli, M. A. Litzow, C. A. O’Leary, and G. Thompson.
4739 2020b. Empirical orthogonal function regression: Linking population biology to spatial varying
4740 environmental conditions using climate projections. *Global Change Biology*, 26(8):4638–4649.
4741 <https://doi.org/10.1111/gcb.15149>
- 4742 Thorson, J. T., A. J. Hermann, K. Siwicke, and M. Zimmermann. 2021. Grand challenge for habitat
4743 science: Stage-structured responses, nonlocal drivers, and mechanistic associations among habitat
4744 variables affecting fishery productivity. *ICES J. Mar. Sci.* 78(6):1956–1968.
4745 <https://doi.org/10.1093/icesjms/fsaa236>
- 4746 Tribuzio, C. A., and K. B. Echave. 2019. Assessment of the other rockfish stock complex in the Gulf of
4747 Alaska. *In* Stock Assessment and Fishery Evaluation Report for the Groundfish Resources of the
4748 Gulf of Alaska. North Pacific Fishery Management Council 1007 West Third, Suite 400
4749 Anchorage, AK 99501.

- 4750 Turner, K., C. N. Rooper, E. A. Laman, S. Rooney, C. W. Cooper, D. W., and M. Zimmermann. 2017.
4751 Model-based essential fish habitat definitions for Aleutian Islands groundfish species. U.S. Dep.
4752 Commer., NOAA Tech. Memo. NMFS-AFSC-360, 239 p.
- 4753 Venables W. N., and B. D. Ripley. 2002. Modern Applied Statistics with S. Fourth Edition. Springer
4754 Science+Business Media, New York, N.Y.
- 4755 von Szalay, P. G., and N. W. Raring. 2018. Data Report: 2017 Gulf of Alaska bottom trawl survey. U.S.
4756 Dep. Commer., NOAA Tech. Memo. NMFS-AFSC-374, 260 p.
- 4757 von Szalay, P. G., and N. W. Raring. 2020. Data Report: 2018 Aleutian Islands bottom trawl survey. U.S.
4758 Dep. Commer., NOAA Tech. Memo. NMFS-AFSC-409, 175 p.
- 4759 Wakabayashi, K., R. G. Bakkala, and M. S. Alton. 1985. Methods of the Japan demersal trawl surveys, p.
4760 7-29. *In* R. G. Bakkala and K. Wakabayashi (Editors), Results of cooperative Japan groundfish
4761 investigations in the Bering Sea during May-August 1979. Int. N. Pac. Fish. Comm. Bull. 44.
- 4762 Walbridge, S., N. Slocum, M. Pobuda, and D. J. Wright. 2018. Unified geomorphological analysis
4763 workflows with Benthic Terrain Modeler. Geosci. 8:94. Version 3.0 is available at:
4764 <http://github.com/EsriOceans/btm>.
- 4765 Walters, G. E., and T. K. Wilderbuer. 2000. Decreasing length at age in a rapidly expanding population of
4766 northern rock sole in the eastern Bering Sea and its effect on management advice. J. Sea Res.
4767 44:17-26.
- 4768 Watson, D. F., and G. M. Philip. 1985. A refinement of inverse distance weighted interpolation. Geo-
4769 processing 2(4):315-327.
- 4770 Weinberg, K. L., and S. Kotwicki. 2008. Factors influencing net width and sea floor contact of a survey
4771 bottom trawl. Fish. Res. 93:265-279.
- 4772 Weiss, A. D. 2001. Topographic Positions and Landforms Analysis (Conference Poster). Proceedings of
4773 the 21st Annual ESRI User Conference. San Diego, CA, July 9-13.
- 4774 Wilson, M. F. J., B. O'Connell, C. Brown, J. C. Guinan, and A. J. Grehan. 2007. Multiscale terrain
4775 analysis of multibeam bathymetry data for habitat mapping on the continental slope. Mar.
4776 Geodesy 30:3-35.
- 4777 Wing, B. L. 1997. Distribution of sablefish, *Anoplopoma fimbria*, larvae in the Eastern Gulf of Alaska. *In*
4778 M. Saunders and M. Wilkins (eds.). Proceedings of the International Symposium on the Biology
4779 and Management of Sablefish. pp 13-26. NOAA Tech. Rep. 130.
- 4780 Wood, S.N. (2003) Thin plate regression splines. J. R. Statist. Soc. B 65(1):95-114.
- 4781 Wood, S.N. 2011. Fast stable restricted maximum likelihood and marginal likelihood estimation of
4782 semiparametric generalized linear models. Journal of the Royal Stat. Soc. (B) 73(1):3-36.
- 4783 Wood, S. N. 2017. Generalized Additive Models: An Introduction with R, Second Edition. CRC Press,
4784 Taylor & Francis Group. 476 pp.
- 4785 Wright, D. J., M. Pendleton, J. Boulware, S. Walbridge, B. Gerlt, D. Eslinger, D. Sampson, et al. 2012.
4786 ArcGIS Benthic Terrain Modeler (BTM), v. 3.0, Environmental Systems Research Institute,
4787 NOAA Coastal Services Center, Massachusetts Office of Coastal Zone Management. Available
4788 at: <http://esriurl.com/5754>.
- 4789 Yang, M. S. 2007. Food Habits and Diet Overlap of Seven Skate Species in the Aleutian Islands. U.S.
4790 Dep. Commer., NOAA Tech. Memo. NMFS-AFSC-177: p. 57.

- 4791 Yang, M. S., and P. A. Livingston. 1986. Food habits and diet overlap of two congeneric species,
4792 *Atheresthes stomias* and *Atheresthes evermanni*, in the eastern Bering Sea. Fish. Bull. 82:615-
4793 623.
- 4794 Yeung, C., and D. W. Cooper, 2020. Contrasting the variability in spatial distribution of two juvenile
4795 flatfishes in relation to thermal stanzas in the eastern Bering Sea. ICES J. Mar. Sci. 77(3):953-
4796 963.
- 4797 Zar, J. H. 1984. Biostatistical Analysis, 2nd Ed., Simon and Schuster Company, New Jersey, USA. 717
4798 pgs.
- 4799 Zevenbergen, L. W., and Thorne, C. R. 1987. Quantitative analysis of land surface topography. Earth
4800 Surface Processes and Landforms, 12: 47–56.
- 4801 Zheng, J., and M. S. M. Siddeek. 2019. Bristol Bay red king crab stock assessment in Fall 2019. **In** Stock
4802 Assessment and Fishery Evaluation Report for the king and tanner crab fisheries of the Bering
4803 Sea and Aleutian Islands Regions. North Pacific Fishery Management Council 1007 West Third,
4804 Suite 400 Anchorage, AK 99501.
- 4805 Zimmermann, M., and J. L. Benson. 2013. Smooth sheets: How to work with them in a GIS to derive
4806 bathymetry, features and substrates. NOAA Tech. Memo. NMFS-AFSC-249. 52 p.
- 4807 Zimmermann, M., M. M. Prescott, and C. N. Rooper. 2013. Smooth Sheet Bathymetry of the Aleutian
4808 Islands. U.S. Dep. Commer., NOAA Tech. Memo. NMFS-AFSC-250, 43p.
- 4809 Zimmerman, M., and P. Goddard. 1996. Biology and distribution of arrowtooth, *Atheresthes stomias*, and
4810 Kamchatka, *A. evermanni*, flounders in Alaskan waters. Fish. Bull. 94: pp. 358-370.
- 4811 Zimmermann, M., M. M. Prescott, and P. J. Haeussler. 2019. Bathymetry and Geomorphology of
4812 Shelikof Strait and the Western Gulf of Alaska. Geosci. 9:409.
4813 <https://doi.org/10.3390/geosciences9100409>.
- 4814 Zuur, A. F., E. N., Ieno, N. J. Walker, A. A. Saveliev, and G. M. Smith. 2009. Mixed Effects Models and
4815 Extensions in Ecology with R. Springer Science+Business Media, LLC. New York, N.Y.